

**RATIONAL DESIGN, SYNTHESIS AND BIOLOGICAL ACTIVITY OF
SOME GLUTAMINE-BASED ANTICANCER HYDROXAMATES AS
PROMISING MATRIX METALLOPROTEINASE-2 INHIBITORS**

Thesis Submitted by

SANDIP KUMAR BAIDYA

Doctor of Philosophy (Pharmacy)

DEPARTMENT OF PHARMACEUTICAL TECHNOLOGY

FACULTY COUNCIL OF ENGINEERING & TECHNOLOGY

JADAVPUR UNIVERSITY

KOLKATA, INDIA

2023

**JADAVPUR UNIVERSITY
KOLKATA – 700032, INDIA**

Registration No. 1021713003

Index No. 255/17/Ph

1. Title of the Thesis:

Rational Design, Synthesis and Biological Activity of Some Glutamine-based Anticancer Hydroxamates as Promising Matrix Metalloproteinase-2 Inhibitors

2. Name, Designation & Institution of the Supervisor/s:

- A) Prof. Tarun Jha, Professor, Department of Pharmaceutical Technology, Jadavpur University, Kolkata 700032, India.
- B) Dr. Nilanjan Adhikari, Assistant Professor, Department of Pharmaceutical Technology, Jadavpur University, Kolkata 700032, India.

3. List of Publication:

Published paper

- [1] **Baidya SK**, Patel T, Himaja A, Banerjee S, Das S, Ghosh B, Jha T, Adhikari N. Biphenylsulfonamides as effective MMP-2 inhibitors with promising antileukemic efficacy: Synthesis, in vitro biological evaluation, molecular docking, and MD simulation analysis. Drug Development Research. 2024 Sep;85(6):e22255. Doi: 10.1002/ddr.22255.
- [2] **Baidya SK**, Banerjee S, Ghosh B, Jha T, Adhikari N. Pinpointing prime structural attributes of potential MMP-2 inhibitors comprising alkyl/arylsulfonyl pyrrolidine scaffold: a ligand-based molecular modelling approach validated by molecular dynamics simulation analysis. SAR and QSAR in Environmental Research. 2024 Aug 30:1-28. Doi: 10.1080/1062936X.2024.2389822.
- [3] Das S, Mondal S, Patel T, Himaja A, Adhikari N, Banerjee S, **Baidya SK**, De AK, Gayen S, Ghosh B, Jha T. Derivatives of D (-) glutamine-based MMP-2 inhibitors as an effective remedy for the management of chronic myeloid leukemia-Part-I: Synthesis, biological screening and in silico binding interaction analysis. European Journal of Medicinal Chemistry. 2024 Jun 1:116563. Doi: 10.1016/j.ejmech.2024.116563.

- [4] Jha T, Jana R, Banerjee S, **Baidya SK**, Amin SA, Gayen S, Ghosh B, Adhikari N. Exploring different classification-dependent QSAR modelling strategies for HDAC3 inhibitors in search of meaningful structural contributors. SAR and QSAR in Environmental Research. 2024 May 18;1-23. Doi: 10.1080/1062936X.2024.2350504.
- [5] **Baidya SK**, Banerjee S, Gutti S, Jha T, Adhikari N. Matrix metalloproteinase-8 (MMP-8) and its inhibitors: A minireview. European Journal of Medicinal Chemistry Reports. 2024 Apr 1;10:100130. Doi: 10.1016/j.ejmcr.2024.100130.
- [6] Banerjee S, **Baidya SK**, Adhikari N, Jha T. An updated patent review of matrix metalloproteinase (MMP) inhibitors (2021-present). Expert Opin Ther Pat. 2023 Oct 3;33(10):631-49. Doi: 10.1080/13543776.2023.2284935.
- [7] Jana S, Banerjee S, **Baidya SK**, Ghosh B, Jha Tarun, Adhikari N. A combined ligand-based and structure-based in silico molecular modeling approach to pinpoint the key structural attributes of hydroxamate derivatives as promising meprin β inhibitors. J Biomol Struct Dyn. 2023 Dec 21:1-7. Doi: 10.1080/07391102.2023.2298394.
- [8] **Baidya SK**, Banerjee S, Ghosh B, Jha T, Adhikari N. A fragment-based exploration of diverse MMP-9 inhibitors through classification-dependent structural assessment. Journal of Molecular Graphics and Modelling. 2024 Jan 126;108671. Doi: 10.1016/j.jmgm.2023.108671.
- [9] **Baidya SK**, Banerjee S, Ghosh B, Jha T, Adhikari N. Assessing structural insights into in house arylsulfonyl L-(+) glutamine MMP-2 inhibitors as promising anticancer agents through ligand-based and structure-based computational modeling approaches. SAR and QSAR in Environmental Research. 2023 Oct 18;1-26. Doi: 10.1080/1062936X.2023.2261842.
- [10] Tamang JDS, Banerjee S, **Baidya SK**, Ghosh B, Adhikari N, Jha T. Employing comparative QSAR techniques for the recognition of dibenzofuran and dibenzothiophene derivatives toward MMP-12 Inhibition. Journal of Biomolecular Structure and Dynamics. 2023;1-17. Doi: 10.1080/07391102.2023.2239923.
- [11] Banerjee S, **Baidya SK**, Ghosh B, Jha T, Adhikari N. Exploration of structural alerts and fingerprints for novel anticancer therapeutics: A robust classification-QSAR dependent structural analysis of drug-like MMP-9 inhibitors. SAR and QSAR in Environmental Research. 2023;1-21. Doi: 10.1080/1062936X.2023.2209737.
- [12] Banerjee S, **Baidya SK**, Adhikari N, Jha T, Ghosh B. Hydrazides as Potential HDAC Inhibitors: Structure-activity Relationships and Biological Implications. Current Topics

in Medicinal Chemistry. 2023 Oct 1;23(25):2343-72. Doi: 10.2174/1568026623666230405124207.

- [13] Banerjee S, **Baidya SK**, Ghosh B, Nandi S, Mandal M, Jha T, Adhikari N. Quantitative structural assessments of potential meprin β inhibitors by non-linear QSAR approaches and validation by binding mode of interaction analysis. New Journal of Chemistry. 2023;47(15):7051-7069. Doi: 10.1039/D2NJ04753E.
- [14] Banerjee S, **Baidya SK**, Adhikari N, Jha T. A comparative quantitative structural assessment of benzothiazine-derived HDAC8 inhibitors by predictive ligand-based drug designing approaches. SAR and QSAR in Environmental Research. 2022;33(12):987-1011. Doi: 10.1080/1062936X.2022.2155241.
- [15] Banerjee S, **Baidya SK**, Adhikari N, Ghosh B, Jha T. Glycyrrhizin as a promising kryptonite against SARS-CoV-2: Clinical, experimental, and theoretical evidences. Journal of Molecular Structure. 2022;1275:134642. Doi: 10.1016/j.molstruc.2022.134642.
- [16] Kundu R, Banerjee S, **Baidya SK**, Adhikari N, Jha T. A quantitative structural analysis of AR-42 derivatives as HDAC1 inhibitors for the identification of promising structural contributors. SAR and QSAR in Environmental Research. 2022;33(11):861-883. Doi: 10.1080/1062936X.2022.2145353.
- [17] **Baidya SK**, Banerjee S, Adhikari N, Jha T. Selective inhibitors of medium-size S1' pocket matrix metalloproteinases: A stepping stone of future drug discovery. Journal of Medicinal Chemistry. 2022;65:10709-10754. Doi: 10.1021/acs.jmedchem.1c01855.
- [18] Banerjee S, **Baidya SK**, Ghosh B, Adhikari N, Jha T. First report on predictive comparative ligand-based multi-QSAR modeling analysis of 4-pyrimidinone and 2-pyridinone based APJ inhibitors. New Journal of Chemistry. 2022;46:11591-11607. Doi: 10.1039/D2NJ01923J
- [19] Yadav V, Banerjee S, **Baidya SK**, Adhikari N, Jha T. Applying comparative molecular modeling techniques on diverse hydroxamate-based HDAC2 inhibitors: An attempt to identify promising structural features for potent HDAC2 inhibition. SAR and QSAR in Environmental Research. 2022;33(1):1-22. Doi: 10.1080/1062936X.2021.2013317.
- [20] Adhikari N, Banerjee S, **Baidya SK**, Ghosh B, Jha T. Ligand-based quantitative structural assessments of SARS-CoV-2 3CLpro inhibitors: An analysis in light of structure-based multi-molecular modeling evidences. Journal of Molecular Structure. 2022;1251:132041. Doi: 10.1016/j.molstruc.2021.132041.

- [21] Guti S, **Baidya SK**, Banerjee S, Adhikari N, Jha T. A robust classification-dependent multi-molecular modelling study on some biphenyl sulphonamide based MMP-8 inhibitors. SAR and QSAR in Environmental Research. 2021;32(10):835-861. Doi: 10.1080/1062936X.2021.1976831.
- [22] **Baidya SK**, Amin SA, Jha T. Outline of gelatinase inhibitors as anti-cancer agents: A patent mini-review for 2010-present. European Journal of Medicinal Chemistry. 2021;213:113044. Doi: 10.1016/j.ejmech.2020.113044.
- [23] Adhikari N, Banerjee S, **Baidya SK**, Ghosh B, Jha T. Robust classification-based molecular modelling of diverse chemical entities as potential SARS-CoV-2 3CL^{pro} inhibitors: theoretical justification in light of experimental evidences. SAR and QSAR in Environmental Research. 2021;32(6):473-493. Doi: 10.1080/1062936X.2021.1914721.
- [24] Adhikari N, **Baidya SK**, Jha T. Effective anti-aromatase therapy to battle against estrogen-mediated breast cancer: Comparative SAR/QSAR assessment on steroidal aromatase inhibitors. European Journal of Medicinal Chemistry. 2020;208:112845. Doi: 10.1016/j.ejmech.2020.112845.
- [25] Banerjee S, Amin SA, **Baidya SK**, Adhikari N, Jha T. Exploring the structural aspects of ureido-amino acid-based APN inhibitors: a validated comparative multi-QSAR modelling study. SAR and QSAR in Environmental Research. 2020;31(5):325-345. Doi: 10.1080/1062936X.2020.1734080.
- [26] **Baidya SK**, Amin SA, Banerjee S, Adhikari N, Jha T. Structural exploration of arylsulfonamide-based ADAM17 inhibitors through validated comparative multi-QSAR modelling studies. Journal of Molecular Structure. 2019;1185:128-142. Doi: 10.1016/j.molstruc.2019.02.081.
- [27] Amin SA, Adhikari N, **Baidya SK**, Gayen S, Jha T. Structural refinement and prediction of potential CCR2 antagonists through validated multi-QSAR modeling studies. Journal of Biomolecular Structure and Dynamics. 2019;37(1):75-94. Doi: 10.1080/07391102.2017.1418679.

Book Chapters

- [1] Banerjee S, **Baidya SK**, Adhikari N, Jha T. 3D-QSAR studies: CoMFA, CoMSIA and Topomer CoMFA methods. In: *Modeling Inhibitors of Matrix Metalloproteinases*. (Ed. T. Jha). Taylor & Francis, CRC Press, 2023; Book ISBN 9781003303282. *In press*

- [2] **Baidya SK**, Banerjee S, Adhikari N, Jha T. Collagenases and their inhibitors. In: *Modeling Inhibitors of Matrix Metalloproteinases*. (Ed. T. Jha). Taylor & Francis, CRC Press, 2023; Book ISBN 9781003303282. *In press*
- [3] **Baidya SK**, Banerjee S, Adhikari N, Jha T. Stromelysins and their inhibitors. In: *Modeling Inhibitors of Matrix Metalloproteinases*. (Ed. T. Jha). Taylor & Francis, CRC Press, 2023; Book ISBN 9781003303282. *In press*
- [4] **Baidya SK**, Banerjee S, Adhikari N, Jha T. Matrilysins and their inhibitors. In: *Modeling Inhibitors of Matrix Metalloproteinases*. (Ed. T. Jha). Taylor & Francis, CRC Press, 2023; Book ISBN 9781003303282. *In press*
- [5] Banerjee S, **Baidya SK**, Adhikari N, Jha T. Membrane-type MMPs and their inhibitors. In: *Modeling Inhibitors of Matrix Metalloproteinases*. (Ed. T. Jha). Taylor & Francis, CRC Press, 2023; Book ISBN 9781003303282. *In press*
- [6] Banerjee S, **Baidya SK**, Adhikari N, Jha T. Other MMPs and their inhibitors. In: *Modeling Inhibitors of Matrix Metalloproteinases*. (Ed. T. Jha). Taylor & Francis, CRC Press, 2023; Book ISBN 9781003303282. *In press*
- [7] **Baidya SK**, Banerjee S, Adhikari N, Ghosh B, Jha T. Modeling inhibitors of Collagenases. In: *Modeling Inhibitors of Matrix Metalloproteinases*. (Ed. T. Jha). Taylor & Francis, CRC Press, 2023; Book ISBN 9781003303282. *In press*
- [8] **Baidya SK**, Banerjee S, Adhikari N, Jha T. Modeling inhibitors of Stromelysins. In: *Modeling Inhibitors of Matrix Metalloproteinases*. (Ed. T. Jha). Taylor & Francis, CRC Press, 2023; Book ISBN 9781003303282. *In press*
- [9] Banerjee S, **Baidya SK**, Adhikari N, Jha T. Modeling inhibitors of Matrilysins. In: *Modeling Inhibitors of Matrix Metalloproteinases*. (Ed. T. Jha). Taylor & Francis, CRC Press, 2023; Book ISBN 9781003303282. *In press*
- [10] Banerjee S, **Baidya SK**, Adhikari N, Jha T. Modeling inhibitors of membrane-type MMPs. In: *Modeling Inhibitors of Matrix Metalloproteinases*. (Ed. T. Jha). Taylor & Francis, CRC Press, 2023; Book ISBN 9781003303282. *In press*
- [11] Banerjee S, **Baidya SK**, Adhikari N, Jha T. Modeling inhibitors of other MMPs. In: *Modeling Inhibitors of Matrix Metalloproteinases*. (Ed. T. Jha). Taylor & Francis, CRC Press, 2023; Book ISBN 9781003303282. *In press*
- [12] Adhikari N, **Baidya SK**, Banerjee S, Jha T. Conclusion and Future Perspectives. In: *Modeling Inhibitors of Matrix Metalloproteinases*. (Ed. T. Jha). Taylor & Francis, CRC Press, 2023; Book ISBN 9781003303282. *In press*

- [13] Adhikari N, **Baidya SK**, Saha A, Jha T. Structural insight into the viral 3C-like protease inhibitors: Comparative SAR/QSAR approaches. In: *Viral Proteases and their inhibitors*. (Ed S. P. Gupta). Academic Press, USA, 2017, p. 317-402.
- [14] Adhikari N, **Baidya SK**, Saha A, Ali N, Jha T. Design and development of matrix metalloproteinase inhibitors containing zinc-binding groups, without zinc-binding groups, and mechanism-based. In: *Advances in studies on enzyme inhibitors as drugs. Volume 2: Miscellaneous drugs*. (Ed S. P. Gupta). Nova Science Publishers, New York, 2017, p. 135-208.

4. List of Patents : NIL

5. List of Presentations in National/International/Conferences/Workshops:

- [1] **Baidya SK**, Amin SA, Banerjee S, Jha T. A comparative multi QSAR modeling and molecular docking studies of some arylsulfonamide based ADAM17 inhibitors as anticancer agents, International Conference of Drug Discovery (ICDD). BITS Pilani, Hyderabad, 29th Feb - 2nd Mar, 2020.
- [2] Workshop on ‘Writing Quality Research article for publication’ at Jadavpur University, Kolkata, West Bengal, India, 13-14th January 2020.
- [3] National Seminar on “Advances in Pharmaceutical Technology: Opportunities and Challenges”, School of Pharmaceutical Technology, Adamas University, Kolkata, West Bengal, India, 22-23rd February 2019.

STATEMENT OF ORIGINALITY

I, SANDIP KUMAR BAIDYA registered on January 19, 2017, do hereby declare that this thesis entitled "Rational Design, Synthesis and Biological Activity of Some Glutamine-based Anticancer Hydroxamates as Promising Matrix Metalloproteinase-2 Inhibitors" contains literature survey and original research work done by the undersigned candidate as part of Doctoral studies.

All information in this thesis have been obtained and presented in accordance with existing academic rules and ethical conduct. I declare that, as required by these rules and conduct, I have fully cited and referred all materials and results that are not original to this work.

I also declare that I have checked this thesis as per the "Policy on Anti Plagiarism, Jadavpur University, 2019", and the level of similarity as checked by iThenticate software is 4% (checked on 12.12.2023).

Sandip Kumar Baidya
14/12/2023

(SANDIP KUMAR BAIDYA)

Certified by Supervisor(s):

Tarun Jha
14.12.23

Prof. Tarun Jha
Department of Pharmaceutical
Technology
Jadavpur University
Kolkata- 700032

TARUN

P

Dept. of

Jadav

Kol

CH.D

ch.

ly

Nilanjan Adhikari
14/12/2023

Dr. Nilanjan Adhikari
Department of Pharmaceutical
Technology
Jadavpur University
Kolkata- 700032

DR. NILANJAN ADHIKARI

Assistant Professor

Dept. of Pharm. Tech.

Jadavpur University

Kolkata - 700 032

CERTIFICATE FROM THE SUPERVISORS

This is to certify that the thesis entitled "Rational Design, Synthesis and Biological Activity of Some Glutamine-based Anticancer Hydroxamates as Promising Matrix Metalloproteinase-2 Inhibitors" submitted by SANDIP KUMAR BAIDYA (Registration No. 1021713003; Index NO.: 255/17/Ph), who got his name registered on 19.01.2017 for the award of **Ph.D. (Pharmacy)** degree of Jadavpur University is absolutely based upon his own work under the joint supervision on **Prof. Tarun Jha** and **Dr. Nilanjan Adhikari** and that neither his thesis nor any part of the thesis has been submitted for any degree/diploma or any other academic award anywhere before.



.....

Prof. Tarun Jha

Department of Pharmaceutical
Technology
Jadavpur University
Kolkata- 700032

TARUN JHA, Ph.D
Professor
Dept. of Pharm. Tech.
Jadavpur University
Kolkata-700 032



.....

Dr. Nilanjan Adhikari

Department of Pharmaceutical
Technology
Jadavpur University
Kolkata- 700032

DR. NILANJAN ADHIKARI
Assistant Professor
Dept. of Pharm. Tech.
Jadavpur University
Kolkata - 700 032

ACKNOWLEDGEMENT

This thesis is the outcome of long rigorous journey in which I have been encouraged and supported by many people. Whatever I have done is a result of their continuous encouragement and assistance. It is indeed a pleasant opportunity to express my gratitude for them.

*At the beginning, I wish to express my sincere thanks, deep gratitude and profoundness to my mentors **Prof. Tarun Jha**, Department of Pharmaceutical Technology, Jadavpur University and **Dr. Nilanjan Adhikari**, Department of Pharmaceutical Technology, Jadavpur University for guiding me well throughout the research work from title's selection to finding the results. Conducting the academic study regarding such a difficult topic couldn't be as simple as they made this for me. They are my mentors and the best advisors for my doctorate study beyond the imagination. I am greatly indebted to their immense knowledge, motivation, fruitful suggestions, patience and inspirations. I must accept that without their novel and innovative ideas, lucid exposition and constructive criticism, this thesis could not be possible.*

*I won't forget to express the gratitude to rest of the team: **Dr. Balaram Ghosh**, BITS-Pilani, Hyderabad, **Dr. Swati Biswas**, BITS-Pilani, Hyderabad, **Dr. Shovanlal Gayen**, Department of Pharmaceutical Technology, Jadavpur University, for sharing insightful suggestions and encouragement. I am grateful to the authorities of Jadavpur University and Indian Association for the Cultivation of Science for providing all the necessary facilities to pursue my work.*

*I owe my deep respect to **Prof. Amalesh Samanta**, Head, Department of Pharmaceutical Technology, Jadavpur University and former Head of the Department **Prof. Sanmoy Karmakar**, **Prof. Kunal Roy**, **Prof. Pulok K. Mukherjee** and **Prof. Biswajit Mukherjee** for their continuous help and encouragement. I am thankful to all of my respected Teachers especially to **Prof. Tapan Kumar Maity**, **Prof. Pallab Kanti Halder**, **Dr. Saikat Dewanjee**, **Dr. Md. Emdad Hossain**, **Dr. Prabir Kumar Ojha**, **Dr. Manas Bhowmick**, **Dr. Nilanjan Ghosh** and non-teaching staffs for their support and help. I am grateful to the authorities of **Jadavpur University, Kolkata** for providing all the necessary facilities to pursue my research work.*

*I would like to convey my sincere thanks to **Junior UPE Phase-II Fellowship (2016-2019)**, **State Government Fellowship Scheme (2019)** of Jadavpur University, Kolkata and **Indian Council of Medical Research (ICMR), New Delhi (2019-2021)** for providing*

Fellowships. I will always remember my fellow lab mates too for the fun-time we spent together, sleepless nights that gave us the courage to complete tasks before deadlines. I am extremely grateful to Mr. Suvankar Banerjee of Department of Pharmaceutical Technology, Jadavpur University for his endless efforts and continuous help. I also express my sincere thanks to all my laboratory seniors and juniors especially to Dr. Amit Kumar Halder, Dr. Avinaba Mukherjee, Dr. Sanchita Datta, Dr. Sk Abdul Amin, Mr. Sanjib Das, Mr. Soumyadip Chakraborty, Ms. Subha Mondal, Mr. JSD Tamang, Mr. Rafiul Jana, Mr. Sandeep Jana, and Mr. Tuhin Samui of Department of Pharmaceutical Technology, Jadavpur University for their valuable cooperation and necessary help.

I would like to acknowledge all my friends and no words can suffice my feelings of gratitude to my Ph.D. colleagues especially Mr. Rudranil Bhowmik, Mr. Avishek Mondal, Mr. Shirsha Basu, Mr. Mithun Majumdar, Mr. Biswarup Pramanik of my University.

At the end, I am grateful to my parents, sister, friends and acquaintances who remembered me in their prayers for the ultimate success. Last but not the least, I would like to thank to my beloved wife Mousumi, who have sacrificed tremendously but always be with me for extending her continuous supporting hands and sharing many moments of joy, sorrow and my dreams. I consider myself nothing without them. They gave me enough moral support, encouragement and motivation to accomplish the personal goals.

Date: 14/12/2023

Place: Jadavpur, Kolkata

Sandip Kumar Baidya
(SANDIP KUMAR BAIDYA)

DEDICATED TO MY SUPERVISORS *PROF*
TARUN JHA & DR. NILANJAN ADHIKARI
(*TOP 2% SCIENTIST* According To
Stanford University) INTRODUCED ME
DRUG DESIGN, SYNTHESIS &
DEVELOPMENT

PREFACE

Among the different subtypes of matrix metalloproteinases (MMPs), MMP-2 is one of the validated potential targets for cancer. It has a crucial role in tumor progression, apoptosis, and angiogenesis. **Chapter 1** provides an outline of different Cancer and its statistics along with MMPs and its classification, and the implication of MMP-2 enzyme and related mechanism regarding cancer especially with relation to chronic myeloid leukemia progression. Moreover, MMP inhibitors entered into different phases of clinical trials have also been discussed. In addition, a brief description of drug design and discovery incorporated. **Chapter 2** extensively highlights MMP-2 inhibitors based on various zinc binding group and their implications as potential anticancer agents. Specific enzyme selectivity issue of hydroxamate-based MMP-2 inhibitors has also been discussed. **Chapter 3** deals with the rationale behind the hydroxamates-based selective MMP-2 inhibitor designing strategies. The aim and objectives of these study also been discussed. **Chapter 4** describes the procedures for performing MMP-2 inhibitor designing strategies along with the organic synthesis and biological screening techniques. **Chapter 5** deals with the results and discussions related to the work describing the detailed designing techniques of hydroxamates-based MMP-2 inhibitors through comparative robust molecular modeling studies (such as regression-based and classification-based QSARs, 3D-QSAR CoMFA and CoMSIA, HQSAR, molecular docking, MD simulations) followed by lead identification and subsequent organic synthesis, characterization as well as biological screening (enzyme inhibition, cytotoxic evaluation, apoptosis analysis, cell cycle analysis, angiogenesis assay, DNA deformation assay). **Chapter 6**, in a nutshell, concludes about the overall results of biphenylsulfonamido hydroxamates-based glutamines as potential MMP-2 inhibitors having effective antileukemic activity particularly CML. **Chapter 7** deals with the future direction of the research work, where the future journey for MMP-2 inhibitors as potential anticancer agents hinges on a multi-faceted approach encompassing structural refinement, translational studies, combination therapies, targeted drug delivery systems, and the elucidation of underlying molecular mechanisms. Therefore, this thesis provides a hallmark of the identified lead novel compound selective towards MMP-2 that may be further evaluated in future for *in vivo* biological studies and pharmacokinetic evaluation along with formulation development to achieve better anti leukemic efficacy. Therefore, this thesis will surely motivate researchers associated with this field both in academia and industry for further development of promising selective MMP-2 inhibitors as potential anticancer agents.

1. Cancer
 - 1.1. Cancer statistics
 - 1.2. Types of cancer
 - 1.2.1. Solid tumor
 - 1.2.1.1. Carcinoma
 - 1.2.1.2. Sarcoma
 - 1.2.2. Hematological cancer
 - 1.2.2.1. Lymphoma
 - 1.2.2.1.1. Hodgkin lymphoma
 - 1.2.2.1.2. Non-Hodgkin lymphoma
 - 1.2.2.2. Leukemia
 - 1.2.2.2.1. Acute lymphocytic leukemia (ALL)
 - 1.2.2.2.2. Acute myelogenous leukemia (AML)
 - 1.2.2.2.3. Chronic lymphocytic leukemia (CLL)
 - 1.2.2.2.4. Chronic myelogenous leukemia (CML)
 - 1.2.2.5. Myeloma
 - 1.2.3. Mixed type
 - 1.3. Risk factors
 - 1.4. Signs and symptoms
 - 1.5. Early detection
 - 1.6. Treatment option
 - 1.6.1. Local therapy
 - 1.6.1.1. Surgery
 - 1.6.1.2. Radiotherapy
 - 1.6.2. Systemic therapy
 - 1.6.2.1. Biological therapy
 - 1.6.2.2. Chemotherapy
 - 1.6.2.3. Hormone therapy
 - 1.6.2.4. Targetted therapy
 - 1.7. MMPs and their classification
 - 1.8. General structure of MMPs
 - 1.9. Biochemistry of MMPs
 - 1.10. Expression of MMPs
 - 1.11. MMPs in cancer and leukemia
 - 1.12. Gelatinases (MMP-2 and MMP-9) in cancer and leukemia
 - 1.13. MMP-2 Crystal structure
 - 1.14. MMP-2 inhibitors
 - 1.15. Classification of MMP-2 inhibitors
 - 1.16. Clinical studies
 - 1.17. Classification of different types of MMPs in clinical trials
 - 1.17.1. Collagen peptidomimetics
 - 1.17.2. Non-peptidomimetics
 - 1.17.3. Bisphosphonates & bisphosphonate esters
 - 1.17.4. Tetracyclines
 - 1.18. Importance of development of MMP-2 inhibitors
 - 1.19. MMP-2 and chronic myeloid leukemia
 - 1.20. Drug design and discovery
 - 1.20.1. Rational drug design

- 1.20.1.1. *Ligand-based drug design*
 - 1.20.1.1.1. *Quantitative structure-activity relationship (QSAR) study*
 - 1.20.1.1.1.1. *Hansch equation and Free-Wilson analysis*
 - 1.20.1.1.1.2. *Significance of QSAR study*
 - 1.20.1.1.1.3. *Different types of QSAR study*
 - 1.20.1.1.1.4. *Software/tool used for QSAR study*
- 1.20.1.2. *Structure-based drug design*
 - 1.20.1.2.1. *Molecular docking study*
 - 1.20.1.2.2. *Molecular dynamics simulation study*
- 1.20.1.3. *Advance approaches*

Chapter 2: Literature Review	51-76
-------------------------------------	--------------

- 2.1. *Literature Search*
- 2.2. *Matrix metalloproteinases-2 (MMP-2): A medicinally important target*
- 2.3. *MMP-2 inhibitors based on different ZBGs*
- 2.4. *Hydroxamic acid-based MMP-2 inhibitors*
- 2.5. *Development of MMP-2 inhibitors*

Chapter 3: Rationale Behind the Work	77-80
---	--------------

- 3.1. *Rationale*
- 3.2. *Aims and objectives*

Chapter 4: Materials and Methods	81-103
---	---------------

- 4.1. *Computational Chemistry*
 - 4.1.1. *Dataset preparation and preprocessing*
 - 4.1.2. *Molecular docking analysis*
 - 4.1.3. *Multiple linear regression (MLR) study*
 - 4.1.4. *2D-QSAR model validation parameters*
 - 4.1.5. *Docking-based 2D-QSAR model development*
 - 4.1.6. *Hologram quantitative structure activity relationship (HQ SAR) study*
 - 4.1.7. *Linear discriminant analysis (LDA)*
 - 4.1.8. *Bayesian classification study*
 - 4.1.9. *3D-QSAR CoMFA and CoMSIA model development*
 - 4.1.10. *Molecular dynamics (MD) simulation analysis study*
 - 4.1.11. *Calculation of Molecular Mechanics Generalized Born and Surface Area (MMGBSA)*
 - 4.1.12. *Free energy landscape (FEL) analysis*
 - 4.1.13. *Dynamic cross-correlation map (DCCM) and principal component analysis (PCA)*
 - 4.1.14. *Probability density function (PDF) analysis*
- 4.2. *Synthetic Organic Chemistry*
 - 4.2.1. *Synthesis procedure of biphenylsulfonyl D(-) glutamic acid (2)*
 - 4.2.2. *Synthesis procedure of biphenylsulfonyl D(-) oxopyrrolidine carboxylic acid (3)*
 - 4.2.3. *Synthesis procedure of 5-N-Substituted 2-(substituted biphenylsulfonyl) D(-) glutamines (4a-4t)*
 - 4.2.4. *Synthesis procedure of methyl ester derivatives of 5-N-Substituted 2-(substituted biphenylsulfonyl) D(-) glutamines (5a-5t)*

- 4.2.5. *Synthesis procedure of hydroxamate derivatives of 5-N-Substituted 2-(substituted biphenylsulfonyl) D(-) glutamines (6a-6t)*
- 4.3. *Characterization of the synthesized molecules*
- 4.4. *Biological Study*
 - 4.4.1. *Enzyme inhibition assay*
 - 4.4.2. *Cell lines*
 - 4.4.3. *Cytotoxicity assay*
 - 4.4.4. *MMP-2 expression analysis*
 - 4.4.5. *Apoptosis analysis in K-562 cell line*
 - 4.4.6. *Cell cycle assay*
 - 4.4.7. *In vitro tube formation assay (Angiogenesis Assay)*
 - 4.4.8. *DNA deformation assay by DAPI staining*
- 4.5. *Statistical analysis*

Chapter 5: Results and Discussions

104-177

Part A

- 5.1. *Molecular Modeling study*
 - 5.1.1. *Multiple linear regression (MLR) analysis*
 - 5.1.2. *Hologram-based quantitative structure-activity relationship (HQSAR) analysis*
 - 5.1.3. *Linear discriminant analysis (LDA) model*
 - 5.1.4. *Bayesian classification modeling analysis*
 - 5.1.5. *Comparative molecular similarity index analysis (CoMSIA) analysis*
 - 5.1.6. *Molecular docking-based 2D-QSAR Model*
 - 5.1.7. *Alignment for field-based 3D-QSAR studies*
 - 5.1.7.1. *Comparative molecular field analysis (CoMFA) study*
 - 5.1.7.2. *Comparative molecular similarity indices analysis (CoMSIA) study*
 - 5.1.8. *Molecular dynamics (MD) simulation study*
 - 5.1.8.1. *Analysis of protein-ligand contacts*
 - 5.1.8.2. *Molecular Mechanics Generalized Born and Surface Area (MMGBSA) calculation*
 - 5.1.8.3. *Analysis of Free energy landscape (FEL)*
 - 5.1.8.4. *Dynamic cross-correlation map (DCCM) and principal component analysis (PCA) study*
 - 5.1.8.5. *Probability density function (PDF) analysis*
 - 5.1.9. *Overview form molecular modeling study*

Part B

- 5.2. *Synthesis of the designed glutamine derivatives and analogs*
 - 5.2.1. *Characterization of the synthesized molecules*

Part C

- 5.3. *Biological Studies*
 - 5.3.1. *Cytotoxicity assay*
 - 5.3.2. *Enzyme inhibition assay*
 - 5.3.3. *MMP-2 expression analysis*
 - 5.3.4. *Apoptosis analysis in K-562 cell line*
 - 5.3.5. *Cell cycle analysis in K-562 cell line*
 - 5.3.6. *In vitro tube formation assay or Angiogenesis assay*
 - 5.3.7. *DNA deformation assay by DAPI staining*

5.4. MD simulation study of the potent MMP-2 inhibitors (DH-15 and DH-18)

5.5. Summary

Chapter 6: Conclusion	178-180
Chapter 7: Future Direction	181-183
References	184-220
Appendix	221-264
Annexure	

Abbreviations

2D-QSAR: Two-Dimensional Quantitative Structure-Activity Relationship

3D: Three-Dimensional

3D-QSAR: Three-Dimensional Quantitative Structure-Activity Relationship

AD: Alzheimer's Disease

ADME: Absorption, Distribution, Metabolism, and Excretion

AI: Artificial Intelligence

AlogP: Octanol-Water Partition Coefficient

AML: Acute Myeloid Leukemia

ANN: Artificial Neural Networks

ANOVA: Analysis of Variance

AP: Accelerated Phase

ARF: Acute Renal Failure

AUC: Area Under the Curve

AUROC: Area Under the Receiver Operating Characteristic Curve

BA: Biological Activity

BC: Blast Crisis

bFGF: Basic Fibroblast Growth Factor

BM-MNC: Bone Marrow Mononuclear Cells

BP: Blast Phase

CAD: Coronary Artery Disease

CHD: Coronary Heart Disease

CML: Chronic Myeloid Leukemia

CoMFA - Comparative Molecular Field Analysis

CoMSIA - Comparative Molecular Similarity Indices Analysis

COPD: Chronic Obstructive Pulmonary Disease

CP: Chronic Phase

CT: Collagen Type

CVD: Cardiovascular Diseases

DAPG: 2, 4-diacetyl phloroglucinol

DAPI: 4',6-Diamidino-2-phenylindole

DCCM: Dynamic Cross-Correlation Map

DMEM: Dulbecco's Modified Eagle Medium

DS: Discovery Studio

DSL: Domestic Substances List

ECFP_6: Extended Connectivity Fingerprint of diameter 6

ECM: Extracellular Matrix

EMMPRIN: Extracellular Matrix Metalloproteinase Inducer

EPIK: Empirical Prediction of Intermolecular Contacts

ERK: Extracellular Signal-Regulated Kinase

EU: European Union

FAK: Focal Adhesion Kinase

FBS: Fetal Bovine Serum

FDA: Food and Drug Administration

FEL: Free Energy Landscape

FN: Fibronectin

GFA: Genetic Function Approximation

HF: Heart Failure

HQSAR: Hologram Quantitative Structure-Activity Relationship

HRMS: High-Resolution Mass Spectrometry

HTS: High Throughput Screening

IBD: Inflammatory Bowel Disease

IC₅₀: Half-maximal Inhibitory Concentration

ICD-O: International Classification of Diseases for Oncology

IGF: Insulin-like Growth Factor

IL-1 β : Interleukin-1 β

JNK: c-Jun N-terminal Kinase

kNN: k-Nearest Neighbors

LBDD: Ligand-Based Drug Design

LDA - Linear Discriminant Analysis

LOO: Leave-One-Out

LR: Linear Regression

LSD - Least Significant Difference

MAPK: Mitogen-Activated Protein Kinase

MCC: Matthew's Correlation Coefficient

MD: Molecular Dynamics

MFPSA: Molecular Fractional Polar Surface Area

MIC: Minimum Inhibitory Concentration

MLR - Multiple Linear Regression

MM/GBSA - Molecular Mechanics Generalised Born and Surface Area

MMP-2: Matrix Metalloproteinase-2

MMPis: Matrix Metalloproteinase Inhibitors

MMPs: Matrix Metalloproteinases

MPN: Myeloproliferative Neoplasms

MSS - Musculoskeletal Syndromes

MTT - 3-(4,5-Dimethylthiazol-2-yl)-2,5-Diphenyltetrazolium Bromide

MW: Molecular Weight

nAR: Number of Aromatic Rings

NF- κ B: Nuclear Factor κ B

nHBA: Number of Hydrogen Bond Acceptors

nHBD: Number of Hydrogen Bond Donors

NMR: Nuclear Magnetic Resonance

nR: Number of Rings

OPLS: Optimized Potentials for Liquid Simulations

OSCC: Oral Squamous Cell Carcinoma

PaDEL: PubChem Assay Data Extended Connectivity Fingerprint Descriptors

PCA: Principal Component Analysis

PDB: Protein Data Bank

PDF: Probability Density Function

PI: Propidium Iodide

PLS: Partial Least-Square

PP2A α : Protein Phosphatase 2A Catalytic Subunit α

PPI: Protein-Protein Interaction

QSAR: Quantitative Structure-Activity Relationship

RA: Rheumatoid Arthritis

ROC: Receiver Operating Characteristic

ROS: Reactive Oxygen Species

RT-PCR: Reverse Transcription Polymerase Chain Reaction

SAR: Structure-Activity Relationship

SBDD: Structure-Based Drug Design

SE: Standard Error

S-MLR: Stepwise Multiple Linear Regression

SPSS: Statistical Package for the Social Sciences

SVM: Support Vector Machines

TACE: Tumor Necrosis Factor-Alpha Converting Enzyme

TIMPs: Tissue Inhibitors of Metalloproteinases

TKIs: Tyrosine Kinase Inhibitors

TLC: Thin Layer Chromatography

TMs: Tumor Markers

TNF- α : Tumor Necrosis Factor α

TTP: Tristetraprolin

VEGF: Vascular Endothelial Growth Factor

WHO: World Health Organization

XP: Extra Precision

ZBGs: Zinc Binding Groups

Chapter 1

INTRODUCTION

1. Cancer

Cancer is defined as abnormal, uncontrolled growth that spreads throughout the body as a result of various genetic, epigenomic, and mutagenic alterations. Moreover, the cell's genome has undergone abnormal modifications that enable it to dodge apoptotic signals and provide growth signals that cause uncontrollable cell division (Fatma and Siddique, 2023). The development of cancer reveals a variety of intricacies that are challenging to analyze and comprehend. Also, to comprehend and categorize common cancer features, Hanahan and Weinberg established a number of hallmarks, such as self-sustaining growth signals and avoidance mechanisms (Hanahan and Weinberg, 2011). Complex molecular changes in cell cycle regulation act as a mediator for cancer metastasis, which is the spread of cancer cells from the primary tumor to neighboring tissues and distant organs (Quintero-Fabián et al., 2019).

1.1. Cancer statistics

Cancer is a major public health problem worldwide and one of the leading causes of death as per the world health organization (<https://www.who.int/>). As populations rise, get older, and adopt lifestyle habits that raise the chance of developing cancer, the number of cancer cases and deaths is anticipated to climb dramatically, adding to the burden already present. In addition, the risk of cancer drastically increases in low- and middle-income nations, which are undergoing economic transitions that involve growing mechanization of labor and transportation, cultural changes in the roles of women, and increased exposure and access to global markets (Torre et al., 2016). Because of this, many of the lifestyle risk factors, which are already prevalent in high-income nations, including tobacco use, physical inactivity, excess body weight, and reproductive patterns, are also becoming more frequent in low- and middle-income nations (Torre et al., 2016).

A report from the International Agency for Research on Cancer of WHO depicts a huge number of populations suffering in different continents (**Figure 1.1**) form different types of cancer (<https://rb.gy/gmhja>). As per Globocan 2020 reports, the population in Asia is much higher than other continents such as Europe, North America, Africa, etc.

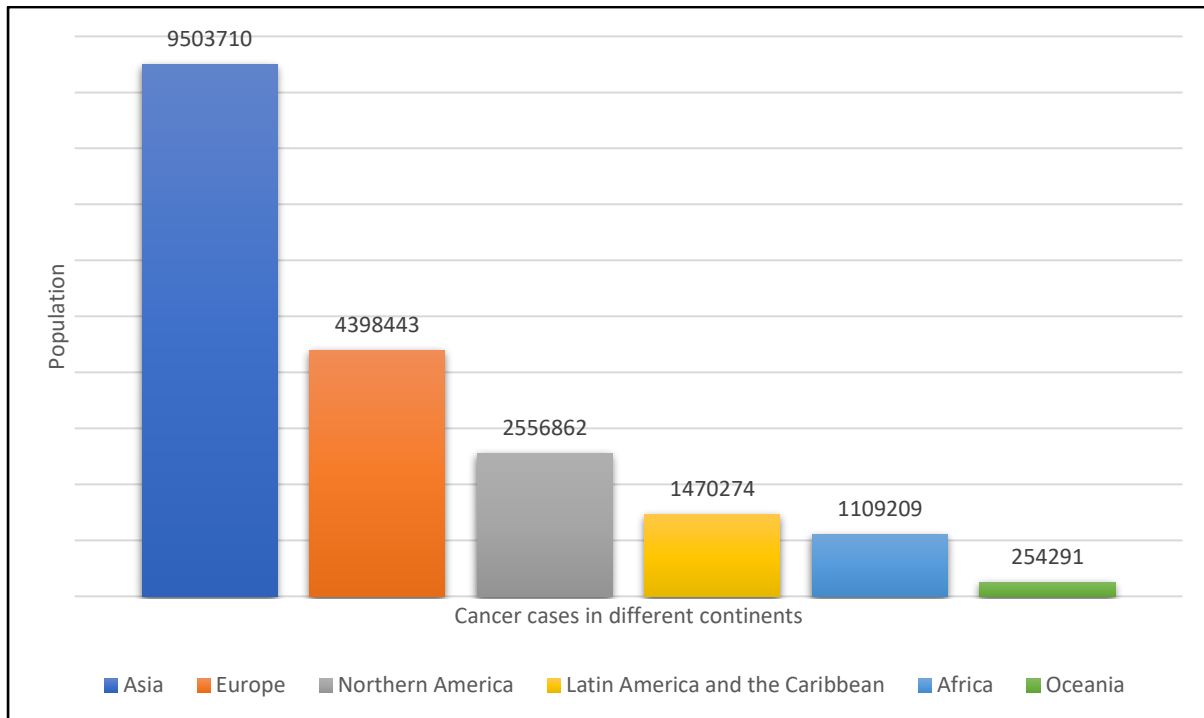


Figure 1.1. Statistical data of the number of cases of cancer in different continents.

Additionally, according to a report by cancer statistics in 2023, an estimated 609,820 people in the United States will die from cancer in 2023, corresponding to 1670 deaths per day (Siegel et al., 2023). The global report of cancer deaths is much higher than the report by the cancer statistic 2023. According to the world health organization, around 10 million deaths, or nearly one in every six, were caused by cancer in 2020, making it the world's top cause of death (<https://www.who.int/>). Another report by global cancer statistic 2020 where the reports are based on the estimation of incidence and mortality for 36 different types of cancer in 185 countries worldwide depicts, including both sexes combined, one-half of all cases and 58.3% of cancer deaths are estimated to occur in Asia, while around 59.5% of the world population locate. Despite making up 9.7% of the world's population, Europe accounts for 22.8% of all cancer cases and 19.6% of all cancer deaths. The Americas come in second with 20.98% incidence and 14.2% worldwide mortality. Because of the distinct distribution of cancer types and greater case fatality rates in these regions, the percentage of cancer deaths in Asia (58.3%) and Africa (7.2%) are larger than the share of incidence (49.3 percent and 5.7 percent, respectively) (Sung et al., 2021). Moreover, statistical data by the world health organization exhibit a massive percentage of deaths by different cancers in different continents (**Figure 1.2**) (<https://www.who.int/>).

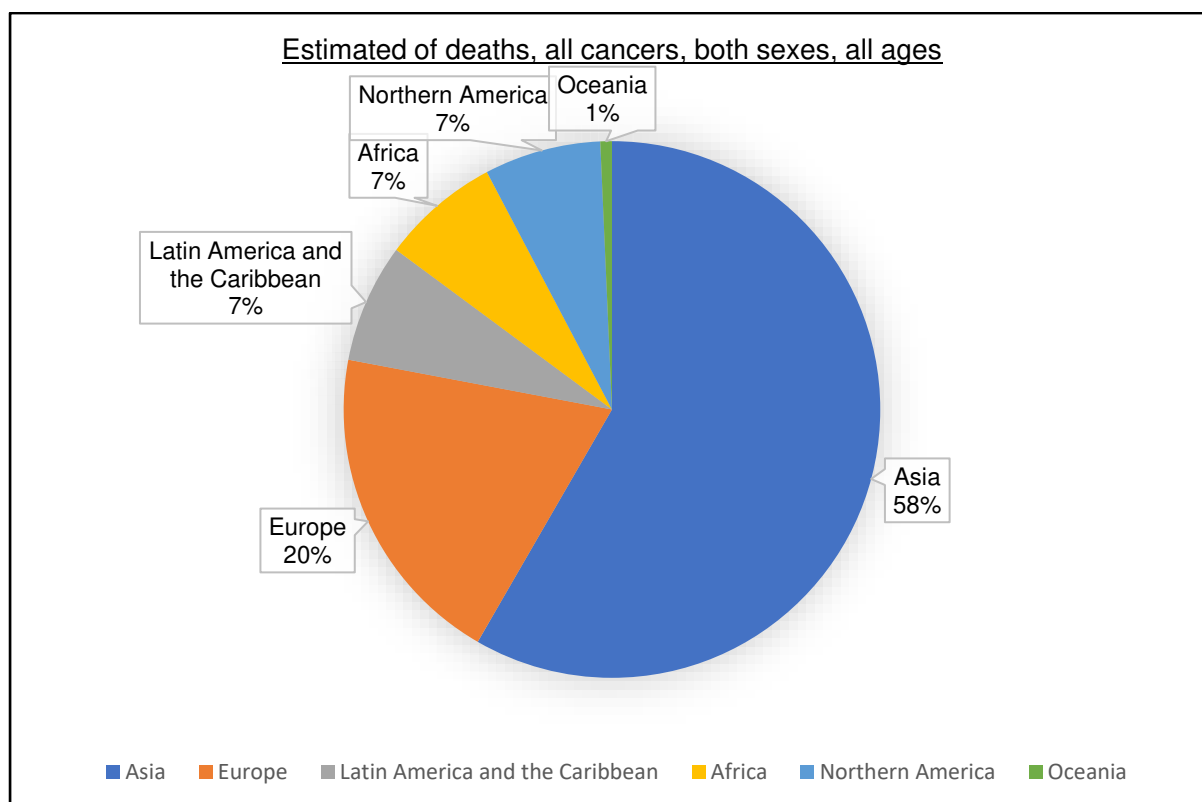


Figure 1.2. Statistical data of the number of deaths by different cancers in different continents.

Therefore, cancer is one of the major diseases as it is increasing in number of cases as well as deaths. Thus, it is of utmost need to manage the disease i.e., cancer. Not only slow down the growth of cancer but also it should have proper drug molecules to prevent the migration of cancerous cells. Moreover, the incredible diversity of cancer continues to provide hints as to its root causes, but it also highlights the need for increased global efforts to combat the illness.

1.2. Types of cancer

Cancer can be categorized based on the tumor type i.e., solid tumor and hematological cancer. However, as per WHO, cancers are divided into two categories: histological types, which refer to the tissue types in which they develop, and primary sites, which refer to the parts of the body where they initially appeared (**Figure 1.3**) (World Health Organization, International classification of diseases for oncology (ICD-O), 2013). Moreover, several body tissue categories give rise to different benign and malignant tumors.

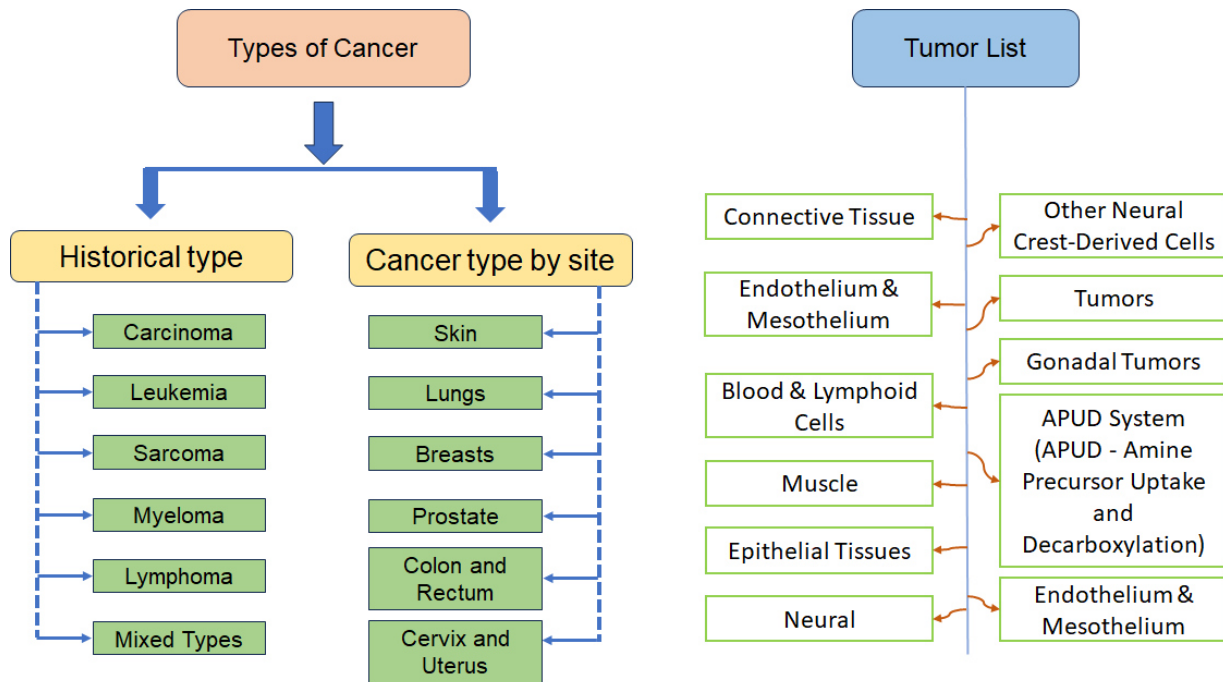


Figure 1.3. Types of cancer along with different types of tumors.

1.2.1. Solid tumor

A solid tumor is an organ made up of stromal and cancerous cells that receive nutrition from a vasculature made up of endothelial cells, all of which are encased in an extracellular matrix. The expression of different genes is regulated by interactions between these cells, their surrounding matrix, and their local microenvironment. These genes by-products, in turn, regulate the pathophysiological characteristics of the tumor. Moreover, the response to different therapies is controlled by tumor pathophysiology, which also controls tumor development, invasion, and metastasis. Sarcomas and carcinomas are the two primary categories of solid tumors. Surgery is frequently used to treat a variety of solid tumors, including carcinoma and sarcoma (Jain, 1990).

1.2.1.1. Carcinoma

A malignant tumor of epithelial origin or cancer of the internal or exterior lining of the body is referred to as a carcinoma. In between 80 and 90 percent of all cancer cases, epithelial tissue malignancies called carcinomas are present

Carcinomas, which are malignancies in epithelial tissues, are commonly found in 80 to 90 percentage of cancer cases, though the specific proportion may vary depending on the cancer type and individual characteristics (<https://rb.gy/b6712p>). Carcinomas are subdivided into two

extensive subtypes i.e., squamous cell carcinoma, which begins in the squamous epithelium, and adenocarcinoma, which appears in an organ or gland, respectively (Chen and Dhahbi, 2021). Moreover, a thicker plaque-like layer of white mucosa is the earliest sign of adenocarcinomas, which typically develop in mucous membranes. They can swiftly spread across the soft tissue where they start, especially in the lungs. Additionally, squamous cell carcinomas can develop in a variety of body parts. The majority of carcinomas involve glands or organs that can secrete, such as the breasts, which produce milk, the lungs, which release mucus, the colon, the prostate, or the bladder. (<https://training.seer.cancer.gov/disease/categories/classification.html>; Chen and Dhahbi, 2021).

1.2.1.2. Sarcoma

Cancer that develops in supporting and connective tissues, such as bones, tendons, cartilage, muscle, and fat, is referred to as sarcoma. The most common sarcoma typically affects young adults and frequently manifests as a painful lump on the bone. They can be divided into two broad categories: primary bone sarcoma and soft tissue sarcoma, each of which has a unique staging and therapeutic strategy (Skubitz and D'Adamo, 2007).

1.2.2. Hematological cancer

A group of blood, bone marrow as well as lymph node disorders known as hematological malignancies are characterized by the clonal growth of blood-forming cells (Huang et al., 2020). Frequently, abnormal hematopoietic and related processes are linked to bone marrow dysfunction. Hematologic malignancies come in three primary categories: lymphoma, leukemia, and myeloma.

1.2.2.1. Lymphoma

Lymphomas grow in the glands or nodes of the lymphatic system. The lymphatic system is a network of tubes, nodes, and organs (particularly the tonsils, spleen, and thymus) that cleans bodily fluids and creates lymphocytes, or white blood cells that fight infection (<https://training.seer.cancer.gov/disease/categories/classification.html>). Moreover, lymphoma is sometimes referred to be a "solid cancer", in contrast to leukemias, which are frequently called "liquid cancers." The stomach, breast, and brain are just a few of the organs where lymphomas can develop. Both Hodgkin lymphoma and Non-Hodgkin lymphoma are subclassified as lymphomas (McCarten et al., 2019). Hodgkin lymphoma can be distinguished from Non-Hodgkin lymphoma by the presence of Reed-Sternberg cells. These large, abnormal

cells are a hallmark characteristic found in Hodgkin lymphoma when examined under a microscope, aiding in its differentiation from the various subtypes of Non-Hodgkin lymphoma.

1.2.2.1.1. Hodgkin lymphoma

Hodgkin lymphoma is largely formed from the B-cell lineage and has two subtypes: classical Hodgkin lymphoma (cHL) and nodular lymphocyte predominate Hodgkin lymphoma. With cHL accounting for about 95% of all HL cases, HL is an uncommon kind of lymphoma that accounts for roughly 10% of lymphomas in the United States (Ullah et al., 2023).

In general, first-line chemotherapy is seen to be highly effective in treating the condition, with or without the inclusion of radiotherapy. Additionally, high-dosage chemotherapy followed by an autologous hematopoietic stem cell transplant is the usual therapeutic option for cHL patients who experience relapses or who do not respond to frontline regimens (AHSCT). Also, several innovative agents are being examined in addition to chimeric antigen receptor (CAR) T-cell therapy, which is also being investigated in clinical trials as a potential treatment option, focused immunotherapy has recently transformed the treatment of cHL (Wang et al., 2017).

1.2.2.1.2. Non-Hodgkin lymphoma

Non-Hodgkin lymphoma (NHL) is a tumor that develops from B cell precursors, mature B cells, T cell progenitors, and mature T cells. It affects the lymphoid tissues. Non-Hodgkin lymphoma has several subtypes, each of which has unique epidemiology, etiology, immunophenotypic makeup, genetic makeup, clinical characteristics, and therapeutic response. Depending on how the disease is expected to progress, it might be classified as either "indolent" or "aggressive." Follicular lymphoma, Burkitt lymphoma, diffuse large B cell lymphoma, Mantle cell lymphoma, marginal zone lymphoma, and primary CNS lymphoma are the most prevalent adult B cell neoplasms. Mycosis fungoides and adult T cell lymphomas are the most prevalent mature T cell lymphomas (Armitage and Weisenburger, 1998). The use of medications including phenytoin, digoxin, and TNF antagonists is linked to non-Hodgkin lymphoma. The development of NHL is also linked to exposure to organic chemicals, pesticides, phenoxy-herbicides, wood preservatives, dust, hair color, solvents, chemotherapy, and radiation (Zhang et al., 2008; Eriksson et al., 2008).

1.2.2.2. Leukemia

Leukemias are bone marrow tumors also known as "liquid cancers" or "blood cancers" (the site of blood cell production). In Greek, leukemia is translated as "white blood." The excessive generation of immature white blood cells is frequently linked to the condition. Since these

immature white blood cells do not function as they should, the patient is frequently vulnerable to infection (<https://training.seer.cancer.gov/disease/categories/classification.html>). Both, acute and chronic leukemia are possible. Compared to acute leukemia, which needs to be treated right away, chronic leukemia advances more slowly. Also, the types of leukemia include lymphocytic and myelogenous. However, white blood cell is known as a lymphocyte that contributes to the immune system, lymphocytic leukemia describes aberrant cell proliferation in the marrow cells that become those lymphocytes. Additionally, the marrow cells that develop into red blood cells, white blood cells, and platelets proliferate abnormally in myelogenous leukemia (<https://www.hematology.org/>). Leukaemia can be broadly categorized into four groups:

- i) Acute lymphocytic leukemia (ALL)
- ii) Acute myelogenous leukemia (AML)
- iii) Chronic lymphocytic leukemia (CLL)
- iv) Chronic myelogenous leukemia (CML)

Leukemia can develop in both children and adults. However, AML is the second most typical type of childhood leukemia, and ALL is the most common type. Additionally, AML and CLL are the two adult leukemias that are most frequent.

1.2.2.2.1. Acute lymphocytic leukemia (ALL)

In the bone marrow, immature leukocytes repeatedly multiply and produce an excessive number of immature leukocytes, which results in acute lymphocytic leukemia (ALL), a kind of WBC cancer (Das et al., 2022). About 25% of all childhood malignancies are ALL, which is mostly prevalent in youngsters. However, it can be challenging to diagnose this malignancy because it exhibits symptoms that are similar to those of the common flu as well as other symptoms including weakness, joint discomfort, exhaustion, etc. One's life is seriously at stake from this sickness. If therapy is delayed, ALL patients have a 3-month survival window. Thus, the patient's life depends on receiving the right care and therapies (Sulaiman et al., 2023). Nonetheless, a skilled doctor or physician is required for the manual detection of this malignancy in order to make an early and correct diagnosis. It is now normal practise to examine blood smear images to find ALL. However, manual detection relies on human interpretation and suffers from issues including noise, blur, weak edges, and the complexity of blood cells (Sulaiman et al., 2023).

1.2.2.2.2. *Acute myelogenous leukemia (AML)*

Acute myeloid leukemia (AML) is a condition of the hematopoietic stem cells that is characterized by a stop in hematopoiesis, leading to the formation of a clonal population of malignant cells or blasts. However, if left untreated, this malignant change in hematopoietic stem cells causes a loss of normal hematopoietic function and often results in mortality within weeks to months of its clinical appearance (Shipley and Butera, 2009). Moreover, AML accounts for 15-20% of childhood leukemias and 33% of those in adolescents and young adults (AYA). Also, independent of other risk variables, age is a highly powerful prognostic factor, with the prognosis getting worse as one gets older (Creutzig et al., 2018). Treatment plans for AML are frequently for kids, adolescents, and adults, but not always, the same. Furthermore, they typically begin with intensive induction courses of cytarabine and anthracyclines at dosages sufficient to achieve remission, followed by post-remission phases that, in recent years, have also included maintenance therapy with novel agents such as tyrosine kinase inhibitors (TKIs) to destroy residual blasts in the bone marrow or other sites (Creutzig et al., 2018).

1.2.2.2.3. *Chronic lymphocytic leukemia (CLL)*

Monoclonal B-cell lymphocytosis (MBL), a protracted pre-malignant stage that precedes chronic lymphocytic leukemia (CLL), is the precursor of the disease (Koliijn et al., 2023). The proliferation of B lymphocytes chosen during clonal expansion through several interactions with (auto) antigens is thought to be the cause of CLL, despite the fact that their levels of activation and maturation vary. This is according to recent advancements in the understanding of CLL biology. Moreover, a diagnosis requires that there be more than 50×10^3 / μ L B lymphocytes per liter of blood present for at least three months (Auen et al., 2023). The kappa/lambda ratio is used in flow cytometry investigations on patients with leukemic cells to determine clonality. The co-expression of CD19, CD20, CD5, and CD23 is the distinguishing characteristic of the B-CLL clone. When compared to normal B cells, the levels of surface immunoglobulin, CD20, and CD79 are often low (Ginaldi et al., 1998). Typically, there is significant bone marrow involvement, with more than 30% of the nucleated cells in the aspirate being lymphoid in origin (García-Muñoz et al., 2012).

1.2.2.2.4. *Chronic myelogenous leukemia (CML)*

Chronic myeloid leukemia (CML), is previously known as chronic granulocytic leukemia (Minciacchi et al., 2021). In the year 1845, Jhon Bennet published a case report of hypertrophy of the spleen and liver of patients along with leukocytosis (Bennett, 1845). Rudolf Virchow, an

independent pathologist, first introduced the term “Leukemia” which means “white blood”. A brief history of CML in a schematic representation is depicted in **Figure 1.4**, which describes the involvement of the Bcr-Abl fusion chromosome (Philadelphia chromosome) responsible for this CML.

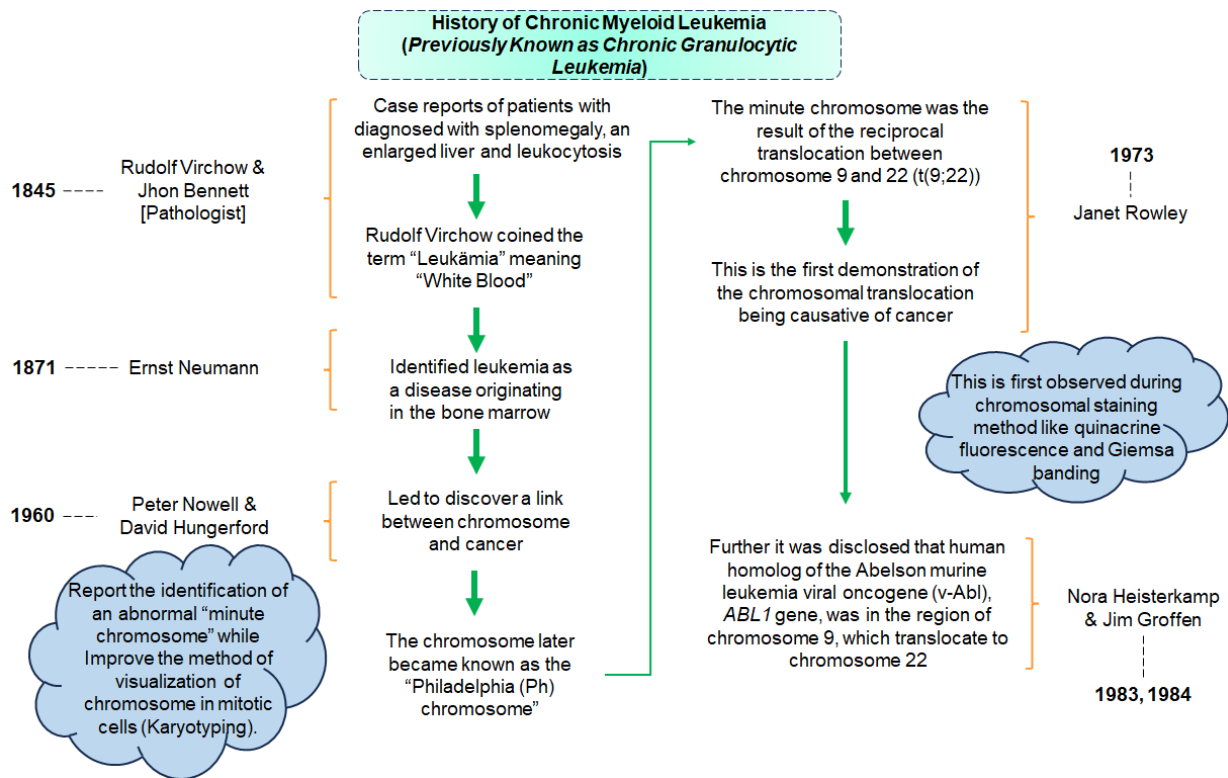


Figure 1.4. A schematic representation of the history of chronic myeloid leukemia.

CML belongs to the class of myeloproliferative neoplasms (MPN) that are defined by the unchecked proliferation of myeloid cells at various stages of maturity. Patients may present in one of three disease phases: the chronic phase (CP), the accelerated phase (AP), or the blast phase (BP) or blast crisis (BC) (Minciacchi et al., 2021). Most CML patients are identified during the chronic phase (CP), which is characterized by a lack of obvious clinical signs other than elevated blood cell counts. The development of tyrosine kinase inhibitors (TKIs) that target the BCR::ABL1 oncoprotein has significantly improved the prognosis for CML, but a small percentage of patients continue to experience blast crisis (BC), which is marked by the proliferation of undifferentiated blasts and a poor prognosis, because of leukemic cells developing resistance to TKI (Hehlmann, 2012; Hochhaus et al., 2020; Radivoyevitch et al., 2020). The Philadelphia (Ph) chromosome and the t(9;22)(q34;q11) chromosomal translocation are characteristics of CML cells. However, a major percentage of CML patients are found Ph-

positive and Philadelphia chromosome translocation occurred. Importantly, the breakpoint cluster region (BCR) of chromosome 22 and the ABL proto-oncogene from chromosome 9 fuse as a result of the Ph translocation (**Figure 1.5**) (Hehlmann, 2012).

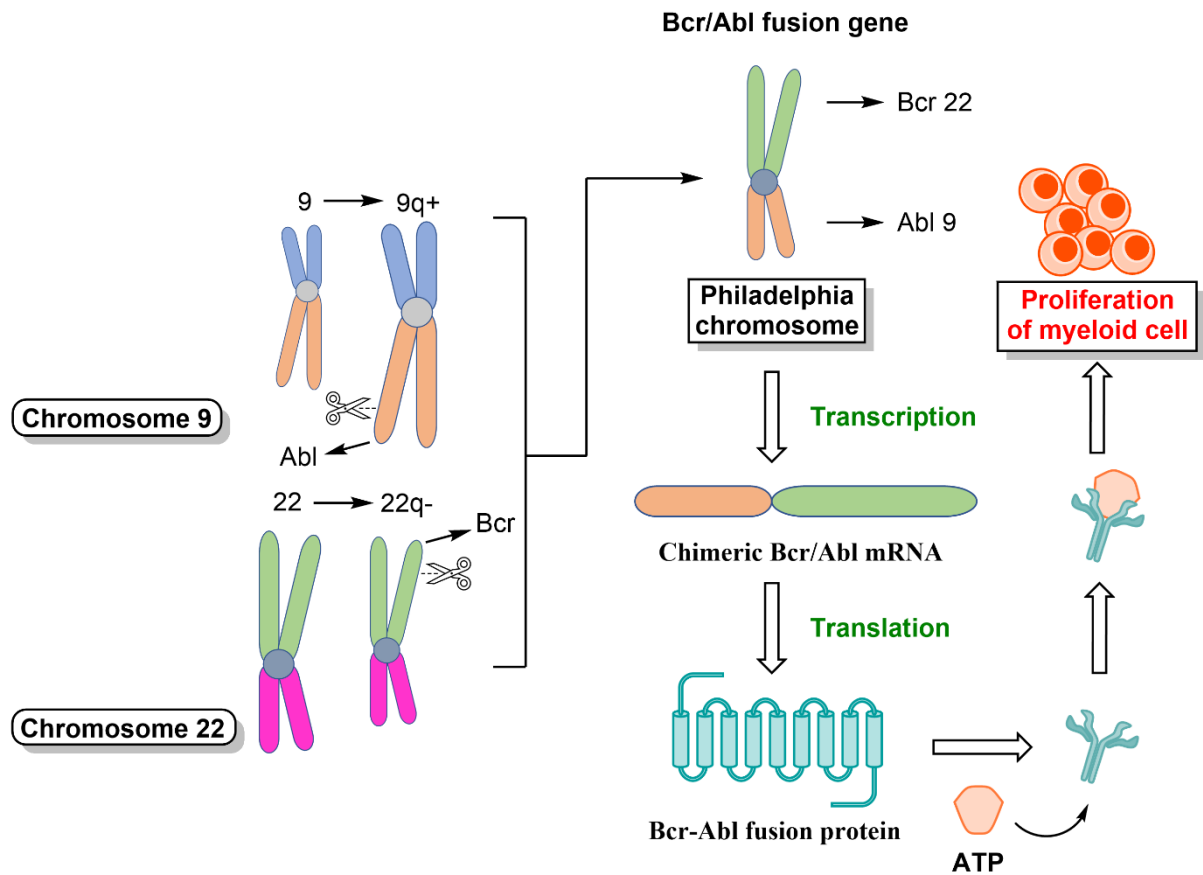


Figure 1.5. BCR protein and ABL gene reciprocal translocation results in an oncogene that constitutively triggers uncontrolled myeloid cell proliferation, which causes CML.

Tyrosine kinase inhibitors (TKIs) are a useful tool for the treatment of CML because they block the tyrosine kinase enzyme in response to the CML and its progression (Bhatia, 2017; Meenakshi Sundaram et al., 2019; Talati and Pinilla-Ibarz, 2018; Saikia, 2018). Additionally, tyrosine kinase enzyme inhibitors are effective in CML progression, boosting chronic phase survival and inducing remission (Bhatia, 2017). Despite having such higher efficacy in slowing CML progression, these TKIs' limitations have become a significant problem in the TKI-mediated treatment of CML. Moreover, TKIs had been held back from being a possible tool in the treatment of CML due to inadequate response-related therapy failures, drug toxicity, and the development of TKI resistance in CML leukemia stem cells (LSCs) (Bhatia, 2017). All of these shortcomings were able to steal the emphasis away from TKIs and encourage research into alternative workable, more recent options for CML progression and treatment. However,

modern leukemia research has been able to pinpoint other biological pathways, cytokines, and enzymes that are connected to the development of CML (Bhatia, 2017; Chaudhary et al., 2013; Ogawa et al., 2000; Yu and Han, 2006).

1.2.2.5. Myeloma

Cancer called myeloma develops in the bone marrow's plasma cells. Some of the proteins contained in the blood are produced by plasma cells. Multiple myeloma, a type of cancer, originates in the bone marrow's plasma cells, which normally produce antibodies essential for the immune system. This cancer leads to the abnormal proliferation of these plasma cells, causing the overproduction of monoclonal proteins or M proteins (Murray et al., 2021). These abnormal proteins can accumulate in the blood, urine, and potentially in organs, leading to various complications. The presence of these anomalous proteins in the blood serves as a crucial diagnostic indicator for multiple myeloma and can result in symptoms such as weakened immunity, anemia, bone pain, and kidney damage (Terpos et al., 2009).

1.2.3. Mixed type

Tumors with mixed-type components encompass a diverse array of tissue types within a single tumor, representing a combination of different categories of tumors. Adenosquamous carcinoma, for instance, features characteristics of both adenocarcinoma and squamous cell carcinoma, while Carcinosarcoma presents elements of both carcinomatous and sarcomatous tissues. These tumors pose diagnostic and treatment challenges due to their complex cellular compositions, which can significantly influence their behavior and response to therapies, making it essential to comprehend their varied elements for effective treatment planning. The mixed-type components could be from one category or several categories (<https://training.seer.cancer.gov/disease/categories/classification.html>). Some examples are (i) Adenosquamous carcinoma, (ii) Mixed mesodermal tumor, (iii) Carcinosarcoma, (iv) Teratocarcinoma, etc.

1.3. Risk factors

The increasing rate of cancer is thought to be influenced by a number of risk factors, such as internal risk factors and external risk factors for both men and women including tobacco smoking, infectious agents, alcohol drinking, dietary factors, obesity or overweight, physical inactivity, occupation, UV radiation, pollution, exogenous hormones, eating habits, and genetic mutation (Collatuzzo and Boffetta, 2023). These risk factors may either directly or indirectly encourage the growth of cancer. Controlling these kinds of internal and external influences,

however, can help to prevent cancer. Therefore, for a preventive intervention to have a significant impact on the treatment of cancer, exposure to the carcinogen must occur frequently. Additionally, for a cancer screening program, the time between avoiding exposure and the result is essential since it allows for potential therapeutic actions and gives a chance for monitoring. The development of targeted protocols, the identification of the subgroups of people who would benefit most from the preventive intervention, and preventative suggestions are all aided by detailed information on changes in other risk or protective factors. Thus, a desirable goal in modern cancer research is to have a better knowledge of how many elements that are related to cancer interact.

More than 25% of known chemical processes, which enzymes in living cells catalyze, include oxidation. This is frequently performed through the transfer of electrons or hydrogen atoms from one molecule to another. These kinds of metabolic reactions are the main source of energy for biological functions (Khan et al., 2010). Although oxygen is necessary for the majority of complex life on the Earth to exist, it is a highly reactive molecule that harms living things by producing reactive oxygen species like hydrogen peroxide (H_2O_2), hypochlorous acid (HOCl), and free radicals like the hydroxyl radical (OH), superoxide anion (O_2^-), and lipid peroxides (Valko et al., 2007). However, the chemical forms of oxygen have the ability to directly or indirectly harm proteins, lipids, and nucleic acids both temporarily and permanently. These biological macromolecules' oxidative damage is linked to the development of a number of illnesses, including cancer (Mayne, 2003; Bagchi and Puri, 1998). Therefore, the body maintains intricate networks of enzymes like catalase (CAT), superoxide dismutase (SOD), glutathione peroxidase (GPx), glutathione reductase (GR), and glutathione-S-transferase in order to protect itself (GST) (Bagchi and Puri, 1998). Henceforth, these parts or enzymes participate in a variety of metabolic processes to stop dangerous oxidative damage. Undoubtedly, a person's vulnerability to DNA damage and risk of developing cancer is associated with the genetic polymorphisms of these enzymes and the various degrees of their production. According to some recent studies, several enzymes, including asparaginase, arginine deiminase, arginase, methionine, lysine oxidase, phenylalanine ammonia lyase, and glutaminase, have been reported for the treatment of cancer (Wang et al, 2021).

1.4. Signs and symptoms

Analysis of serum tumor markers (TMs) is primarily recommended for patients being monitored for certain forms of cancer (Sturgeon et al., 2008). Tumor markers' sensitivity is typically poor in patients with confined tumors, whereas high TM concentrations are typically

found in individuals with bulky tumors or metastases (Molina et al., 2005; Duffy et al., 2010; Trapé et al., 2012; Duffy et al., 2007; Mattar et al., 2002). Many cancer patients who seek medical attention don't exhibit any particular symptoms or indicators. Moreover, a significant number of tests may be necessary for differential diagnosis with other illnesses (Pavlidis et al., 2003). In addition, the tests may be challenging to administer and interpret in some underlying illnesses, such as liver disease, kidney failure, or chronic obstructive pulmonary disease (COPD). It is interesting to note that, the patient has an underlying disease like liver disease or renal failure, which can also cause high serum TM concentrations in the absence of tumors, or when they have other disorders like pneumonia, diverticulitis, cholelithiasis, etc., the differential diagnosis of cancer is made (Trapé et al., 2011). Additionally, the serum TM concentrations were higher in those who finally had tumors diagnosed among the individuals with signs or symptoms suggesting malignancy. Since this diagnosis was severe, the specificity was set to 100 percent. With a sensitivity of 46.6 percent, a positive predictive value of above 99 percent, and a negative predictive value of 70.4 percent, the cut-off points for TMs obtained were therefore high across the board. These findings imply that patients who test positive have a very high risk of presenting with a confirmed cancer diagnosis. Significantly different cut-off points for TMs were found after subclassifying patients into two groups based on their bilirubin and creatinine levels (Trapé et al., 2015).

1.5. Early detection

Early cancer detection leads to more successful therapy and significantly higher survival rates. However, only about 50% of tumors are still found after they are already advanced. Improved early cancer detection may significantly improve survival rates. Recent improvements in early detection have undoubtedly saved lives, but more advancements and development of early cancer detection techniques are required. Due to improvements in biological understanding and a faster speed of technology advancement, the subject is evolving quickly (Crosby et al., 2022). Both healthy and high-risk groups can benefit from screening because it can help find cancer early when there is a greater chance that it can be treated and cured. Nonetheless, some cancer types currently have a clear function for screening, but each screening test has drawbacks, and better screening techniques are urgently required. Unfortunately, there are currently ineffective screening guidelines for many malignancies, or the benefits of screening are sometimes insignificant when compared to the risk of harm (Schiffman et al., 2015). The possibility of overdiagnosis is still a major worry in screening because it is possible to find lesions with no clinical significance and force the clinician and patient to make challenging treatment choices.

Patients may experience morbidity from a course of treatment that might not actually be beneficial if treatment is pursued after an overdiagnosis.

1.6. Treatment option

The present strategy for treating cancer is still reductionist, despite significant advancements. Single molecular aberrations or cancer pathways have been the focus of effective treatment therapies that have only slightly impacted some malignancies' survival rates. The "magic bullet" approach of using a single medicine to target a specific characteristic or route, however, is unlikely to result in the cure of cancer (Zugazagoitia et al., 2016). There are a number of cancer treatment options. Also, the type of cancer and its stage will determine the types of treatment. Some cancer patients will only receive one treatment. However, the majority of patients have a mix of therapies, including surgery, chemotherapy, and radiation therapy. Depending on the various treatment preferences the treatment options for cancer can be categorized into two broad groups such as (i) local therapy and (ii) systemic therapy.

1.6.1. Local therapy

There are numerous methods and medications for treating cancer, and many more are being researched. Some treatments are performed "locally," like surgery and radiation therapy, to treat a particular tumor or region of the body.

1.6.1.1. Surgery

In order to treat their cancer, about 60% of patients will have surgery of some kind. Surgery is the sole treatment necessary in some circumstances. As part of a comprehensive treatment strategy, it may also be used with radiation therapy or chemotherapy. Moreover, cancer is frequently taken out of the body during surgery and removed. For cancers that aren't advanced and haven't spread to other parts of the body, surgery is typically a good option. Depending on the sort of cancer you have, there are numerous surgical options. Additionally, there are various cancer surgeries such as curative surgery, reconstructive surgery, preventive surgery, staging surgery, palliative surgery, etc (Lange et al., 2009; Hanasono, 2014; Scheuer et al., 2002; Coburn et al., 2018; Hope and Pothuri, 2013).

1.6.1.2. Radiotherapy

About half of all cancer patients receive radiation therapy at some point during their illness, and it accounts for 40% of all curative cancer treatments. Radiation therapy is still a crucial part of cancer treatment. Radiation therapy's primary objective is to deprive cancer cells of

their capacity for cell division and proliferation (Baskar et al., 2012). Moreover, radiation creates ions (electrically charged particles) and deposits energy in the cells of the tissues it passes through, the radiation employed is known as ionizing radiation. This accumulated energy has the power to kill cancer cells by damaging the genetic materials (DNA) or damaging them by changing their genetic makeup (Jackson and Bartek, 2009).

1.6.2. Systemic therapy

Because they can have an impact on the entire body, drug therapies (such as biological therapy, chemotherapy, or hormone therapy) are frequently referred to as "systemic" treatments.

1.6.2.1. Biological therapy

Biological cancer therapy uses synthetic or naturally occurring chemicals created by the body or in the laboratory for cancer treatment. These treatments either support the immune system's defense against cancer or target the disease directly. These types of cancer therapy include the use of monoclonal antibodies, adoptive cell transfer, gene therapy, oncolytic viruses, cytokine therapy, cancer vaccines, immunoconjugates, along with different targeted therapies (Papież and Krzyściak, 2021). Moreover, the use of biological therapies for cancer treatment is currently on the rise and is a perfect fit for the new field of precision oncology, which uses the results of next-generation sequencing (NGS) techniques to identify novel, uncommon mutations in cancer cells in order to customize treatment for a particular patient (Han et al., 2020).

1.6.2.2. Chemotherapy

Chemotherapy works to stop tumor growth and cell division, which prevents invasion and metastasis. However, because chemotherapy also has an impact on normal cells, this leads to hazardous side effects. Tumor growth can be slowed down at various levels both inside the cell and in its surroundings. By interfering with the production of DNA, RNA, or proteins or by impairing the proper operation of the preformed molecule, traditional chemotherapeutic drugs largely disrupt the macromolecular synthesis and function of malignant cells (Amjad et al., 2023). Combination chemotherapy is frequently used to get sufficient results. They seem to promote cytotoxicity in resting and dividing cells, which appears to stop the emergence of resistant clones (Baserga, 1981). Additionally, chemotherapy is possible in neoadjuvant, adjuvant, combination, and metastatic settings. A treatment administered before the main therapy is called neoadjuvant therapy. Also, adjuvant therapy, which is a form of secondary treatment used in conjunction with primary therapy, has the ability to slow or stop the growth

of occult cancer cells. Breast, lung, colorectal, and ovarian cancer adjuvant therapy is increasingly the norm. Before surgery or other curative treatments for malignancies of the head and neck, lung, or anal, combined therapies like chemotherapy and radiation are utilized to reduce the tumor (Amjad et al., 2023).

1.6.2.3. Hormone therapy

Hormone treatment has recently been employed more frequently for the treatment of cancer like breast, prostate gland, uterus, lymphatic, and hematopoietic cancer. Importantly, patients having neoplastic diseases who choose to receive hormone therapy must take medications that block the biological function of certain hormones or lower their levels in the body in order to stop or slow the spread of the disease (Mitra et al., 2022). Furthermore, inhibiting hormone production or preventing hormones from increasing the number and division of cancer cells are two ways that hormone therapy works to treat cancer. In recent years, there has been a tremendous advancement in the treatment of individuals with gynecological cancers (Chaudhry and Asselin, 2009; Mitra et al., 2022).

1.6.2.4. Targetted therapy

One another kind of cancer treatment is called targeted therapy. Drugs are used to specifically target the genes and proteins that support the growth and survival of cancer cells. Moreover, the tissue environment in which cancer cells grow can be changed by targeted therapy, or it can focus on cells like blood cells that are associated with cancer growth (Tsimberidou, 2015). There are most common targeted therapies for the treatment of cancer such as antibody-targeted therapy (monoclonal antibody), targeted therapy by small molecules, ligand-targeted therapy, etc (Wu et al., 2006).

1.7. MMPs and their classification

Matrix metalloproteinases (MMPs) are zinc-dependent endopeptidases. These are responsible for the degradation of the extracellular matrix (ECM). There are several enzymes, that are involved in ECM remodeling, but the MMPs have a major role in it (Bonnans et al., 2014). Numerous physiological processes, including tissue repair, morphogenesis, development, tissue homeostasis, etc, depend on tissue remodeling. It could be a component of several clinical disorders, neurological diseases, arthritis, cardiovascular diseases along with cancer. Interestingly, by modulating ECM, MMPs are involved in growth factor availability and play an extensive role in the functioning of cell surface signaling systems such that way MMPs influence proliferation, migration, and cell death (Djuric and Zivkovic, 2017). In general, all

the MMPs are secreted as inactive forms. However, one of the main methods for activating MMP is the "cysteine switch" process, in which the thiol group is left unpaired and the cysteine is switched out for a water molecule (Van Wart and Birkedal-Hansen, 1990). Additionally, it permits pro-peptide hydroxylation of partially activated MMPs in this stepwise activation pathway. All the MMPs are activated intercellularly other than MT-MMPs, MMP-11, -23, and -28 (Djuric and Zivkovic, 2017). There are 26 different types of MMPs had been reported to this date, and sequence homology along with the biological effects have been reported (Mondal et al., 2020).

MMPs are classified into six different classes (**Table 1.1**) based on their substrate specificity i.e., (i) collagenase, (ii) gelatinases, (iii) stromelysins, (iv) matrilysins, (v) membrane type (MT-MMP), and (vi) Others MMPs. MMPs play significant roles in the tumor development and invasion of inflammatory cells (Abbas et al., 2015). Additionally, the major number of MMPs are responsible for the different types of disease (**Table 1.1**).

Table 1.1. Classification of MMPs along with their substrate and associated diseases

<i>Subfamily/Class</i>	<i>MMPs</i>	<i>Substrate</i>	<i>Related Disease</i>	<i>References</i>
Collagenases	MMP-1	CT I-III, VII-VIII, X, aggrecan, gelatin and MMP-2, -9	Cancer, RA	(Hu et al., 2007; Arakaki et al., 2009)
	MMP-8	CT I-III, V, VII-VIII, X, laminin, gelatine, fibronectin, aggrecan and elastin	Periodontitis, Cancer, RA, Asthma	(Hu et al., 2007; Alahö and Kähäri, 2005; Romero et al., 2013)
	MMP-13	CT I-IV, aggrecan, gelatin and MMP-9	Cancer, IBD, Osteoarthritis, RA, Obesity	(Hu et al., 2007; Alahö and Kähäri, 2005; Rath et al., 2006; Shih and Ajuwon, 2015; Li, 2017)
	MMP-18	Unknown	--	--
Gelatinases	MMP-2	CT I-V, VII, X-XI, XIV, aggrecan, gelatine, fibronectin, laminin, elastin, and MMP-9, -13	Cancer, CVD, Asthma, HF	(Hu et al., 2007; Overall and López-Otín, 2002)
	MMP-9	CTIV-V, VII, X, XIV; elastin; fibronectin; aggrecan and gelatin	Cancer, Asthma, RA, IBD, HF, Liver fibrosis	(Hu et al., 2007; Kurzepa et al., 2014; Radosinska et al., 2017; Siloşi et al., 2014; Huang, 2018)
Stromelysins	MMP-3	CT II-IV, IX-XI; elastin; aggrecan; fibronectin;	Atherosclerosis, CAD, IBD, Periodontitis	(Hu et al., 2007; Romero et al., 2013;

		laminin; gelatin and MMP-1,-7,-8,-9,-13		Siloşi et al., 2014; Beton et al., 2016)
	MMP-10	CT III-V; fibronectin; laminin; aggrecan; gelatin; elastin and MMP-1,-8	COPD, Atherothrombosis	(Gharib et al., 2018; Rodriguez et al., 2008)
	MMP-11	Fibronectin; a-1 antitrypsin; laminin and aggrecan	Ovarian Cancer, OSCC	(Périgny et al., 2008; Hsin et al., 2014)
	MMP-27	Unknown	--	--
Matrilysins	MMP-7	CT IV, X, elastin; fibronectin, aggrecan, laminin; gelatin and MMP-1, -2, -9	Cancer, IBD, Lung fibrosis	(Hu et al., 2007; Rath et al., 2006; Overall and López-Otín, 2002)
	MMP-26	pro-MMP-9	Periodontitis, Colon cancer	(Emingil et al., 2006; Bister et al., 2004)
Membrane type (MT-MMP)	MMP-14	CT I-III; elastin; aggrecan; fibronectin; laminin; gelatin and MMP-2,-13	Cancer, ARF	(Solovyeva et al., 2015; Covington et al., 2006)
	MMP-15	Gelatin; laminin; fibronectin and MMP-2	Ovarian Cancer	(Lin et al., 2013)
	MMP-16	MMP-2	--	--
	MMP-17	Unknown	--	--
	MMP-24	Pro-MMP-2,-9, and gelatine	Arthritis, AD	(Sugimoto et al., 2020)
	MMP-25	CT IV; fibrin; fibronectin; and gelatine	Periodontitis, COPD	(Emingil et al., 2006; Blumenthal et al., 2010)
Others MMPs	MMP-12	CT IV; casein; elastin; gelatin; fibronectin; fibrin fibrinogen; vitronectin and plasminogen	COPD, Neurological diseases	(Hu et al., 2007; Chelluboina et al., 2018)
	MMP-19	Type-I collagen	Colon Cancer	(Bister et al., 2004)
	MMP-20	Aggrecan; gelatin; amelogenin (dentine) and COMP	RA	(Kontinen et al., 1999)
	MMP-21	Not determined	Cancer	(Boyd et al., 2009)
	MMP-22	Casein and gelatin	CHD	(Jin et al., 2017)
	MMP-23	Not determined	Melanoma	(Moogk et al., 2014)
	MMP-28	Casein	Colon Cancer	(Bister et al., 2004)
	MMP-29	Not determined	CHD	(Jin et al., 2017)

RA = Rheumatoid arthritis, IBD = Inflammatory bowel disease, CVD = Cardiovascular diseases, HF = Heart failure, COPD = Chronic obstructive pulmonary disease, CAD = Coronary artery disease, OSCC = Oral Squamous Cell Carcinoma, ARF = Acute renal failure, AD = Alzheimer's disease, CHD = Coronary heart disease, CT = Collagen type.

1.8. General structure of MMPs

MMPs are made up entirely of a single peptide. MMPs are functionally different, despite their structural similarity. There are four primary domains in MMPs such as (i) signal peptide

domain, (ii) pro-peptide domain, (iii) catalytic domain, and (iv) hemopexin domain (**Figure 1.6**). The one peptide domain (17–29 amino acids), which dissociated from the N-terminal amino acids (except from MMP–23), is responsible for its release from the cells. Moreover, a transmembrane domain binds the majority of MMPs to the cell surface (excluding MT-MMPs) (Baidya et al., 2021). Until or unless the enzyme is activated, the pro-peptide domain, which has 80 amino acids, inhibits the catalytic area. This area contains residues of cysteine. The catalytic domain contains 170 amino acids in total. Along with the calcium ion, this domain also contains the zinc-binding motif HEXXHXXGXXH, which is in charge of preserving the three-dimensional MMP structure for stability and enzyme function (Djuric and Zivkovic, 2017). Hemopexin-like domains the hinge region, and the fibronectin (FN) domain are also present in the MMP structure (**Figure 1.6**).

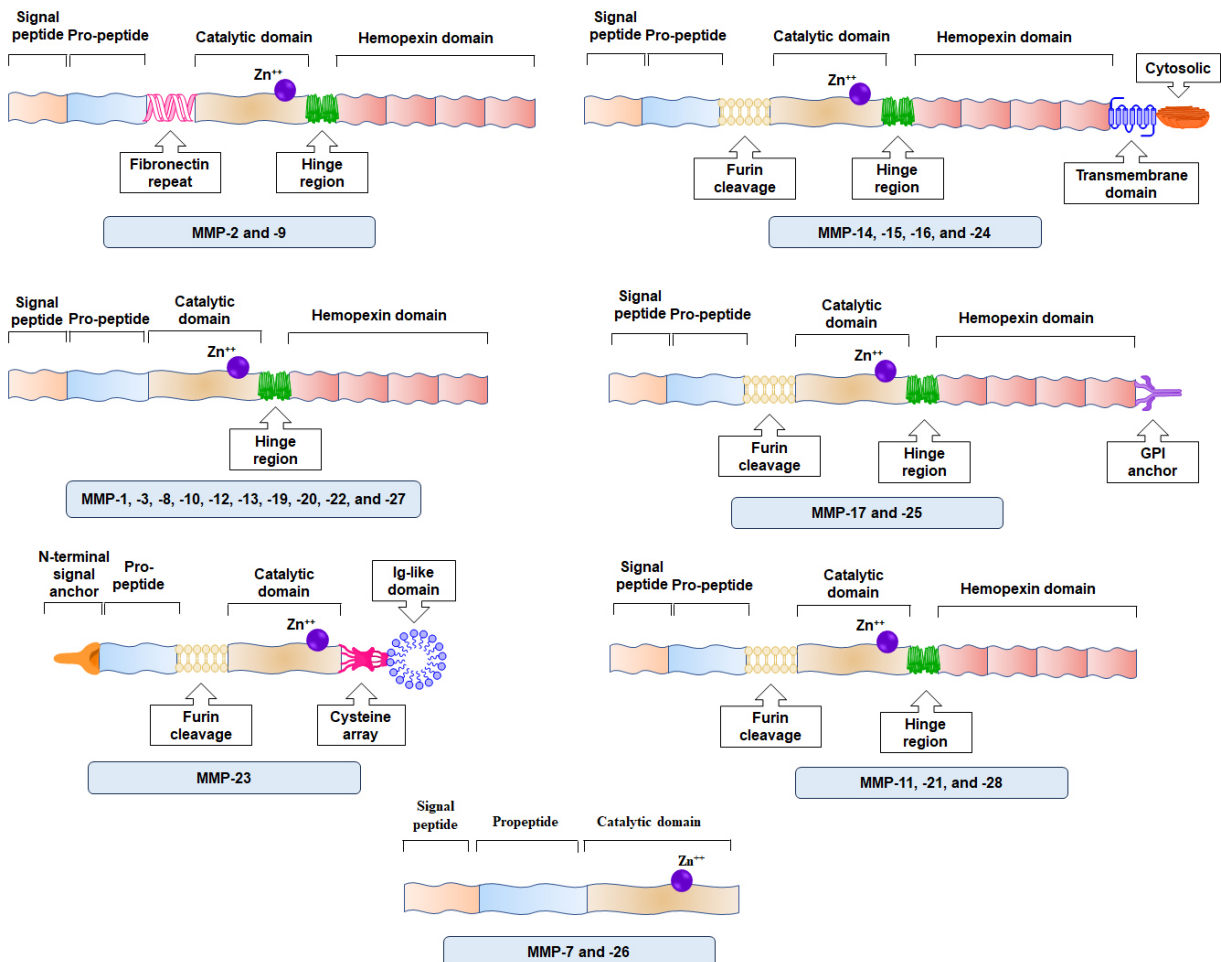


Figure 1.6. Representation of different structural domains of the MMP family members.

Moreover, For the creation of more potent and selective MMPiS, the X-ray crystal structure of gelatinases with their inhibitors provided data on the structure-activity relationship (SAR) (**Figure 1.7**). It has been revealed that the complex hydroxamic acid-based inhibitor (SC-74020) has the 3D crystal structure of MMP-2 (PDB: 1HOV) (Feng et al., 2002). By forming a hydrogen bond connection with the amide protons and sulfonyl oxygen atom, the inhibitor SC-74020 attaches to the enzyme. The large hydrophobic portion is inserted into the substantial S1' pocket. Again, another group of researchers provided information about the broad-spectrum hydroxamate-based inhibitor (CC27) crystal structure in combination with the MMP-9 catalytic region (PDB: 4H3X) (Antoni et al., 2013).

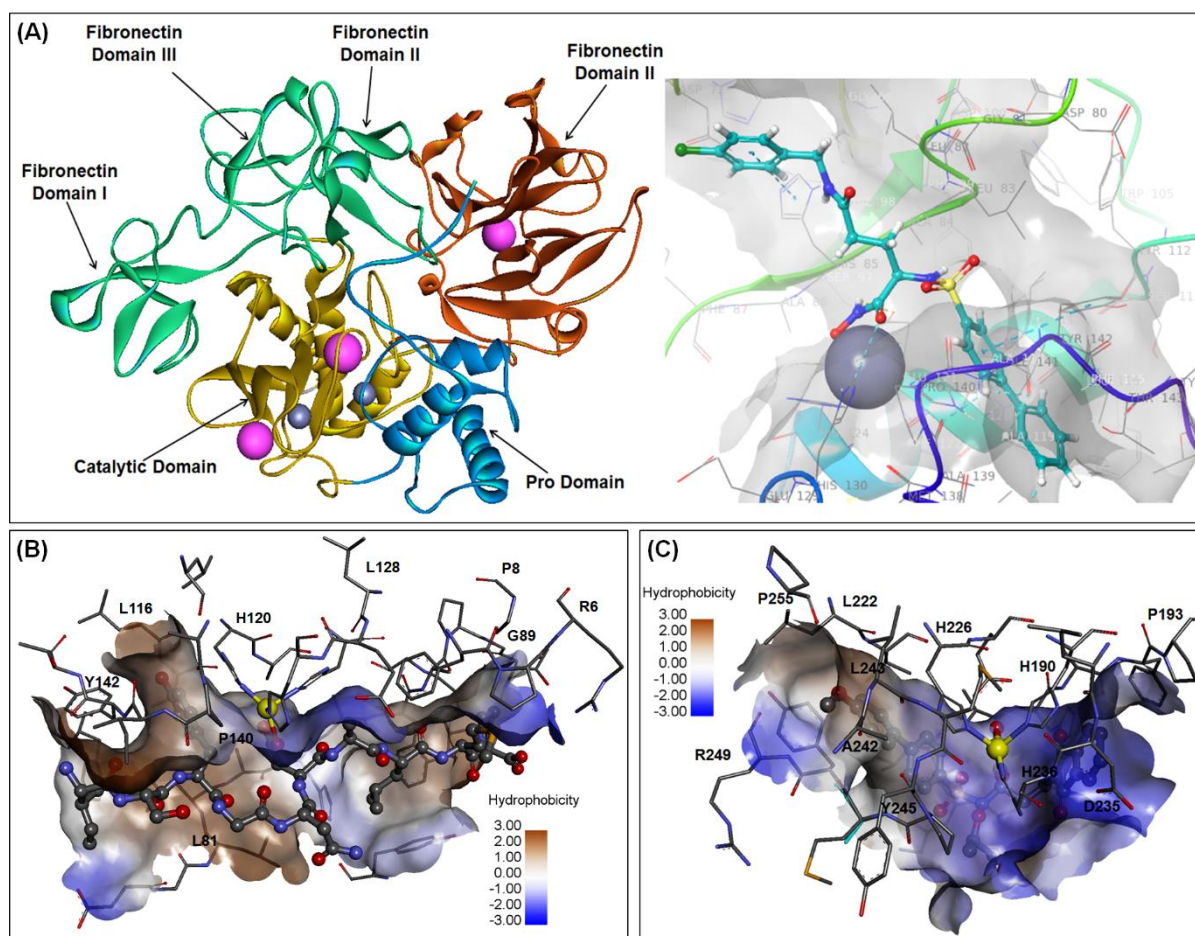


Figure 1.7. (A) Structure of different domain of MMP-2 enzyme and binding site (PDB: 1HOV) of MMP-2 enzyme; Structure-based hydrophobic contour at the (B) MMP-2 binding site (PDB: 3AYU) and (C) MMP-9 binding site (PDB: 4WZV), mapped with inhibitor (shown in Ball and stick). Catalytic amino acid residues are shown in stick and the catalytic zinc ion is shown in yellow ball.

Another group of workers validated the binding mode of the MMP-9 complex with the two distinct inhibitors (Nutti et al., 2015). The catalytic domain of MMP-9 is complexed with the hydroxamate-based inhibitors APR101 and EN140 in both crystal structures (PDB: 4XCT and 4WZV). Moreover, another group of researchers revealed the crystal structure of another hydroxamate-based inhibitor, LT4 and MMP-9 complex (PDB: 5CUH) (Camodeca et al., 2016). The asymmetric structure is made up of the catalytic domain of MMP-9 without the repetition of FN-II. Three α -helices, a twisted five-strand β -sheet, eight intervening loops, and a deep S1' pocket where the inhibitor LT4 is attached are all present in this conformation of the domain. The catalytic domains of gelatinases are homologous with hydrophobic subsites, and the S1' site is medium in size when taken collectively. Recently, the Dept. of Pharm Tech, Jadavpur University, provided an explanation for the variation in the S1' pocket among medium-size pocket MMPs, which offers information for the development of MMP inhibitors (Baidya et al., 2022).

1.9. Biochemistry of MMPs

The cellular conditions necessary for development and morphogenesis are created by extracellular matrix (ECM) macromolecules. Moreover, proteinases known as MMPs, also known as matrixins, are involved in the breakdown of ECM (Kwon, 2023). The transcription of MMPs, activation of the precursor zymogens, interaction with particular ECM components, and inhibition by endogenous inhibitors are all tightly regulated under normal physiological conditions (Sternlicht and Werb, 2001). Therefore, diseases like arthritis, cancer, atherosclerosis, aneurysms, nephritis, tissue ulcers, and fibrosis may be brought on by a loss of activity control (Visse and Nagase, 2003; Kwon, 2023). Tissue inhibitors of metalloproteinases (TIMPs) are particular matrixins inhibitors that help to regulate the local MMP activity in tissues (Visse and Nagase, 2003). Additionally, it has been reported that MMPs with medium-sized S1' pockets, such as MMP-2, MMP-8, MMP-9, MMP-12, and MMP-14, are involved in modifying a number of disease states, including malignancies, cardiovascular illnesses, neurological disorders, inflammatory diseases, and viral infections (Baidya et al., 2022). Nevertheless, not only medium-sized S1' pockets MMPs, but also all different classes of MMPs like collagenases, stromelysin, matrilysins, membrane-type MMPs, and other types of MMPs are associated with the various types of diseases (**Figure 1.8**).

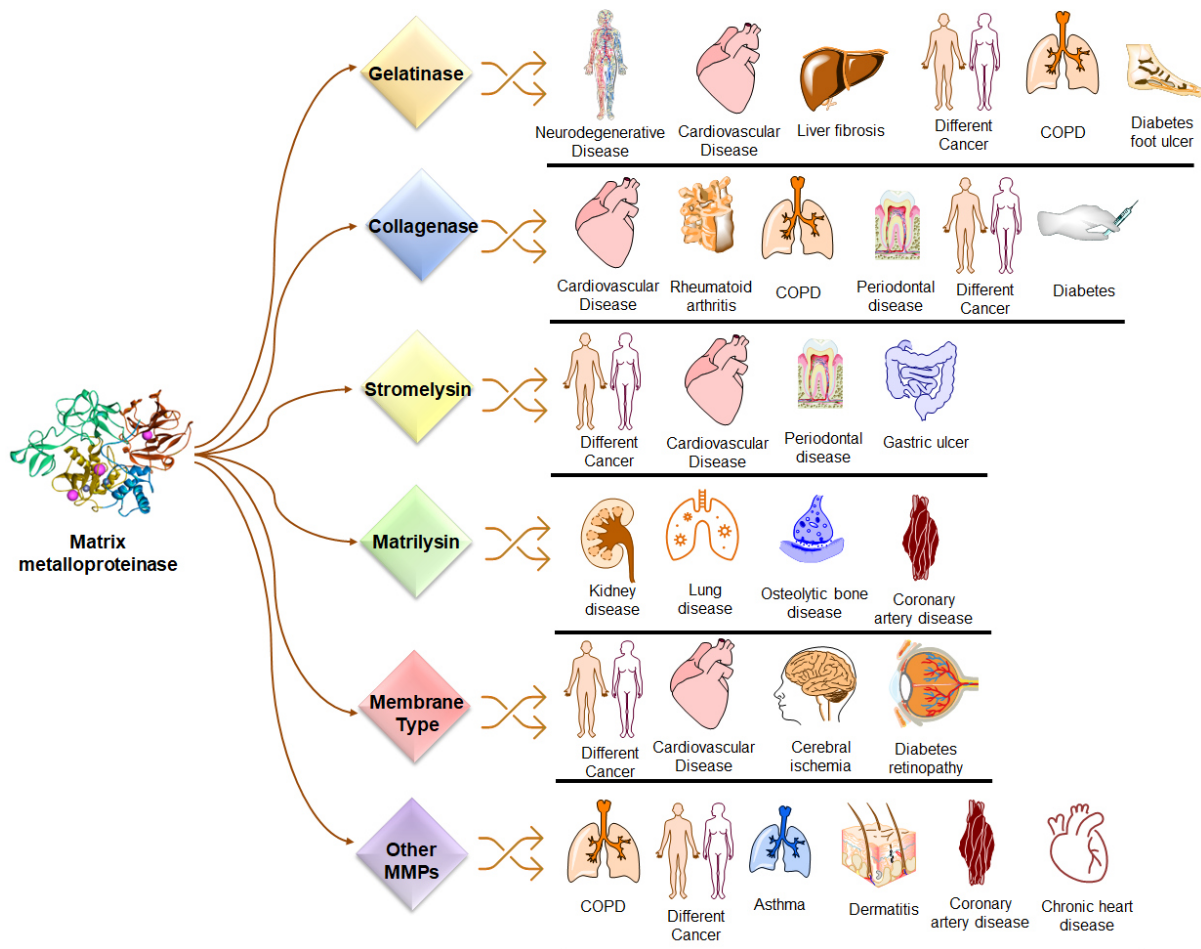


Figure 1.8. The implication of all different classes of MMPs consisting of various disease conditions.

Moreover, MMPs can be triggered by proteinases or chemical triggers like oxidized glutathione, SDS chaotropic compounds, reactive oxygens, and thiol-modifying agents (4-aminophenylmercuric acetate, HgCl_2 , and N-ethylmaleimide). Additionally, activation may result from heat treatment and low pH. The disruption of the cysteine-zinc connection of the cysteine switch is most likely how these substances function (Nagase, 1997). MMPs that have been activated can take part in processing other MMPs. Given that TIMPs may obstruct activation by engaging with the intermediate MMP before it is fully activated, the stepwise activation system may have evolved to accommodate finer regulatory mechanisms to control destructive enzymes (Visse and Nagase, 2003).

The elimination of ECM during tissue resorption is regarded to be one of MMPs' main functions. In addition to serving as an extracellular structure, the ECM also stores physiologically active chemicals like growth factors (Sternlicht and Werb, 2001). On proteolysis, several ECM components can display cryptic biological roles. As a result, MMP

destruction of ECM components can change the phenotype and behavior of cells. For example, the activation of osteoclasts, keratinocyte migration during re-epithelialization, and epithelial cell death prior to the start of labor are all linked to the degradation of type I collagen by collagenase. The cleavage sites of protein substrates or a variety of synthetic peptide substrates have both been used to study the substrate specificities of MMPs. The S1' specificity pocket, whose size and shape varied significantly among MMPs, can fit the hydrophobic residues (Bode et al., 1999, Baidya et al., 2022). In addition, the substrate selectivity of the enzyme is also influenced by other substrate interaction sites (subsites) besides the S1' pocket.

1.10. Expression of MMPs

Growth factors and cytokines released by both tumor or stromal cells and tumor-infiltrating inflammatory cells control the production of MMPs in tumors in a paracrine way. Research suggests that during the invasion process, tumor cells, stromal cells, and inflammatory cells continuously interact with one another (Westermarck and Kähäri, 1999). As a result, substances produced by tumor cells that boost the expression of a number of MMPs in stromal cells have been isolated. One of these elements, called EMMPRIN, was first discovered in the cell membrane of LX-1 carcinoma cells and has been demonstrated to cause fibroblasts to express MMP-1, MMP-3, and MMP-2 (Zhao et al., 2013). Aside from destroying ECM components, MMPs, and TIMPs may also control the availability and activity of inflammatory cytokines at the site of the tumor invasion due to their capacity to degrade and inactivate interleukin-1 β (IL-1 β), cleave the precursor of tumor necrosis factor α (TNF- α) into a biologically active form, and inhibit TNF- α activation (Ito et al., 1996).

Different malignant tumors have high levels of expression for both MMP-2 and MMP-9 (Li et al., 2017). Additionally, breast, colon, and stomach adenocarcinomas have an increased abundance of the immunoreactive enzyme at the neoplastic epithelium, according to an immunohistochemistry study of the expression of MMP-2. However, *in situ* hybridizations demonstrate an increase in MMP-2 mRNA mostly in the stromal component of tumors, in contrast to the immunohistochemistry data. Discoveries that the MMP-2 interacts with cell membrane-associated MT1-MMP to bind to the cell surface of malignant cells may help to explain this discrepancy (Westermarck and Kähäri, 1999). Additionally, through the α V β 3 integrin, active MMP-2 attaches to the cell surface of invasive melanoma and endothelial cells (Jiao et al., 2012). Findings suggest that MT1-MMP binds to and activates MMP-2 at the cell surface of fibroblasts, as both MMP-2 and MT1-MMP mRNAs are expressed by stromal fibroblasts of human vulvar, breast, lung, and head and neck carcinomas. In SCCs, MMP-13,

which may in turn be activated by MT1-MMP, can also activate MMP-2 and MMP-9 (Westermarck and Kähäri, 1999). They significantly increase in vivo cell surface localized proteolytic activity and suggest that selective inhibition of one MMP may be sufficient to prevent activation cascades and ECM degradation during tumor invasion. These types of activation cascades may be necessary to ensure cooperation between tumor and stromal cells.

1.11. MMPs in cancer and leukemia

MMP has crucial functions in the development of cancer. The advancement of cancer goes through various stages, including the development of the tumor and the multi-step processes of invasion, metastasis, and angiogenesis, all of which can be influenced by MMPs. MMPs are expressed in the tumor microenvironment in conjunction with nearby stromal cells as well as cancer cells (Gialeli et al., 2011). Nonetheless, angiogenesis, tumor cell invasion, and metastasis are made easier by MMPs' proteolytic action, which breaks down the physical barriers. The enhanced accessibility of signaling molecules, such as growth factors and cytokines, to cancer cells and the tumor microenvironment, is made possible by MMPs. This is also essential for tumor growth and angiogenesis. In order to do this, either IGF, bFGF, and VEGF are released from the ECM or the cell sheds them (Gialeli et al., 2011).

Due to their potential to function as both positive and negative regulators of angiogenesis depending on the time point of expression during tumor angiogenesis and vasculogenesis as well as the availability of the substrates, MMPs exhibit a dual role in tumor vasculature. MMP-2, -9, and MMP-14 are the main MMP family members involved in tumor angiogenesis, with MMP-1 and -7 playing a less significant role (Rundhaug, 2003). Furthermore, new blood vessels must develop in order for cancer cells to multiply and begin moving. By degrading the ECM, the physical barriers are first removed, which is followed by the production of pro-angiogenic factors. VEGF, the most potent mediator of tumor vasculature, and basic fibroblast growth factor (bFGF) are two important factors in the angiogenic switch, and MMP-9 contributes to this process by increasing their bioavailability through the degradation of extracellular components like collagen type IV, XVIII, and perlecan, respectively (Gialeli et al., 2011).

1.12. Gelatinases (MMP-2 and MMP-9) in cancer and leukemia

Currently, the focus of cancer research is on determining the underlying functional processes of cell transformation, tumor growth, and metastasis (Gonzalez-Avila et al., 2019). However, complex molecular changes in cell cycle regulation act as a mediator for cancer metastasis, which is the spread of cancer cells from the primary tumor to neighboring tissues and distant

organs (Gonzalez-Avila et al., 2019). Epithelial-mesenchymal transition (EMT) is one of the primary underlying functional processes of cancer progression, according to newly available research (Gonzalez-Avila et al., 2019). EMT enables polarised epithelial cells to go through a number of biochemical changes that allow them to adopt a mesenchymal cell phenotype with increased invasiveness, motility, and resistance to apoptosis (Kalluri and Weinberg, 2009). Also, MMP-2 and MMP-9 participate in biochemical reactions, which cause cancer cells to invade and migrate (Gonzalez-Avila et al., 2019; Li et al., 2020; Li and Luo, 2019). Angiogenesis is the process by which new blood vessels develop from pre-existing ones. Malignant cells need oxygen and nutrients to survive and multiply, and they cluster around blood vessels, hence the beginning of tumor angiogenesis is necessary for tumor progression (Lugano et al., 2020). In cases of solid tumors, such as malignancies of the breast, lung, gastric, hepatic, colorectal, prostate, ovarian, oesophageal, melanoma, thyroid, and head and neck cancer, the gelatinolytic action leads to tumor invasion and metastasis. The literature's Pythora of data indicated that gelatinases are closely related to solid tumor malignancies. The association between gelatinases and hematological cancers has not been well investigated to date (Das et al., 2021; Baidya et al., 2021). Despite the fact that over 5,000 gelatinase inhibitors had been recorded in the ChEMBL database, only a small portion had been tested against leukemia or other hematological malignancies (<https://www.ebi.ac.uk/chembl>).

However, some groups of researchers indicated the correlation of gelatinase expression in CML cells. Through *in silico* and *in vitro* experiments, Veena and coworkers revealed the anti-leukemic potential of the microbial polyketide 2, 4-diacetyl phloroglucinol (DAPG) (Veena et al., 2016). DAPG interacted with proteins associated with metastasis, including MMP-2 and MMP-9. Furthermore, Arg 149 of the MMP-2 enzyme interacts with one hydroxyl functional group of DAPG at a bond distance of 2.075 Å (PDB: 1HOV). With Thr 143, the carboxyl group of DAPG forms a hydrogen bond. However, three hydroxyl groups of DAPG are implicated in hydrogen bonding interactions with Leu 188, Ala 189, and Glu 402 the residues of MMP-9 (PDB: 1GKC). It inhibited the MMP-2 ($IC_{50} = 5.82 \pm 1.6 \mu M$) and MMP-9 ($IC_{50} = 6.75 \pm 1.2 \mu M$) in a dose-dependent manner followed by NF- κ B ($IC_{50} = 10.82 \pm 1.5 \mu M$). In addition to inhibiting MMP-2, MMP-9, and NF-B, DAPG also inhibits the Bcl-2 protein family's antiapoptotic members and causes leukemic cells to undergo apoptosis. Additionally, DAPG also inhibited human cancer cell lines such as A549 ($IC_{50} = 0.06 \pm 0.02 \mu M$), MDA MB-231 ($IC_{50} = 0.08 \pm 0.01 \mu M$), K562 ($7.67 \pm 0.73 \mu M$), Raji ($IC_{50} = 10.72 \pm 0.92 \mu M$) and HL-60 ($IC_{50} = 16.31 \pm 1.82$) in a dose-dependent manner.

Amsacrine [4-(9-acridinylamino)-N-(methanesulfonyl)-m-anisidine hydrochloride] reduces the amount of MMP-2/MMP-9 protein expression and mRNA level in U937, Jurkat, HL-60, K562, KU812, and MEG-01 cells lines (Liu et al., 2013). Results from Liu and coworkers reported that amsacrine (m-AMSA) may have an anti-leukemic impact by decreasing the expression of MMP-2/MMP-9 in leukemic cells (Liu et al., 2013). Amsacrine also decreased the activity of the MMP-2/MMP-9 promoter luciferase in leukemia cells. The molecular mechanism of CIL-102-induced MMP-2/MMP-9 down-regulation in human leukemia K562 cells was better understood as a result of additional work by the group of scientists (Liu et al., 2012). Moreover, in K562 cells, ROS production caused by CIL-102 promoted ERK inactivation, which resulted in the reduction of MMP-2/MMP-9 gene transcriptional activity. Additionally, p38 MAPK/JNK activation caused by CIL-102-induced ROS production caused PP2A α up-regulation and consequently TTP breakdown. When TTP was downregulated, KSRP protein complexes containing TTP were formed, which aided in the MMP-2/MMP-9 mRNA degradation process. Together, MMP-2/MMP-9 genetic transcription and mRNA stability were markedly inhibited by CIL-102, which ultimately prevented K562 cells from migrating and invading other cells.

Doxycycline significantly affected the migration of AML (KG1a) and CML (K562) cells, according to Wang et al (Wang et al., 2015). These findings suggested that doxycycline-induced leukemic cell migration may benefit from the inhibition of MMP-2/-9 and the expression and phosphorylation of FAK. Data suggested that MMP-2/MMP-9 expression may be reduced by m-AMSA to improve leukemia treatment. Furthermore, MMP-2/MMP-9 expression has been linked to the pathophysiology of leukemia (Bruchova et al., 2002; Lin et al., 2002; Kaneta et al., 2003; Baran et al., 2007; Paupert et al., 2008).

1.13. MMP-2 Crystal structure

MMP-2 enzyme has so far had 11 different structures determined by nuclear magnetic resonance (NMR), solution structures, and X-ray diffraction (XRD) structures (although high resolution). The different structures of MMP-2 are summarised in **Table 1.2**. Only a few of these structures have been primarily used in docking and molecular dynamics simulation-based studies for the exploration of potential newer drug interactions as well as for finding novel compound or substructural features. Although, these structures may provide an in-depth knowledge of the overall protein structure of MMP-2 as well as their roles in the protein function.

Table 1.2. Details of the crystal structures of MMP-2 (<https://www.rcsb.org/>).

Sl no	PDB ID	Type	Structure	Resolution	Sequence length	Substrate/ Inhibitor	Year
1	1RTG	X-Ray	C-terminal domain	2.60	210	--	1996
2	1GEN	X-Ray	C-terminal domain	2.15	218	--	1996
3	1CK7	X-Ray	Full length	2.80	631	--	1999
4	1QIB	X-Ray	Catalytic domain	2.80	161	--	1999
5	1CXW	Solution NMR	Fibronectin Type II Module	--	60	--	1999
6	1HOV	Solution NMR	Haemopexin-like domain	--	163	SC-74020	2001
7	1J7M	Solution NMR	Fibronectin Type II Module	--	72	--	2001
8	1EAK	X-Ray	Catalytic domain	2.66	421	--	2001
9	1KS0	Solution NMR	Fibronectin Type II Module	--	63	--	2002
10	1GXD	X-Ray	--	3.10	631	--	2002
11	3AYU	X-Ray	Active site mutant	2.00	167	Decapeptide inhibitor	2011

1.14. MMP-2 inhibitors

MMP-2, a member of the gelatinase subfamily and one of the most important targets for cancer, has been discovered among the several MMP subtypes, whereas MMP-9 has been linked as an anti-target in the advanced stages of cancer (Adhikari et al., 2017A; Overall and Kleifeld, 2006).

1.15. Classification of MMP-2 inhibitors

A number of molecules have been designed and tested as effective MMP-2 inhibitors, but most of the compounds have shown adverse effects as well as failed in cytotoxic studies. However, these molecules can be categorized based on their structure into two broad sections, such as (i) hydroxamate-based inhibitors, and (ii) non-hydroxamate-based inhibitors. Furthermore, non-hydroxamate-based inhibitors can be classified into five different segments such as carboxylic acid-based inhibitors, phosphonate-based inhibitors, pyrimidine-2,4,6-triones based inhibitors, n-hydroxyformamides-based inhibitors and thiols and mercaptosulfide-based inhibitors.

1.16. Clinical studies

A number of MMPs have been designed and developed based on the zinc ion and substrate binding pocket analysis. MMPs can be classified as hydroxamates, carboxylates, sulfhydryls, amino carboxylates, and phosphoric acid-based derivatives depending on whether a zinc-binding group is present (Baidya et al., 2021). For the clinical development of MMPs, hydroxamates are used because of their strong zinc-binding properties. Through hydrogen bonds, the hydroxamates' NH and OH groups can join with the Glu and Ala residues, respectively (Mondal et al., 2020). MMP inhibitory activity of the clinical trial compounds is depicted in **Table 1.3**.

Table 1.3. MMP inhibitory activity of the clinical trial compounds (Baidya et al., 2022)

<i>Name</i>	<i>MMP-1</i>	<i>MMP-2</i>	<i>MMP-3</i>	<i>MMP-7</i>	<i>MMP-8</i>	<i>MMP-9</i>	<i>MMP-12</i>	<i>MMP-13</i>	<i>MMP-14</i>
Batimastat	3	4	20	6	10	1		1	3
Prinomastat	8.3	0.05	0.3	54	-	0.26	-	0.03	0.33
Marimastat	5	6	200	20	2	3	< 5	0.74	1.8
BB1101	10 (8)	5 (4)	30 (30)	30 (60)	3 (3)	3 (3)	-(5)	-(7)	-(10)
CGS-27023A	33 (33)	11 (20)	13 (43)	-	-(1.9)	8 (8)	7.7	6	-
Ilomastat (GM 6001)	1.5 (0.4)	1.1 (0.39)	1.9 (27)	-	-(0.18)	0.5 (0.2)	-	-	13.4
Doxycycline	>4,00,000	56,000	32,000	28,000	26,000- 50,000	-	-	20,000- 50,000	-
Minocycline	--	--	2,90,000	1,25,000	--	1,80,000	--	--	--
Tanomastat/ BAY 12-9566	(>5000)	(11)	(134)	-	-	(301)	-	(1,47,000)	-
Rebimastat/ BMS 275291	25	41	157	-	-	25	-	4	-
Solimastat/B B-3644	10	80	30	5	-	70	-	-	-
RO-32-3555	(3)	(154)	(527)	-	(4)	(59)	-	(3)	-
RS-130830	(590)	(0.22)	(9.3)	(1200)	-	(0.58)	-	(0.52)	-

The respective K_i values are provided in the first bracket wherever the data is available.

1.17. Classification of different types of MMPs in clinical trials

MMPs can be categorized into four pharmacologic categories, such as (i) collagen peptidomimetics, (ii) non-peptidomimetics, (iii) bisphosphonates & bisphosphonate esters, and (iv) tetracycline derivatives. MMP-mediated clinical conditions have been treated using chemically diverse ZBGs and peptidomimetic or non-peptidomimetic scaffolds with a variety of synthesized MMPs (Li and Wu, 2010).

1.17.1. Collagen peptidomimetics

The earliest generation of MMPs with a hydroxamic moiety is collagen peptidomimetics. The peptidomimetic inhibitors include Ilomastat (GM-6001), Batimastat (BB-94), and Marimastat (BB-2516), (Krüger et al., 2010; Vandenbroucke et al., 2011; Whittaker et al., 1999). Batimastat (BB-94), is a peptide analog based on hydroxamate having a low molecular weight (**Figure**

1.9). British Biotech created this initially for patients with cancer in clinical trials (Wang et al., 1994; Sledge et al., 1995).

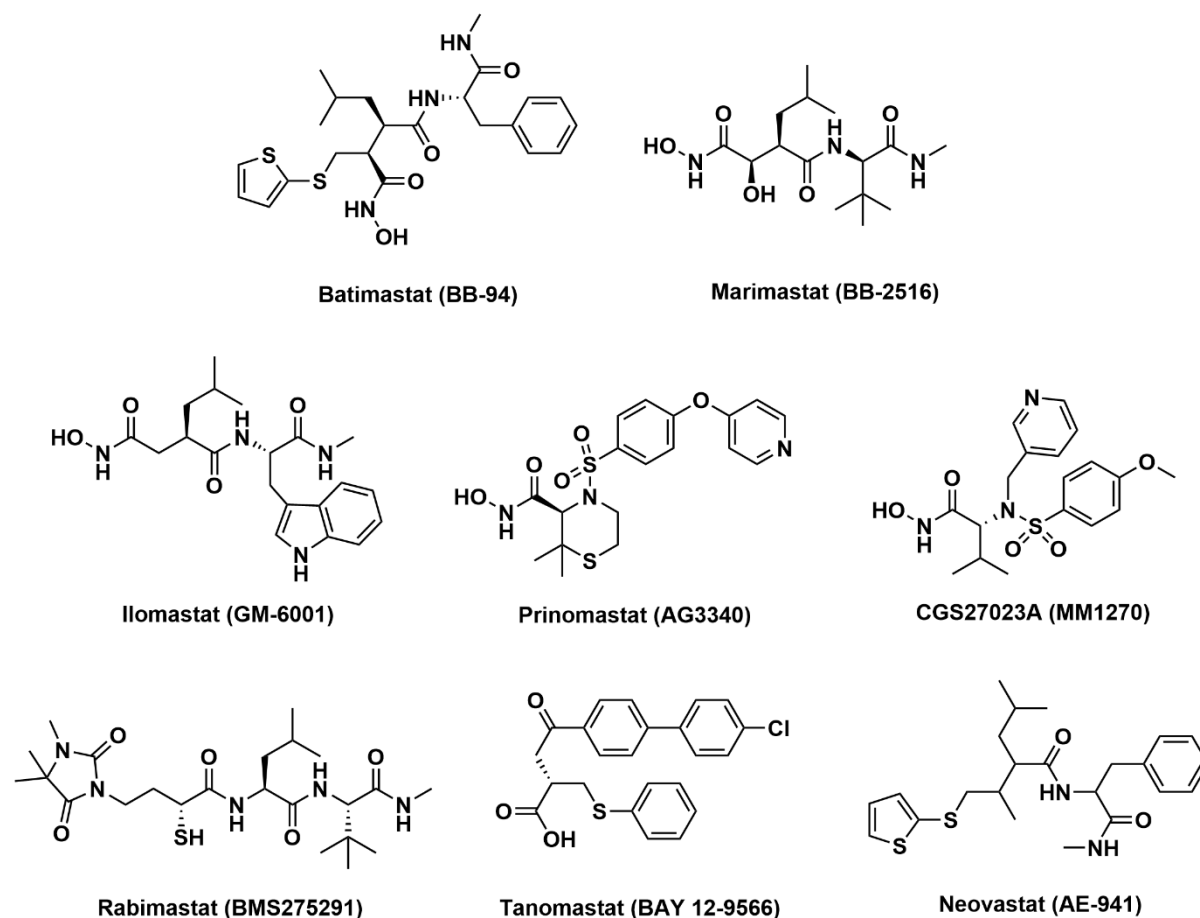


Figure 1.9. Structures of MMPIs evaluated in clinical trials.

It has very promising results against animal tumor models, tumor development, angiogenesis, and metastasis. Additionally, when combined with captopril and docetaxel, batimastat demonstrated antiproliferative, anti-angiogenic, and pro-apoptotic effects (Hidalgo and Eckhardt, 2001). However, due to weak solubility and undesirable effects, further development was put on hold years ago (Macaulay et al., 1999).

Additionally, British Biotech created marimastat (BB-2516, **Figure 1.9**). This extensive range of MMPIs participated in pre-clinical research and successfully completed Phase I, II, and some Phase III trials for various tumor development and metastasis (Thomas and Steward, 2000). Marimastat water solubility was made easier by the inclusion of *tert*-butyl and hydroxyl groups (Whittaker et al., 1999). However, in phase II clinical research, just 5% of patients with various cancer kinds responded (Nelson et al., 2000). Marimastat manifested several adverse side effects, including GI-tract toxicity, inflammation, weight loss, fibrosis, necrosis tissue, and

bleeding.(Wojtowicz-Praga et al., 1997). Ultimately, this molecule's performance in that study did not improve, which resulted in the discontinuation of additional clinical trials (Shepherd et al., 2002).

Ilomastat (GM-6001) is a member of the first generation of MMPIs based on collagen peptidomimetics (**Figure 1.9**). It was a broad-spectrum MMP subtype inhibitor, inhibiting MMP-2 and MMP-9 (Agren et al., 2001; Hao et al., 1999). It was applied topically to treat corneal ulcers and act as a skin collagenase inhibitor (Galardy et al., 1994). Nevertheless, ilomastat's poor oral bioavailability caused the clinical studies to fail.

1.17.2. Non-peptidomimetics

Non-peptidomimetics MMPIs were developed and manufactured using a structural approach in comparison to peptidomimetics inhibitors in order to increase oral bioavailability and have substantial pharmacokinetic features. The non-peptidomimetic class of drugs includes prinomastat (AG3340), CGS27023A (MM1270), rabimastat (BMS275291), tanomastat (BAY 12-9566), and neovastat (AE-941) (**Figure 1.9**).

Agouron Pharmaceutical Inc. was the first to develop prinomastat (AG3340) (**Figure 1.9**). This medication showed good results against MMPs of all types, including MMP-2,-3,-9, and -13 (Shalinsky et al., 1999a). It demonstrated a moderate level of gelatinase-specific inhibitory action. Prinomastat has lipophilic properties and may pass the blood-brain barrier (BBB) as a result. Although it might slow the growth of an implanted tumor, there were no appreciable effects on the proliferation of cells in culture. Additionally, it reduced angiogenesis and apoptosis expression in a variety of cancers, including non-small cell lung, breast, colon, and prostate carcinoma, in the xenograft mice model (Shalinsky et al., 1999b; Shalinsky et al., 1999c). Phase I clinical trials revealed acute and long-term harm at various levels. Although joint and muscle pain have been identified as the predominant symptoms at this stage (Li et al., 2013). Additionally, phase III clinical trials for patients with prostate and non-small lung cancer have been discontinued because they were ineffective (Peterson, 2004).

A broad-spectrum sulfonamide derivative called CGS-27023A (MM1270) (**Figure 1.9**) that was also efficient against gelatinases was known as an inhibitor of MMPs. It was a non-peptidomimetic inhibitor based on hydroxamate that, according to preclinical studies, reduced angiogenesis and tumor growth (Overall and López-Otín, 2002; Nakamura et al., 2003). It demonstrated synergistic benefits when used in combination therapy with the cytotoxic agent. MMP-1 ($IC_{50} = 33$ nM), MMP-13 ($IC_{50} = 6$ nM), MMP-3 ($IC_{50} = 13$ nM), MMP-2 ($IC_{50} = 11$ nM), and MMP-9 ($IC_{50} = 8$ nM) were all inhibited by CGS-27023A (Baidya et al., 2021).

However, CGS-27023A did not have any anti-proliferative effects on tumor cells, but at nanomolar (nM) concentrations, it decreased the activity of MMPs in the proteasome (Li et al., 2010). Unfortunately, due to its adverse effects and the resulting muscle and joint discomfort, the therapeutic potential was uncertain and failed in multiple clinical trials (Cathcart et al., 2015).

Bayer, Inc. was the company that first created tanomastat (BAY 12-9566) (**Figure 1.9**). It is an orally accessible homolog of biphenyl non-peptide butanoic acid. It demonstrated strong and precise inhibition of MMP-13, gelatinase A, and gelatinase B. In the phase, I clinical investigation, tanomastat's efficacy with a combined therapy of carboplatin and paclitaxel was safe (Gatto et al., 1999). However, patients with lung, ovarian, and pancreatic cancer received unsatisfactory results in phase III clinical trials (Nelson et al., 2000). Additionally, it demonstrated a relatively low rate of survival for patients with small-cell lung cancer in the clinical trials, which led to the termination of future research (Thomas and Steward, 2000).

Third-generation inhibitor rabimastat (BMS275291) (**Figure 1.9**) was orally accessible and has a broad range. The MMPs (MMP-1, -2, -3, -9, -13, and -14) are inhibited in a number of cancer types, including breast, lung, ovarian, and pancreatic cancer (Somani and Bhanushali, 2013). However, the tested substance was toxic, so this agent was also removed from clinical trials (Lara et al., 2006).

Neovastat (AE-941) (**Figure 1.9**), a non-peptidomimetics compound, is a naturally occurring multifunctional angiogenic inhibitor. MMP-2 was shown to have gelatinolytic activity compared to other MMPs (i.e., MMP-1, -7, -9 and -13). In addition to MMP-12, it demonstrated elastinolytic action against gelatinase (Gingras et al., 2001). The phase III clinical trials of this molecule for non-small cell lung carcinoma, breast, renal, and colorectal cancer had started, but the study was later stopped due to unfavorable side effects (Gingras et al., 2001).

1.17.3. Bisphosphonates & bisphosphonate esters

Bisphosphonates were developed in the previous three decades (O'Carrigan et al., 2017). It is unclear how these synthetic bisphosphonates work, although it may involve a direct inhibition of osteoclast function, assimilation into the skeletal matrix, or inhibition of the generation of the osteoclast cytokines (Rodan and Fleisch, 1996). Additionally, bisphosphonates precisely induced apoptosis and reduced prostate cancer cell gene expression. The study provided data that chelating with zinc ions can prevent MMPs from invading tumor cells (O'Carrigan et al., 2017). The bisphosphonates class of MMPIs includes BP-7033, minodronate (YM529),

risedronate, alendronate, incadronate, ibandronate, pamidronate, zoledronate (CGP 42446), and clodronate (**Figure 1.10**).

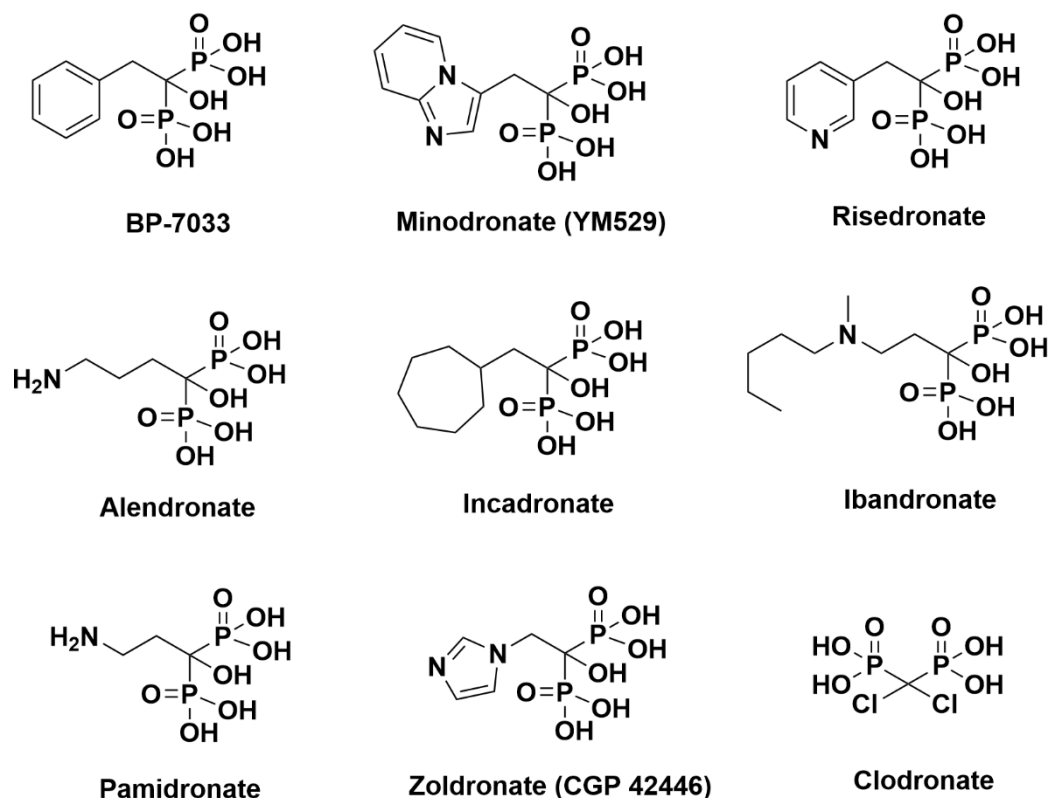


Figure 1.10. Structures of bisphosphonate derivatives

Due to their extreme hydrophilicity, these substances displayed very limited membrane permeability, which resulted in a reduced drug concentration in the soft tissue (Li et al., 2010). By esterifying the hydroxyl group, one or more ionized groups of bisphosphonates were covered in order to avoid these issues. Camdronate, tryptdronate, BKM1740, and Me-BP7033 are all members of the bisphosphonate ester family (**Figure 1.11**).

It was discovered that the bisphosphonate, BP-7033, which doesn't contain nitrogen atoms, works well in treating cancer (Li et al., 2010). Its impact on human umbilical vein endothelial cells was positive (Ledoux et al., 2006). Additionally, it was reducing the VEGF and MMP-2 synthesis. The third-generation bisphosphonate minodronate (YM529) inhibited osteoclastic bone resorption, which had an impact on lung cancer. It demonstrated its anticancer effects by activating the mitochondria-dependent apoptotic pathway (Ohishi and Matsuyama, 2018). A bone resorption inhibitor called risedronate is effective in treating Paget's disease, osteoporosis, bone metastases, and hypercalcemia. Moreover, MMP's proteolytic activity was suppressed by it. It did not stop MMP from being produced (Nutti, 2014). For the treatment of osteoporosis, alendronate was incredibly effective. Rather than preventing MMP-2 or TIMP-free plasmin

from degrading, it allowed TIMP-2 to ensure that MMP-2 would degrade by plasmin (Farina et al., 1998). The adverse consequences were a low calcium level and bone discomfort (Deliberador et al., 2018).

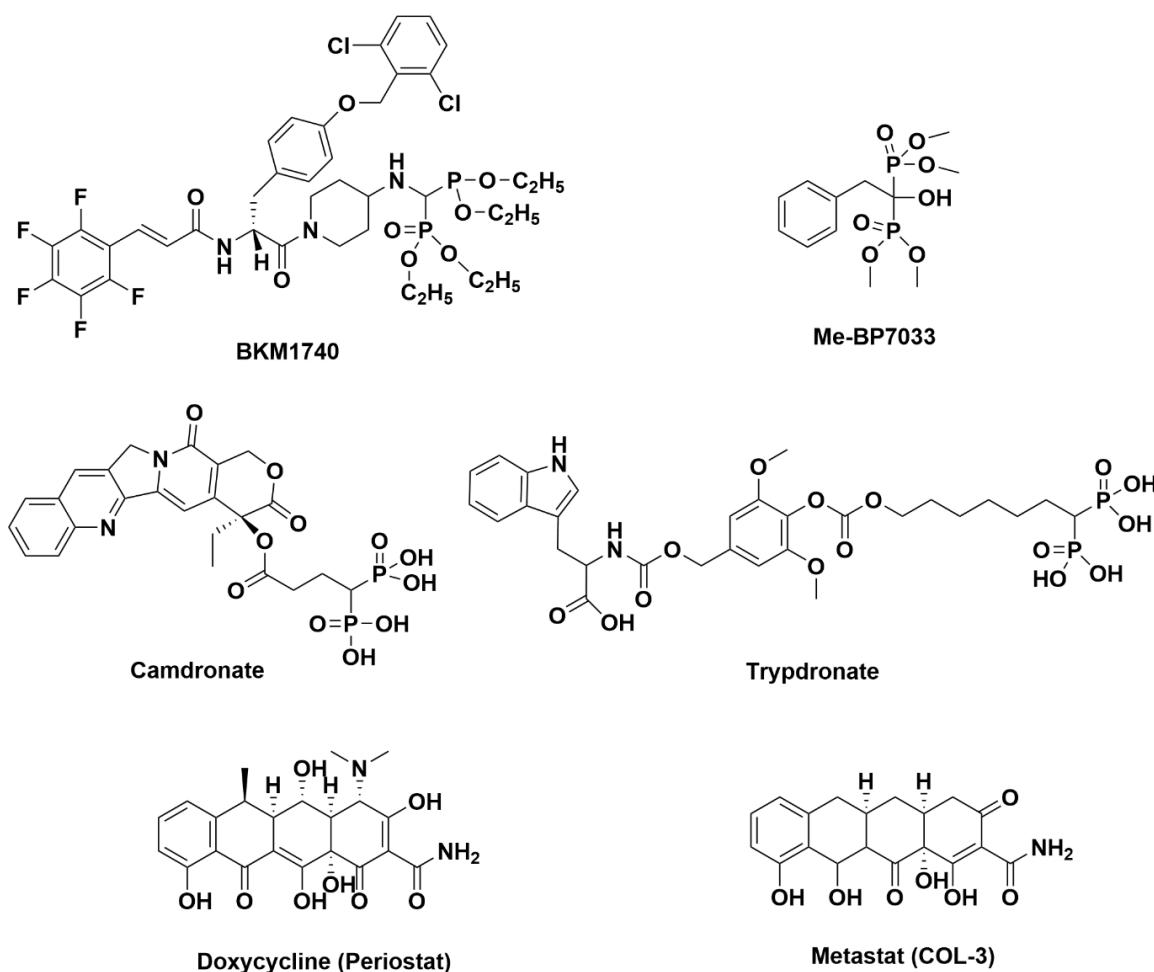


Figure 1.11. Structures of BKM1740, Me-BP7033, Camdronate, Trypdronate, Doxycycline (Periostat), and Metastat (COL-3).

Incadronate is a member of the aminomethylidenebisphosphonic acid family. In an animal model, it proved a very effective osteoporosis inhibitor (Nasulewicz-Goldeman et al., 2019). Moreover, ibandronate is one of the most effective nitrogen-containing bisphosphonates that can be used to treat bone metastases, osteoporosis, and hypercalcemia of malignancy (Li et al., 2010). Pamidronate is essential in controlling osteoclast activity and treating osteoporosis patients with malignancies that spread to the bone (Doroshov and Gaur, 2020). Novartis pharmaceutical originally introduced the bisphosphonate zoledronate (CGP 42446). By entering macrophages, this nitrogen-containing medication reduced the expression of MMP-9 (Giraud et al., 2004). In rat vascular smooth muscle cells (VSMCs), MMP-2, -9, and -13 expression were affected by zoledronate, according to Arun et al., (2016). Clodronate has

quickly been employed for its osteoactive and antiresorptive properties as well as its ability to reduce endothelial cell proliferation at low doses. Interestingly, patients with low serum MMP-2 and MMP-9 levels experience negative effects (Leppä et al., 2005). Compared to its predecessor, ME-BP7033 had greater pharmacokinetic action. In vivo investigations showed antitumoral and antiangiogenic action, but no evidence of deleterious consequences. Additionally, ME-BP7033 reduced the growth of human cancer A431 cell lines (Ledoux et al., 2006). Both carbonate and tryptidronate had strong bone tissue binding properties while being less harmful. In human prostate cancer cells, BKM1740 clearly suppressed survivin and promoted apoptosis (Li et al., 2010).

1.17.4. Tetracyclines

Tetracycline derivatives inhibited MMPs by chelating with the catalytic zinc ion in the enzyme's active site to impede its activity. Additionally, these substances controlled how pro-MMP became active (Li et al., 2010). As a result, these compounds were extremely beneficial for treating conditions including cancer and osteoarthritis. Tetracycline derivatives were doxycycline (periostat) and metastat (COL-3) (**Figure 1.11**).

Inhibiting breast cancer metastasis with the antibiotic doxycycline (periostat) may be beneficial for both MMP production and tumor cell proliferation (Ali et al., 2017). In the MDA-MB-435 cell line, it reduced MMP-2 and MMP-9 secretion (Fife and Sledge, 1995). Notably, this substance is a periodontitis medication that has received FDA approval (Samartzis et al., 2019). A non-antimicrobial tetracycline called metastat (COL-3) is created by changing the elemental structure of tetracycline. It was utilized to prevent tumor metastasis since it can reduce MMP activity. Additionally, COL-3 can prevent the thermal hyperalgesia caused by paclitaxel, suggesting that it may be useful in the prevention of chemotherapy-induced painful neuropathy (Parvathy and Masocha, 2013).

1.18. Importance of development of MMP-2 inhibitors

MMPs have been identified as crucial biomolecular targets in connection with several disease states. As a result, research is currently being done to learn more about the mechanism of action on these MMPs during the past 40 years. There are a number of MMPIs that have been created and are now going through various stages of clinical testing. However, because of serious side effects, many substances either stopped working or were taken out of trial phases. Despite this, there are currently no medication candidates for these MMPs on the market. Although there is a pressing need to create target-specific and selective MMPIs, the structural similarity of the

various MMPs makes the task of devising strategies difficult and time-consuming. Therefore, efforts to discover new MMP-2 inhibitors in the field of medicinal chemistry are still ongoing. However, MMPs are an attractive target for drug discovery against a number of illness situations due to the diversity and distinctive characteristics of the S1' pocket and the catalytic Zn^{2+} ion. The key amino acid residues of the S1' pocket and zinc chelating capacity have thus been used to design a number of prospective and selective inhibitors. However, due to the higher hydrophobic character and higher zinc chelating activity of such compounds, obtaining specificity and druggability is a serious challenge. This could result in a wide range of inhibition and serious off-target negative consequences. Department of Pharm. Tech., Jadavpur University has been involved in the development of powerful and targeted MMP-2 inhibitors in recent years (Halder et al., 2013; Halder et al., 2015; Adhikari et al., 2016; Jha et al., 2017; Adhikari et al., 2017A; Adhikari et al., 2018; Mukherjee et al., 2017; Sanyal et al., 2019; Das et al., 2021).

However, it is also true that MMPIs are only taken into account when it comes to treating a variety of solid tumors, whereas their role in the invasion of hematological neoplastic diseases is mostly ignored. None of these MMPIs used in various stages of clinical investigations have been examined to date for the management of leukemia. Furthermore, research has looked at the relationship between MMPs and leukemia, where invasion is a crucial feature. Therefore, in this research work, I am focusing on developing potential and promising MMP-2 inhibitors, which may be selective over other MMPs, and may totally change the course of the development of anticancer as well as antileukemic agents.

1.19. MMP-2 and chronic myeloid leukemia

Although there is evidence suggesting gelatinases (MMP-2 and MMP-9) are a potential target for the therapy of CML, the biological role of gelatinases (MMP-2 and MMP-9) in CML is not fully understood. However, a study found that MMP-2 was present in only 3 of the 6 peripheral blood MNC samples taken from 6 CML patients, while MMP-9 was expressed in all 6 samples. Additionally, it was shown that murine FL5.12 cells transfected with the Bcr-Abl constructs expressed both gelatinases. The study also noted that the angiogenic factor VEGF increased the expression of MMP-9 in primary CML cells, contradicting the observation described in the case of CLL, albeit the mechanism by which VEGF increased MMP-9 expression by primary CML cells has not been identified (Ugarte-Berzal et al., 2010, Janowska-Wieczorek et al., 2002). Another study found an increasing amount of MMP-2 enzyme was much higher in CML patients during the measurement of the production of bone marrow mononuclear cells of

normal individuals and patients having CML (Ries et al., 1999). In addition to MMP-9, the study found that MMP-2 enzyme release was present in bone marrow mononuclear cells (BM-MNC) from a diversity of myeloid leukemia and preleukemia patients, but not in specimens from healthy people. Therefore, due to the presence of MMP-2 and MMP-9 in these samples, it is highly likely that the leukemic blast cell population released these enzymes. The absence of this enzyme in samples from healthy individuals supports the hypothesis that MMP-2 is generated by leukemic cells in bone marrow. MMP-2 transcripts were also found by RT-PCR in the BM-MNC fractions from healthy individuals and CML patients, even though zymography was unable to detect the enzyme's activity in these samples. This could be attributed to the fact that RT-PCR can only detect a small subset of the mRNA molecules produced by MMP-2-expressing cells, which are present in these BM-MNC fractions but may not necessarily secrete detectable levels of this enzyme (Ries et al., 1999). Another study found that the results indicate that MMP-2 and MMP-14 are not expressed in adult bone marrow mononuclear cells normally, but TIMP-2 is. In contrast, all bone marrow mononuclear cells from CML patients express TIMP-2, whereas 90% express MMP-2 and MMP-14 (Song et al., 2009). Given that the chronic phase in CML patients is in a self-balanced state in comparison to acute leukemia, TIMP-2 may be a factor in suppressing disease development; however, if the balance is lost, MMP-2 cannot be inhibited, and its excessive production causes disease progression (Huang et al., 2017). Therefore, MMP-2 inhibition might be a helpful therapeutic strategy for the treatment of diseases like CML.

1.20. Drug design and discovery

Drug discovery is a lengthy, expensive, risky, multi-step process that starts with target identification and is followed by validation, hit-to-lead production, lead optimization, preclinical research, and various stages of clinical trials. To transfer a novel medicine candidate from a basic research laboratory to the shelf of a chemist's shop, a journey of 10 to 15 years and an investment of more than a billion are needed (Tautermann, 2020; Hu et al., 2011; Gurung et al., 2021). High-throughput screening and combinatorial techniques were developed in the 1990s to expedite the synthesis and screening of huge libraries and decrease the times and costs associated with drug discovery. Unfortunately, there was little progress made in the creation of new chemical entities and no notable successes were reported (Baig et al., 2018). Later, improved computer tools, chemical synthesis, and biological research were combined to speed up the discovery process (Baig et al., 2018). Amazingly, the Fortune magazine cover story from 1981, headed "The next industrial revolution: developing pharmaceuticals by computer at

Merck," was released. Computer-aided drug discovery (CADD) has been showing signs of progress since 1981 (Brown et al., 2017). The previous ten years have seen the development of many impressive initiatives as well as the gratifying emergence of sophisticated computational approaches. All preclinical drug development stages can now be advanced using computational methods, including target selection and validation, lead finding and optimization, and preclinical tests (Anwar et al., 2021). A schematic representation of computer-aided drug discovery (CADD) workflows based on the available structural information, a structure- or ligand-based approach selected for drug design is depicted in **Figure 1.12**.

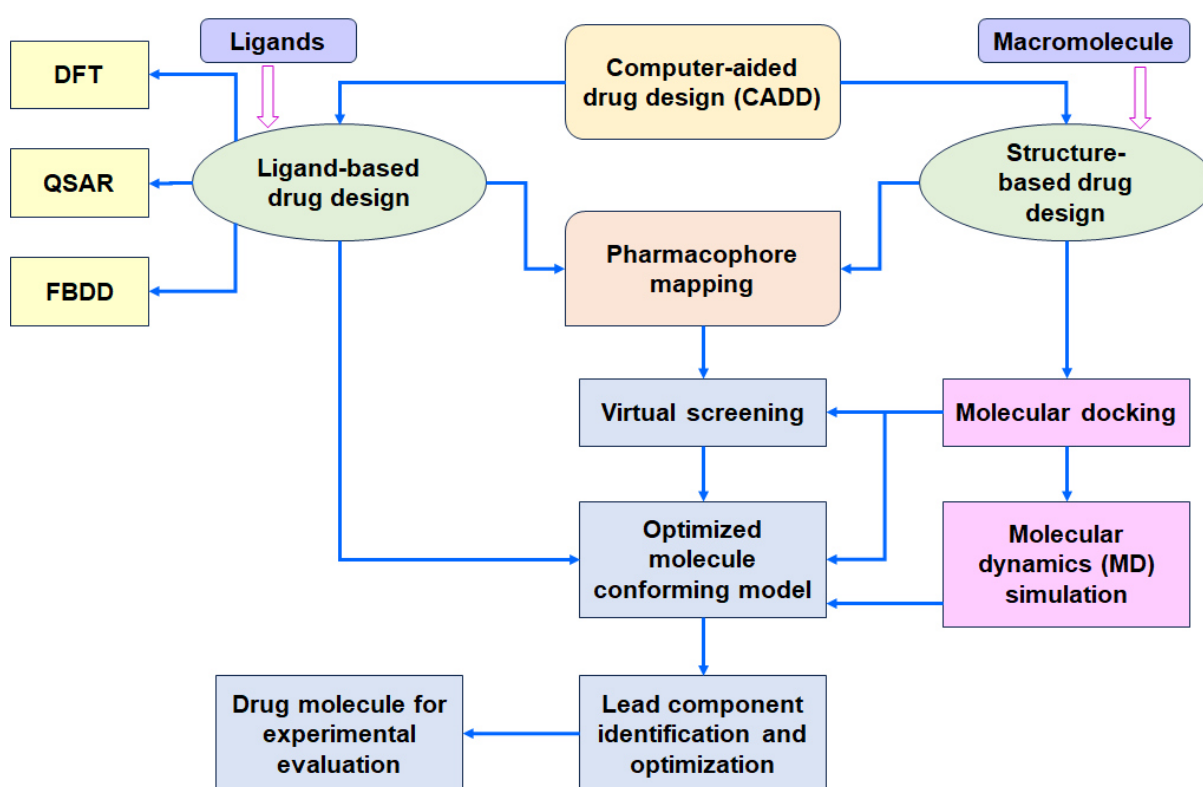


Figure 1.12. Schematic representation of computer-aided drug discovery (CADD) workflows, based on the available structural information, a structure- or ligand-based approach is selected for drug design. Following the successful discovery of lead compounds, a number of lead optimization cycles produce one or more drug-like molecules.

Structure-based drug design (SBDD) and ligand-based drug design (LBDD) are two primary categories for CADD. Drug target structural knowledge is a requirement for structure-based drug design (SBDD). Several computational methods, including homology modeling, molecular docking, and molecular dynamic (MD) simulation, were used by SBDD. Using these computational methods for SBDD, target molecules that may be enzymes linked to the disease

of interest are found and new, functionally active compounds may be developed (Baig et al., 2018).

Again the LBDD seeks to establish a generic method for evaluating how physicochemical and structural characteristics of substances or ligands affect their biological effects (Baig et al., 2018). In the case of LBDD, currently existing information on ligands and their biological functions is used to create new, successful therapeutic candidates (Baig et al., 2018). The LBDD is typically predicated on the idea that molecules with comparable structural traits interact with or inhibit molecules with similar biological characteristics (Baig et al., 2018). Quantitative structure-activity relationships (QSARs), pharmacophore modeling, and artificial intelligence (AI) are among the key methods employed in LBDD (Gurung et al., 2021).

1.20.1. Rational drug design

There are essentially two types of rational drug design:

- (i) Development of small compounds with desired properties for biomolecules (proteins or nucleic acids) with known 3D structures and functional roles in biological processes as targets. The pharmaceutical industry frequently uses this strategy in medication design, which is well-established.
- (ii) Development of small molecules with predefined properties for targets, whose cellular functions and their structural information may be known or unknown. Using cutting-edge computational technologies, it is possible to identify unknown targets (genes and proteins) by examining the global gene expression data of samples that have not been treated and that have been treated with a drug.

Both strategies (i) and (ii) for the development of small molecules must be examined after a target has been identified. In addition to the evaluation of binding scores (affinity/specificity), absorption, distribution, metabolism, and excretion (ADME), electrophilic, nucleophilic, and radical attack (biodegradation), toxicity of the parent small molecules, and products due to biotransformation in the various phases of metabolism, quantitative structure-activity relationship (QSAR), and quantitative structure-property relationship (QSPR) respectively (Mandal and Mandal, 2009). The majority of these processes, including designing a small molecule, might be initially carried out using computer methods. To learn more about gene expression patterns after the first assessment and identification of lead compounds, gene expression profiling, and bioinformatics analysis would be especially crucial. This knowledge can then be used to develop drugs that have desired properties like disease-free survival, disease

eradication, elimination or reduction of toxic side effects, reduction of undesirable biotransformation, improvement in distribution (bioavailability), defeating drug resistance, and enhancement of immune responses. In order to develop and discover new drugs, rational drug design would therefore be a key strategy (Mandal and Mandal, 2009).

1.20.1.1. Ligand-based drug design

When 3D structures of macromolecules are unavailable, drug discovery and lead compound optimization become difficult. In contrast to conventional procedures, which are considered to be time- and cost-effective, the development of computer-aided drug designing and high-throughput virtual screening has opened new possibilities for major therapeutic approaches in contemporary technology. This appears to be an issue that needs improvement everywhere. Due to this issue, the concept of ligand-based drug designing (LBDD) has shed light on the similarity principle, which states that molecules with comparable structural characteristics will have similar biological capabilities. These approaches were combined, which resulted in an increase in the complexity of the R&D process and an expansion of the chemical and biological data field (Ajjarapu et al., 2022).

1.20.1.1.1. Quantitative structure-activity relationship (QSAR) study

A data-driven approach, the modern pipeline for finding hit compounds is dependent on the biological activity data produced by high throughput screening (HTS) programs (Nantasenamat et al., 2015). The quantitative structure-activity relationship (QSAR) study is a ligand-based chemometric drug discovery technique that quantitatively shows a mathematical association between changes in chemical compound structures and corresponding changes in biological activities (Sharma and Bhatia, 2021). The potency, effectiveness, and selectivity of the lead compounds intended for clinical investigations are all enhanced by the QSAR approaches, which play important roles in the drug discovery process (Sharma and Bhatia, 2021). Moreover, due to its high and quick throughput and good hit rate from ligand-based virtual screening (LBVS) studies of huge databases of compounds, the QSAR analysis is a potent and cost-effective in-silico drug discovery approach (Neves et al., 2018). QSAR modeling is essential for minimizing the number of compounds that must be created and biologically assessed. However, QSAR models are helpful for lead optimization, hit-to-lead conversion, and hit discovery (Neves et al., 2018). It has been noted that QSAR techniques have dominated lead optimization in recent decades. Not only is QSAR modeling used in academia and/or industry, but it is also acknowledged on a global scale by regulatory bodies including the FDA, Health

Canada, and European Union (EU) authorities (Kar et al., 2020). Additionally, under the New Substances Provisions of the Canadian Environmental Protection Act, the regulatory body of Canada uses QSAR models to evaluate and prioritize the Canadian inventory of existing substances (i.e., domestic substances list, DSL, 1999). Also, the Danish Environmental Protection Agency (EPA), which is part of the EU, uses QSAR models to foretell the endpoint of ecological and health-risking compounds for which experimental results are not yet available (Kar et al., 2020).

1.20.1.1.1.1. Hansch equation and Free-Wilson analysis

The Hansch approach, which examines the structure-activity relationship in many biological systems, has gained widespread acceptance and recognition as a flexible method of comprehending drug action. This method makes the assumption that the electronic, hydrophobic, and steric components can be used to account for the physicochemical parameters influencing the transport and drug-receptor interaction. In general, one might assume that the corresponding changes in these physicochemical parameters determine the variations in biological activity brought on by structural alterations in congeneric medications. In *Equation 1.1* parameters for the factored physicochemical qualities, E, H, and S, respectively, sum up the assumption (Hansch and Fujita, 1964).

$$\Delta BA = f(\Delta E, \Delta H, \Delta S) \quad 1.1$$

$$BA = f(\Delta E, \Delta H, \Delta S) + \text{constant} \quad 1.2$$

The biological activity, BA, of a reference chemical, remains constant throughout a group of congeners. *Equation 1.2* therefore applies to every member of the series. The value of BA is typically assumed to be inversely proportional to the drug concentration C that produces a typical biological response, such as EC₅₀, IC₅₀, minimum inhibitory concentration (MIC), etc., on a molar basis. Practically speaking, the parameters relating to free energy are employed, such as log 1/C for BA, π or log P for ΔH , σ , σ^* , σ' , or $\Delta \log K_A$ for ΔE and E_8 or E_8^C for ΔS . π is the hydrophobic substituent constant derived from the partition coefficient, P, which is usually determined with the use of a 1-octanol/water system, σ is the Hammett constant, σ' is an electronic parameter for radical reactions, σ^* and E_8 are the Taft's polar and steric constants for aliphatic systems, and E_8^C is the Hancock corrected steric constant.

$$\log 1/C = -a (\log P)^2 + b \log P + \rho \sigma + \delta E_8 + c \quad 1.3$$

The formula for the most popular equation in this method is *Equation 1.3*, where $a(\geq 0)$, b , ρ , δ , and c are constants that are determined by the least-squares analysis (Hansch and Fujita, 1964).

The Free Wilson model is a quick and effective way to describe structure-activity correlations quantitatively. In contrast to Hansch analysis, which correlates physicochemical attributes with biological activity values, it is the only numerical method that directly links structural features with biological properties. However, both approaches have a close relationship with one another, both theoretically and in terms of how they might be used in real-world situations. Both models can frequently be used to create a mixed approach that uses physicochemical characteristics to characterize the impact of various substituents on the biological activity (*Equation 1.4*) and Free Wilson-type variables to describe the activity contributions of specific structural alterations. This combination model is the most potent tool of conventional QSAR, as shown by numerous successful applications, especially from the work of Hansch and his team on the structure-activity correlations of enzyme inhibitors (Kubinyi, 1988).

$$BA = \sum a_i + \mu \quad 1.4$$

BA represents the biological activity values (on a linear scale) where a_i are the activity contributions of the substituents X_i which refer to the overall mean of the biological activity values, μ .

Both models can frequently be used to create a mixed approach that uses physicochemical parameters to characterize the impact of various substituents on the biological activity and Free Wilson-type variables to describe the activity contributions of specific structural alterations. This combination model is the most potent tool of conventional QSAR, as shown by numerous successful applications, especially from the work of Hansch and his team on the structure-activity correlations of enzyme inhibitors (Kubinyi, 1988).

1.20.1.1.1.2. Significance of QSAR study

QSARs are concerned with creating and developing prediction models that connect chemical bioactivity with characteristics or descriptors that are indicative of molecular structure (Amin and Gayen, 2016). Similar analogs with minute differences in their chemical structures may exhibit varying levels of a specific biological activity or may generate radically different forms of biological potential. The QSAR model's goal is to quantitatively comprehend how changes in biological activity and their corresponding molecular structures are related (Roy et al., 2009; Cherkasov et al., 2014). Nevertheless, the association between biological activity and the structural and physicochemical characteristics of substances is investigated using statistical

approaches as a preliminary tool in the QSAR research (Amin et al., 2016). Several regressions and classification-based methods are available to produce QSAR equations. Different diagnostic statistics are used to determine the accuracy and predictability of generated QSAR models. One may be able to forecast the biological activities of novel compounds using the QSAR equations that have been developed (Cherkasov et al., 2014).

1.20.1.1.1.3. Different types of QSAR study

There are three approaches to characterize the QSAR methodologies: by the number of targets, by the chemometric methods, and by the dimension of descriptors (**Figure 1.13**).

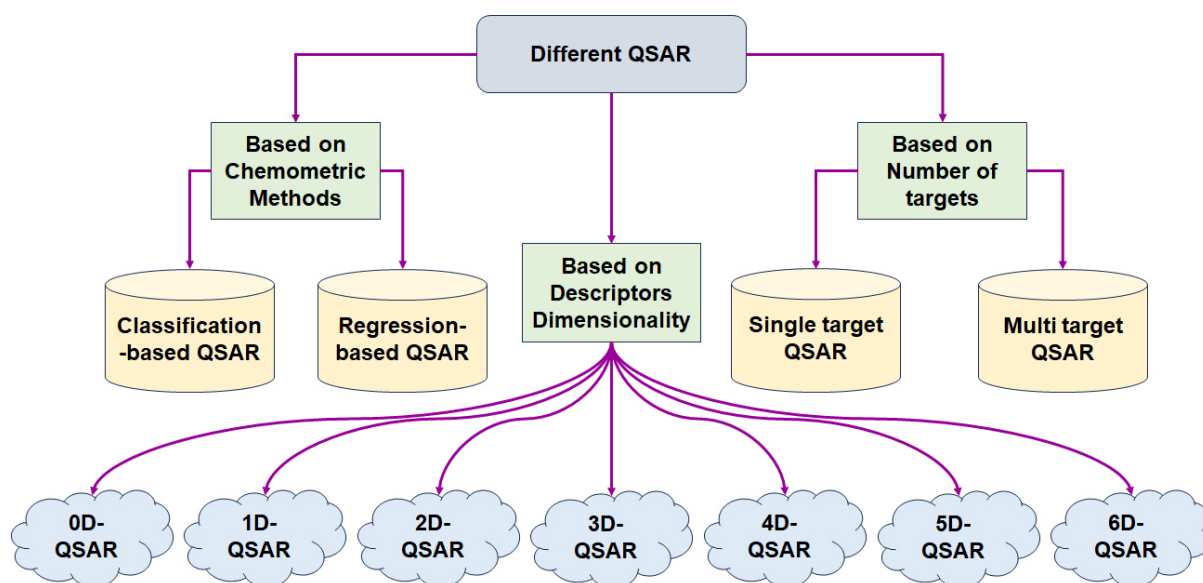


Figure 1.13. Schematic representation of different types of QSAR techniques.

The chemical information that represents the behavior of the substance is encoded by molecular descriptors in QSAR analysis. The appropriate algorithm is utilized to calculate the descriptors in numerical form, and they are then employed as the independent variables for the construction of QSAR models (Roy and Das, 2014). In contrast, the dimension of an object can be defined as the smallest set of coordinates necessary to explain a point within it. Dimension is an inherent quality that is independent of an object's space (Crilly and Johnson, 1999). Therefore, a higher level of structural information is acquired when dimensions are added to descriptors in QSAR analysis. The QSAR approach uses the dimension as a constraint to control how the analysis is conducted. The complexity of the modeling technique is correlated with the dimensional increment of descriptors used in building QSAR models. A descriptor's dimension corresponds to the compound's dimension, which specifically describes that molecular property. As a result, the dimension of the computed descriptors, which is used to create the

QSAR model, includes the dimension of the QSAR analysis (Roy and Das, 2014). According to the number of dimensions in the descriptors, there are six different types of QSAR methodologies: zero-dimensional (0D), one-dimensional (1D), two-dimensional (2D), three-dimensional (3D), four-dimensional (4D), five-dimensional (5D), and six-dimensional (6D). The 0D-QSAR model is built using descriptors derived from knowledge of molecules, including molecular weight, atom counts and kinds, and the sum of atomic attributes. The 1D-QSAR model correlates the activity or attribute with the overall parameters of the molecules, such as the pKa, solubility, hydrophobic parameter, and functional groups (Todeschini and Consonni, 2009). The 2D-QSAR model also reveals a correlation between activity and structural ornamentation. The fundamental predictor variables utilized for 2D-QSAR model generation are the descriptors derived from the topological portrayal of a molecule. Different topological indices that take into account the internal atomic arrangement of molecules are employed as 2D descriptors for the creation of successful QSAR models (Roy and Das, 2014). Topological parameters encode information about the amount of heteroatoms, numerous bonds, and molecular size, shape, and branching. These 2D descriptors play an important role in describing a variety of biological outcomes as well as the physicochemical properties of molecules. The mathematical symbol for a molecular graph, which depicts the topology of a chemical compound is $G = (V, E)$ where V is a collection of vertices that represent the compound's atoms and E is a collection of elements that correspond to the binary associations between pairs of vertices. These molecular diagrams show the chemical structure in a non-numeric way. Chemical graphs must be numerically transformed. Topological indices are calculated using specific algorithms (Danishuddin and Khan 2016). Additionally, there are many other topological descriptors, such as the connection indices, Wiener index, Kier shape, Zagreb indices, and Balaban J index are the most often used topological indices. Furthermore, connectivity indices are the most successful descriptors in QSAR investigations (Danishuddin and Khan 2016). Other physicochemical characteristics of molecules are also regarded as an essential component of the 2D-QSAR study, in addition to topological descriptors. The hydrophobic, electronic, and steric characteristics are the three main groups of physicochemical descriptors that are frequently utilized in 2D-QSAR modeling. These physicochemical characteristics can be determined experimentally or even computed from the compound's structure without taking conformational analysis or energy minimization into account. Numerous physicochemical characteristics of the substance, such as the acid dissociation constant (pKa), partition coefficient (logP), molar refractivity (MR), spectroscopic signals, rate constants, etc may be used to describe the entire molecule or may highlight certain molecular

components. Other structural features that can be directly computed from the molecular structure or formula are also included in the 2D-QSAR analysis. These include the molecular weight (MW), the number of hydrogen bond donors (nHBD), the number of hydrogen bond acceptors (nHBA), and the number of various additional atoms, fragments, and links (Roy and Das, 2014). On the other hand, the 3D-QSAR approach visualizes the molecular organization in 3D space and links the activity or characteristic to the molecules' steric and electrostatic non-covalent interaction fields (Tosco and Balle, 2011; Cramer, 2011; Cramer, 2012). In a similar fashion to the 3D-QSAR study, the 4D-QSAR analysis extends the number of ligand configurations by labeling each chemical in a variety of conformations, stereoisomers, orientations, tautomers, or protonation states. The numerous induced-fit models in the 4D-QSAR study, however, are perfectly designated by 5D-QSAR analysis. Once more, the 6D-QSAR approach includes a variety of solvation models in the 5D-QSAR study (Scior et al., 2012).

QSAR assessments can be divided into linear and non-linear categories depending on the type of chemometric techniques used. In the case of linear approaches, these include partial least-square (PLS), principal component analysis (PCA), stepwise multiple linear regression (S-MLR), multiple linear regression (MLR), linear regression (LR), and genetic function approximation (GFA) (GFA) (Fisher, 1980). Yet again, more recent developments in chemometrics have led to a variety of fresh methods for building predictive models that include nonlinear and algorithmic methodologies like support vector machines (SVM) (Nantasenamat et al., 2008; Nantasenamat et al., 2013), artificial neural networks (ANN) (Nantasenamat et al., 2013; Worachartcheewan et al., 2009), k-nearest neighbors (kNN) (Ajmani et al., 2006), and Bayesian neural nets (Klon et al., 2006). The classification of QSAR as single-target or multi-target depends on the number of dependent variables, such as the number of biological targets (**Figure 1.13**). Recent studies have demonstrated the potency of multi-target pharmacological molecules in treating conditions like Alzheimer's disease (AD), cancer, diabetes, malaria, and tuberculosis. This work demonstrates that multi-target drug development strategy is a current study topic in the field of drug discovery (Ling et al., 2020; Benek et al., 2020; Makhoba et al., 2020).

1.20.1.1.1.4. Software/tool used for QSAR study

Various QSAR modeling software and tools have been released during the past 20 years, including commercial, non-commercial, and open-source versions. **Table 1.4** provides a summary of some of these significant programs and technologies.

Table 1.4. A list of various applications and web services, both paid and free, for QSAR studies.

<i>Sl No</i>	<i>Software</i>	<i>Description</i>	<i>Paid/Free</i>
1	cQSAR	A database of regression-based QSAR models having more than 21,000 QSAR equations relating bio-chemical and physic-chemical activities to molecular descriptors.	Paid
2	QSARPro	QSAR software for calculation of molecular descriptors QSAR model building (linear or non-linear regression) and also used for predicting the activities of the test or new set of molecules. It offers another patent pending QSAR technique named group-based QSAR (GQSAR). Works on Linux and Windows.	Paid
3	MedChem Studio (Formerly ClassPharmer)	Used for QSAR model building and ADMET property prediction.	Paid
4	Codessa	Procures molecular descriptors using quantum mechanical results from AMPAC which are then used to develop QSAR/QSPR models.	Paid
5	OpenMolGRID	Grid-enabled QSAR approach for modeling large and complex datasets.	Paid
6	CODESSA Pro	Program for calculating descriptors, developing multi-linear and non-linear QSAR/QSPR models, and interpreting the developed model.	Paid
7	MCASE	Machine learning-based QSAR software for modeling and predicting toxicities of chemicals.	Paid
8	smirep	SAR/QSAR tool for predicting the structural activity of chemical compounds. It works on the Linux platform.	Free
9	AutoWeka	Automated data mining software for QSAR.	Free
10	DTC Lab tools	2D QSAR tools.	Free
11	MOLE db	Online molecular descriptors database comprised of 1124 molecular descriptors which are calculated for 234773 molecules.	Free
12	Datasets of Milano Chemometrics and QSAR Research Group	Reference data sets.	Free
13	OCHEM Database	Online database of experimental measurements of chemical and biological data integrated with a modeling environment. Users can submit experimental data or use the data uploaded by other users to build predictive QSAR models.	Free
14	ChemSAR	Web-based pipeline platform for classification-based models of small molecules. It includes standardization and validation of molecules, calculation of descriptors (1D, 2D, and FP), feature selection, model building, and interpretation.	Free
15	Chembench	Chembench provides robust model building, property and activity predictions, and virtual libraries of available compounds with predicted biological activities and drug-like properties. It also provides special tools for designing chemical libraries.	Free
16	Partial Least Squares Regression (PLSR)	Construct QSAR/QSPR models and predict activity/property using the Partial Least Squares (PLS) regression technique.	Free

1.20.1.2. Structure-based drug design

When the target structure is known, structure-based drug discovery is crucial. The key methods for structure-based drug discovery include molecular dynamics (MD) simulations and molecular docking studies.

1.20.1.2.1. Molecular docking study

Drug and target protein interactions resemble a secure connection in which each party tries to accommodate the other to some extent. One of the effective methods for comprehending

protein-ligand interactions is molecular docking (Kalyaanamoorthy and Chen, 2011). Currently, molecular docking study is used often in many stages of the drug design process (Tripathi and Bankaitis, 2017). In order to evaluate binding interaction poses, a potential ligand, a target of interest, and a technique are usually needed in protein-ligand docking.

In a molecular docking study, the proposed ligand could be a small molecule, DNA, peptide, or perhaps even a protein. The main repository for protein structures that may be retrieved for molecular docking study is the RSCB Protein Data Bank (PDB) (<https://www.rcsb.org/>; Burley et al., 2018). There are currently more than 62,000 entries for protein-ligand complexes in the RSCB Protein Data Bank, of which 60,000 were resolved using X-ray techniques and 1,700 using NMR techniques. There are numerous open-source and commercial molecular docking methods that can compute binding energies and predict protein-ligand poses. **Table 1.5** displays a collection of protein-ligand docking software/tools.

Table 1.5. List of various protein-ligand docking software/tools

<i>Sl No</i>	<i>Software/tools</i>	<i>Method</i>	<i>Types</i>	<i>Source^a</i>
1	3D-Dock Suite	Fourier correlation algorithm, self-consistent mean field optimization procedure, single distance constraint empirically derived pair potential	PLI	http://www.sbg.bio.ic.ac.uk/docking/index.html
2	ArgusLab	Genetic algorithm and ArgusDock	PLI	http://www.arguslab.com
3	AutoDock	Lamarckian genetic algorithm	PLI	http://autodock.scripps.edu/
4	BiGGER	Soft-docking	PLI	http://www.cqfb.fct.u.nl.pt/
5	ClusPro	10 most populated low energy clusters, irmsd > 9 Å	automatic docking web servers	https://cluspro.org/
6	Dock Vision	Hybrid evolutionary algorithm	PLI	http://dockvision.com/
7	DOT	Fast Fourier transforms	PLI	http://www.sdsc.edu/CCMS/DOT/
8	FlexX	Sequential importance sampling (SIS)-algorithm	PLI	http://www.biosolveit.de/FlexX/
9	FRED	Directed docking with SMiles ARbitrary target specification (SMARTS) patterns	PLI	http://www.eyesopen.com/fred
10	Gold	Genetic algorithm	PLI	http://www.ccdc.cam.ac.uk/
11	GRAMM-X	Up to 300 lowest energy conformations	automatic docking web servers	http://vakser.compbio.ku.edu/resources/gramm/grammx/
12	HADDOCK	Fully flexible for interacting residues of peptide and protein	automatic docking web servers	https://wenmr.science.uu.nl/haddock2.4/

13	HADDOCK	Uses ambiguous interaction restraints of NMR	PLI	http://www.nmr.chem.uu.nl/haddock/
14	HDOCK	Top 100 lowest energy clusters, lmrstd > 5 Å	automatic docking web servers	http://hdock.phys.hust.edu.cn/
15	Hex	Similar to conventional fast Fourier transform (FFT)	PLI	http://www.loria.fr/ritchied/hex/
16	InterPred	No conformational search (template-based)	automatic docking web servers	http://bioinfo.ifm.liu.se/inter/interpred/
17	LZerD	Up to 50,000 generated geometries	automatic docking web servers	https://lzerd.kiharalab.org/
18	MDockPP	Up to 3000 generated geometries; clustering cutoff adjustable	automatic docking web servers	https://zougrouptoolkit.missouri.edu/MDockPP/
19	PatchDock	Up to 100 top-ranking candidates; clustering cutoff adjustable	automatic docking web servers	http://bioinfo3d.cs.tau.ac.il/PatchDock/
20	pyDockWEB	Top 100 lowest energy conformations	automatic docking web servers	http://life.bsc.es/servlet/pydock
21	rDock	Weighted sum of intermolecular, ligand intramolecular, site intramolecular, and external restraint terms	PLI	http://www.ysbl.york.ac.uk/rDock
22	RosettaDock	1000 decoys can be downloaded	automatic docking web servers	http://rosettadock.graylab.jhu.edu
23	Surflex-Dock	Hammerhead docking system	PLI	http://www.tripos.com/
24	ZDOCK	Top 10 lowest energy conformations; possibility to retrieve top 500	automatic docking web servers	https://zdock.umassmed.edu/

^aas accessed in 30th April, 2023; PLI, protein-ligand interactions

Protein-ligand docking has been effectively applied in numerous real-world scenarios since its debut fifty years ago, including the subsequent approval of new drugs created with the help of structure-based drug design. These novel drugs include ion channel blockers, receptor antagonists and agonists, and enzyme inhibitors. As the practical applications of molecular models grow as a result of the quality enhancement in computational power, the field is quickly evolving with approximations that offer a better balance between accuracy and computing cost.

Investigating protein-protein interaction (PPI) networks is necessary for pathophysiology understanding and drug discovery (Andreani and Guerois, 2014; Ohue et al., 2013; Ohue et al., 2014; Shin et al., 2017; Vakser, 2014). As a result, the protein-protein docking problem is one of the trendiest subjects in computational biophysics and structural biology. In general, it is more difficult to estimate the 3D structure of a protein-protein complex than it is to do so for a single protein. Effective

computational algorithms to predict protein interactions are crucial as more and more protein structures, particularly in light of structural genomics, are known. A structural foundation for drug development is provided by docking study, which also provides resources for basic research on protein interactions. Protein-protein docking can be used to deduce the structure of a complex from the individual protein structures. Steric and physicochemical complementarity at the protein-protein interaction is the foundation of docking technology. **Table 1.6** provides a selection of protein-peptide and protein-protein docking software/tools.

Table 1.6. List of different protein-peptide and protein-protein docking software/tools.

<i>Sl No</i>	<i>Software/tools</i>	<i>Method</i>	<i>Source^a</i>
1	ClusPro PeptiDock	Fast Fourier Transform (FFT)-based docking method, Clustering by structure scoring and CAPRI peptide docking criteria	https://peptidock.cluspro.org/
2	DOCK	Geometric matching algorithm	http://dock.compbio.ucsf.edu/
3	DynaDock	Combined Optimized Potential Molecular dynamics (OPMD) with a soft-core potential	Not available to the public
4	GalaxyPepDock	Use similarity search (known template structures) as scaffolds for prediction	http://galaxy.seoklab.org/pepdock
5	GRAMM	Empirical approach	http://vakser.bioinformatics.ku.edu/main/resources_gramm.php
6	HPEPDOCK	Ensemble peptide conformation by MODPEP	http://huanglab.phys.hust.edu.cn/hpepdock/
7	ICM-Docking	Flexible docking	http://www.molsoft.com/docking.html
8	PBRpredict-Suite	Integrated six machine learning algorithms (model stacking)	http://cs.uno.edu/~{ }tamjid/Software/PBRpredict/pbrpredict-suite.zip
9	pepATTRACT	Rigid-body peptide docking within the binding pocket	http://bioserv.rpbs.univ-parisdiderot.fr/services/pepATTRACT/
10	PepComposer	Motif similarity search to defined binding interfaces from monomeric protein databases PepX (http://pepx.switchlab.org)	https://cassandra.med.uniroma1.it/pepcomposer/webserver/pepcomposer.php
11	PepCrawler	Rapidly exploring Random Tree (RRT) algorithm	http://bioinfo3d.cs.tau.ac.il/PepCrawler
12	PepSite 2.0	Coarse-grained peptide orientation by spatial position-specific scoring matrix (S-PSSM)	http://pepsite2.russelllab.org
13	Rosetta FlexPepDock	Rosetta energy function-based clustering and scoring	http://flexpepdock.furmanlab.cs.huji.ac.il
14	Situs	Correlation-based rigid body docking and density filtering, ARD	http://situs.biomachina.org/index.html
15	SPRINT-Str	Use SVM with optimized parameters	http://sparks-lab.org/server/SPRINT-Str

^aas accessed on 30th April 2023

Additionally, molecular docking study consists mostly of two stages: sampling and scoring functions. Furthermore, the sampling procedure successfully searches the conformational space depicted by the free energy landscape. Also, the scoring function, on the other hand, assigns a score to each expected pose from the free energy landscape (Huang and Zou, 2010; Abagyan and Totrov, 2001; Kitchen et al., 2004). It may be said that the scoring function makes it possible to link the native bound conformation to the energy hypersurface's global minimum.

1.20.1.2.2. Molecular dynamics simulation study

Many drug development processes, from hit identification to lead optimization and beyond, now use molecular dynamics (MD) simulations as their primary tool (Parrill and Reddy, 1999; Sussman and Silman, 2020). MD simulations have a considerable impact on molecular biology as well as medication discovery. By retaining the movements of macromolecules in their complete atomic detail while keeping a good temporal resolution, it analyses the time-resolved motion of proteins and other biomolecules. An intuitive and quick understanding of dynamics and function is made possible by the visualization of MD trajectories (Hollingsworth and Dror, 2018). It can produce a wealth of data on interactions between proteins and ligands as well as dynamic structural data on biomacromolecules (Adcock and McCammon et al., 2006). This information is essential for determining the target's structure-function relationship, understanding the basics of protein-ligand interactions, and guiding drug development and design strategies.

Because of this, MD simulations have been widely and dependably utilized throughout all phases of modern drug discovery research (Liu et al., 2018). It also forecasts how each molecule in a protein or other molecular system would move over time based on a broad model of the physics governing interatomic interactions (Karplus and McCammon, 2002). These simulations are capable of simulating a variety of important biomolecular events, including protein folding, conformational change, and ligand binding. It can show all atoms' locations with femtosecond temporal resolution (Hildebrand et al., 2019). Additionally, these simulations could predict how biomolecules will react to changes like mutation, phosphorylation, protonation, or the atomic-scale addition or removal of a ligand (Hollingsworth and Dror, 2018).

1.20.1.3. Advanced approaches

Due to the crystal-specific packing of ligand-receptor complexes, structure-based pharmacophore models created from a single 3D coordinate set collected from X-ray structures

may or may not incorporate a number of properties. Multiple crystal structures of active ligand complexes can be used for the same function as a solution to this issue. Every ligand-ligand interaction is identified and connected to a more precise pharmacophore theory. This approach is nonetheless restricted to ligand-target complexes for which several crystal structures are known, and each ligand must have a unique binding mechanism. Another method to produce a number of precise sets of atomic coordinates without being constrained by the availability of numerous experimental structures is to run molecular dynamics (MD) simulations of the system under study. For pharmacophore modeling and pharmacophore-based virtual screening, the enormous amount of data gathered can be applied in numerous ways:

(i) Methods combining the concept of a 3D pharmacophore with molecular docking and MD simulations

The docking approach analyses the effects of protein mutations on ligand binding by supplying mutational cues that support the robust survival of drug-resistant infections. It also offers novel mechanistic insights into protein-ligand binding mechanisms. The discipline is developing quickly as ongoing advances in computing power broaden the useful applications of molecular models, providing a better balance between accuracy and computational expense. Future work will definitely result in many more interesting applications (Wieder et al., 2017).

(ii) Integrated pharmacophore and docking-based virtual screening

The pharmacophore model (query) is utilized in this search as a characteristic of the pharmacophore model since it is used to filter and get the initial set of hits from a huge database. One can either obtain molecules with characteristics that are similar to those of the pharmacophore or entirely distinct scaffolds. Then, hits are gathered from molecules that have received higher scores and better fit for the pharmacophore model. Additional research using various modeling techniques is necessary in this case. For example, the highest-scoring perfect match compounds found in a pharmacophore-based screen can be docked into the putative binding pocket of a specific target of interest to reduce the number of active hits. This approach is also called docking-based virtual screening. Therefore, the combination of pharmacophore and docking-based virtual screening followed by MD simulation has proven to be a powerful approach to incorporating all available information into computational hit identification (Molla et al., 2023).

Chapter 2

LITERATURE REVIEW

2.1. Literature Search

MMPs, which are Zn^{2+} and Ca^{2+} dependent endopeptidases, aid in the breakdown of the basement membrane's gelatin, elastin, fibronectin, collagen, and laminin as well as the extracellular matrix (Agrawal and Pulendran 2004; Murphy et al., 1991; Nagase and Woessner 1999; Page-McCaw et al., 2007). MMPs have been revealed to be essential for a number of vital physiological processes, such as angiogenesis, tissue remodeling, wound healing, and embryo development (Nelson et al., 2000; Skiles et al., 2004; Whittaker et al., 1999). MMP-2, also known as gelatinase A, is one of the MMPs that has been linked to a number of diseases, including cancer, angiogenesis, cardiovascular disease, neurodegenerative disease, aortic aneurysms, obesity, asthma, sepsis, kidney disease, inflammatory bowel disease, rheumatoid arthritis, viral infections, and liver fibrosis (Baidya et al., 2022).

A number of studies have been conducted for the finding of potent and selective MMP-2 inhibitors for the management of those diseases. However, in this work, a drastic search for potential MMP-2 inhibitors for the management of cancer has been carried out. Furthermore, the Department of Pharmaceutical Technology at Jadavpur University in Kolkata, India, has been working on developing glutamate-based small-molecule anticancer drugs over the past decades. Target identification, however, is the most important step in drug design strategies because it pinpoints the specific mechanism by which a molecule inhibits a specific enzyme. Therefore, it is essential but difficult to develop such glutamate-based hydroxamate derivatives as anticancer agents with target selectivity and higher efficacy.

2.2. Matrix metalloproteinases-2 (MMP-2): A medically important target

MMP-2, a member of the gelatinase subfamily and one of the most lucrative targets for cancer, has been found among the 26 subtypes of MMPs, whereas MMP-9 has been linked to an antitarget in advanced stages of cancer (Fabre et al., 2013; Fabre et al., 2014; Overall and Kleinfeld, 2006; Serra et al., 2012; Zapico et al., 2015). Besides that, other studies using MMP-2 knockout mice have shown that MMP-2 is connected to the development of cancer in humans. Additionally, MMP-2 is essential for angiogenesis and neovascularization (Cathcart et al., 2015, Kessenbrock et al., 2011). Additionally, MMP-2 overexpression has been linked to the development of a variety of cancers (Chien et al., 2013; Herszényi et al., 2012; Liu et al. 2006). Therefore, it is vital to develop an MMP-2 inhibitor that is efficacious and selective compared to other MMPs, particularly MMP-9. MMPIs have been investigated in significant areas of medication development and research due to their involvement in a variety of

significant medical disorders. Several MMPIs (Table 1.3, *Chapter 1*) were introduced into various stages of clinical trials (Section 1.15) but were not successful because of serious side effects or unsatisfactory pharmacokinetics efficacy. The main factor hindering MMP selective drug discovery methods may be the lack of selectivity or rather the broad spectrum of inhibition of MMPIs. However, a number of MMPIs have previously been examined, and this process is ongoing because achieving target specificity for a given MMP is crucial for the development of novel, potent therapeutic candidates for treating a variety of medical conditions. Here, in this review, various MMP-2 inhibitors are presented for creating new MMP-2 inhibitors.

2.3. MMP-2 inhibitors based on different ZBGs

Zinc binding groups (ZBGs), which are important for MMP inhibition, may control the process by which the substrate is cleaved by MMPs by interfering with the catalytic Zn^{2+} ion (Hangauer et al., 1984; Lovejoy et al., 1999; Matthews, 1988). A charge transfer mechanism from a conserved glutamic acid residue and the scissile bond amide nitrogen atom results in the cleavage of peptide when a water molecule coordinates to the Zn^{2+} ion during attachment to the substrate (Lovejoy et al., 1999; Matthews, 1988; Skiles et al., 2001). Therefore, enzyme activation may not occur until and unless the zinc-bound water molecule is not displaced by the ZBGs (Rao, 2005). Additionally, ZBGs coordinate the exact binding pockets by directing the associated inhibitor's backbone structure. ZBGs are essential for creating strong and targeted MMPIs. With the enzyme, ZBGs' oxygen, nitrogen, and sulfur atoms can form monodentate, bidentate, and tridentate chelates. These ZBGs' atomic constituents exhibit a wide range of diversity and affinity for the catalytic Zn^{2+} ion. However, the binding pattern of MMPIs may be significantly influenced by the structural orientation of ZBGs and the corresponding backbone structure. The structures of the MMP-2 inhibitors contain a wide range of ZBGs, including hydroxamic acids, carboxylic acids and related esters, thiols, mercaptosulfides, phosphonates, carbamoylphosphonates, nitrogen-based ZBGs, heterocyclic ZBGs, etc (Baidya et al., 2022). It is interesting to note that, hydroxamate groups, the ZBG, produce trigonal-bipyramidal geometry to attach to the catalytic Zn^{2+} ion. Furthermore, the hydrophobic contacts of MMPIs created a stable enzyme-inhibitor complex with broad-spectrum inhibition, and the amide group developed a possible hydrogen bonding interaction with the adjacent functional groups of amino acids of MMP enzymes (Verma, 2012).

2.4. Hydroxamic acid-based MMP-2 inhibitors

Through coordination with a number of metal ions, including Zn^{2+} , hydroxamate has been shown to produce strong bidentate chelates. It is one of the efficient ZBGs that can interact with the Zn^{2+} ion and nearby amino acid residues in the MMP active site via hydrogen bonds. With the residues of alanine and glutamic acid, respectively, the amino and hydroxyl groups of the hydroxamate moiety create hydrogen bonds (Rao, 2005). Hydroxamate may make it more difficult to develop selective MMPs because of its strong zinc chelating activity and causes undesirable adverse effects against unintended MMPs (Georgiadis and Yiotakis, 2008; Overall and Kleifeld, 2006; Rao, 2005). However, one of the factors contributing to the MMPs' greater activity is the existence of the hydroxamate moiety.

A number of α gem-disubstituted succinimide hydroxamates have been reported by Abbott Laboratory researchers as potential broad-spectrum MMPs (Curtin et al., 1998). Most of these molecules exhibited robust and specific MMP-2 inhibition over MMP-1 and -3. Compound 1 (**Figure 2.1**) produced around 4-fold and 74-fold MMP-2 selectivity over MMP-1 and -3, respectively, and was a highly powerful MMP-2 inhibitor ($\text{IC}_{50} = 2.3 \text{ nM}$).

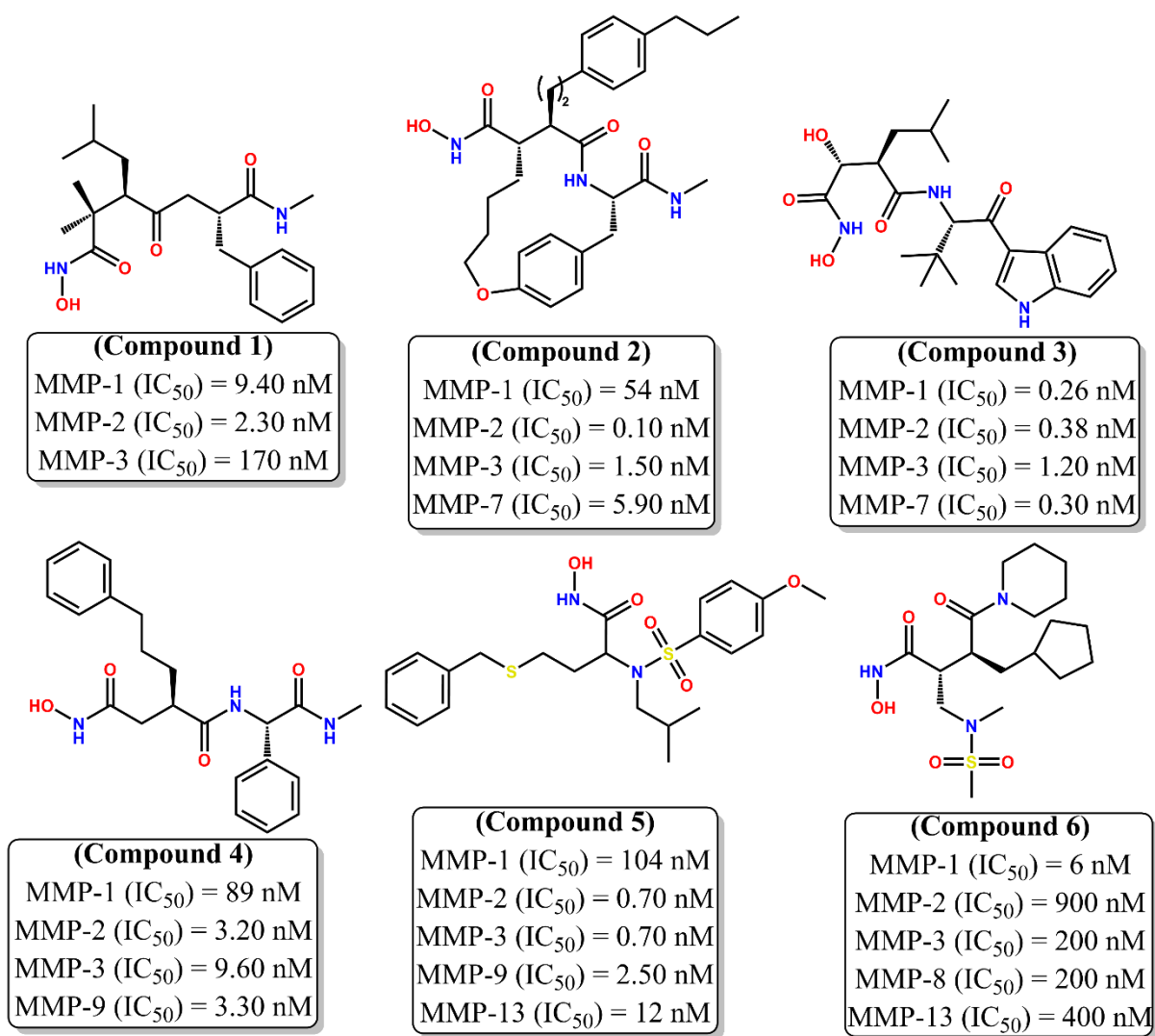


Figure 2.1. Hydroxamate-based MMP-2 inhibitors (Compounds 1-6).

Likewise, the Abbott researchers developed a number of potent macrocyclic rings containing succinimide hydroxamates (Steinman et al., 1998). Compound 2 (**Figure 2.1**) showed a minimum 15-fold selectivity over MMP-1, -3, and -7 while exhibiting significant MMP-2 inhibition (IC_{50} = 0.1 nM). Another study described a series of succinyl hydroxamate MMPIs that substituted C-terminal amino acid amides with an arylaminoketone moiety (Sheppard et al., 1998). Many of these molecules were powerful broad-spectrum MMPIs but lacked selectivity. A highly effective but nonselective broad-spectrum inhibitor, compound 3 (**Figure 2.1**) had IC_{50} values for MMP-1, MMP-2, MMP-3, and MMP-7 of 0.26 nM, 0.38 nM, 1.20 nM, and 0.30 nM, respectively. When compared to marimastat (**Figure 1.16**, Chapter 1), compound 3 had high oral bioavailability at a dose of 10 mg/kg. Again, a series of promising hydroxamates-based MMPIs had been reported by researchers of Kanebo Limited (Yamamoto et al., 1998). Compound 4 produced a minimum of 2.5-fold selectivity over MMP-1 and -3

but produced robust but nonselective gelatinase inhibition (**Figure 2.1**). It has been reported that a group of acyclic sulfonamide-based hydroxamates are highly potent MMPs that selectively inhibit MMP-9 rather than MMP-1, -2, -3, and -13 (Hanessian et al., 1999). Moreover, the selectivity of compound 5 over MMP-9 and -13 was 3.5-fold and 17-fold, respectively, with higher MMP-2 inhibition ($IC_{50} = 0.70$ nM) (**Figure 2.1**). Some sulfonamide-based hydroxamates have been reported by British Biotech researchers as powerful MMPs (Martin et al., 1999). A minimum 33-fold selectivity over other MMPs, such as MMP-2 ($IC_{50} = 900$ nM), was maintained by compound 6 (**Figure 2.1**), which exhibited effective MMP-1 inhibition. In comparison to marimastat (**Figure 1.16, Chapter 1**), compound 6 had higher oral bioavailability in rats ($C_{max} = 171.8$ ng/mL after 30 min, $AUC = 662$ ng/mL.hr). Furthermore, a number of arylsulfonamido thiazine and thiazepine-based hydroxamates have been identified by Procter & Gamble Pharmaceuticals researchers as powerful and broad-spectrum MMPs (Almstead et al., 1999). The majority of compounds were potent, broad-spectrum MMPs. A minimum of 2.3-fold selectivity over other MMPs was maintained by compound 7 (**Figure 2.2**), which produced potent MMP-2 inhibition ($IC_{50} = 1$ nM) over other MMPs (such as MMP-1, -2, -3 and -13).

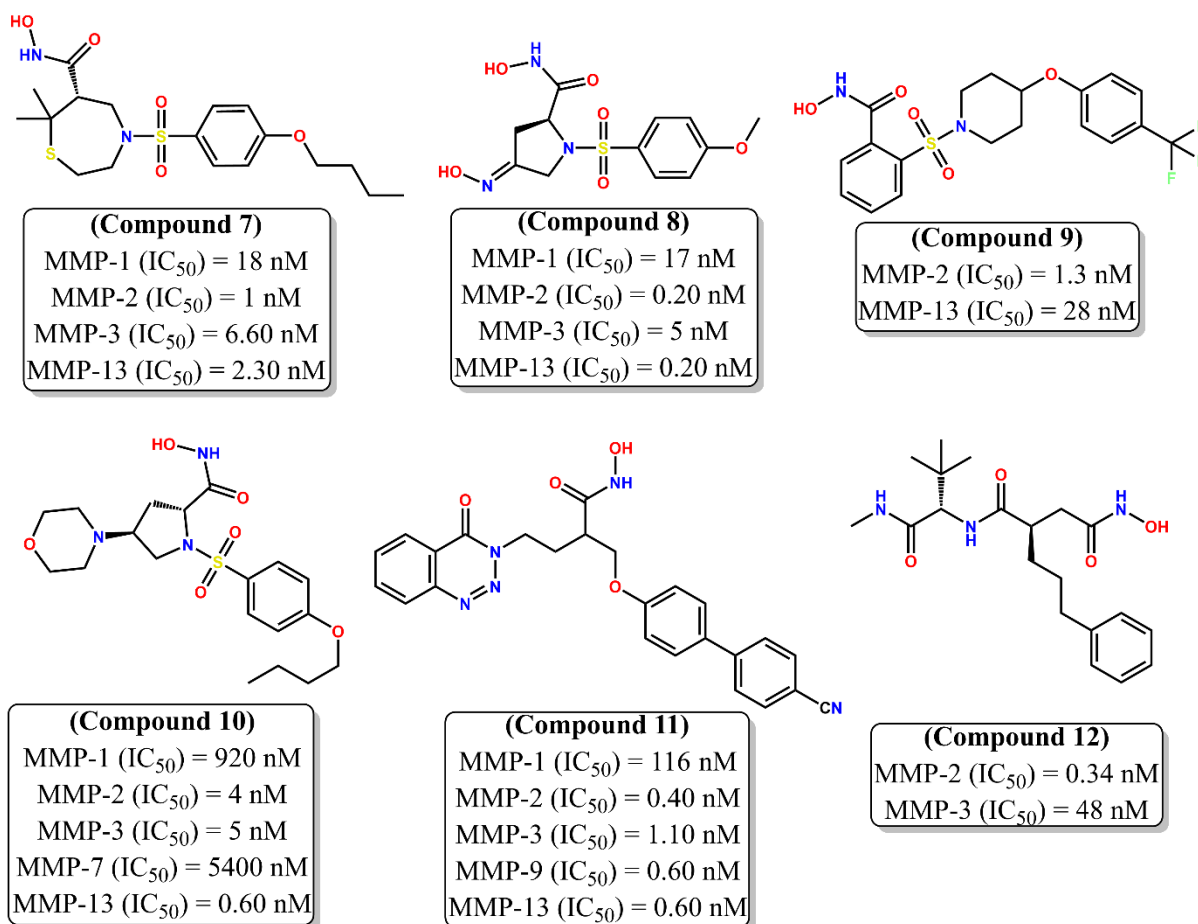


Figure 2.2. Hydroxamate-based MMP-2 inhibitors (Compounds 7-12).

In a different study, a group of hydroxamates based on arylsulfonamido proline were described as robust, broad-spectrum MMPIs that contained oxime, hydrazone, and exomethylene moieties (Cheng et al. 1999). All of these inhibitors showed higher affinities for MMP-2 and -13 while still exhibiting strong selectivity for MMP-1, -3, and -7. Compound 8 (**Figure 2.2**) exhibited at least 25-fold selectivity over other MMPs with higher but nonselective inhibition for MMP-2 and -13. In 2000, Barta and colleagues reported a number of arylhydroxamate sulfonamides and tested their activity against MMP-1, -2, and -13. The majority of substances exhibited effective and selective MMP-2 inhibition over MMP-13 sparing MMP-1. With a selectivity of over 21-fold over MMP-13, compound 9 (**Figure 2.2**) exhibited the potential MMP-2 inhibition (IC_{50} = 1.3 nM). Again, a series of arylsulfonamido hydroxamates with functionalized 4-aminoproline moiety have been reported by researchers from Procter and Gamble Pharmaceuticals to have high potency, nonselectivity between MMP-2 and -13, but the higher selectivity over other MMPs (Natchus et al., 2000). Compound 10 (**Figure 2.2**) displayed a 7-fold selectivity over MMP-2 (IC_{50} = 4 nM) and substantial MMP-13 inhibition (IC_{50} = 0.6 nM). In a rat arthritis model generated by iodoacetate, compound 10 also reduced

articular damage by 26%. There have also been reports of several 3-aryloxy propionic acid hydroxamates as possible MMPIs by a group of workers (Chollet et al., 2001). Most compounds were incredibly potent and selective MMP-2 inhibitors compared to other MMPs. When compared to MMP-3, -9, and -13, compound 11 (**Figure 2.2**) showed a higher affinity for MMP-2 ($IC_{50} = 0.4$ nM). The degradation of proteoglycans was similarly effectively inhibited by compound 11 ($IC_{50} = 0.1$ M). Despite having a favorable pharmacokinetic profile, it also produced a 40% tumor decrease in mice using the B16F10 melanoma model at a dose of 100 mg/kg i.p. Succinylhydroxamates have been described by Pfizer researchers as very effective and selective MMP-2 inhibitors over MMP-3 (Fray et al., 2001a). With the 141-fold selectivity over MMP-3, compound 12 (**Figure 2.2**) showed the strongest MMP-2 inhibition ($IC_{50} = 0.34$ nM).

Another set of succinylhydroxamates was reported by Fray and Dickinson (2001b) as robust and highly selective MMP-3 inhibitors over MMP-2. Compound 13 (**Figure 2.3**) exhibited the highest dual MMP-2 and MMP-3 inhibition.

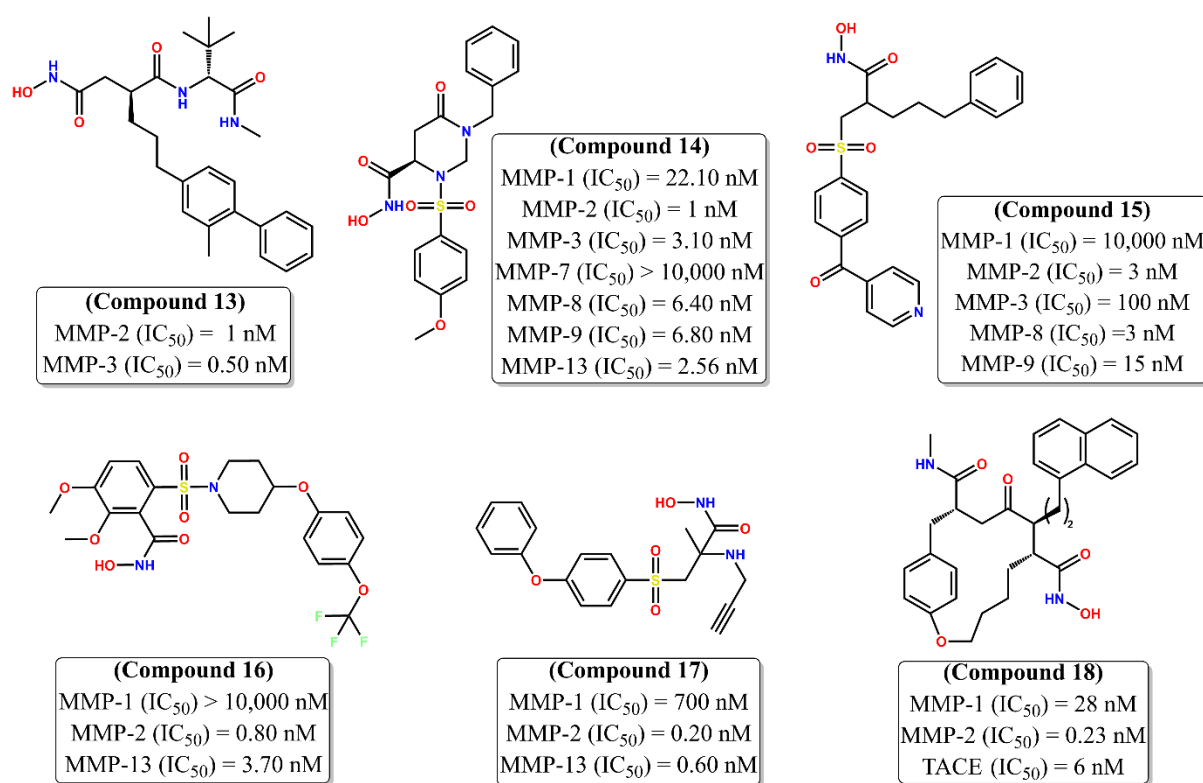


Figure 2.3. Hydroxamate-based MMP-2 inhibitors (Compounds 13-18).

The researchers at Procter and Gamble Pharmaceuticals revealed several arylsulfonamide-based hydroxamates with 6-oxohexahydropyridine and diazepine moieties as potent MMPIs

(Pikul et al., 2001). Inhibition of MMP-2 by compound 14 (**Figure 2.3**) was very effective ($IC_{50} = 1$ nM) and at least 2.5 times more selective than inhibition of other MMPs. Arylsulfonyl hydroxamates have been found by researchers at Celltech Chiroscience as effective MMPis (Baxter et al., 2001). When compared to MMP-8, compound 15 (**Figure 2.3**) showed effective but non-selective MMP-2 inhibition ($IC_{50} = 3$ nM for both), while still exhibiting better selectivity over MMP-3 and -9. After oral administration in rats (10 mg/kg), compound 15 showed a significant plasma level concentration (300 ng/ml). Comparatively better than marimastat (**Figure 1.16, Chapter 1**), compound 15 produced 50% and 80% inhibition in the adjuvant arthritis model and the B16F10 melanoma mouse model, respectively, at a dose of 3 mg/kg. Pharmacia researchers reported some arylhydroxamate sulfonamides are powerful inhibitors of MMP-2 and -13 (Barta et al., 2001). The majority of substances produced strong and specific MMP-2 inhibition over MMP-13. Compound 16 (**Figure 2.3**) exhibited favorable pharmacokinetic characteristics in rats ($C_{max} = 5.16$ g/ml, $t_{1/2} = 1.5$ hours), effective MMP-2 inhibition ($IC_{50} = 0.8$ nM), and around 5-fold selectivity over MMP-13. It has been suggested that a group of hydroxamates of -alkyl-amino-sulfone could inhibit MMP-2 and -13 (Becker et al., 2001). The best MMP-2 inhibition was obtained by compound 17 (**Figure 2.3**), which also had a selectivity over MMP-13. A number of macrocyclic amide and ketone-based hydroxamates have been identified by Abbott laboratories researchers as effective inhibitors of TACE as well as MMP-1 and -2 (Holms et al., 2001). Compound 18 (**Figure 2.3**) produced significant MMP-2 inhibition ($IC_{50} = 0.23$ nM) and had a selectivity of more than 26 times over TACE. In addition, MMP-2 activity is better than prinomastat (**Figure 1.16, Chapter 1**). The THP-1 cellular assay showed that it inhibited TNF production in a promising way. Some N-aryl sulfonyl aziridine hydroxamates were described by Hanessian and colleagues (2001a) as potent MMPis. The most potent MMP-2 inhibitor ($IC_{50} = 237$ nM, **Figure 2.4**) was compound 19, which was nonselective toward MMP-3 and -13 and nearly three times less active against MMP-9 ($IC_{50} = 83$ nM).

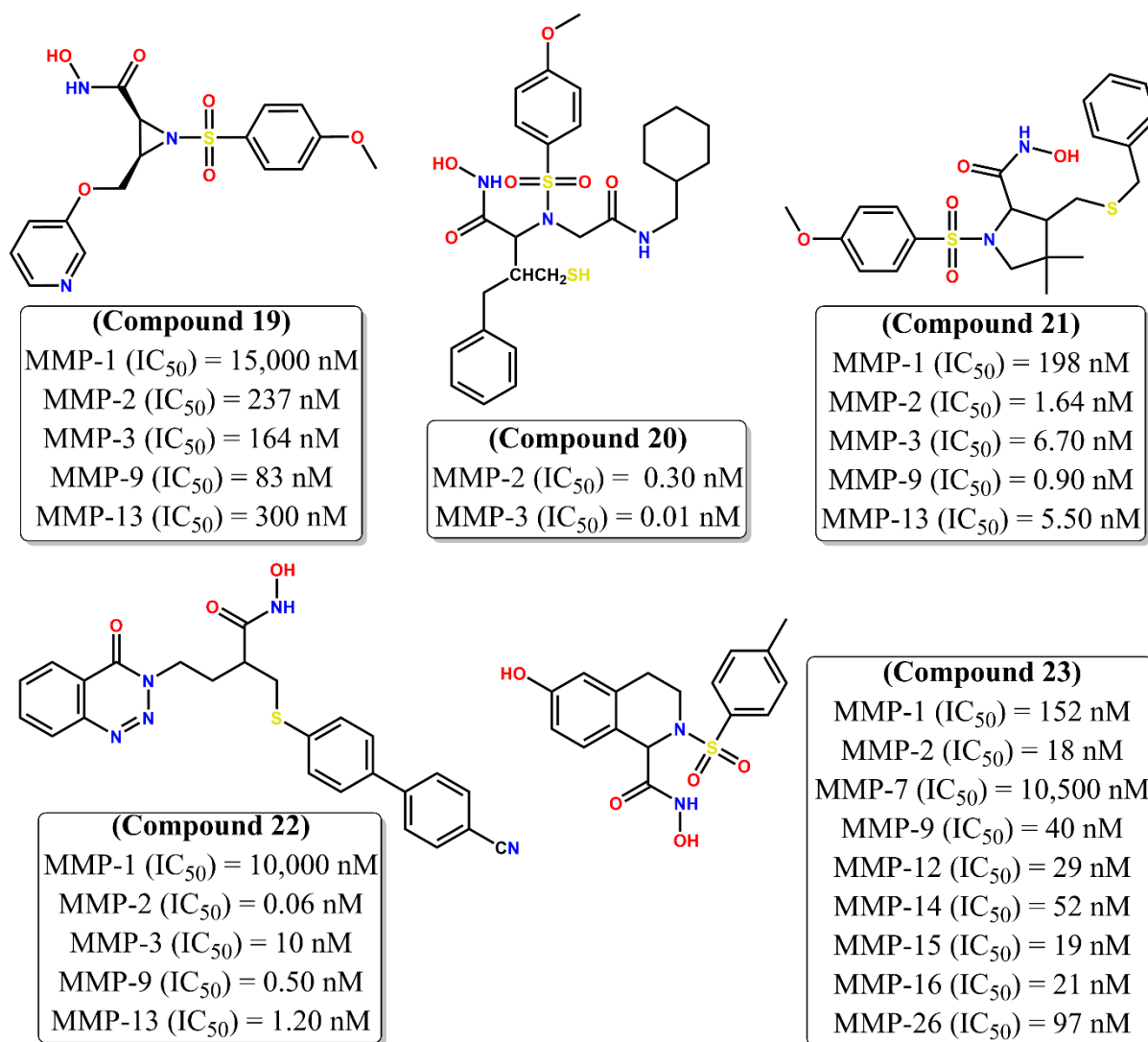


Figure 2.4. Hydroxamate-based MMP-2 inhibitors (Compounds 19-23).

Additionally, Hanessian et al. (2001b) revealed that a few arylsulfonyl homocysteine hydroxamates were efficient MMPIs. The majority of these compounds exhibited strong and focused MMP-9 inhibition in comparison to other MMPs. Compound 20 (**Figure 2.4**) produced strong MMP-2 inhibition (IC_{50} = 0.3 nM), but it had a 30 times stronger affinity for MMP-9 (IC_{50} = 0.01 nM). Hanessian et al. (2001c) reported certain arylsulfonyl hydroxamates as possible MMPIs in a different report. The highest MMP-2 inhibition was shown by compound 21 (**Figure 2.4**), which also had a nearly higher affinity for MMP-9 (IC_{50} = 0.9 nM). Some bisarylthio N-hydroxy propionamides with α -substitutions were described by Chollet et al. (2002) as potential MMPIs. Most compounds show excellent and selective MMP-2 inhibitory activity as compared to other MMPs. The best MMP-2 inhibition (IC_{50} = 0.06 nM) was seen with compound 22 (**Figure 2.4**), which had the minimum 8-fold selectivity over other MMPs. Additionally, Compound 22 showed a significant reduction in the metastatic spread and a 55

percent tumor reduction at 200 mg/kg ip dose in the B16F10 mouse melanoma model. Also, it (compound 22) demonstrated high absorption (92 percent) in the permeability investigation using the caco-2 cell line monolayer and intermediate metabolic stability (20 percent) in human hepatic microsomes. Tetrahydroisoquinoline-based hydroxamates have been reported to be effective broad-spectrum MMPs (Ma et al., 2004). Compared to MMP-15 ($IC_{50} = 19$ nM) and MMP-16 ($IC_{50} = 21$ nM), compound 23 (**Figure 2.4**) inhibited MMP-2 potently but nonselectively ($IC_{50} = 18$ nM).

When compared to other MMPs, a group of N-arylsulfonyl-N-alkyloxy aminoaceto hydroxamic acids have been found to be effective and selective MMP-2 inhibitors (Rossello et al., 2004). Compound 24 (**Figure 2.5**), which had the minimum 17-fold selectivity over MMP-3 and -9, had strong MMP-2 inhibitory action ($IC_{50} = 12$ nM). Additionally, compound 24 was also found to reduce fibrosarcoma HT1080 cells at a concentration of 50 nM, in addition to a decreased invasion as revealed by the matrigel assay.

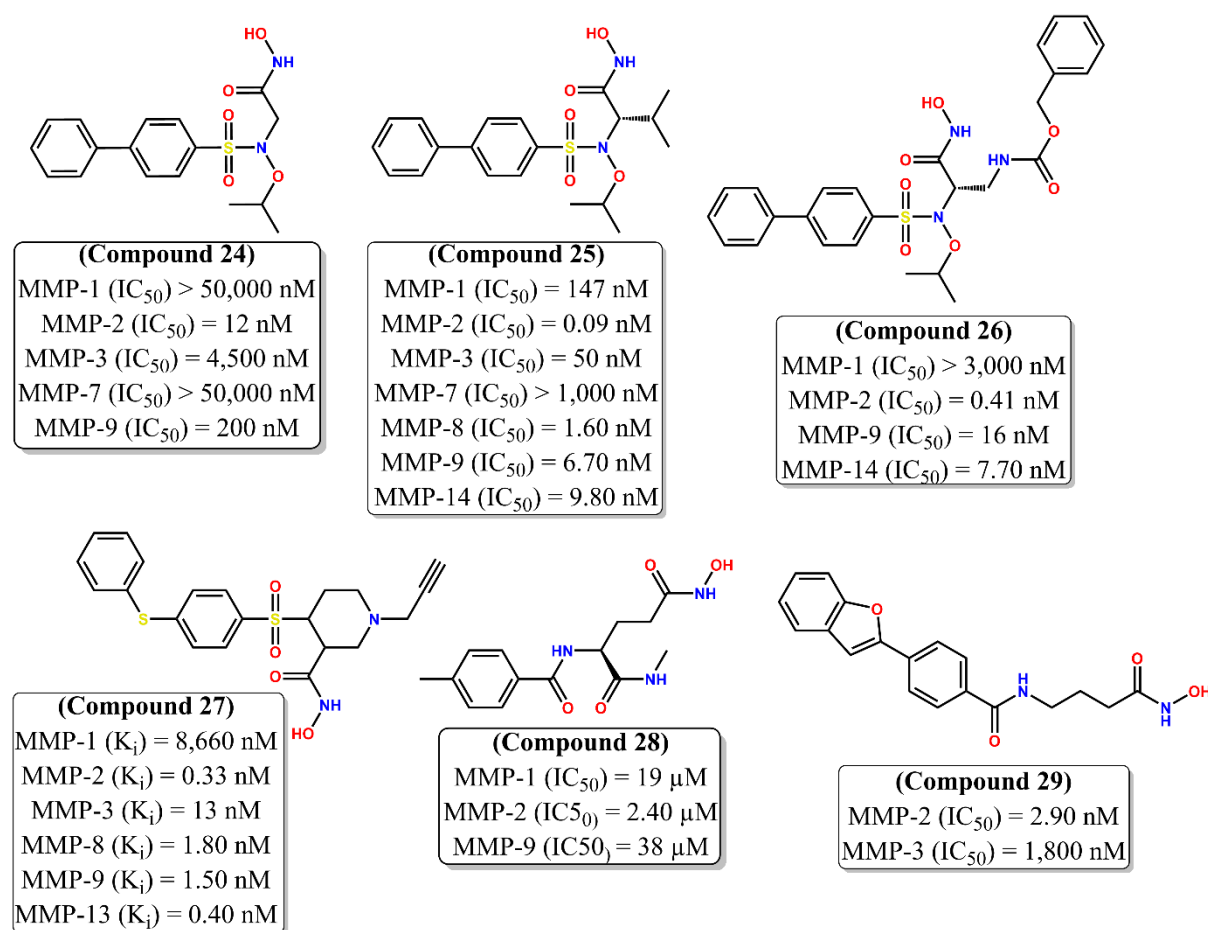


Figure 2.5. Hydroxamate-based MMP-2 inhibitors (Compounds 24-29).

The report of N-isopropoxy-N-biphenylsulphonyl-aminobutylhydroxamic acids as potent and specific MMP-2 inhibitors over other MMPs was the result of research by Rossello and coworkers (2005a). With a stronger selectivity for MMP-2 than the other compounds, compound 25 (**Figure 2.5**) demonstrated the strongest MMP-2 inhibitory efficacy ($IC_{50} = 0.09$ nM). Compound 25 also showed a significant reduction in HUVEC cells' chemoinvasion after they crossed the matrigel barrier. In addition, it has been found that some arylsulfonamido hydroxamic acids are more effective and specific MMP-2 inhibitors than other MMPs (Rossello et al., 2005b). Compound 26 (**Figure 2.5**), which had the minimum 19-fold selectivity over other MMPs, exhibited higher MMP-2 inhibition ($IC_{50} = 0.41$ nM). Compound 26 also showed potential as the cytotoxic agent against HT1080 in a Trypan Blue test (35% cytotoxicity at 10 μ M dosage). A group of α - and β -piperidine-sulfone hydroxamic acids were reported by Pfizer researchers to be effective MMPi (Becker et al., 2005). Compound 27 (**Figure 2.5**), however, showed strong selectivity against other MMPs while exhibiting robust but nonselective MMP inhibition (MMP-2 $IC_{50} = 0.33$ nM, MMP-13 $IC_{50} = 0.40$ nM). It also showed a fantastic C_{max} of 281 ng/ml after 6 hr of treatment in rats. In the mouse model of corneal neovascularization, compound 27 reduced neovascularization by 50% at the dose of 50 mpk, indicating a promising antiangiogenic action. Nevertheless, compound 27 with paclitaxel improved mice's median survival time by roughly 46.7 days, which strongly supported compound 27 potential for tumor reduction. Another work by Ono Pharmaceuticals researchers identified a number of γ -aminobutyric acid derivatives as potential MMP-2 inhibitors using an in silico fragment-based methodology (Takahashi et al., 2005). The highest MMP-2 inhibitory efficacy ($IC_{50} = 2.4$ M) and maximum selectivity for MMP-2 were exhibited by compound 28 (**Figure 2.5**). The same research laboratory conducted additional studies that resulted in the creation of N-benzyl γ -aminobutyric acid hydroxamates as highly effective and selective MMP-2 inhibitors (Ikura et al., 2006). Compound 29 (**Figure 2.5**), which has 620-fold selectivity over MMP-3, showed the highest MMP-2 inhibition ($IC_{50} = 2.9$ nM). Once again, the Ono workers created a number of N-benzoyl γ -aminobutyric acid hydroxamates that show potential as MMP-2 inhibitors (Nakatani et al., 2006). Compound 30 (**Figure 2.6**) displayed the highest selectivity for MMP-2 and the strongest MMP-2 inhibition ($IC_{50} = 0.73$ nM).

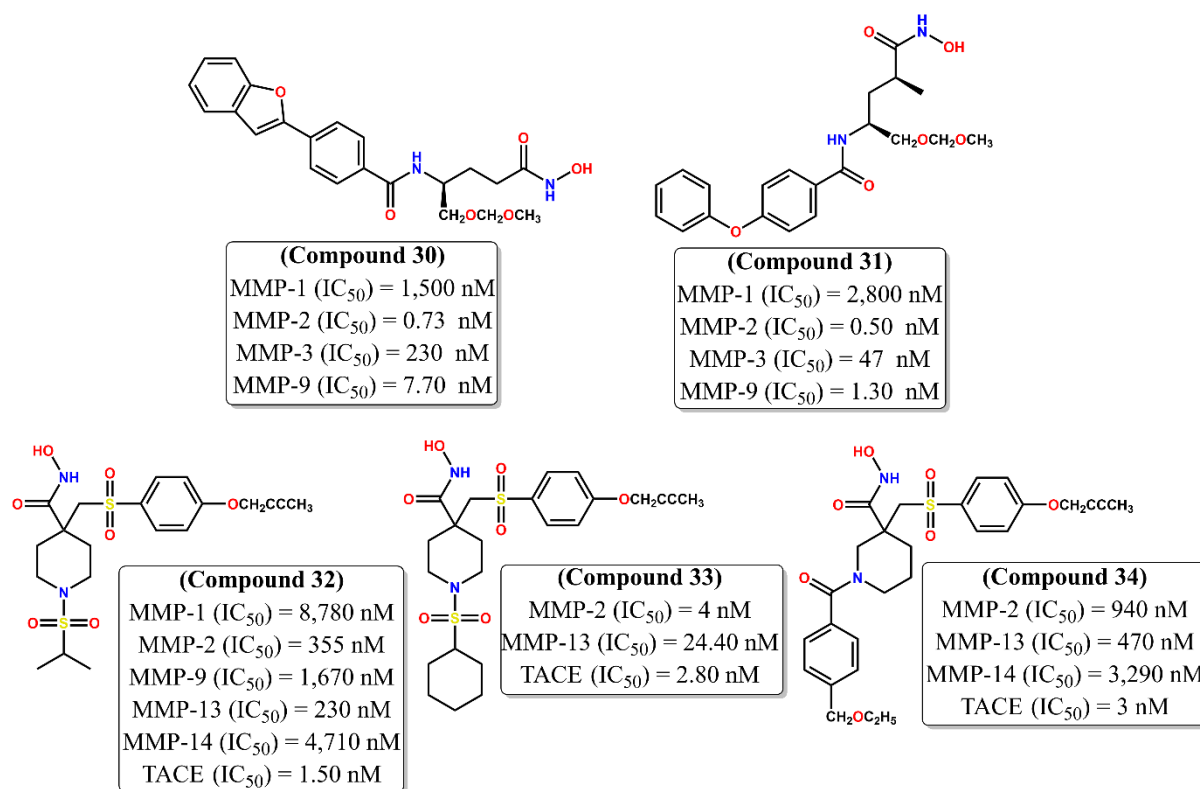


Figure 2.6. Hydroxamate-based MMP-2 inhibitors (Compounds 30-34).

The Ono researchers carried out some more studies that resulted in the creation of N-phenoxy benzyl γ -aminobutyric acid hydroxamates (Yamamoto et al., 2006). Compound 31 (**Figure 2.6**) exhibited impressive MMP-2 (IC_{50} = 0.5 nM) inhibition with selectivity over other MMPs. Researchers at Wyeth Research created a number of butynyloxyphenyl-sulphone piperidine hydroxamates as potential TACE inhibitors selective for MMPs (Park et al., 2006). Compound 32 (**Figure 2.6**), the highly effective TACE inhibitor with a selectivity of 237-fold over MMP-2 (IC_{50} = 355 nM), had an IC_{50} value of 1.5 nM. The Wyeth researchers carried out more work that resulted in the discovery of TACE inhibitors that are specifically effective against MMP-2 and MMP-13 (Condon et al. 2007). Compound 33 (**Figure 2.6**) showed potent MMP-2 inhibition (IC_{50} = 4 nM) with a selectivity of nearly 6 times that of MMP-13 (IC_{50} = 24.4 nM). A series of butynyloxyphenyl and butynylaminophenyl *o*-sulfone piperidine hydroxamates were described by Lombart and colleagues (2007) as potent and selective TACE inhibitors over MMP-2, -13, and -14. Compound 34 (**Figure 2.6**) resulted in MMP-2 inhibition (IC_{50} = 940 nM) but potent and selective TACE inhibition (IC_{50} = 3 nM).

Researchers from Pfizer Global Research reported a series of 4-biaryl piperidine sulfonamide hydroxamates as potent and selective MMP-3 inhibitors over MMP-2 (Whitlock et al. 2007).

Among these molecules, compound 35 (**Figure 2.7**) had the highest MMP-2 inhibition ($IC_{50} = 9$ nM), while it was nonselective over MMP-3 ($IC_{50} = 6$ nM).

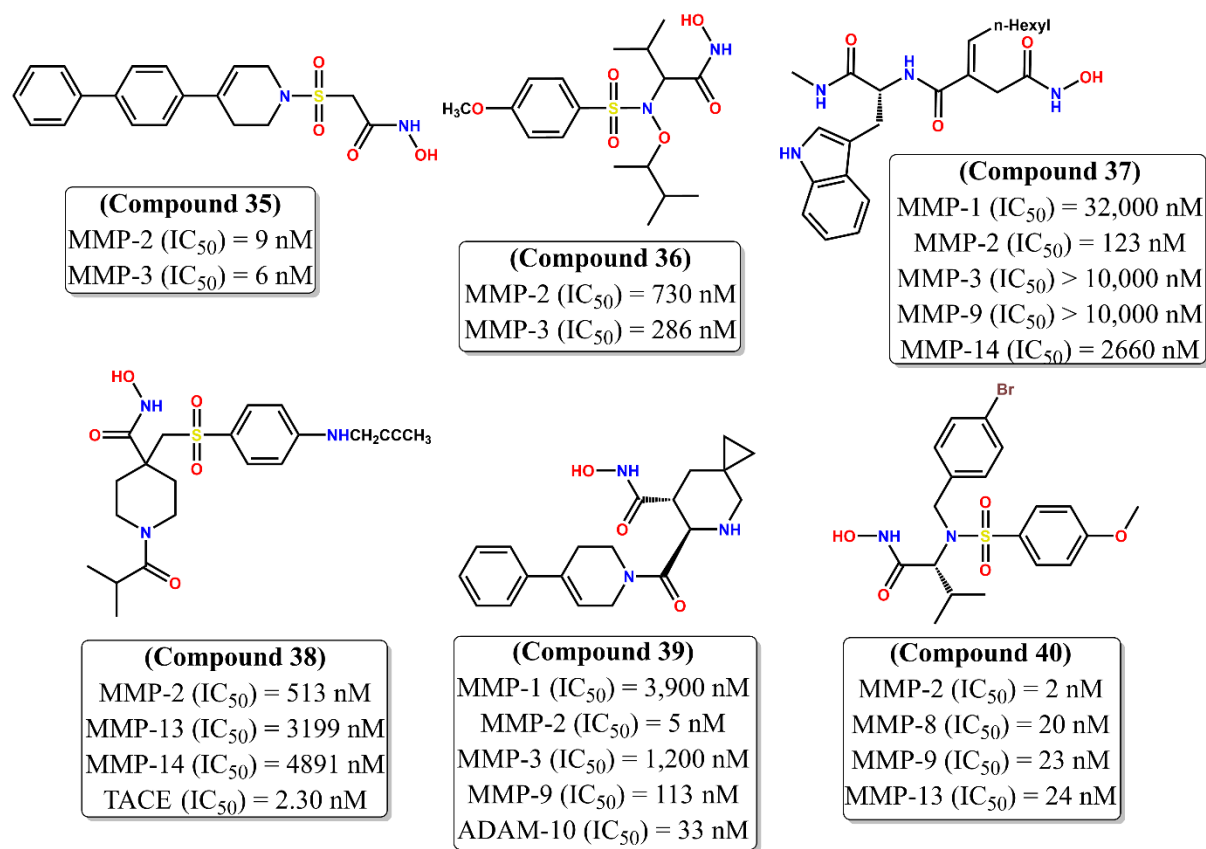


Figure 2.7. Hydroxamate-based MMP-2 inhibitors (Compounds 35-40).

Arylsulfonamide hydroxamates have been identified by Nuti and co-workers (2007) as MMP and carbonic anhydrase inhibitors (CAs). The most effective compound 36 (**Figure 2.7**), MMP-9 inhibitor ($IC_{50} = 286$ nM) exhibits potential inhibitory activity over MMP-2 ($IC_{50} = 730$ nM). Moroy and colleagues (2007) produced some ilomastat (**Figure 1.16, Chapter 1**) analogs and tested them against various MMPs. Inhibitory activity against MMP-2 ($IC_{50} = 123$ nM) was produced by compound 37 (**Figure 2.7**), which was more effective against other MMPs. Again, some β -sulfonyl hydroxamates have been identified by Wyeth Research as potential and stronger MMP inhibitors than TACE inhibitors (Huang et al., 2007). Compound 38 (**Figure 2.7**) exhibited remarkable TACE inhibition with greater selectivity than MMP-2 ($IC_{50} = 513$ nM) and the IC_{50} of 2.3 nM. Researchers at Incyte Corporation described a number of N-hydroxy-6-carboxamide-5-azaspiro [2.5] octane-7-carboxamides as strong and specific inhibitors of MMPs and ADAM-10 (Yao et al., 2007). Compound 39 (**Figure 2.7**) showed significant MMP-2 inhibitory effects with the IC_{50} of 39 nM and better selectivity over other

MMPs and ADAM-10. Additionally, compound 39 was shown to reduce HER-2 overexpressed human breast cancer, as indicated by the mouse xenograft model BT-474-SC1. The tumor size of models was also reduced, which improved the effectiveness in combination with trastuzumab. A number of arylsulfonamido hydroxamates were described by Wagner et al. (2007) as promising broad-spectrum MMPIs. It's interesting to note that compound 40 (**Figure 2.7**) inhibited MMP-2 ($IC_{50} = 2 \text{ nM}$) more effectively than other MMPs.

Incyte Corporation researchers also further disclosed a series of 7-[(hydroxylamino) carbonyl]-6-carboxamide-5-azasprin [2.5] octane-5-carboxylates as ADAM-10 as well as MMPIs inhibitors (Yao et al., 2008). With the higher selectivity over various MMPs, such as MMP-2 ($IC_{50} = 488 \text{ nM}$), compound 41 (**Figure 2.8**) produced significant ADAM-10 inhibitory action ($IC_{50} = 26 \text{ nM}$).

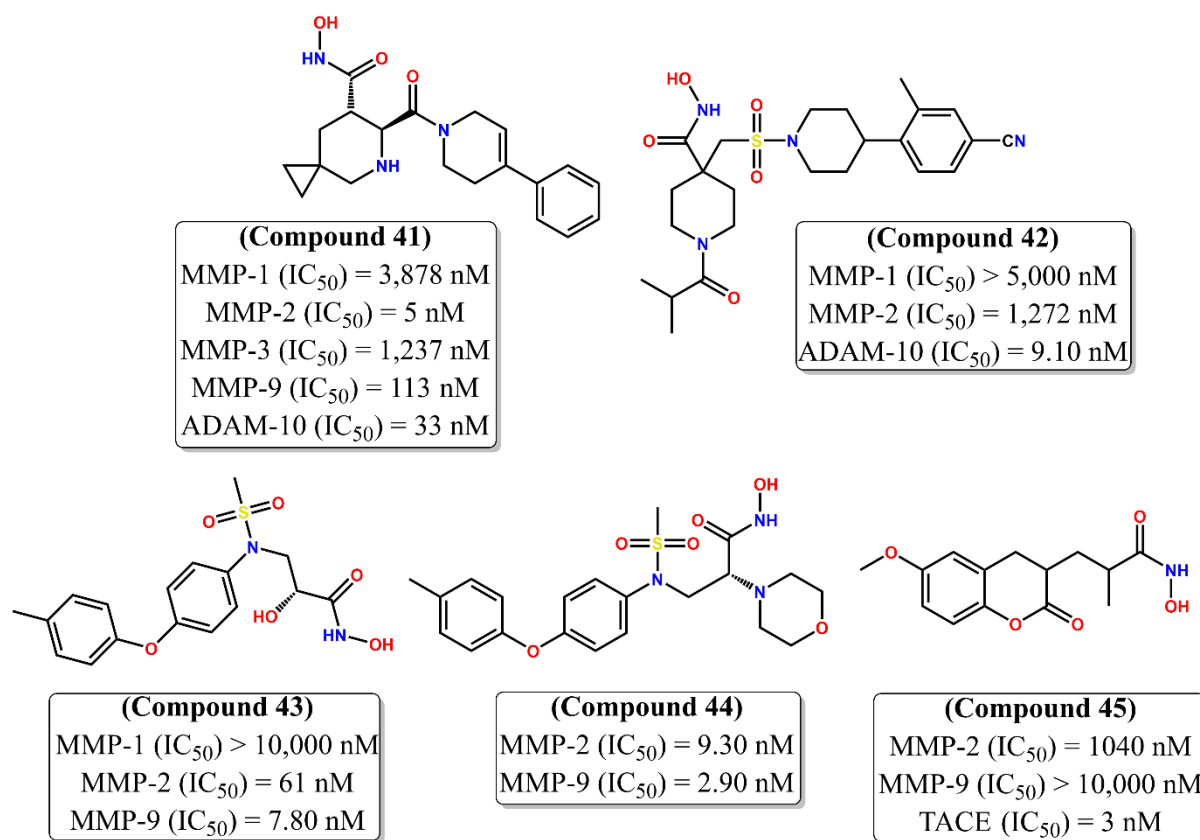


Figure 2.8. Hydroxamate-based MMP-2 inhibitors (Compounds 41-45).

In additional research conducted by the same laboratory, potent MMPIs and ADAM-10 inhibitors known as β -sulfonamido piperidine hydroxamates were developed (Burns et al., 2008). With a stronger selectivity over MMP-2 ($IC_{50} = 1,272 \text{ nM}$) than any other molecule, compound 42 (**Figure 2.8**) demonstrated potent ADAM-10 inhibitory action ($IC_{50} = 9.1 \text{ nM}$).

Johnson and Johnson's Pharmaceutical researchers investigated several hydroxamates based on β -N biarylether sulfonamide as potent gelatinase inhibitors (Yang et al., 2008a). However, inhibition of MMP-9 by compound 43 (**Figure 2.8**) was highly effective ($IC_{50} = 7.8$ nM) and 7.8-fold more selective than MMP-2 ($IC_{50} = 61$ nM). The same research team conducted additional research that led to the development of β -N biarylether sulfonamido hydroxamates, which are powerful and selective MMP-9 inhibitors over MMP-2 (Yang et al., 2008b). Compound 44 (**Figure 2.8**) displayed strong MMP-9 inhibitory activity and exhibited selectivity over MMP-2 ($IC_{50} = 9.3$ nM). Chun and coworkers (2008) reported certain chromene-based hydroxamates as possible TACE inhibitors. Compound 45 (**Figure 2.8**) showed a 347-fold selectivity over MMP-2 ($IC_{50} = 1040$ nM) having promising TACE inhibitory activity.

Some L-lysine derivatives have been found by Wang et al. (2008) to be powerful and selective MMP-2 inhibitors over aminopeptidase N (APN). The highest MMP-2 inhibitory activity ($IC_{50} = 3.54$ M) was exhibited by compound 46 (**Figure 2.9**) with a 161-fold selectivity over APN.

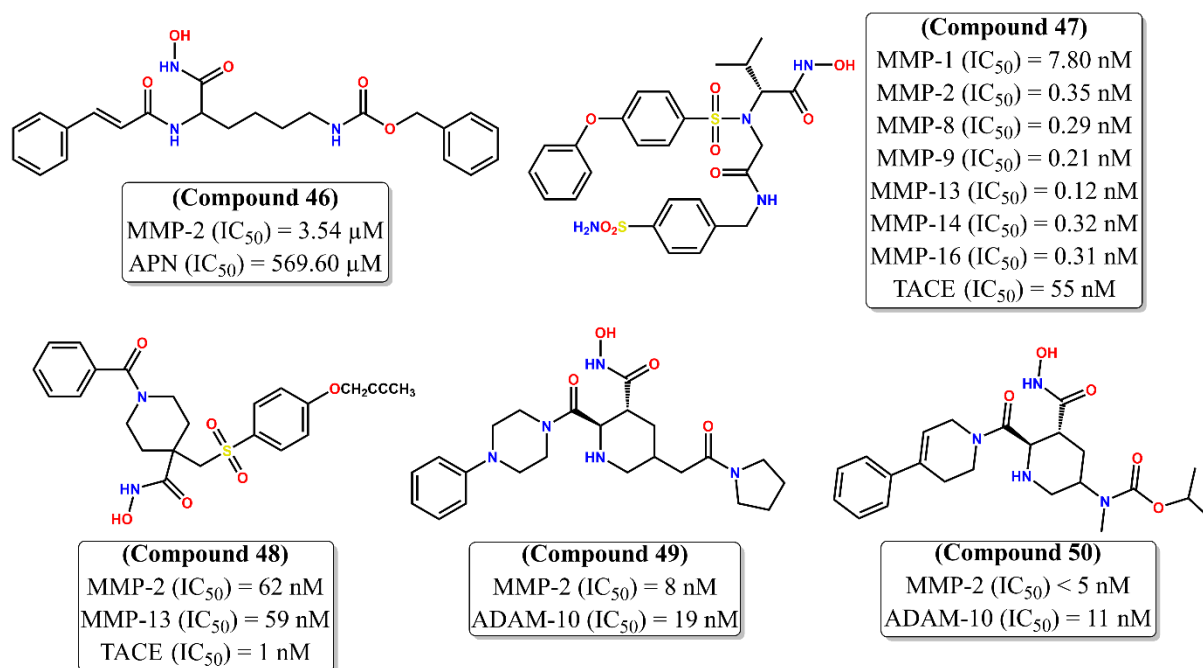


Figure 2.9. Hydroxamate-based MMP-2 inhibitors (Compounds 46-50).

Some iminodiacetyl-based arylsulfonamido hydroxamates were reported by Marques et al. (2008) acting as both MMP and CA inhibitors. Compound 47 (**Figure 2.9**) exhibits potent MMP-13 inhibitory activity ($IC_{50} = 0.12$ nM) in addition to promising CA inhibitory activity, surpassing that of other MMPs like MMP-2 ($IC_{50} = 0.35$ nM). The Wyeth Research group

reported a number of α -sulfone piperidine hydroxamates as powerful inhibitors of MMP-2, -13, and TACE (Zhang et al., 2009). Compound 48 (**Figure 2.9**) showed the 62-fold selectivity for MMP-2 ($IC_{50} = 62$ nM) and powerful TACE inhibitory activity. Also, as powerful MMPs and ADAM-10 inhibitors, Incyte Corporation researchers created a series of 2-carboxamide-3-hydroxamic acid piperidines (Burns et al. 2009). The MMP-2 ($IC_{50} = 8$ nM) enzyme was effectively inhibited by compound 49 (**Figure 2.9**) as compared to ADAM-10. Researchers from Incyte Corporation explored several carboxamate derivatives as effective ADAM-10 inhibitors that are also selective for MMPs in a separate research (Li et al. 2009). Moreover, when compared to ADAM-10 ($IC_{50} = 11$ nM), compound 50 (**Figure 2.9**) showed robust and selective MMP-2 inhibition ($IC_{50} < 5$ nM).

Mou and coworkers (2009) suggested a number of L-arginine-based compounds as possible APN and MMP-2 inhibitors. Compound 51 (**Figure 2.10**) displayed 191-fold selectivity for APN and significant MMP-2 inhibitory action ($IC_{50} = 8.7$ M).

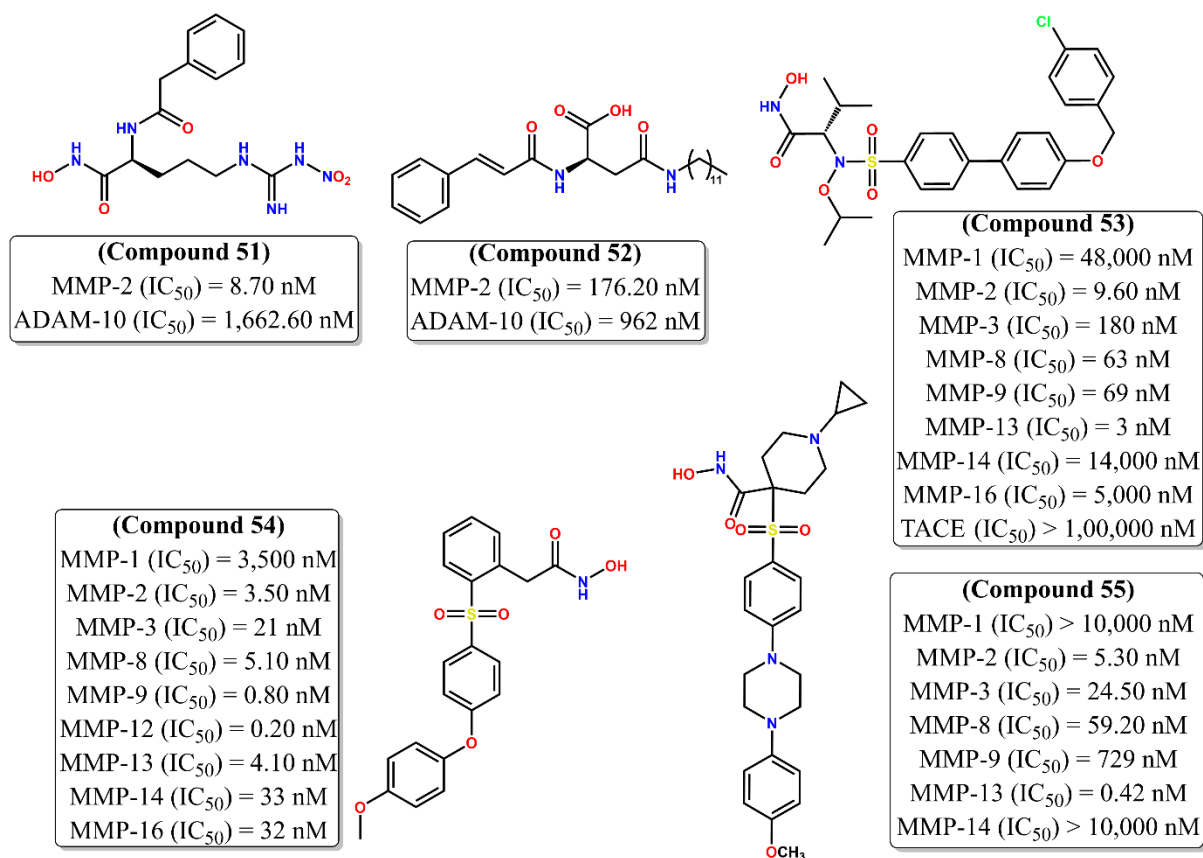


Figure 2.10. Hydroxamate-based MMP-2 inhibitors (Compounds 51-55).

APN and MMP-2 are both inhibited by certain N-cinnamoyl-L-aspartic acids, according to Liu et al. (2009). With a selectivity of 5.5-fold over APN, compound 52 (**Figure 2.10**) showed significant MMP-2 inhibition ($IC_{50} = 176.5$ M) among such molecules. Nuti and coworkers

(2009a) reported certain N-O-isopropyl sulfonamide-based hydroxamates as potential MMPIs. Compound 53 (**Figure 2.10**) exhibited impressive MMP-13 inhibitory activity with 3.2-fold selectivity over MMP-2 ($IC_{50} = 9.6$ nM), and its IC_{50} value was only 3 nM. Arylsulfone-based hydroxamates were developed as potential MMPIs as a result of further research by Nuti et al. (2009b). Despite having a strong inhibitory effect on MMP-2 ($IC_{50} = 3.5$ nM) in compound 54 (**Figure 2.10**), it was more selective for MMP-12 ($IC_{50} = 0.20$ nM). Some phenylpiperidine α -sulfone hydroxamates have been described by Pfizer researchers as orally bioavailable and selective MMP-13 inhibitors. (Kolodziej et al., 2010a). A minimum of 12.5-fold selectivity over all MMPs, including MMP-2 ($IC_{50} = 5.3$ nM), was obtained by compound 55 (**Figure 2.10**), which exhibited strong MMP-13 inhibitory action ($IC_{50} = 0.42$ nM).

Kolodziej et al. (2010b) developed a host of N-aryl isonipecotamide α -sulfone hydroxamates as potential and effective MMP-13 inhibitors that are selective compared to other MMPs. With the minimum of 41-fold selectivity over other MMPs, including MMP-2 ($IC_{50} = 400$ nM), compound 56 (**Figure 2.11**) produced strong MMP-13 inhibitory activity ($IC_{50} = 9$ nM).

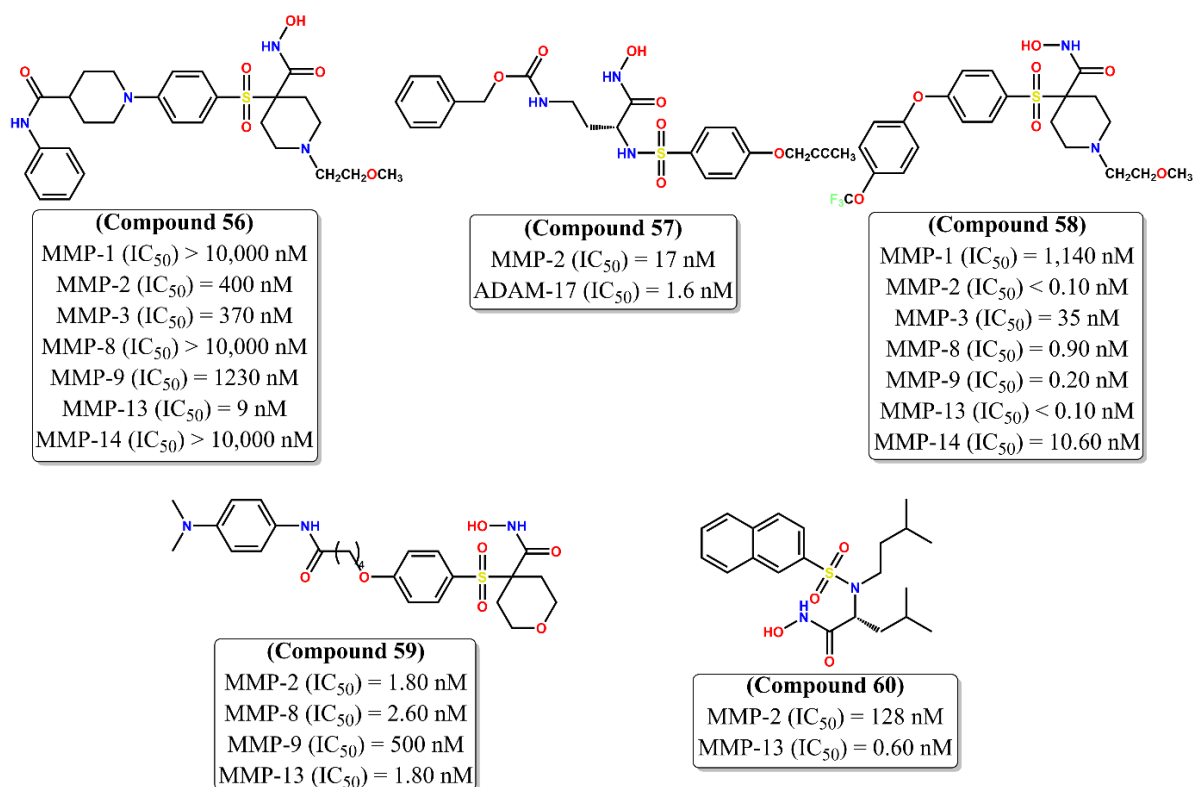


Figure 2.11. Hydroxamate-based MMP-2 inhibitors (Compounds 56-60).

A variety of arylsulfonamides were also reported by Nuti and colleagues (2010) as powerful inhibitors of MMPs as well as ADAM-17 and -10. A minimum of 10.6-fold selectivity over various MMPs, including MMP-2 ($IC_{50} = 17$ nM), was exhibited by compound 57 (**Figure**

2.11), which demonstrated potent ADAM-17 inhibition ($IC_{50} = 1.6$ nM). The epithelial ovarian (A2774 and SKOV3), breast (MCF-7 and MDAMB-486), and neuroblastoma (GI-CA-N) cancers were all responded well with it. Additionally, it effectively reduced the release of sALCAM from a variety of cell lines, including the A2774 cell line ($IC_{50} = 11$ nM). Pfizer Research scientists produced a number of α -sulfone α -piperidine and α -tetrahydropyranyl hydroxamates as possible MMPs (Becker et al., 2010). Strong but nonselective MMP inhibition was demonstrated by compound 58 (**Figure 2.11**) (IC_{50} : MMP-2 = 0.1 nM, MMP-13 = 0.1 nM). The same research team conducted additional studies that resulted in the discovery of α -sulfone hydroxamates as potent MMPs (Fobian et al., 2011). Despite being nonselective toward MMP-8 and -13, compound 59 (**Figure 2.11**) had strong MMP-2 inhibitory action ($IC_{50} = 0.18$ nM). A group of 2-naphthyl sulfonamide-based hydroxamates has been identified by Novartis researchers (Tommasi et al., 2011) as effective MMP-13 inhibitors that are selective for MMP-2. Compound 60 (**Figure 2.11**) showed excellent MMP-2 inhibition ($IC_{50} = 128$ nM), but it was 213-fold more selective for MMP-13 ($IC_{50} = 0.6$ nM). Nuti and coworkers (2011) reported a number of (ethylthiophene) sulfonamide-based hydroxamates that are effective MMPs. A minimum of 16.5-fold selectivity over other MMPs was shown by compound 61 (**Figure 2.12**), which exhibited strong MMP-2 inhibitory activity ($IC_{50} = 2.3$ nM). In U87MG glioma cells, compound 61 displayed 12 percent cell viability and decreased 42.6 percent cellular invasion in a dose-dependent manner.

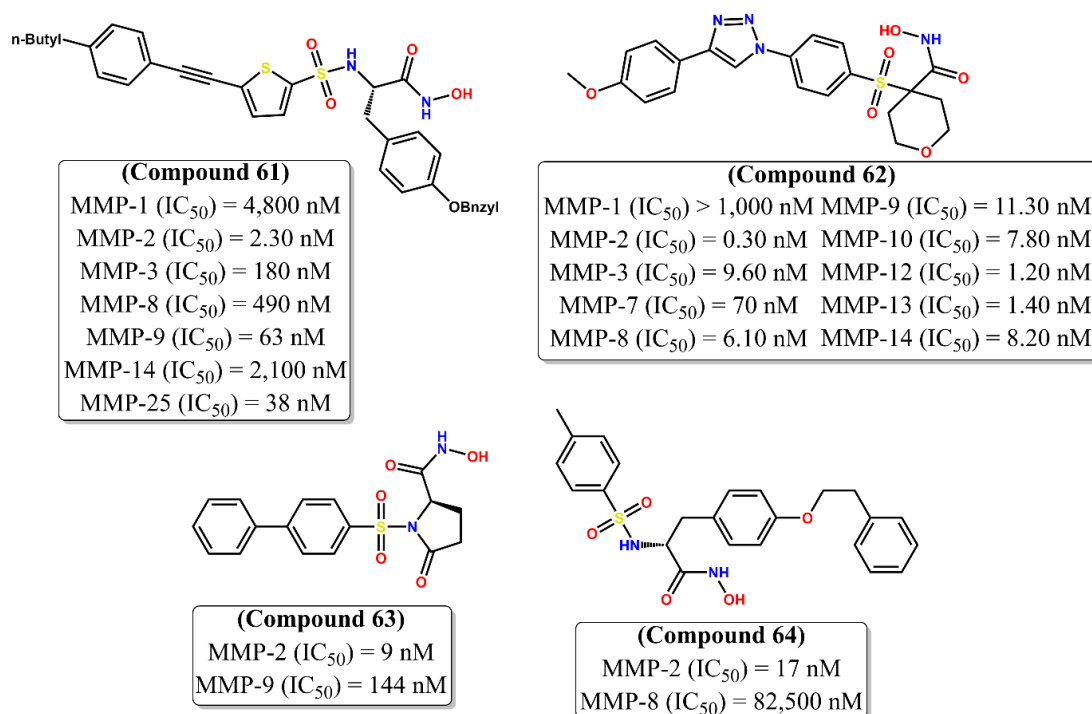


Figure 2.12. Hydroxamate-based MMP-2 inhibitors (Compounds 61-64).

Some arylsulfonyl hydroxamates based on α -tetrahydropyranyl were reported to be strong and selective MMP-2 inhibitors over MMP-9 (Zapico et al., 2011). The highest MMP-2 inhibitory action was obtained by compound 62 (**Figure 2.12**), which also maintained a minimum 4-fold selectivity over other MMPs ($IC_{50} = 0.03$ nM). Topai and coworkers (2012) suggested several gelatinase inhibitors using a number of scaffolds using an *in silico* pharmacophore-based method and the virtual screening strategy. An efficient gelatinase inhibitory pyroglutamine analog was found to be a promising hit. In order to create several arylsulfonamido hydroxamate derivatives, the pyroglutamate moiety was first changed by various bioisosteric scaffolds (specifically proline, hydroxyproline, thiazolidine, and thiazolidinedione). The majority of these substances have greater potency and selectivity for MMP-2 than MMP-9. Compound 63 (**Figure 2.12**), which maintained the minimum 17.8-fold selectivity over other MMPs, demonstrated strong MMP-2 inhibitory action ($IC_{50} = 9$ nM). Ltyrosine-containing dual inhibitors of HDAC-8 and MMP-2 were developed by Cheng et al. in 2012. Compound 64 (**Figure 2.12**) demonstrated more than 4,850-fold selectivity over HDAC-8 and significant MMP-2 inhibitory action ($IC_{50} = 17$ nM).

Some triazole-substituted hydroxamates were described by Hugenberg et al. (2012) as potent MMPIs. Compound 65 (**Figure 2.13**) exhibited strong MMP-2 inhibition ($IC_{50} = 0.13$ nM), however, it was 21 times more selective for MMP-13 ($IC_{50} = 0.006$ nM). Compound 65 may be a potential MMP-targeted radiotracer for non-invasive positron emission tomography (PET) imaging of activated MMPs, according to the *in vivo* investigation.

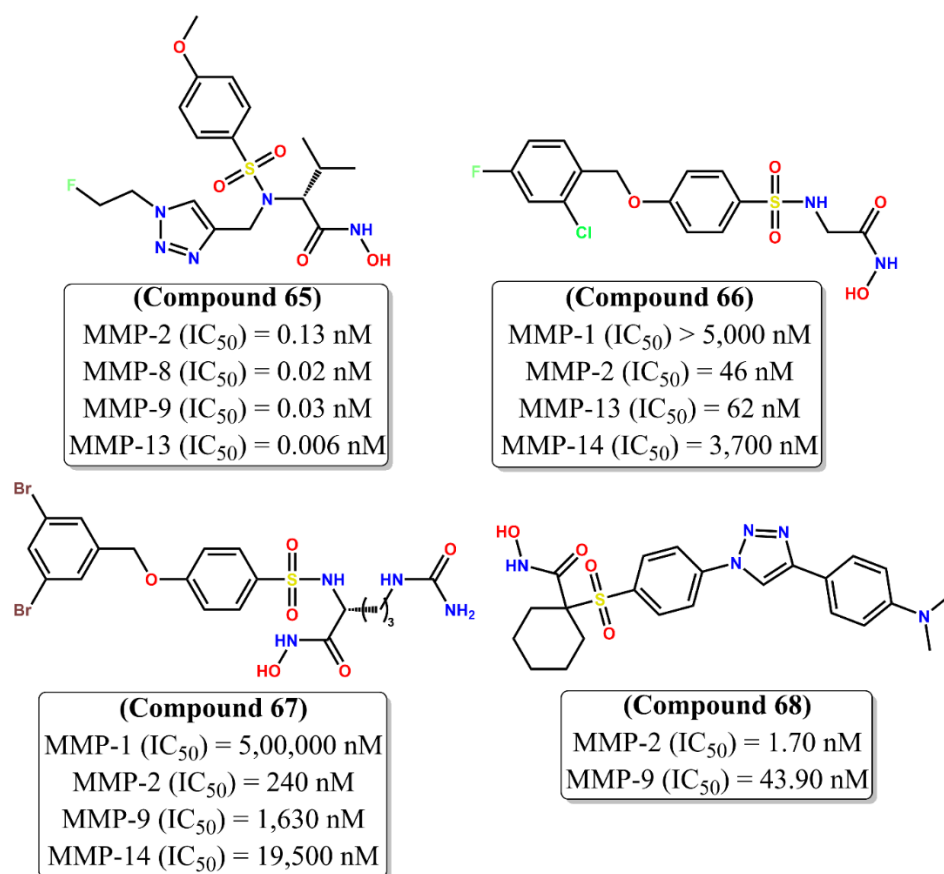


Figure 2.13. Hydroxamate-based MMP-2 inhibitors (Compounds 65-68).

A number of arylsulfonamido hydroxamates with potential MMP and aggrecanase inhibitory actions were reported by Nuti and colleagues in 2013a. In comparison to MMP-2 (IC_{50} = 46 nM), compound 66 (**Figure 2.13**) showed significantly greater affinity for aggrecanase-2 (IC_{50} = 35 nM). Additional research by Nuti and colleagues (2013b) prompted the development of a number of arylsulfonamides that are promising MMPI and ADAM-17 inhibitors. Compound 67 (**Figure 2.13**) showed excellent MMP-2 inhibition (IC_{50} = 240 nM) with a minimum selectivity of 6.8-fold over MMP-9 and -14. It was also revealed to strongly decrease sALCAM shedding at lower concentrations in a variety of ovarian cancer cell lines (such as A2774, SKOV3-luc, and A2780). Some triazolyl-substituted arylsulfonyl hydroxamates were described by Fabre et al. (2013) as strong and highly selective inhibitors of MMP-2 over MMP-9. Compound 68 (**Figure 2.13**) showed 25.8-fold selectivity over MMP-9 and strong MMP-2 inhibition (IC_{50} = 1.7 nM). It also exhibited promising water solubility and caco-2 cellular permeability *in vitro* in the HT1080 cell line, where it inhibited invasive behavior by 37% at a 10 μ M dose.

Some α -sulfonyl γ -(glycynylamino) proline peptidomimetic analogs were reported by Zhang and coworkers (2014) as dual inhibitors of MMP-2 and APN-sparing HDACs. Inhibition of

MMP-2 by compound 69 (**Figure 2.14**) was highly selective against APN ($IC_{50} = 72.29$ nM) and displayed significant activity. Compound 69 also exhibited antiproliferative properties *in vitro* against the human ovarian cell line (SKOV3) with an IC_{50} value of 196.37 nM, however, it had no effect on the HL60 leukemia cell line or the A549 lung carcinoma cell line.

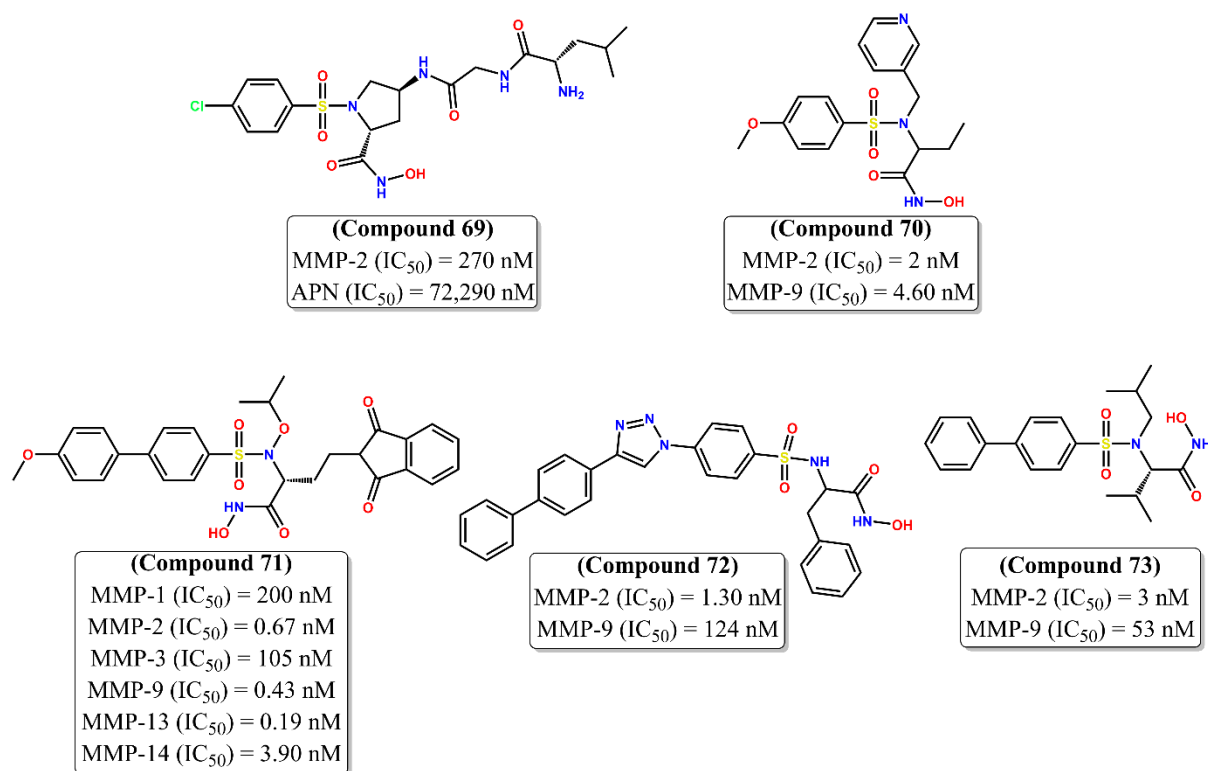


Figure 2.14. Hydroxamate-based MMP-2 inhibitors (Compounds 69-73).

Behrends and coworkers (2015) reported a series of effective gelatinase inhibitors called γ -fluorinated α -aminocarboxylic and α -aminohydroxamic acids. Compound 70 (**Figure 2.14**) demonstrated strong MMP-2 inhibition ($IC_{50} = 2$ nM) with 2.3-fold selectivity over MMP-9. Additionally, N-isopropoxy-arylsulfonamido hydroxamates were reported by Nuti et al. (2015) as promising and selective MMP-2 inhibitors in comparison to other MMPs. MMP-2 inhibition ($IC_{50} = 0.67$ nM) by compound 71 (**Figure 2.14**) was significant, but its MMP-9 and MMP-13 inhibitory actions were higher. According to the *in vitro* study, compound 71 drastically lowered HUVEC migration and invasion at lower concentrations (1 nM). However, in a dose-dependent manner, it also prevented HUVEC cells from undergoing FBS-induced morphogenesis, indicating that it may have antiangiogenic properties. Further evidence that compound 71 could block gelatinase activity came from the western blot and gelatine zymography analyses. Additionally, it demonstrated potential cytotoxicity and an ability to cause apoptosis in endothelial cells. However, the matrigel sponge assay model in mice

revealed that it also responded favorably to the evaluation of antiangiogenic efficacy *in vivo*. According to Zapico et al., (2015), a group of arylsulfonamido hydroxamates is effective gelatinase inhibitor. Compound 72 (**Figure 2.14**) demonstrated strong MMP-2 inhibitory activity ($IC_{50} = 1.3 \text{ nM}$) with a maximal 95-fold selectivity over other MMPs. Some hydroxamates have been identified by Sjolli et al. (2016) as potential gelatinase and ADAM-17 inhibitors. Compound 73 (**Figure 2.14**) produced strong MMP-2 inhibition ($IC_{50} = 0.003 \text{ nM}$) with selectivity for MMP-2 greater than 17.6 times that of MMP-9.

2.5. Development of MMP-2 inhibitors

For the past decade, the Natural Science Laboratory at Jadavpur University's Department of Pharmaceutical Technology has been focused on developing carboxylic acid derivatives based on arylsulfonamide and arylcarboxamide as efficient MMP-2 inhibitors as possible anticancer agents (Dutta et al., 2019; Mukherjee et al., 2017; Adhikari et al., 2016; Halder et al., 2015; Dutta et al., 2022; Adhikari, 2018). The arylcarboxamide derivatives were shown to have both MMP-2 and HDAC8 inhibitory capabilities, whilst the arylsulfonamides were discovered to be more effective and selective MMP-2 inhibitors. The study has discovered that the biphenyl sulfonyl scaffold may be a key fragment for exerting potential MMP-2 inhibition through the use of several ligand-based drug designing methodologies (specifically 2D-QSAR, classification-based QSARs, pharmacophore mapping, as well as 3D-QSAR CoMFA and CoMSIA) (Adhikari et al., 2016). Various biphenyl sulfonyl L(+) glutamic acid derivatives were designed and synthesized based on this discovery and molecular docking validation (Adhikari et al., 2016). It's interesting to note that all of them have the potential to inhibit MMP-2 with a high level of selectivity for MMP-2 over MMP-9 (>10-fold), sparing MMP-1. The biphenyl group attached to the sulfonamido moiety directed toward the S1' pocket played significant roles in the MMP-2 selectivity, according to several molecular modeling studies using these *in-house* molecules (Baidya et al., 2023; Adhikari et al., 2017; Adhikari et al., 2018a; Jha et al., 2018; Adhikari et al., 2018b).

Biphenyl sulfonyl L-(+) glutamine (compound 74, **Figure 2.15**) was shown to be a powerful and selective MMP-2 inhibitor when compared to MMP-9 and MMP-14 in the initial observation (Adhikari et al., 2016).

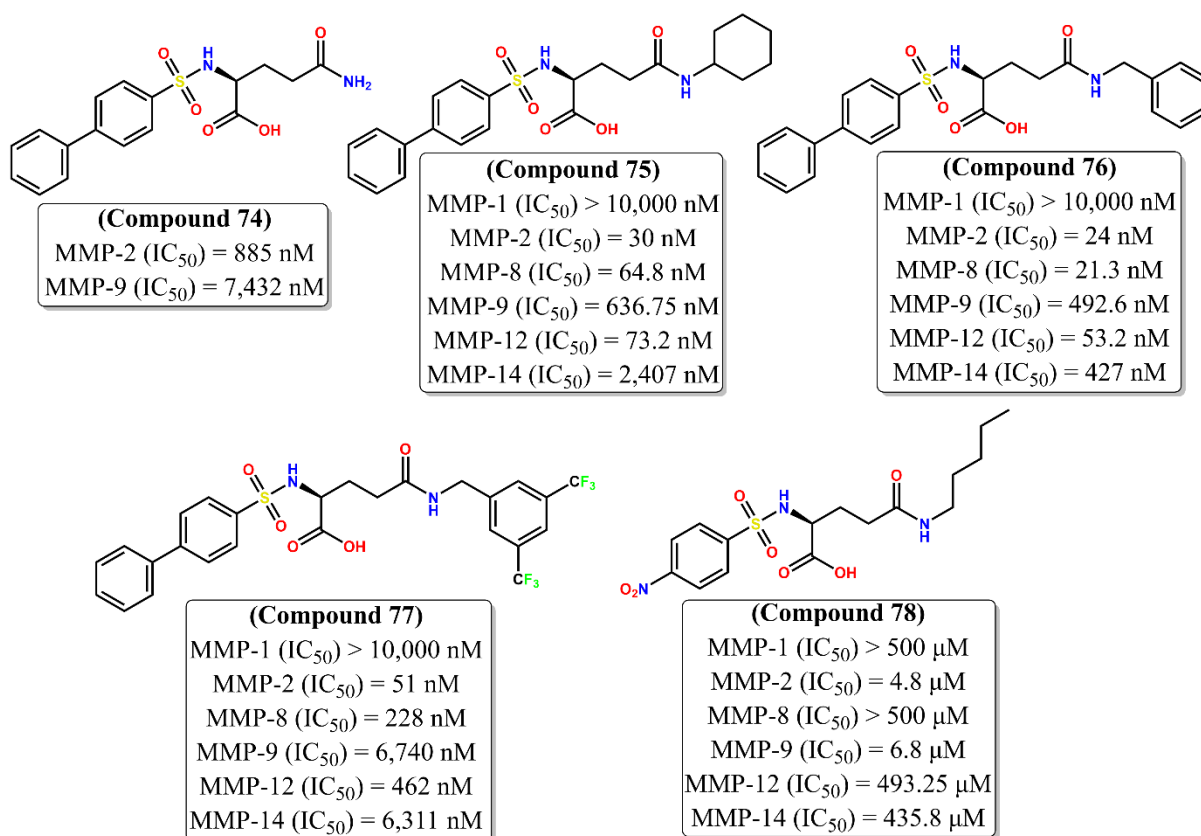


Figure 2.15. Structures of glutamic acid-based potent and selective MMP-2 inhibitors (Compound 74-78).

Similar to this, the free amine group was substituted with cyclohexyl (compound 75, **Figure 2.15**) and benzyl (compound 76, **Figure 2.15**) groups to produce very effective and selective MMP-2 inhibitors over MMP-9 and MMP-14. However, when evaluated against other medium-sized S1' pocket MMPs, the MMP-2 selectivity of each of these compounds was found to be significantly lower (namely MMP-8 and MMP-12). When tested against all other medium-size S1' pocket MMPs, the 3,5-bis(trifluoromethyl)benzyl moiety (compound 77, **Figure 2.15**) produced a strong and relatively selective MMP-2 inhibition. None of these compounds, with the exception of compound 77 (IC_{50} = 270 M), had any cytotoxicity (>200 nM) against the lung cancer cell line A549. Interestingly, it was shown that compounds 76 and 77 both decreased the cellular MMP-2 expression in the A549 cell line by up to 60.50 and 78.90%, respectively. Similarly, it was found that both of these compounds had effective anti-invasive activities (> 50%) and decreased migration in the A549 cell line at a dose of 50 μ M. When these compounds (74-76) were tested for cytotoxicity against the leukemia cell line K562, they did not perform well. In this situation, it is reasonable to suppose that while being

extremely strong and selective for MMP-2, the biphenyl scaffold's greater hydrophobicity and poor solubility may have restricted cellular permeability and caused poor cytotoxicity.

To test whether this change would affect MMP-2 inhibitory potency, selectivity, or cytotoxic characteristics, structural alterations were made by substituting the terminal phenyl group of the biphenyl scaffold with an electron-withdrawing nitro group (Mukherjee et al., 2017). It was noteworthy to find that although exerting cytotoxicity against multiple cancer cell lines (such as A549, MDA-MB-231, K-562, and U-937), these compounds MMP-2 inhibitory efficacy and selectivity were reduced several fold when compared to the earlier ones. In contrast to other medium-sized S1' pocket MMPs, Compound 78 (**Figure 2.15**), a dual selective gelatinase inhibitor, showed good cytotoxic potential against leukemia cell lines K-562 ($IC_{50} = 17.90$ M) and U-937 ($IC_{50} = 32.14$ M) as well as breast cancer cell lines MDA-MB-231 ($IC_{50} = 162$ M) and A549 ($IC_{50} = 205.80$ M).

The benzyl analog (compound 79, **Figure 2.16**) had significant cytotoxic potential against the K-562 cell line and demonstrated MMP-2 selectivity ($IC_{50} = 210$ nM) over other medium-size S1' pocket MMPs.

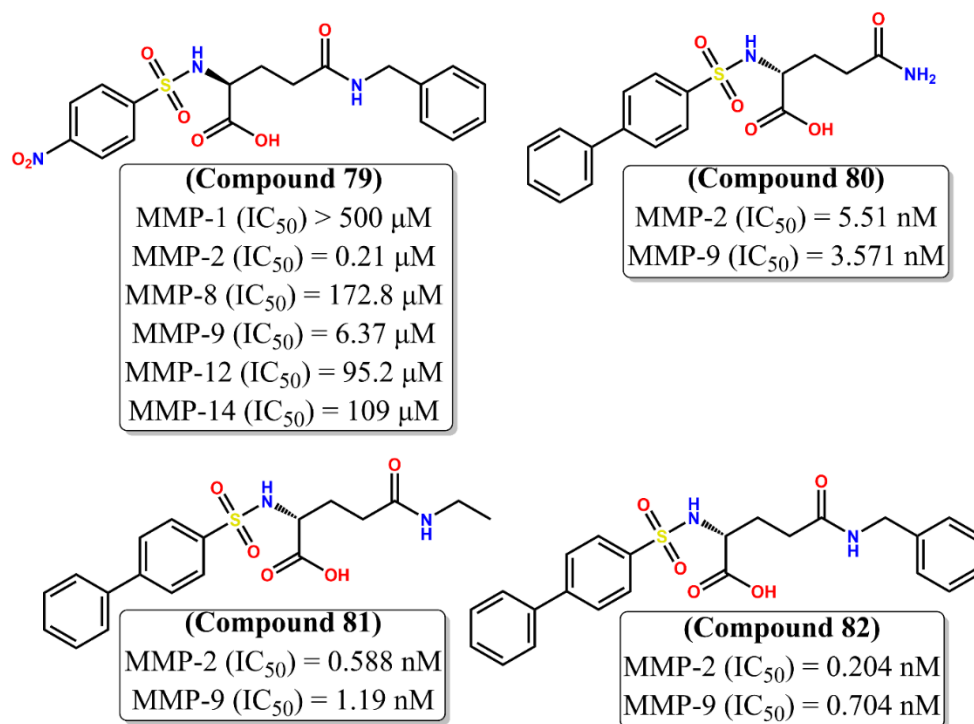


Figure 2.16. Structures of glutamic acid-based potent and selective MMP-2 inhibitors (Compound 79-82).

In the K-562 cell line, compound 78 also resulted in sub-G1 cellular arrest and produced a dose-dependent anti-invasive action. Again, flow cytometry analysis indicated that compound

78 downregulated MMP-2 expression (80.10 percent) at the dose of 10 μ M. It is reasonable to assume that the decreased hydrophobicity of such compounds may be a regulating factor for altering their ability to damage leukemia and solid tumor cell lines. Again, it was noticed that compound 80 (**Figure 2.16**) showed highly potent gelatinase inhibition. Despite being a nonselective inhibitor, compound 80 was found to have a greater affinity for MMP-9 than MMP-2 in terms of gelatinase inhibition. Ethyl analog (compound 81, **Figure 2.16**) yielded better MMP-2 inhibition ($IC_{50} = 0.588$ nM) than the other analog but it was only 2-fold MMP-2 selective over MMP-9. Last but not least, compound 82 (**Figure 2.16**) benzyl substitution analog exhibits potential gelatinase inhibition, but non selective against MMP-2 enzyme inhibition.

According to the binding mode of interaction investigation, both MMP-2 and MMP-9 allowed the biphenyl group to reach the S1' pocket in an aligned manner (**Figures 2.17A and 2.17B**). The benzyl group (compound 76) and 3,5-bis-trifluoromethyl benzyl group (compound 77) against MMP-2, on the other hand, created a π - π stacking interaction with His85 at the S2' pocket. When compared to the amino (compound 74) and cyclohexyl (compound 75) analogs, these molecules (compounds 76 and 77) may inhibit MMP-2 more potently due to this type of interaction. Contrarily, compounds 78 and 79, which lack the phenyl moiety but have the nitro group in their place, were less effective against MMP-2 in comparison but more effective MMP-2 inhibitors than MMP-9 enzyme.

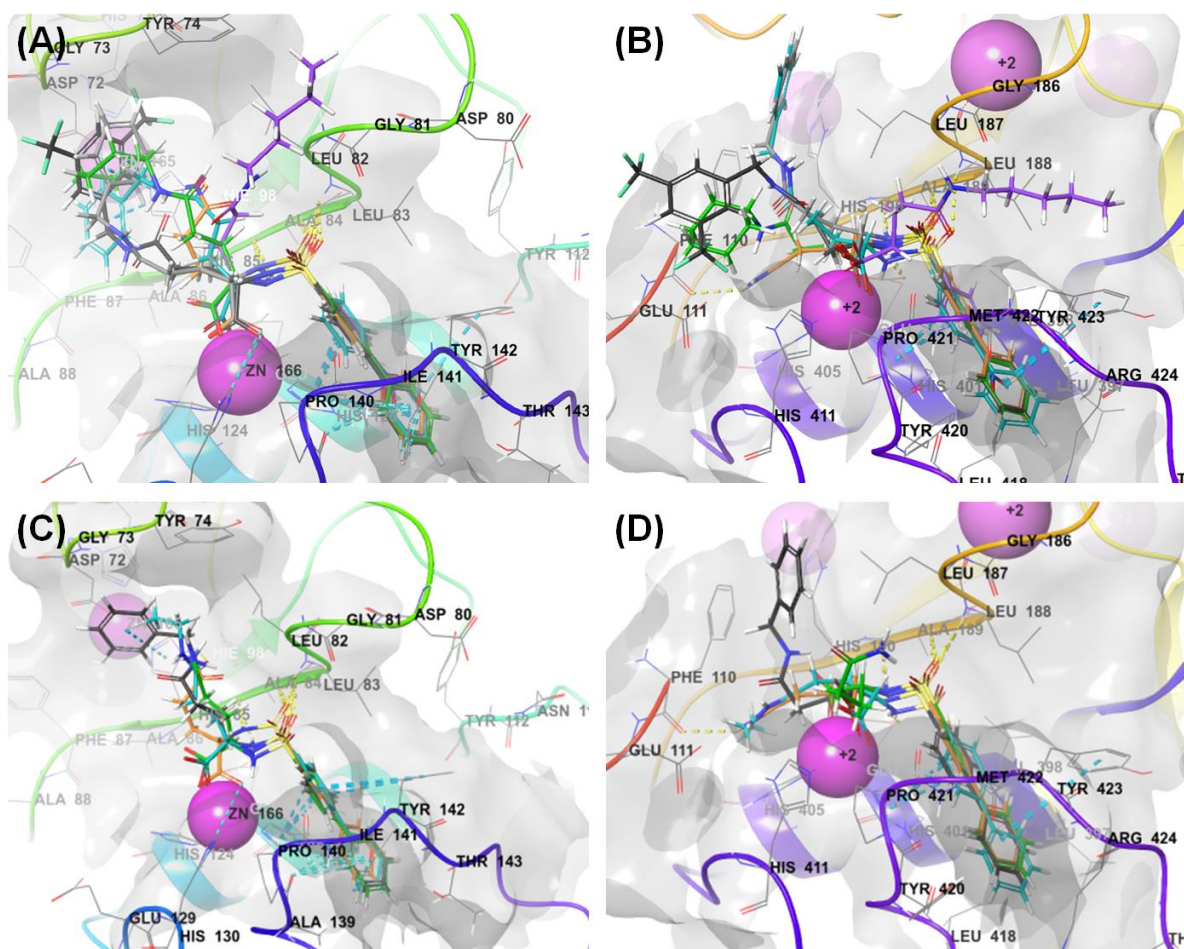


Figure 2.17. (A) Binding mode of interactions of compounds 74-79 at the active site of MMP-2 (PDB ID: 1HOV); (B) Binding mode of interactions of compounds 74-79 at the active site of MMP-9 (PDB ID: 1GKC) (C) Binding mode of interactions of compounds 74 and 80-82 at the active site of MMP-2 (PDB ID: 1HOV); (D) Binding mode of interactions of compounds 74 and 80-82 at the active site of MMP-9 (PDB ID: 1GKC) [Compounds 74, 75, 76, 77, 78 and 79 are shown in orange, green, cyan, black, violet and grey ball and stick, respectively; Compounds 77, 80, 81, 82 are shown in orange, green, cyan, black ball and stick, respectively]

Henceforth, it is possible to argue that the large aryl groups in the S1' pocket are also in part to blame for the selectivity provided over MMP-9 in addition to their role in the increased MMP-2 inhibitory potency. All of these changes from all of these compounds were noticeably absent from the S2' pocket upon binding to MMP-9, giving a possible explanation for the increased MMP-2 selectivity of these molecules over MMP-9 (Figure 2.17A and 2.17B).

Chapter 3

RATIONALE BEHIND THE WORK

3.1. Rationale

The Department of Pharmaceutical Technology at Jadavpur University, Kolkata, India, has dedicated the last 30 years to designing glutamate-based small molecule anticancer agents, as evidenced by a substantial body of research publications (De et al., 1984, 1985; Debnath AK et al., 1989; Debnath B et al., 2002, 2005, 2006; Gayen et al., 2005; Halder et al., 2013, 2015; Jha et al., 1986, 1987a, 1987b, 1999, 2003, 2017; Panda et al., 2006; Samanta et al., 2004, 2007, 2009; Srikanth et al., 2001, 2002a, 2002b). This significant research emphasizes on the critical importance of target identification in the drug design process, particularly in understanding the pathways and specific mechanisms by which these molecules interact with enzymes to inhibit cancer progression. Designing and developing glutamate-based anticancer agents with both precise target specificity and heightened efficacy poses a complicated challenge. Therefore, a deep understanding of the biological pathways, drug-target interactions, comprehensive efficacy and safety evaluations, as well as continual refinement of these molecules to address issues such as specificity, bioavailability, and toxicity while utilizing advanced methodologies to enhance the development of safer and more effective anticancer agents. A thorough review of the literature confirms that glutamic acid is associated with hydroxamates, which could make it a viable and efficient ZBG (Adhikari et al., 2017c). The type of ZBG and the pattern of binding between the ZBG and the catalytic Zn^{2+} of the metalloenzyme may have a significant correlation with the rate of metalloenzyme inhibition as well as the potentiality of the ligand (Adhikari et al., 2017a; Baidya et al., 2022). To maintain greater efficacy and selectivity between these isoenzymes containing Zn^{2+} ions, ZBG's presence in the molecule is not as significant as its related groups/functions and structural orientation (Adhikari et al., 2017c).

A number of hydroxamate analogs having potential MMP-2 inhibitory activity have already been discussed in detail in *Chapter 2*. Taking into account this important fact, the hydroxamates of the glutamic acid analogs may be considered as potential ZBG. Interestingly, hydroxamate is an effective ZBG as it may form hydrogen bonding interaction with the Zn^{2+} ion as well as the neighboring amino acid residues in MMP enzyme active sites. Moreover, the $-\text{NH}$ group and the $-\text{OH}$ group of the hydroxamate group are found to form hydrogen bonds with alanine and glutamic acid residues respectively (Rao, 2005). Hydroxamate, a potent chelator, may make it difficult to create selective MMPIs because of unfavorable side effects against off-target MMPs (Rao 2005; Overall and Kleifeld, 2006; Georgiadis and Yiotakis 2008). Despite these serious problems, hydroxamates (ZBG1) and carboxylates (ZBG2) containing MMPIs

were reported to exhibit selectivity among MMPs (Rossello et al. 2005a; Nakatani et al. 2006; Whitlock et al. 2007). It was also proven that strong ZBGs may not impart off-target metalloenzyme inhibition inherently. Moreover, the off-target activity of ZBGs may not necessarily produce the overall reflection of the off-target activity of an inhibitor compared to the same ZBG (Jacobsen et al. 2008). Despite being potent MMPIs, none of the hydroxamate analogs were approved by the FDA due to unwanted musculoskeletal syndromes (MSS) in clinical studies (Brown et al. 2004) for nonselective MMP inhibition as discussed in *Chapter 1*. However, in case of improvement of selectivity, strong metal chelating groups may impede the development of highly selective MMPIs because of the conserved Zn^{2+} ion across all MMPs, even if devolve powerful and selective MMPIs. Achieving MMPIs selectivity for a particular isoenzyme over various MMPs is a difficult challenge. Therefore, to improve the physicochemical characteristics of these MMPIs, pharmacokinetic and bioavailability studies may need to be taken into account. In addition to MMPIs with ZBGs, effective methods for achieving MMPI selectivity for compounds without ZBGs were reported.

It is an extremely tough undertaking to build a molecule with better potency towards MMP-2 and simultaneously higher selectivity over other different MMPs with respect to efficacy and selectivity towards MMP-2. The structure and amino acid residues of the S1' pocket of these MMPs that show structural similarities are the only factors contributing to this issue. In addition, it is well known that the hydrophobic S1' pocket is the single most important and inevitable component in maintaining the efficacy of MMPIs. Thus, while creating powerful MMPIs, the essential hydrophobicity of the S1' pocket must be taken into account (Baidya et al., 2022). However, creating a druggable MMPI with a superior pharmacokinetic profile and less harmful characteristics is equally challenging. However, the selectivity profile should be given the highest importance or priority in order to obtain or construct target-specific MMPIs, given the significant biological implications.

The key structural components of arylsulfonamide compounds that enable them to inhibit MMP-2 enzyme selectively and effectively are displayed in **Figure 3.1** (Adhikari et al., 2017a). This SAR study could be helpful in the development of more effective and selective MMP-2 inhibitors.

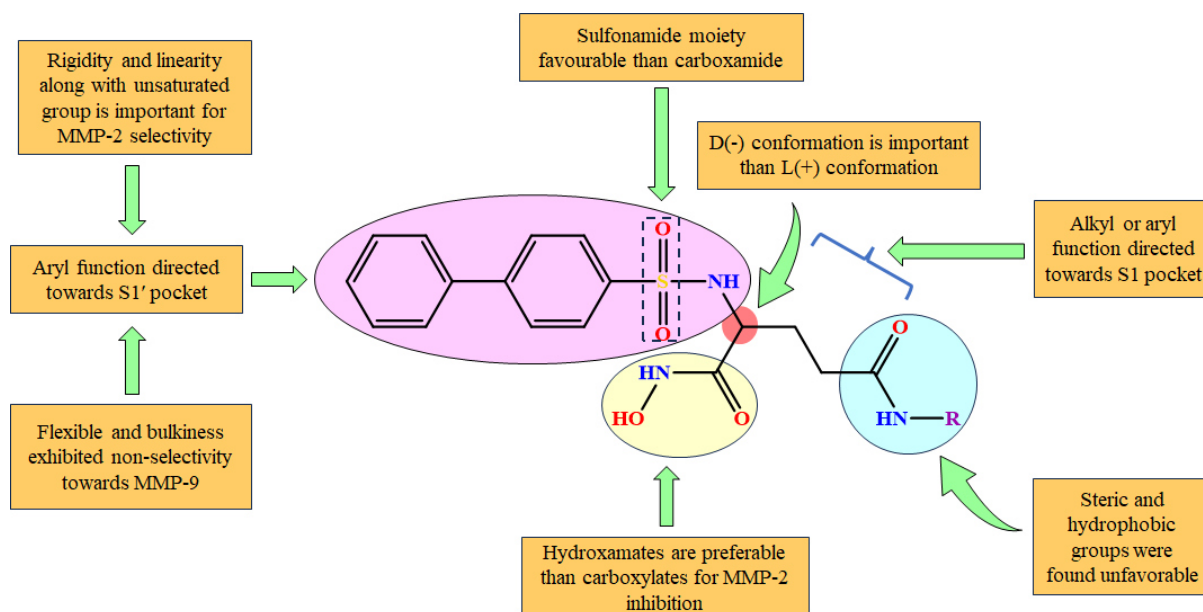


Figure 3.1. Structural exploration of hydroxamates-based arylsulfonamides moiety for exerting MMP-2 selectivity.

3.2. Aims and objectives

This present research has been using a variety of molecular modeling approaches such as docking-based 2D-QSAR, HQSAR, Linear discriminant analysis (LDA), Bayesian classification, and 3D-QSAR (i.e., CoMFA and CoMSIA) to design various biphenylsulfonamide hydroxamates-based glutamine analogs. These molecules were synthesized and characterized by different analytical techniques followed by biological evaluation through enzymatic assay and cytotoxicity studies. To combat terrible diseases like cancer, especially hematological cancer, the goal of this work was to create and identify a potential lead molecule as a metalloenzyme (MMP-2) inhibitor that may also offer selectivity over other MMPs. It has long been known that glutamines may effectively cure cancer. One of the most crucial requirements for metalloenzyme inhibition is that glutamines act as an effective zinc binding group, which is made possible by the presence of hydroxamates. Molecular modeling research and a thorough review of the literature, however, indicated that glutamine compounds would work well as MMP-2 inhibitors. The initial hit molecule was found to be an efficient MMP-2 inhibitor using extensive multiple molecular modeling and structure-activity relationship (SAR) studies. Subsequent structural modification resulted in the lead molecule, which exhibited MMP-2 inhibitory activity at nM concentrations. However, these molecules did not exhibit any significant cytotoxicity and did show some typical antiinvasive and antimigratory properties. Moreover, these molecules can effectively be used

as adjuvant cancer therapy in combination with first-line anticancer treatments to treat diseases like cancer. Though our in-house molecules did not show MMP-2 selectivity in contrast to MMP-9, they were more cytotoxic in many cancer cell types. Again, some compounds were achieved through conformational alteration of the lead molecule and these were found to be highly selective towards MMP-2 as well as cytotoxic towards leukemia K-562 cell line and non-cytotoxic in normal human cell line. In terms of creating selective and cytotoxic MMP-2 inhibitors, this might be the biggest accomplishment. Additionally, this research contained significant hints that might offer some helpful information for future improvements and adjustments to the methods used to design selective MMP-2 inhibitors.

Therefore, this research work's aims and objectives may be briefly summarized as follows:

- To develop promising therapy against cancer by targeting selective inhibition against MMP-2 through evaluation of small molecule biphenylsulfonamides hydroxamates-based glutamine derivatives.
- To conduct molecular modeling studies using docking-based multiple linear regression (MLR), HQSAR study, linear discriminant analysis (LDA), bayesian classification study (molecules developed by Shandong University) and docking-based 2D-QSAR and 3D-QSAR (i.e., CoMFA and CoMSIA) study of MMP-2 inhibitors (*in-house* molecules) required for the design and development of promising MMP-2 inhibitors.
- To synthesize and characterize 5-N-Substituted 2-(substituted biphenylsulfonyl) D(-) glutamines.
- To synthesize and characterize hydroxamate derivatives of 5-N-Substituted 2-(substituted biphenylsulfonyl) D(-) glutamines.
- The most effective and potential hydroxamate-based MMP-2 inhibitor(s) was subjected to biological evaluation like cytotoxicity assay, MMP-2 expression analysis, enzyme assay, cell cycle analysis, angiogenesis assay, apoptosis analysis in K-562 cell line, and DNA deformation assay by DAPI staining for the management of cancer, especially hematological malignancy.

Chapter 4

MATERIALS AND METHODS

Target identification and subsequent validation are the first steps in the lengthy, expensive, dangerous, and multistep process of drug development. Thereafter, hit-to-lead production, lead optimization, preclinical research, and various stages of clinical trials come afterward. High-throughput screening and combinatorial techniques were developed in the 90s to expedite the synthesis and screening of huge libraries and decrease the time and costs associated with drug discovery. Consequently, there was little progress made in the creation of new chemical entities or any notable successes were reported. Later, advanced computational tools, chemical synthesis, and biological research were combined to speed up the discovery process (Baig et al., 2018). The current study is based on three basic specialized fields viz (i) computational chemistry (molecular modeling), (ii) synthetic organic chemistry, and (iii) biological studies. This chapter discusses the resources and methods employed in each field.

4.1. Computational Chemistry

The Quantitative structure-activity relationships (QSAR) technique aids in the correlation between biological activity and the structural and physicochemical characteristics of the molecules, which may be useful in discovering crucial structural and physicochemical characteristics essential for imparting the increased inhibitory action (Gini, 2022). From a simpler perspective, the QSAR methodologies help in developing the correlation between a set of chemical quantifiable structural variances or similarity and their biological activity. The acceptance of computational chemistry has been demonstrated in various fields (Gasteiger, 2020). Using reliable statistical and machine learning techniques, QSAR is primarily concerned with the connection of chemical descriptors with certain biological end objectives. Additionally, it decreases the cost and length of the drug development process. In recent years, the quick development of computer technology, the accessibility of potent artificial intelligence (AI) algorithms, and the quick collection of molecular data have opened the way for the exponential rise of chemical knowledge and molecular modeling (Wei et al., 2022). Hence, in this work, different QSAR studies have been conducted based on modern computational techniques for the development of promising molecules to combat diseases like cancer.

In this context, the computational study includes sulfonyl pyrrolidine-based MMP-2 inhibitors having diverse zinc-binding motifs. This dataset would serve as the foundation for building predictive models such as multiple linear regression (MLR), HQSAR study (Baidya et al., 2019),

linear discriminant analysis (LDA) (Guti et al., 2021), bayesian classification study (Baidya et al., 2019) and comparative molecular similarity index analysis (CoMSIA) (Baidya et al., 2023; Adhikari et al., 2013; Halder et al., 2017), that elucidate the structure-activity relationships, aiding in the design and development of more potent MMP-2 inhibitors.

In addition, another computational study was done concerning molecular docking-based 2D-QSAR analysis (Baidya et al., 2019; Adhikari et al., 2016), and the 3D-QSAR study which deals with the comparative molecular field analysis (CoMFA) and comparative molecular similarity index analysis (CoMSIA) techniques (Baidya et al., 2023; Adhikari et al., 2013; Halder et al., 2017) to identify the important structural parameters from *in-house* arylsulfonyl L-(+) glutamine derivatives required for the higher MMP-2 inhibitory activity. Moreover, a molecular docking study was performed to know the important enzyme-ligand interactions at the enzyme active site required for enzyme inhibitory activity. Apart from different docking-based 2D-QSAR and 3D-QSAR studies, also performed molecular dynamics (MD) simulation analysis associated with molecular mechanics generalized born and surface area (MM/GBSA), free energy landscape (FEL) analysis, dynamic cross-correlation map (DCCM), principal component analysis (PCA) and probability density function (PDF) analysis. All the procedures have been discussed and depicted in detail as follows:

4.1.1. Dataset preparation and preprocessing

The first dataset comprising 65 sulfonyl pyrrolidine-based promising MMP-2 inhibitors (compound 1a-65a) with different zinc binding moieties was collected data curation from the literature (**Table 5.1, Chapter 5**) (Cheng et al., 2008a; Cheng et al., 2008b; Zhang et al., 2014; Zhang et al., 2018). These molecules were taken into consideration for robust multi-QSAR modeling analyses. Before carrying out the molecular modeling study, the variable biological endpoint, i.e., the MMP-2 inhibitory activity (IC_{50} ranging from 2 nM to 9,500 nM) of these molecules was converted into their respective negative logarithm values [$pIC_{50} = -\log (IC_{50}/10^9)$] for normal data point distribution (Adhikari et al., 2021). Noticeably, there was a high variation of pIC_{50} values of these molecules (pIC_{50} ranging from 8.699 to 5.022).

Before descriptor calculation, these 65 compounds (compound 1a-65a) of this dataset were subjected to scrutiny through the ‘*Prepare ligands for QSAR*’ protocol of Discovery studio (DS) 3.0 (<http://www.accelrys.com>). Next, the ‘PaDEL’ Descriptor software (Yap, 2011) was utilized

to compute 1,444 PaDEL descriptors for these dataset MMP-2 inhibitors. Not only that, but the PubChem fingerprint features (881 bits), the Klekota–Roth fingerprint (4860 bits), 2D-atom-pair fingerprint (780 bits), and substructure fingerprints (307 bits) were computed (ftp://ftp.ncbi.nlm.nih.gov/pubchem/specifications/pubchem_fingerprints.txt; Klekota and Roth, 2008; Openbabel's SMARTS_InteLigand.txt).

Again, the dataset pretreatment was carried out with the help of DTC laboratory software (<https://dtclab.webs.com/software-tools>) to remove highly correlated descriptors. Descriptors with correlation higher than 0.99 and covariance lower than 0.001 were removed in this process. Additionally, for the general physicochemical property-activity analysis, several molecular features such as molecular weight, lipophilicity, hydrogen bond forming capability, molecular surface areas as well as the number of aromatic and aliphatic groups were calculated using the DS 3.0 software (<http://www.accelrys.com>).

The total dataset consisting of 65 molecules (compound 1a-65a) was divided based on the ‘*generate training and test data*’ protocol with the random method by using Discovery Studio 3.0 (<http://www.accelrys.com>) where 70% molecules ($n_{\text{Train}} = 49$) were considered as the training set molecules and the remaining 30% molecules ($n_{\text{Test}} = 16$) were considered as the test set molecules. Depending upon the average (Avg) pIC_{50} value of the total dataset molecules (Avg $pIC_{50} = 6.3$), a threshold pIC_{50} of 6.3 ($IC_{50} = 5.01$ nM) was considered to increase the benchmark to binarize the dataset molecules into actives ($pIC_{50} \geq 6.300$) and inactive ($pIC_{50} < 6.300$). It was noticed that among the 49 training set compounds, 22 molecules had a pIC_{50} value ≥ 6.300 , and therefore, these were considered actives. The remaining 27 molecules had a pIC_{50} value < 6.300 and were considered inactive. Similarly, for the 16 test set molecules, 7 molecules had a pIC_{50} value ≥ 6.300 , and the remaining 9 molecules had a pIC_{50} value < 6.300 . Therefore, the test set comprised 7 molecules as actives and 9 molecules as inactives. The training set compounds were used to construct the statistically validated classification models which were externally validated on the test set molecules.

In addition, another molecular modeling study was conducted on the second dataset for a total of 32 (compound 1b-32b) *in-house* arylsulfonyl L-(+) glutamine derivatives having definite MMP-2 inhibitory activity values was taken into consideration for structure-based drug designing studies (Adhikari et al., 2016; Mukherjee et al., 2017). The common scaffold of these *in-house* MMP-2 inhibitors and their respective inhibitory activity are listed in **Table 5.2, Chapter 5**.

Before conducting the structure-based designing studies, the 2D structure of these molecules was drawn by using Chem Draw 5.0 software (<http://www.cambridgesoft.com>) and then converted respectively into their 3D counterparts (.mol). The '*prepare ligand for QSAR*' protocol incorporated in Discovery Studio 3.0 (DS 3.0) software (<http://www.accelrys.com>) was then utilized to minimize the energy as well as structural and geometrical refinement of these molecules. Simultaneously, the MMP-2 inhibitory activity of these molecules (IC_{50} in nM) was also transformed into their respective negative logarithmic value (pIC_{50}) for utilization as the dependent parameter.

After such a dataset refinement process, the 32 dataset compounds (compound 1b-32b) were grouped into the training set and the test set for internal and external validation purposes. The *Diverse Molecules* method from the '*Generate Training and Test Data*' protocol of DS 3.0 software (<http://www.accelrys.com>) was adopted to generate a training set of 24 compounds ($N_{\text{Training}} = 24$) as well as a test set comprising 8 compounds ($N_{\text{Test}} = 08$) (**Table 5.1, Chapter 5**), using the fundamental molecular characteristics such as lipophilicity ($AlogP$), molecular weight (MW), number of hydrogen bond donor and hydrogen bond acceptor groups ($nHBD$ and $nHBA$, respectively), number of rotatable bonds (nRB), molecular polar surface area ($MPSA$), number of aromatic rings (nAR) of these *in house* MMP-2 inhibitors.

4.1.2. Molecular docking analysis

The molecular docking analysis was performed as per the protocol conducted earlier (Adhikari et al., 2016; Mukherjee et al., 2017; Adhikari et al., 2017b; Adhikari et al., 2018b). For the molecular docking study, initially, the NMR solution structure of the MMP-2 enzyme (PDB: 1HOV) was retrieved from the Protein Data Bank (<https://www.rcsb.org/>). The '*protein preparation wizard*' protocol incorporated in the Schrodinger Maestro v12.1 software (<https://www.schrodinger.com>) was considered for the preparation and optimization of the MMP-2 structure. During protein preparation, the water molecules were eliminated from the protein structure. Moreover, the missing atoms were incorporated into the side chain of the MMP-2 structure. While preparing the protein structure, the OPLS2005 force field was taken into consideration to conduct the restrained minimization of the MMP-2 enzyme structure (<https://www.schrodinger.com>). Next, with the help of the protocol '*receptor grid generation*' incorporated in the Schrodinger Maestro v12.1 software (<https://www.schrodinger.com>), the receptor grid generation was performed. The ligand-binding

region of the MMP-2 enzyme was estimated by choosing the active site amino acid residues (<https://www.schrodinger.com>). The centroid of the selected amino acid residues was considered for defining the grid of the receptor for molecular docking analysis. During receptor grid generation, the specific ligand diameter midpoint box (10Å X 10Å X 10Å) was made and other different parameters such as constraints, rotatable groups, and excluded volumes were considered unaltered. Then the compounds were prepared for the molecular docking analysis by using the *LigPrep* protocol of Schrodinger Maestro v12.1 software (<https://www.schrodinger.com>) along with *EPIK* module and OPLS_2005 forcefield while desalting, adding metal binding sites and retaining all the specific chirality for individual compounds without generating any tautomer. After that, the molecular docking analysis was conducted by using the extra-precision (XP) method of the *GLIDE* protocol. Finally, the post-docking interaction analysis was visualized through the *Pose Viewer* protocol incorporated in Schrodinger Maestro v12.1 software (<https://www.schrodinger.com>).

4.1.3. Multiple linear regression (MLR) study

Multiple linear regressions (MLR) based 2D-QSAR study was employed to correlate molecular descriptors with biological activity. In this context, MLR was done by internal and external matrices were used to assess the predictability of the generated model (<https://dtclab.webs.com/software-tools>). The correlation coefficient (R) explains how closely the observed data follows the fitted regression line. The squared correlation coefficient (R^2) was determined as per *Equation 4.1*.

$$R^2 = 1 - \frac{\sum(y_{obs} - y_{calc})^2}{\sum(y_{obs} - y_{mean})^2} \quad 4.1$$

Where, Y_{obs} and Y_{calc} represent the actual and predicted biological activity of training set molecules, respectively and Y_{mean} represents the average biological activity of the training set molecules.

Again, adjusted R^2 (R^2_{adj}) was calculated using *Equation 4.2* where n is the number of scores and p is the number of descriptors, to avoid the limitations associated with the value the value of R^2 .

$$R^2_{adj} = \frac{(n-1) \times R^2 - p}{n-p-1} \quad 4.2$$

In addition, the F statistic, generated using R^2 , and the number of data points that were used to examine the significance of the regression equation at specific degrees of freedom (df) were also considered. The standard error of estimate (SEE) was also calculated for the residuals as per Equation 4.3.

$$SEE = \sqrt{\frac{\sum (y_{obs} - y_{calc})^2}{n - p - 1}} \quad 4.3$$

Where y_{obs} and y_{calc} are the actual and predicted activity of molecules in the training set, n denotes the total number of data points, and p denotes the total number of descriptors. The lower the value of SEE , the better the model quality.

4.1.4. 2D-QSAR model validation parameters

The predictive ability of 2D-QSAR models can be evaluated by cross-validation Q^2 /standard deviation of error of predictions (SDEP) statistics. Each molecule was deleted from the training set at each time and the prediction of activity of the deleted molecule was done simultaneously by the model constructed from the remaining train set compounds. The leave-one-out (LOO) Q^2 value was calculated as per Equation 4.4.

$$Q^2 = 1 - \frac{\sum (y_{obs} - y_i)^2}{\sum (y_{obs} - y_{mean})^2} \quad 4.4$$

Where y_{obs} and y_i are the actual and predicted biological activity of the i^{th} molecule respectively belong to the training set, and y_{mean} denotes the average biological activity of training set molecules.

Further, PRESS (the sum of squared deviations between the actual and predicted biological activities of the test set molecules) and SDEP (the sum of squared deviations error of prediction) values were determined in order to judge the internal predictability of the model.

The external predictability of the developed QSAR models was also justified by external validation of test set molecules. The R^2_{pred} is the external validation parameter which was calculated as per Equation 4.5.

$$R^2_{pred} = 1 - \frac{\sum (y_{obs} - y_i)^2}{\sum (y_{obs} - y_{mean})^2} \quad 4.5$$

Where y_{obs} and y_i are the actual and predicted biological activity of the i^{th} molecule respectively belong to the training set, and y_{mean} is the average biological activity of test set molecules.

The R^2_{pred} value is not sufficient enough to confirm the external predictability of a model. The value of R^2_{pred} is mainly controlled by the sum of squared differences between observed biological activities of the test set compounds and mean observed activities of the training set compounds. Therefore, it may not truly reflect the predictability of the model, and a modified r^2_m value was calculated (Roy et al., 2012). The calculation of r^2_m metrics [$r^2_{m(LOO)}$, $r^2_{m(test)}$ and $r^2_{m(Overall)}$] was used to estimate the closeness between the values of the predicted and the corresponding observed biological activities of the training set, test set, and the total dataset respectively. The r^2_m metrics should have a minimum value of 0.50 (Roy et al., 2012) and were calculated as per Equation 4.6.

$$r^2_{m(test)} = r^2 \times (1 - \sqrt{r^2 - r_0^2}) \quad 4.6$$

Where r^2 and r_0^2 are the squared correlation coefficients between the actual and predicted biological activities of the test set compounds with and without the intercept respectively.

4.1.5. Docking-based 2D-QSAR model development

Here, the XP descriptors obtained from the molecular docking study have been considered as independent parameters and these were utilized for correlating the MMP-2 inhibitory activity of these *in-house* compounds. This model can be able to provide an idea about the important parameters related to the binding pattern of compounds at the active site of MMP-2. Regarding the calculated XP descriptors, the 318 independent parameters were primarily reduced by applying an intercorrelation cutoff of 0.90 and a covariance threshold of 0.001 to remove the feature dimension and multicollinearity as well. The remaining 150 features were processed through a two-step feature selection process to identify the most relevant features that influence the activity. In the first step, the *CSF_Subset_Eval* attribute selector protocol with the *BestFirst* search method from WEKA 3.8 was applied to the pretreated features. Then the selected features from the first step of feature selection were used for a *Best Subset Selection* process where the best multiple linear regression (MLR) model was chosen on the basis of their internal leave-one-out (*LOO*) cross-validated squared correlation coefficient (Q^2) and externally cross-validated R^2_{pred} values obtained for the test set population.

The judgment of the model reliability and robustness of the final MLR model was also evaluated through the estimation of several other statistical parameters. For the MLR model, the squared correlation coefficient (R^2), standard error of estimate (SEE), predicted residual sum of square ($PRESS$), F -ratio, adjusted R^2 (R^2_A) values along with Q^2 were evaluated to analyze the model performance and predictability. The external predictability was judged by calculating the R^2_{pred} values provided by the model for the test set compounds. Additionally, the calculation of r_m^2 (Ojha and Roy, 2011), and Golbraikh and Tropsha (2002) matrices as well as the Y -scrambling test (Adhikari et al., 2017b; Adhikari et al., 2018b) were also done to estimate the robustness and reliability of the final model predictions (Adhikari et al., 2017b; Adhikari et al., 2018b).

4.1.6. Hologram quantitative structure-activity relationship (HQSAR) study

As far as drug design and development are concerned, molecular substructures or fragments of drug molecules play crucial roles in imparting biological potency (Banerjee et al., 2020). Therefore, pinpointing crucial molecular fragments (either good or bad) of any chemical entities may aid in enhancing both the potency and selectivity of these molecules (Banerjee et al., 2020). In this context, the application of fragment-based methods may provide fruitful outcomes and become popular over the years (Adhikari et al., 2022). The hologram-dependent QSAR (HQSAR) methodology applies the molecular hologram or molecular fragments with various lengths as the independent parameters that are correlated with the biological endpoint of molecules through partial least square (PLS) analysis (Adhikari et al., 2022). The HQSAR method, employing a chemometric technique, generates an expanded form of fingerprint encoding that encompasses various molecular fragments, including linear, cyclic, branched, and overlapping features present within the molecules under study.

To ensure the importance of such molecular substructures or fragments of these dataset compounds, in this study, several HQSAR models were constructed on the training set arylsulfonyl and alkylsulfonyl pyrrolidine derivatives (compound 1a-65a) with the help of SYBYL-X 2.0 software (<http://www.certara.com>) by using various combinations of fragment distinction features such as atomic number (A), bond type (B), hydrogen (H), atomic connections (C), chirality (Ch), and electron donor-acceptor groups (DA). The best HQSAR model among all these HQSAR models developed was selected depending on the highest Leave-One-Out (LOO) cross-validated R^2 (Q^2) as well as the lower standard error (SE) value. However, to assess its predictive capability

beyond the training data, the optimal HQSAR model underwent external validation using a separate test set of molecules, evaluating the R^2_{Pred} value for external predictability (Banerjee et al., 2020; Adhikari et al., 2022). This approach incorporates distinct molecular fingerprints of varied lengths (referred to as molecular holograms) as independent variables, aligning them with the specific biological properties of the compounds using the partial least square (PLS) method (Yu et al., 2015), thus enhancing the model's robustness and reliability in predicting the biological activities of novel compounds.

4.1.7. Linear discriminant analysis (LDA)

Linear discriminant analysis (LDA) has been established among the popular classification methods for feature selection and dimension reduction (Adhikari et al., 2015). The LDA model helps to distribute the data points in a binary group-based manner by applying linear formalism (Adhikari et al., 2021). Here, in this study, LDA was successfully utilized on these arylsulfonamido pyrrolidine derivatives for model building in order to point out crucial structural and physicochemical properties contributing to MMP-2 inhibitory properties. The average MMP-2 inhibitory activity of the dataset compounds was considered as the threshold value for binarizing these compounds into active class (activity equal to or higher than the threshold value) and inactive class (activity lower than the threshold value) (Adhikari et al., 2021) before the development of LDA model. Here, for constructing the LDA model through a stepwise fashion with the help of STATISTICA 7.1 software (<http://www.statsoft.com>), some parameters were used ($F = 4.0$ for inclusion; $F = 3.9$ for exclusion; tolerance = 0.001). As far as the LDA model was concerned, the model with a lower number of parameters with a lower Wilk's λ value was taken into consideration for model selection and further statistical validation (Adhikari et al., 2021). Regarding the LDA model validation, the receiver operating characteristic (ROC) curve analysis was carried out on both the discrimination set and the test set to evaluate the quality of discrimination capability of the developed LDA model (Adhikari et al., 2015). Further, the robustness of the LDA model was also considered for justification with the help of various classification-dependent validation parameters namely accuracy, sensitivity, specificity, precision, and F-measure values. On the other hand, several other validation parameters such as Wilk's λ parameter (Gálvez-Llompart et al., 2011), Matthew's correlation coefficient (MCC) (Matthews, 1975), squared Mahalanobis distance

(Matthews, 1975) and ROC graph (Fawcett, 2006) along with the area under the ROC (AUROC) were also taken into account to judge the performance of the LDA model (Adhikari et al., 2015). Moreover, the statistical property of sensitivity, specificity, precision, accuracy, *F1*-measure (Equations 4.7- 4.11) as well as Matthews's correlation coefficient (*MCC*) was computed as per Equation 4.12.

$$Sensitivity = \frac{TP}{(TP+FN)} \quad 4.7$$

$$Specificity = \frac{TN}{(TN+FP)} \quad 4.8$$

$$Precision = \frac{TP}{(TP+FP)} \quad 4.9$$

$$Accuracy = \frac{(TP+TN)}{(TP+FP+TN+FN)} \quad 4.10$$

$$F1 = \frac{2TP}{(2TP+FP+FN)} \quad 4.11$$

$$MCC = \frac{(TP \times TN) - (FP \times FN)}{\sqrt{(TP+FP)(TP+FN)(TN+FP)(TN+FN)}} \quad 4.12$$

Where *TP* is the true positive or the number of known 'active' compounds that appeared as 'active' in the model. The *FN* is the false negative which is known as an 'active' compound that appeared 'inactive'. The *TN* denotes the true negative which is the total number of known 'inactive' molecules predicted as 'inactive'. The *FP* is false positive which is the number of known 'inactive' predicted as 'active'.

Nevertheless, the ROC graph Euclidean distance (ROCED) and the corrected Fitness Function (FIT (λ)) (ROCFIT) (Perez-Garrido et al., 2011; Murcia-Soler et al., 2003) were also computed for validation purposes. The following formulae (Equations 4.13-4.15) were used for the construction of the LDA model.

$$d_i = \sqrt{(1 - Sensitivity)^2 + (1 - Specificity)^2} \quad 4.13$$

$$ROCED = (|d_1 - d_2| + 1)(d_1 + d_2)(d_2 + 1) \quad 4.14$$

$$ROCFIT = \frac{ROCED}{\lambda} \quad 4.15$$

Where $i = 1$ denotes the training set, $i = 2$ denotes the test set, and λ = Wilk's parameter. The performance of the LDA-QSAR model was judged by the determination of the area under the receiver operating characteristic curve (AUROC) (Adhikari et al., 2018; Fawcett, 2006).

4.1.8. Bayesian classification study

The Bayesian classification study employs Bayes' theorem to predict probabilities of sufficient data (Adhikari et al., 2021; Chen et al., 2011). Here in this study, the fragment-dependent Bayesian classification modeling was carried out with the help of the '*Create Bayesian Model*' protocol incorporated in DS 3.0 software (<http://www.accelrys.com>) utilizing '*default settings*' to judge the performance of internal as well as external cross-validation (Banerjee et al., 2023). The fundamental molecular properties namely hydrophobicity (*AlogP*), molecular fractional polar surface area (*MFPSA*), number of rings (*nR*), molecular weight (*MW*), number of hydrogen bond acceptors (*nHBA*), number of hydrogen bond donors (*nHBD*), number of aromatic rings (*nAR*) along with extended connectivity fingerprint feature of diameter 6 (*ECFP_6*) were employed to build the Bayesian classification model. The developed model was subjected to internal and external validation by judging the predictability by analyzing the receiver operating characteristics (ROC) as well as statistical parameters namely the sensitivity (*Se*), specificity (*Sp*), precision (*Pr*), and accuracy (*Acc*) on both the training and test set (Adhikari et al., 2021, Banerjee et al., 2023).

4.1.9. 3D-QSAR (CoMFA and CoMSIA) model development

The application and evaluation of several three-dimensional (3D) field-dependent molecular properties, such as electrostatic, steric, hydrophobic, hydrogen bond acceptor, and hydrogen bond donor fields toward a particular biomolecular target, is extremely important in terms of drug designing and discovery (Adhikari et al., 2017b; Jha et al., 2018). Here, in order to gain insight into the crucial 3D molecular fields needed to modify the MMP-2 inhibition of these drugs, two field-dependent 3D-QSAR experiments were conducted: comparative molecular field analysis (CoMFA) and comparative molecular similarity indices analysis (CoMSIA) (Adhikari et al., 2017b; Adhikari et al., 2018a; Jha et al., 2018). Regarding these types of field-dependent 3D-QSAR investigations, these molecules' alignment in 3D space is essential (Adhikari et al., 2017b). Consequently, the development of 3D-QSAR (CoMFA and CoMSIA) models using the Sybyl-X v2.0 software was accomplished here by means of the molecular docking-dependent alignment of all these molecules in 3D space (<http://www.certara.com>). Here, using the previously published techniques, the CoMFA and CoMSIA molecular interaction field parameters were calculated in a three-dimensional cubic grid (Adhikari et al., 2017b; Adhikari et al., 2018a; Jha et al., 2018). The Tripos force field was used to calculate the van der Waals and Coulombic parameters. A +1

charged sp^3 hybridized carbon atom was used as the probe atom while calculating the steric and electrostatic fields. Moreover, as the independent parameters for the creation of the CoMFA model, the Coulomb potential and Lennard-Jones technique were used to calculate the field interaction energies (Adhikari et al., 2017b; Jha et al., 2018). However, assessing the degree of similarity between these molecules is made easier by the CoMSIA study. A Gaussian function with a bell shape was used to calculate the similarity indices between molecules and the probe atom (Adhikari et al., 2017b). The CoMSIA model investigates additional important similarity fields, such as hydrophobic, hydrogen bond donor, and hydrogen bond acceptor fields, in addition to the steric and electrostatic fields. These fields are important because they correlate with the MMP-2 inhibitory property of these proprietary compounds. The CoMSIA independent parameters were calculated using Sybyl-X v2.0 software with the aid of a methyl probe atom with the corresponding particular properties such as Charge: +1; hydrophobicity: +1; hydrogen bond acceptor: +1; hydrogen bond donor: +1, at each lattice and grid spacing of 2\AA (<http://www.certara.com>). Then, using internal validation parameters (such *SEE*, F-ratio, R^2 , Q^2 , R^2_{10-CV} , and R^2_{20-BS}) and external validation parameters, the PLS analysis was carried out to create statistically reliable CoMFA and CoMSIA models (namely R^2_{pred}) (Adhikari et al., 2017b; Adhikari et al., 2018a; Jha et al., 2018). Additionally, Y-scrambled testing was performed on each of these models to assess the robustness of the CoMFA and the CoMSIA.

4.1.10. Molecular dynamics (MD) simulation analysis study

Compounds 29b and 22b, which are the most and least active compounds complexed with MMP-2 (PDB ID: 1HOV), had their docked conformations analyzed using the Desmond module of the Schrodinger Suite for 200 ns, with two runs for each molecule (<https://www.schrodinger.com>). The complexes were generated using the Schrodinger Maestro v12.1 software's Protein Preparation program prior to the MD simulation investigation (<https://www.schrodinger.com>). The preparation of the protein-ligand complexes for the simulation study followed a similar approach to that employed in the molecular docking study. The simulation study's system was created using the System Builder application from the v12.1 software (<https://www.schrodinger.com>). For a periodic boundary, an orthorhombic system with a buffer distance of 10\AA was constructed using the *TIP3P* water model and the OPLS2005 forcefield. While Na^+ and Cl^- ions were added to the system to create isotonicity (a NaCl concentration of 0.15 M), Na^+ counter ions were utilized to

neutralize the system (Banerjee et al., 2023). With the use of the RESPA integrator and a 2 fs timestep, a system relaxation procedure was chosen prior to starting the simulation study. For the relaxation protocol, the Langevin thermostat and Langevin barostat were employed with an isotropic coupling mechanism (Grønbech-Jensen and Farago, 2014). In addition, the *NPT* ensemble was used for the 200 ns MD simulation investigation of each of the complexes twice each employing the Desmond application of the Schrodinger suite (<https://www.schrodinger.com>) at 310.15 K (37°C) temperature and 1.01325 atm pressure (Guttikonda et al., 2015).

4.1.11. Calculation of Molecular Mechanics Generalised Born and Surface Area (MM/GBSA)

One popular technique for determining the free binding energy of protein-ligand complexes is the molecular mechanics generalized born and surface area (MM/GBSA) analysis (Rizzo et al., 2004; Genheden and Ryde, 2015). The binding free energy value ($\Delta G_{\text{Binding}}$) of the MMGBSA is determined by deducting the optimized energy of the protein-ligand complex (E_{Complex}) from the optimized energy of the free ligand (E_{Ligand}) and the optimized free protein (E_{Protein}). The following is the equation (Equation 4.16) for the $\Delta G_{\text{Binding}}$ calculation.

$$\Delta G_{\text{binding}} = E_{\text{complex}} - (E_{\text{protein}} + E_{\text{ligand}}) \quad 4.16$$

Here, the $\Delta G_{\text{Binding}}$ of each of the 200 ns simulations of our *in-house* MMP-2 inhibitors was calculated using the *thermal_mmgsa.py* script from the Schrodinger suite's Prime tool (<https://www.schrodinger.com>) (two 200 ns simulations performed for each of the complexes).

4.1.12. Free energy landscape (FEL) analysis

By applying the thermodynamics methodology, the free energy landscape (FEL) analysis allows one to visualize the stable conformations of a protein structure in terms of Gibb's free energy. This approach makes protein conformation mapping and energy levels possible (Papaleo et al., 2009). The simulation studies utilized for each of the complexes with the best and least active compounds (MMP-2-Compound 29b and MMP-2-Compound 22b complexes) (Table 5.2, Chapter 5), the FEL computation, the first two main components (PC1 and PC2) were employed. The *g_sham* script of Gromacs v2020.6 (<https://www.gromacs.org>; Berendsen et al., 1995) was used to calculate Gibb's free energy. The PC1 and PC2 were also calculated using the Boltzmann inversion approach for a multi-dimensional histogram.

4.1.13. Dynamic cross-correlation map (DCCM) and principal component analysis (PCA)

The MD simulation study's cross-correlation matrix of C- α chain displacement revealed intricate motions of protein residues that are both correlated and anti-correlated (Aier et al., 2016). The protein-atom fluctuation-based covariance matrix generation is calculated as part of the principal component analysis (PCA) of the MD simulation study. By diagonalizing the covariance matrix, the eigenvalues and eigenvectors provided the relevant information on the correlated motion of the protein atoms. Here, the Bio3D module (Grant et al., 2006) in RStudio (<https://github.com/rstudio/rstudio>) was used to carry out each simulation for the MMP-2 along with the most and least active complexes.

4.1.14. Probability density function (PDF) analysis

The probability density function (PDF) for the MD simulation studies is based on the kernel density estimate (KDE) and evaluates the frequency of likelihood of a trajectory event. Here, the Geo Measures v0.9 (Kagami et al., 2020) PyMol plug-in was utilized for the PDF analysis using the free and open-source PyMol software (<https://github.com/schrodinger/pymol-open-source>) for every simulation study.

4.2. Synthetic Organic Chemistry

All starting materials D(-) glutamic acid and biphenylsulfonyl chlorides were commercially available and hence these compounds were utilized without further purification. Precoated plates containing silica gel F254 from Merck Millipore Co., USA were utilized for thin layer chromatography (TLC) to monitor every reaction.

4.2.1. Synthesis procedure of biphenylsulfonyl D(-) glutamic acid (2)

In a 250 ml conical flask, D(-) glutamic acid was taken. 2(N) sodium hydroxide was added dropwise till the D(-) glutamic acid completely dissolved into it. The reaction was carried out in a just alkaline condition at a pH of 8-9. The biphenylsulfonyl chlorides were taken in small portions and added to the alkaline solution individually with continuous stirring at 80°C with a magnetic stirrer. 2(N) sodium hydroxide solution was added from time to time to maintain the alkalinity of the solution. The reaction was carried out until a homogenous clear solution was obtained (Adhikari et al., 2016; Mukherjee et al., 2017). Completion of the reaction was confirmed by

detection in thin layer chromatography (TLC) as mentioned previously. After cooling for a while at room temperature, the mixture was filtered to remove any remaining undissolved solids. The filtrate obtained was acidified with conc. hydrochloric acid after the solution was saturated by using sodium chloride. Then, the solution was extracted three times using 50 ml of ethyl acetate each. After that, the organic layer was carefully cleaned three times using 10 ml of brine solution each time. The organic layer was kept overnight under anhydrous sodium sulfate. After distillation of ethyl acetate, the respective substituted biphenylsulfonyl D(-) glutamic acids were individually obtained as crude solids. These solid products were separately purified by recrystallization with hot water. Each step of the synthetic scheme has been depicted in *Scheme 4.1*.

4.2.2. Synthesis procedure of biphenylsulfonyl D(-) oxopyrrolidine carboxylic acid (3)

In a 100 ml round bottom flask, 2N-substituted biphenylsulfonyl D(-) glutamic acids were separately refluxed by using acetyl chloride in a water bath for 2-3 hr (Adhikari et al., 2016; Mukherjee et al., 2017). The completion of the reaction was determined by using a TLC plate. After cooling to room temperature, the reaction mixture was transferred into crushed ice. To obtain the intended results, the resulting product was filtered and thoroughly washed. Finally, the synthesized compound biphenylsulfonyl D(-) oxopyrrolidine carboxylic acid (*Scheme 4.1*) was recrystallized with water.

4.2.3. Synthesis procedure of 5-N-Substituted 2-(substituted biphenylsulfonyl) D(-) glutamines (4a-4t)

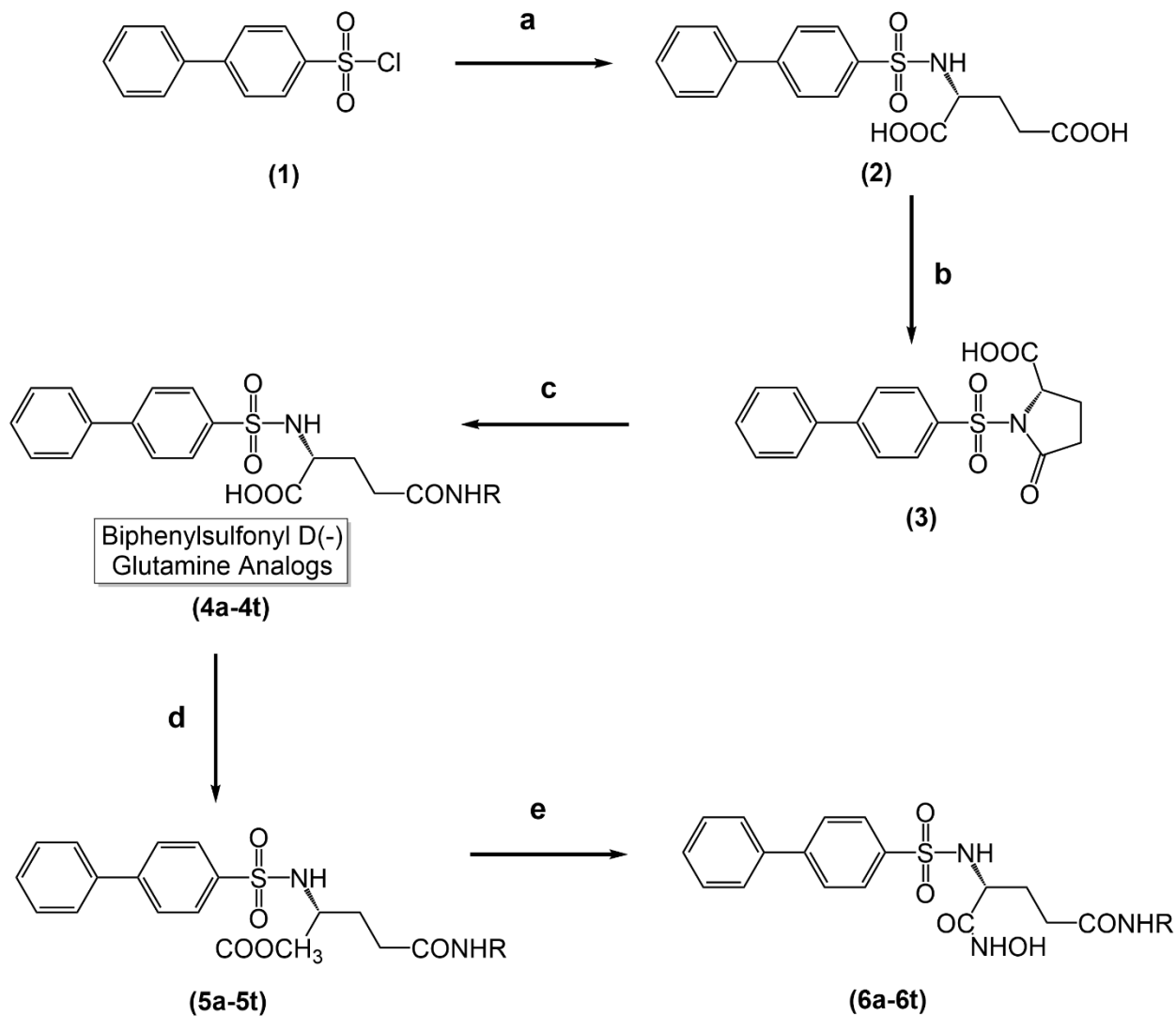
The substituted biphenylsulfonyl oxopyrrolidine carboxylic acid (*Scheme 4.1*) was suspended in 20 ml water. Excess amines were added individually with a gram mol ratio of 1:2.5 into these suspensions. After being left at room temperature overnight, the reaction mixture was heated in a water bath to eliminate any remaining amines. Then the mixture was cooled and 6(N) hydrochloric acid was added to an ice bath. To get the biphenylsulfonyl D(-) glutamine analogs, the precipitated solid product was filtered off, rinsed thoroughly with cold water, and then recrystallized with 70% ethanol (Adhikari et al., 2016; Mukherjee et al., 2017).

4.2.4. Synthesis procedure of methyl ester derivatives of 5-N-Substituted 2-(substituted biphenylsulfonyl) D(-) glutamines (5a-5t)

The biphenylsulfonyl D(-) glutamine analogs were individually taken in an iodine flask and added dry methanol. Then thionyl chloride was added to the solution in an ice-cold condition. The reaction mixture was kept for a continuous stirrer by magnetic stirrer for about 2-3 hr. Remove the excess methanol and unreacted thionyl chloride by heating the reaction mixture in the water bath. Then, 50 ml of ethyl acetate was added and dissolved the final product. The solution was then washed off by the 1(N) sodium bicarbonate solution and separated the ethyl acetate solution by using a separating funnel and kept overnight by adding sodium sulfate. Filter the ethyl acetate solution and distill the solution mixture to remove the ethyl acetate and dry the ester derivatives of 5-N-Substituted 2-(substituted biphenylsulfonyl) D(-) glutamines (*Scheme 4.1*) completely and lastly recrystallized with 70% ethanol. The completion of the reaction was determined by using a TLC plate.

4.2.5. Synthesis procedure of hydroxamate derivatives of 5-N-Substituted 2-(substituted biphenylsulfonyl) D(-) glutamines (6a-6t)

The ester derivatives of 5-N-Substituted 2-(substituted biphenylsulfonyl) D(-) glutamines were individually taken in an RB flask and anhydrous methanol to mix the compound completely. Then 50% aqueous hydroxyl amine was added in a gram-mole ratio of 1:18 into the solution mixture. 10% sodium hydroxide solution was added from time to time to maintain the alkalinity of the solution. Then the reaction mixture was kept stirring for approximately 24 hr by using a magnetic stirrer. The 2(N) hydrochloric acid was added after the reaction and kept in a cool dry place. Then filter the final desired hydroxamate derivatives of 5-N-Substituted 2-(substituted biphenylsulfonyl) D(-) glutamines (*Scheme 4.1*) and wash with diethyl ether and lastly recrystallized with 70% ethanol.



Scheme 4.1. Reagents and conditions: (a) i. D(-) glutamic acid ii. 2(N) NaOH; (b) acetyl chloride; (c) i. RNH₂ ii. 6(N) HCl (d) i. anhydrous methanol ii. Thionyl chloride; (e) i. 50% aqueous hydroxyl amine ii. anhydrous methanol iii. 10% NaOH solution.

4.3. Characterization of the synthesized molecules

The melting point of these final glutamine compounds was estimated by using a capillary melting point apparatus and Mel-Temp Electrothermal apparatus. These compounds were verified further in CTRONICS, a digital melting point apparatus.

High-resolution mass spectrometry (HRMS) serves as a fundamental tool for characterizing synthesized molecules within this research. The procedure involves multiple crucial steps,

commencing with the purification of samples and their dissolution in a suitable solvent. Employing a precisely calibrated high-resolution mass spectrometer, ionization techniques such as electrospray ionization (ESI) or atmospheric pressure chemical ionization (APCI) are utilized. The subsequent analysis of the resultant mass spectra provides accurate molecular weight determination and offers insights into the structural composition of the compounds. Interpretation of the data involves peak identification and fragmentation analysis, contributing to the confirmation of proposed structures and the detection of potential impurities. It's vital to integrate the outcomes of HRMS with complementary analytical methods to comprehensively understand the molecules' structural characteristics.

Again, proton nuclear magnetic resonance (^1H NMR) and carbon-13 nuclear magnetic resonance (^{13}C NMR) spectroscopy stand as fundamental techniques within this research for characterizing synthesized molecules. The process entails sample preparation involving the dissolution of the compound in a deuterated solvent to ensure cleanliness and optimal analysis. Employing a meticulously calibrated NMR spectrometer, both ^1H and ^{13}C NMR spectra are obtained, illuminating distinct peaks that represent varied hydrogen and carbon environments within the synthesized molecules. Detailed analysis of these peaks contributes to the identification of functional groups, molecular connectivity, and structural attributes, pivotal in unveiling the compound's overarching configuration. Validation of the proposed structure is carried out by cross-referencing obtained spectra with established databases. A comprehensive documentation of these spectra and their comprehensive analysis constitutes an integral component of this work, offering a detailed characterization of the synthesized compounds. High-resolution mass spectroscopy was carried out on Xevo G2-XS QToF mass spectrometry system (Waters Corporation, MA, USA) in positive ESI mode operated by Waters Informatics software. Nonetheless, ^1H and ^{13}C NMR spectra were performed in DMSO- d_6 solvent using Nuclear Magnetic Resonance (NMR) Spectrophotometer High Performance-400 MHz (Bruker Biospin, Switzerland).

4.4. Biological Study

The synthesized final compounds were screened for different MMP inhibition as well as cytotoxicity against different cancer cell lines (such as K562, A549, U87MG, HT1080, and HEK-293). Moreover, an enzyme inhibition assay was performed on MMP-2, MMP-9, and MMP-8

enzymes. Additionally, MMP-2 enzyme assay, cell cycle assay, apoptosis analysis in the K562 cell line, in vitro tube formation assay (Angiogenesis Assay), and DNA deformation assay by DAPI staining were performed to determine the efficacy of synthesized molecules.

4.4.1. Enzyme inhibition assay

MMP-2 and MMP-9 inhibitory assays of these compounds were carried out as per our earlier reported methods (Adhikari et al., 2016; Mukherjee et al., 2017) following the protocols provided by Enzo Life Science International, USA. The concentration of the substrate was measured with the help of absorbance at 410 nm in a microplate photometer of Thermo Scientific Multiscan FC, USA. The enzyme reactions (100 μ l final volume) of six concentrations of inhibitor individually were carried out for 1 hr at 37°C. After the addition of the proper volume of substrate (10 μ l) to each well containing different concentrations of inhibitors along with the control, the absorbance of each well was recorded at 1 min intervals for about 30 min. Optical density (OD) vs time for each sample was plotted in order to obtain the reaction velocity (V) in OD/min. The percentage of residual activity for each compound was calculated according to *Equation 3.17*.

$$\% \text{ of remaining activity} = \frac{\text{Reaction velocity (V) in presence of inhibitor}}{\text{reaction velocity (V) of control}} \times 100 \quad 3.17$$

The IC₅₀ values for each compound were evaluated by semi-logarithmic dose-response plots (Graph Pad Prism 5.0 for Windows, Graph Pad Software Inc., San Diego, California, USA, 2007) (Adhikari et al., 2016; Mukherjee et al., 2017).

4.4.2. Cell lines

Human cancer cell line, K562 (chronic myeloid leukemia cell line), A549 (non-small cell lung cancer cell line), U87MG (human glioblastoma cell line), and HT1080 (fibrosarcoma cell line) were collected from National Centre for Cell Science (NCCS), Pune, India. Additionally, normal healthy human embryonic kidney cell line HEK-293 was isolated.

The cell lines A549 was grown in Dulbecco's Modified Eagle Medium (DMEM) (Gibco) supplemented with 10% heat-inactivated FBS (Invitrogen, USA) and Penicillin–Streptomycin (100 IU ml⁻¹ to 100 mg ml⁻¹) (Adhikari et al., 2016; Mukherjee et al., 2017). Likewise, the K562 was grown in RPMI-1640 media. This cell line was subsequently maintained at carefully controlled conditions (37°C temperature with 5% CO₂ in a humidified incubator). Adherent cell

(A549) was harvested with 0.025% trypsin and 0.52 mM EDTA in phosphate buffer saline, plated at requisite cell numbers, and allowed to stick to a minimum of around 24 hours before treatment. Non-small cell lung cancer cells (A549) in Dulbecco's Modified Eagle Medium/ Nutrient Mixture F-12 Ham (DMEM/F12, 1:1 mixture, Himedia Laboratories Pvt. Ltd., Mumbai, India) supplemented with 10% heat-inactivated fetal bovine serum (Himedia Laboratories Pvt. Ltd., Mumbai, India) and 1 % of Antibiotic solution (10000 U penicillin and 10 mg streptomycin per ml, Himedia Laboratories Pvt. Ltd., Mumbai, India). The cells were grown at 37°C in a humidified environment with 5% CO₂. All synthesized compounds were stored as stock solutions in DMSO at a concentration of 100 mM. Moreover, the U87MG human glioblastoma cell line is typically cultured by thawing the frozen cells in a 37°C water bath, then resuspending them in Dulbecco's Modified Eagle's Medium (DMEM) or Eagle's Minimum Essential Medium (EMEM) supplemented with 10% fetal bovine serum (FBS). The cells are seeded into culture vessels at a suitable density and maintained in a 37°C incubator with 5% CO₂. Regular medium changes every 2-3 days, and subculturing at 80-90% confluency ensures healthy growth. For passaging, cells are detached using trypsin-EDTA, neutralized, and transferred to new flasks or plates. Quality control checks for mycoplasma contamination and authentication tests are periodically performed to ensure the cells' identity and purity. Again, HT1080 human fibrosarcoma cell line is grown by rapidly freezing cells in a 37°C water bath, followed by dilution in Dulbecco's Modified Eagle's Medium (DMEM) or Minimum Essential Medium (MEM) containing 10% foetal bovine serum (FBS). Seeded at an appropriate density in culture vessels, these cells are incubated at 37°C with 5% CO₂. Regular medium changes every 2-3 days and subculturing at 80-90% confluency facilitates growth. For passaging, cells are detached using trypsin-EDTA, neutralized, and transferred to new flasks or plates. Routine checks for mycoplasma contamination and authentication tests are performed to ensure the cells' identity and purity are maintained. HEK-293 (Human Embryonic Kidney 293) cells are also cultured by rapidly thawing in a 37°C water bath, then diluting in Dulbecco's Modified Eagle Medium (DMEM) with 10% fetal bovine serum (FBS). Seeded into culture vessels at a suitable density, cells are incubated at 37°C with 5% CO₂. Medium changes every 2-3 days and subculturing at 80-90% confluency supports growth. For passaging, cells are detached using trypsin-EDTA, neutralized, and transferred to new flasks or plates. Routine checks for mycoplasma contamination and authentication tests are conducted to ensure the cells' identity and purity are maintained.

4.4.3. Cytotoxicity assay

The MTT assay was used to determine the cytotoxicity. Before the individual chemicals were added, the cells were first seeded into 96-well plates at a density of 5000 cells per well and left to adhere for 18 to 24 hours. The final compounds (diluted with DMEM or RPMI-1640 media) were added in different concentrations and kept for 48 hr. 10 ml of MTT solution (10 mg ml⁻¹) was added to each well before 4 hr at the end of incubation. Following a 4-hour incubation period, 100 μ l of DMSO was used to dissolve the formazan crystal. The microplate photometer (Thermo Scientific Multiscan FC, USA) was used to measure the absorbance at 570 nm. Since the control contained 0.1 percent DMSO as the solvent control, it was assumed to be 100% viable for estimating the viability of the cells. The IC₅₀ value was determined as the concentration that reduced the cell viability by 50% (Adhikari et al., 2016; Mukherjee et al.; 2017).

4.4.4. MMP-2 expression analysis

K562 cells were grown into 6-well culture plates (about 2x10⁴ cells per well) with phenol-free RPMI-1650 medium (HIMedia Laboratories Pvt. Ltd. in Mumbai, India) containing 10% FBS and left for 24 hours. Monensin sodium (1 μ M) (Sisco Research Laboratories Pvt. Ltd., Mumbai, India) also was added to K562 cells (1 x 10⁴ cells/ml) before they were plated. Compounds at IC₅₀ dose were then added to the cells (apart from the untreated control). Because the synthesized compounds were poorly soluble in cell culture media (phenol-free RPMI-1650) and hydrophobic by nature, 0.1% tissue culture grade DMSO was added into the cell culture medium while preparing the drug solution separately. The control groups are treated with solvent only (0.1% DMSO in phenol-free RPMI-1650 medium). Monensin sodium increases the number of intracellular proteins, enhancing the ability to differentiate between autofluorescence-induced background signals and positive cells (Oviedo-Orta et al., 2008). Following a 48-hour treatment period, cells were collected, twice cleaned in a cold wash buffer, and then fixed for 20 minutes using 0.5 mL of fixation solution. Bovine serum albumin (BSA) (Sisco Research Laboratories Pvt. Ltd., Mumbai, India) at 1% in PBS (pH 7.4) made up the wash buffer. 0.4% paraformaldehyde solution in PBS (pH 7.4) was the fixing solution. After that, the cells were subjected to a blocking solution (5% BSA in PBS) for an hour after being twice washed in wash buffer-saponin solution (0.1% saponin in wash buffer). The suppliers of paraformaldehyde and saponin were HIMedia Laboratories Pvt. Ltd. in Mumbai, India. After two rounds of washing, the cells were treated with anti-MMP2 primary antibody

(1:250 dilutions) overnight. Following washing, cells were exposed to FITC-labelled secondary antibodies at 1:250 dilutions for a duration of 1 hr. The secondary antibody conjugated with FITC and the anti-MMP2 antibody was obtained from Santa Cruz Biotechnology Inc. (CA, USA). Following one wash, the cells were examined for MMP2 expression by flow cytometry (BD-FACS) (Oviedo-Orta et al., 2008; Dutta et al., 2019; Datta et al., 2022).

4.4.5. Apoptosis analysis in K562 cell line

The apoptosis assay was done by using an annexin V-FITC apoptosis detection kit which was purchased from Calbiochem, Germany. Briefly, the K562 cells ($\sim 2 \times 10^4$) were treated with synthesized novel molecules for 72 hr. Cells were harvested and washed with phosphate buffer saline (PBS). The harvested cells were incubated with annexin V-FITC (100 ng/ml) and PI (50 mg/ml) at room temp for 15 min in the dark and analyzed using a FACS Calibur (BD Bioscience) taking a minimum of 10,000 cells in each sample.

4.4.6. Cell cycle assay

Briefly, $\sim 2 \times 10^4$ K562 cells were seeded and treated with the synthesized novel molecules for 72 hr. Cells were recovered, washed twice with cold PBS, and fixed in 70% chilled ethanol. Cells were washed twice in PBS, and incubated for 1 hr. at room temp with 100 mg/ml RNase A. After that 50 mg/ml PI was added and cells were incubated for 15 min in the dark and were analyzed using a FACS Calibur flow cytometer (BD Bioscience). Ten thousand events were analyzed for each sample using the appropriate gate to select a single cell population and the same gate was used for all these samples.

4.4.7. In vitro tube formation assay (Angiogenesis Assay)

The *in vitro* morphogenesis experiment was carried out in the presence of IC_{50} concentrations of chosen compounds. Cells after 3-4 passages were used for the experiment. In a nutshell, a 12-microwell plate was carefully filled with 200 μ L /well of Cultrex at 4°C using a pipette after being pre-chilled at -20°C. The cells were trypsinized and then suspended in 100 μ L of complete media in the absence or presence of inhibitors of IC_{50} values. Following the polymerization of the basement membrane matrix for 1 h at 37°C, cells were carefully stacked on top of the polymerized basement membrane matrix. The arrangement of the cells was evaluated under a microscope after 72 hours of incubation on Cultrex. Using the Angiogenesis tool and ImageJ software, the number

of meshes, tubes, branches, and nodes were counted as a direct measurement for tubulogenic efficiency. For statistical analysis, two wells were seeded for each test inhibitor.

4.4.8. DNA deformation assay by DAPI staining

Six-well culture plates were populated with K562 cells (about 2×10^4), which were left to grow for 24 hours. Then cells were treated with compounds at IC_{50} dose for 48 hours (except the control group). The control groups are treated with solvent only (0.1% DMSO in phenol-free RPMI-1650 medium). Cells were taken from both the control and treated groups (compounds at IC_{50} dose) and fixed for one hour using 70% cooled ethanol. They were then rinsed twice with PBS and stained with 10 μ M DAPI for 30 minutes. Following that, the fixed cells were examined under a fluorescent microscope (Leica Fluorescence microscope, Germany) to see the nuclear morphology of k562 cells (Das et al., 2022; Mukherjee et al., 2017).

4.5. Statistical analysis

All these data reported were the arithmetic mean of data of independent experiments performed in triplicate where each group was six in number. Results were expressed as mean \pm SD (standard deviation) unless otherwise stated. Statistical analysis was made by the one-way analysis of variance (ANOVA) with LSD post-hoc test using SPSS 16 software. Statistical significance was considered as P-value < 0.001 .

Chapter 5

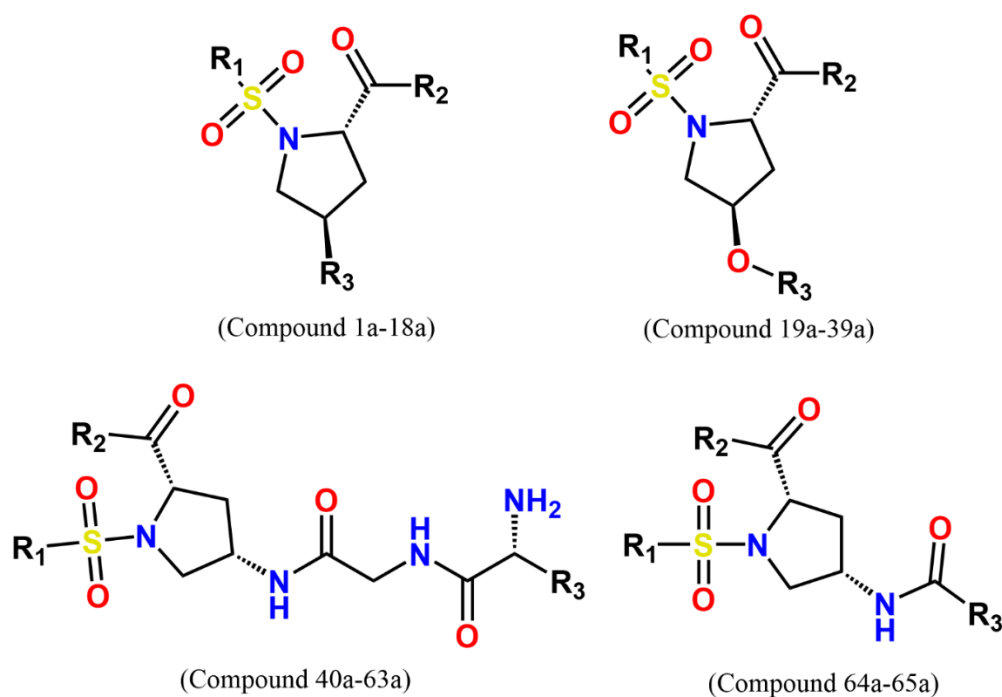
RESULTS AND DISCUSSIONS

The outcomes of the research have been divided into three different parts i.e., (i) Part A, (ii) Part B, and (iii) Part C. Part A deals with the designing of the arylsulfonamide-containing hydroxamate-based glutamine analogs with the help of molecular modeling techniques. Part B deals with the synthesis and characterization of the screened molecules, and Part C discusses the biological study associated with the activities of compounds and further molecular modeling studies to accelerate the development of potential MMP-2 inhibitors for anticancer drug development.

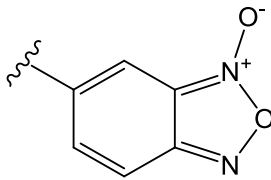
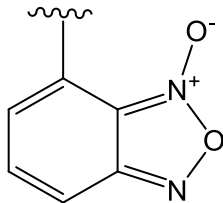
Part A

5.1. Molecular Modeling study

In this research work, two different molecular modeling study was conducted on different datasets of molecules. One computation study was conducted on 65 sulfonyl pyrrolidine-based promising MMP-2 inhibitors (compound 1a-65a) (**Table 5.1**) and data curation was done successfully as all the enzyme inhibition data of these molecules were collected from the same laboratory. Several molecular modeling approaches such as multiple linear regression (MLR), hologram QSAR (HQSAR) study, linear discriminant analysis (LDA), bayesian classification modeling, and comparative molecular similarity index analysis (CoMSIA) were conducted on this dataset and all the results are discussed in this chapter.

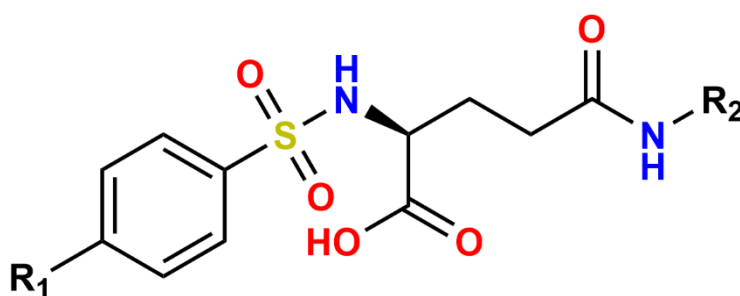
Table 5.1. Sulfonyl pyrrolidine derivatives as effective MMP-2 inhibitors

Compound	R_1	R_2	R_3	MMP-2 IC_{50} (nM)	pIC_{50}
1a	<i>p</i> -Tosyl	NHOH	O-(CH ₂) ₂ -O	3	8.523
2a	<i>p</i> -Tosyl	NHOH	O-(CH ₂) ₃ -O	6	8.222
3a	Ph	NHOH	O-(CH ₂) ₂ -O	8	8.097
4a	<i>p</i> -Tosyl	NHOH	O-(CH ₂) ₄ -O	8	8.097
5a	Ph	NHOH	O-(CH ₂) ₃ -O	11	7.959
6a	Ph	NHOH	O-(CH ₂) ₄ -O	12	7.921
7a	<i>p</i> -Tosyl	OMe	OH	100	7
8a	<i>p</i> -Tosyl	OMe	O-(CH ₂) ₂ -O	100	7
9a	Ph	OMe	O-(CH ₂) ₂ -O	200	6.699
10a	<i>p</i> -Tosyl	OMe	O-(CH ₂) ₃ -O	200	6.699
11a	<i>p</i> -Tosyl	OMe	O-(CH ₂) ₄ -O	300	6.523
12a	<i>p</i> -Tosyl	OMe	C=O	400	6.398
13a	Ph	OMe	OH	800	6.097
14a	Ph	OMe	O-(CH ₂) ₃ -O	1,100	5.959
15a	Ph	OMe	O-(CH ₂) ₄ -O	1,500	5.824
16a	Ph	OMe	C=O	2,000	5.699
17a	Me	OMe	OH	7,100	5.149
18a	Me	OMe	C=O	9,500	5.022
19a	Ph	NHOH	H	4	8.398
20a	<i>p</i> -Tosyl	OMe	<i>p</i> -TosylSO ₂	7	8.155
21a	Ph	OMe	PhSO ₂	10	8
22a	Me	NHOH	H	20	7.699
23a	Ph	OMe	<i>p</i> -TosylSO ₂	40	7.398
24a	<i>p</i> -Tosyl	OMe	(<i>E</i>)PhCH=CHCO	40	7.398
25a	<i>p</i> -Tosyl	OMe	PhSO ₂	50	7.301
26a	Ph	OMe	(<i>E</i>)PhCH=CHCO	90	7.046
27a	Me	OMe	<i>p</i> -TosylSO ₂	200	6.699

28a	<i>p</i> -Tosyl	OMe	CH ₃ SO ₂	200	6.699
29a	Me	OMe	(E)PhCH=CHCO	500	6.301
30a	Me	OMe	PhSO ₂	700	6.155
31a	Ph	OMe	CH ₃ SO ₂	1,300	5.886
32a	Me	OMe	<i>p</i> -ClPhCO	1,500	5.824
33a	<i>p</i> -Tosyl	OMe	<i>p</i> -ClPhCO	2,200	5.658
34a	Ph	OMe	<i>p</i> -ClPhCO	2,700	5.569
35a	<i>p</i> -Tosyl	OMe	PhCO	3,200	5.495
36a	Ph	OMe	PhCO	3,500	5.456
37a	Me	OMe	PhCO	5,200	5.284
38a	Me	OMe	CH ₃ SO ₂	8,900	5.051
39a	<i>p</i> -Tosyl	NHOH	H	2	8.699
40a	<i>p</i> -ClPh	NHOH	<i>i</i> -But	270	6.569
41a	<i>p</i> -ClPh	NHOH	Bnz	430	6.367
42a	<i>p</i> -ClPh	NHOH	CH ₂ CH ₂ SCH ₃	460	6.337
43a	<i>p</i> -OMePh	NHOH	<i>i</i> -But	520	6.284
44a	<i>p</i> -OMePh	NHOH	Bnz	720	6.143
45a	<i>p</i> -OMePh	NHOH	CH ₂ CH ₂ SCH ₃	760	6.119
46a	<i>p</i> -MePh	NHOH	<i>i</i> -But	870	6.06
47a	<i>p</i> -MePh	NHOH	Bnz	980	6.009
48a	<i>p</i> -MePh	NHOH	CH ₂ CH ₂ SCH ₃	1,030	5.987
49a	<i>p</i> -ClPh	NHOH	CH(CH ₃)CH ₂ CH ₃	1,280	5.893
50a	Ph	NHOH	<i>i</i> -But	1,520	5.818
51a	<i>p</i> -ClPh	NHOH	<i>i</i> -Pr	1,810	5.742
52a	<i>p</i> -OMePh	NHOH	CH(CH ₃)CH ₂ CH ₃	1,940	5.712
53a	<i>p</i> -MePh	NHOH	CH(CH ₃)CH ₂ CH ₃	2,050	5.688
54a	Ph	NHOH	Bnz	2,070	5.684
55a	Ph	NHOH	CH ₂ CH ₂ SCH ₃	2,320	5.635
56a	<i>p</i> -OMePh	NHOH	<i>i</i> -Pr	2,710	5.567
57a	<i>p</i> -MePh	NHOH	<i>i</i> -Pr	2,950	5.53
58a	<i>p</i> -ClPh	NHOH	Me	3,360	5.474
59a	<i>p</i> -OMePh	NHOH	Me	4,190	5.378
60a	<i>p</i> -MePh	NHOH	Me	4,360	5.361
61a	Ph	NHOH	CH(CH ₃)CH ₂ CH ₃	5,210	5.283
62a	Ph	NHOH	<i>i</i> -Pr	5,760	5.24
63a	Ph	NHOH	Me	7,430	5.129
64a	PhOPh	NHOH		102	6.991
65a	PhOPh	NHOH		182	6.74

For structure-based drug designing studies, a total of 32 *in house* arylsulfonyl L(+) glutamine derivatives with MMP-2 inhibitory activity (compounds 1b-32b) (**Table 5.2**) were subjected to another computational analysis. The computational study was done on this dataset of molecules concerning molecular docking-based 2D-QSAR analysis, and the 3D-QSAR study namely comparative molecular field analysis (CoMFA) and comparative molecular similarity index analysis (CoMSIA) techniques to identify the important structural parameters from these arylsulfonyl L(+) glutamine derivatives required for the higher MMP-2 inhibitory activity discussed in this chapter.

Table 5.2. *In house* Arylsulfonyl-based L(+) glutamine analogs



(Compound 1b-32b)

<i>Compound</i>	<i>R₁</i>	<i>R₂</i>	<i>MMP-2 IC₅₀ (nM)</i>	<i>pIC₅₀</i>
1b	Ph	<i>n</i> -Hex	103	6.987
2b*	Ph	β-PhEt	123	6.910
3b	Ph	<i>n</i> -Pr	177	6.752
4b	Ph	<i>t</i> -But	186	6.730
5b	Ph	<i>p</i> -OMeBnz	193	6.714
6b	Ph	Et	203	6.693
7b	Ph	<i>i</i> -Pr	208	6.682
8b	Ph	<i>p</i> -ClBnz	263	6.580
9b*	Ph	<i>p</i> -NO ₂ Bnz	291	6.536
10b	Ph	<i>c</i> -Hex	30	7.523
11b	Ph	3,4-diClBnz	806	6.094
12b	Ph	Me	843	6.074
13b*	Ph	H	885	6.053
14b*	NO ₂	Bnz	210	6.678
15b*	NO ₂	H	1,650	5.783
16b	NO ₂	<i>i</i> -Pr	2,120	5.674
17b	NO ₂	Me	2,850	5.545
18b	NO ₂	<i>n</i> -But	4,070	5.390
19b	Ph	<i>o</i> -ClBnz	31	7.509
20b*	NO ₂	<i>n</i> -Pent	4,800	5.319
21b	NO ₂	Et	5,340	5.272
22b	NO ₂	<i>i</i> -But	8,520	5.070

23b	Ph	<i>n</i> -Pent	41	7.387
24b	Ph	<i>n</i> -But	45	7.347
25b *	Ph	3,5-diCF ₃ Bnz	51	7.292
26b	Ph	<i>p</i> -FBnz	76	7.119
27b	Ph	Ph	79	7.102
28b	Ph	<i>i</i> -But	98	7.009
29b	Ph	Bnz	24	7.620
30b	<i>p</i> -BrPhO	Bnz	419	6.378
31b *	<i>p</i> -BrPhO	<i>n</i> -Pent	472	6.326
32b	<i>p</i> -BrPhO	<i>c</i> -Hex	672	6.173

*Marked compounds are considered as the test set molecules

5.1.1. Multiple linear regression (MLR) analysis

The MLR model was developed on the first dataset comprising 65 molecules (compound 1a-65a) (**Table 5.1**). The equation obtained from the dataset:

$$pIC_{50} = 4.791 (\pm 0.141) + 0.732 (\pm 0.123) PubchemFP346 + 1.901 (\pm 0.179) PubchemFP682 - 1.154 (\pm 0.188) PubchemFP698 + 0.285 (\pm 0.031) SubFPC287 - 0.405 (\pm 0.124) KRFP2820 \quad 5.1$$

$N_{train} = 49$, $R = 0.938$, $R^2 = 0.879$, $R^2_A = 0.865$, $Q^2 = 0.835$, $SEE = 0.365$, $PRESS = 5.739$, $F(5, 43) = 62.664$, $Avg. r_{m^2_{LOO}} = 0.776$, $cR^2_p = 0.831$, $N_{test} = 16$, $R^2_{pred} = 0.912$; $Avg. r_{m^2_{test}} = 0.887$, $p < 0.05$

The statistical analysis of the MLR model (*Equation 5.1*) revealed, that the model demonstrated an R^2_{pred} of 0.912 for the test set compounds and could explain 86.50% and predict 83.50% in the training set, respectively. Additionally, the model fulfilled the Golbraikh and Tropsha model acceptability criteria (**Table 5.3**) (Golbraikh and Tropsha, 2002).

Table 5.3. Docking-based MLR model (*Equation 5.1*) acceptability criteria proposed by Golbraikh and Tropsha

<i>Parameter</i>	<i>Threshold</i>	<i>Equation 5.1</i>
Q^2	$Q^2 > 0.5$	0.835
r^2	$r^2 > 0.6$	0.918
$r_0^2 - r'^2$	$ r_0^2 - r'^2 < 0.3$	0.003
k	$0.85 < k < 1.15$	0.991
k'	$0.85 < k' < 1.15$	1.006
$(r^2 - r_0^2)/r^2$	$[(r^2 - r_0^2)/r^2] < 0.1$	0.004
$(r^2 - r'^2)/r^2$	$[(r^2 - r'^2)/r^2] < 0.1$	0.000

r^2 = Squared correlation coefficient between observed vs predicted response of the test set compounds; r_0^2 = The values for regression through the origin (observed vs predicted); r'^2 = The values for regression through the origin (predicted vs observed); k = Slope of the regression lines through the origin for observed vs predicted; k' = Slope of the regression lines through the origin for predicted vs observed.

Equation 5.1 revealed the importance of three PubChem fingerprint features (i.e., *PubchemFP346*, *PubchemFP682*, and *PubchemFP698*) as well as one substructural fingerprint feature (*SubFPC287*) and one Klekota-Roth fingerprint feature (*KRFP2820*) affecting MMP-2 inhibition. The PubChem fingerprint feature *PubchemFP346* indicates the function (-C-CH-O). The positive coefficient of *PubchemFP346* implied that compounds were identified to be highly efficient MMP-2 inhibitors (compounds 1a-6a, 19a-25a, 39a). On the other hand, the absence of such a feature resulted in lower efficacy (compounds 18a, 56a-63a). Therefore, it may be implicated that pyrrolidine derivatives with ether function were far better compared to the respective pyrrolidine derivatives with amide function. Again, *PubchemFP682* is another PubChem fingerprint feature denoting the topological distance between oxygen and nitrogen atoms separated by four carbon atoms. The positive coefficient of *PubchemFP682* revealed that only 9 compounds in this dataset bearing such fragment features were maximum effective MMP-2 inhibitors (compounds 1a-6a, 19a, 22a, 39a). It also suggested that the distance between the amide group of hydroxamate function and the oxygen atom substituted at the pyrrolidine ring is crucial for MMP-2 inhibition. On the other hand, *PubchemFP698* is another PubChem fingerprint feature implicating the fragment with seven carbon units attached to one oxygen atom. The negative coefficient of *PubchemFP698* revealed that molecules with such fragments were lower active MMP-2 inhibitors. It was observed that compounds possessing *p*-chlorophenylcarbonyl or phenylcarbonyl moieties (compounds 32a-37a) were poor inhibitors of MMP-2. Again, *KRFP2820* is a Klekota-Roth fingerprint feature representing phenylsulfonyl moiety. The negative coefficient of

KRFP2820 implicated that phenylsulfonyl moiety may have an unfavorable impact on MMP-2 inhibition though many of these dataset compounds possess such structures to become potential MMP-2 inhibitors (compounds 3a, 5a-6a, 19a) probably due to the presence of hydroxamate moiety. However, several compounds containing such a feature were lower effective MMP-2 inhibitors (compounds 13a-16a, 34a, 36a, 50a, 54a). Therefore, it can be inferred that *p*-tosyl derivatives were preferable to the corresponding phenylsulfonyl analogs (compound 7a vs compound 13a; compound 10a vs compound 14a; compound 11a vs compound 15a; compound 20a vs compound 23a; compound 24a vs compound 26a). Again, *SubFPC287* is a substructural fingerprint representing the total count of conjugated double bonds. The positive coefficient of *SubFPC287* revealed that compounds with a higher number of conjugated double bonds were highly effective MMP-2 inhibitors (compounds 20a-21a, 23a-26a). The observed vs predicted MMP-2 inhibitory activity for all molecules as per the MLR model is provided in **Table A1** (Appendix).

5.1.2. Hologram-based quantitative structure-activity relationship (HQSAR) analysis

As far as the HQSAR study was concerned, all these possible fragment distinctions (such as atom, bond, connection, hydrogen, chirality, and donor-acceptor) were utilized to generate 50 probable HQSAR models (**Table 5.4**) on the first dataset.

Table 5.4. All the possible HQSAR models were generated with different fragment distinction parameters.

<i>Model</i>	<i>Fragment distinction</i>	<i>R²_{cv}</i>	<i>R²</i>	<i>SE</i>	<i>Length</i>	<i>Component</i>
*1	A	0.793	0.882	0.366	97	6
2	B	0.396	0.652	0.628	83	6
3	C	0.786	0.892	0.349	199	6
4	H	0.228	0.497	0.775	61	6
5	Ch	0.228	0.497	0.775	61	6
6	DA	0.666	0.782	0.485	83	4
7	A/B	0.784	0.888	0.356	151	6
8	A/C	0.772	0.884	0.363	151	6
9	A/H	0.732	0.865	0.39	83	6
10	A/Ch	0.767	0.873	0.379	97	6
11	A/DA	0.744	0.848	0.415	59	6
12	B/C	0.792	0.908	0.323	401	6
13	B/H	0.396	0.652	0.628	83	6
14	B/Ch	0.396	0.652	0.628	83	6
15	B/DA	0.643	0.822	0.448	199	6
16	C/H	0.786	0.892	0.349	199	6
17	C/Ch	0.786	0.892	0.349	199	6
18	C/DA	0.739	0.865	0.39	53	6
19	H/Ch	0.228	0.497	0.755	61	6
20	H/DA	0.666	0.782	0.485	83	4
21	Ch/DA	0.666	0.782	0.485	83	4

22	A/B/C	0.78	0.898	0.34	401	6
23	A/B/H	0.787	0.905	0.329	97	6
24	A/B/Ch	0.787	0.894	0.346	307	6
25	A/B/DA	0.723	0.837	0.424	83	5
26	B/C/H	0.792	0.908	0.323	401	6
27	B/C/Ch	0.792	0.908	0.323	401	6
28	B/C/DA	0.761	0.882	0.361	257	5
29	C/H/Ch	0.786	0.892	0.349	199	6
30	C/Ch/DA	0.739	0.865	0.39	53	6
31	A/B/C/H	0.761	0.903	0.331	307	6
32	A/B/C/Ch	0.78	0.902	0.333	401	6
33	A/B/C/DA	0.751	0.894	0.346	59	6
34	A/B/H/Ch	0.782	0.896	0.343	97	6
35	A/B/H/DA	0.721	0.877	0.369	59	5
36	A/B/Ch/DA	0.739	0.849	0.409	71	5
37	A/C/H/Ch	0.732	0.88	0.369	257	5
38	A/C/H/DA	0.734	0.899	0.335	151	5
39	A/C/Ch/DA	0.706	0.86	0.394	97	5
40	A/H/Ch/DA	0.707	0.894	0.347	257	6
41	B/C/H/Ch	0.792	0.908	0.323	401	6
42	B/C/H/DA	0.761	0.882	0.361	257	5
43	B/H/Ch/DA	0.643	0.822	0.448	199	6
44	C/H/Ch/DA	0.739	0.865	0.39	53	6
45	A/B/C/H/Ch	0.758	0.89	0.353	401	6
46	A/B/C/Ch/DA	0.753	0.88	0.364	307	5
47	A/B/C/H/DA	0.75	0.881	0.363	257	5
48	A/B/H/Ch/DA	0.712	0.889	0.355	61	6
49	B/C/H/Ch/DA	0.761	0.882	0.361	257	5
50	A/B/C/H/Ch/DA	0.791	0.922	0.297	83	6

*The best model was shown in bold

Among these 50 models developed, 44 HQSAR models were found to exhibit a Q^2 value > 0.60. Among these 44 HQSAR models, model-1 comprising 6 components as well as a length of 97 was selected as the best one due to the highest Q^2 value of 0.793 (**Table 5.4**). This model-1 also possessed a good R^2 value of 0.882. As this model was the best one among all these models, it was further subjected to optimize with various atom counts (**Table 5.5**).

Table 5.5. Various HQSAR models were developed by optimizing the HQSAR model 1 using different atom counts.

<i>Model</i>	<i>Atom Count</i>	R^2_{CV}	R^2	<i>SE</i>	<i>Length</i>	<i>Component</i>
1-a	1 to 4	0.686	0.802	0.474	53	6
1-b	2 to 5	0.653	0.788	0.49	61	6
1-c	3 to 6	0.724	0.853	0.408	401	6
*1-d	4 to 7	0.793	0.883	0.366	97	6
1-e	5 to 8	0.719	0.848	0.414	59	6
1-f	6 to 9	0.714	0.828	0.436	151	5
1-g	7 to 10	0.717	0.866	0.389	71	6

*The best model was shown in bold

It was observed that model 1-d having atom count 4 to 7, resulted in the highest Q^2 of 0.793 along with the lowest SE of 0.366. As a result, the best model was determined to be HQSAR model 1-d, which was then validated using a test set of compounds to determine external predictability. An R^2_{Pred} value of 0.890 was reported for model 1-d, which has 6 components and a length of 97. As this model 1-d validated these MMP-2 inhibitors through both internal and external validation methods, it can be a statistically stable and robust model. The observed vs predicted activity plot for the dataset molecules is shown in **Figure A1** (Appendix). Furthermore, the observed vs predicted MMP-2 inhibitory activity for all these molecules as per the HQSAR model is provided in **Table A1** (Appendix).

Regarding the contribution made by the best active compound (compound 39a), it was observed that some of the fragments of this molecule exhibited either green-blue (0.1480545 to 0.2467575) or green-blue (>0.2467575) as colour well as yellow colour (0.098703 to 0.1480545) reflecting the utility of these fragments toward higher MMP-2 inhibition (**Figure 5.1**).

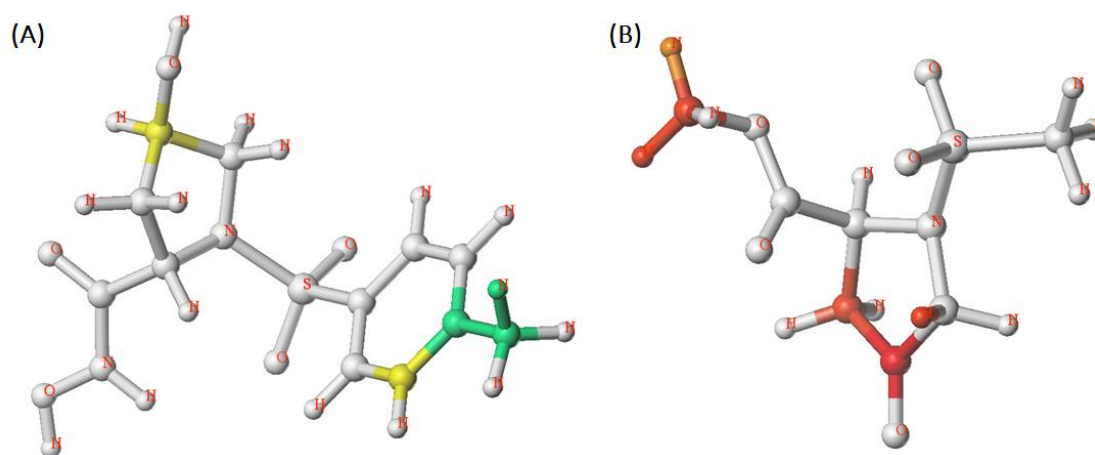


Figure 5.1. Fragment contributions of (A) the most active molecule (compound 39a) and (B) the least active molecule (compound 18a) compounds as per the optimized HQSAR model (Model 1-d).

It was noticed that the methyl carbon and the associated phenyl carbon of the *p*-tolyl moiety exhibited green fragments. Not only that, the adjacent carbon to the *p*-tolyl carbon atom exhibited the implication of a good yellow fragment. Apart from these two fragments, other fragments of this compound were found white (-0.11629967 to 0.098703) implicating their moderate effects on MMP-2 inhibition. Importantly, no such bad fragments (either red or orange-red) were observed in the best active molecule (compound 39a).

On the other hand, the least active molecule of this dataset (compound 18a) disclosed no such good and very good fragments (yellow or green). Most of these fragments of this molecule exhibited white fragments reflecting their moderate implication toward MMP-2 inhibition. However, the red (-0.1744495 to -0.11629967) and orange-red (-0.29074917 to -0.1744495) fragments explored the bad effect on MMP-2 inhibition. In terms of the increased MMP-2 inhibitory activity, it was also indicated that such red and orange-red fragments shouldn't be present in the molecular structure. Here, in the least active molecule (compound 18a), it was noticed that two of the pyrrolidine carbon atoms along with an adjacent hydrogen atom exhibited bad red-colored fragments. Nevertheless, the terminal methoxy carbon atom as well as two hydrogen atoms was shown as red or red-colored fragments implicating that ester function was not favorable as far as the zinc-chelation was concerned. Subsequently, it also pointed out that the presence of ester function may be responsible for the lower MMP-2 inhibitory activity of this compound (compound 18a).

5.1.3. Linear discriminant analysis (LDA) model

The LDA model (*Equation 5.2*) was generated on the first dataset with five descriptors. The capacity to discriminate between *active* and *inactive* MMP-2 inhibitors was noticed using the LDA model. The discrimination function (*DF*) for these alkyl and arylsulfonamido pyrrolidine MMP-2 inhibitors is provided in *Equation 5.2*.

$$DF = -5.951 + 12.012 * KRFP504 + 8.180 * SubFPC85 - 4.674 * PubchemFP726 - 3.357 * KRFP3328 - 0.748 * PubchemFP709 \quad 5.2$$

$$n_{\text{Train}} = 49, \lambda = 0.319, R_C = 0.825, DM^2 = 8.278, F(5, 43) = 18.361, p < 0.000, \chi^2 = 50.847, \\ MCC_{\text{Train}} = 0.767, AUROC_{\text{Train}} = 0.981, n_{\text{Test}} = 16, MCC_{\text{Test}} = 0.630, AUROC_{\text{Test}} = 0.921$$

It was observed from the LDA model that it explored significant discriminating ability as evidenced by the low Wilk's lambda value ($\lambda = 0.319$) as well as good canonical correlation coefficient value ($R_C = 0.825$). The high value of χ^2 (50.847) reflected that the LDA model is statistically significant in terms of distinctly discriminating both the *active* and *inactive* compounds. It was observed from the LDA model that 21 *active* molecules of the discrimination set were predicted as truly *active* (TP) while 22 *inactive* molecules were predicted as truly *inactive* (TN). Interestingly, only 5 *inactive* compounds of the discrimination set were predicted as falsely *active* (FP) whereas only one *active* compound was predicted as falsely *inactive* (FN). Similarly, in the case of the test set, 6 *active* molecules

were predicted as truly *active* (TP) whereas only one *active* molecule was predicted as falsely *inactive* (FN). Again, 7 *inactive* molecules were predicted as truly *inactive* while only 2 *inactive* molecules were predicted to be falsely *active* (FP). Various statistical parameters were estimated to validate the internal as well as external predictive performance of the LDA model as shown in **Table 5.6**. Again, the ROC plot for the developed LDA model is displayed in **Figure 5.2A**.

Table 5.6. Statistical performance of the classification-based QSAR models

<i>Model</i>	<i>Dataset</i>	<i>ROC</i>	<i>TP</i>	<i>TN</i>	<i>FP</i>	<i>FN</i>	<i>Se</i>	<i>Sp</i>	<i>Pr</i>	<i>Acc</i>	<i>F-measure</i>	<i>MCC</i>
LDA	Training	0.981	21	22	5	1	0.955	0.815	0.808	0.878	0.875	0.767
	Test	0.921	6	7	2	1	0.857	0.778	0.750	0.813	0.800	0.630
Bayesian classification	Training	0.759	18	24	3	4	0.818	0.889	0.857	0.857	0.837	0.804
	Test	0.937	6	7	2	1	0.857	0.778	0.750	0.813	0.800	0.630

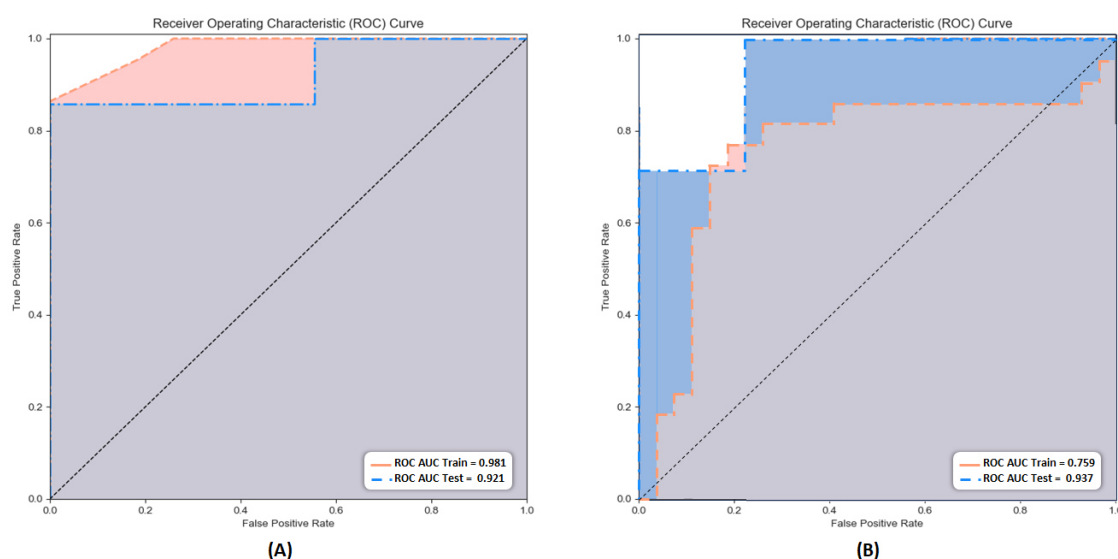


Figure 5.2. ROC plots of (A) the LDA model (*Equation 5.2*) for the training and test sets, and (B) the Bayesian classification model for the training and test sets.

From **Table 5.6**, it was noticed that the discrimination set was predicted as statistically reliable as per the LDA model ($Se = 0.955$, $Sp = 0.815$, $Acc = 0.878$, $Pr = 0.808$, $F\text{-measure} = 0.875$). Again, the external predictive performance of the test set was also statistically significant as per the LDA model ($Se = 0.857$, $Sp = 0.778$, $Acc = 0.813$, $Pr = 0.750$, $F\text{-measure} = 0.800$). Moreover, the values of the Matthews correlation coefficient (MCC) for both the discrimination set and test set (0.767 and 0.630, respectively) suggested that both

these sets were supposed to be good classifiers. Nevertheless, the values of the area under the receiver operating characteristic curve (AUROC) for both the discrimination set and test set (0.981 and 0.921, respectively) justified the accuracy of the LDA model. The LDA model depicted the importance of five descriptors (*KRFP504*, *KRFPC3328*, *SubFPC85*, *PubchemFP726*, and *PubchemFP709*) implicating their discriminating ability from *actives* to *inactives*.

PubchemFP726 is a PubChem fingerprint feature, denoting the fragment *p*-chlorophenyl group associated with a sulfur atom. The negative contribution of this feature suggested that compounds bearing such a structural feature (compounds 49a, 51a, 58a) were MMP-2 inhibitors with lower efficacy. Therefore, it may be postulated that the *p*-chloro phenyl group associated with the sulfur atom directed toward the S1' pocket may not be favorable for MMP-2 inhibition. Again, *PubchemFP709* is another Pubchem fingerprint feature representing the structure comprising six carbon atoms with one branching, i.e., C-C(C)-C-C-C. Such a fragment was also not favorable for MMP-2 inhibition as evidenced by the LDA model. Though many of these promising MMP-2 inhibitors in this dataset possess such a fragment, it was interesting to note that compounds with *p*-chlorophenyl carbonyl moiety directed toward the S2' pocket (compound 32a-34a), phenyl carbonyl moiety (compound 35a-37a) as well as a bulky linear branched chain (50a, 53a-54a, 57a) were lower effective MMP-2 inhibitors. On the other hand, *KRFP504* is a Klekota-Roth fingerprint feature denoting the methylene carbonyl fragment (-CH₂CO-). This fragment feature has the ability to discriminate the *actives* from the *inactives*. Compounds comprising such a fragment (compounds 48a-50a, 52a-60a, 62a-63a) were lower effective MMP-2 inhibitors. On the other hand, compounds with no such fragment feature were promising MMP-2 inhibitors (compounds 1a-4a, 19a-21a, 39a). Again, another Klekota-Roth fingerprint feature is *KRFPC3328* denoting the ester functions. The negative contribution of this feature implied that compounds bearing such ester function as ZBG were lower effective MMP-2 inhibitors (compounds 14a-18a, 31a-38a). It further suggested that the hydroxamate function was better zinc chelator compared to the respective ester function as far as MMP-2 inhibition is concerned. Therefore, compounds with hydroxamate function were potent MMP-2 inhibitors (compounds 1a-6a, 19a, 22a, 39a). Again, *SubFPC85* is a substructure fingerprint feature denoting the number of carboxylic acid ester functions present in the molecule. The positive coefficient of *SubFPC85* suggested that such a feature exhibited a higher ability to discriminate *actives* from *inactives*. It is obvious that the carboxylic acid ester function as ZBG was weaker compared to the respective hydroxamate function. However, several

compounds apart from the carboxylic acid ester ZBG group also possess another carboxylic acid ester function associated with bulky aryl moieties (compounds 24a, 26a, and 29a). The second carboxylic acid ester function may guide the associated aryl moiety to interact at the S2' pocket for imparting higher MMP-2 inhibition. Interestingly, it was also noticed that compound 29a exhibited more than 10-fold less potency compared to both compounds 24a and 26a. Additionally, it was suggested that in order to perform higher MMP-2 inhibition, the bulky aryl group linked to the sulfonyl moiety and directed toward the S1' pocket is essential. Simply said, simply two carboxylic acid ester activities were insufficient. A similar observation was noted for other compounds (compounds 32a, 37a) where there is a smaller methyl function associated with the sulfonyl group resulting in lower efficacy instead of possessing two carboxylic acid ester functions. This further suggested that bulky aryl functions associated with the sulfonyl group were the most crucial feature for enhancing MMP-2 inhibition. On the other hand, compounds with one carboxylic acid ester function were found effective MMP-2 inhibitors probably due to the presence of the phenyl and *p*-tosyl functions (compounds 20a, 23a, and 25a).

5.1.4. Bayesian classification modeling analysis

As far as the Bayesian modeling study was concerned on the first dataset, it exhibited a ROC_{LOO} of 0.753 and a 5-fold ROC score (ROC_{5-CV}) of 0.759 for the training set molecules. However, for the training set molecules, the Bayesian model also expressed the sensitivity, specificity, and accuracy of 0.818, 0.889, and 0.857, respectively. Again, the model's ROC score (ROC_{Test}) of 0.937 for the test set molecules confirmed the high quality of this Bayesian model. Moreover, the sensitivity, specificity, and accuracy of the test were found to be 0.857, 0.778, and 0.813, respectively. **Table 5.6** provides the comprehensive statistics for the Bayesian classification model, whereas **Figure 5.2B** displays the ROC curves..

It was observed that the Bayesian classification modeling study disclosed various good substructural fragments (**Figure A2**) (Appendix) that may be responsible for imparting efficacious MMP-2 inhibition. Substructural fragments such as sulfonyl pyrrolidine group with sulfonyloxy substituent (G1, G18), carboxamido substituted sulfonyl pyrrolidine group (G2), sulfonyl or arylsulfonyl substituted 3-hydroxy pyrrolidine group (G9, G10), sulfonyl pyrrolidine group with -CONHOH group substituted at the 2nd position of the pyrrolidine ring (G8), carboxamido substituted arylsulfonyl pyrrolidine with dimethoxy substitution (G5), -CONHOH group substituted arylsulfonyl pyrrolidine with dimethoxy substitution (G7), carboxamido substituted sulfonyl pyrrolidine with 1,3-dioxane moiety (G6) were found

preferable for higher MMP-2 inhibitory efficacy. On the other hand, substructural fragments like substituted arylsulfonyloxy substitution (G3, G4, G14, G16, and G17), 1,3-dioxolane moiety (G11), substituted pyrrolidine group with dioxolane moiety (G12), arylsulfonyloxy cyclopentyl moiety (G15 and G20) were found favorable for higher MMP-2 inhibition. Compounds 20a, 21a, and 23a comprising substructural fingerprint sulfonyl pyrrolidine group with sulfonyloxy substituent (G1 and G18) exhibited highly potent MMP-2 inhibition. Again, compounds bearing carboxamido substituted sulfonyl pyrrolidine group (G2) also displayed highly potent MMP-2 inhibitory efficacy (compounds 1a-6a). A similar type of substructural fingerprint (G8) was noted for the same compounds (compounds 1a-6a) revealing the importance of hydroxamate moiety apart from the sulfonyl pyrrolidine group. On the other hand, compounds comprising sulfonyl or arylsulfonyl substituted 3-hydroxy pyrrolidine group (G9, G10) were potent MMP-2 inhibitors (compounds 19a, 22a, and 39a). Again, compounds bearing substructural fragments substituted arylsulfonyloxy substitution (G3, G4, G14, G16 and G17) were highly effective MMP-2 inhibitors (compounds 20a-21a, 23a, 25a). On the other hand, various bad substructural fragments (**Figure A3**) (Appendix) such as aryl ester or substituted aryl ester group (B7, B8, B11, B18, and B20), aryl ester functions with various groups like cyclopentyl and pyrrolidinyl groups (B4-B6), linear alkyl amino carboxamide group with amine substitution (B1, B2), amine substituted alkyl function (B3), methoxy substituted aryl groups (B12-B16) was found unfavorable for MMP-2 inhibitory activity.

5.1.5. Comparative molecular similarity index analysis (CoMSIA) analysis

Prior to generating the CoMSIA model, all these molecules were aligned keeping in consideration the best active MMP-2 inhibitor of the first dataset (compound 39a). The aligned structures of the dataset MMP-2 inhibitors are depicted in **Figure 5.3**.

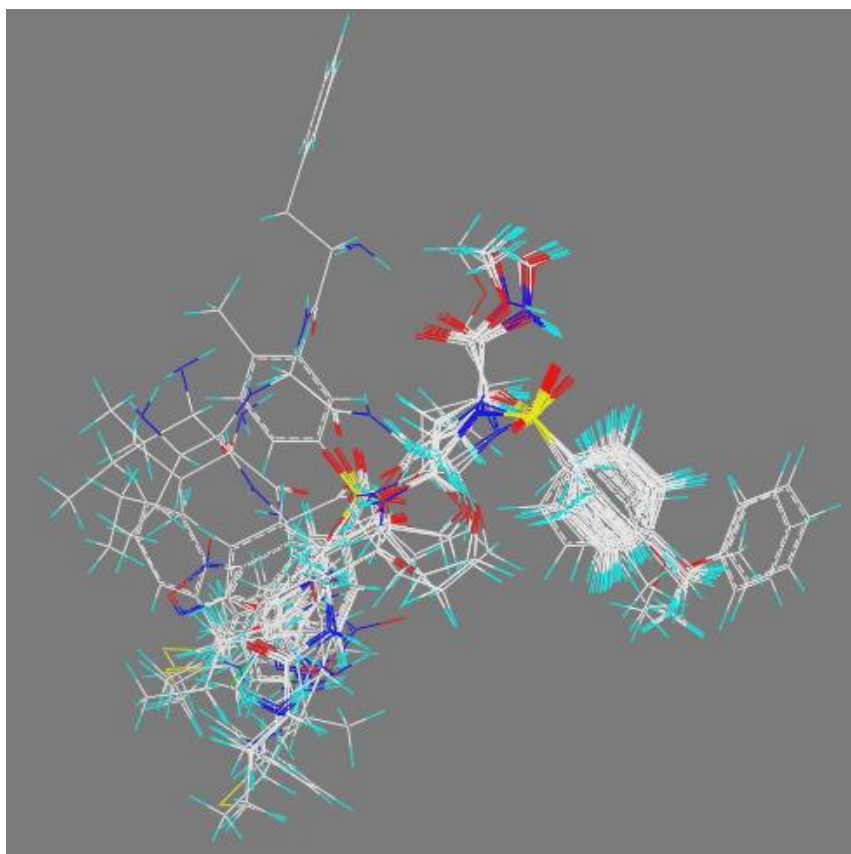


Figure 5.3. Aligned structures of all these MMP-2 inhibitors of the dataset.

With reference to the CoMSIA model, it was generated with 4 components on 49 training set molecules and this was subsequently validated on 16 test set compounds. This CoMSIA model was statistically significant as it yielded a leave-one-out Q^2 value of 0.538 and an R^2 value of 0.809. Not only that, this CoMSIA model also resulted in an acceptable 10-fold cross-validation ($R^2_{10-CV} = 0.529$) as well as a good external prediction result ($R^2_{Pred} = 0.640$). The observed vs predicted MMP-2 inhibitory activity for all these molecules as per the CoMSIA model is provided in **Table A1** (Appendix).

Not only that, the other statistical validation parameters (such as bootstrapping and Y-scrambling) also revealed the CoMSIA model to be a reliable one. Importantly, it was noticed that the CoMSIA model displayed the importance of four fields (i.e., steric, electrostatic, hydrophobic, and donor) having an impact on MMP-2 inhibition. The contributions of steric, electrostatic, hydrophobic, and donor fields were found to be 10.20%, 21.20%, 30.10%, and 38.50%, respectively, towards MMP-2 inhibitory activity. Regarding the CoMSIA contour maps, the implication of all these fields was noticed (Green: steric favorable; Yellow: steric unfavorable; Blue: electrostatic favorable; Red: electrostatic unfavorable; Magenta:

hydrophobic favorable Cyan: hydrophobic unfavorable; Black: donor favorable; Orange: donor unfavorable). All the statistical results of the CoMSIA model are shown in **Table 5.7**.

Table 5.7. Statistical results from the CoMSIA model.

<i>Parameters</i>	<i>CoMSIA</i>
Features	S, E, H, D
Q^2	0.538
Component	4
R^2	0.809
SEE	0.455
F	46.468
R^2_{10-CV}	0.529
R^2_{20-BS}	0.849
R^2_{scr}	0.405
$cSDEP$	0.802
dq^2/dr_{yy}^2	0.839
r^2_{Pred}	0.640
<i>Field</i>	<i>Field distribution (%)</i>
Steric	10.20
Electrostatic	21.20
Hydrophobic	30.10
Hydrogen bond donor	38.50

For the best effective molecule of the dataset (compound 39a), it was noticed that the *p*-tolyl group associated with the sulphonamide moiety was inserted into the steric favorable region (green polyhedron) (**Figure 5.4**). Not only that, a small favorable hydrophobic region (magenta polyhedron) was also observed near the terminal end, i.e., near the *p*-tolyl group. It suggested that steric and hydrophobic substituents are preferable at this position, i.e., towards the S1' pocket of the MMP-2 enzyme. Likewise, the steric unfavorable domain (yellow polyhedrons) were found located opposite as well as far away from this molecule (compound 39a). Importantly, it was also interesting to note that a bigger favorable hydrophobic region (magenta polyhedron) was found closely associated with the hydroxyl group substituted at the pyrrolidine ring. It suggested that hydrophobic substitutions at this position i.e., towards the S2' pocket may be suitable for enhancing the MMP-2 inhibitory activity. Therefore, in a nutshell, it may be inferred that hydrophobic and steric groups/substituents were found suitable towards the S1' pocket whereas only hydrophobic substituents with less or no steric effect were preferable towards the S2' pocket for higher MMP-2 inhibition. Conversely, the hydroxamate group was found inserted into a bulky hydrophobic unfavorable region (cyan

polyhedron). It suggested that no such hydrophobic groups or substituents were favored at this position. It was obvious that in this region the zinc-binding group (ZBG) (here hydroxamate function) chelates to the catalytic Zn^{2+} ion and thus, no such hydrophobic interactions were favorable at this region. Again, a smaller unfavorable hydrophobic group (cyan polyhedron) was located near the terminal *p*-tolyl group adjacent to the sulfonyl moiety. It suggested that hydrophobic substituents are not favored in this region. As far as the electrostatic contours were concerned, the favorable regions (blue polyhedrons) were away from this molecule. However, two bigger unfavorable electrostatic regions (red polyhedrons) were located close to the molecule suggesting that no such electrostatic groups were favorable in these positions (one region near the terminal *p*-tosyl moiety and another region at the center of this molecule). Importantly, only one favorable donor region (black polyhedron) group was found near the terminal *p*-tosyl moiety but it was away from the sulfonyl function. It suggested that donor substituents may be favored near the terminal aryl moiety for higher MMP-2 inhibition. It appears that no such acceptor groups were appropriate at these places, though, because the unfavourable donor groups (orange polyhedrons) were located far from the molecule.

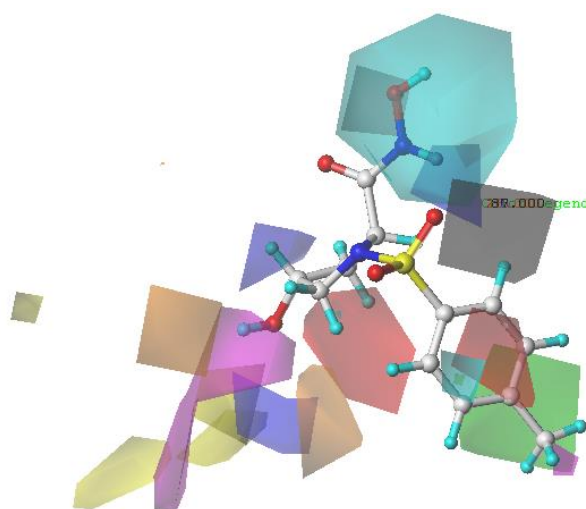


Figure 5.4. CoMSIA contour plot of the best active molecule (compound 39a)

As far as the contour maps of the least active molecule (compound 18a) were concerned, it was noticed that the methyl group attached to the sulfonyl moiety was far away from the favorable steric and hydrophobic regions (green and magenta, respectively) (**Figure 5.5**).

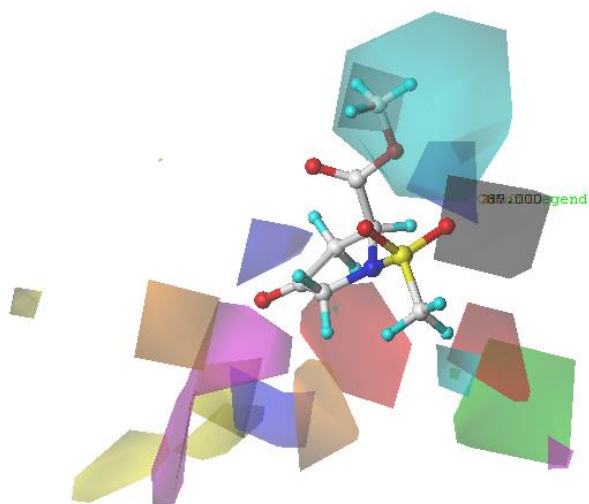


Figure 5.5. CoMSIA contour plot of the least active molecule (compound 18a)

On the other hand, the carbonyl moiety attached to the pyrroline moiety was also away from the favorable hydrophobic region (magenta polyhedron). Importantly, the methoxy group of the ester function (ZBG) was inserted into the unfavorable hydrophobic region (cyan polyhedron). It again suggested that no such hydrophobic interactions were favoured near the zinc-binding region. However, other contours (i.e., electrostatic and donor) were found mostly away from this molecule. Therefore, comparing the contours of both the best active (compound 39a) and least active (compound 18a) compounds, it may be inferred that aryl functionality associated with the sulphonamido moiety conferring both favorable steric and hydrophobic interactions toward the S1' pocket of the MMP-2 enzyme was the most crucial for the enhancement of MMP-2 inhibitory efficacy.

[The work was communicated for publication.]

5.1.6. Molecular docking-based 2D-QSAR Model

For the second dataset (**Table 5.2**):

The thirty-two *in house* molecules (compounds 1b-32b) (**Table 5.2**) were docked at the MMP-2 enzyme active site (PDB ID: 1HOV), and the method of docking was confirmed by re-docking the inbound molecule. The incoming and re-docked inbound molecule's alignment is shown in **Figure 5.6A** (RMSD of the re-docked conformation = 3.84). Furthermore, the alignment of the *in house* molecules at the MMP-2 active region (PDB ID: 1HOV) is shown in **Figure 5.6B**.

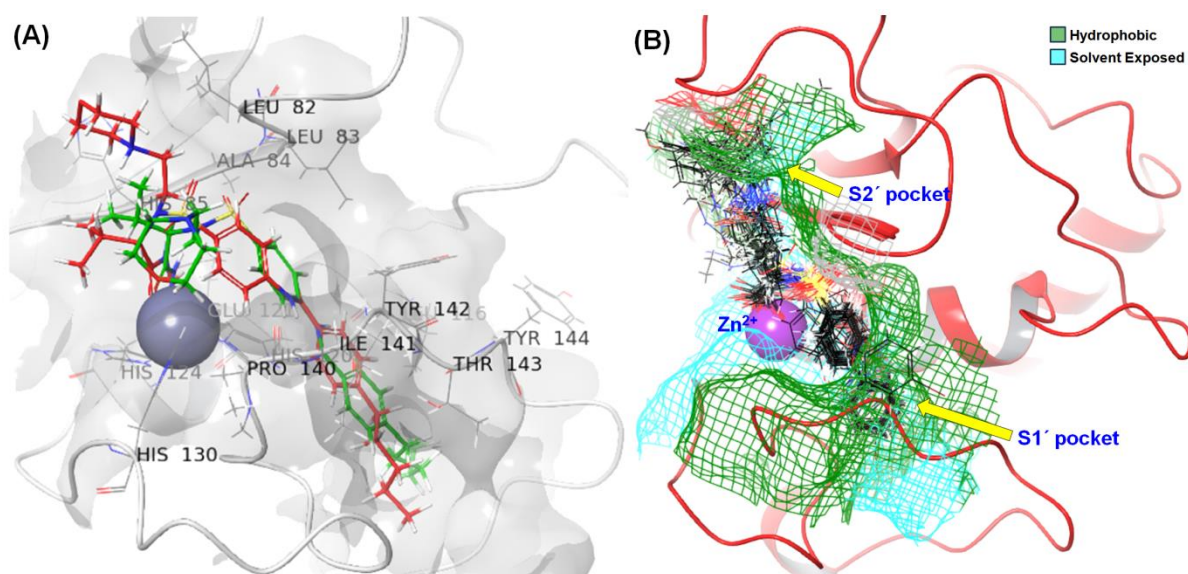


Figure 5.6. (A) Alignment of the inbound MMP-2 inhibitor with the active site residues at MMP-2 (PDB ID: 1HOV) and its re-docked conformation; (B) Alignment of docked conformers derived from the molecular docking analysis at the MMP-2 active site (PDB ID: 1HOV).

The docking-based 2D-QSAR model was developed using the *XP* (extra precision) descriptors produced by GLIDE docking from the molecular docking study. The training set population was used to create this model, and 19 features were chosen in the initial stage of the feature selection process before being put through the *Best Subset Selection (BSS)* procedure. Subsequently, three *XP* descriptors made up the optimal model, which was determined by analyzing its internally cross-validated Q^2 and R^2_{pred} values (Equation 5.3).

$$pIC_{50}(M) = 5.915 (\pm 0.257) + 3.824 (\pm 0.725) r_{\text{glide_XP_LowMW}} - 0.461 (\pm 0.185) r_{\text{glide_res:A142_coul}} - 0.210 (\pm 0.05549) r_{\text{glide_res:A84_Eint}} \quad 5.3$$

$N_{\text{train}} = 24$, $R = 0.854$, $R^2 = 0.729$, $R^2_A = 0.688$, $Q^2 = 0.629$, $SEE = 0.406$, $PRESS = 3.294$, $F(3, 20) = 17.911$, $\text{Avg. } r_{m^2\text{LOO}} = 0.509$, $cR^2_p = 0.675$, $N_{\text{test}} = 8$, $R^2_{\text{pred}} = 0.610$; $\text{Avg. } r_{m^2\text{test}} = 0.520$, $p < 0.05$

Equation 5.3, which represents the docking-based 2D-QSAR model, underwent statistical analysis to show that the model demonstrated an R^2_{pred} of 0.610 for the test set compounds and could explain 68.8 % and predict 62.9 % in the training set. Additionally, the model fulfilled the Golbraikh and Tropsha model acceptability criteria (**Table 5.8**) (Golbraikh and Tropsha, 2002).

Table 5.8. Golbraikh and Tropsha criteria for the docking-based MLR model (Equation 5.3)

<i>Parameter</i>	<i>Threshold</i>	<i>Equation 5.3</i>
Q^2	$Q^2 > 0.5$	0.629
r^2	$r^2 > 0.6$	0.711
$r_0^2 - r_0'^2$	$ r_0^2 - r_0'^2 < 0.3$	0.113
k	$0.85 < k < 1.15$	0.967
k'	$0.85 < k' < 1.15$	1.031
$(r^2 - r_0^2)/r^2$	$[(r^2 - r_0^2)/r^2] < 0.1$	0.000
$(r^2 - r_0'^2)/r^2$	$[(r^2 - r_0'^2)/r^2] < 0.1$	0.159

The observed *vs* predicted activities for the dataset molecules are listed in **Table 5.9** and **Figure 5.7A**.

Table 5.9. Measured (actual) and predicted activity for the *in house* compounds obtained from the molecular modeling studies along with the values of the features used to develop the docking-based MLR model, CoMFA model, and CoMSIA model.

Compound	r_glide_XP_Low MW	r_glide_res: A142_coul	r_glide_res:A 84_Eint	pIC ₅₀	Predicted Activity		
					MLR	CoMFA	CoMSIA
1b	-0.01482	-1.2159	-3.45422	6.987	7.143	7.039	7.144
*2b	0	-1.36576	-2.29474	6.910	7.026	7.036	7.197
3b	-0.15509	-1.1868	-3.65949	6.752	6.637	6.934	6.761
4b	-0.10834	-1.36722	-3.45499	6.730	6.856	6.819	6.553
5b	0	-1.26502	-1.47154	6.714	6.807	6.926	6.894
*6b	-0.20185	-1.28083	-2.8999	6.693	6.342	6.445	6.505
7b	-0.15509	-1.43324	-3.08052	6.682	6.629	6.725	6.599
8b	0	-1.21389	-2.62341	6.580	7.025	6.831	6.731
*9b	0	-1.23196	-2.88881	6.536	7.089	6.965	6.833
10b	-0.02154	-1.31868	-2.16107	7.523	6.894	6.851	6.967
*11b	0	-1.33015	-2.01415	6.094	6.951	6.947	7.055
12b	-0.2486	-1.35017	-3.46262	6.074	6.313	6.643	6.239
13b	-0.29536	-1.44914	-4.27765	6.053	6.351	6.402	6.283
14b	-0.09861	-0.23693	-2.9558	6.678	6.268	--	--
15b	-0.39902	-0.71537	-3.76485	5.783	5.509	5.503	5.800
*16b	-0.25875	-0.18308	-4.79436	5.674	6.016	5.640	5.317
17b	-0.35226	-0.17202	-3.51379	5.545	5.385	5.304	5.391
18b	-0.212	-0.34617	-2.4145	5.390	5.771	5.344	5.280
*19b	0	-1.14164	-3.6634	7.509	7.210	6.779	6.830
20b	-0.1686	-1.22011	0.993335	5.319	5.624	5.072	5.215
*21b	-0.30551	-0.16359	-3.42976	5.272	5.542	5.158	5.172
22b	-0.212	-0.08811	-0.68809	5.070	5.290	5.849	5.228
23b	-0.06158	-1.24124	-1.28648	7.387	6.522	6.892	7.122
24b	-0.10834	-1.15058	-4.56454	7.347	6.989	6.902	7.275
25b	0	-0.8363	-5.70331	7.292	7.497	7.254	7.476
*26b	0	-0.77956	-5.45381	7.119	7.419	6.821	6.931
27b	-0.0417	-1.17993	-3.75765	7.102	7.088	6.974	7.191
28b	-0.10498	-0.78906	-5.2435	7.009	6.978	7.100	7.027
29b	0	-1.28269	-2.92326	7.620	7.120	7.185	7.505
30b	0	0.134814	-1.67531	6.378	6.205	6.610	6.383
31b	0	-0.88733	-3.77901	6.326	7.117	6.618	6.256
32b	0	-1.03678	-0.51127	6.173	6.500	6.059	6.515

*Test set molecules are in **Bold**.

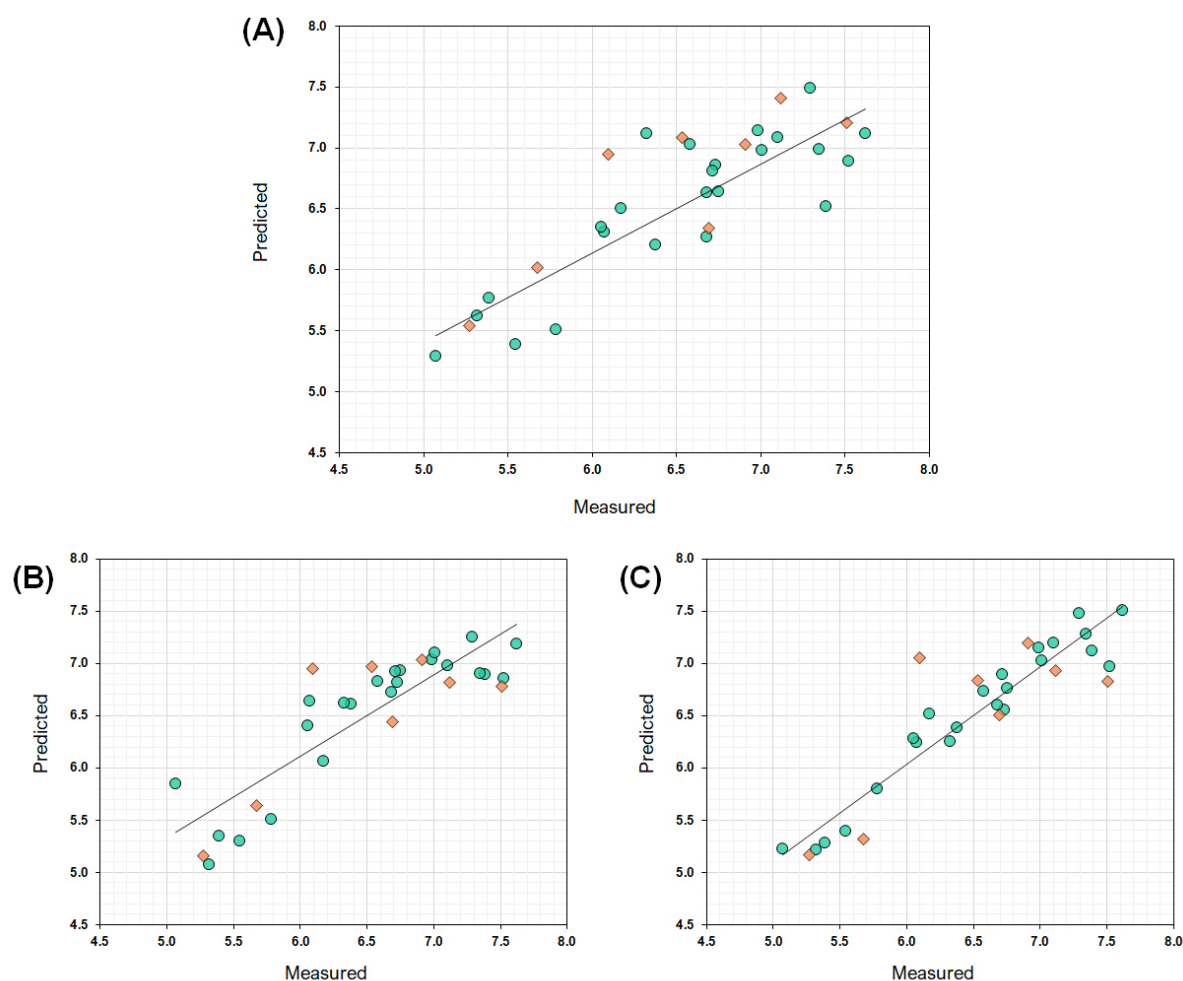


Figure 5.7. Measured (actual) versus predicted activity of (A) Docking-based MLR model; (B) CoMFA model; (C) CoMSIA model.

The assessment and validation of a 2D-QSAR model (*Equation 5.3*) in a computational chemistry context, involves three key analyses depicted in **Figures 5.8A**, **5.8B**, and **5.8C**, respectively. Firstly, the correlation matrix (**Figure 5.8A**) illustrates the relationships between various molecular descriptors employed in the model, providing insights into the interrelations among these features. Secondly, the applicability domain analysis, demonstrated in **Figure 5.8B**, uses the Euclidean distance-based method to evaluate how closely new compounds align with the known dataset used to construct the model, ensuring the model's reliability for predicting properties of similar compounds. Lastly, the Y-randomization test (**Figure 5.8C**) involves creating multiple random models (50 models in this case) to validate the robustness of the original model by comparing its performance against these random models, thereby confirming the meaningful relationships within the

original model and ensuring its predictive significance and reliability for practical applications.

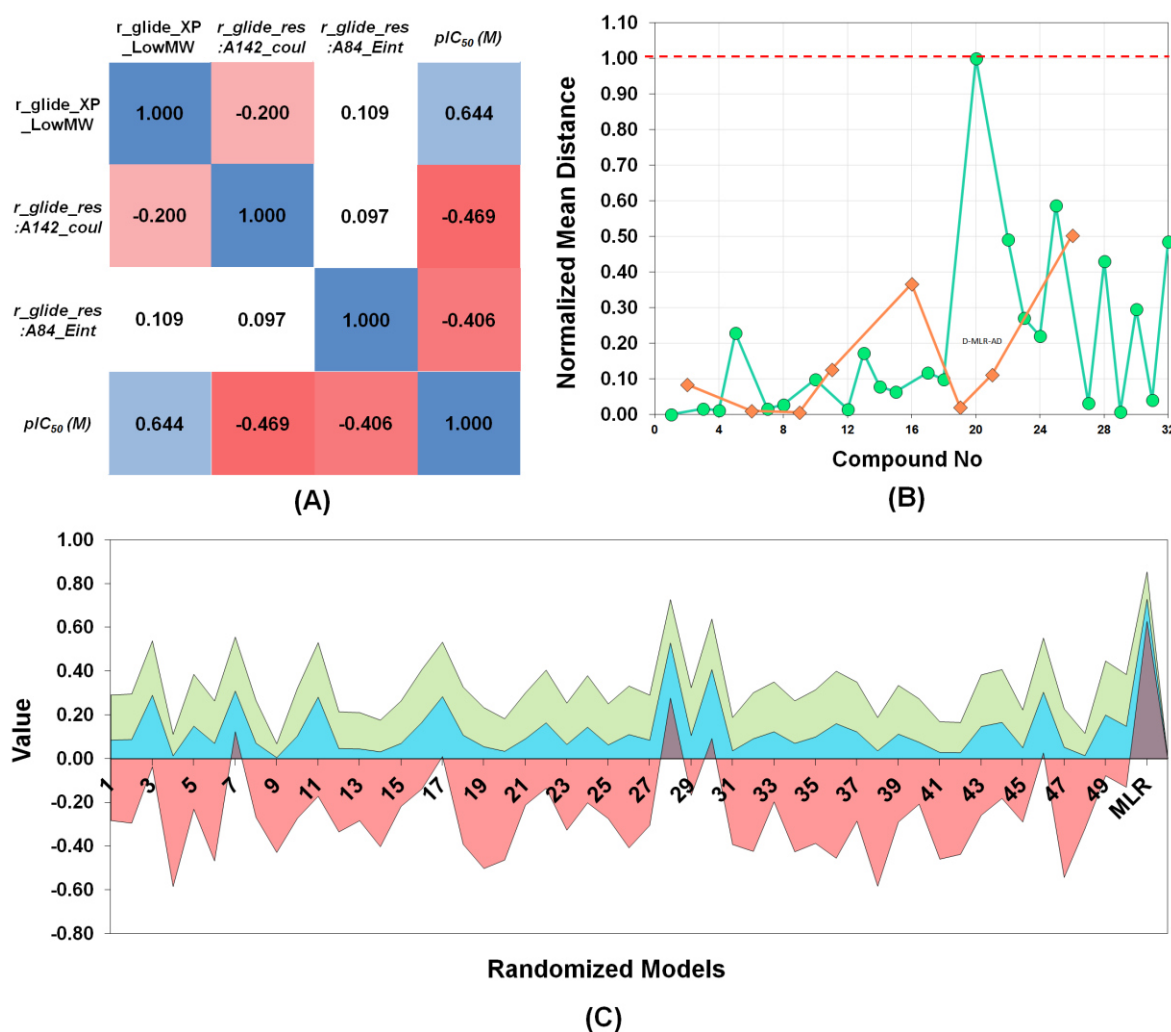


Figure 5.8. (A) Correlation matrix heatmap for the descriptors utilized for the docking-based MLR (Equation 5.3) model; (B) Normalized mean distance values for the training (green circle) and the test set (orange square) compounds; (C) Comparison of R , R^2 , Q^2 values of Equation 5.3 and the 50 random models.

From the docking-based 2D-QSAR model (Equation 5.3), the analysis concerned the model and its correlation with the inhibitory activity of MMP-2. Three specific XP parameters derived from the model, namely $r_glide_XP_LowMW$, $r_glide_res:A142_coul$, and $r_glide_res:A84_Eint$, were found to have a strong relationship with the MMP-2 inhibitory activity.

The descriptor $r_glide_XP_LowMW$, in particular, revealed an intriguing relationship with the inhibitory potential. A positive coefficient associated with this descriptor implies that lower molecular weight compounds might negatively impact the inhibition of MMP-2.

Analysis of various molecules reveals that those with lower values of *r_glide_XP_LowMW*, indicative at the R₂ position (**Table 5.7**), smaller linear or branched alkyl groups and being relatively distant from the S2' pocket, showed reduced effectiveness in inhibiting MMP-2 (compounds 12b-13b, 15b-18b, and 21b-22b). On the contrary, compounds with higher values of *r_glide_XP_LowMW*, marked at the R₂ position (**Table 5.7**) by a bulky benzyl substitution or a halogen-substituted bulky benzyl substitution, were associated with a positive impact on MMP-2 inhibition by effectively fitting into the S2' pocket (compounds 19b, 25b-26b, and 29b).

Additionally, this analysis also suggests that the nature of the substitution at the R₂ position (**Table 5.7**) plays a crucial role in determining the effectiveness of compounds in inhibiting MMP-2. Compounds with smaller alkyl groups or those situated away from the S2' pocket exhibited reduced inhibitory potential. In contrast, compounds with larger, bulky substitutions at the R₂ position, capable of fitting properly into the S2' pocket, were more effective in interacting with the specific amino acid residues within that pocket, leading to enhanced MMP-2 inhibitory activity. This insight provides valuable guidance for designing or selecting compounds with the potential to interact effectively at the S2' pocket for improved MMP-2 inhibition in drug development or medicinal chemistry efforts.

In addition, another parameter derived from a docking-based 2D-QSAR model (*Equation 5.3*), *r_glide_res:Ala142_coul*, reflecting the Coulomb energy associated with the Ala142 residue, was scrutinized. Findings suggest that the magnitude of this Coulombic energy associated with Ala142 significantly influences the effectiveness of compounds in inhibiting MMP-2. Lower negative values of this energy parameter related to Ala142 appear to correlate with reduced efficacy in inhibiting MMP-2, observed in compounds 15b-18b and 21b-22b. Conversely, higher negative values of this energy parameter are linked to more effective inhibition of MMP-2, evidenced in compounds 2b, 4b-5b, 10b, 23b, and 29b. These observations imply that the electrostatic interactions governed by the Coulomb energy attributed to the Ala142 residue within the MMP-2 binding site play a pivotal role in determining the effectiveness of the compounds in inhibiting the enzyme, offering valuable insights for optimizing future drug development endeavors targeting MMP-2. Moreover, in this context, the model specifically examined compounds 29b, 22b, 10b, and 14b aiming to identify significant residues within a biological structure (likely a protein) and determine their distances from these compounds (**Figure 5.9**).

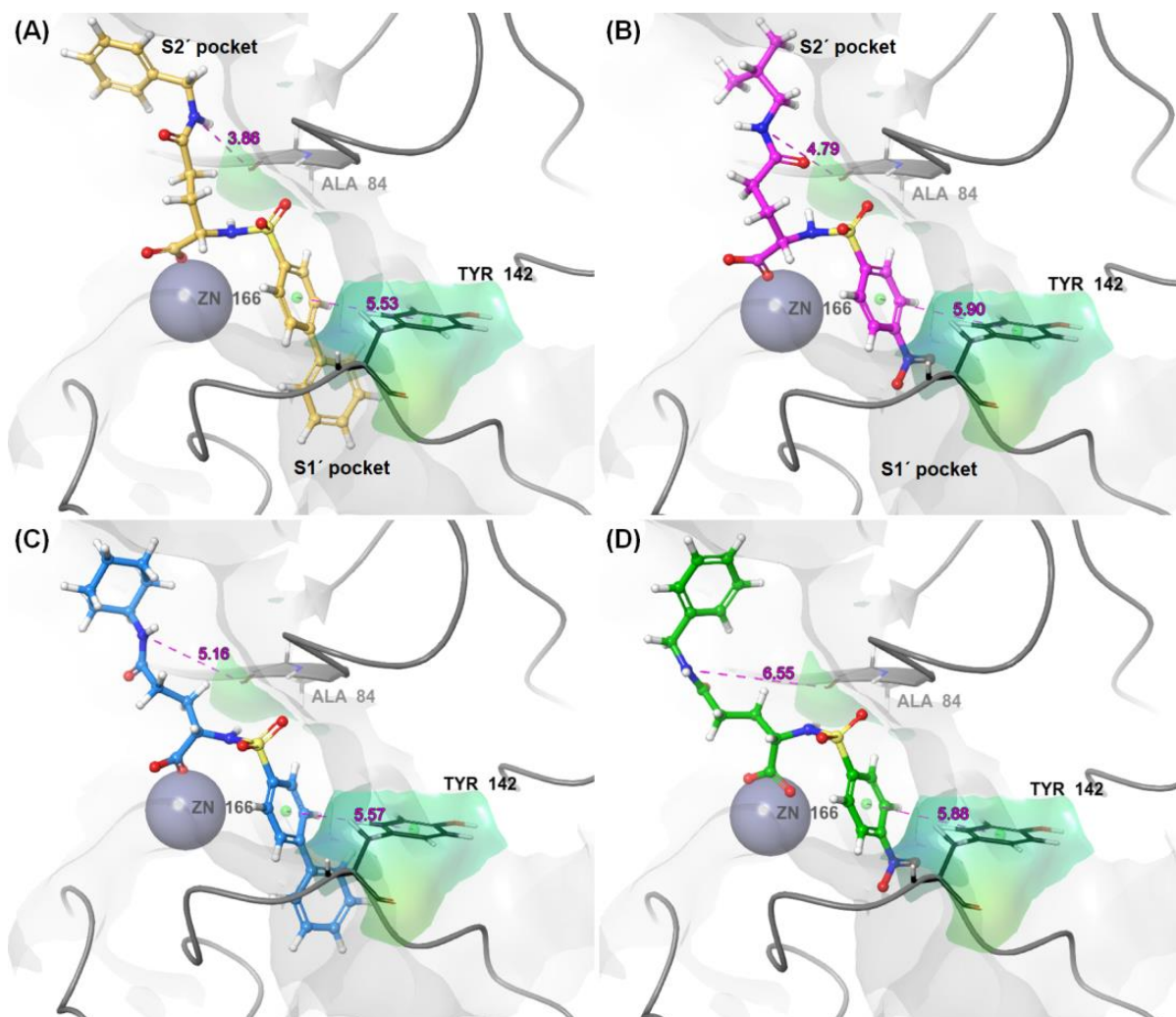


Figure 5.9. The docking-based MLR model identified important residues and their distance with (A) compound 29b; (B) compound 22b; (C) compound 10b; and (D) compound 14b.

Furthermore, the parameter $r_glide_res:A84_Eint$, characterizing the total interaction energy involving Coulomb, van der Waals, and hydrogen bonding scores and minimum distance calculations between the ligand and the Ala84 residue, has unveiled significant insights. Notably, the model (*Equation 5.3*) revealed a distinct relationship between the scores attributed by Ala84 and the effectiveness of compounds in inhibiting MMP-2. Compounds displaying higher negative scores, denoted by Ala84 (compounds 19b, and 24b-28b), were notably more favorable in their MMP-2 inhibitory potential compared to compounds demonstrating lower negative scores by the same residue (compounds 11b, 20b, 22b, and 32b). These findings highlight the critical impact of the total interaction energy, particularly concerning the scores associated with the Ala84 residue, in dictating the efficacy of compounds in inhibiting MMP-2. Compounds with more robust interactions, as indicated by higher negative scores derived from Ala84, demonstrated enhanced effectiveness in inhibiting

the targeted enzyme. Understanding and harnessing these specific interactions comprising various energetic contributions and distance calculations with Ala84 could significantly inform the design and optimization of compounds for MMP-2 inhibition.

5.1.7. Alignment for field-based 3D-QSAR studies

For the development of field-dependent CoMFA and CoMSIA models, the 3D conformations of the second dataset (**Table 5.2**) and the *in house* MMP-2 inhibitors (compounds 1b–32b) following molecular docking studies were taken into consideration. **Figure 5.10** shows the aligned geometrical orientation of each of these molecules.

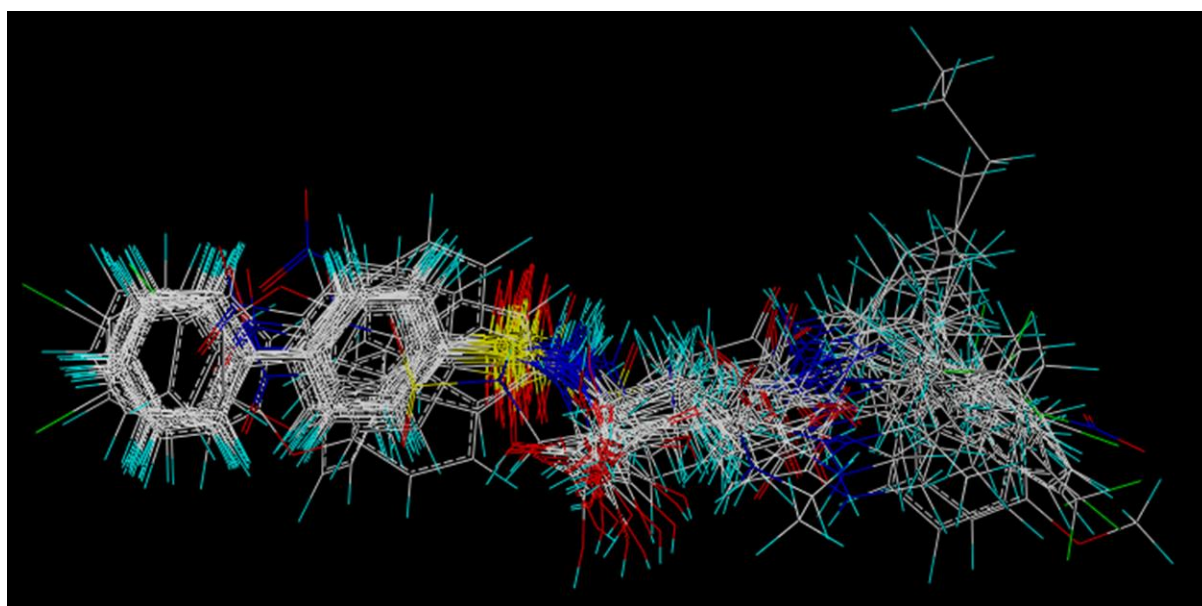


Figure 5.10. Docking-based alignment of all 32 *in house* MMP-2 inhibitors (compounds 1b–32b).

5.1.7.1. Comparative molecular field analysis (CoMFA) study

The CoMFA model, constructed on the same 23 training set molecules and validated using 8 test set compounds (**Table 5.2**), demonstrates moderate predictive ability ($Q^2 = 0.501$) and a good fit to the training data ($R^2 = 0.780$). Moreover, these values indicate that approximately 50.10% of the variability in biological activity can be explained by the model and that it effectively captures the relationship between molecular structure and activity in the training compounds. Furthermore, the model exhibits satisfactory 10-fold cross-validation ($R^2_{10-CV} = 0.526$) and external prediction ($R^2_{Pred} = 0.591$), showing its consistency and reasonable capability to predict the activities of new compounds. While it shows promise in predicting the biological activity of molecules, there remains an opportunity for improvement in

precision. The observed *vs* CoMFA-predicted activity for these compounds is provided in **Table 5.9** and **Figure 5.7B**. Several other statistical characteristics demonstrated the statistical reliability and dependability of the CoMFA model (**Table 5.10**).

Table 5.10. Statistical results from the CoMFA and CoMSIA models.

<i>Parameters</i>	<i>CoMFA</i>	<i>CoMSIA</i>
Features	S, E	S, E, H, A, D
Q^2	0.501	0.560
Component	1	2
r^2	0.780	0.931
SEE	0.356	0.204
F	74.448	135.669
R^2_{10-CV}	0.526	0.607
R^2_{20-BS}	0.808	0.927
R^2_{scr}	0.470	0.496
$cSDEP$	0.552	0.570
dq^2/dr_{yy}^2	0.359	0.484
r^2_{Pred}	0.591	0.556
<i>Field</i>	<i>Field distribution (%)</i>	
Steric	44.00	9.00
Electrostatic	56.00	36.00
Hydrophobic	--	18.80
Hydrogen bond acceptor	--	13.00
Hydrogen bond donor	--	23.20

In addition, in the CoMFA analysis pertaining to MMP-2 inhibition, the model defines that steric and electrostatic fields contribute significantly, with respective contributions of 44% and 56% (**Table 5.10**). Specifically, for the most potent compound (compound 29b), the CoMFA contour plot (depicted in **Figure 5.11A**) highlights the positioning of the biphenyl moiety, the terminal phenyl group in close proximity to a region indicating favorable steric interactions, represented by a green polyhedron. This spatial relationship suggests that smaller steric substituents in this specific area might be conducive to enhancing the inhibition of MMP-2. Besides, these findings provide critical insights into the structural determinants governing interactions with MMP-2. Notably, the model's suggestion to favor smaller steric groups in proximity to the identified region implies a potential strategy for augmenting the inhibitory potency against MMP-2. Such insights are invaluable for the rational design or optimization of novel compounds targeting MMP-2 inhibition.

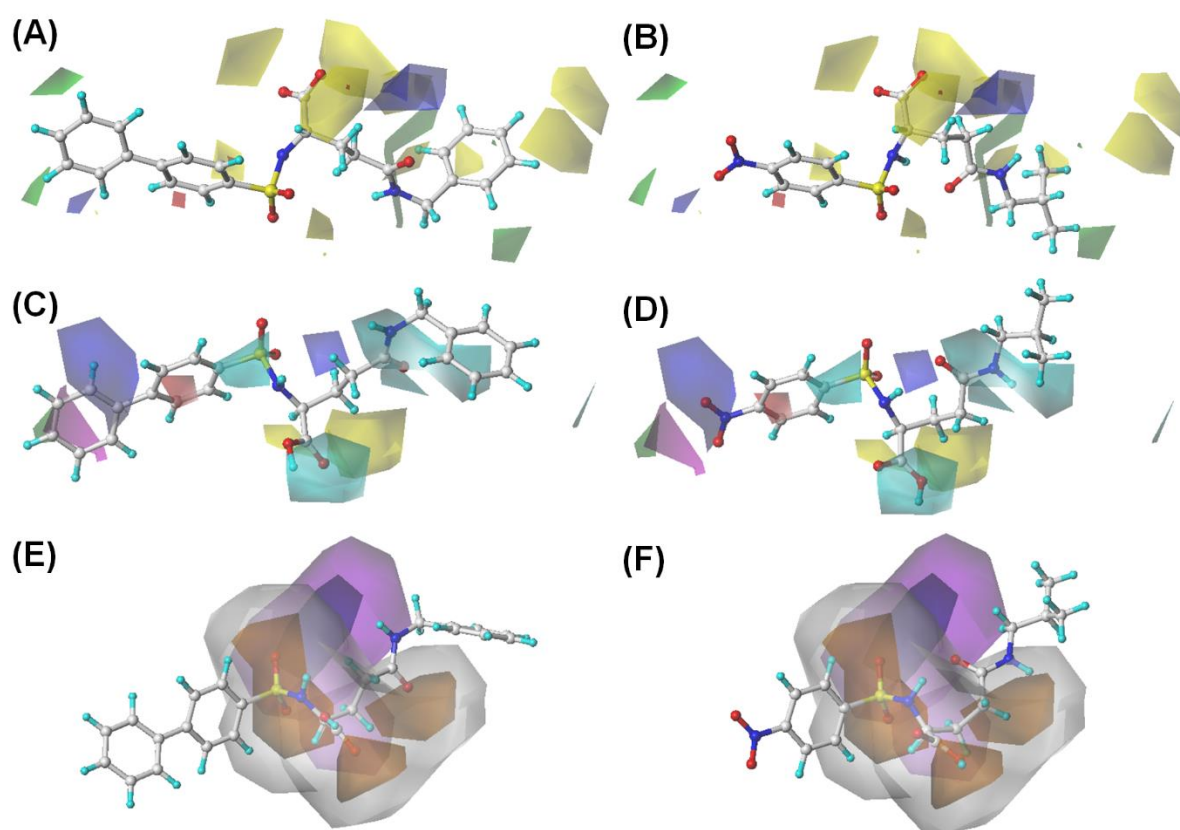


Figure 5.11. CoMFA steric and electrostatic generated contour plots with (A) compound 29b, and (B) compound 22b; CoMSIA steric, electrostatic, hydrophobic contour plots with (C) compound 29b, and (D) compound 22b; CoMSIA donor and acceptor contour plots with (E) compound 29b, (F) compound 22b.

Interestingly, all the biphenyl derivatives revealed a distinct correlation between their structural features and their effectiveness as MMP-2 inhibitors. The terminal phenyl group, common among these molecules, consistently aligns in close proximity to a favorable steric region, as indicated by the green polyhedron (**Figure 5.11A**). This implies that smaller steric substituents are more conducive to achieving higher MMP-2 inhibition. Conversely, in the least active molecule (compound 22b), the beneficial steric field is located far from the nitro replacement (**Figure 5.11B**). For the *p*-nitrophenyl analogs, not only is the favorable steric region distant from the nitro group but the biphenyl derivatives exhibit promising effectiveness as MMP-2 inhibitors compared to their *p*-nitrophenyl counterparts.

Unfavorable steric regions (yellow polyhedrons) are appreciable, and dispersed apart from these molecules, indicating that no steric substituents are beneficial in such regions (**Figure 5.11A** and **5.11B**). In addition, it was observed that an electrostatic favorable region (blue polyhedron) was displayed away from the terminal phenyl ring. Furthermore, a potential

preference for positively charged groups in this position is suggested by a smaller electrostatic favorable region relatively close to the biphenyl moiety's terminal phenyl ring. Conversely, the unfavorable electrostatic regions (red polyhedrons) were notably adjacent to the phenyl ring linked to the sulfonamide group, implying that negative charges in this position might enhance the activity (**Figure 5.11A** and **5.11B**).

Despite having a similar active site orientation to compound 22b, which is the least active, compound 14b has a comparatively strong MMP-2 inhibitory effect ($IC_{50} = 210$ nM). This discrepancy between its structural arrangement and its activity, classifying compound 14b as an outlier, challenges the model's explanatory capacity for this specific compound. Therefore, compound 14b is considered an outlier within this structural-activity relationship analysis.

5.1.7.2. Comparative molecular similarity indices analysis (CoMSIA) study

The CoMSIA model on the second dataset compounds (**Table 5.2**), employing steric, electrostatic, hydrophobic, hydrogen bond acceptor, and hydrogen bond donor fields, constructed with 2 components, depicted different contributions from these features: steric (S) at 9%, electrostatic (E) at 36%, hydrophobic (H) at 18.80%, hydrogen bond acceptor (A) at 13%, and hydrogen bond donor (D) at 23.20% (**Table 5.10**). Moreover, the model's robust statistical validation was evidenced by a Q^2 value of 0.560, signifying its reliability in predicting biological activity within the dataset. Additionally, the r^2_{pred} value of 0.556 from external validation confirms its credibility in predicting the activity of compounds. Notably, the substantially high R^2 value of 0.931 (**Table 5.10**) reflects the model's strong correlation with observed data, indicating an exceptional quality in fitting the known data points. The comparative analysis between observed versus predicted activity, depicted in **Table 5.9** and **Figure 5.7C**, further affirms the robustness of the model and reliability in predicting compound activities. These validation parameters collectively endorse the model's accuracy, reliability, and robust predictive capability, suggesting its potential utility in guiding rational drug design and development processes. The insights derived from this CoMSIA model provided a comprehensive understanding of the molecular features influencing compound activity, offering valuable guidance for designing new compounds with optimized biological effects.

The terminal phenyl group of the biphenyl scaffold for the best active molecule, compound 29b, was found to be in close proximity to the favorable electrostatic fields (blue contour) and steric (green polyhedron) (**Figure 5.11C**). Additionally, the terminal phenyl ring was situated in close proximity to the magenta polyhedron, a hydrophobic contour that was advantageous

(**Figure 5.11C**). It was observed that in this region, positively charged, hydrophobic, and steric groups were favorable for enhanced MMP-2 inhibitory efficiency of such molecules.

Likely, the least active molecule, compound 22b, it was noted that the position of the *p*-nitro group was distanced from regions that are favorable in terms of steric and hydrophobic characteristics, as depicted in **Figure 5.11D**. Thus, the analysis pointed out that to enhance MMP-2 inhibition, it's crucial to have steric and hydrophobic substituents positioned advantageously within the molecular structure. The red polyhedron in the CoMFA contour plots indicated an electrostatically unfavorable region close to the phenyl ring connected to the sulfonyl group. This result revealed that the presence of negatively charged substituents in this particular location may have a beneficial effect on MMP-2 inhibition (**Figures 5.11C and 5.11D**).

Further analysis revealed additional insights into MMP-2 inhibition among different compounds. An unfavorable hydrophobic contour (cyan polyhedrons) at one end suggested that hydrophobic substituents in those positions might hinder MMP-2 inhibition (**Figure 5.11C and 5.11D**). Similarly, a sterically unfavorable region (yellow polyhedrons) close to the dimethylene groups indicated that steric groups in those regions could potentially hinder the MMP-2 inhibition. Although these findings were consistent for compound 14b compared to the least active compound 22b, compound 14b exhibited unexpectedly higher MMP-2 inhibitory activity. This discrepancy led to considering compound 14b as an outlier in the CoMSIA model developed. Understanding these small differences is crucial for understanding the complex relationships between molecular structures and MMP-2 inhibition.

In Addition, it was noticed that the most active compound (compound 29b), the sulfonyl oxygen atoms, and other oxygen atoms all fitted into favorable acceptor regions (orange polyhedrons), indicating their potential for forming hydrogen bonds, contributing to increased MMP-2 inhibition (**Figure 5.11E**). Conversely, the least active molecule (compound 22b) showed a contrasting orientation of the oxygen atom at the gamma terminal compared to the same carbon in the most active compound (compound 29b) (**Figure 5.11E vs. 5.11F**). This suggested the significance of the gamma terminal's orientation in forming crucial hydrogen bonds at the active site, impacting MMP-2 inhibition. An unfavorable hydrogen bond acceptor region (white polyhedron) covered the total area for all compounds, suggesting that smaller hydrogen bond acceptor groups might be preferable, while bulkier ones were not conducive for higher MMP-2 inhibitory activity. Furthermore, both favorable (deep blue polyhedron) and unfavorable (violet polyhedron) hydrogen bond donor regions were

positioned away from the molecular structure, indicating that such donor groups were not advantageous in those positions for increased MMP-2 inhibitory efficacy. Despite similarities in orientations and contour regions between the least active compound (compound 22b) and the relatively effective compound 14b, the CoMSIA model couldn't justify these differences. Consequently, compound 14b was regarded as an outlier within this analysis. These findings emphasize the importance of specific molecular orientations, hydrogen bonding capabilities, and optimal functional groups in designing compounds for effective MMP-2 inhibition.

5.1.8. Molecular dynamics (MD) simulation study

The molecular dynamics simulation study on the second dataset (**Table 5.2**), involved subjecting the best active and least active molecules of the dataset i.e., compounds 29b and 22b respectively, along with MMP-2 (PDB ID: 1HOV), to two separate 200 nanosecond MD simulations using the Schrodinger Suite (Schrodinger Suite). Post-simulation analysis files were generated for the four 200 ns runs (two for each compound), revealing that two independent simulations for each complex exhibited promising outcomes (**Figure 5.12**). The study implies that the observed dynamics potentially mirror the actual behavior of these complexes. However, it was important to consider factors such as force field accuracy and initial conditions impacting simulation reliability. The consistent results across these parallel runs increase confidence in the findings' validity. Further validation and in-depth analysis will be imperative to confirm and leverage these results for understanding the interactions between compounds 29b and 22b with MMP-2.

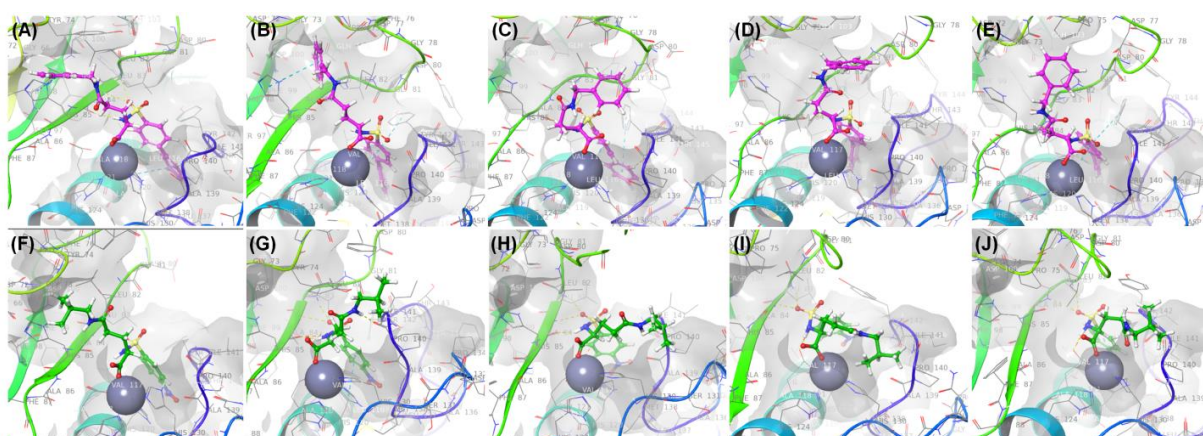


Figure 5.12. The binding mode of compound 29b at the MMP-2 binding site at (A) 0 ns (B) 50 ns (C) 100 ns (D) 150 ns (E) 200 ns; The binding mode of compound 22b at the MMP-2 binding site at (F) 0 ns (G) 50 ns (H) 100 ns (I) 150 ns (J) 200 ns

In the trajectory analysis of the conducted MD simulation studies, fundamental analyses were performed. Key metrics such as the root mean square deviation (RMSD) of the protein and ligand (compound 29b, **Figure 5.13A** and compound 22b, **Figure 5.13B**), as well as the assessment of ligand atom fluctuations concerning both the protein and the ligand (compound 29b, **Figure 5.13C**, and compound 22b, **Figure 5.13D**), were carried out. Additionally, the root mean square fluctuation (RMSF) for the C- α chain in MMP-2 (PDB ID: 1HOV) was computed (compound 29b, **Figure 5.13E** and compound 22b, **Figure 5.13F**). These analyses are pivotal in understanding the stability, deviations, and fluctuations in the protein-ligand complex throughout the simulation period. RMSD provides insights into overall structural changes, while RMSF identifies specific regions undergoing significant fluctuations, aiding in comprehending the dynamic behavior of the complex, critical for evaluating the interaction dynamics between the protein MMP-2 and the ligands under study.

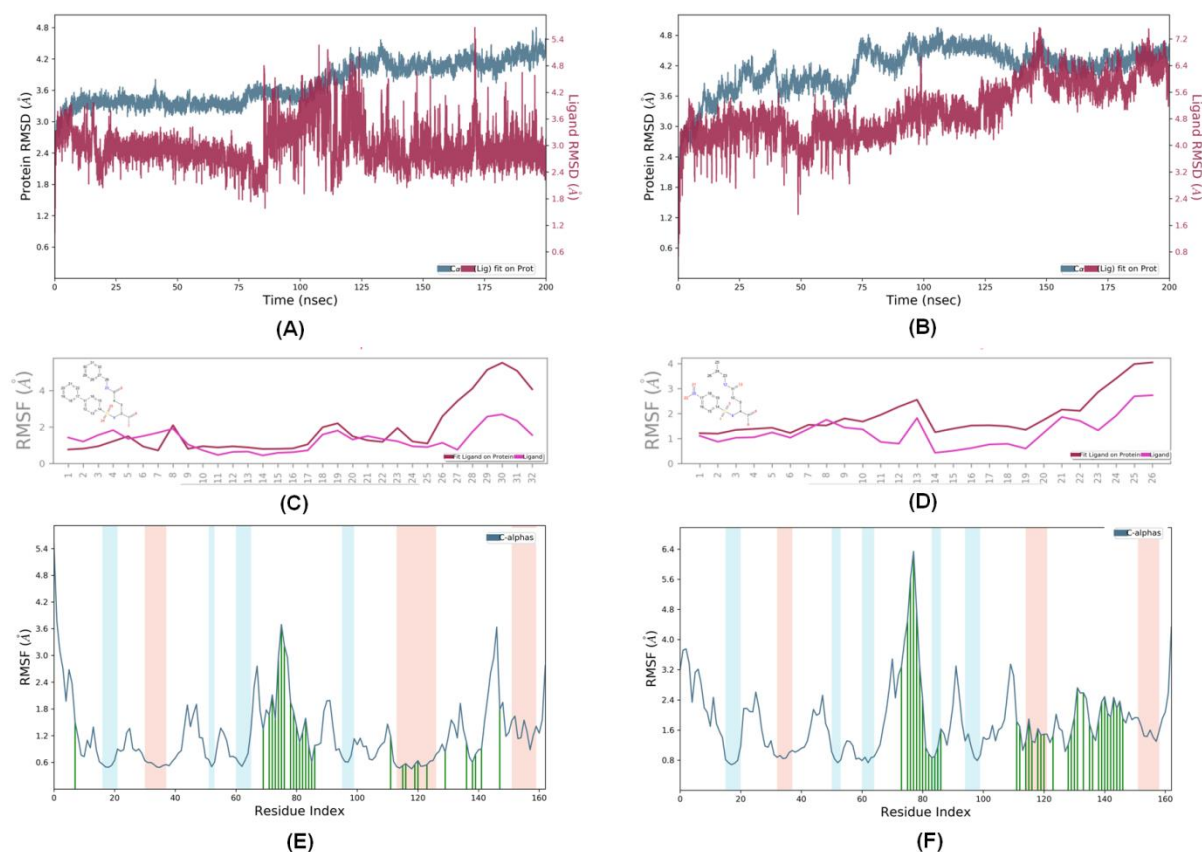


Figure 5.13. The RMSD generated from the MD simulation of (A) MMP-2 (PDB ID: 1HOV) and compound 29b complex, (B) MMP-2 (PDB ID: 1HOV) and compound 22b complex, the RMSD of the atoms of (C) compound 29b, (D) compound 22b, the RMSF of the C- α chain residues of MMP-2 produced from the MD simulation study of (E) MMP-2 (PDB ID:

1HOV) and compound 29b complex, (F) MMP-2 (PDB ID: 1HOV) and compound 22b complex.

The RMSD analysis showed that the protein connected to compound 29b had a lower RMSD than the protein connected to compound 22b, although both compounds had similar fluctuations (compound 29b, **Figure 5.13A** and compound 22b, **Figure 5.13B**). The RMSD of the connected parts of the compounds revealed that a specific section called the P2' substituent in both compounds 29b and 22b moved a lot, more than 3(Å), while another part called the S1' pocket substituent (P1') had less movement, less than 3(Å). This suggests that the P1' part of the compounds is more stable inside the S1' pocket. The atoms from the biphenyl P1' portion of compound 29b fluctuated less than 1(Å) than the P1' part of compound 22b, according to a comparison of the stability of the S1' pocket substituent in the two compounds (**Figure 5.13C** vs **5.13D**). This indicates that the biphenyl P1' part has greater stability inside the MMP-2 S1' pocket (PDB ID: 1HOV) compared to the 4-NO₂-phenyl P1' part of compound 22b.

The RMSF (Root Mean Square Fluctuation) analysis for the C- α chain of MMP-2 when connected with compounds 29b and 22b (**Figure 5.13E** and **5.13F**) displayed similar fluctuations among the amino acid residues, yet some differences were noticed. Specifically, in the MMP-2-compound 22b complex, certain amino acids such as Pro75 (3.96 Å), Phe76 (4.48 Å), Asp77 (5.62 Å), Gly78 (6.34 Å), and Lys79 (4.79 Å) showed higher fluctuations compared to the MMP-2-compound 29b complex (**Figure 5.13E** and **5.13F**, respectively). This difference could potentially result from the influence of the alkyl P2' part of compound 22b, which might have had a greater impact on the loop forming the S2' pocket, compared to the benzyl P2' part of compound 29b. This difference could affect how well each compound binds to the S2' pocket of MMP-2.

5.1.8.1. Analysis of protein-ligand contacts

An important factor in defining an inhibitor's inhibitory activity is its interaction with a ligand through its active site residues. To assess this, a post-MD simulation analysis of protein-ligand interactions was conducted for the simulated complexes (**Figure 5.14**). This analysis aimed to understand and evaluate how the protein and the ligand molecules were interacting after the molecular dynamics (MD) simulations. Identifying and analyzing these interactions is essential as they play a significant role in the effectiveness of inhibitors in binding to the target protein's active site.

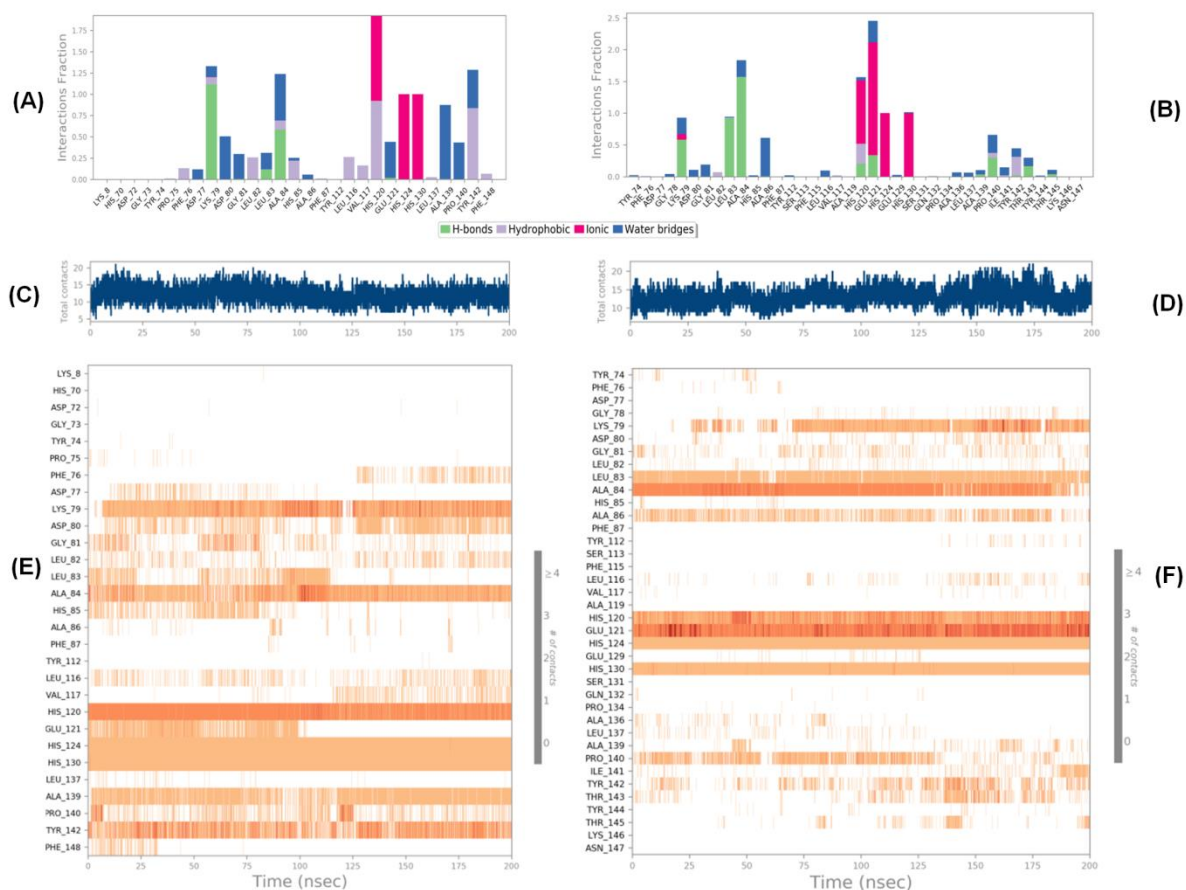


Figure 5.14. The interaction fractions of (A) compound 29b and (B) compound 22b with MMP-2 (PDB ID: 1HOV) active site residues; Total contacts vs time plot for the simulation studies of (C) MMP-2-compound 29b complex and (D) MMP-2-compound 29b complex; The interaction frequencies of individual residues between (E) MMP-2 and compound 29b and (F) MMP-2 and compound 22b for 200 ns

It was found from the MD simulation study that compound 29b interacted through hydrogen bonds with particular residues such as Lys79, Leu83, Ala84, and Glu121 at the MMP-2 active site. It also interacted with a number of other important residues from binding sites, including Tyr112, His120, Phe76, Leu82, Ala84, His85, Fhe87, Tyr137, Tyr142, and Phe148. In addition to these interactions, compound 29b was found to interact with significant Ω -loop residue Pro140 of MMP-2 as well as critical active site residues such as His85, Ala84, His120, Glu121, His124, and His130. These interactions were also observed by ionic water-mediated interactions. Conversely, the less active compound 22b interacted with several key active site residues of MMP-2, yet the bond formation extent of its P1' substituent was notably lower compared to compound 29b (Figure 5.14A vs 5.14B). Additionally, compared to compound 22b, compound 29b had more stable connections with active site residues based

on the overall number of contacts between the protein and ligands (**Figure 5.14C** and **5.14D**). This suggests that compound 29b displayed more stable and stronger interactions at the active site of the MMP-2 protein compared to compound 22b.

Furthermore, the frequency of individual interactions between residues (**Figure 5.14E** and **5.14F**) clearly demonstrates the differences in the development of contacts between MMP-2 amino acid residues and the compounds that are most and least active (compound 29b and 22b, respectively). Notably, compound 29b displayed frequent interactions with key active site residues such as Ala84, His120, His124, His130, and Tyr142 (**Figure 5.14E**). Conversely, compound 22b exhibited a high frequency of contact with residues such as His120, Glu121, Leu83, Ala84, His124, and His130 (**Figure 5.14F**). Compound 22b did not bind with Tyr142 and Thr143, two more essential hydrophobic S1' pocket residues, but it did interact more frequently with catalytic Glu121 and Ω -loop Pro140 residues than compound 29b did. The absence of these interactions might affect the stability of compound 22b at the hydrophobic S1' pocket, potentially leading to reduced inhibitory activity against MMP-2. Therefore, this difference in interaction frequency could contribute to the lower inhibitory potential of compound 22b compared to compound 29b.

In the comprehensive analysis of interactions derived from the MD simulation study (**Figure 5.15**), it was observed that in compound 29b, one of the phenyl rings from the biphenyl S1' pocket section established a stable π - π interaction with the His120 residue, occurring about 88% of the time. Furthermore, it formed water-mediated hydrogen bond interactions with Tyr142, Glu121, and Ala84 residues through water-mediated (**Figure 5.15A**). In contrast, compound 22b did not interact with the particular residues required for establishing the S1' pocket, although it did exhibit direct hydrogen bond interactions with the residues Leu83 (86 % occurrence), Ala84 (88 % and 67 % occurrence), and Glu121 (33 % occurrence) (**Figure 5.15B**). This distinct difference in interactions suggests that compound 29b formed more stable and specific interactions with key residues essential for S1' pocket formation compared to compound 22b.

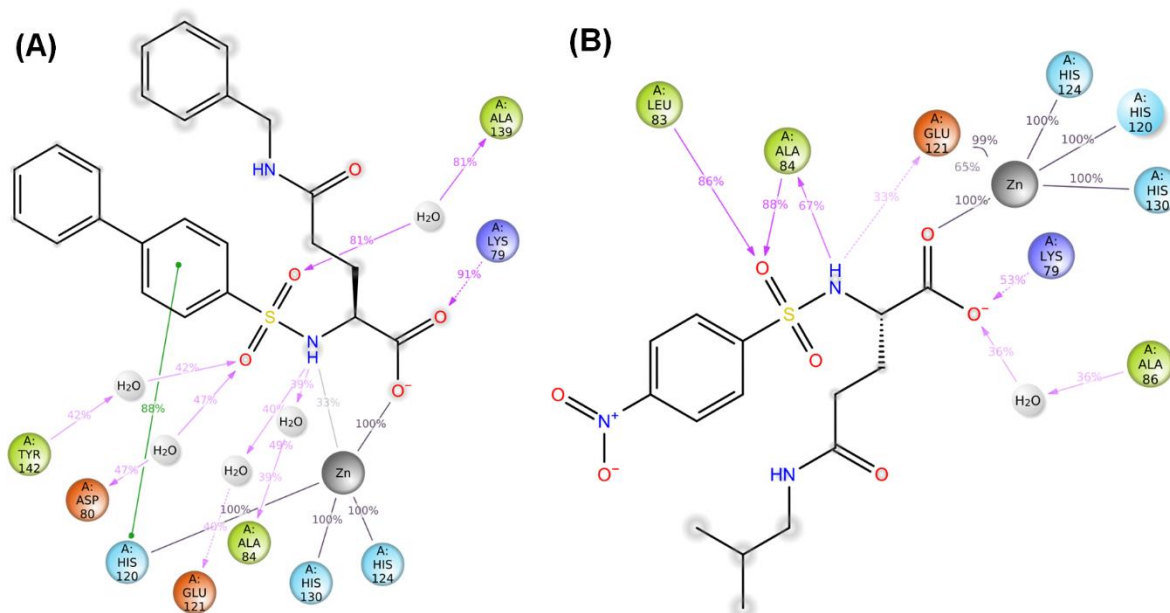


Figure 5.15. The overall interaction occupancies obtained from the MD simulation study of (A) MMP-2-compound 29b complex and (B) MMP-2-compound 22b complex.

5.1.8.2. Molecular Mechanics Generalized Born and Surface Area (MM/GBSA) calculation

The Schrodinger Suite's Prime MM/GBSA module was utilized to calculate the $\Delta G_{\text{binding}}$ values of the complexes obtained from the 200 nanosecond MD simulation study. The average $\Delta G_{\text{binding}}$ for compound 29b complexed with MMP-2 (PDB ID: 1HOV) was determined to be -38.975 kcal/mol, with a standard deviation (SD) of 9.91. The $\Delta G_{\text{binding}}$ values were found to be between -57.345 and -11.958 kcal/mol. Again, the range of $\Delta G_{\text{binding}}$ for compound 22b complexed with MMP-2 (PDB ID: 1HOV) was -51.444 kcal/mol to -16.000 kcal/mol. The average $\Delta G_{\text{binding}}$ value for this complex was determined as -34.510 kcal/mol, with a standard deviation of 8.52. These values provide insight into the energetics of binding for the two complexes, suggesting that compound 29b displayed a higher average binding affinity compared to compound 22b towards MMP-2.

5.1.8.3. Analysis of Free energy landscape (FEL)

Gibb's free energy was calculated for both complexes using the first two principal components (PC1 and PC2) of a 200 nanosecond simulation, which also produced the Free Energy Landscape (FEL) graph (**Figure 5.16**). The MMP-2-compound 22b and MMP-2-compound 29b complexes both showed the formation of multiple clusters, according to the FEL graphs. In contrast to the MMP-2-compound 29b complex, the MMP-2-compound 22b complex (**Figure 5.16A**) showed more stable conformations, which are shown by darker

violet/blue regions (**Figure 5.16B**). This suggests that, although both complexes exhibited different clusters indicating different conformations, the MMP-2-compound 22b complex generally maintained more stable structural arrangements throughout the simulation compared to the MMP-2-compound 29b complex.

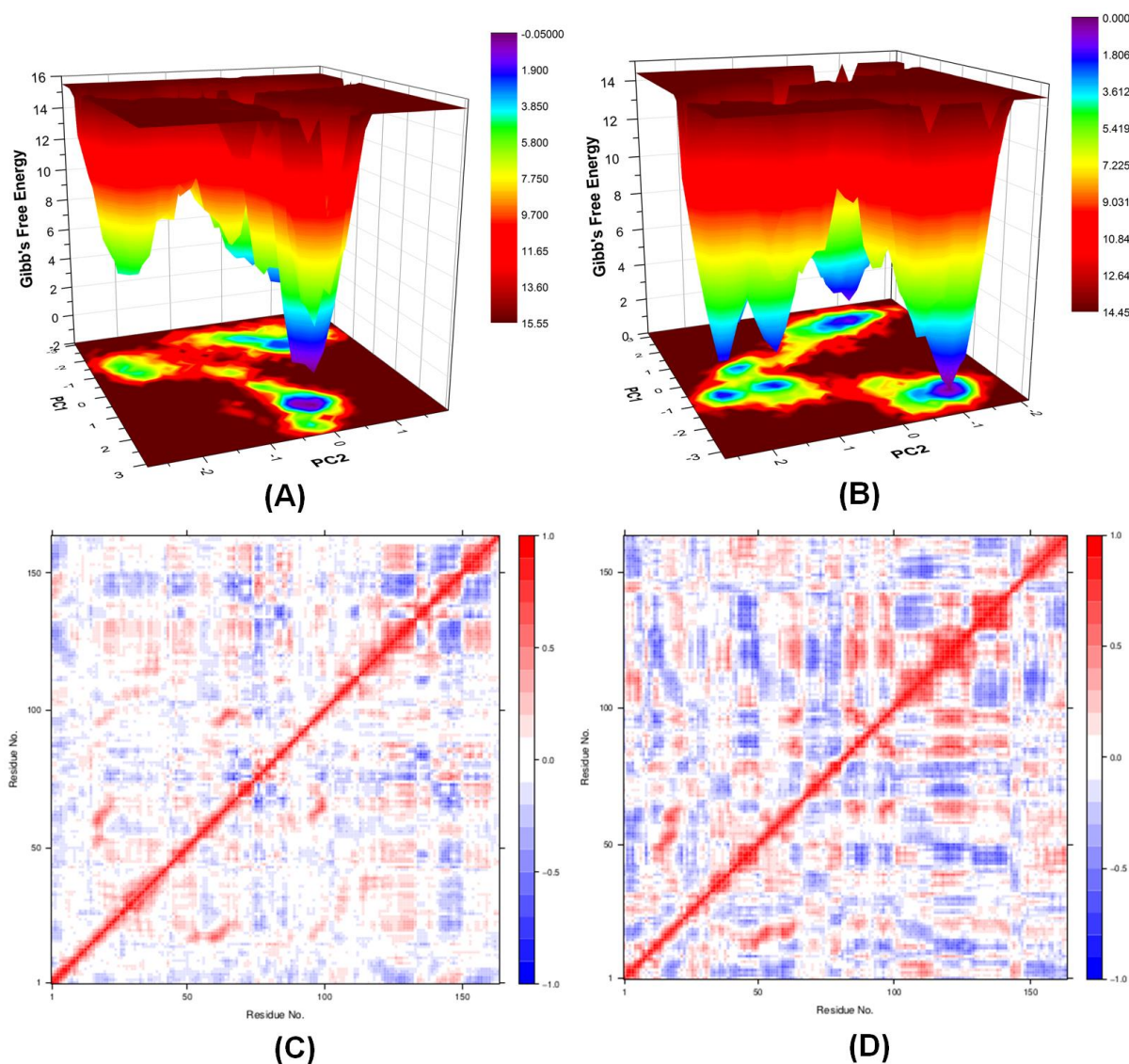


Figure 5.16. Free energy landscape (FEL) of (A) MMP-2-compound 29b complex and (B) MMP-2-compound 22b complex; The dynamic cross- correlation matrix (DCCM) for the C- α chain of (C) MMP-2-compound 29b complex, and (D) MMP-2-compound 22b complex.

5.1.8.4. Dynamic cross-correlation map (DCCM) and principal component analysis (PCA) study

For every simulated complex, the covariance matrix from the atoms' movements in the C- α chain of MMP-2 was computed to generate the Dynamic Cross-Correlation Map (DCCM). Their eigenvalues and eigenvectors were used in this procedure. **Figure 5.16C** and **Figure**

5.16D show the DCCM developed for the MMP-2-compound 29b and MMP-2-compound 22b complexes, respectively. These maps provided insights into the correlated motions among the atoms in the protein structure and the ligands over the course of the simulations, offering information about how different parts of the complexes move in relation to each other.

The PCA of the simulation trajectories, as shown in **Figure 5.17**, distinctly highlights the differences between the two systems under study. Notably, the study showed that PC1 and PC2 together accounted for 43.7 % of the diversity in the protein trajectories for the MMP-2-compound 29b complex (**Figure 5.17A**). This indicates that these two principal components captured a significant portion of the variability and behavior of the protein within this specific complex throughout the simulation.

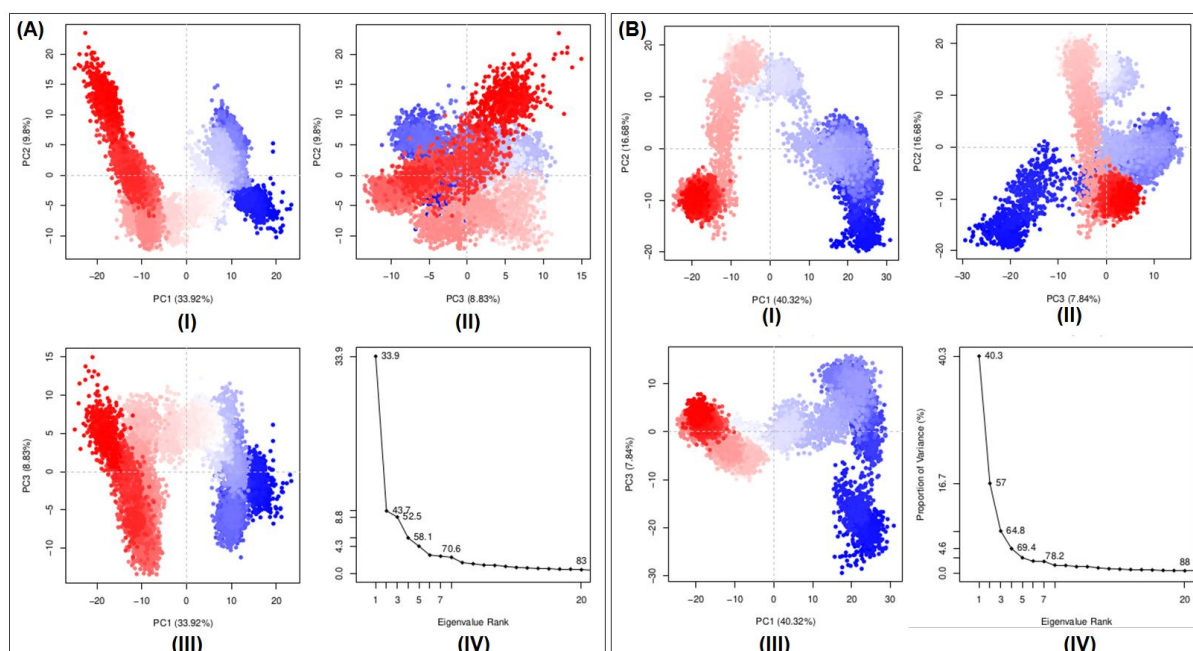


Figure 5.17. PCA analysis for the C- α chain of MMP-2 in complex with (A) compound 29b and (B) compound 22b.

Moreover, the MMP-2-compound 29b complex, PC1 independently accounted for 33.9% of the variance in the protein trajectory. However, for the MMP-2-compound 22b complex, PC1 and PC2 together explained 57% of the variance, with PC1 accounting for 40% of the variation in the protein trajectory (as depicted in **Figure 5.17B**). According to this data, compared to the MMP-2-compound 29b complex, where PC1 alone held a lower but still significant portion of variance, both PC1 and PC2 collectively contributed to a larger

percentage of explained variance in the protein's trajectory in the context of the MMP-2-compound 22b complex.

5.1.8.5. Probability density function (PDF) analysis

Protein trajectories' chance of occurring is displayed by the Probability Density Function (PDF) analysis, which is based on Kernel Density Estimation (KDE). For the MMP-2-compound 29b and MMP-2-compound 22b complexes, the PDF plots were created using the radius of gyration (R_g) and the root mean square deviation (RMSD), as shown in **Figures 5.18A** and **5.18B**, respectively. These plots provided insights into the distribution and likelihood of different conformations or structural states adopted by the protein in these two distinct complexes over the course of the simulation.

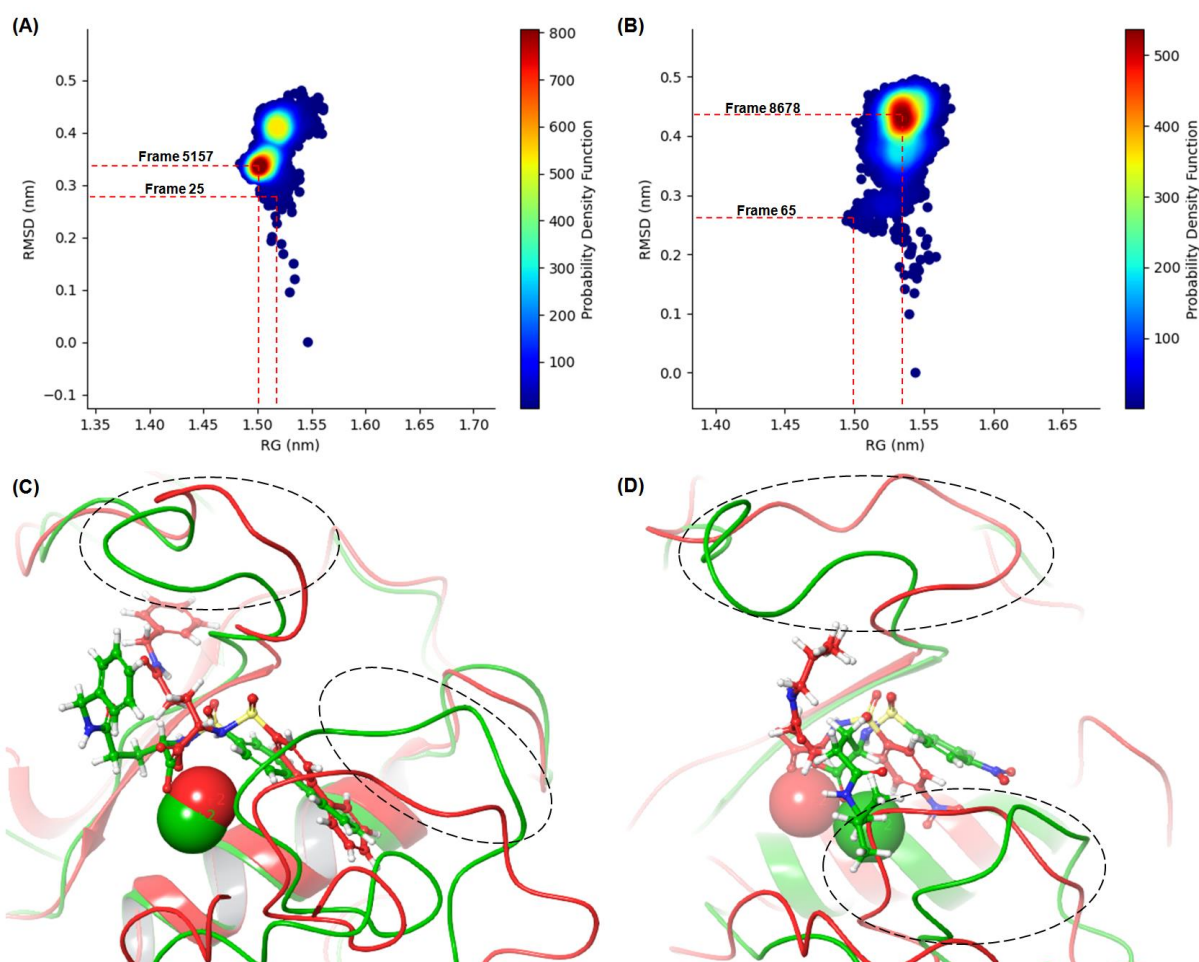


Figure 5.18. Probability density function (PDF) of (A) MMP-2-compound 29b complex and (B) MMP-2-compound 22b complex; The least (red) and the most (green) developed

conformations for **(C)** MMP-2-compound 29b complex and **(D)** MMP-2-compound 22b complex.

The PDF analysis of the MMP-2-compound 29b complex revealed an interesting finding: the most common conformations were linked to a R_g value of 1.50 nm and an RMSD value of 0.34 nm, respectively. Conversely, the less common conformations were associated with a R_g of 1.52 nm and an RMSD of 0.28 nm, respectively (depicted in **Figure 5.18A**). The predominant conformations of the MMP-2-compound 22b complex, on the other hand, were determined to have an RMSD value of 0.44 nm and a R_g value of 1.53 nm, respectively. The MMP-2-compound 22b complex was found to have less frequent conformations with corresponding R_g values of 1.50 nm and RMSD values of 0.27 nm (**Figure 5.18A**). These observations highlight the prevalence and distribution of specific conformations for each complex, offering insights into their structural behavior and variability during the simulation. A significant change in the protein conformation was seen in the analysis of the most (green ribbon) and least (red ribbon) populated conformations of the MMP-2-compound 29b and MMP-2-compound 22b complexes (**Figure 5.18C** and **5.18D**, respectively). This was particularly noticeable in the MMP-2-compound 22b complex. Both the loop forming the MMP-2 S2' pocket and the S1' loop showed notable changes in this complex. In contrast to the least crowded conformation, where the Ω -loop active site appeared to have moved away from the entrance of MMP-2's S1' pocket, the most populated conformation showed a broader S1' pocket. This led to an enlargement of the S1' pocket and a potential destabilization of the binding of the P1' substituent for compound 22b. The presence of a polar NO₂-group within the hydrophobic S1' pocket of MMP-2 or the extremely flexible P2' substituent of compound 22b, which shifted away from the S2' pocket and into the Ω -loop, could be the reason of this conformational change (**Figure 5.18D**). In comparison, the positions of the S1' loop, Ω -loop, and S2' pocket forming loops in the MMP-2-compound 29b complex did not significantly alter. This stability facilitated a consistent binding of the molecule within the S1' pocket, potentially contributing to its high inhibitory activity against MMP-2.

[The work was published in *SAR QSAR Environmental Research*, 2023, 34(10):1-26.]

5.1.9. Overview form molecular modeling study

The research delves into the significance of MMP-2 in cancer regulation, proposing it as a promising target for the development of anticancer drugs. The study focused on the two

datasets i.e., conducted on sulfonyl pyrrolidine-based MMP-2 inhibitors (compounds 1a-65a) (**Table 5.1**) and *in house* 32 specific arylsulfonyl L(+) glutamine molecules (compounds 1b-32b) (**Table 5.2**), employing various quantitative structure-activity relationship (QSAR) models (such as multiple linear regression, HQSAR study, LDA model, bayesian classification study, CoMSIA, docking based 2D-QSAR study, 3D-QSAR, MD simulation) to identify crucial structural features essential for inhibiting MMP-2 effectively.

From the MLR and classification-based model it was found that arylsulfonamide moiety and hydroxamates were crucial for the MMP-2 inhibition. Moreover, hydroxamates are better zinc chelators than ester function and may be favorable for the MMP-2 inhibitory efficacy. From the CoMFA and CoMSIA, it was found that steric and hydrophobic substituents were favorable at the terminal phenyl ring position. Furthermore, the findings from docking-based 2D-QSAR models underscored the significance of specific energies associated with amino acids such as Tyr142 and Ala84 in the inhibition of MMP-2. Moreover, the results highlighted the preference for steric and hydrophobic attributes at the terminal phenyl ring, while indicating an adverse effect on P2' substituents. Additionally, the molecular modeling revealed that smaller hydrogen bond groups were beneficial, whereas hydrogen bond donor groups did not contribute to inhibiting MMP-2. The crucial structural features of MMP-2 inhibitors are provided in **Figure 5.19**.

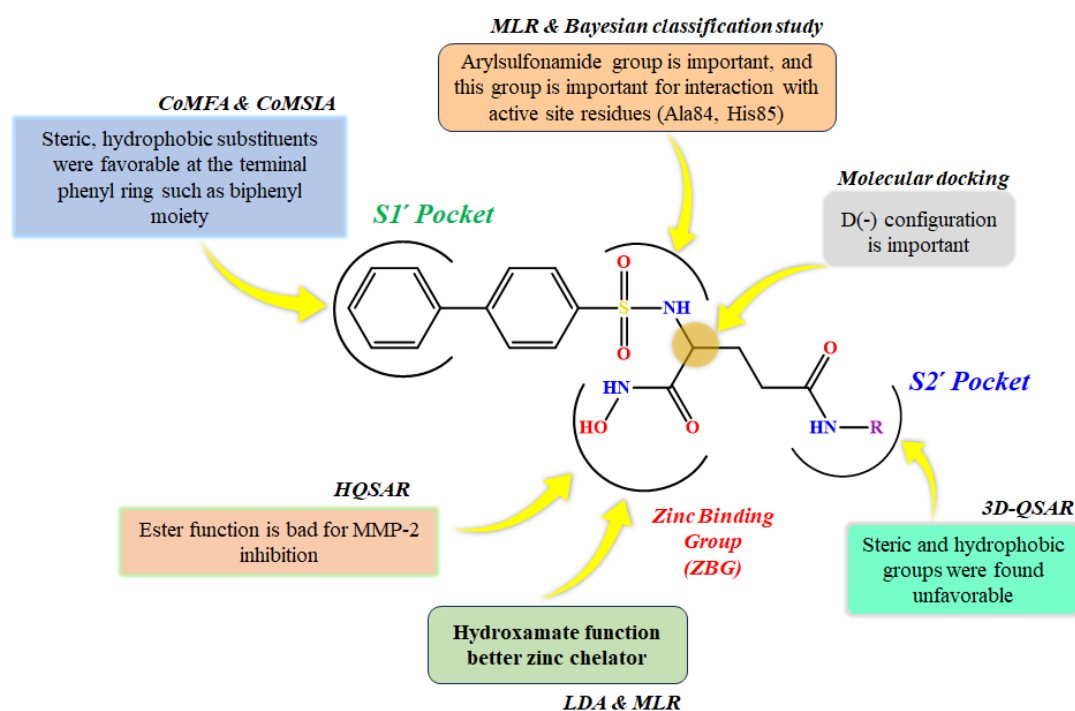


Figure 5.19. Crucial structural features finding from molecular modeling study of MMP-2 inhibitors

Molecular dynamics (MD) simulations showcased stable interactions between MMP-2 and the tested inhibitors, displaying minimal fluctuations in parameters such as RMSD, RMSF, and Rg values. This analysis also identified specific amino acid residues responsible for potential hydrogen bonding, further contributing to inhibiting MMP-2.

In summary, the study suggests that the insights obtained from these multi-QSAR modeling approaches and the analysis of binding interactions hold promise for the development of more effective MMP-2 inhibitors with heightened potential for combating cancer in the future.

5.1.10. Designing of MMP-2 inhibitors

The designing of potential MMP-2 inhibitors as anticancer agents, in this context, a series of arylsulfonamido glutamine analogs had been designed. Hydroxamates, a class of compounds renowned for their ability to chelate metal ions, have emerged as promising MMP-2 inhibitors with potential applications in cancer therapy. By binding to the active site of MMP-2, these hydroxamate-based inhibitors hinder the enzyme's role in degrading the extracellular matrix, thereby showing promise in impeding tumor invasion, angiogenesis, and metastasis. Their mechanism of action involves specifically targeting MMP-2, which plays a crucial role in cancer progression. Although these inhibitors exhibit potential as anti-cancer agents by suppressing metastasis, inhibiting angiogenesis, and potentially limiting tumor growth, further research is necessary to enhance their specificity, efficacy, and safety profile for future clinical use in combating cancer. Therefore, from the initial molecular modeling study, it has been found that hydroxamates were a potential zinc binder and exhibited a good rigid binding mode of interaction at the active site of the MMP-2 enzyme (**Figure 5.20**).

In this work, the synthesized molecules were designed from the outcome of these two series (*in house* molecules and molecules from Shandong University) of molecular modeling study. Henceforth, the molecules were designed in such a way that this analog can fit perfectly at the MMP-2 enzyme active site for obtaining potential and selective efficacy. It is interesting to note that, the designed compound should have arylsulfonamide group having steric and hydrophobic substituents. Moreover, these compounds must contain hydroxamates that function as Zn^{2+} chelators, rather than esters of any carboxylate function for achieving better efficacy. Docking interactions of the preliminary compound (DH-1) (**Table 5.11**) were depicted in **Figure 5.20** along with designing approaches of proposed molecules.

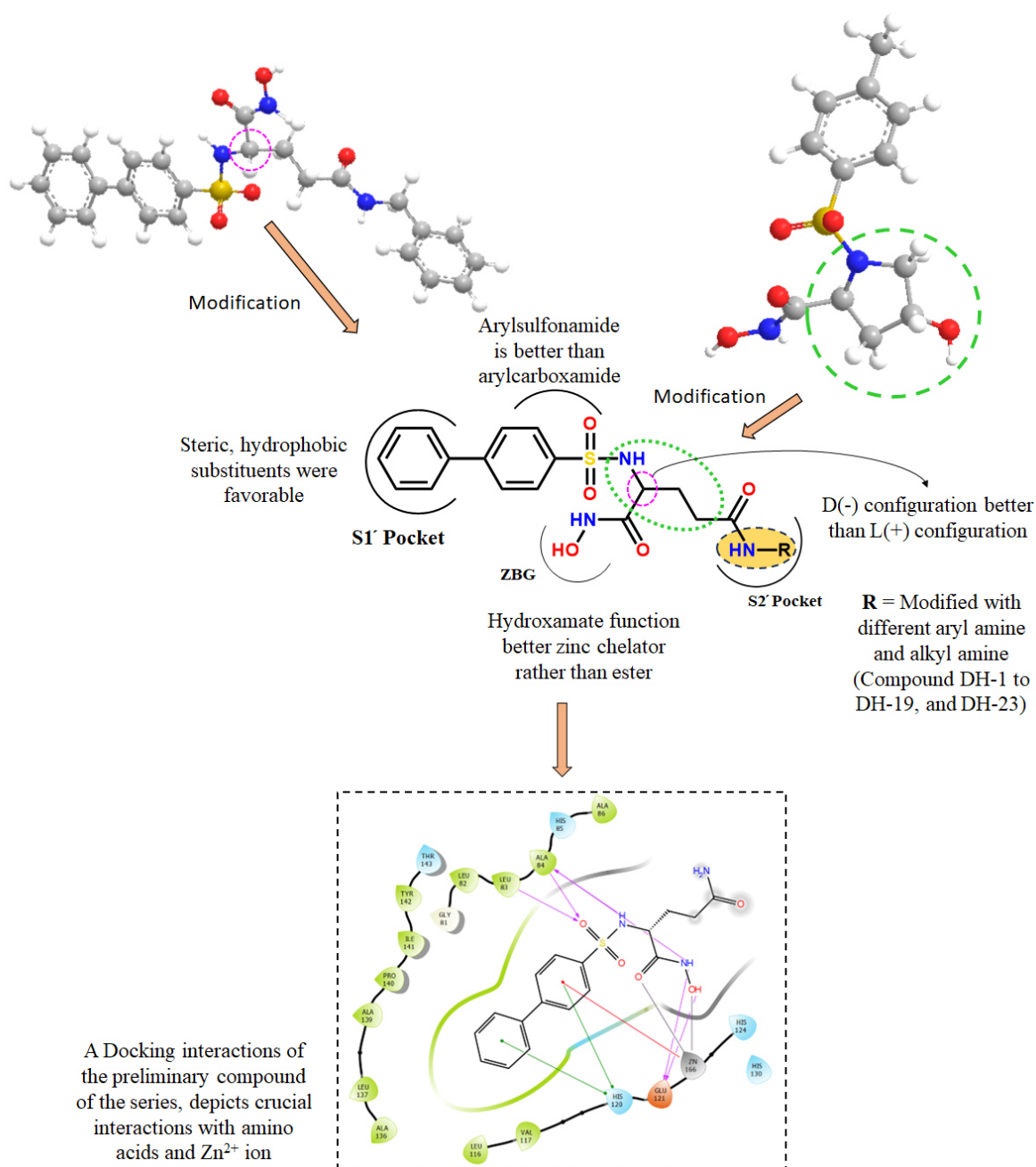


Figure 5.20. Designing approaches for the proposed arylsulfonamide hydroxamates-based D(-) glutamic analogs as potential MMP-2 inhibitors.

One previous study conducted by Adhikari and colleagues in 2016 focused on investigating the potential of biphenylsulfonyl L(+) glutamines as inhibitors of Matrix Metalloproteinase-2 (MMP-2), showing selectivity over MMP-9. Therefore, in this study, it has been explored from this molecular modeling study whether the mirror-image versions of biphenylsulfonyl L(+) glutamines, known as the corresponding biphenylsulfonyl D(-) glutamine analogs,

might exhibit stronger inhibition of MMP-2 or if their different molecular structure would have an impact on inhibitory activity. Henceforth, before synthesizing these compounds, the biphenylsulfonyl D(-) glutamine analogs were computationally modeled and docked into the active site of MMP-2 to predict how they might interact with the enzyme (**Figure 5.20**). A docking interaction of a preliminary compound (DH-1) from the series is shown in **Figure 5.20** where it depicts crucial interaction with the amino acids such as Leu83, Ala84, and His120 along with hydroxamates moiety conjugate with the Zn^{2+} ion of the MMP-2 enzyme active site.

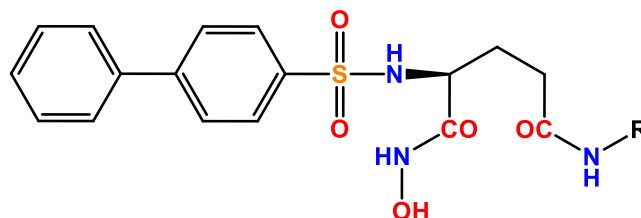
Surprisingly, the computational simulations suggested that these biphenylsulfonyl D(-) glutamines could potentially be more effective inhibitors of MMP-2 compared to their mirror-image biphenylsulfonyl L(+) glutamine analogs, indicating that the different stereochemistry or conformation might significantly influence their ability to inhibit MMP-2 activity. This finding is promising as it suggests a potential for developing more potent and selective MMP-2 inhibitors by considering the specific molecular structures or stereochemical properties of these compounds. Further experimental validation and synthesis of these biphenylsulfonyl D(-) compounds could provide valuable insights into their actual inhibitory potential and pave the way for more effective anti-cancer agents.

Part B

5.2. Synthesis of the designed glutamine derivatives and analogs

Derivatives of sulfonamide containing hydroxamates-based D(-)glutamic acid and its analogs were synthesized in different steps. In the synthesis procedure, the biphenylsulfonyl chloride was condensed with glutamic acid to prepare the corresponding biphenylsulfonyl glutamic acids. These analogs were further cyclized to prepare their corresponding monoacids which on subsequent amination produced the desired substituted biphenylsulfonyl glutamine analogs. After those biphenylsulfonyl glutamine analogs were prepared for the esterification and finally hydroxamates containing biphenylsulfonyl glutamic acid derivatives were prepared by amination with the hydroxyl amine of the ester compounds. The detailed of the synthesis procedure has been discussed in Chapter 5 (*Scheme 5.1*). However, the final steps of the synthesis procedure compounds' i.e., hydroxamates-based analogs (*6a-6t*) physical properties are depicted in **Table 5.11**.

Table 5.11. Physical properties of hydroxamates-based analogs 5-N-Substituted 2-(substituted biphenylsulfonyl) D(-) glutamines.



Serial No	Compound	R	Mol. Wt.	% Yield	Melting Point (°C)
1	DH-1	H	377.41	55.81	165-167
2	DH-2	CH ₃	391.44	76.92	164-168
3	DH-3	C ₂ H ₅	405.47	73.53	174-177
4	DH-4	<i>n</i> -Propyl	419.49	48.16	171-174
5	DH-5	<i>i</i> -Propyl	419.49	61.23	175-179
6	DH-6	<i>n</i> -butyl	433.52	73.41	171-175
7	DH-7	<i>i</i> -butyl	433.17	47.29	170-175
8	DH-8	<i>n</i> -Pentyl	447.55	61.81	175-178
9	DH-9	<i>c</i> -hexyl	459.56	75.50	180-185
10	DH-10	<i>n</i> -hexyl	461.57	76.67	190-192
11	DH-11	Phenyl	453.51	47.76	204-208
12	DH-12	Benzyl	467.54	69.52	198-204
13	DH-13	β-Phenylethyl	481.56	63.63	198-202

14	DH-14	2-Cl Bnz	501.98	78.85	201-203
15	DH-15	4-Cl Bnz	501.98	71.42	183-186
16	DH-16	3,4-diCl Bnz	536.43	70.00	194-197
17	DH-17	4-OCH ₃ Bnz	497.56	65.52	196-199
18	DH-18	3,5-diCF ₃ Bnz	603.53	73.11	195-199
19	DH-19	4-FBnz	485.53	71.56	187-190
20	DH-20	t-but	433.52	68.44	178-182

5.2.1. Characterization of the synthesized molecules

All the final products were characterized through high-resolution mass spectroscopy (HRMS), ¹H NMR, and ¹³C NMR (**Figure A4–Figure A43**) (Appendix). Spectral data of These analytical data are given below:

2-([1,1'-biphenyl]-4-sulfonamido)-N¹-hydroxypentanediamide (**DH-1**)

MS (ESI Positive) *m/z* [M+H⁺]: 378.05. ¹H NMR (400 MHz, MeOD₄) - δ 7.90 – 7.85 (m, 2H), 7.84 – 7.79 (m, 2H), 7.72 – 7.67 (m, 3H), 7.60 – 7.55 (m, 3H), 7.41 – 7.35 (m, 3H), 7.33 – 7.28 (m, 1H), 3.64 (dd, *J* = 8.5, 5.7 Hz, 1H), 2.17 – 1.99 (m, 1H), 1.89 – 1.70 (m, 1H).

¹³C NMR (101 MHz, MeOD₄) - δ 177.17, 176.85, 172.33, 149.33, 143.20, 132.65, 132.04, 131.18, 131.01, 130.85, 57.48, 54.74, 33.30, 32.99, 31.90.

2-([1,1'-biphenyl]-4-sulfonamido)-N¹-hydroxy-N⁵-methylpentanediamide (**DH-2**)

MS (ESI Positive) *m/z* [M+H⁺]: 392.35. ¹H NMR (400 MHz, Methanol-*d*₄) δ 7.79 (d, *J* = 8.6 Hz, 1H), 7.66 (d, *J* = 8.6 Hz, 1H), 7.57 (d, *J* = 7.0 Hz, 1H), 7.42 – 7.38 (m, 2H), 7.34 – 7.31 (m, 1H), 7.10 – 7.04 (m, 2H), 7.01 – 7.98 (m, 1H), 3.77 (dd, *J* = 5.1, 5.1 Hz, 1H), 3.50 (s, 3H), 1.93 – 1.83 (m, 1H), 1.78 – 1.66 (m, 1H), 1.24 – 1.19 (m, 2H).

¹³C NMR (101 MHz, Methanol-*d*₄) δ 172.93, 172.33, 145.89, 141.28, 139.97, 129.12, 128.34, 128.10, 127.91, 127.15, 54.60, 29.04, 27.41.

2-([1,1'-biphenyl]-4-sulfonamido)-N⁵-ethyl-N¹-hydroxypentanediamide (**DH-3**)

MS (ESI Positive) *m/z* [M+H⁺]: 405.02. ¹H NMR (400 MHz, MeOD₄) - δ 7.82 (dd, *J* = 8.5, 3.4 Hz, 2H), 7.70 (dd, *J* = 8.6, 2.1 Hz, 2H), 7.58 (dd, *J* = 9.4, 2.3 Hz, 2H), 7.39 (t, *J* = 7.4 Hz, 3H), 7.31 (t, *J* = 7.3 Hz, 1H), 3.57 (dd, *J* = 8.1, 5.7 Hz, 1H), 3.25 (s, 2H), 2.97 – 2.82 (m, 2H), 2.06 (m, 1H), 2.01 – 1.91 (m, 1H), 0.88 (t, *J* = 7.3 Hz, 3H).

¹³C NMR (101 MHz, MeOD₄) - δ 173.37, 171.25, 145.43, 139.11, 128.76, 128.16, 127.51, 127.16, 126.87, 55.95, 50.79, 33.78, 29.28, 27.99, 13.13.

2-([1,1'-biphenyl]-4-sulfonamido)-N¹-hydroxy-N⁵-propylpentanediamide (DH-4)

MS (ESI Positive) m/z [M+H⁺]: 420.26. ¹H NMR (400 MHz, Methenol-*d*₄) δ 7.81 (d, J = 8.6 Hz, 2H), 7.69 (d, J = 8.7 Hz, 2H), 7.59 – 7.55 (m, 2H), 7.39 – 7.35 (m, 2H), 7.32 – 7.28 (m, 1H), 3.62 (dd, J = 5.6, 5.6 Hz, 1H), 3.02 – 2.93 (m, 2H), 2.14 – 2.06 (m, 2H), 1.85 – 1.66 (m, 2H), 1.41 – 1.32 (m, 2H), 0.78 (t, J = 7.4 Hz, 3H).

¹³C NMR (101 MHz, Methenol-*d*₄) δ 173.04, 168.55, 145.35, 139.20, 128.70, 128.10, 127.26, 127.22, 126.92, 126.34, 54.00, 39.09, 31.19, 28.81, 22.00, 12.93.

2-([1,1'-biphenyl]-4-sulfonamido)-N¹-hydroxy-N⁵-isopropylpentanediamide (DH-5)

MS (ESI Positive) m/z [M+H⁺]: 420.09. ¹H NMR (400 MHz, MeOD₄) - δ 7.84-7.80 (m, 1H), 7.72-7.69 (m, 1H), 7.64 – 7.50 (m, 2H), 7.42 – 7.30 (m, 4H), 7.12 (dd, J = 8.6, 2.5 Hz, 1H), 5.27 – 5.22 (m, 1H), 4.48 (s, 1H), 4.12 (dd, J = 5.7, 2.0 Hz, 1H), 3.49 (s, 2H), 3.25 (s, 1H), 2.27 – 2.20 (m, 2H), 2.20 – 2.13 (m, 2H), 1.24 (s, 6H).

¹³C NMR (101 MHz, MeOD₄) - δ 170.60, 167.90, 148.03, 147.71, 147.36, 128.72, 128.11, 127.40, 127.18, 126.88, 126.74, 125.02, 124.50, 55.55, 55.47, 44.61, 33.64, 31.67, 30.41, 29.66, 29.36, 29.30, 29.21, 29.07, 29.02, 28.92, 26.71, 24.73, 22.34.

2-([1,1'-biphenyl]-4-sulfonamido)-N⁵-butyl-N¹-hydroxypentanediamide (DH-6)

MS (ESI Positive) m/z [M+H⁺]: 434.00. ¹H NMR (400 MHz, MeOD₄) - δ 7.90 – 7.84 (m, 1H), 7.81 – 7.76 (m, 2H), 7.73 – 7.67 (m, 3H), 7.58 (m, 3H), 7.42 – 7.35 (m, 3H), 7.34 – 7.28 (m, 1H), 4.49 (s, 1H), 3.83 (m, 1H), 3.31 (s, 3H), 2.18 (t, J = 7.4 Hz, 2H), 1.94 (m, 2H), 1.79 – 1.67 (m, 2H), 0.82 (t, J = 7.2 Hz, 3H).

¹³C NMR (101 MHz, MeOD₄) - δ 172.86, 171.71, 145.32, 139.20, 128.76, 128.14, 127.41, 127.09, 126.87, 126.34, 55.41, 51.18, 38.79, 31.24, 31.06, 29.36, 28.33, 19.68, 12.67.

2-([1,1'-biphenyl]-4-sulfonamido)-N¹-hydroxy-N⁵-isobutylpentanediamide (DH-7)

MS (ESI Positive) m/z [M+H⁺]: 434.50. ¹H NMR (400 MHz, Methenol-*d*₄) δ 7.81 (d, J = 8.8 Hz, 2H), 7.69 (d, J = 8.9 Hz, 2H), 7.58 (d, J = 7.0 Hz, 2H), 7.37 (d, J = 7.6 Hz, 2H), 7.31 (d, J = 7.5 Hz, 1H), 3.62 (dd, J = 8.6, 5.6 Hz, 1H), 2.85 – 2.82 (m, 1H), 2.13 (t, J = 7.8 Hz, 2H), 1.87 – 1.57 (m, 4H), 0.77 (d, J = 1.6 Hz, 3H), 0.76 (d, J = 1.8 Hz, 3H).

¹³C NMR (101 MHz, Methenol-*d*₄) δ 173.19, 168.54, 145.35, 139.20, 128.69, 128.10, 127.26, 127.22, 126.92, 126.35, 54.03, 46.60, 31.22, 29.36, 28.99, 28.17, 19.08.

2-([1,1'-biphenyl]-4-sulfonamido)-N¹-hydroxy-N⁵-pentylpentanediamide (DH-8)

MS (ESI Positive) m/z [M+H⁺]: 448.68. ¹H NMR (400 MHz, Methenol-*d*₄) δ 7.84 (dd, J = 8.76, 8.6 Hz, 2H), 7.69 (d, J = 8.6 Hz, 2H), 7.60 – 7.55 (m, Hz, 2H), 7.40 – 7.36 (m, 2H), 7.32 – 7.28 (m, 1H), 3.61 (dd, J = 5.6, 5.6 Hz, 1H), 3.06 – 2.94 (m, 2H), 2.14 – 2.07 (m, 2H), 1.84 – 1.65 (m, 2H), 1.38 – 1.31 (m, 2H), 1.24 – 1.14 (m, 4H), 0.79 (t, J = 6.8 Hz, 3H).

¹³C NMR (101 MHz, Methenol-*d*₄) δ 173.04, 168.55, 145.35, 139.20, 128.70, 128.10, 127.26, 127.22, 126.92, 126.34, 54.00, 39.09, 31.19, 28.91, 28.81, 28.61, 22.00, 12.93.

2-([1,1'-biphenyl]-4-sulfonamido)-N⁵-cyclohexyl-N¹-hydroxypentanediamide (DH-9)

MS (ESI Positive) m/z [M+H⁺]: 460.12. ¹H NMR (400 MHz, Methenol-*d*₄) δ 7.82 (d, J = 8.6 Hz, 2H), 7.70 (d, J = 8.6 Hz, 2H), 7.60 – 7.55 (m, 2H), 7.41 – 7.36 (m, 2H), 7.34 – 7.29 (m, 1H), 3.62 (dd, J = 5.6, 5.6 Hz, 1H), 3.51 – 3.43 (m, 1H), 2.23 – 2.01 (m, 2H), 1.84 – 1.67 (m, 3H), 1.65 – 1.60 (m, 3H), 1.28 – 0.93 (m, 6H).

¹³C NMR (101 MHz, Methenol-*d*₄) δ 172.18, 168.54, 145.35, 139.19, 128.69, 128.10, 127.26, 127.22, 126.92, 54.02, 48.39, 32.31, 31.30, 28.97, 25.22, 24.71.

2-([1,1'-biphenyl]-4-sulfonamido)-N⁵-hexyl-N¹-hydroxypentanediamide (DH-10)

MS (ESI Positive) m/z [M+H⁺]: 461.92. ¹H NMR (400 MHz, Methenol-*d*₄) δ 7.81 (d, J = 8.6 Hz, 2H), 7.69 (d, J = 8.6 Hz, 2H), 7.59 – 7.56 (m, 2H), 7.40 – 7.35 (m, 2H), 7.32 – 7.28 (m, 1H), 3.61 (dd, J = 5.6, 5.6 Hz, 1H), 3.05 – 2.94 (m, 2H), 2.21 – 2.05 (m, 2H), 1.83 – 1.67 (m, 2H), 1.38 – 1.30 (m, 2H), 1.24 – 1.14 (m, 6H), 0.79 (t, J = 6.7 Hz, 3H).

¹³C NMR (101 MHz, Methenol-*d*₄) δ 173.04, 168.56, 145.35, 139.20, 128.70, 128.10, 127.26, 127.22, 126.92, 54.00, 39.12, 31.26, 28.89, 26.29, 22.23, 12.96.

2-([1,1'-biphenyl]-4-sulfonamido)-N¹-hydroxy-N⁵-phenylpentanediamide (DH-11)

MS (ESI Positive) m/z [M+H⁺]: 454.43. ¹H NMR (400 MHz, Methenol-*d*₄) δ 7.81 (d, J = 8.6 Hz, 2H), 7.63 (d, J = 8.7 Hz, 2H), 7.54 – 7.48 (m, 2H), 7.43 – 7.34 (m, 3H), 7.33 – 7.27 (m, 2H), 7.19 – 7.13 (m, 2H), 6.98 – 6.94 (m, 1H), 3.71 (dd, J = 5.4, 5.4 Hz, 1H), 2.34 – 2.25 (m, 2H), 1.95 – 1.87 (m, 1H), 1.83 – 1.74 (m, 1H).

¹³C NMR (101 MHz, Methenol-*d*₄) δ 171.47, 168.68, 145.35, 139.16, 138.38, 128.64, 128.35, 128.03, 127.23, 126.90, 123.72, 119.84, 53.90, 31.77, 28.42.

2-([1,1'-biphenyl]-4-sulfonamido)-N⁵-benzyl-N¹-hydroxypentanediamide (DH-12)

MS (ESI Positive) m/z [M+H⁺]: 467.36. ¹H NMR (400 MHz, Methanol-*d*₄) δ 7.87 (d, J = 8.7 Hz, 1H), 7.78 (d, J = 8.7 Hz, 2H), 7.69 (dd, J = 2, 1.8 Hz, 3H), 7.59 – 7.58 (m, 1H), 7.57 – 7.56

(m, 1H), 7.41 – 7.35 (m, 3H), 7.34 – 7.29 (m, 1H), 3.92 – 3.88 (m, 1H), 3.52 (s, 2H), 2.38 – 2.28 (m, 2H), 2.02 – 1.89 (m, 1H), 1.77 – 1.68 (m, 1H), 1.24 – 1.12 (m, 2H).

¹³C NMR (101 MHz, Methanol-*d*₄) δ 172.66, 172.35, 145.89, 141.28, 139.97, 138.87, 129.12, 128.48, 128.34, 128.10, 127.91, 127.74, 127.15, 54.60, 40.62, 29.25, 28.12.

2-([1,1'-biphenyl]-4-sulfonamido)-N^I-hydroxy-N⁵-phenethylpentanediamide (DH-13)

MS (ESI Positive) *m/z* [M+H⁺]: 481.11. ¹H NMR (400 MHz, Methanol-*d*₄) δ 7.78 (d, *J* = 8.6 Hz, 2H), 7.69 (d, *J* = 8.3 Hz, 2H), 7.58 (dd, *J* = 1.52, 1.12 Hz, 2H), 7.42 – 7.29 (m, 3H), 7.18 – 7.13 (m, 2H), 7.12 – 7.05 (m, 3H), 3.83 (dd, *J* = 5.2, 5.12 Hz, 1H), 2.66 (t, *J* = 7.4 Hz, 2H), 2.16 (t, *J* = 7.4 Hz, 2H), 1.99 – 1.87 (m, 1H), 1.75 – 1.66 (m, 1H), 1.22 (m, 2H).

¹³C NMR (101 MHz, Methanol-*d*₄) δ 172.96, 171.74, 145.34, 139.14, 139.10, 128.78, 128.40, 128.17, 128.09, 127.42, 127.11, 126.88, 126.35, 125.93, 55.40, 40.67, 35.08, 37.25, 28.29.

2-([1,1'-biphenyl]-4-sulfonamido)-N⁵-(2-chlorobenzyl)-N^I-hydroxypentanediamide (DH-14)

MS (ESI Positive) *m/z* [M+H⁺]: 502.47. ¹H NMR (400 MHz, Methanol-*d*₄) δ 7.80 (d, *J* = 8.6 Hz, 2H), 7.66 (d, *J* = 8.7 Hz, 2H), 7.58 (dd, *J* = 1.5, 1.2 Hz, 2H), 7.42 – 7.36 (m, 2H), 7.35 – 7.30 (m, 1H), 7.21 – 7.16 (m, 1H), 7.14 – 6.97 (m, 3H), 3.80 (dd, *J* = 5.1, 5.0 Hz, 1H), 2.34 – 2.15 (m, 2H), 1.96 – 1.84 (m, 1H), 1.81 – 1.67 (m, 1H), 1.24 – 1.19 (m, 2H).

¹³C NMR (101 MHz, Methanol-*d*₄) δ 173.35, 171.69, 145.36, 139.01, 135.03, 132.84, 128.98, 128.75, 128.43, 127.45, 127.16, 126.95, 126.73, 55.87, 40.62, 29.25, 28.12.

2-([1,1'-biphenyl]-4-sulfonamido)-N⁵-(4-chlorobenzyl)-N^I-hydroxypentanediamide (DH-15)

MS (ESI Positive) *m/z* [M+H⁺]: 502.05. ¹H NMR (400 MHz, Methanol-*d*₄) δ 7.82 – 7.75 (m, 2H), 7.74 – 7.63 (m, 2H), 7.59 – 7.53 (m, 2H), 7.44 – 7.31 (m, 3H), 7.30 – 7.09 (m, 2H), 7.09 – 7.03 (m, 1H), 7.01 – 6.95 (m, 1H), 3.74 – 3.70 (m, 1H), 2.41 – 2.02 (m, 2H), 1.94 – 1.81 (m, 1H), 1.79 – 1.67 (m, 1H), 1.25 – 1.16 (m, 2H).

¹³C NMR (101 MHz, Methanol-*d*₄) δ 174.19, 172.35, 145.35, 141.28, 139.19, 137.46, 132.80, 128.71, 128.62, 128.14, 127.42, 127.16, 126.92, 56.24, 41.93, 29.36, 22.34.

2-([1,1'-biphenyl]-4-sulfonamido)-N⁵-(3,4-dichlorobenzyl)-N^I-hydroxypentanediamide (DH-16)

MS (ESI Positive) *m/z* [M+H⁺]: 537.00. ¹H NMR (400 MHz, Methanol-*d*₄) δ 7.81 (d, *J* = 8.6 Hz, 2H), 7.66 (d, *J* = 8.7 Hz, 2H), 7.58 (dd, *J* = 1.5, 1.2 Hz, 2H), 7.42 – 7.36 (m, 2H), 7.35 – 7.30 (m, 1H), 7.21 – 7.16 (m, 1H), 7.14 – 6.97 (m, 2H), 3.80 (dd, *J* = 5.1, 5.0 Hz, 1H), 2.34 – 2.15 (m, 2H), 1.96 – 1.84 (m, 1H), 1.81 – 1.67 (m, 1H), 1.24 – 1.19 (m, 2H).

^{13}C NMR (101 MHz, Methanol- d_4) δ 173.40, 171.28, 158.96, 145.27, 139.11, 129.81, 128.81, 128.40, 128.20, 127.43, 127.16, 127.07, 126.93, 126.35, 54.18, 42.16, 29.37, 28.29.

2-([1,1'-biphenyl]-4-sulfonamido)- N^1 -hydroxy- N^5 -(4-methoxybenzyl)pentanediamide (DH-17)

MS (ESI Positive) m/z $[\text{M}+\text{H}]^+$: 498.51. ^1H NMR (400 MHz, Methanol- d_4) δ 7.79 (d, J = 8.7 Hz, 2H), 7.66 (d, J = 8.6 Hz, 2H), 7.58 (dd, J = 1.5, 1.2 Hz, 2H), 7.50 – 7.27 (m, 3H), 6.88 (d, J = 8.7 Hz, 2H), 6.60 (d, J = 8.7 Hz, 2H), 3.99 (dd, J = 14.7, 14.7 Hz, 2H), 3.76 (dd, J = 5.1, 5.1 Hz, 1H), 3.53 (s, 3H), 1.92 – 1.82 (m, 1H), 1.78 – 1.67 (m, 1H), 1.24 – 1.19 (m, 2H).

^{13}C NMR (101 MHz, Methanol- d_4) δ 173.40, 171.28, 158.96, 145.27, 139.11, 129.81, 128.81, 128.40, 128.20, 127.43, 127.16, 126.93, 113.45, 55.88, 54.18, 42.16, 29.37, 28.29.

2-([1,1'-biphenyl]-4-sulfonamido)- N^5 -(3,5-dimethylbenzyl)- N^1 -hydroxypentanediamide (DH-18)

MS (ESI Positive) m/z $[\text{M}+\text{H}]^+$: 604.06. ^1H NMR (400 MHz, Methanol- d_4) δ 7.81 (d, J = 8.6 Hz, 2H), 7.66 (d, J = 8.7 Hz, 2H), 7.58 (dd, J = 1.5, 1.2 Hz, 2H), 7.42 – 7.36 (m, 2H), 7.35 – 7.30 (m, 1H), 7.21 – 7.16 (m, 1H), 7.14 – 6.97 (m, 2H), 4.35 (d, J = 4.4 Hz, 2H), 3.95 (m, 1H), 1.90 (m, 1H), 1.74 (m, 1H), 1.24 – 1.19 (m, 2H).

^{13}C NMR (101 MHz, Methanol- d_4) δ 173.35, 171.69, 145.36, 139.01, 135.03, 128.98, 128.75, 128.43, 128.19, 127.45, 127.16, 126.95, 126.73, 55.87, 50.79, 29.25, 28.12.

2-([1,1'-biphenyl]-4-sulfonamido)- N^5 -(4-fluorobenzyl)- N^1 -hydroxypentanediamide (DH-19)

MS (ESI Positive) m/z $[\text{M}+\text{H}]^+$: 486.00. ^1H NMR (400 MHz, Methanol- d_4) δ 7.89 (s, 4H), 7.78 (d, J = 8.6 Hz, 2H), 7.69 (dd, J = 8.6, 1.8 Hz, 2H), 7.60 – 7.57 (m, 1H), 7.42 – 7.35 (m, 2H), 7.32 – 7.27 (m, 2H), 3.32 (s, 2H), 2.32 (t, J = 7.2 Hz, 1H), 1.25 – 1.10 (m, 4H).

^{13}C NMR (101 MHz, Methanol- d_4) δ 173.21, 171.70, 145.34, 144.86, 142.30, 139.38, 139.19, 128.74, 128.08, 127.39, 127.10, 126.97, 126.35, 116.58, 54.99, 51.26, 29.03, 27.40.

2-([1,1'-biphenyl]-4-sulfonamido)- N^5 -(tert-butyl)- N^1 -hydroxypentanediamide (DH-20)

MS (ESI Positive) m/z $[\text{M}+\text{H}]^+$: 434.00. ^1H NMR (400 MHz, Methanol- d_4) δ 7.77 (s, 4H), 7.70 (d, J = 8.6 Hz, 2H), 7.59–7.29 (m, 3H), 2.33 (t, J = 7.2 Hz, 1H), 1.24–1.12 (m, 4H), 0.80 (s, 9H).

^{13}C NMR (101 MHz, Methanol- d_4) δ 173.21, 171.70, 145.34, 139.20, 128.77, 128.15, 127.39, 127.10, 126.87, 54.99, 50.93, 31.43, 29.03, 27.41.

Part C

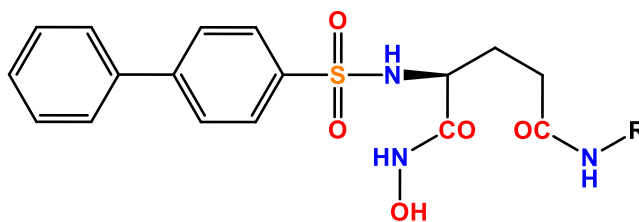
5.3. *Biological Studies*

The synthesized compounds underwent comprehensive biological assessments employing diverse methods. These evaluations included cytotoxicity analysis to measure cell impact, enzyme assays targeting MMP-2 inhibition, and DNA nick generation tests. Furthermore, apoptosis and cell cycle analyses in K562 cells were conducted to understand cell-specific responses, along with in vitro tube formation assays assessing angiogenesis. These assays collectively provided insights into the compounds' toxicity, their effects on critical enzymes and DNA integrity, their impact on cell-specific behaviors like apoptosis and cell cycle progression, and their potential role in angiogenesis regulation. This thorough evaluation aimed to comprehend the compounds' diverse biological effects and their potential for therapeutic applications. All the synthesized compounds were biologically evaluated using different methods:

- Cytotoxicity assay
- Enzyme assay (MMP-2 inhibition assay)
- MMP-2 expression analysis
- Apoptosis analysis in K562 cell line
- Cell cycle analysis in K562 cell line
- In vitro tube formation assay or Angiogenesis assay
- DNA deformation assay by DAPI staining

5.3.1. *Cytotoxicity assay*

The cytotoxicity analysis of the novel screened compounds has been determined against a variety of cancer cell lines. All the cytotoxicity assay results have been depicted in **Table 5.12**.

Table 5.12. Cytotoxicity of the novel synthesized molecules against a variety of cancer cell lines

Compound	R	K562 (IC ₅₀) μM	A549 (IC ₅₀) μM	U87MG (IC ₅₀) μM	HT1080 (IC ₅₀) μM	HEK-293 (IC ₅₀) μM
DH-1	H	0.541	13.818	16.325	42.461	299.943
DH-2	CH ₃	1.253	20.552	24.872	16.565	411.044
DH-3	C ₂ H ₅	1.334	15.394	22.151	29.504	307.880
DH-4	<i>n</i> -Propyl	1.546	58.309	47.483	52.905	1166.177
DH-5	<i>i</i> -Propyl	1.258	14.436	37.154	30.594	308.029
DH-6	<i>n</i> -butyl	1.586	25.866	50.098	39.944	517.325
DH-7	<i>i</i> -butyl	1.401	9.887	16.271	19.070	197.733
DH-8	<i>n</i> -Pentyl	2.253	15.608	18.117	27.558	311.912
DH-9	<i>c</i> -hexyl	3.651	6.751	17.438	23.795	235.846
DH-10	<i>n</i> -hexyl	7.199	16.139	23.910	37.581	322.786
DH-11	Phenyl	6.175	27.552	30.994	27.552	551.015
DH-12	Benzyl	6.541	9.656	15.155	22.641	192.458
DH-13	β-Phenylethyl	6.791	5.615	16.772	23.734	209.491
*DH-14	2-Cl Bnz	0.395	3.378	18.327	38.342	470.596
*DH-15	4-Cl Bnz	0.315	2.694	13.703	23.633	670.292
*DH-16	3,4-diCl Bnz	0.474	6.383	16.325	31.238	277.861
DH-17	4-OCH ₃ Bnz	0.847	8.155	18.506	20.660	335.090
*DH-18	3,5-diCF₃Bnz	0.338	4.770	22.360	24.389	266.568
*DH-19	4-FBnz	0.398	4.229	18.398	22.134	213.817
DH-20	t-but	0.941	6.137	19.800	28.171	388.367

*Best active (K562 cell line) are in bold

The biological evaluation of the synthesized compounds (DH-1 to DH-20) through multiple cell-based assays provides valuable insights into their inhibitory effects across different cell lines, assessed by their IC₅₀ values measured in micromoles (μM) concentration. The IC₅₀ values represent the concentration at which each compound inhibits cell growth by 50% in various cell lines, including K562, A549, U87MG, HT1080, and HEK-293. Several notable patterns emerge from the data: Compounds DH-14, DH-15, DH-16, DH-18, and DH-19 demonstrate lower IC₅₀ values, indicating potent inhibitory effects in K-562 cell lines compared to the other compounds (**Table 5.12**). Moreover, compounds DH-14, DH-15, DH-

16, DH-18, and DH-19 exhibit considerable effectiveness, showing notably moderately good IC_{50} values in the A549 cell line, suggesting potential suitability for targeting these specific cell types. Additionally, compounds DH-1 and DH-20 also display promising inhibitory effects, particularly evident in the K-562 cell line. These lower IC_{50} values imply higher potency, indicating these compounds' ability to more effectively impede the growth of these cells. Conversely, other compounds show less potent inhibitory effects, highlighting varied levels of effectiveness in different cell lines. Overall, the diverse range of IC_{50} values signifies the differing efficacy of these compounds against various cell types, underscoring the importance of understanding the compound-cell interactions for targeted and effective therapeutic applications. In this context, the screened synthesized biphenyl sulfonamides hydroxamates-based derivatives exhibit potential results against hematological malignancy such as chronic myeloid leukemia cell line K-562 than solid cancer cell line A549. However, The log concentration of the dose-response curve of K-562 and A549 cell lines, and the cell viability assay results for 72 hr are shown in **Figure 5.21**. NNGH was considered as a prototype standard inhibitor.

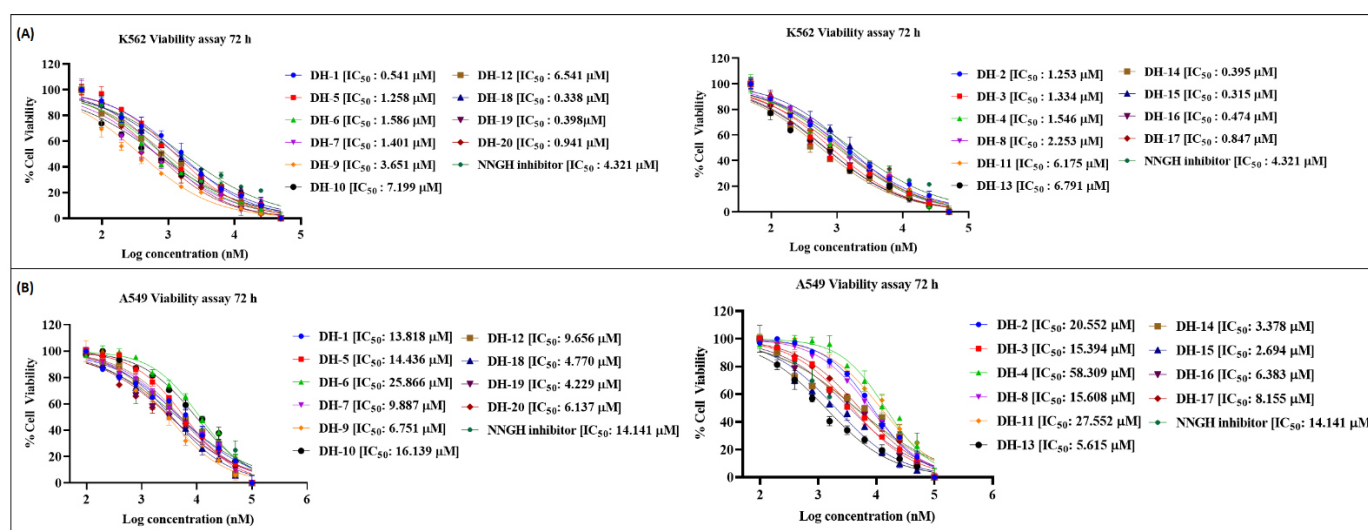


Figure 5.21. IC_{50} results of the compounds by cell viability assay using presto blue in (A) K562 cells at a concentration range of 0.048 μ M to 50 μ M for 72 hr. (B) A549 cells at a concentration range of 0.097 μ M to 100 μ M. Data represent mean \pm SD, $n = 2$.

Therefore, it is interesting to note that, the compound having benzyl group having halogen substitution such as 2-Cl Bnz (DH-14), 4-Cl Bnz (DH-15), DH-16 (3,4-diCl Bnz), DH-18 (3,5-diCF₃Bnz), and DH-19 (4-FBnz) exhibit promising result in K-562 cell line. Nonetheless, compounds having n-hexyl (DH-10), phenyl (DH-11), benzyl (DH-12), and β -phenylethyl (DH-13) showed poor contribution against hematological malignancy (**Table**

5.12). Furthermore, from this cytotoxicity assay, the HEK-293 cell line results also imply the non-cytotoxicity properties of all the synthesized biphenylsulfonamides hydroxamates-based derivatives which might be beneficial for the treatment of hematological malignancy.

5.3.2. Enzyme inhibition assay

A comprehensive enzyme assay analysis was conducted on the best active compounds (DH-1, DH-14, DH-15, DH-16, DH-17, DH-18, DH-19, and DH-20) and their inhibitory efficacy on MMP-2, MMP-9, and MMP-8. Each compound, denoted by different labels such as DH-1, DH-14, DH-15, and so forth, is associated with an R-group or side chain linked to a common base structure (**Table 5.13**). The inhibitory potential of these compounds against MMP-2, MMP-9, and MMP-8 is quantified through IC_{50} values, measured in nanomolar concentrations. Notably, the selectivity of each compound's inhibition for MMP-2 over MMP-9 and MMP-2 over MMP-8 is also highlighted, providing critical insights into their differential effects. For instance, DH-15 (4-Cl Bnz) demonstrates an IC_{50} of 23.28 nM against MMP-2, 55.14 nM against MMP-9, and 1162.79 nM against MMP-8. The selectivity values reveal a preference for inhibiting MMP-2 over MMP-9 with a ratio of 2.36 and an exceptionally higher selectivity of 49.94 for MMP-2 over MMP-8. Conversely, DH-20 (t-butyl) exhibits an IC_{50} of 81.10 nM for MMP-2, 738.42 nM for MMP-9, and 43.05 nM for MMP-8, indicating a substantial selectivity of 9.10 fold for MMP-2 over MMP-9 and a notably lower selectivity of 0.53 for MMP-2 over MMP-8. Understanding the differential inhibitory effects of these compounds on MMPs is essential for designing targeted therapeutics and furthering insights into the intricate roles of MMPs in diseases and biological mechanisms.

Table 5.13. MMP-2 inhibition of best active compounds (K562) and selectivity profile over MMP-9 and MMP-8.

Compound	R	MMP-2 (IC ₅₀ in nM)	MMP-9 (IC ₅₀ in nM)	MMP-8 (IC ₅₀ in nM)	Selectivity (MMP-9/ -2)	Selectivity (MMP-8/ -2)
DH-1	H	118.5	238.46	1041.67	2.01	8.79
DH-14	2-Cl Bnz	109.74	531.33	--	4.84	--
DH-15	4-Cl Bnz	23.28	55.14	1162.79	2.36	49.94
DH-16	3,4-diCl Bnz	108.16	470.07	438.58	4.35	4.05
DH-17	4-OCH ₃ Bnz	105.78	983.89	425.00	9.30	4.02
DH-18	3,5- diCF ₃ Bnz	139.45	518.11	833.34	3.71	5.98
DH-19	4-FBnz	115.16	336.60	1273.89	2.92	11.06
DH-20	t-butyl	81.10	738.42	43.05	9.10	0.53

5.3.3. MMP-2 expression analysis

The lead compounds' ability to modulate MMP-2 expression was examined using flow cytometry. The changes in MMP-2 expression levels in K562 cells before and after treatments with DH-14 and DH-15 for 48 hr at their respective IC₅₀ doses were estimated by flow cytometry analysis (Halder et al., 2015; Mukherjee et al., 2017; Dutta et al., 2019; Dutta et al., 2022). The treated and untreated cells were fixed and stained with MMP-2 primary antibody followed by treatment with secondary antibody conjugated with FITC. The K562 cell population with MMP-2 cells was found to be reduced after treatment with DH-14 and DH-15. After 48 hr of drug treatments, flow cytometric data revealed that cellular MMP-2 expression levels were reduced by 15.8% (**Figure 5.22**) in the case of DH-14 (at IC₅₀ dose, 0.395μM) and 18.4% (**Figure 5.22**) in the case of compound DH-15 (at IC₅₀ dose, 0.315μM) in comparison with untreated control. Therefore, this data indicates that the synthesized lead compounds (DH-14 and DH-15) also have the potential to inhibit the cell MMP-2 expression.

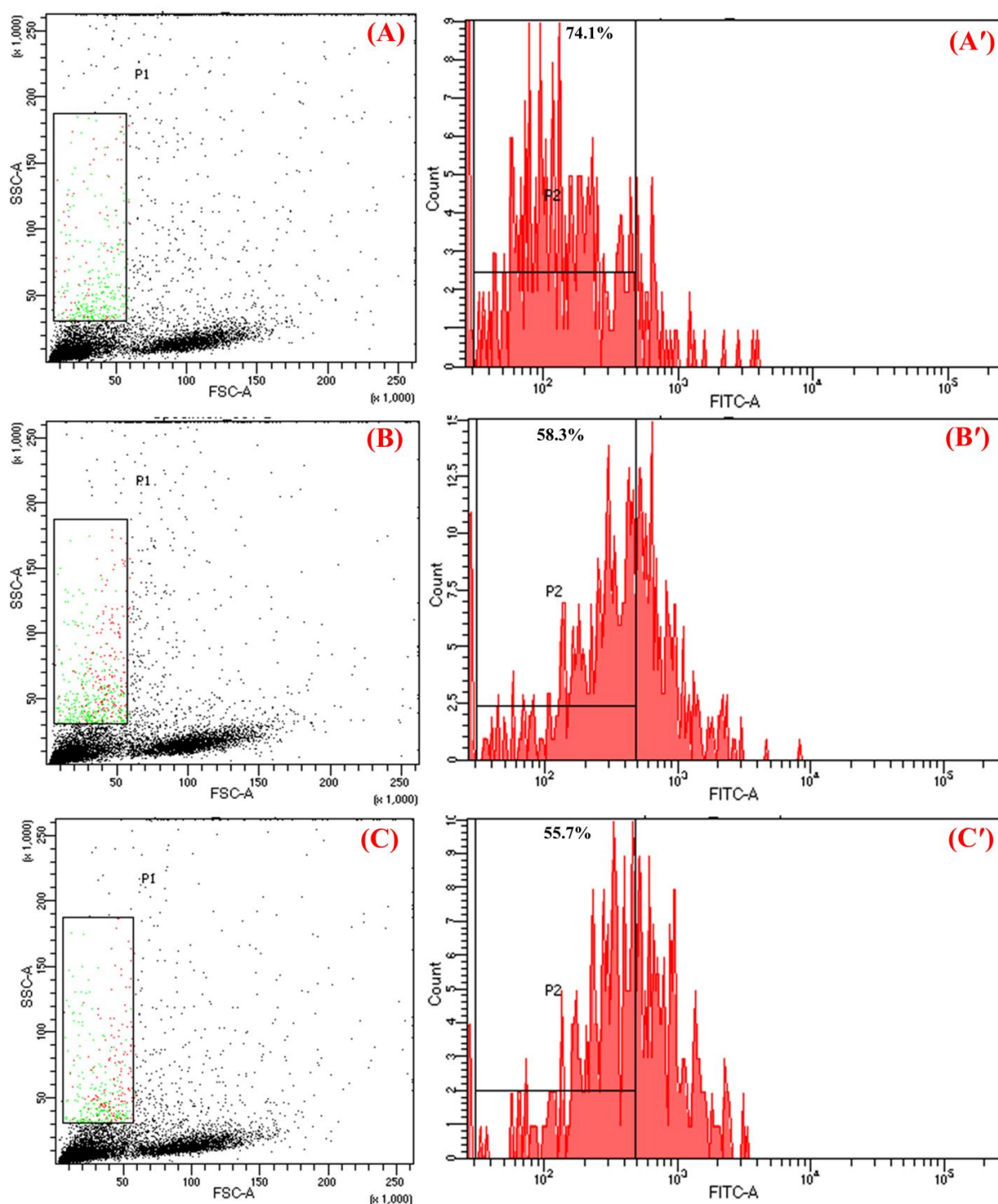


Figure 5.22. MMP-2 expression analysis of K562 cells by fluorescence-activated cell sorting (FACS) after 48 hr of treatments and followed by incubation with primary (anti-MMP2) and secondary antibody (FITC conjugated anti-MMP2). **(A)** (dot plot) and **(A')** (histogram plot) represent the Control, **(B)** (dot plot) and **(B')** (histogram plot) represent the treatment by DH-14 with IC_{50} dose (0.395 μ M), and **(C)** (dot plot) and **(C')** (histogram plot) represent the treatment by DH-15 with IC_{50} dose (0.315 μ M).

In addition, the lead compounds' ability to modulate MMP-2 expression was also examined using flow cytometry. The changes in MMP-2 expression levels in K562 cells before and after treatments with DH-18 and DH-19 for 48 hr at their respective IC₅₀ doses were estimated by flow cytometry analysis (Halder et al., 2015; Mukherjee et al., 2017; Dutta et al., 2019; Dutta et al., 2022). The treated and untreated cells were fixed and stained with MMP-2 primary antibody followed by treatment with secondary antibody conjugated with FITC. The K562 cell population with MMP-2 cells was found to be reduced after treatment with DH-18 and DH-19. After 48 hr of drug treatments, flow cytometric data revealed that cellular MMP-2 expression levels were reduced by 21.3% (**Figure 5.23**) in the case of DH-18 (at IC₅₀ dose, 0.338 μ M) and 17.8% (**Figure 5.23**) in the case of compound DH-19 (at IC₅₀ dose, 0.398 μ M) in comparison with untreated control. Therefore, this data indicates that the synthesized lead compounds (DH-18 and DH-19) also have the potential to inhibit the cell MMP-2 expression.

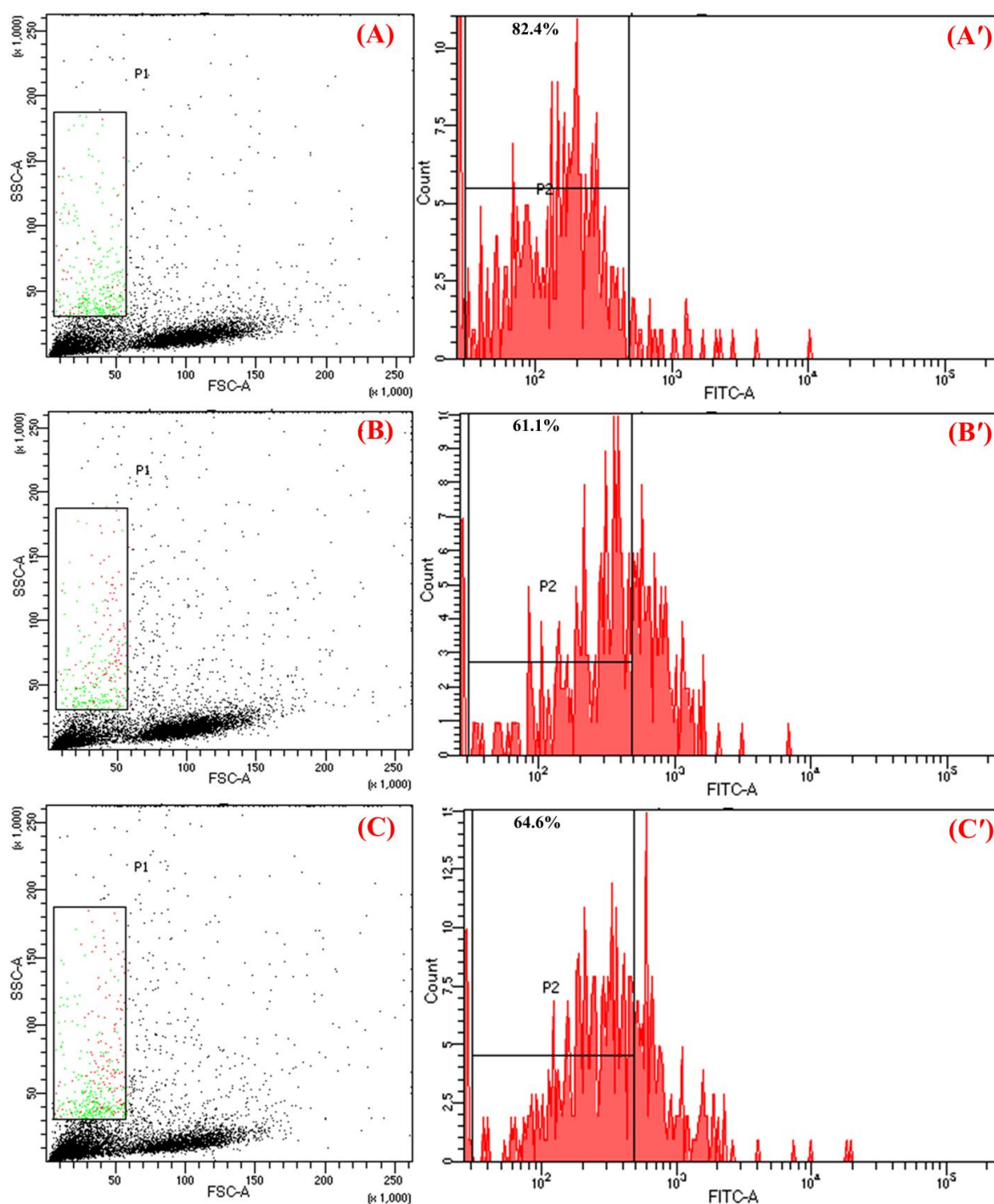


Figure 5.23. MMP-2 expression analysis of K562 cells by fluorescence-activated cell sorting (FACS) after 48 hr of treatments and followed by incubation with primary (anti-MMP2) and secondary antibody (FITC conjugated anti-MMP2). **(A)** (dot plot) and **(A')** (histogram plot) represent the Control, **(B)** (dot plot) and **(B')** (histogram plot) represent the treatment by DH-18 with IC_{50} dose ($0.338 \mu M$), and **(C)** (dot plot) and **(C')** (histogram plot) represent the treatment by DH-19 with IC_{50} dose ($0.398 \mu M$).

5.3.4. Apoptosis analysis in K-562 cell line

The apoptosis assay has been conducted in the K562 cell line on DH-14, DH-15, DH-18, and DH-19. The analysis results imply that the compounds showed a substantial impact in apoptosis compared to control (**Figure 5.24**).

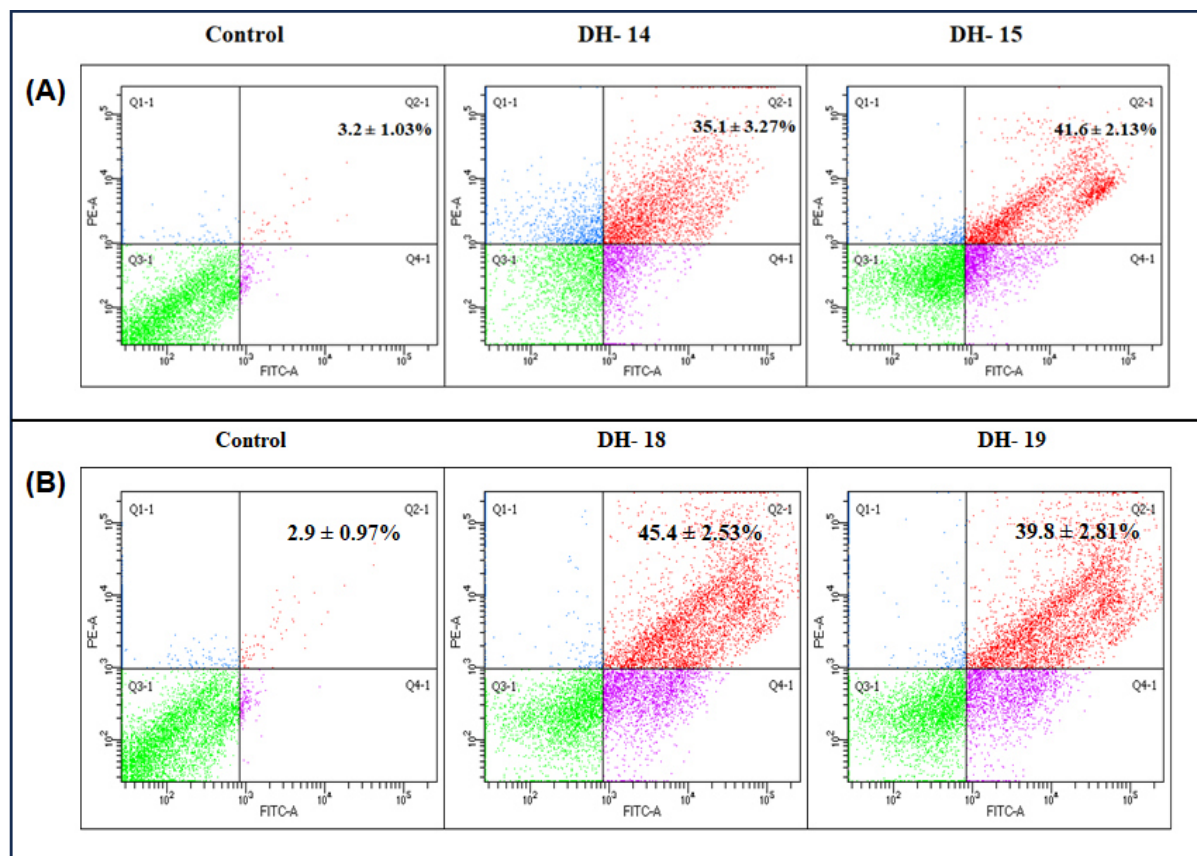


Figure 5.24. Apoptosis analysis in K562 cell line for (A) DH-14 (0.395 μ M) and DH-15 (0.315 μ M) (B) DH-18 (0.338 μ M) and DH-19 (0.398 μ M); X and Y-axis represent the intensities of annexin-V and propidium iodide respectively). Data represents mean \pm standard deviation, n=3.

In the control group, the total apoptosis was measured at 3.2%. In the presence of compound DH-14, the total apoptosis showed significantly to 35.1%, and with compound DH-15, it further rose to 41.6% (**Figure 5.24A**). This suggests that both DH-14 and DH-15 compounds have a substantial impact on promoting apoptosis, showing a considerable increase compared to the control group. Apoptosis, or programmed cell death, is a crucial process in the regulation of cell growth and development. The notable increase in apoptosis induced by DH-14 and DH-15 may imply their potential role in affecting cellular mechanisms or signaling pathways related to programmed cell death. On the other hand, the total apoptosis rate was

measured at 2.9%. In the presence of compound DH-18, the total apoptosis notably increased to 45.4%, while DH-19 resulted in a slightly lower but still significant apoptosis rate of 39.8% (**Figure 5.24B**). These results suggest that both DH-18 and DH-19 compounds have a considerable impact on promoting apoptosis compared to the control group. Apoptosis is a controlled and programmed cell death mechanism crucial for various physiological processes. The substantial increase in apoptosis induced by DH-18 and DH-19 implies their potential influence on cell signaling pathways or mechanisms related to programmed cell death. The total percentage of apoptosis with respect to the control of compounds DH-14, DH-15, DH-18, and DH-19 is shown in **Figure 5.25**.

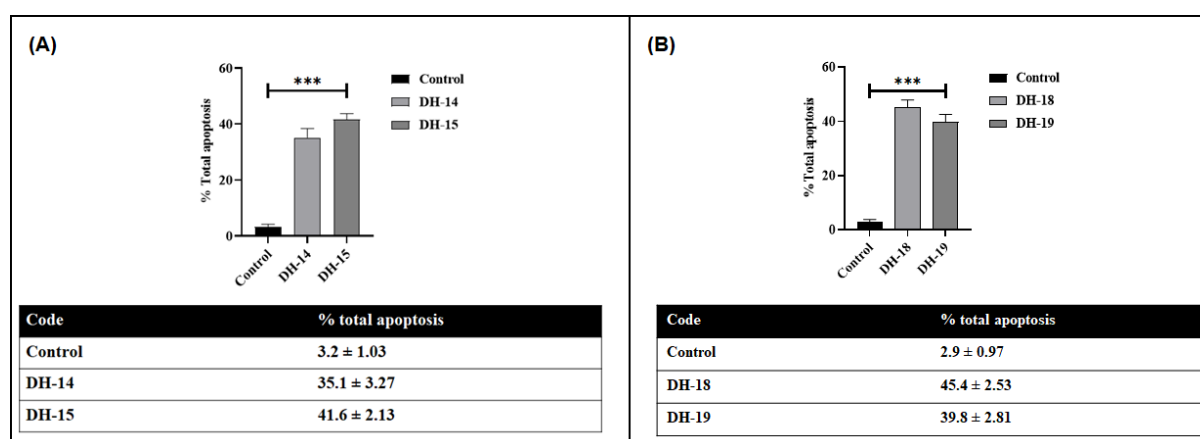


Figure 5.25. Total percentage of apoptosis with respect to control and (A) DH-14 and DH-15 (B) DH-18 and DH-19.

5.3.5. Cell cycle analysis in K562 cell line

The cell cycle analysis was conducted on K562 cells treated with different compounds at their respective IC₅₀ concentrations for 72 hr. This analysis aimed to assess the impact of these compounds (DH-14, DH-15, DH-18, and DH-19) on the cell cycle progression of K562 cells. The cell cycle analysis was performed using flow cytometry, specifically the BD Aria III, a common flow cytometer used for cell analysis and sorting based on specific characteristics such as size, granularity, and fluorescence (**Figure 5.26**). Also, the results of this cell cycle analysis would provide insights into how these compounds at their respective IC₅₀ concentrations influence the distribution of cells in different phases of the cell cycle. Typically, the cell cycle is divided into phases: G1 (gap 1), S (synthesis), G2 (gap 2), and M (mitosis). Alterations in the cell cycle phases or the distribution of cells in these phases can indicate the compounds' effects on cell growth, proliferation, or potential cell cycle arrest.

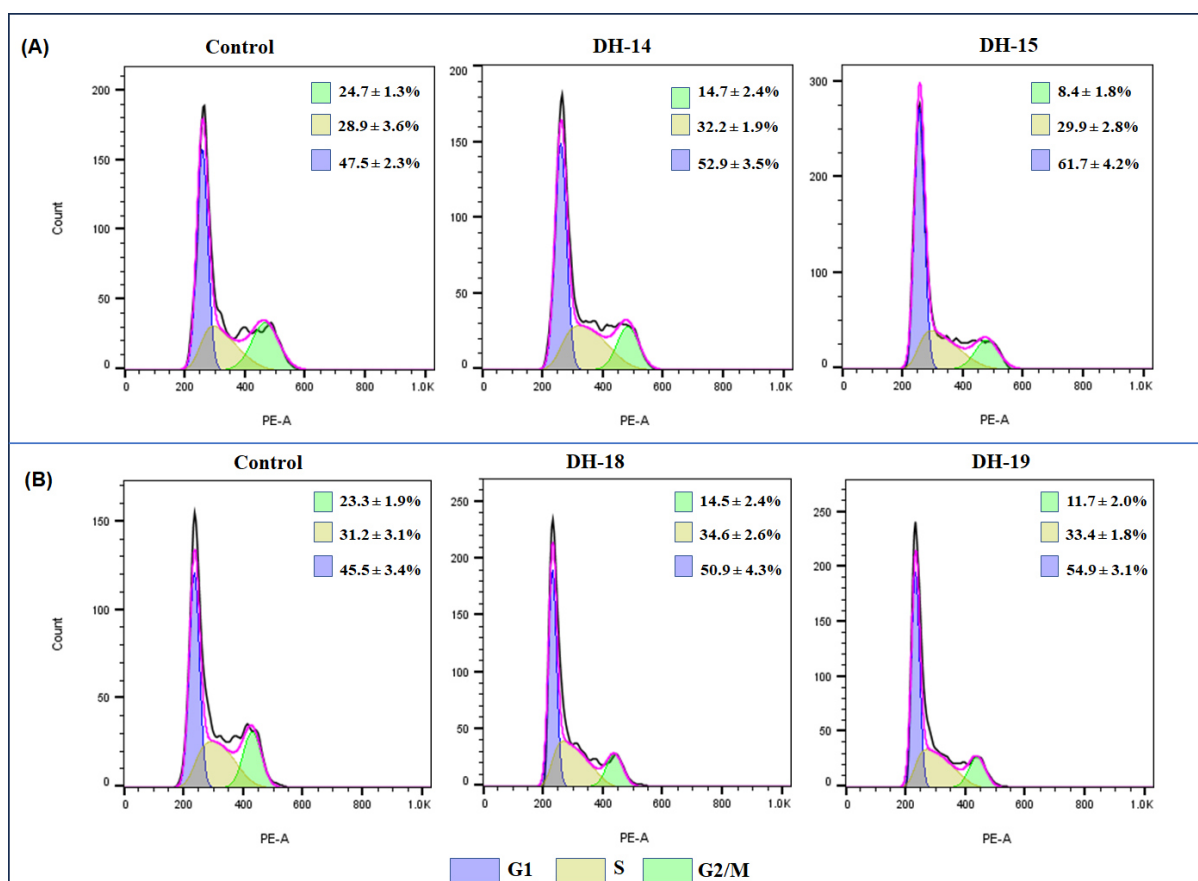


Figure 5.26. Cell cycle analysis in K562 cells treated with vehicle (control), **(A)** DH-14 (0.395 μ M), and DH-15 (0.315 μ M); **(B)** DH -18 (0.338 μ M), and DH-19 (0.398 μ M) at IC₅₀ concentration of the compounds for 72 h. The cell cycle analysis was carried out by Flow cytometry (BD Aria III). Data represent mean \pm standard deviation, n=3.

Moreover, the specific outcomes of the analysis could include information about any changes observed in the percentage of cells in the G1, S, G2, or M phases, compared to the control group (**Figure 5.26**).

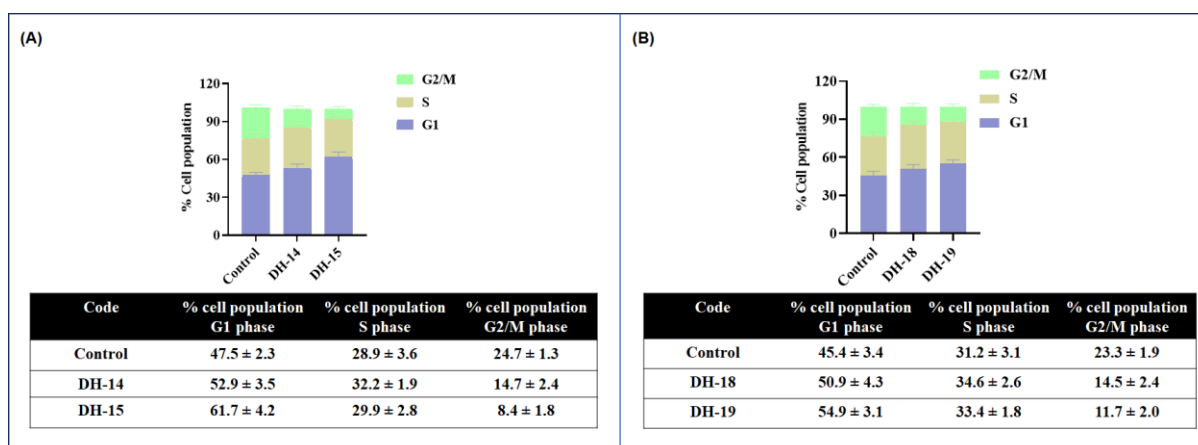


Figure 5.27. Graphical representation of the % cell population of K562 cells at various phases, i.e., G1, S, and G2/M phases of (A) DH-14 and DH-15 (B) DH-18 and DH-19. Data represent mean \pm standard deviation, $n=3$.

The graphical representation of the distribution of K562 cells at different cell cycle phases (G1, S, and G2/M) under varying treatments: control, DH-14, and DH-15 (**Figure 5.27**). In the control group, the G1 phase constitutes 47.5% of the cell population, with 28.9% in the S phase and 24.7% in the G2/M phase (**Figure 5.27A**). Under DH-14 treatment, there's an increase in the G1 phase (52.9%), a slight rise in the S phase (32.2%), and a decrease in the G2/M phase (14.7%). DH-15 treatment notably shows a substantial increase in the G1 phase (61.7%) and lower percentages in the S (29.9%) and G2/M phases (8.4%). These results suggest an accumulation of cells in the G1 phase under both DH-14 and DH-15 treatments, with DH-15 exhibiting the most prominent impact, indicating a potential cell cycle arrest or delay at this phase and reduced progression into the G2/M phase. On the other hand, the percentage of the cell population distribution of K562 cells across G1, S, and G2/M phases for control, DH-18, and DH-19 conditions. Control cells exhibit 45.4% in G1, 31.2% in S, and 23.3% in G2/M phases (**Figure 5.27B**). In contrast, DH-18 displays 50.9% in G1, 34.6% in S, and 14.5% in G2/M phases, while DH-19 depicts 54.9% in G1, 33.4% in S, and 11.7% in G2/M phases. These variations indicate an altered cell phase distribution, with DH-19 showing a higher proportion in the G1 phase and a lower percentage in the G2/M phase compared to Control and DH-18. This data signifies the influence of these compounds on cell cycle dynamics, potentially affecting cell proliferation and regulatory mechanisms associated with cell division and growth.

5.3.6. *In vitro* tube formation assay or Angiogenesis assay

In the angiogenesis assay comparing compounds DH-14 and DH-15 to the control, the analysis involves image processing using software such as ImageJ or FIJI to segment and analyze the images. Segregation of images for each group enables the assessment of meshes, branches, and nodes, representing the blood vessel network's density, complexity, and connectivity. Quantitative measurements are then extracted to compare the control and test groups, focusing on parameters like total vessel length, junctions (nodes), and branching points. Statistical tests are applied to discern significant differences, ultimately providing insights into the angiogenic potential of DH-14 and DH-15 compared to the control (**Figure 5.28**).

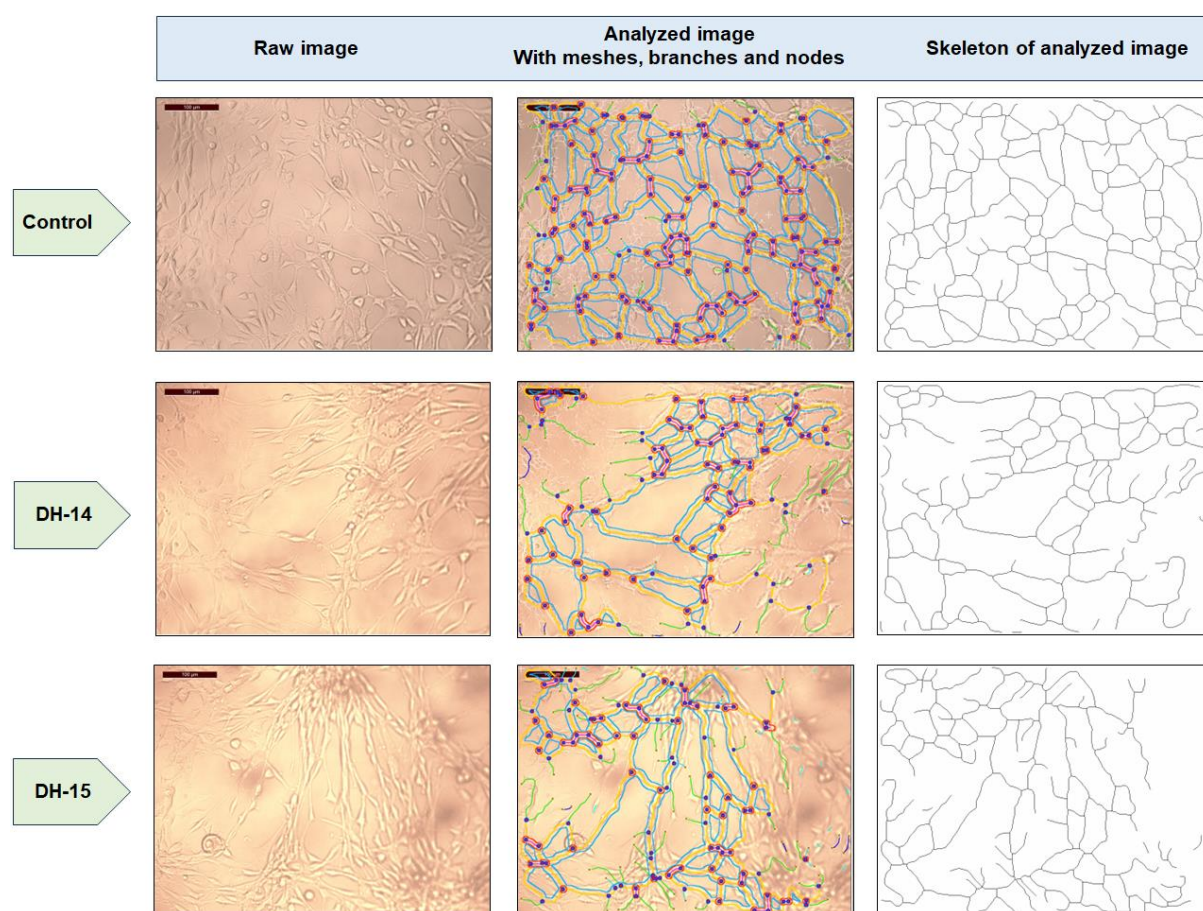


Figure 5.28. Angiogenesis assay of compound DH-14 and DH-15 compared to control having a raw image, analyzed image with meshes, branches, and nodes.

Similarly, the angiogenesis assay comparing compounds DH-18 and DH-19 to the control involves the initial acquisition of high-quality raw images, followed by image processing using software like ImageJ or FIJI to analyze and segment the images, distinguishing blood vessels from the background. Quantification of meshes, branches, and nodes representing the

vessel network's density and complexity is carried out. Statistical analysis is then applied to compare these parameters across the control, DH-18, and DH-19 groups. The resulting analyzed images highlight these structural features, allowing for visual comparison and insights into the angiogenic potential of DH-18 and DH-19 compared to the control, aiding in understanding their effects on angiogenesis (**Figure 5.29**).

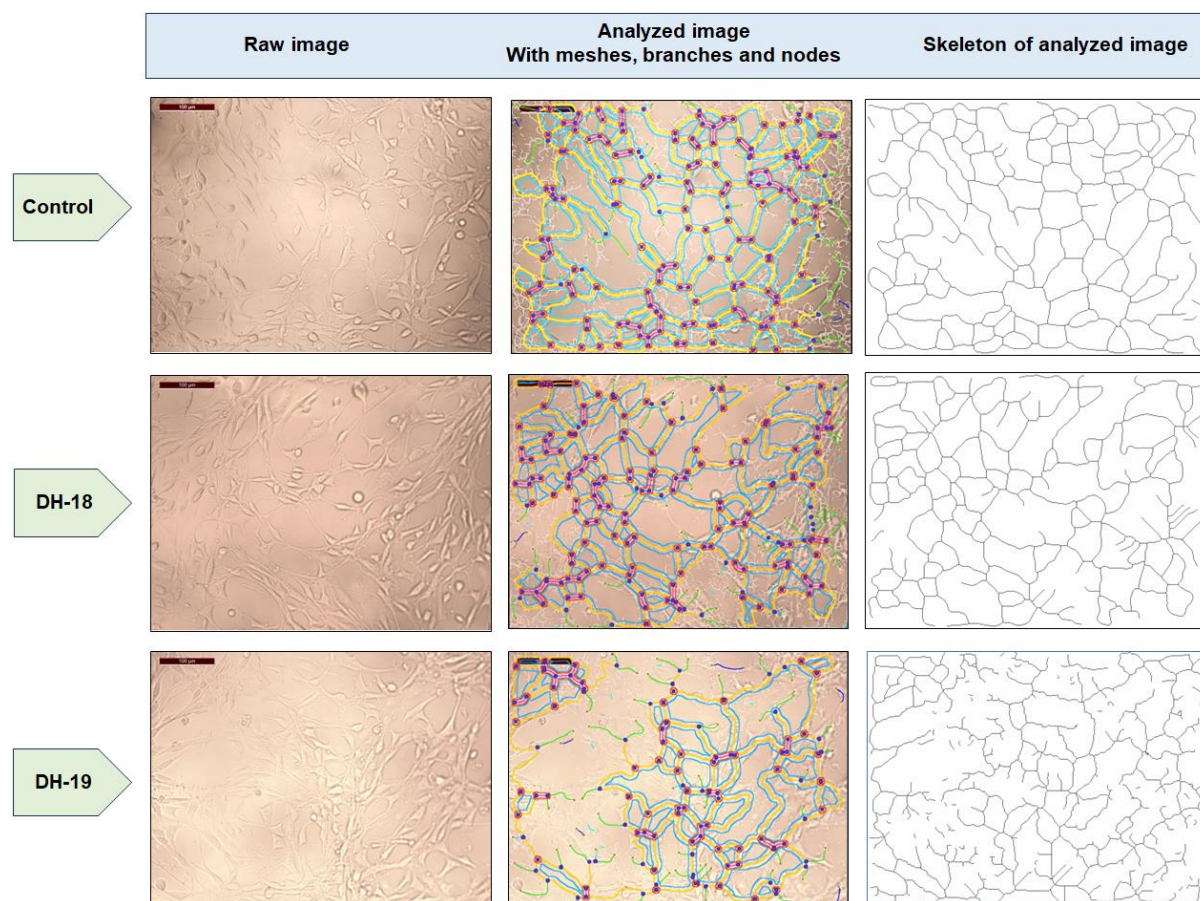


Figure 5.29. Angiogenesis assay of compound DH-18 and DH-19 compared to control having a raw image, analyzed image with meshes, branches, and nodes.

The comparative measurement of parameters obtained from image analysis in ACHN cells involves culturing separate groups for DH-14 and DH-15 and DH-18 and DH-19 in Cultrex for 72 hr, both with and without treatment (**Figure 5.30**). After image acquisition and analysis using software like ImageJ or FIJI, specific cellular parameters such as cell count, morphology, and other relevant characteristics are quantified. The comparison is drawn between the treated and untreated groups within each compound category, aiming to identify significant differences in cellular responses induced by DH-14, DH-15, DH-18, and DH-19 within the Cultrex environment. This analysis facilitates the understanding of the impact of

these treatments on ACHN cells, potentially revealing distinct effects and aiding in the determination of each compound's influence on cell behavior and characteristics.

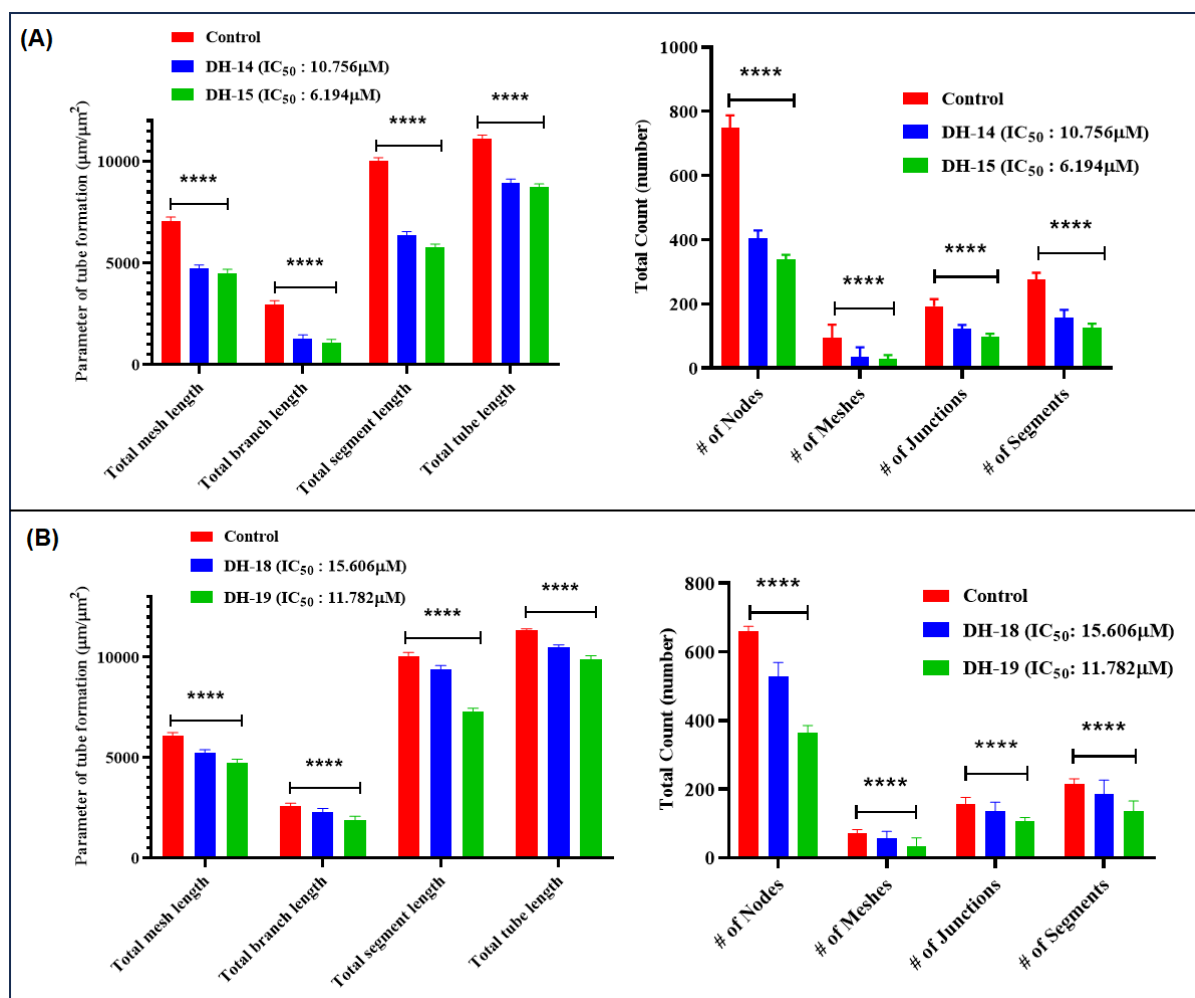


Figure 5.30. Comparative measurement of parameters obtained from image analysis in ACHN cells (A) DH-14 and DH-15 (B) DH-18 and DH-19 which were cultured for 72hr in Cultrex with and without treatment

5.3.7. DNA deformation assay by DAPI staining

DNA deformation assay is a widely used technique to observe the morphology of the cell nucleus. DAP (4',6-diamidino-2- phenylindole dihydrochloride) is a dye that can be used to visualize nuclear alterations and evaluate apoptosis (Das et al., 2022). In the minor groove of DNA's adenine-thymine sections, DAPI attaches firmly and preferentially. Light with an ultraviolet wavelength of 359 nm is absorbed by DAPI when it is attached to double-stranded DNA, and it produces fluorescent blue light at 461 nm. The fluorescence intensity of bound DAPI is about 20 times higher than that of unbound DAPI. Increased DAPI entry and deeper blue staining of the nucleus are caused by the apoptotic cell which has a damaged cell

membrane (Chazotte, 2011). The visual identification of apoptotic cells labeled with DAPI is aided by the distinct nuclear morphology of these cells, which includes margination of the nucleus, chromosomal condensation, and nuclear degeneration (Atale et al., 2014). DNA condensation is a distinct process that occurs during apoptosis; necrosis is not the result of any similar event (Kai et al., 2022). Furthermore, DAPI-stained apoptotic cells may have visible membrane blebbing, which is a characteristic feature of apoptotic cells (Wickman et al., 2013). The nuclear morphology of untreated K562 cells as well as treated K562 cells with lead compounds (DH-14 and DH-15) was evaluated after staining the nucleus individually with DAPI under a fluorescence microscope to know the exact mechanism of cytotoxicity (Das et al., 2022). In the case of lead compounds (DH-14 and DH-15) treated K562 cells (**Figure 5.31; B-C'**); margination of the nucleus, membrane blebbing, chromatin condensation, and nuclear fragmentation was observed whereas in the case of untreated K562 cells (**Figure 5.31; A-A'**); such kind of nuclear deformations were absent and the nuclei of untreated K562 cells were intact and having normal morphology. margination of the nucleus, membrane blebbing, chromatin condensation, and nuclear fragmentation all are associated with apoptosis-mediated cell death (Das et al., 2022; Pajaniradje et al., 2014).

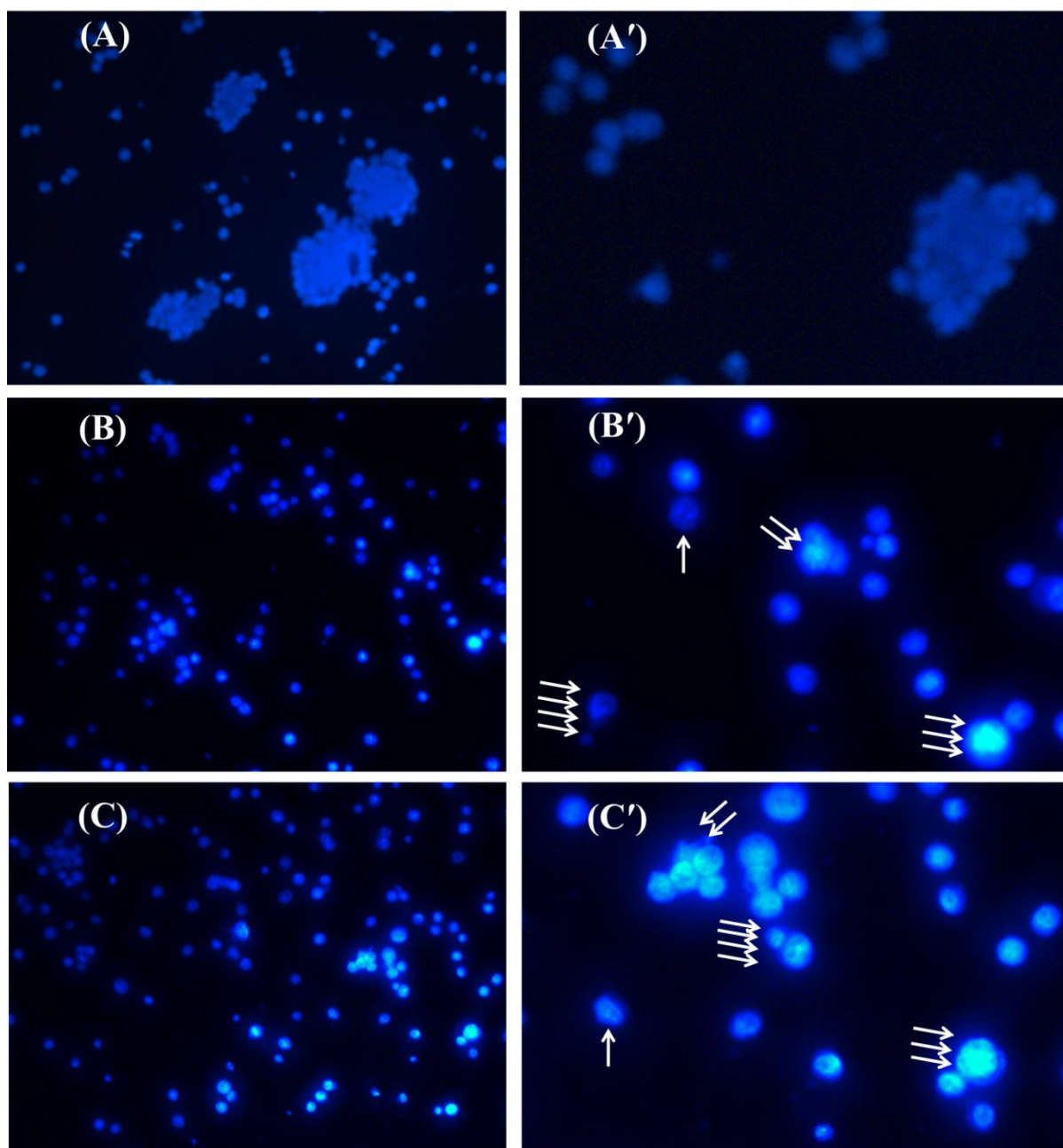


Figure 5.31. Fluorescence microscopic images of K562 cell nucleus after 48 hr of treatments and followed by DAPI staining. ; (A) represents the Control, (B) represents the treatment by DH-14 ($0.395 \mu\text{M}$) with IC_{50} dose, and (C) represents the treatment by DH-15 with IC_{50} dose ($0.315 \mu\text{M}$) whereas (A'), (B'), and (C') are the zoomed view of (A), (B), and (C). The single arrow indicates the margination of the nucleus, the double arrow indicates membrane blebbing, the triple arrow indicates chromatin condensation, and the quadruple arrow indicates nuclear fragmentation, all are associated with apoptosis-mediated cell death.

Conversely, K562 cells treated with another lead compound DH-18 and DH-19 displayed significant alterations in nuclear structure. These changes included margination of the nucleus, membrane blebbing, chromatin condensation, and nuclear fragmentation. Notably, these alterations are recognized characteristics associated with apoptosis-induced cell death, as reported in prior studies (Das et al., 2022; Pajaniradje et al., 2014). In the case of compounds (DH-18 and DH-19) treated K562 cells (**Figure 5.32; B-C'**); margination of the nucleus, membrane blebbing, chromatin condensation, and nuclear fragmentation was observed whereas in the case of untreated K562 cells (**Figure 5.32; A-A'**); such kind of nuclear deformations were absent and the nuclei of untreated K562 cells were intact and having normal morphology. Moreover, the observed morphological changes in the nuclei of treated cells, such as chromatin condensation and nuclear fragmentation, align with known indicators of apoptosis. In this context, these alterations provide valuable insights into the mechanism by which the lead compounds induce cytotoxic effects on K562 cells, shedding light on the apoptosis-mediated pathway responsible for cell death.

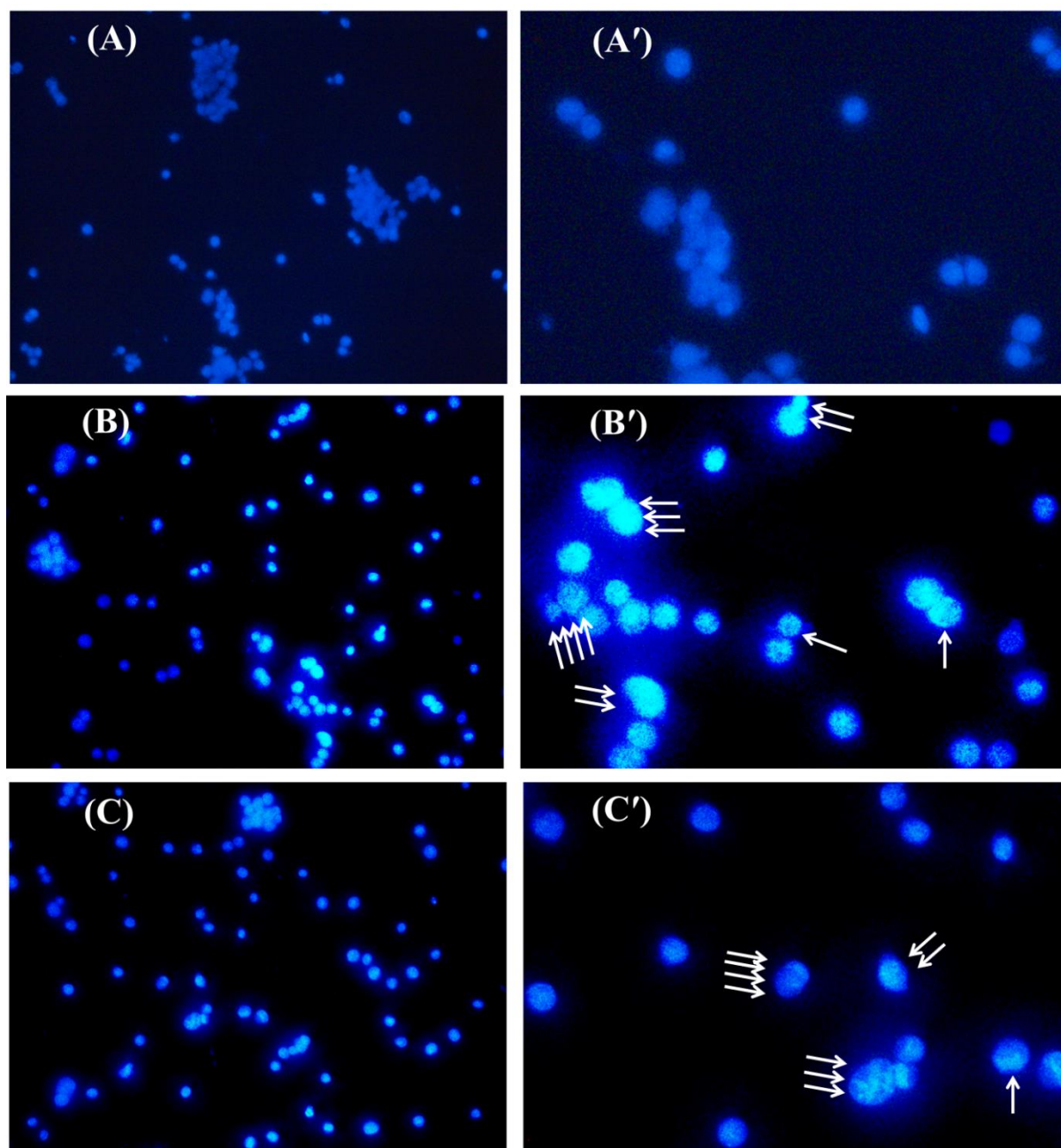


Figure 5.32. Fluorescence microscopic images of K562 cell nucleus after 48 hr of treatments and followed by DAPI staining. (A) represents the Control, (B) represents the treatment by DH-18 with IC_{50} ($0.338 \mu M$) dose, and (C) represents the treatment by DH-19 ($0.398 \mu M$) with IC_{50} dose whereas (A'), (B'), and (C') are the zoomed view of (A), (B), and (C). The single arrow indicates the margination of the nucleus, the double arrow indicates membrane blebbing, the triple arrow indicates chromatin condensation, and the quadruple arrow indicates nuclear fragmentation, all are associated with apoptosis-mediated cell death.

[This work was communicated for publication.]

5.4. MD simulation study of the potent MMP-2 inhibitors (DH-15 and DH-18)

The binding pattern of the most potent MMP-2 inhibitors of this series (DH-15 and DH-18) was predicted by performing 100ns MD simulation studies at the active site of MMP-2 (PDB ID: 1HOV). Simulation of each of the DH-15, DH-18, and MMP-2 complexes was performed using the *Desmond* module of Schrodinger Suite (<https://www.schrodinger.com>) using *OPLS_2005* forcefield.

From the trajectory RMSD analysis of the simulated complexes (**Figures 5.33A** and **5.33B**), it is noticed that the molecule showed very little deviation in their trajectory, unlike the ligand molecules that have shown comparatively higher deviation at the MMP-2 active site (PDB ID: 1HOV). Also, despite depicting comparatively similar fluctuation, the compound DH-15 showed comparatively more stable binding in comparison to the DH-18 (**Figure 5.33A** vs **5.33B**) at the MMP-2 binding site (PDB ID: 1HOV). Regarding the RMS fluctuation of the C- α chain residue, some key active site residues such as Leu 82, Leu83, Ala84, His85, Glu121, His120, Pro140, and Tyr142 showed similar fluctuation while complexed with both DH-15 (**Figure 5.33C**) and DH-18 (**Figure 5.33D**). This might suggest their almost similar MMP-2 inhibitory activities due to similar binding to the enzyme.

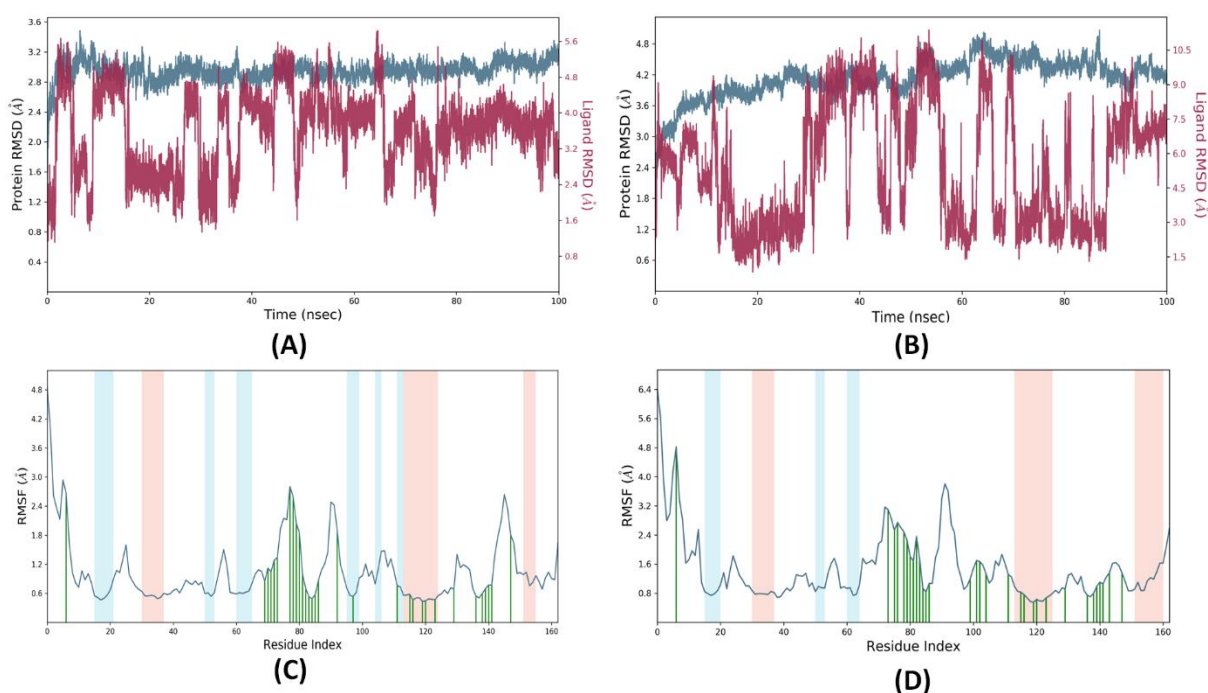


Figure 5.33. The RMSD obtained from the MD simulation study of (A) MMP-2 (PDB ID: 1HOV) and DH-15 complex, (B) MMP-2 (PDB ID: 1HOV) and DH-18 complex; the RMSF

of the C- α chain residues of MMP-2 obtained from the MD simulation study of **(C)** MMP-2 (PDB ID: 1HOV) and DH-15 complex, **(D)** MMP-2 (PDB ID: 1HOV) and DH-18 complex.

Regarding the interactions formed by the simulated compounds at the MMP-2 active site (PDB ID: 1HOV), it is visible that both the compounds DH-15 and DH-18 (**Figure 5.34A** and **5.34B**, respectively) formed similar hydrophobic, ionic, and water-mediated hydrogen bond interactions with active site residues such as His120, Glu121, His124, His130, Pro140, and Tyr142 residues. Interestingly, all these aforementioned residues are in association with each other to shape the S1' pocket of MMP-2. Therefore, the similar interactions between the S1' pocket and Ω -loop residues with DH-15 and DH-18 indicate an identical and stable binding of the biphenyl P1; substituents of these compounds inside the hydrophobic S1' pocket. On the other hand, it is also visible that the compound DH-15 has shown a higher extent of hydrogen bond interactions with the Leu82, Leu83, and Ala84, as well as His85 (using both hydrophobic and hydrogen bond interactions with His85) suggesting the reason behind a slight increase in the MMP-2 inhibitory activity of compound DH-15 compared to compound DH-18 (**Figure 5.34A** vs **5.34B**, respectively). This may occur due to the presence of 4-Cl benzyl P2' substituent that may be providing an advantage to the P2' moiety of DH-15 to enter into/near the solvent-exposed S2' pocket of MMP-2 (PDB ID: 1HOV) unlike the higher hydrophobic 3,5-bis trifluoromethyl benzyl P2; moiety of compound DH-18. The occupancy/proximity of the P2' substituent of compound DH-15 may have influenced greater stability of the molecule by interacting with His85 residues near the S2' pocket which in turn facilitated the formation of hydrogen bond interactions between the sulfonamide and the Leu82, Leu83, and Ala84 residues of MMP-2 throughout the simulation time. This is also clearly observable in the frequency of interactions formed between the DH-15, DH-18, and the individual active site residues of MMP-2 (PDB ID: 1HOV) (**Figure 5.34C** and **5.34D**, respectively).

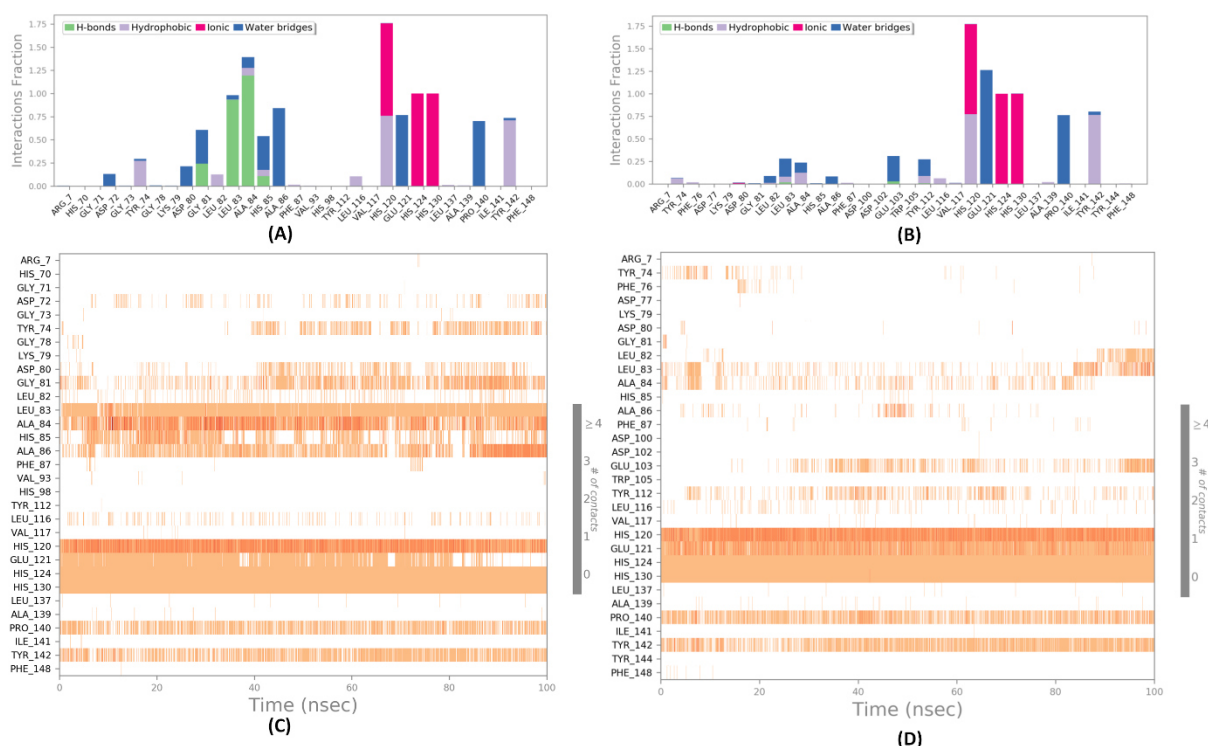


Figure 5.34. The interaction fractions of (A) DH-15 and (B) DH-18 with MMP-2 (PDB ID: 1HOV) active site residues; The interaction frequencies of individual residues between (C) MMP-2 and DH-15 and (D) MMP-2 and DH-18 for 100 ns

Regarding the bond occupancy throughout the simulated 100ns timeframe, it is observable that the common interactions formed between the DH-15, DH-18, and MMP-2 active site residues showed almost similar occupancy of formed interactions (**Figure 5.35A** and **5.35B**). However, the higher hydrogen bond forming occupancy between the compound DH-15 and Leu83 (93%), Ala84 (80%), and His85 (30%) residues of MMP-2 were absent between the same residues and compound DH-18. This slightly higher activity of DH-15 compared to DH-18 may be due to the extra interactions made by the DH-15 that might provide extra stability to the binding of DH-15 at the MMP-2 active site than DH-18.

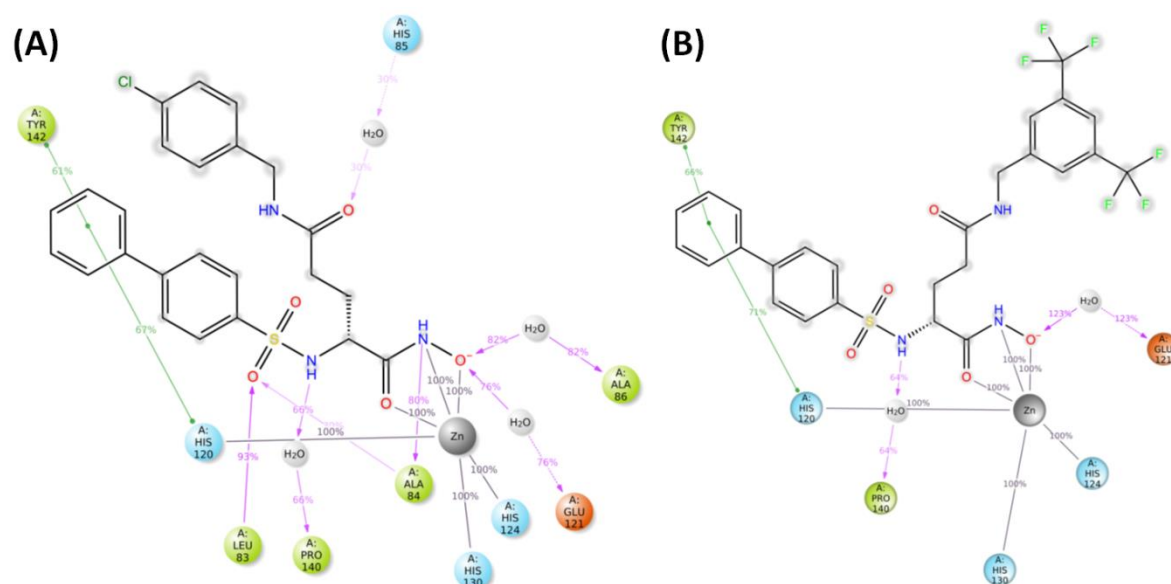


Figure 5.35. The overall interaction occupancies obtained from the MD simulation study of (A) MMP-2-DH-15 complex and (B) MMP-2-DH-18 complex.

5.5. Summary

The biological evaluation of newly synthesized compounds (DH-1 to DH-20) encompasses a broad spectrum of assays designed to comprehensively understand their potential applications in therapy against cancer, especially hematological malignancy. These biological assessments aim to provide crucial insights into the biphenyl sulfonamide-based hydroxamates, effects on various cellular processes, from cytotoxicity to their influence on specific enzymatic activities, apoptosis induction, cell cycle regulation, and even angiogenesis modulation. One significant aspect of this evaluation is the compound's impact on different cancer cell lines (K562, A549, U87MG, HT1080), shedding light on their potential in treating specific types of cancer. Notably, the results highlighted specific novel compounds, DH-14, DH-15, DH-18, and DH-19, displaying pronounced inhibitory effects on the K562 cell line, indicating a promising prospect for combating specific types of cancer such as CML. Moreover, DH-14 and DH-15 revealed substantial effectiveness even in the A549 cell line, emphasizing their potential across different cancer types. The enzyme inhibition assay aimed to assess these molecules' potential in targeting specific MMPs, such as MMP-2, MMP-9, and MMP-8, crucial enzymes involved in various physiological and pathological processes. This assay identified compounds displaying selective inhibition, providing insights into potential targeted therapeutic strategies against the MMP-2 enzyme. For example, DH-15 showed a preference for inhibiting MMP-2 over MMP-8 and MMP-9 with a significant selectivity

ratio. Understanding this selectivity is instrumental in designing therapies targeting specific MMPs, paving the way for more precise and effective treatments. Moreover, the assessment of MMP-2 expression in K562 cells post-treatment with specific compounds revealed a reduction in MMP-2 levels, indicating the novel compounds' potential to modulate MMP enzymes. This reduction in MMP-2 expression might have significant implications in controlling metastasis and tumor invasion. The apoptosis and cell cycle analyses were pivotal in understanding these novel synthesized analogs' impact on cell death and proliferation. Furthermore, compounds DH-14, DH-15, DH-18, and DH-19 exhibited notable effects on inducing apoptosis in K562 cells, a crucial mechanism in controlling cell growth. The cell cycle analysis showed alterations in the distribution of cells in different phases, indicating potential impacts on cell division and growth regulation. Henceforth, these findings suggest the novel compounds' potential to interfere with crucial cellular mechanisms, potentially influencing disease progression and treatment strategies. The analysis included modulation of angiogenesis, which is important in many clinical situations, such as cancer. Through *in vitro* tube formation assays, compounds DH-14, DH-15, DH-18, and DH-19 showed varying effects on blood vessel network density and complexity. Additionally, the DNA deformation assay, utilizing DAPI staining, revealed distinct morphological changes in the nuclei of treated K562 cells. The observed morphological alterations, characteristic of apoptosis-induced cell death, shed light on these novel compounds' cytotoxic effects and potential mechanisms behind cellular responses. Moreover, MD simulations study was conducted on best active molecules DH-15 and DH-18, formed hydrophobic, ionic, and water-mediated hydrogen bond interactions with active site residues such as His120, Glu121, His124, His130, Pro140, and Tyr142 residues. The interaction revealed the stable binding interactions at the active site of MMP-2 enzyme which validate the biological assay results. In summary, the diverse assays provided profound insights into the biological effects of these compounds [hydroxamates-based analogs 5-N-substituted 2-(substituted biphenylsulfonyl) D(-) glutamines], suggesting these novel molecules have potential for targeted therapeutic applications across different cancer types, CML. These findings highlight these analogs' diverse effects on specific cellular processes and mechanisms, paving the way for potential novel therapeutic strategies.

Chapter 6

CONCLUSION

Cancer continues to be one of the most difficult challenges in modern medicine, with its multifaceted nature demanding innovative approaches to treatment and management. Matrix metalloproteinases (MMPs), a family of enzymes implicated in various physiological and pathological processes, have emerged as potential targets for developing anticancer drugs. Among these MMPs, MMP-2 plays a crucial role in cancer progression, making it an attractive focus for research and drug development. The research presented in this study explores the significance of MMP-2 in cancer regulation and proposes it as a promising target for the development of anticancer drugs. Through the design, synthesis, and evaluation of specific compounds, including arylsulfonyl D(-) glutamine-based hydroxamate analogs, a multi-faceted approach has been employed to explore their potential as MMP-2 inhibitors and their effects on various cellular processes and mechanisms. Additionally, these findings particularly reveal the promise of these compounds for the development of targeted therapeutic strategies across different cancer types, particularly hematological malignancies. A diverse range of analytical techniques and assays, from quantitative structure-activity relationship (QSAR) models to molecular dynamics simulations and a plethora of biological assessments, has been employed to provide a comprehensive understanding of the compounds' effects on MMP-2, cancer cells, and various cellular processes.

In the realm of QSAR study, the regression and classification-based QSAR analysis played a crucial role in revealing the significant structural aspects of the MMP-2 enzyme. Various models like MLR, LDA, and Bayesian classification shed light on molecular characteristics affecting MMP-2 inhibitor efficacy, aiding in predictive analysis and understanding structure-activity relationships. In addition, the docking-based 2D-QSAR and 3D-QSAR analyses have also played a pivotal role in identifying the structural features crucial for inhibiting MMP-2 effectively. These models have elucidated the importance of specific amino acid residues, such as Tyr142 and Ala84, in MMP-2 inhibition. Furthermore, the model also has highlighted the significance of steric and hydrophobic attributes at specific regions of the compounds while suggesting an adverse effect on certain substituents. The preference for smaller hydrogen bond groups and the limited contribution of hydrogen bond donor groups have also been described. These findings lay a solid foundation for the rational design and optimization of MMP-2 inhibitors, potentially leading to more effective anticancer drugs. The integration of molecular dynamics (MD) simulations into the research framework has not only validated the findings from the QSAR models but also provided insight into the stability of interactions between MMP-2 and the tested inhibitors. The minimal fluctuations in parameters like RMSD, RMSF, and R_g values during MD simulations indicate robust and consistent binding between the

compounds and the MMP-2 enzyme. Furthermore, the simulations have identified specific amino acid residues responsible for potential hydrogen bonding, reinforcing the compounds' inhibitory potential. The convergence of findings from the computational models and MD simulations strengthens the foundation for the potential development of MMP-2 inhibitors.

The biological evaluation of the newly synthesized compounds represents a crucial phase of the study, shedding light on their effects on various cellular processes and mechanisms, *in vitro*. This evaluation encompasses a broad spectrum of assays, from cytotoxicity assessments to the influence on specific enzymatic activities, apoptosis induction, cell cycle regulation, DNA deformation assay by DAPI staining, and angiogenesis modulation. These assessments collectively provide profound insights into the compounds' potential for therapeutic applications in cancer, particularly hematological malignancies. One of the key outcomes from the biological evaluations is the synthesized novel molecule's ability to exert pronounced inhibitory effects on specific cancer cell lines, notably the K562 cell line. From this cytotoxicity analysis compounds such as DH-14 ($IC_{50} = 0.395 \mu M$), DH-15 ($IC_{50} = 0.315 \mu M$), DH-18 ($IC_{50} = 0.338 \mu M$), and DH-19 ($IC_{50} = 0.398 \mu M$) exhibit promising activity against K562 cell line, whereas the compounds showed non-toxic against normal cell line like HEK-293. Therefore, this observation holds significant promise for combating leukemia, indicating that these compounds may have a targeted and selective impact on chronic myeloid leukemia. Furthermore, compounds like DH-14, DH-15, DH-18, and DH-19 have exhibited substantial effectiveness in additional cancer cell lines, such as A549, underscoring their potential applicability across different cancer types, while these compounds exhibit non-cytotoxicity in normal human kidney cell line such as HEK-293. Therefore, this broad-spectrum efficacy adds to the compounds' attractiveness as candidates for future cancer therapies.

The enzyme inhibition assay conducted as part of the biological evaluations has provided crucial insights into the compounds' selectivity in targeting specific matrix metalloproteinases (MMPs), including MMP-2, MMP-9, and MMP-8. Selectivity is a vital consideration in drug development, as it enables the design of therapies that precisely target specific molecular pathways. In this context, DH-15 has demonstrated a preference for inhibiting MMP-2 ($IC_{50} = 23.28 \text{ nM}$) over MMP-9 ($IC_{50} = 55.14 \text{ nM}$) and MMP-8 ($IC_{50} = 1162.79 \text{ nM}$) with a significant selectivity ratio. This selectivity can be instrumental in designing therapies that specifically target MMP-2, thereby potentially increasing their effectiveness while minimizing off-target effects.

A significant aspect of the study has been evaluating MMP-2 expression in K562 cells following treatment with these molecules. It is interesting to note that, lower MMP-2 levels

can have significant implications in controlling metastasis and tumor invasion, which are often associated with diseases like cancer. The ability to modulate MMP-2 expression further strengthens the potential of these compounds as anticancer agents. In addition, the apoptosis and cell cycle analyses, integral to the biological evaluations, have offered crucial insights into the compounds' impact on cell death and proliferation. DH-14, DH-15, DH-18, and DH-19 have been particularly notable in inducing apoptosis in K562 cells, a fundamental mechanism in controlling cell growth and preventing uncontrolled proliferation. The cell cycle analysis has revealed alterations in the distribution of cells in different phases, suggesting potential impacts on cell division and growth regulation. These results highlight the molecules' capacity to alter essential cellular processes, which may impact the course of a disease like leukemia, and the approaches used to treat it. Furthermore, through *in vitro* tube formation assays, compounds DH-14, DH-15, DH-18, and DH-19 displayed varying effects on blood vessel network density and complexity. These effects on angiogenesis have the potential to disrupt the vascular supply to tumors, ultimately hampering their growth and progression. Additionally, the DNA deformation assay, utilizing DAPI staining, revealed distinct morphological changes in the nuclei of treated K562 cells, indicative of apoptosis-induced cell death. These changes in morphology provide information about the cytotoxic effects of these novel molecules and possible processes behind cellular reactions. The journey from the initial exploration of MMP-2 inhibition to the biological evaluations of these novel compounds has revealed the intricate interplay between structural features, molecular interactions, and biological responses. The integration of computational modeling and experimental assays has offered a holistic perspective on the compounds' potential, making a strong case for their further development and optimization as antileukemic agents. In addition, MD simulation study was conducted on best active compounds (DH-15 and DH-18), formed hydrophobic, ionic, and water-mediated hydrogen bond interactions with active site residues. The interaction revealed the stable binding interactions at the active site of MMP-2 enzyme which validate the biological assay results. In conclusion, the insights gained from this comprehensive study are poised to catalyze the development of more effective MMP-2 inhibitors, offering a new frontier in the fight against cancer, especially leukemia. The intricate understanding of molecular interactions, structural requirements, and biological effects of these compounds represents a significant leap forward in the pursuit of novel anticancer strategies. The potential for these compounds to translate into clinical applications presents a hopeful outlook for future advancements in cancer therapeutics, offering renewed possibilities in the ongoing battle against this complex and challenging disease.

Chapter 7

FUTURE DIRECTIONS

The research into MMP-2 inhibitors as potential anticancer agents holds substantial promise, laying the groundwork for a future marked by innovative steps in cancer therapy. Building upon the discoveries made in this study, the forthcoming trajectory in this field will encompass a concerted effort toward refining the structural makeup of these compounds to optimize their efficacy and specificity. Computational models and sophisticated algorithms will aid in a deeper understanding of the critical structural features highlighted in this research (**Figure 7.1**), guiding the rational design of new molecules and the modification of existing compounds. By precisely tailoring these inhibitors to target MMP-2, researchers aim to enhance their selectivity, potency, and ability to disrupt the critical pathways involved in cancer progression.

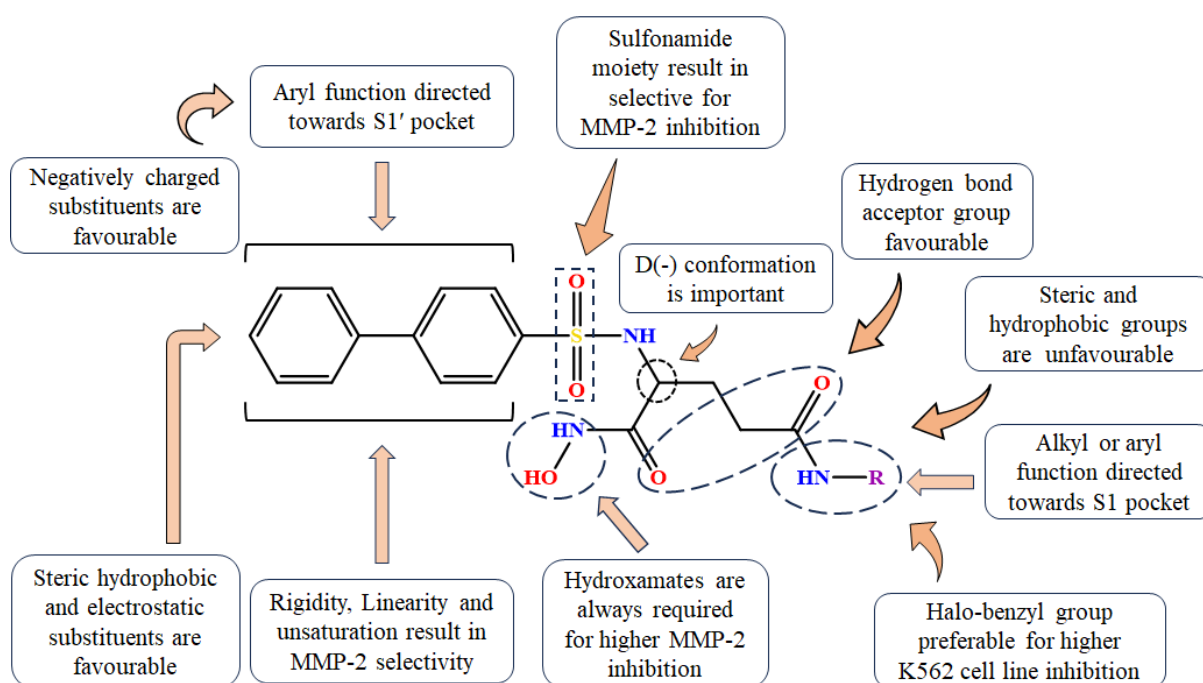


Figure 7.1. Structural requirements of glutamine analogs for obtaining higher efficacy.

Translating laboratory findings into practical clinical applications stands as a pivotal milestone in the future of this research. To bridge this gap, rigorous *in vivo* studies using animal models will be instrumental in assessing those novel compounds' effects on a systemic level. These studies will not only provide insights into the efficacy and safety profiles but also help determine the potential toxicities and optimal dosages necessary for human clinical trials. These preclinical trials will also serve as a stepping stone toward evaluating these inhibitors' pharmacokinetics, bioavailability, and interactions within living organisms, ultimately guiding the direction of human trials.

Upon successful validation in preclinical studies, the next phase would involve human clinical trials, where these compounds will be evaluated in diverse patient populations. These trials will focus on assessing their therapeutic effects, safety, and efficacy against specific cancer types, particularly hematological malignancies. Observing and quantifying the compounds' impacts on patient outcomes, including tumor regression, remission rates, and overall survival, will be pivotal in determining their clinical viability.

Furthermore, exploring the potential synergistic effects of these MMP-2 inhibitors in combination with existing cancer treatments, such as chemotherapy, immunotherapy, or other targeted therapies, presents a promising avenue. Combining these inhibitors with established treatments aims to leverage their complementary actions, potentially enhancing treatment efficacy while minimizing adverse side effects. Such synergistic approaches may provide a comprehensive strategy for combating cancer with improved outcomes.

An additional frontier in research involves targeted drug delivery systems to optimize the delivery of these inhibitors specifically to cancer cells. Innovative technologies like nanotechnology-based approaches or conjugation with specific carriers will aim to enhance the compounds' bioavailability at tumor sites while minimizing off-target effects. This targeted approach holds the potential to increase the local concentration of the compounds within cancerous tissues, maximizing their therapeutic effects. Understanding the molecular mechanisms underlying these inhibitory actions is fundamental for their further development and optimization. Deeper insights into how these inhibitors modulate MMP-2 expression, induce apoptosis, alter cell cycle progression, and impact angiogenesis will provide the necessary guidance for improving their effectiveness and potentially overcoming drug resistance.

Moreover, further studies can investigate the broad-spectrum impacts of the best active compounds on a variety of zinc-dependent metalloenzymes like other MMPs, HDACs, APNs, ADAMs, meprins, etc. This approach helps in the identification of potential therapeutic uses for a variety of disorders associated with these enzymes. Preliminary works in this direction were done, paving the way for comprehensive evaluations.

In conclusion, the future journey for MMP-2 inhibitors as potential anticancer agents hinges on a multi-faceted approach encompassing structural refinement, translational studies, combination therapies, targeted drug delivery systems, and the elucidation of underlying molecular mechanisms. These inhibitors hold promise for revolutionizing cancer therapy, but their true impact will depend on successful translation from laboratory findings to tangible clinical benefits for patients. The ultimate goal remains the development of safe, effective, and

accessible treatments that can significantly transform cancer management and patient outcomes on a global scale.

REFERENCES

- Abagyan R, Totrov M. High-throughput docking for lead generation. *Curr Opin Chem Biol.* 2001;5(4):375-382.
- Abbasi M, Ramezani F, Elyasi M, Sadeghi-Aliabadi H, Amanlou M. A study on quantitative structure-activity relationship and molecular docking of metalloproteinase inhibitors based on L-tyrosine scaffold. *Daru.* 2015;23(1):29.
- Adcock SA, McCammon JA. Molecular dynamics: Survey of methods for simulating the activity of proteins. *Chem Rev.* 2006;106(5):1589-1615.
- Adhikari N, Amin SA, Saha A, Jha T. Exploring in house glutamate inhibitors of matrix metalloproteinase-2 through validated robust chemico-biological quantitative approaches. *Struc Chem.* 2018a;29:285-297.
- Adhikari N, Amin SA, Saha A, Jha T. Structural exploration for the refinement of anticancer matrix metalloproteinase-2 inhibitor designing approaches through robust validated multi-QSARs. *J Mol Struc.* 2018b;1156:501-515.
- Adhikari N, Amin SA, Saha A, Jha T. Understanding chemico-biological interactions of glutamate MMP-2 inhibitors through rigorous alignment-dependent 3D-QSAR analyses. *ChemistrySelect.* 2017b;2(26):7888-7898.
- Adhikari N, Baidya S, Saha A, Jha T. Advances in studies on enzyme inhibitors as drugs. Volume 2: Miscellaneous drugs. Eds., S. P. Gupta. Design and development of matrix metalloproteinase inhibitors containing zinc-binding groups, without zinc-binding groups, and mechanism-based. Nova Science Publishers, New York, USA. 2017c;135-208.
- Adhikari N, Banerjee S, Baidya SK, Ghosh B, Jha T. Ligand-based quantitative structural assessments of SARS-CoV-2 3CLpro inhibitors: An analysis in light of structure-based multi-molecular modeling evidences. *J Mol Struct.* 2022;1251:132041.
- Adhikari N, Banerjee S, Baidya SK, Ghosh B, Jha T. Robust classification-based molecular modelling of diverse chemical entities as potential SARS-CoV-2 3CLpro inhibitors: theoretical justification in light of experimental evidences. *SAR QSAR Environ Res.* 2021;32(6):473-493.
- Adhikari N, Halder AK, Mallick S, Saha A, Saha KD, Jha T. Robust design of some selective matrix metalloproteinase-2 inhibitors over matrix metalloproteinase-9 through in silico/fragment-based lead identification and de novo lead modification: Syntheses and biological assays. *Bioorg Med Chem.* 2016;24(18):4291-4309.

- Adhikari N, Halder AK, Mondal C, Jha T. Exploring structural requirements of aurone derivatives as antimalarials by validated DFT-based QSAR, HQSAR, and COMFA–COMSIA approach. *Medicinal Chemistry Research*. 2013;22:6029-6045.
- Adhikari N, Halder AK, Saha A, Das Saha K, Jha T. Structural findings of phenylindoles as cytotoxic antimitotic agents in human breast cancer cell lines through multiple validated QSAR studies. *Toxicol In Vitro*. 2015;29(7):1392-1404.
- Adhikari N, Mukherjee A, Saha A, Jha T. Arylsulfonamides and selectivity of matrix metalloproteinase-2: An overview. *Eur J Med Chem*. 2017a;129:72-109.
- Adhikari N, Ph.D. Thesis, entitled “glutamine derivatives and analogs as matrix metalloproteinase-2 inhibitors: Rational design, synthesis, biological screening and molecular modeling studies”, Jadavpur University, Kolkata, 2018.
- Agrawal A, Pulendran B. Anthrax lethal toxin: A weapon of multisystem destruction. *Cell Mol Life Sci*. 2004;61(22):2859-2865.
- Agren MS, Mirastschijski U, Karlsmark T, Saarialho-Kere UK. Topical synthetic inhibitor of matrix metalloproteinases delays epidermal regeneration of human wounds. *Exp Dermatol*. 2001;10(5):337-348.
- Aier I, Varadwaj PK, Raj U. Structural insights into conformational stability of both wild-type and mutant EZH2 receptor. *Sci Rep*. 2016;6:34984.
- Ajjarapu SM, Tiwari A, Ramteke PW, Singh DB, Kumar S. Ligand-based drug designing. In *Bioinformatics*. Academic Press. 2022;233-252.
- Ajmani S, Jadhav K, Kulkarni SA. Three-dimensional QSAR using the k-nearest neighbor method and its interpretation. *J Chem Inf Model*. 2006;46(1):24-31.
- Ala-aho R, Kähäri VM. Collagenases in cancer. *Biochimie*. 2005;87(3-4):273-286.
- Ali I, Alfarouk KO, Reshkin SJ, Ibrahim ME. Doxycycline as potential anti-cancer agent. *Anticancer Agents Med Chem*. 2017;17(12):1617-1623.
- Almstead NG, Bradley RS, Pikul S, De B, Natchus MG, Taiwo YO, Gu F, Williams LE, Hynd BA, Janusz MJ, Dunaway CM, Mielsing GE. Design, synthesis, and biological evaluation of potent thiazine- and thiazepine-based matrix metalloproteinase inhibitors. *J Med Chem*. 1999;42(22):4547-4562.
- Amin SA, Gayen S. Modelling the cytotoxic activity of pyrazolo-triazole hybrids using descriptors calculated from the open source tool “PaDEL-descriptor”. *J Taibah Univ Sci*. 2016;10(6):896-905.
- Amjad MT, Chidharla A, Kasi A. Cancer chemotherapy. In: *StatPearls*. Treasure Island (FL): StatPearls Publishing; 2023. PMID: 33232037.

- Andreani J, Guerois R. Evolution of protein interactions: From interactomes to interfaces. *Arch Biochem Biophys*. 2014;554:65-75.
- Antoni C, Vera L, Devel L, Catalani MP, Czarny B, Cassar-Lajeunesse E, Nuti E, Rossello A, Dive V, Stura EA. Crystallization of bi-functional ligand protein complexes. *J Struct Biol*. 2013;182(3):246-254.
- Anwar T, Kumar P, Khan AU. Modern tools and techniques in computer-aided drug design. In *Molecular docking for computer-aided drug design*. Academic Press. 2021;1-30.
- Arakaki PA, Marques MR, Santos MC. MMP-1 polymorphism and its relationship to pathological processes. *J Biosci*. 2009;34(2):313-320.
- Armitage JO, Weisenburger DD. New approach to classifying non-Hodgkin's lymphomas: Clinical features of the major histologic subtypes. Non-hodgkin's lymphoma classification project. *J Clin Oncol*. 1998;16(8):2780-2795.
- Arun MZ, Reel B, Sala-Newby GB, Bond M, Tsaousi A, Maskell P, Newby AC. Zoledronate upregulates MMP-9 and -13 in rat vascular smooth muscle cells by inducing oxidative stress. *Drug Des Devel Ther*. 2016;10:1453-1460.
- Atale N, Gupta S, Yadav UC, Rani V. Cell-death assessment by fluorescent and nonfluorescent cytosolic and nuclear staining techniques. *J Microsc*. 2014;255(1):7-19.
- Auen T, Renavikar P, Habib E, Koepsell SA. Therapeutic leukocytapheresis for leukostasis in chronic lymphocytic leukemia: A case report and literature review. *J Clin Apher*. 2023.
- Bagchi K, Puri S. Free radicals and antioxidants in health and disease: A review. *EMHJ*. 1998;4(2):350-360.
- Baidya SK, Amin SA, Banerjee S, Adhikari N, Jha T. Structural exploration of arylsulfonamide-based ADAM17 inhibitors through validated comparative multi-QSAR modelling studies. *J Mol Struct*. 2019;1185:128-142.
- Baidya SK, Amin SA, Jha T. Outline of gelatinase inhibitors as anti-cancer agents: A patent mini-review for 2010-present. *Eur J Med Chem*. 2021;213:113044.
- Baidya SK, Banerjee S, Adhikari N, Jha T. Selective inhibitors of medium-size S1' pocket matrix metalloproteinases: A stepping stone of future drug discovery. *J Med Chem*. 2022;65(16):10709-10754.
- Baidya SK, Banerjee S, Ghosh B, Jha T, Adhikari N. Assessing structural insights into in house arylsulfonyl L-(+) glutamine MMP-2 inhibitors as promising anticancer agents through ligand-based and structure-based computational modeling approaches. *SAR QSAR Env Res*. 2023;34(10):1-26.

- Baig MH, Ahmad K, Rabbani G, Danishuddin M, Choi I. Computer aided drug design and its application to the development of potential drugs for neurodegenerative disorders. *Curr Neuropharmacol*. 2018;16(6):740-748.
- Banerjee S, Adhikari N, Amin SA, Jha T. Structural exploration of tetrahydroisoquinoline derivatives as HDAC8 inhibitors through multi-QSAR modeling study. *J Biomol Struct Dyn*. 2020;38(5):1551-1564.
- Banerjee S, Dumawat S, Jha T, Lanka G, Adhikari N, Ghosh B. Fragment-based structural exploration and chemico-biological interaction study of HDAC3 inhibitors through non-linear pattern recognition, chemical space, and binding mode of interaction analysis. *J Biomol Struct Dyn*. 2023:1-23.
- Banerjee S, Kejriwal S, Ghosh B, Lanka G, Jha T, Adhikari N. Fragment-based investigation of thiourea derivatives as VEGFR-2 inhibitors: a cross-validated approach of ligand-based and structure-based molecular modeling studies. *J Biomol Struct Dyn*. 2023:1-17.
- Baran Y, Ural AU, Gunduz U. Mechanisms of cellular resistance to imatinib in human chronic myeloid leukemia cells. *Hematology*. 2007;12(6):497-503.
- Barta TE, Becker DP, Bedell LJ, De Crescenzo GA, McDonald JJ, Mehta P, Munie GE, Villamil CI. Selective, orally active MMP inhibitors with an aryl backbone. *Bioorg Med Chem Lett*. 2001;11(18):2481-2483.
- Barta TE, Becker DP, Bedell LJ, De Crescenzo GA, McDonald JJ, Munie GE, Rao S, Shieh HS, Stegeman R, Stevens AM, Villamil CI. Synthesis and activity of selective MMP inhibitors with an aryl backbone. *Bioorg Med Chem Lett*. 2000;10(24):2815-2817.
- Baserga R. The cell cycle. *N Engl J Med*. 1981;304(8):453-459.
- Baskar R, Lee KA, Yeo R, Yeoh KW. Cancer and radiation therapy: Current advances and future directions. *Int J Med Sci*. 2012;9(3):193.
- Baxter AD, Bhogal R, Bird J, Keily JF, Manallack DT, Montana JG, Owen DA, Pitt WR, Watson RJ, Wills RE. Arylsulphonyl hydroxamic acids: potent and selective matrix metalloproteinase inhibitors. *Bioorg Med Chem Lett*. 2001;11(11):1465-1468.
- Becker DP, Barta TE, Bedell LJ, Boehm TL, Bond BR, Carroll J, Carron CP, Decrescenzo GA, Easton AM, Freskos JN, Funckes-Shippy CL, Heron M, Hockerman S, Howard CP, Kiefer JR, Li MH, Mathis KJ, McDonald JJ, Mehta PP, Munie GE, Sunyer T, Swearingen CA, Villamil CI, Welsch D, Williams JM, Yu Y, Yao J. Orally active MMP-1 sparing α -tetrahydropyranyl and α -piperidinyl sulfone matrix metalloproteinase (MMP) inhibitors with efficacy in cancer, arthritis, and cardiovascular disease. *J Med Chem*. 2010;53(18):6653-6680.

- Becker DP, DeCrescenzo G, Freskos J, Getman DP, Hockerman SL, Li M, Mehta P, Munie GE, Swearingen C. α -Alkyl- α -amino- β -sulphone hydroxamates as potent MMP inhibitors that spare MMP-1. *Bioorg Med Chem Lett*. 2001;11(20):2723-2725.
- Becker DP, Villamil CI, Barta TE, Bedell LJ, Boehm TL, Decrescenzo GA, Freskos JN, Getman DP, Hockerman S, Heintz R, Howard SC, Li MH, McDonald JJ, Carron CP, Funckes-Shippy CL, Mehta PP, Munie GE, Swearingen CA. Synthesis and structure-activity relationships of β - and α -piperidine sulfone hydroxamic acid matrix metalloproteinase inhibitors with oral antitumor efficacy. *J Med Chem*. 2005;48(21):6713-6730.
- Behrends M, Wagner S, Kopka K, Schober O, Schäfers M, Kumbhar S, Waller M, Haufe G. New matrix metalloproteinase inhibitors based on γ -fluorinated α -aminocarboxylic and α -aminohydroxamic acids. *Bioorg Med Chem*. 2015;23(13):3809-3818.
- Benek O, Korabecny J, Soukup O. A Perspective on Multi-target Drugs for Alzheimer's Disease. *Trends Pharmacol Sci*. 2020;41(7):434-445.
- Bennett JH. Case of hypertrophy of the spleen and liver, in which death took place from suppuration of the blood. *Edinburgh Med Sug J*. 1845;64:413-23.
- Berendsen HJ, van der Spoel D, van Drunen R. GROMACS: A message-passing parallel molecular dynamics implementation. *Comput Phys Commun*. 1995;91(1-3):43-56.
- Beton O, Arslan S, Acar B, Ozbilum N, Berkan O. Association between MMP-3 and MMP-9 polymorphisms and coronary artery disease. *Biomed Rep*. 2016;5(6):709-714.
- Bhatia R. Novel approaches to therapy in CML. *Hematology Am Soc Hematol Educ Program*. 2017;2017(1):115-120.
- Bister VO, Salmela MT, Karjalainen-Lindsberg ML, Uria J, Lohi J, Puolakkainen P, Lopez-Otin C, Saarialho-Kere U. Differential expression of three matrix metalloproteinases, MMP-19, MMP-26, and MMP-28, in normal and inflamed intestine and colon cancer. *Dig Dis Sci*. 2004;49(4):653-661.
- Blumenthal MN, Zhong W, Miller M, Wendt C, Connett JE, Pei D. Serum metalloproteinase leukolysin (MMP-25/MT-6): A potential metabolic marker for atopy-associated inflammation. *Clin Exp Allergy*. 2010;40(6):859-866.
- Bode W, Fernandez-Catalan C, Tschesche H, Grams F, Nagase H, Maskos K. Structural properties of matrix metalloproteinases. *Cell Mol Life Sci*. 1999;55(4):639-652.
- Bonnans C, Chou J, Werb Z. Remodelling the extracellular matrix in development and disease. *Nat Rev Mol Cell Biol*. 2014;15(12):786-801.

- Boyd S, Virolainen S, Pärssinen J, Skoog T, van Hogerlinden M, Latonen L, Kyllönen L, Toftgard R, Saarialho-Kere U. MMP-10 (Stromelysin-2) and MMP-21 in human and murine squamous cell cancer. *Exp Dermatol*. 2009;18(12):1044-1052.
- Brown FK, Sherer EC, Johnson SA, Holloway MK, Sherborne BS. The evolution of drug design at Merck research laboratories. *J Comput Aided Mol Des*. 2017;31(3):255-266.
- Brown S, Meroueh SO, Fridman R, Mobashery S. Quest for selectivity in inhibition of matrix metalloproteinases. *Curr Top Med Chem*. 2004;4(12):1227-1238.
- Bruchova H, Borovanova T, Klamova H, Brdicka R. Gene expression profiling in chronic myeloid leukemia patients treated with hydroxyurea. *Leuk Lymphoma*. 2002;43(6):1289-1295.
- Burley SK, Berman HM, Christie C, Duarte JM, Feng Z, Westbrook J, Young J, Zardecki C. RCSB Protein Data Bank: Sustaining a living digital data resource that enables breakthroughs in scientific research and biomedical education. *Protein Sci*. 2018;27(1):316-330.
- Burns DM, He C, Li Y, Scherle P, Liu X, Marando CA, Covington MB, Yang G, Pan M, Turner S, Fridman JS, Hollis G, Vaddi K, Yeleswaram S, Newton R, Friedman S, Metcalf B, Yao W. Conversion of an MMP-potent scaffold to an MMP-selective HER-2 sheddase inhibitor via scaffold hybridization and subtle P1' permutations. *Bioorg Med Chem Lett*. 2008;18(2):560-564.
- Burns DM, Li YL, Shi E, He C, Xu M, Zhuo J, Zhang C, Qian DQ, Li Y, Wynn R, Covington MB, Katiyar K, Marando CA, Fridman JS, Scherle P, Friedman S, Metcalf B, Yao W. Compelling P1 substituent affect on metalloprotease binding profile enables the design of a novel cyclohexyl core scaffold with excellent MMP selectivity and HER-2 sheddase inhibition. *Bioorg Med Chem Lett*. 2009;19(13):3525-3530.
- Camodeca C, Nuti E, Tepshi L, Boero S, Tuccinardi T, Stura EA, Poggi A, Zocchi MR, Rossello A. Discovery of a new selective inhibitor of A Disintegrin And Metalloprotease 10 (ADAM-10) able to reduce the shedding of NKG2D ligands in Hodgkin's lymphoma cell models. *Eur J Med Chem*. 2016;111:193-201.
- Cathcart J, Pulkoski-Gross A, Cao J. Targeting matrix metalloproteinases in cancer: Bringing new life to old ideas. *Genes Dis*. 2015;2(1):26-34.
- Chaudhary AK, Pandya S, Ghosh K, Nadkarni A. Matrix metalloproteinase and its drug targets therapy in solid and hematological malignancies: an overview. *Mutat Res*. 2013;753(1):7-23.

- Chaudhry P, Asselin E. Resistance to chemotherapy and hormone therapy in endometrial cancer. *Endocr Relat Cancer*. 2009;16(2):363-380.
- Chazotte B. Labeling nuclear DNA using DAPI. *Cold Spring Harb Protoc*. 2011 Jan 1;2011(1):pdb.prot5556.
- Chelluboina B, Nalamolu KR, Klopfenstein JD, Pinson DM, Wang DZ, Vemuganti R, Veeravalli KK. MMP-12, a promising therapeutic target for neurological diseases. *Mol Neurobiol*. 2018;55(2):1405-1409.
- ChemDraw ultra 5.0. Cambridge Soft Corporation, USA, 2010; software available at <http://www.cambridgesoft.com>.
- Chen JW, Dhahbi J. Lung adenocarcinoma and lung squamous cell carcinoma cancer classification, biomarker identification, and gene expression analysis using overlapping feature selection methods. *Sci Rep*. 2021;11(1):13323.
- Chen L, Li Y, Zhao Q, Peng H, Hou T. ADME evaluation in drug discovery. 10. Predictions of P-glycoprotein inhibitors using recursive partitioning and naive Bayesian classification techniques. *Mol Pharm*. 2011;8(3):889-900.
- Cheng M, De B, Almstead NG, Pikul S, Dowty ME, Dietsch CR, Dunaway CM, Gu F, Hsieh LC, Janusz MJ, Taiwo YO, Natchus MG, Hudlicky T, Mandel M. Design, synthesis, and biological evaluation of matrix metalloproteinase inhibitors derived from a modified proline scaffold. *J Med Chem*. 1999;42(26):5426-5436.
- Cheng XC, Wang Q, Fang H, Tang W, Xu WF. Design, synthesis and evaluation of novel sulfonyl pyrrolidine derivatives as matrix metalloproteinase inhibitors. *Bioorg Med Chem*. 2008a;16(10):5398-5404.
- Cheng XC, Wang Q, Fang H, Tang W, Xu WF. Synthesis of new sulfonyl pyrrolidine derivatives as matrix metalloproteinase inhibitors. *Bioorg Med Chem*. 2008b;16(17):7932-7938.
- Cheng XC, Wang RL, Dong ZK, Li J, Li YY, Li RR. Design, synthesis and evaluation of novel metalloproteinase inhibitors based on L-tyrosine scaffold. *Bioorg Med Chem*. 2012;20(19):5738-5744.
- Cherkasov A, Muratov EN, Fourches D, Varnek A, Baskin II, Cronin M, Dearden J, Gramatica P, Martin YC, Todeschini R, Consonni V, Kuz'min VE, Cramer R, Benigni R, Yang C, Rathman J, Terfloth L, Gasteiger J, Richard A, Tropsha A. QSAR modeling: Where have you been? Where are you going to?. *J Med Chem*. 2014;57(12):4977-5010.
- Chien MH, Lin CW, Cheng CW, Wen YC, Yang SF. Matrix metalloproteinase-2 as a target for head and neck cancer therapy. *Expert Opin Ther Targets*. 2013;17(2):203-216.

- Chollet AM, Le Diguarher T, Kucharczyk N, Loynel A, Bertrand M, Tucker G, Guilbaud N, Burbridge M, Pastoureau P, Fradin A, Sabatini M, Fauchère JL, Casara P. Solid-phase synthesis of alpha-substituted 3-bisarylthio N-hydroxy propionamides as specific MMP inhibitors. *Bioorg Med Chem*. 2002;10(3):531-544.
- Chollet AM, Le Diguarher T, Murray L, Bertrand M, Tucker GC, Sabatini M, Pierré A, Atassi G, Bonnet J, Casara P. General synthesis of alpha-substituted 3-bisaryloxy propionic acid derivatives as specific MMP inhibitors. *Bioorg Med Chem Lett*. 2001;11(3):295-299.
- Chun K, Park SK, Kim HM, Choi Y, Kim MH, Park CH, Joe BY, Chun TG, Choi HM, Lee HY, Hong SH, Kim MS, Nam KY, Han G. Chromen-based TNF-alpha converting enzyme (TACE) inhibitors: design, synthesis, and biological evaluation. *Bioorg Med Chem*. 2008;16(1):530-535.
- Coburn N, Cosby R, Klein L, Knight G, Malthaner R, Mamazza J, Mercer CD, Ringash J. Staging and surgical approaches in gastric cancer: A systematic review. *Cancer Treat. Rev*. 2018;63:104-115.
- Collatuzzo G, Boffetta P. Cancers attributable to modifiable risk factors: A road map for prevention. *Annu Rev Public Health*. 2023;44:279-300.
- Condon JS, Joseph-McCarthy D, Levin JL, Lombart HG, Lovering FE, Sun L, Wang W, Xu W, Zhang Y. Identification of potent and selective TACE inhibitors via the S1 pocket. *Bioorg Med Chem Lett*. 2007;17(1):34-39.
- Covington MD, Burghardt RC, Parrish AR. Ischemia-induced cleavage of cadherins in NRK cells requires MT1-MMP (MMP-14). *Am J Physiol Renal Physiol*. 2006;290(1):F43-F51.
- Cramer RD. Rethinking 3D-QSAR. *J Comput Aided Mol Des*. 2011;25(3):197-201.
- Cramer RD. The inevitable QSAR renaissance. *J Comput Aided Mol Des*. 2012;26(1):35-38.
- Creutzig U, Kutny MA, Barr R, Schlenk RF, Ribeiro RC. Acute myelogenous leukemia in adolescents and young adults. *Pediatric Blood Cancer*. 2018;65(9):e27089.
- Crilly T, Johnson DM. The emergence of topological dimension theory. *History Topol*. 1999:1-24.
- Crosby D, Bhatia S, Brindle KM, Coussens LM, Dive C, Emberton M, Esener S, Fitzgerald RC, Gambhir SS, Kuhn P, Rebbeck TR. Early detection of cancer. *Science*. 2022;375(6586):eaay9040.
- Curtin ML, Garland RB, Davidsen SK, Marcotte PA, Albert DH, Magoc TJ, Hutchins C. Broad spectrum matrix metalloproteinase inhibitors: an examination of succinamide

- hydroxamate inhibitors with P1 C alpha gem-disubstitution. *Bioorg Med Chem Lett*. 1998;8(12):1443-1448.
- Danishuddin, Khan AU. Descriptors and their selection methods in QSAR analysis: Paradigm for drug design. *Drug Discov Today*. 2016;21(8):1291-1302.
 - Das PK, Diya VA, Meher S, Panda R, Abraham A. A systematic review on recent advancements in deep and machine learning based detection and classification of acute lymphoblastic leukemia. *IEEE access*. 2022;10:81741-81763.
 - Das S, Amin SA, Datta S, Adhikari N, Jha T. Synthesis, biological activity, structure activity relationship study and liposomal formulation development of some arylsulfonyl pyroglutamic acid derivatives. *J Mol Struct*. 2022;1248:131512.
 - Das S, Amin SA, Jha T. Inhibitors of gelatinases (MMP-2 and MMP-9) for the management of hematological malignancies. *Eur J Med Chem*. 2021;223:113623.
 - Das S, Amin SA, Jha T. Insight into the structural requirement of aryl sulphonamide based gelatinases (MMP-2 and MMP-9) inhibitors - Part I: 2D-QSAR, 3D-QSAR topomer CoMFA and Naïve Bayes studies - First report of 3D-QSAR Topomer CoMFA analysis for MMP-9 inhibitors and jointly inhibitors of gelatinases together. *SAR QSAR Environ Res*. 2021;32(8):655-687.
 - Datta S, Halder AK, Adhikari N, Amin SA, Das S, Jha T. Synthesis, anticancer activity, SAR and binding mode of interaction studies of substituted pentanoic acids: part II. *Future Med Chem*. 2022;14(1):17-34.
 - De AU, Jha T, Majumdar A, Debnath AK. Possible antineoplastic agents: Part IX- Synthesis, antineoplastic activity and quantitative structure-activity relationship of 5-N-substituted-2-(chlorosubstituted benzenesulphonyl)-L-glutamines. *Ind J Pharm Sci*. 1985;47:93-96.
 - De AU, Majumdar A, Jha T, Debnath AK. Possible antineoplastic agents: Part VIII- Synthesis and antineoplastic activity of 5-N-substituted-3-substituted phenylglutaramic acids and 5-Nsubstituted-2- benzenesulphonyl-3-phenyl-1-L-glutamines. *Ind J Chem*. 1984;23B:97.
 - Debnath AK, Jha T, Majumdar A, De AU. Rational design of 4-(4'-substituted benzoyl)aminobenzenesulphonyl-L-glutamines as potential antineoplastic agents: Synthesis, biological evaluation and quantitative structure-activity relationship studies. *Ind J Chem*. 1989;28B:843-847.
 - Debnath B, Gayen S, Samanta S, Basu A, Ghosh B, Jha T. QSAR study on some synthesized and biologically evaluated glutamine analogs as possible anticancer agents. *Ind J Chem A*. 2006;45A:93-99.

- Debnath B, Samanta S, Gayen S, Basu A, Ghosh B, Jha T. QSAR study on 5–N–substituted–2–(substituted benzenesulphonyl) glutamines as antitumor agents through synthesis and biological evaluation: Part III, Internet Electron J Mol Des. 2005;4:393-412.
- Debnath B, Srikanth K, Banarjee S, Jha T. Glutamamides as Antitumor Agents. Part 2. Synthesis, biological activity and QSAR study. Internet Electron J Mol Des. 2002;1:488-502.
- Deliberador FR, Sebastiani AM, Gerber J, Bonetto L, Tórtora G, Giovanini AF, Deliberador TM, Zielak JC, Scariot R. Effect of local application of alendronate and parathyroid hormone on craniofacial bone repair - a preliminary study. Braz Dent J. 2018;29(5):435-445.
- Discovery studio 3.0 (DS 3.0). Accelrys Inc, CA, USA, 2015; software available at <http://www.accelrys.com>.
- Djuric T, Zivkovic M. Overview of MMP biology and gene associations in human diseases. In: The role of matrix metalloproteinase in human body pathologies. In Tech open, London. 2017;3-33
- Doroshov JH, Gaur S. Role of reactive oxygen species in the cytotoxicity of arsenic trioxide and pamidronate for human prostate cancer cells. React Oxyg Species (Apex). 2020;9(26):81-94.
- Duffy MJ, Sturgeon C, Lamerz R, Haglund C, Holubec VL, Klapdor R, Nicolini A, Topolcan O, Heinemann V. Tumor markers in pancreatic cancer: A European group on tumor markers (EGTM) status report. Ann Oncol. 2010;21(3):441-447.
- Duffy MJ, van Dalen A, Haglund C, Hansson L, Holinski-Feder E, Klapdor R, Lamerz R, Peltomaki P, Sturgeon C, Topolcan O. Tumour markers in colorectal cancer: European Group on Tumour Markers (EGTM) guidelines for clinical use. Eur J Cancer. 2007;43(9):1348-1360.
- Dutta S, Halder AK, Adhikari N, Amin SA, Das S, Saha A, Jha T. Synthesis, anticancer activity, structure–activity relationship and binding mode of interaction studies of substituted pentanoic acids. Future Med Chem. 2019;11(14):1679-1702.
- Emingil G, Kuula H, Sorsa T, Atilla G. Gingival crevicular fluid matrix metalloproteinase-25 and -26 levels in periodontal disease. J Periodontol. 2006;77(4):664-671.
- Eriksson M, Hardell L, Carlberg M, Akerman M. Pesticide exposure as risk factor for non-Hodgkin lymphoma including histopathological subgroup analysis. Int J Cancer. 2008;123(7):1657-1663.

- Fabre B, Filipiak K, Díaz N, Zapico JM, Suárez D, Ramos A, de Pascual-Teresa B. An integrated computational and experimental approach to gaining selectivity for MMP-2 within the gelatinase subfamily. *Chembiochem*. 2014;15(3):399-412.
- Fabre B, Filipiak K, Zapico JM, Díaz N, Carbajo RJ, Schott AK, Martínez-Alcázar MP, Suárez D, Pineda-Lucena A, Ramos A, de Pascual-Teresa B. Progress towards water-soluble triazole-based selective MMP-2 inhibitors. *Org Biomol Chem*. 2013;11(38):6623-6641.
- Farina AR, Tacconelli A, Teti A, Gulino A, Mackay AR. Tissue inhibitor of metalloproteinase-2 protection of matrix metalloproteinase-2 from degradation by plasmin is reversed by divalent cation chelator EDTA and the bisphosphonate alendronate. *Cancer Res*. 1998;58(14):2957-2960.
- Fatma H, Siddique HR. Research and patents status of selected phytochemicals against cancer: How close and how far?. *Recent Pat Anticancer Drug Discov*. 2023;18(4):428-447.
- Fawcett T. An introduction to ROC analysis. *Pattern recognition letters*. 2006;27(8):861-874.
- Feng Y, Likos JJ, Zhu L, Woodward H, Munie G, McDonald JJ, Stevens AM, Howard CP, De Crescenzo GA, Welsch D, Shieh HS, Stallings WC. Solution structure and backbone dynamics of the catalytic domain of matrix metalloproteinase-2 complexed with a hydroxamic acid inhibitor. *Biochim Biophys Acta*. 2002;1598(1-2):10-23.
- Fife RS, Sledge GW Jr. Effects of doxycycline on in vitro growth, migration, and gelatinase activity of breast carcinoma cells. *J Lab Clin Med*. 1995;125(3):407-411.
- Fisher FM. Multiple regression in legal proceedings. *Colum. L. Rev.*. 1980;80:702.
- Fobian YM, Freskos JN, Barta TE, Bedell LJ, Heintz R, Kassab DJ, Kiefer JR, Mischke BV, Molyneaux JM, Mullins P, Munie GE, Becker DP. MMP-13 selective alpha-sulfone hydroxamates: identification of selective P1' amides. *Bioorg Med Chem Lett*. 2011;21(10):2823-2825.
- Fray MJ, Burslem MF, Dickinson RP. Selectivity of inhibition of matrix metalloproteases MMP-3 and MMP-2 by succinyl hydroxamates and their carboxylic acid analogues is dependent on P3' group chirality. *Bioorg Med Chem Lett*. 2001a;11(4):567-570.
- Fray MJ, Dickinson RP. Discovery of potent and selective succinyl hydroxamate inhibitors of matrix metalloprotease-3 (stromelysin-1). *Bioorg Med Chem Lett*. 2001b;11(4):571-574.
- ftp://ftp.ncbi.nlm.nih.gov/pubchem/specifications/pubchem_fingerprints.txt
- Galaray RE, Cassabonne ME, Giese C, Gilbert JH, Lapierre F, Lopez H, Schaefer ME, Stack R, Sullivan M, Summers B, Tressler R, Tyrrell D, Wee J, Allen SD, Castellot JJ, Barletta JP, Schultz GS, Fernandez LA, Fisher S, Cui TY, Foellmer HG, Grobelny D, Holleran

- WH. Low molecular weight inhibitors in corneal ulceration. *Ann N Y Acad Sci.* 1994;732:315-323.
- Galvez-Llompart M, Zanni R, García-Domenech R. Modeling natural anti-inflammatory compounds by molecular topology. *Int J Mol Sci.* 2011;12(12):9481-9503.
 - García-Muñoz R, Roldan Galiacho V, Llorente L. Immunological aspects in chronic lymphocytic leukemia (CLL) development. *Ann Hematol.* 2012;91(7):981-996.
 - Gasteiger J. Chemistry in times of artificial intelligence. *Chemphyschem.* 2020;21:2233-2242.
 - Gatto C, Rieppi M, Borsotti P, Innocenti S, Ceruti R, Drudis T, Scanziani E, Casazza AM, Taraboletti G, Giavazzi R. BAY 12-9566, a novel inhibitor of matrix metalloproteinases with antiangiogenic activity. *Clin Cancer Res.* 1999;5(11):3603-3607.
 - Gayen S, Debnath B, Samanta S, Ghosh B, Basu A, Jha T. Glutamamide analogues as anticancer agents. Part 3. Synthesis, biological screening and QSAR study. *Internet Electron J Mol Des.* 2005;4:556-578.
 - Genheden S, Ryde U. The MM/PBSA and MM/GBSA methods to estimate ligand-binding affinities. *Expert Opin Drug Discov.* 2015;10(5):449-461.
 - Georgiadis D, Yiotakis A. Specific targeting of metzincin family members with small-molecule inhibitors: progress toward a multifarious challenge. *Bioorg Med Chem.* 2008;16(19):8781-8794.
 - Gharib SA, Manicone AM, Parks WC. Matrix metalloproteinases in emphysema. *Matrix Biology.* 2018;73:34-51.
 - Gialeli C, Theocharis AD, Karamanos NK. Roles of matrix metalloproteinases in cancer progression and their pharmacological targeting. *FEBS J.* 2011;278(1):16-27.
 - Ginaldi L, De Martinis M, Matutes E, Farahat N, Morilla R, Catovsky D. Levels of expression of CD19 and CD20 in chronic B cell leukaemias. *Journal of clinical pathology.* 1998;51(5):364-369.
 - Gingras D, Batist G, Béliveau R. AE-941 (Neovastat): A novel multifunctional antiangiogenic compound. *Expert Rev Anticancer Ther.* 2001;1(3):341-347.
 - Gingras D, Renaud A, Mousseau N, Beaulieu E, Kachra Z, Béliveau R. Matrix proteinase inhibition by AE-941, a multifunctional antiangiogenic compound. *Anticancer Res.* 2001;21(1A):145-155.
 - Gini G. QSAR Methods. *Methods Mol Biol.* 2022;2425:1-26.

- Giraudo E, Inoue M, Hanahan D. An amino-bisphosphonate targets MMP-9-expressing macrophages and angiogenesis to impair cervical carcinogenesis. *J Clin Invest.* 2004;114(5):623-633.
- Golbraikh A, Tropsha A. Beware of q²! *J Mol Graph Model.* 2002;20(4):269-276.
- Gonzalez-Avila G, Sommer B, Mendoza-Posada DA, Ramos C, Garcia-Hernandez AA, Falfan-Valencia R. Matrix metalloproteinases participation in the metastatic process and their diagnostic and therapeutic applications in cancer. *Crit Rev Oncol Hematol.* 2019;137:57-83.
- Grant BJ, Rodrigues AP, ElSawy KM, McCammon JA, Caves LS. Bio3d: An R package for the comparative analysis of protein structures. *Bioinformatics.* 2006;22(21):2695-2696.
- Grønbech-Jensen N, Farago O. Constant pressure and temperature discrete-time Langevin molecular dynamics. *J Chem Phys.* 2014;141(19):194108.
- Groningen machine for chemical simulations. software available at <https://www.gromacs.org>.
- Gurung AB, Ali MA, Lee J, Farah MA, Al-Anazi KM. An updated review of computer-aided drug design and its application to COVID-19. *Biomed Res Int.* 2021;2021:8853056.
- Gutti S, Baidya SK, Banerjee S, Adhikari N, Jha T. A robust classification-dependent multi-molecular modelling study on some biphenyl sulphonamide based MMP-8 inhibitors. *SAR QSAR Environ Res.* 2021;32(10):835-861.
- Guttikonda V, Raavi D, Maadwar SK, Gade DR. Molecular insights of benzodipyrzole as CDK2 inhibitors: combined molecular docking, molecular dynamics, and 3D QSAR studies. *J Recept Signal Transduct Res.* 2015;35(5):439-449.
- Halder AK, Amin SA, Jha T, Gayen S. Insight into the structural requirements of pyrimidine-based phosphodiesterase 10A (PDE10A) inhibitors by multiple validated 3D QSAR approaches. *SAR QSAR Environ Res.* 2017;28(3):253-273.
- Halder AK, Mallick S, Shikha D, Saha A, Saha KD, Jha T. Design of dual MMP-2/HDAC-8 inhibitors by pharmacophore mapping, molecular docking, synthesis and biological activity. *RSC advances.* 2015;5(88):72373-72386.
- Halder AK, Saha A, Jha T. Exploring QSAR and pharmacophore mapping of structurally diverse selective matrix metalloproteinase-2 inhibitors. *J Pharm Pharmacol.* 2013;65(10):1541-1554.
- Han XJ, Ma XL, Yang L, Wei YQ, Peng Y, Wei XW. Progress in neoantigen targeted cancer immunotherapies. *Front Cell Dev Biol.* 2020;8:728.

- Hanahan D, Weinberg RA. Hallmarks of cancer: The next generation. *Cell*. 2011;144(5):646-674.
- Hanasono MM. Reconstructive Surgery for Head and Neck Cancer Patients. *Adv Med*. 2014;2014:795483.
- Hanessian S, Bouzbouz S, Boudon A, Tucker GC, Peyroulan D. Picking the S1, S1' and S2' pockets of matrix metalloproteinases. A niche for potent acyclic sulfonamide inhibitors. *Bioorg Med Chem Lett*. 1999;9(12):1691-1696.
- Hanessian S, MacKay DB, Moitessier N. Design and synthesis of matrix metalloproteinase inhibitors guided by molecular modeling. Picking the S(1) pocket using conformationally constrained inhibitors. *J Med Chem*. 2001c;44(19):3074-3082.
- Hanessian S, Moitessier N, Cantin LD. Design and synthesis of MMP inhibitors using N-arylsulfonylaziridine hydroxamic acids as constrained scaffolds. *Tetrahedron*. 2001a;57(32):6885-6900.
- Hanessian S, Moitessier N, Gauchet C, Viau M. N-Aryl sulfonyl homocysteine hydroxamate inhibitors of matrix metalloproteinases: further probing of the S(1), S(1)', and S(2)' pockets. *J Med Chem*. 2001b;44(19):3066-3073.
- Hangauer DG, Monzingo AF, Matthews BW. An interactive computer graphics study of thermolysin-catalyzed peptide cleavage and inhibition by N-carboxymethyl dipeptides. *Biochemistry*. 1984;23(24):5730-5741.
- Hansch C, Fujita T. ρ - σ - π Analysis. A Method for the Correlation of Biological Activity and Chemical Structure. *Journal of the American Chemical Society*. 1964;86(8):1616-1626.
- Hao JL, Nagano T, Nakamura M, Kumagai N, Mishima H, Nishida T. Effect of galardin on collagen degradation by *Pseudomonas aeruginosa*. *Exp Eye Res*. 1999;69(6):595-601.
- Hehlmann R. How I treat CML blast crisis. *Blood*. 2012;120(4):737-747.
- Herszényi L, Hritz I, Lakatos G, Varga MZ, Tulassay Z. The behavior of matrix metalloproteinases and their inhibitors in colorectal cancer. *Int J Mol Sci*. 2012;13(10):13240-13263.
- Hidalgo M, Eckhardt SG. Development of matrix metalloproteinase inhibitors in cancer therapy. *J Natl Cancer Inst*. 2001;93(3):178-193.
- Hildebrand PW, Rose AS, Tiemann JKS. Bringing molecular dynamics simulation data into view. *Trends Biochem Sci*. 2019;44(11):902-913.
- Hochhaus A, Baccarani M, Silver RT, Schiffer C, Apperley JF, Cervantes F, Clark RE, Cortes JE, Deininger MW, Guilhot F, Hjorth-Hansen H, Hughes TP, Janssen JJWM, Kantarjian HM, Kim DW, Larson RA, Lipton JH, Mahon FX, Mayer J, Nicolini F,

- Niederwieser D, Pane F, Radich JP, Rea D, Richter J, Rosti G, Rousselot P, Saglio G, Sauße S, Soverini S, Steegmann JL, Turkina A, Zaritskey A, Hehlmann R. European LeukemiaNet 2020 recommendations for treating chronic myeloid leukemia. *Leukemia*. 2020;34(4):966-984.
- Hollingsworth SA, Dror RO. Molecular dynamics simulation for all. *Neuron*. 2018;99(6):1129-1143.
 - Holms J, Mast K, Marcotte P, Elmore I, Li J, Pease L, Glaser K, Morgan D, Michaelides M, Davidsen S. Discovery of selective hydroxamic acid inhibitors of tumor necrosis factor- α converting enzyme. *Bioorg Med Chem Lett*. 2001;11(22):2907-2910.
 - Hope JM, Pothuri B. The role of palliative surgery in gynecologic cancer cases. *Oncol*. 2013;18(1):73-79.
 - Hsin CH, Chen MK, Tang CH, Lin HP, Chou MY, Lin CW, Yang SF. High level of plasma matrix metalloproteinase-11 is associated with clinicopathological characteristics in patients with oral squamous cell carcinoma. *PLoS One*. 2014;9(11):e113129.
 - <https://rb.gy/b6712p> as accessed on 15th July 2023.
 - <https://rb.gy/gmhja> as accessed on 30th July 2023.
 - <https://www.ebi.ac.uk/chembl> as accessed on 30th August 2023
 - <https://www.hematology.org/> as accessed on 30th July 2023.
 - <https://www.rcsb.org/> as accessed on 30th August 2023
 - <https://www.who.int/> as accessed on 30th July 2023.
 - Hu J, Van den Steen PE, Sang QX, Opdenakker G. Matrix metalloproteinase inhibitors as therapy for inflammatory and vascular diseases. *Nat Rev Drug Discov*. 2007;6(6):480-498.
 - Hu ZZ, Huang H, Wu CH, Jung M, Dritschilo A, Riegel AT, Wellstein A. Omics-based molecular target and biomarker identification. *Methods Mol Biol*. 2011;719:547-71.
 - Huang A, Joseph-McCarthy D, Lovering F, Sun L, Wang W, Xu W, Zhu Y, Cui J, Zhang Y, Levin JI. Structure-based design of TACE selective inhibitors: manipulations in the S1'-S3' pocket. *Bioorg Med Chem*. 2007;15(18):6170-6181.
 - Huang H. Matrix Metalloproteinase-9 (MMP-9) as a cancer biomarker and MMP-9 biosensors: recent advances. *Sensors (Basel)*. 2018;18(10):3249.
 - Huang L, Huang J, Huang J, Xue H, Liang Z, Wu J, Chen C. Nanomedicine - a promising therapy for hematological malignancies. *Biomater Sci*. 2020;8(9):2376-2393.
 - Huang SY, Zou X. Advances and challenges in protein-ligand docking. *Int J Mol Sci*. 2010;11(8):3016-34.

- Huang X, Qi L, Lu W, Yang G, Chen Y, Zhang R, Rao J, Ji D, Huang R, Chen G. miRNA-301a induces apoptosis of chronic myelogenous leukemia cells by directly targeting TIMP2/ERK1/2 and AKT pathways. *Oncol Rep.* 2017;37(2):945-952.
- Hugenberg V, Breyholz HJ, Riemann B, Hermann S, Schober O, Schäfers M, Gangadharmath U, Mocharla V, Kolb H, Walsh J, Zhang W, Kopka K, Wagner S. A new class of highly potent matrix metalloproteinase inhibitors based on triazole-substituted hydroxamates: (radio)synthesis and *in vitro* and first *in vivo* evaluation. *J Med Chem.* 2012;55(10):4714-4727.
- Ikura M, Nakatani S, Yamamoto S, Habashita H, Sugiura T, Takahashi K, Ogawa K, Ohno H, Nakai H, Toda M. Discovery of a new chemical lead for a matrix metalloproteinase inhibitor. *Bioorg Med Chem.* 2006;14(12):4241-4252.
- Ito A, Mukaiyama A, Itoh Y, Nagase H, Thøgersen IB, Enghild JJ, Sasaguri Y, Mori Y. Degradation of interleukin 1 β by matrix metalloproteinases. *Journal of Biological Chemistry.* 1996;271(25):14657-60.
- Jackson SP, Bartek J. The DNA-damage response in human biology and disease. *Nature.* 2009;461(7267):1071-1078.
- Jain RK. Vascular and interstitial barriers to delivery of therapeutic agents in tumors. *Cancer Meta Rev.* 1990;9:253-266.
- Janowska-Wieczorek A, Majka M, Marquez-Curtis L, Wertheim JA, Turner AR, Ratajczak MZ. Bcr-abl-positive cells secrete angiogenic factors including matrix metalloproteinases and stimulate angiogenesis *in vivo* in Matrigel implants. *Leukemia.* 2002;16(6):1160-1166.
- Jha T, Adhikari N, Saha A, Amin SA. Multiple molecular modelling studies on some derivatives and analogues of glutamic acid as matrix metalloproteinase-2 inhibitors. *SAR QSAR Environ Res.* 2018;29(1):43-68.
- Jha T, Basu S, Halder AK, Adhikari N, Samanta S. Possible anticancer agents: Synthesis, pharmacological activity, and molecular modeling studies on some 5-N-Substituted-2-N-(substituted benzenesulphonyl)-L (+) glutamines. *Med Chem Res.* 2017;26:1437-1458.
- Jha T, Debnath AK, Majumdar A, De AU. Possible antineoplastic agents XI: QSAR analogs of glutamines: synthesis and biological activity of 5-N-alkyl-2-(substituted benzenesulphonyl)-Lglutamines. *Ind J Chem.* 1987a;26B: 542-545.
- Jha T, Debnath AK, Majumdar A, De AU. Possible antineoplastic agents X: Synthesis, antineoplastic activity and QSAR study of 5-N-substituted-2-(chlorosubstituted benzenesulphonyl)-Lglutamines and 5-N-alkyl-2-(2',5'-dichlorobenzenesulphonyl)-L-glutamines. *Ind J Pharm Sci.* 1987b;49:133-136.

- Jha T, Debnath AK, Majumdar A, Sengupta C, De AU. Hansch analysis of antineoplastic 5-Nsubstituted-2-(substituted benzenesulphonyl)-L- glutamines. *Ind J Chem.* 1986;25B:169.
- Jha T, Debnath B, Samanta S, De AU. QSAR studies on some substituted glutamine analogs as possible anticancer agents. *Internet Electron J Mol Des.* 2003;2:539.
- Jha T. Rational design of glutamine analogs as possible anticancer agents, In: *Frontiers of Pharmaceutical Technology*, Gupta JK and Jha T. Eds., Jadavpur University, Kolkata, 1999;87-95.
- Jiao Y, Feng X, Zhan Y, Wang R, Zheng S, Liu W, Zeng X. Matrix metalloproteinase-2 promotes $\alpha\beta 3$ integrin-mediated adhesion and migration of human melanoma cells by cleaving fibronectin. *PLoS One.* 2012;7(7):e41591.
- Jin DY, Liu CL, Tang JN, Zhu ZZ, Xuan XX, Zhu XD, Wang YZ, Zhang TX, Shen DL, Wang XF, Shi GP, Zhang JY. Interleukin-18, matrix metalloproteinase-22 and -29 are independent risk factors of human coronary heart disease. *J Zhejiang Univ Sci B.* 2017;18(8):685-695.
- Kagami LP, das Neves GM, Timmers LFSM, Caceres RA, Eifler-Lima VL. Geo-Measures: A PyMOL plugin for protein structure ensembles analysis. *Comput Biol Chem.* 2020 Jun 24;87:107322.
- Kalluri R, Weinberg RA. The basics of epithelial-mesenchymal transition. *J Clin Invest.* 2009;119(6):1420-1428.
- Kalyaanamoorthy S, Chen YP. Structure-based drug design to augment hit discovery. *Drug Discov Today.* 2011;16(17-18):831-839.
- Kaneta Y, Kagami Y, Tsunoda T, Ohno R, Nakamura Y, Katagiri T. Genome-wide analysis of gene-expression profiles in chronic myeloid leukemia cells using a cDNA microarray. *Int J Oncol.* 2003;23(3):681-691.
- Kar S, Sanderson H, Roy K, Benfenati E, Leszczynski J. Ecotoxicological assessment of pharmaceuticals and personal care products using predictive toxicology approaches. *Green Chem.* 2020;22(5):1458-1516.
- Kari S, Subramanian K, Altomonte IA, Murugesan A, Yli-Harja O, Kandhavelu M. Programmed cell death detection methods: a systematic review and a categorical comparison. *Apoptosis.* 2022;27(7-8):482-508.
- Karplus M, McCammon JA. Molecular dynamics simulations of biomolecules. *Nat Struct Biol.* 2002;9(9):646-52.
- Kessenbrock K, Plaks V, Werb Z. Matrix metalloproteinases: regulators of the tumor microenvironment. *Cell.* 2010;141(1):52-67.

- Khan Asaduzzaman M, Tania M, Zhang DZ, Chen HC. Antioxidant enzymes and cancer. *Chin. J. Cancer Res.* 2010;22:87-92.
- Kitchen DB, Decornez H, Furr JR, Bajorath J. Docking and scoring in virtual screening for drug discovery: methods and applications. *Nat Rev Drug Discov.* 2004;3(11):935-949.
- Klekota J, Roth FP. Chemical substructures that enrich for biological activity. *Bioinformatics.* 2008;24(21):2518-2525.
- Klon AE, Lowrie JF, Diller DJ. Improved naïve Bayesian modeling of numerical data for absorption, distribution, metabolism and excretion (ADME) property prediction. *J Chem Inf Model.* 2006;46(5):1945-1956.
- Kolijn PM, Späth F, Khouja M, Hengeveld PJ, Van Der Straten L, Darzentas N, Hultdin M, McKay J, Pott C, Vermeulen RCH, Langerak AW. Genetic drivers in the natural history of chronic lymphocytic leukemia development as early as 16 years before diagnosis. *Blood.* 2023:blood.2023019609.
- Kolodziej SA, Hockerman SL, Boehm TL, Carroll JN, DeCrescenzo GA, McDonald JJ, Mischke DA, Munie GE, Fletcher TR, Rico JG, Stehle NW, Swearingen C, Becker DP. Orally bioavailable dual MMP-1/MMP-14 sparing, MMP-13 selective alpha-sulfone hydroxamates. *Bioorg Med Chem Lett.* 2010a;20(12):3557-3560.
- Kolodziej SA, Hockerman SL, DeCrescenzo GA, McDonald JJ, Mischke DA, Munie GE, Fletcher TR, Stehle N, Swearingen C, Becker DP. MMP-13 selective isonipecotamide alpha-sulfone hydroxamates. *Bioorg Med Chem Lett.* 2010b;20(12):3561-3564.
- Konttinen YT, Ainola M, Valleala H, Ma J, Ida H, Mandelin J, Kinne RW, Santavirta S, Sorsa T, López-Otín C, Takagi M. Analysis of 16 different matrix metalloproteinases (MMP-1 to MMP-20) in the synovial membrane: Different profiles in trauma and rheumatoid arthritis. *Ann Rheum Dis.* 1999;58(11):691-697.
- Krüger A, Kates RE, Edwards DR. Avoiding spam in the proteolytic internet: future strategies for anti-metastatic MMP inhibition. *Biochim Biophys Acta.* 2010;1803(1):95-102.
- Kubinyi H. Free Wilson analysis. Theory, applications and its relationship to Hansch analysis. *QSAR.* 1988;7(3):121-133.
- Kurzepa J, Mądro A, Czechowska G, Kurzepa J, Celiński K, Kazmierak W, Slomka M. Role of MMP-2 and MMP-9 and their natural inhibitors in liver fibrosis, chronic pancreatitis and non-specific inflammatory bowel diseases. *Hepatobiliary Pancreat Dis Int.* 2014;13(6):570-579.

- Kwon MJ. Matrix metalloproteinases as therapeutic targets in breast cancer. *Front Oncol.* 2023;12:1108695.
- Lange MM, Rutten HJ, Van de Velde CJ. One hundred years of curative surgery for rectal cancer: 1908–2008. *Eur J Surg Oncol (EJSO).* 2009;35(5):456-463.
- Lara PN Jr, Stadler WM, Longmate J, Quinn DI, Wexler J, Van Loan M, Twardowski P, Gumerlock PH, Vogelzang NJ, Vokes EE, Lenz HJ, Doroshow JH, Gandara DR. A randomized phase II trial of the matrix metalloproteinase inhibitor BMS-275291 in hormone-refractory prostate cancer patients with bone metastases. *Clin Cancer Res.* 2006;12(5):1556-1563.
- Ledoux D, Hamma-Kourbali Y, Di Benedetto M, Foucault-Bertaud A, Oudar O, Sainte-Catherine O, Lecouvey M, Kraemer M. A new dimethyl ester bisphosphonate inhibits angiogenesis and growth of human epidermoid carcinoma xenograft in nude mice. *Anticancer Drugs.* 2006;17(4):479-485.
- Leppä S, Saarto T, Vehmanen L, Blomqvist C, Elomaa I. Clodronate treatment influences MMP-2 associated outcome in node positive breast cancer. *Breast Cancer Res Treat.* 2005;90(2):117-125.
- Li H, Qiu Z, Li F, Wang C. The relationship between MMP-2 and MMP-9 expression levels with breast cancer incidence and prognosis. *Oncol Lett.* 2017;14(5):5865-5870.
- Li H. Detection distance calculation model of flying target and atmospheric influence analysis. *Optik.* 2017;129:248-255.
- Li S, Luo W. Matrix metalloproteinase 2 contributes to aggressive phenotype, epithelial-mesenchymal transition and poor outcome in nasopharyngeal carcinoma. *Onco Targets Ther.* 2019;12:5701-5711.
- Li W, Saji S, Sato F, Noda M, Toi M. Potential clinical applications of matrix metalloproteinase inhibitors and their future prospects. *Int J Biol Markers.* 2013;28(2):117-130.
- Li X, Wu JF. Recent developments in patent anti-cancer agents targeting the matrix metalloproteinases (MMPs). *Recent Pat Anticancer Drug Discov.* 2010;5(2):109-141.
- Li Y, He J, Wang F, Wang X, Yang F, Zhao C, Feng C, Li T. Role of MMP-9 in epithelial-mesenchymal transition of thyroid cancer. *World J Surg Oncol.* 2020;18(1):181.
- Li YL, Shi E, Burns D, Li Y, Covington MB, Pan M, Scherle P, Friedman S, Metcalf B, Yao W. Discovery of novel selective HER-2 sheddase inhibitors through optimization of P1 moiety. *Bioorg Med Chem Lett.* 2009;19(17):5037-5042.

- Lin A, Xu HH, Xu DP, Zhang X, Wang Q, Yan WH. Multiple steps of HLA-G in ovarian carcinoma metastasis: Alter NK cytotoxicity and induce matrix metalloproteinase-15 (MMP-15) expression. *Hum Immunol.* 2013;74(4):439-446.
- Lin LI, Lin DT, Chang CJ, Lee CY, Tang JL, Tien HF. Marrow matrix metalloproteinases (MMPs) and tissue inhibitors of MMP in acute leukaemia: Potential role of MMP-9 as a surrogate marker to monitor leukaemic status in patients with acute myelogenous leukaemia. *Br J Haematol.* 2002;117(4):835-841.
- Ling Y, Liu J, Qian J, Meng C, Guo J, Gao W, Xiong B, Ling C, Zhang Y. Recent advances in multi-target drugs targeting protein kinases and histone deacetylases in cancer therapy. *Curr Med Chem.* 2020;27(42):7264-7288.
- Liu FC, Pan CH, Lai MT, Chang SJ, Chung JG, Wu CH. Gan-Lu-Yin inhibits proliferation and migration of murine WEHI-3 leukemia cells and tumor growth in BALB/C allograft tumor model. *Evid Based Complement Alternat Med.* 2013;2013:684071.
- Liu SC, Yang SF, Yeh KT, Yeh CM, Chiou HL, Lee CY, Chou MC, Hsieh YS. Relationships between the level of matrix metalloproteinase-2 and tumor size of breast cancer. *Clin Chim Acta.* 2006;371(1-2):92-96.
- Liu WH, Chen YL, Chang LS. CIL-102 induces matrix metalloproteinase-2 (MMP-2)/MMP-9 down-regulation via simultaneous suppression of genetic transcription and mRNA stability. *Int J Biochem Cell Biol.* 2012;44(12):2212-2222.
- Liu X, Shi D, Zhou S, Liu H, Liu H, Yao X. Molecular dynamics simulations and novel drug discovery. *Expert Opin Drug Discov.* 2018;13(1):23-37.
- Liu Y, Shang L, Fang H, Zhu H, Mu J, Wang Q, Wang X, Yuan Y, Xu W. Design, synthesis, and preliminary studies of the activity of novel derivatives of N-cinnamoyl-L-aspartic acid as inhibitors of aminopeptidase N/CD13. *Bioorg Med Chem.* 2009;17(20):7398-7404.
- Lombart HG, Feyfant E, Joseph-McCarthy D, Huang A, Lovering F, Sun L, Zhu Y, Zeng C, Zhang Y, Levin J. Design and synthesis of 3,3-piperidine hydroxamate analogs as selective TACE inhibitors. *Bioorg Med Chem Lett.* 2007;17(15):4333-4337.
- Lovejoy B, Welch AR, Carr S, Luong C, Broka C, Hendricks RT, Campbell JA, Walker KA, Martin R, Van Wart H, Browner MF. Crystal structures of MMP-1 and -13 reveal the structural basis for selectivity of collagenase inhibitors. *Nat Struct Biol.* 1999;6(3):217-221.
- Lugano R, Ramachandran M, Dimberg A. Tumor angiogenesis: Causes, consequences, challenges and opportunities. *Cell Mol Life Sci.* 2020;77(9):1745-1770.

- Ma D, Wu W, Yang G, Li J, Li J, Ye Q. Tetrahydroisoquinoline based sulfonamide hydroxamates as potent matrix metalloproteinase inhibitors. *Bioorg Med Chem Lett*. 2004;14(1):47-50.
- Macaulay VM, O'Byrne KJ, Saunders MP, Braybrooke JP, Long L, Gleeson F, Mason CS, Harris AL, Brown P, Talbot DC. Phase I study of intrapleural batimastat (BB-94), a matrix metalloproteinase inhibitor, in the treatment of malignant pleural effusions. *Clin Cancer Res*. 1999;5(3):513-520.
- Makhoba XH, Viegas C Jr, Mosa RA, Viegas FPD, Poole OJ. Potential impact of the multi-target drug approach in the treatment of some complex diseases. *Drug Des Devel Ther*. 2020;14:3235-3249.
- Mandal S, Mandal SK. Rational drug design. *Eur J Pharmacol*. 2009;625(1-3):90-100.
- Marques SM, Nuti E, Rossello A, Supuran CT, Tuccinardi T, Martinelli A, Santos MA. Dual inhibitors of matrix metalloproteinases and carbonic anhydrases: iminodiacetyl-based hydroxamate-benzenesulfonamide conjugates. *J Med Chem*. 2008;51(24):7968-7979.
- Martin FM, Beckett RP, Bellamy CL, Courtney PF, Davies SJ, Drummond AH, Dodd R, Pratt LM, Patel SR, Ricketts ML, Todd RS, Tuffnell AR, Ward JW, Whittaker M. The synthesis and biological evaluation of non-peptidic matrix metalloproteinase inhibitors. *Bioorg Med Chem Lett*. 1999;9(19):2887-2892.
- Mattar R, Alves de Andrade CR, DiFavero GM, Gama-Rodrigues JJ, Laudanna AA. Preoperative serum levels of CA 72-4, CEA, CA 19-9, and alpha-fetoprotein in patients with gastric cancer. *Rev Hosp Clin Fac Med Sao Paulo*. 2002;57(3):89-92.
- Matthews BW. Comparison of the predicted and observed secondary structure of T4 phage lysozyme. *Biochim Biophys Acta*. 1975;405(2):442-451.
- Matthews BW. Structural basis of the action of thermolysin and related zinc peptidases. *Accounts of Chemical research*. 1988;21(9):333-340.
- Mayne ST. Antioxidant nutrients and chronic disease: use of biomarkers of exposure and oxidative stress status in epidemiologic research. *J Nutr*. 2003;133 Suppl 3:933S-940S.
- McCarten KM, Nadel HR, Shulkin BL, Cho SY. Imaging for diagnosis, staging and response assessment of Hodgkin lymphoma and non-Hodgkin lymphoma. *Pediatr Radiol*. 2019;49(11):1545-1564.
- Meenakshi Sundaram DN, Jiang X, Brandwein JM, Valencia-Serna J, Remant KC, Uludağ H. Current outlook on drug resistance in chronic myeloid leukemia (CML) and potential therapeutic options. *Drug Discov Today*. 2019;24(7):1355-1369.

- Minciacchi VR, Kumar R, Krause DS. Chronic myeloid leukemia: A model disease of the past, present and future. *Cells*. 2021;10(1):117.
- Mitra S, Lami MS, Ghosh A, Das R, Tallei TE, Fatimawali, Islam F, Dhama K, Begum MY, Aldahish A, Chidambaram K, Emran TB. Hormonal therapy for gynecological cancers: How far has science progressed toward clinical applications?. *Cancers (Basel)*. 2022;14(3):759.
- Molina R, Barak V, van Dalen A, Duffy MJ, Einarsson R, Gion M, Goike H, Lamerz R, Nap M, Sölétormos G, Stieber P. Tumor markers in breast cancer- European group on tumor markers recommendations. *Tumour Biol*. 2005;26(6):281-293.
- Molla MHR, Aljahdali MO, Sumon MAA, Asseri AH, Altayb HN, Islam MS, Alsaiani AA, Opo FADM, Jahan N, Ahammad F, Mohammad F. Integrative Ligand-Based Pharmacophore Modeling, Virtual Screening, and Molecular Docking Simulation Approaches Identified Potential Lead Compounds against Pancreatic Cancer by Targeting FAK1. *Pharmaceuticals (Basel)*. 2023;16(1):120.
- Mondal S, Adhikari N, Banerjee S, Amin SA, Jha T. Matrix metalloproteinase-9 (MMP-9) and its inhibitors in cancer: A minireview. *Eur J Med Chem*. 2020;194:112260.
- Moogk D, da Silva IP, Ma MW, Friedman EB, de Miera EV, Darvishian F, Scanlon P, Perez-Garcia A, Pavlick AC, Bhardwaj N, Christos PJ, Osman I, Krogsgaard M. Melanoma expression of matrix metalloproteinase-23 is associated with blunted tumor immunity and poor responses to immunotherapy. *J Transl Med*. 2014;12:342.
- Moroy G, Denhez C, El Mourabit H, Toribio A, Dassonville A, Decarme M, Renault JH, Mirand C, Bellon G, Sapi J, Alix AJ, Hornebeck W, Bourguet E. Simultaneous presence of unsaturation and long alkyl chain at P'1 of Ilomastat confers selectivity for gelatinase A (MMP-2) over gelatinase B (MMP-9) inhibition as shown by molecular modelling studies. *Bioorg Med Chem*. 2007;15(14):4753-4766.
- Mou J, Fang H, Jing F, Wang Q, Liu Y, Zhu H, Shang L, Wang X, Xu W. Design, synthesis and primary activity evaluation of L-arginine derivatives as amino-peptidase N/CD13 inhibitors. *Bioorg Med Chem*. 2009;17(13):4666-4673.
- Mukherjee A, Adhikari N, Jha T. A pentanoic acid derivative targeting matrix metalloproteinase-2 (MMP-2) induces apoptosis in a chronic myeloid leukemia cell line. *Eur J Med Chem*. 2017;141:37-50.
- Murcia-Soler M, Pérez-Giménez F, García-March FJ, Salabert-Salvador MT, Díaz-Villanueva W, Medina-Casamayor P. Discrimination and selection of new potential

- antibacterial compounds using simple topological descriptors. *J Mol Graph Model*. 2003;21(5):375-390.
- Murphy GJ, Murphy G, Reynolds JJ. The origin of matrix metalloproteinases and their familial relationships. *FEBS Lett*. 1991;289(1):4-7.
 - Murray DL, Puig N, Kristinsson S, Usmani SZ, Dispenzieri A, Bianchi G, Kumar S, Chng WJ, Hajek R, Paiva B, Waage A, Rajkumar SV, Durie B. Mass spectrometry for the evaluation of monoclonal proteins in multiple myeloma and related disorders: an International Myeloma Working Group Mass Spectrometry Committee Report. *Blood Cancer J*. 2021;11(2):24.
 - Nagase H, Woessner JF Jr. Matrix metalloproteinases. *J Biol Chem*. 1999;274(31):21491-21494.
 - Nagase H. Activation mechanisms of matrix metalloproteinases. *Biol Chem*. 1997;378(3-4):151-160.
 - Nakamura ES, Koizumi K, Yamaura T, Saiki I. Anti-tumor angiogenic effect of a matrix metalloproteinase inhibitor MMI270. *Anticancer Res*. 2003;23(1A):411-417.
 - Nakatani S, Ikura M, Yamamoto S, Nishita Y, Itadani S, Habashita H, Sugiura T, Ogawa K, Ohno H, Takahashi K, Nakai H, Toda M. Design and synthesis of novel metalloproteinase inhibitors. *Bioorg Med Chem*. 2006;14(15):5402-5422.
 - Nantasenamat C, Isarankura-Na-Ayudhya C, Naenna T, Prachayasittikul V. Prediction of bond dissociation enthalpy of antioxidant phenols by support vector machine. *J Mol Graph Model*. 2008;27(2):188-196.
 - Nantasenamat C, Prachayasittikul V. Maximizing computational tools for successful drug discovery. *Expert Opin Drug Discov*. 2015;10(4):321-329.
 - Nantasenamat C, Worachartcheewan A, Prachayasittikul S, Isarankura-Na-Ayudhya C, Prachayasittikul V. QSAR modeling of aromatase inhibitory activity of 1-substituted 1,2,3-triazole analogs of letrozole. *Eur J Med Chem*. 2013;69:99-114.
 - Nasulewicz-Goldeman A, Goldeman W, Mrówczyńska E, Wietrzyk J. Biological effects of aromatic bis[aminomethylidenebis(phosphonic)] acids in osteoclast precursors in vitro. *Chem Biol Drug Des*. 2019;94(4):1835-1848.
 - Natchus MG, Bookland RG, De B, Almstead NG, Pikul S, Janusz MJ, Heitmeyer SA, Hookfin EB, Hsieh LC, Dowty ME, Dietsch CR, Patel VS, Garver SM, Gu F, Pokross ME, Mielsing GE, Baker TR, Foltz DJ, Peng SX, Bornes DM, Strojnowski MJ, Taiwo YO. Development of new hydroxamate matrix metalloproteinase inhibitors derived from functionalized 4-aminoproline. *J Med Chem*. 2000;43(26):4948-4963.

- Nelson AR, Fingleton B, Rothenberg ML, Matrisian LM. Matrix metalloproteinases: Biologic activity and clinical implications. *J Clin Oncol.* 2000;18(5):1135-1149.
- Neves BJ, Braga RC, Melo-Filho CC, Moreira-Filho JT, Muratov EN, Andrade CH. QSAR-based virtual screening: Advances and applications in drug discovery. *Front Pharmacol.* 2018;9:1275.
- Nuti E, Cantelmo AR, Gallo C, Bruno A, Bassani B, Camodeca C, Tuccinardi T, Vera L, Orlandini E, Nencetti S, Stura EA, Martinelli A, Dive V, Albini A, Rossello A. N-O-Isopropyl sulfonamido-based hydroxamates as matrix metalloproteinase inhibitors: Hit selection and in vivo antiangiogenic activity. *J Med Chem.* 2015;58(18):7224-7240.
- Nuti E, Casalini F, Avramova SI, Santamaria S, Cercignani G, Marinelli L, La Pietra V, Novellino E, Orlandini E, Nencetti S, Tuccinardi T, Martinelli A, Lim NH, Visse R, Nagase H, Rossello A. N-O-isopropyl sulfonamido-based hydroxamates: design, synthesis and biological evaluation of selective matrix metalloproteinase-13 inhibitors as potential therapeutic agents for osteoarthritis. *J Med Chem.* 2009a;52(15):4757-4773.
- Nuti E, Casalini F, Avramova SI, Santamaria S, Fabbi M, Ferrini S, Marinelli L, La Pietra V, Limongelli V, Novellino E, Cercignani G, Orlandini E, Nencetti S, Rossello A. Potent arylsulfonamide inhibitors of tumor necrosis factor- α converting enzyme able to reduce activated leukocyte cell adhesion molecule shedding in cancer cell models. *J Med Chem.* 2010;53(6):2622-2635.
- Nuti E, Casalini F, Santamaria S, Fabbi M, Carbotti G, Ferrini S, Marinelli L, La Pietra V, Novellino E, Camodeca C, Orlandini E, Nencetti S, Rossello A. Selective arylsulfonamide inhibitors of ADAM-17: hit optimization and activity in ovarian cancer cell models. *J Med Chem.* 2013b;56(20):8089-8103.
- Nuti E, Casalini F, Santamaria S, Gabelloni P, Bendinelli S, Da Pozzo E, Costa B, Marinelli L, La Pietra V, Novellino E, Margarida Bernardo M, Fridman R, Da Settimo F, Martini C, Rossello A. Synthesis and biological evaluation in U87MG glioma cells of (ethynylthiophene)sulfonamido-based hydroxamates as matrix metalloproteinase inhibitors. *Eur J Med Chem.* 2011;46(7):2617-2629.
- Nuti E, Orlandini E, Nencetti S, Rossello A, Innocenti A, Scozzafava A, Supuran CT. Carbonic anhydrase and matrix metalloproteinase inhibitors. Inhibition of human tumor-associated isozymes IX and cytosolic isozyme I and II with sulfonylated hydroxamates. *Bioorg Med Chem.* 2007;15(6):2298-2311.
- Nuti E, Panelli L, Casalini F, Avramova SI, Orlandini E, Santamaria S, Nencetti S, Tuccinardi T, Martinelli A, Cercignani G, D'Amelio N, Maiocchi A, Uggeri F, Rossello A.

- Design, synthesis, biological evaluation, and NMR studies of a new series of arylsulfones as selective and potent matrix metalloproteinase-12 inhibitors. *J Med Chem.* 2009b;52(20):6347-6361.
- Nuti E, Santamaria S, Casalini F, Yamamoto K, Marinelli L, La Pietra V, Novellino E, Orlandini E, Nencetti S, Marini AM, Salerno S, Taliani S, Da Settimo F, Nagase H, Rossello A. Arylsulfonamide inhibitors of aggrecanases as potential therapeutic agents for osteoarthritis: synthesis and biological evaluation. *Eur J Med Chem.* 2013a;62:379-394.
 - Nuti R. Updates on mechanism of action and clinical efficacy of risedronate in osteoporosis. *Clin Cases Miner Bone Metab.* 2014;11(3):208-214.
 - O'Carrigan B, Wong MH, Willson ML, Stockler MR, Pavlakis N, Goodwin A. Bisphosphonates and other bone agents for breast cancer. *Cochrane Database Syst Rev.* 2017;10(10):CD003474.
 - Ogawa M, Kawamoto M, Yamanaka N. Matrix metalloproteinase and tissue inhibitor of metalloproteinase in human bone marrow tissues-an immunohistochemical study. *J Nippon Med Sch.* 2000;67(4):235-241.
 - Ohishi T, Matsuyama Y. Minodronate for the treatment of osteoporosis. *Ther Clin Risk Manag.* 2018;14:729-739.
 - Ohue M, Matsuzaki Y, Shimoda T, Ishida T, Akiyama Y. Highly precise protein-protein interaction prediction based on consensus between template-based and de novo docking methods. *BMC Proc.* 2013;7(Suppl 7):S6.
 - Ohue M, Matsuzaki Y, Uchikoga N, Ishida T, Akiyama Y. MEGADOCK: An all-to-all protein-protein interaction prediction system using tertiary structure data. *Protein Pept Lett.* 2014;21(8):766-778.
 - Ojha PK, Roy K. Comparative QSARs for antimalarial endochins: importance of descriptor-thinning and noise reduction prior to feature selection. *Chemometrics and Intelligent Laboratory Systems.* 2011;109(2):146-161.
 - Openbabel's SMARTS_InteLigand.txt
 - Overall CM, Kleifeld O. Tumour microenvironment-opinion: validating matrix metalloproteinases as drug targets and anti-targets for cancer therapy. *Nat Rev Cancer.* 2006;6(3):227-239.
 - Overall CM, López-Otín C. Strategies for MMP inhibition in cancer: Innovations for the post-trial era. *Nat Rev Cancer.* 2002;2(9):657-672.

- Oviedo-Orta E, Bermudez-Fajardo A, Karanam S, Benbow U, Newby AC. Comparison of MMP-2 and MMP-9 secretion from T helper 0, 1 and 2 lymphocytes alone and in coculture with macrophages. *Immunology*. 2008;124(1):42-50.
- Page-McCaw A, Ewald AJ, Werb Z. Matrix metalloproteinases and the regulation of tissue remodelling. *Nat Rev Mol Cell Biol*. 2007;8(3):221-233.
- Pajaniradje S, Mohankumar K, Pamidimukkala R, Subramanian S, Rajagopalan R. Antiproliferative and apoptotic effects of *Sesbania grandiflora* leaves in human cancer cells. *Biomed Res Int*. 2014;2014:474953.
- Panda P, Samanta S, Alam SM, Basu S, Jha T. QSAR for Analogs of 1,5 N, N-disubstituted-2-(substituted benzenesulphonyl) glutamamides as possible antitumor agents. *Internet Electron J Mol Des*. 2006;6:280-301.
- Papaleo E, Mereghetti P, Fantucci P, Grandori R, De Gioia L. Free-energy landscape, principal component analysis, and structural clustering to identify representative conformations from molecular dynamics simulations: the myoglobin case. *J Mol Graph Model*. 2009;27(8):889-899.
- Papież MA, Krzyściak W. Biological therapies in the treatment of cancer-update and new directions. *Int J Mol Sci*. 2021;22(21):11694.
- Park K, Aplasca A, Du MT, Sun L, Zhu Y, Zhang Y, Levin JI. Design and synthesis of butynyloxyphenyl beta-sulfone piperidine hydroxamates as TACE inhibitors. *Bioorg Med Chem Lett*. 2006;16(15):3927-3931.
- Parrill AL, Reddy MR, Eds. *Rational drug design: Novel methodology and practical applications*. Am Chem Soc. 1999.
- Parvathy SS, Masocha W. Matrix metalloproteinase inhibitor COL-3 prevents the development of paclitaxel-induced hyperalgesia in mice. *Med Princ Pract*. 2013;22(1):35-41.
- Paupert J, Mansat-De Mas V, Demur C, Salles B, Muller C. Cell-surface MMP-9 regulates the invasive capacity of leukemia blast cells with monocytic features. *Cell Cycle*. 2008;7(8):1047-1053.
- Pavlidis N, Briasoulis E, Hainsworth J, Greco FA. Diagnostic and therapeutic management of cancer of an unknown primary. *Eur J Cancer*. 2003;39(14):1990-2005.
- Pérez-Garrido A, Helguera AM, Borges F, Cordeiro MN, Rivero V, Escudero AG. Two new parameters based on distances in a receiver operating characteristic chart for the selection of classification models. *J Chem Inf Model*. 2011 Oct 24;51(10):2746-2759.

- Périgny M, Bairati I, Harvey I, Beauchemin M, Harel F, Plante M, Têtu B. Role of immunohistochemical overexpression of matrix metalloproteinases MMP-2 and MMP-11 in the prognosis of death by ovarian cancer. *Am J Clin Pathol*. 2008;129(2):226-231.
- Peterson JT. Matrix metalloproteinase inhibitor development and the remodeling of drug discovery. *Heart Fail Rev*. 2004;9(1):63-79.
- Pikul S, Dunham KM, Almstead NG, De B, Natchus MG, Taiwo YO, Williams LE, Hynd BA, Hsieh LC, Janusz MJ, Gu F, Mieling GE. Heterocycle-based MMP inhibitors with P2' substituents. *Bioorg Med Chem Lett*. 2001;11(8):1009-1013.
- Protein data Bank, <https://www.rcsb.org/> as accessed in May 2023.
- PyMOL. Software available at <https://github.com/schrodinger/pymol-open-source>.
- QSAR tools. DTC laboratory, India, 2020; software available at <https://dtclab.webs.com/software-tools>.
- Quintero-Fabián S, Arreola R, Becerril-Villanueva E, Torres-Romero JC, Arana-Argáez V, Lara-Riegos J, Ramírez-Camacho MA, Alvarez-Sánchez ME. Role of matrix metalloproteinases in angiogenesis and cancer. *Front Oncol*. 2019;9:1370.
- Radivoyevitch T, Weaver D, Hobbs B, Maciejewski JP, Hehlmann R, Jiang Q, Hochhaus A, Gale RP. Do persons with chronic myeloid leukaemia have normal or near normal survival?. *Leukemia*. 2020;34(2):333-335.
- Radosinska J, Barancik M, Vrbjar N. Heart failure and role of circulating MMP-2 and MMP-9. *Panminerva Medica*. 2017;59(3):241-253.
- Rao BG. Recent developments in the design of specific Matrix Metalloproteinase inhibitors aided by structural and computational studies. *Curr Pharm Des*. 2005;11(3):295-322.
- Rath T, Roderfeld M, Graf J, Wagner S, Vehr AK, Dietrich C, Geier A, Roeb E. Enhanced expression of MMP-7 and MMP-13 in inflammatory bowel disease: A precancerous potential?. *Inflamm Bowel Dis*. 2006;12(11):1025-1035.
- Ries C, Loher F, Zang C, Ismail MG, Petrides PE. Matrix metalloproteinase production by bone marrow mononuclear cells from normal individuals and patients with acute and chronic myeloid leukemia or myelodysplastic syndromes. *Clin Cancer Res*. 1999;5(5):1115-1124.
- Rizzo RC, Toba S, Kuntz ID. A molecular basis for the selectivity of thiadiazole urea inhibitors with stromelysin-1 and gelatinase-A from generalized born molecular dynamics simulations. *J Med Chem*. 2004;47(12):3065-3074.
- Rodan GA, Fleisch HA. Bisphosphonates: Mechanisms of action. *J Clin Invest*. 1996;97(12):2692-2696.

- Rodriguez JA, Orbe J, Martinez de Lizarrondo S, Calvayrac O, Rodriguez C, Martinez-Gonzalez J, Paramo JA. Metalloproteinases and atherothrombosis: MMP-10 mediates vascular remodeling promoted by inflammatory stimuli. *Front Biosci.* 2008;13:2916-2921.
- Romero AM, Mastromatteo-Alberga P, Escalona L, Correnti M. Niveles de MMP-3 y MMP-8 en pacientes con periodontitis crónica antes y después del tratamiento periodontal no quirúrgico [MMP-3 and MMP-8 levels in patients with chronic periodontitis before and after nonsurgical periodontal therapy]. *Invest Clin.* 2013;54(2):138-148.
- Rossello A, Nuti E, Carelli P, Orlandini E, Macchia M, Nencetti S, Zandomeneghi M, Balzano F, Uccello Barretta G, Albini A, Benelli R, Cercignani G, Murphy G, Balsamo A. N-i-Propoxy-N-biphenylsulfonylaminobutylhydroxamic acids as potent and selective inhibitors of MMP-2 and MT1-MMP. *Bioorg Med Chem Lett.* 2005a;15(5):1321-1326.
- Rossello A, Nuti E, Catalani MP, Carelli P, Orlandini E, Rapposelli S, Tuccinardi T, Atkinson SJ, Murphy G, Balsamo A. A new development of matrix metalloproteinase inhibitors: twin hydroxamic acids as potent inhibitors of MMPs. *Bioorg Med Chem Lett.* 2005b;15(9):2311-2314.
- Rossello A, Nuti E, Orlandini E, Carelli P, Rapposelli S, Macchia M, Minutolo F, Carbonaro L, Albini A, Benelli R, Cercignani G, Murphy G, Balsamo A. New N-arylsulfonyl-N-alkoxyaminoacetohydroxamic acids as selective inhibitors of gelatinase A (MMP-2). *Bioorg Med Chem.* 2004;12(9):2441-2450.
- Roy K, Das RN. A review on principles, theory and practices of 2D-QSAR. *Curr Drug Metab.* 2014;15(4):346-379.
- Roy K, Mitra I, Kar S, Ojha PK, Das RN, Kabir H. Comparative studies on some metrics for external validation of QSPR models. *J Chem Inf Model.* 2012;52(2):396-408.
- Roy PP, Paul S, Mitra I, Roy K. On two novel parameters for validation of predictive QSAR models. *Molecules.* 2009;14(5):1660-1701.
- R-Studio. Software available at <https://github.com/rstudio/rstudio>.
- Rundhaug JE. Matrix metalloproteinases, angiogenesis, and cancer: Commentary in: AC Lockhart et al., Reduction of wound angiogenesis in patients treated with BMS-275291, a broad spectrum matrix metalloproteinase inhibitor. *Clin Cancer Res.* 2003;9(2):551-554.
- Saikia T. The cure of chronic myeloid leukemia: Are we there yet?. *Curr Oncol Rep.* 2018;20(2):12.
- Samanta S, Alam SM, Basu S, Maji T, Roy DK, Jha T. Chemoimmunotherapeutic approach to prolonged survival time in combination with immunization and glutamic acid derivatives with antitumor activity in tumor-bearing mice. *Biol Pharm Bull.* 2007;30:2334-2339.

- Samanta S, Alam SM, Panda P, Jha T. Possible anticancer agents: QSAR analogs of glutamamide: synthesis and pharmacological activity of 1, 5-N, N'-disubstituted-2-(substituted benzenesulphonyl) glutamamides. *Eur J Med Chem.* 2009;44:70-82.
- Samanta S, Srikanth K, Banerjee S, Debnath B, Gayen S, Jha T; 5-N-substituted-2-(substituted benzenesulphonyl) glutamines as antitumor agents ii: synthesis, biological activity and QSAR study. *Bioorg Med Chem.* 2004;12:1413-1423.
- Samartzis EP, Fink D, Stucki M, Imesch P. Doxycycline reduces MMP-2 activity and inhibits invasion of 12Z epithelial endometriotic cells as well as MMP-2 and -9 activity in primary endometriotic stromal cells in vitro. *Reprod Biol Endocrinol.* 2019;17(1):38.
- Sanyal S, Amin SA, Adhikari N, Jha T. QSAR modelling on a series of arylsulfonamide-based hydroxamates as potent MMP-2 inhibitors. *SAR QSAR Environ Res.* 2019;30(4):247-263.
- Scheuer L, Kauff N, Robson M, Kelly B, Barakat R, Satagopan J, Ellis N, Hensley M, Boyd J, Borgen P, Norton L. Outcome of preventive surgery and screening for breast and ovarian cancer in BRCA mutation carriers. *J. Clin. Oncol.* 2002;20(5):1260-1268.
- Schiffman JD, Fisher PG, Gibbs P. Early detection of cancer: Past, present, and future. *Am Soc Clin Oncol Educ Book.* 2015;35(1):57-65.
- Schrodinger Suite. Schrodinger LLC, New York, USA, 2019; software available at <https://www.schrodinger.com>.
- Scior T, Bender A, Tresadern G, Medina-Franco JL, Martínez-Mayorga K, Langer T, Cuanalo-Contreras K, Agrafiotis DK. Recognizing pitfalls in virtual screening: A critical review. *J Chem Inf Model.* 2012;52(4):867-881.
- Serra P, Bruczko M, Zapico JM, Puckowska A, Garcia MA, Martin-Santamaria S, Ramos A, de Pascual-Teresa B. MMP-2 selectivity in hydroxamate-type inhibitors. *Curr Med Chem.* 2012;19(7):1036-1064.
- Shalinsky DR, Brekken J, Zou H, Bloom LA, McDermott CD, Zook S, Varki NM, Appelt K. Marked antiangiogenic and antitumor efficacy of AG3340 in chemoresistant human non-small cell lung cancer tumors: single agent and combination chemotherapy studies. *Clin Cancer Res.* 1999c;5(7):1905-1917.
- Shalinsky DR, Brekken J, Zou H, Kolis S, Wood A, Webber S, Appelt K. Antitumor efficacy of AG3340 associated with maintenance of minimum effective plasma concentrations and not total daily dose, exposure or peak plasma concentrations. *Invest New Drugs.* 1998-1999b;16(4):303-313.

- Shalinsky DR, Brekken J, Zou H, McDermott CD, Forsyth P, Edwards D, Margosiak S, Bender S, Truitt G, Wood A, Varki NM, Appelt K. Broad antitumor and antiangiogenic activities of AG3340, a potent and selective MMP inhibitor undergoing advanced oncology clinical trials. *Ann N Y Acad Sci.* 1999a;878:236-270.
- Sharma S, Bhatia V. Recent trends in QSAR in modelling of drug-protein and protein-protein interactions. *Comb Chem High Throughput Screen.* 2021;24(7):1031-1041.
- Shepherd FA, Giaccone G, Seymour L, Debruyne C, Bezjak A, Hirsh V, Smylie M, Rubin S, Martins H, Lamont A, Krzakowski M, Sadura A, Zee B. Prospective, randomized, double-blind, placebo-controlled trial of marimastat after response to first-line chemotherapy in patients with small-cell lung cancer: A trial of the National Cancer Institute of Canada-Clinical Trials Group and the European Organization for Research and Treatment of Cancer. *J Clin Oncol.* 2002;20(22):4434-4439.
- Sheppard GS, Florjancic AS, Giesler JR, Xu L, Guo Y, Davidsen SK, Marcotte PA, Elmore I, Albert DH, Magoc TJ, Bouska JJ, Goodfellow CL, Morgan DW, Summers JB. Aryl ketones as novel replacements for the C-terminal amide bond of succinyl hydroxamate MMP inhibitors. *Bioorg Med Chem Lett.* 1998;8(22):3251-3256.
- Shih CL, Ajuwon KM. Inhibition of MMP-13 prevents diet-induced obesity in mice and suppresses adipogenesis in 3T3-L1 preadipocytes. *Mol Biol Rep.* 2015;42(7):1225-1232.
- Shin WH, Christoffer CW, Kihara D. In silico structure-based approaches to discover protein-protein interaction-targeting drugs. *Methods.* 2017;131:22-32.
- Shipley JL, Butera JN. Acute myelogenous leukemia. *Experimental hematology.* 2009;37(6):649-658.
- Siegel RL, Miller KD, Wagle NS, Jemal A. Cancer statistics, 2023. *CA Cancer J Clin.* 2023;73(1):17-48.
- Siloși I, Boldeanu MV, Mogoantă SȘ, Ghiluși M, Cojocaru M, Biciușcă V, Cojocaru IM, Avrănescu CS, Gheonea DI, Siloși CA, Turculeanu A. Matrix metalloproteinases (MMP-3 and MMP-9) implication in the pathogenesis of inflammatory bowel disease (IBD). *Rom J Morphol Embryol.* 2014;55(4):1317-1324.
- Sjøli S, Nuti E, Camodeca C, Bilotto I, Rossello A, Winberg JO, Sylte I, Adekoya OA. Synthesis, experimental evaluation and molecular modelling of hydroxamate derivatives as zinc metalloproteinase inhibitors. *Eur J Med Chem.* 2016;108:141-153.
- Skiles JW, Gonnella NC, Jeng AY. The design, structure, and clinical update of small molecular weight matrix metalloproteinase inhibitors. *Curr Med Chem.* 2004;11(22):2911-2977.

- Skiles JW, Gonnella NC, Jeng AY. The design, structure, and therapeutic application of matrix metalloproteinase inhibitors. *Curr Med Chem*. 2001;8(4):425-474.
- Skubitz KM, D'Adamo DR. Sarcoma. *Mayo Clin Proc*. 2007;82(11):1409-1432.
- Sledge GW Jr, Qulali M, Goulet R, Bone EA, Fife R. Effect of matrix metalloproteinase inhibitor batimastat on breast cancer regrowth and metastasis in athymic mice. *J Natl Cancer Inst*. 1995;87(20):1546-1550.
- Solovyeva NI, Timoshenko OS, Gureeva TA, Kugaevskaya EV. Matrix metalloproteinases and their endogenous regulators in squamous cervical carcinoma. *Biomed Khim*. 2015;61(6):694-704.
- Somani RR, Bhanushali UV. Targeting angiogenesis for treatment of human cancer. *Indian J Pharm Sci*. 2013;75(1):3-10.
- Song JH, Kim SH, Cho D, Lee IK, Kim HJ, Kim TS. Enhanced invasiveness of drug-resistant acute myeloid leukemia cells through increased expression of matrix metalloproteinase-2. *Int J Cancer*. 2009;125(5):1074-1081.
- Srikanth K, Debnath B, Jha T. Synthesis, biological evaluation and QSAR study on antitumor activity of 1,5-N, N'-distubuted-2-(substituted benzenesulphonyl) glutamamides. *Bioorg Med Chem*. 2002a;10:1841-1854.
- Srikanth K, Kumar CA, Ghosh B, Jha, T. Synthesis, screening and quantitative structure activity relationship (QSAR) study on some glutamine analogues for possible anticancer activity. *Bioorg Med Chem*. 2002b;10:2119-2131.
- Srikanth K, Kumar CA, Goswami D, De AU, Jha T. Quantitative structure activity relationship (QSAR) studies of some substituted benzenesulphonyl glutamines as tumor suppressors. *Ind J Biochem Biophys* 2001;38:120-123.
- STATISTICA Version 7. Statistical Software of StatSoft, Inc., Tulsa, USA; software available at <http://www.statsoft.com>.
- Steinman DH, Curtin ML, Garland RB, Davidsen SK, Heyman HR, Holms JH, Albert DH, Magoc TJ, Nagy IB, Marcotte PA, Li J, Morgan DW, Hutchins C, Summers JB. The design, synthesis, and structure-activity relationships of a series of macrocyclic MMP inhibitors. *Bioorg Med Chem Lett*. 1998;8(16):2087-2092.
- Sternlicht MD, Werb Z. How matrix metalloproteinases regulate cell behavior. *Annu Rev Cell Dev Biol*. 2001;17:463-516.
- Sturgeon CM, Duffy MJ, Stenman UH, Lilja H, Br  nner N, Chan DW, Babaian R, Bast RC Jr, Dowell B, Esteva FJ, Haglund C, Harbeck N, Hayes DF, Holten-Andersen M, Klee GG, Lamerz R, Looijenga LH, Molina R, Nielsen HJ, Rittenhouse H, Semjonow A, Shih IeM,

- Sibley P, Sölétormos G, Stephan C, Sokoll L, Hoffman BR, Diamandis EP; National Academy of Clinical Biochemistry laboratory medicine practice guidelines for use of tumor markers in testicular, prostate, colorectal, breast, and ovarian cancers. *Clin Chem*. 2008;54(12):e11-79.
- Sugimoto W, Itoh K, Hirata H, Abe Y, Torii T, Mitsui Y, Budirahardja Y, Tanaka N, Kawauchi K. MMP24 as a target of YAP is a potential prognostic factor in cancer patients. *Bioengineering (Basel)*. 2020;7(1):18.
 - Sulaiman A, Kaur S, Gupta S, Alshahrani H, Reshan MSA, Alyami S, Shaikh A. ResRandSVM: Hybrid approach for acute lymphocytic leukemia classification in blood smear images. *Diagnostics (Basel)*. 2023;13(12):2121.
 - Sung H, Ferlay J, Siegel RL, Laversanne M, Soerjomataram I, Jemal A, Bray F. Global cancer statistics 2020: GLOBOCAN estimates of incidence and mortality worldwide for 36 cancers in 185 countries. *CA Cancer J Clin*. 2021;71(3):209-249.
 - Sussman JL, Silman I. Computational studies on cholinesterases: Strengthening our understanding of the integration of structure, dynamics and function. *Neuropharmacol*. 2020;179:108265.
 - SYBYL-X 2.0 software. Tripos Inc, St. Louis. MO, USA, 2012; software available at <http://www.certara.com>.
 - Takahashi K, Ikura M, Habashita H, Nishizaki M, Sugiura T, Yamamoto S, Nakatani S, Ogawa K, Ohno H, Nakai H, Toda M. Novel matrix metalloproteinase inhibitors: generation of lead compounds by the in silico fragment-based approach. *Bioorg Med Chem*. 2005 Jul 15;13(14):4527-4543.
 - Talati C, Pinilla-Ibarz J. Resistance in chronic myeloid leukemia: Definitions and novel therapeutic agents. *Curr Opin Hematol*. 2018;25(2):154-161.
 - Tautermann CS. Current and future challenges in modern drug discovery. *Methods Mol Biol*. 2020;2114:1-17.
 - Terpos E, Cibeira MT, Blade J, Ludwig H. Management of complications in multiple myeloma. *Semin Hematol*. 2009;46(2):176-189.
 - Thomas AL, Steward WP. Marimastat: The clinical development of a matrix metalloproteinase inhibitor. *Expert Opin Investig Drugs*. 2000;9(12):2913-2922.
 - Todeschini R, Consonni V. Molecular descriptors for chemoinformatics. In: Mannhold R, Kubinyi H, Folkers G, Eds., *Methods and Principles in Medicinal Chemistry*, Wiley-VCH. Weinheim, Germany, 2009.

- Tommasi RA, Weiler S, McQuire LW, Rogel O, Chambers M, Clark K, Doughty J, Fang J, Ganu V, Grob J, Goldberg R, Goldstein R, Lavoie S, Kulathila R, Macchia W, Melton R, Springer C, Walker M, Zhang J, Zhu L, Shultz M. Potent and selective 2-naphthylsulfonamide substituted hydroxamic acid inhibitors of matrix metalloproteinase-13. *Bioorg Med Chem Lett*. 2011;21(21):6440-6445.
- Topai A, Breccia P, Minissi F, Padova A, Marini S, Cerbara I. In silico scaffold evaluation and solid phase approach to identify new gelatinase inhibitors. *Bioorg Med Chem*. 2012;20(7):2323-2337.
- Torre LA, Siegel RL, Ward EM, Jemal A. Global cancer incidence and mortality rates and trends--an update. *Cancer Epidemiol. Biomarkers Prev*. 2016;25(1):16-27.
- Tosco P, Balle T. Open3DQSAR: A new open-source software aimed at high-throughput chemometric analysis of molecular interaction fields. *J Mol Model*. 2011;17(1):201-208.
- Trapé J, Filella X, Alsina-Donadeu M, Juan-Pereira L, Bosch-Ferrer Á, Rigo-Bonnin R; Oncology section of the catalan association of clinical laboratory science. increased plasma concentrations of tumour markers in the absence of neoplasia. *Clin Chem Lab Med*. 2011;49(10):1605-1620.
- Trapé J, Montesinos J, Catot S, Buxó J, Franquesa J, Sala M, Domenech M, Sant F, Badal JM, Arnau A. A prognostic score based on clinical factors and biomarkers for advanced non-small cell lung cancer. *Int J Biol Markers*. 2012;27(3):e257-e262.
- Trapé J, Sala M, Franquesa F, Ordeig JM, Soler-Bel JM, Bustamante E, Pérez R, Aligué J, Montesinos J, Arnau A, Ordeig-Villanueva R. Clinical utility of determining tumor markers in patients with signs and symptoms of cancer. *Clin Chem Lab Med*. 2015;53(3):485-491.
- Tripathi A, Bankaitis VA. Molecular Docking: From Lock and Key to Combination Lock. *J Mol Med Clin Appl*. 2017;2(1):10.16966/2575-0305.106.
- Tsimberidou AM. Targeted therapy in cancer. *Cancer Chemother Pharmacol*. 2015;76:1113-1132.
- Ugarte-Berzal E, Redondo-Muñoz J, Eroles P, Del Cerro MH, García-Marco JA, Terol MJ, García-Pardo A. VEGF/VEGFR2 interaction down-regulates matrix metalloproteinase-9 via STAT1 activation and inhibits B chronic lymphocytic leukemia cell migration. *Blood*. 2010;115(4):846-849.
- Ullah F, Dima D, Omar N, Ogbue O, Ahmed S. Advances in the treatment of Hodgkin lymphoma: Current and future approaches. *Front Oncol*. 2023;13:1067289.
- Vakser IA. Protein-protein docking: From interaction to interactome. *Biophys J*. 2014;107(8):1785-1793.

- Valko M, Leibfritz D, Moncol J, Cronin MT, Mazur M, Telser J. Free radicals and antioxidants in normal physiological functions and human disease. *Int J Biochem Cell Biol.* 2007;39(1):44-84.
- Van Wart HE, Birkedal-Hansen H. The cysteine switch: A principle of regulation of metalloproteinase activity with potential applicability to the entire matrix metalloproteinase gene family. *Proc Natl Acad Sci U S A.* 1990;87(14):5578-5582.
- Vandenbroucke RE, Dejonckheere E, Libert C. A therapeutic role for matrix metalloproteinase inhibitors in lung diseases?. *Eur Resp J.* 2011;38(5):1200-1214.
- Veena VK, Kennedy K, Lakshmi P, Krishna R, Sakthivel N. Anti-leukemic, anti-lung, and anti-breast cancer potential of the microbial polyketide 2, 4-diacetylphloroglucinol (DAPG) and its interaction with the metastatic proteins than the antiapoptotic Bcl-2 proteins. *Mol Cell Biochem.* 2016;414(1-2):47-56.
- Verma RP. Hydroxamic acids as matrix metalloproteinase inhibitors. *Exp Suppl.* 2012;103:137-176.
- Visse R, Nagase H. Matrix metalloproteinases and tissue inhibitors of metalloproteinases: structure, function, and biochemistry. *Circ Res.* 2003;92(8):827-839.
- Wagner S, Breyholz HJ, Law MP, Faust A, Höltke C, Schröer S, Haufe G, Levkau B, Schober O, Schäfers M, Kopka K. Novel fluorinated derivatives of the broad-spectrum MMP inhibitors N-hydroxy-2(R)-[[[(4-methoxyphenyl)sulfonyl](benzyl)- and (3-picolyl)-amino]-3-methyl-butanamide as potential tools for the molecular imaging of activated MMPs with PET. *J Med Chem.* 2007 Nov 15;50(23):5752-5764.
- Wang C, Xiang R, Zhang X, Chen Y. Doxycycline inhibits leukemic cell migration via inhibition of matrix metalloproteinases and phosphorylation of focal adhesion kinase. *Mol Med Rep.* 2015;12(3):3374-3380.
- Wang CM, Wu ZQ, Wang Y, Guo YL, Dai HR, Wang XH, Li X, Zhang YJ, Zhang WY, Chen MX, Zhang Y, Feng KC, Liu Y, Li SX, Yang QM, Han WD. Autologous T cells expressing CD30 chimeric antigen receptors for relapsed or refractory Hodgkin lymphoma: An open-label phase I trial. *Clin Cancer Res.* 2017;23(5):1156-1166.
- Wang Q, Chen M, Zhu H, Zhang J, Fang H, Wang B, Xu W. Design, synthesis, and QSAR studies of novel lysine derives as amino-peptidase N/CD13 inhibitors. *Bioorg Med Chem.* 2008 May 15;16(10):5473-5481.
- Wang X, Fu X, Brown PD, Crimmin MJ, Hoffman RM. Matrix metalloproteinase inhibitor BB-94 (batimastat) inhibits human colon tumor growth and spread in a patient-like orthotopic model in nude mice. *Cancer Res.* 1994;54(17):4726-4728.

- Wang Z, Xie Q, Zhou H, Zhang M, Shen J, Ju D. Amino acid degrading enzymes and autophagy in cancer therapy. *Front Pharmacol.* 2021;11:582587.
- Wei GW, Soares TA, Wahab H, Zhu F. Computational chemistry in Asia. *J Chem Inf Model.* 2022 Nov 14;62(21):5035-5037.
- Westermarck J, Kähäri VM. Regulation of matrix metalloproteinase expression in tumor invasion. *FASEB J.* 1999;13(8):781-792.
- Whitlock GA, Dack KN, Dickinson RP, Lewis ML. A novel series of highly selective inhibitors of MMP-3. *Bioorg Med Chem Lett.* 2007;17(24):6750-6753.
- Whittaker M, Floyd CD, Brown P, Gearing AJ. Design and therapeutic application of matrix metalloproteinase inhibitors. *Chem Rev.* 1999;99(9):2735-2776.
- Wickman GR, Julian L, Mardilovich K, Schumacher S, Munro J, Rath N, Zander SA, Mleczak A, Sumpton D, Morrice N, Bienvenut WV, Olson MF. Blebs produced by actin-myosin contraction during apoptosis release damage-associated molecular pattern proteins before secondary necrosis occurs. *Cell Death Differ.* 2013;20(10):1293-1305.
- Wieder M, Garon A, Perricone U, Boresch S, Seidel T, Almerico AM, Langer T. Common hits approach: Combining pharmacophore modeling and molecular dynamics simulations. *J Chem Inf Model.* 2017;57(2):365-385.
- Wojtowicz-Praga SM, Dickson RB, Hawkins MJ. Matrix metalloproteinase inhibitors. *Investig New Drugs.* 1997;15:61-75.
- Worachartcheewan A, Nantasenamat C, Naenna T, Isarankura-Na-Ayudhya C, Prachayasittikul V. Modeling the activity of furin inhibitors using artificial neural network. *Eur J Med Chem.* 2009;44(4):1664-1673.
- World Health Organization. International classification of diseases for oncology (ICD-O). World Health Organization; 2nd update, ICD-O-3.2. 2019.
- Wu HC, Chang DK, Huang CT. Targeted therapy for cancer. *J Cancer Mol.* 2006;2(2):57-66.
- Yamamoto M, Tsujishita H, Hori N, Ohishi Y, Inoue S, Ikeda S, Okada Y. Inhibition of membrane-type 1 matrix metalloproteinase by hydroxamate inhibitors: an examination of the subsite pocket. *J Med Chem.* 1998;41(8):1209-1217.
- Yamamoto S, Nakatani S, Ikura M, Sugiura T, Nishita Y, Itadani S, Ogawa K, Ohno H, Takahashi K, Nakai H, Toda M. Design and synthesis of an orally active matrix metalloproteinase inhibitor. *Bioorg Med Chem.* 2006;14(18):6383-6403.
- Yang SM, Scannevin RH, Wang B, Burke SL, Huang Z, Karnachi P, Wilson LJ, Rhodes KJ, Lagu B, Murray WV. beta-N-Biaryl ether sulfonamide hydroxamates as potent gelatinase

- inhibitors: part 2. Optimization of alpha-amino substituents. *Bioorg Med Chem Lett*. 2008b;18(3):1140-1145.
- Yang SM, Scannevin RH, Wang B, Burke SL, Wilson LJ, Karnachi P, Rhodes KJ, Lagu B, Murray WV. beta-N-Biaryl ether sulfonamide hydroxamates as potent gelatinase inhibitors: part 1. Design, synthesis, and lead identification. *Bioorg Med Chem Lett*. 2008a;18(3):1135-1139.
 - Yao W, Zhuo J, Burns DM, Li YL, Qian DQ, Zhang C, He C, Xu M, Shi E, Li Y, Marando CA, Covington MB, Yang G, Liu X, Pan M, Fridman JS, Scherle P, Wasserman ZR, Hollis G, Vaddi K, Yeleswaram S, Newton R, Friedman S, Metcalf B. Design and identification of selective HER-2 sheddase inhibitors via P1' manipulation and unconventional P2' perturbations to induce a molecular metamorphosis. *Bioorg Med Chem Lett*. 2008;18(1):159-163.
 - Yao W, Zhuo J, Burns DM, Xu M, Zhang C, Li YL, Qian DQ, He C, Weng L, Shi E, Lin Q, Agrios C, Burn TC, Caulder E, Covington MB, Fridman JS, Friedman S, Katiyar K, Hollis G, Li Y, Liu C, Liu X, Marando CA, Newton R, Pan M, Scherle P, Taylor N, Vaddi K, Wasserman ZR, Wynn R, Yeleswaram S, Jalluri R, Bower M, Zhou BB, Metcalf B. Discovery of a potent, selective, and orally active human epidermal growth factor receptor-2 sheddase inhibitor for the treatment of cancer. *J Med Chem*. 2007;50(4):603-606.
 - Yap CW. PaDEL-descriptor: an open source software to calculate molecular descriptors and fingerprints. *J Comput Chem*. 2011;32(7):1466-1474.
 - Yu L, Hong Y, Geng L, Zhou Y, Zhu Q, Cao J, Nie Y. Hyperspectral estimation of soil organic matter content based on partial least squares regression. *Transactions of the Chinese Society of Agricultural Engineering*. 2015;31(14):103-109.
 - Yu XF, Han ZC. Matrix metalloproteinases in bone marrow: Roles of gelatinases in physiological hematopoiesis and hematopoietic malignancies. *Histol Histopathol*. 2006;21(5):519-531.
 - Zapico JM, Puckowska A, Filipiak K, Coderch C, de Pascual-Teresa B, Ramos A. Design and synthesis of potent hydroxamate inhibitors with increased selectivity within the gelatinase family. *Org Biomol Chem*. 2015;13(1):142-156.
 - Zapico JM, Serra P, García-Sanmartín J, Filipiak K, Carbajo RJ, Schott AK, Pineda-Lucena A, Martínez A, Martín-Santamaría S, de Pascual-Teresa B, Ramos A. Potent "clicked" MMP2 inhibitors: synthesis, molecular modeling and biological exploration. *Org Biomol Chem*. 2011;9(12):4587-4599.

- Zhang C, Lovering F, Behnke M, Zask A, Sandanayaka V, Sun L, Zhu Y, Xu W, Zhang Y, Levin JJ. Synthesis and activity of quinolinylmethyl P1' alpha-sulfone piperidine hydroxamate inhibitors of TACE. *Bioorg Med Chem Lett*. 2009;19(13):3445-3448.
- Zhang H, Wang X, Mao J, Huang Y, Xu W, Duan Y, Zhang J. Synthesis and biological evaluation of novel benzofuroxan-based pyrrolidine hydroxamates as matrix metalloproteinase inhibitors with nitric oxide releasing activity. *Bioorg Med Chem*. 2018;26(15):4363-4374.
- Zhang J, Li X, Jiang Y, Feng J, Li X, Zhang Y, Xu W. Design, synthesis and preliminary evaluation of α -sulfonyl γ -(glycinyloxy)proline peptidomimetics as matrix metalloproteinase inhibitors. *Bioorg Med Chem*. 2014;22(11):3055-3064.
- Zhang Y, Sanjose SD, Bracci PM, Morton LM, Wang R, Brennan P, Hartge P, Boffetta P, Becker N, Maynadie M, Foretova L, Cocco P, Staines A, Holford T, Holly EA, Nieters A, Benavente Y, Bernstein L, Zahm SH, Zheng T. Personal use of hair dye and the risk of certain subtypes of non-Hodgkin lymphoma. *Am J Epidemiol*. 2008;167(11):1321-1331.
- Zhao Y, Chen S, Gou WF, Niu ZF, Zhao S, Xiao LJ, Takano Y, Zheng HC. The role of EMMPRIN expression in ovarian epithelial carcinomas. *Cell Cycle*. 2013;12(17):2899-2913.
- Zugazagoitia J, Guedes C, Ponce S, Ferrer I, Molina-Pinelo S, Paz-Ares L. Current challenges in cancer treatment. *Clinical therapeutics*. 2016;38(7):1551-1566.

APPENDIX

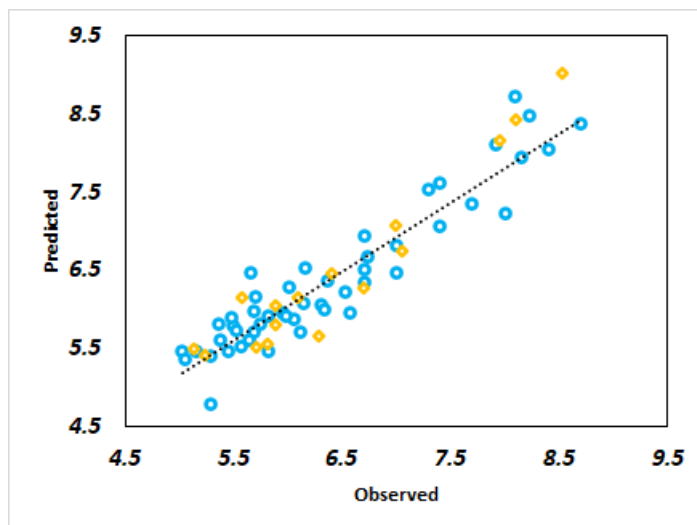


Figure A1. Observed vs predicted activity plot of HQSAR model.

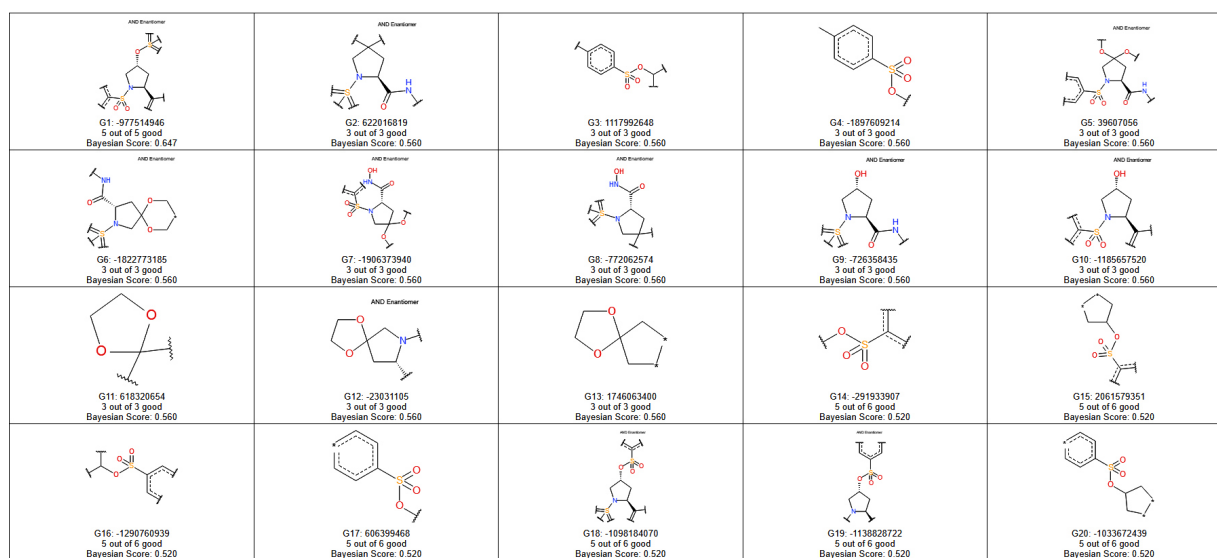


Figure A2. Good molecular substructural fragments were obtained from the Bayesian classification model.

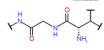
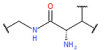

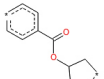
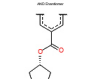
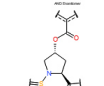
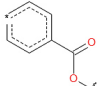
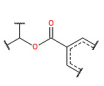
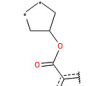
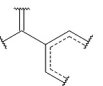
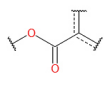
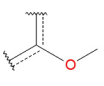
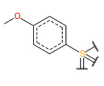
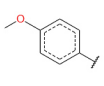
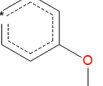
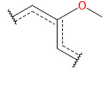
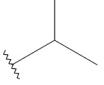
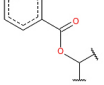
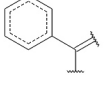
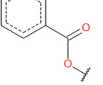
 <p>B1: 435352650 0 out of 5 good Bayesian Score: -1.144</p>	 <p>B2: -1692990643 0 out of 5 good Bayesian Score: -1.144</p>	 <p>B3: -621924532 0 out of 5 good Bayesian Score: -1.144</p>	 <p>B4: -715262484 0 out of 5 good Bayesian Score: -1.144</p>	 <p>B5: -1835013855 0 out of 5 good Bayesian Score: -1.144</p>
 <p>B6: 1355492337 0 out of 5 good Bayesian Score: -1.144</p>	 <p>B7: -586619256 0 out of 5 good Bayesian Score: -1.144</p>	 <p>B8: -1785583741 0 out of 5 good Bayesian Score: -1.144</p>	 <p>B9: 830534047 0 out of 5 good Bayesian Score: -1.144</p>	 <p>B10: -175146122 0 out of 5 good Bayesian Score: -1.144</p>
 <p>B11: 1430791942 0 out of 5 good Bayesian Score: -1.144</p>	 <p>B12: 1307307440 0 out of 4 good Bayesian Score: -0.998</p>	 <p>B13: -360736333 0 out of 4 good Bayesian Score: -0.998</p>	 <p>B14: 693720869 0 out of 4 good Bayesian Score: -0.998</p>	 <p>B15: -1271104377 0 out of 4 good Bayesian Score: -0.998</p>
 <p>B16: 2055803015 0 out of 4 good Bayesian Score: -0.998</p>	 <p>B17: 864518973 1 out of 10 good Bayesian Score: -0.971</p>	 <p>B18: 551030807 0 out of 3 good Bayesian Score: -0.826</p>	 <p>B19: 1451403962 0 out of 3 good Bayesian Score: -0.826</p>	 <p>B20: -837988472 0 out of 3 good Bayesian Score: -0.826</p>

Figure A3. Bad molecular substructural fragments were obtained from the Bayesian classification model.

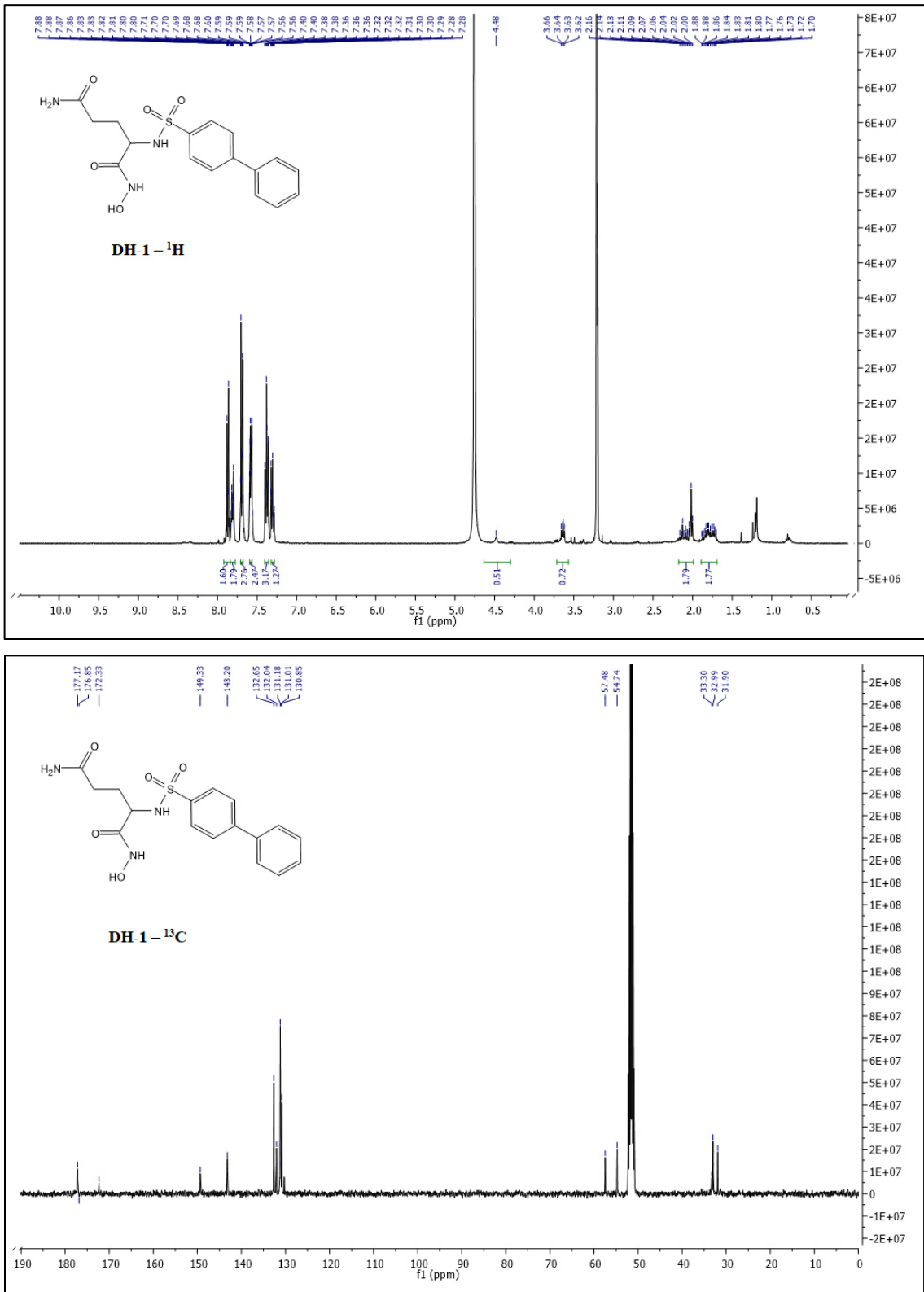


Figure A4. ^1H and ^{13}C NMR Spectra of Compound DH-1.

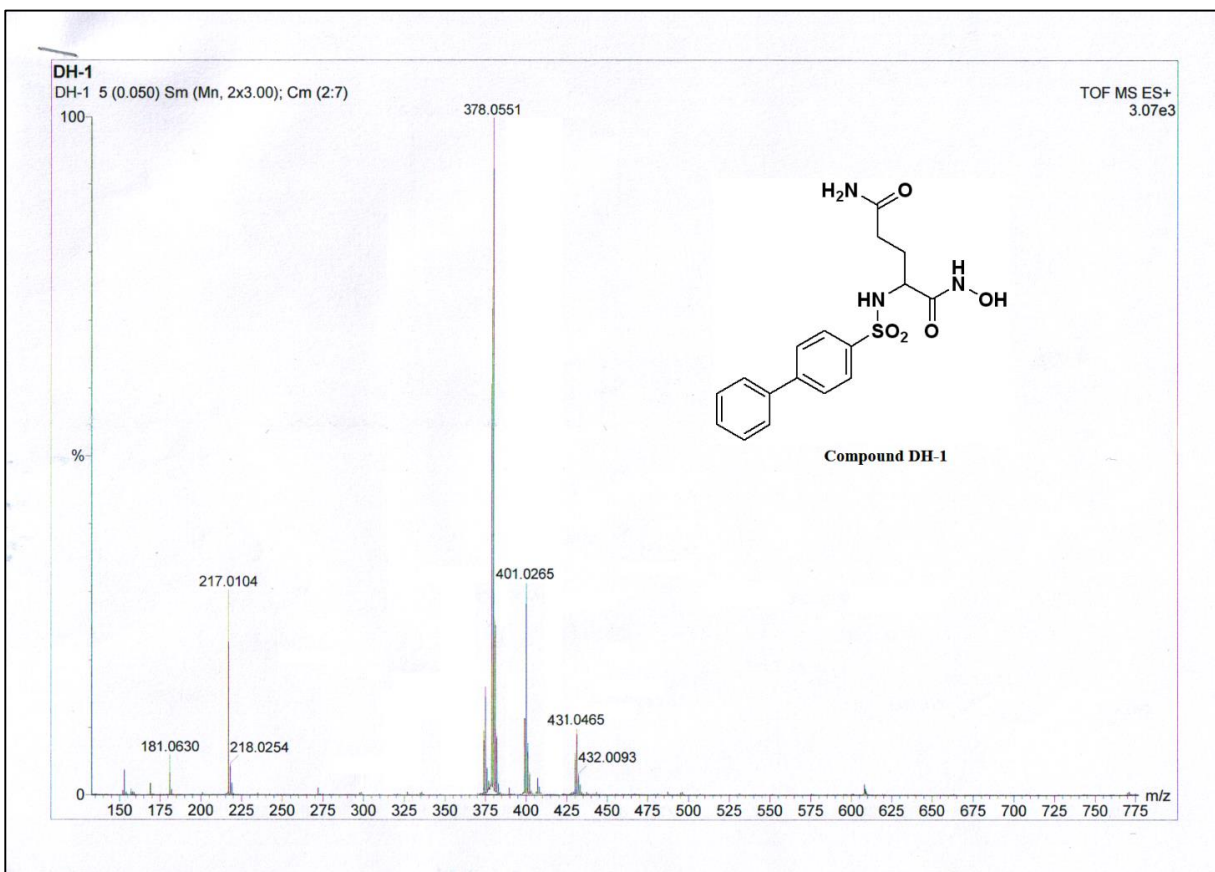


Figure A5. HRMS Spectra of Compound DH-1.

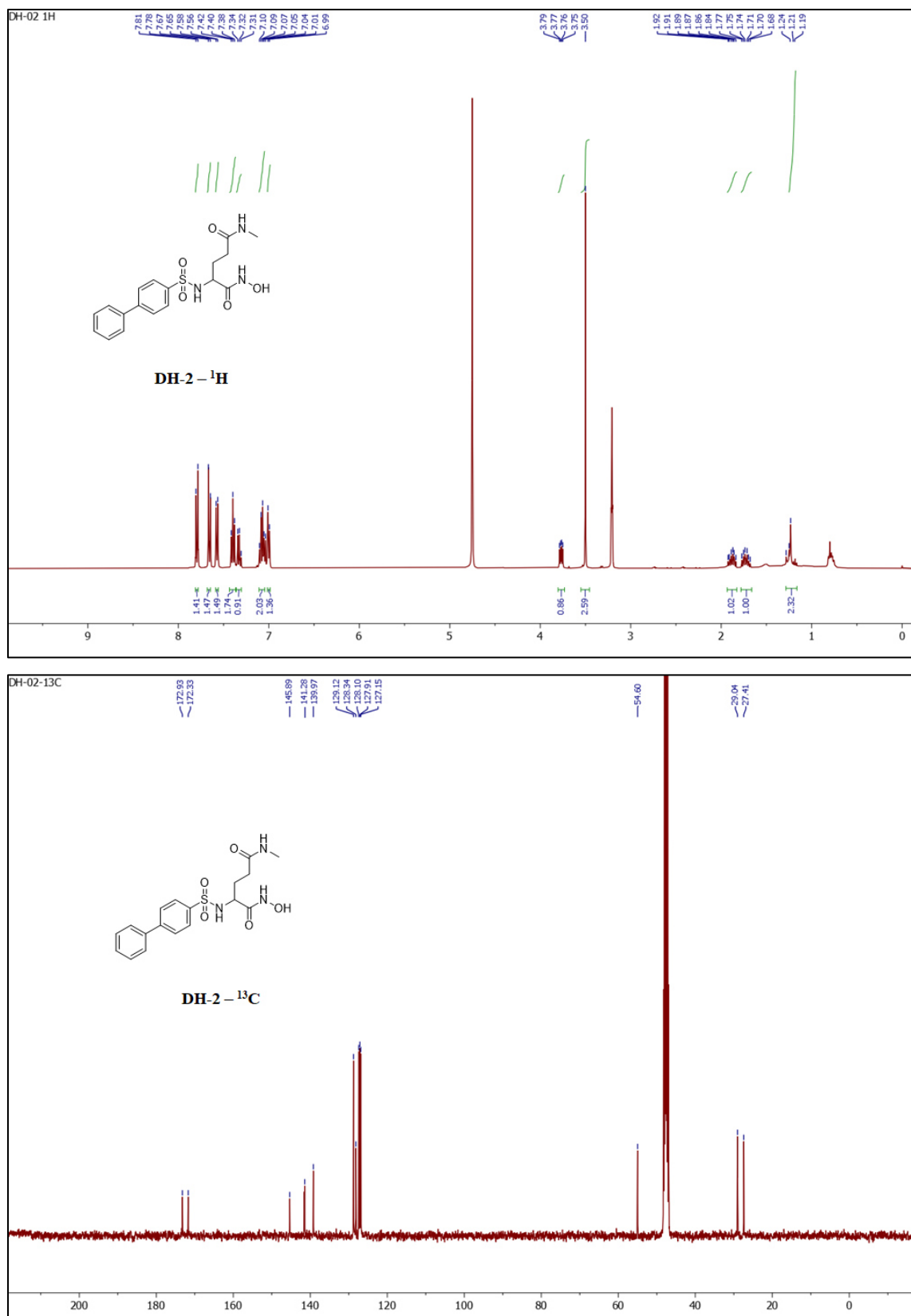


Figure A6. ^1H and ^{13}C NMR Spectra of Compound DH-2.

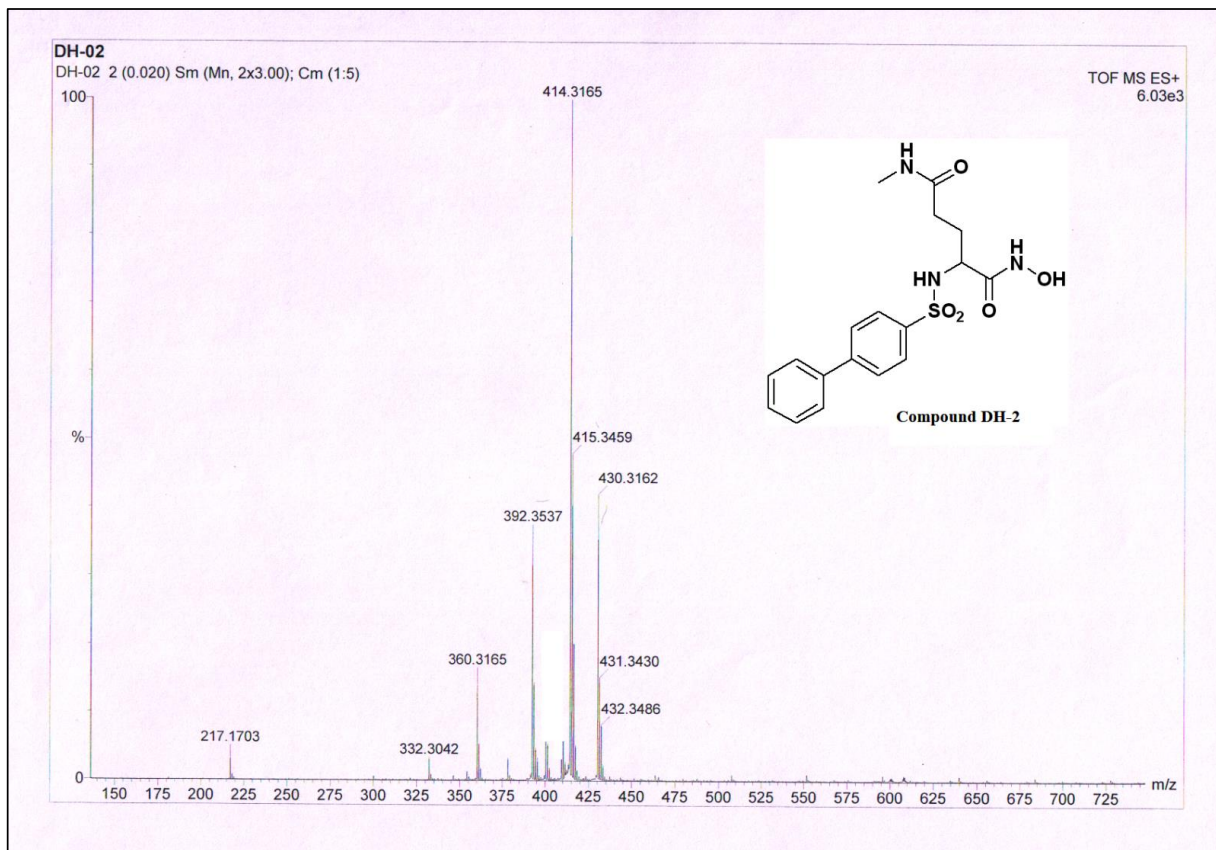


Figure A7. HRMS Spectra of Compound DH-2.

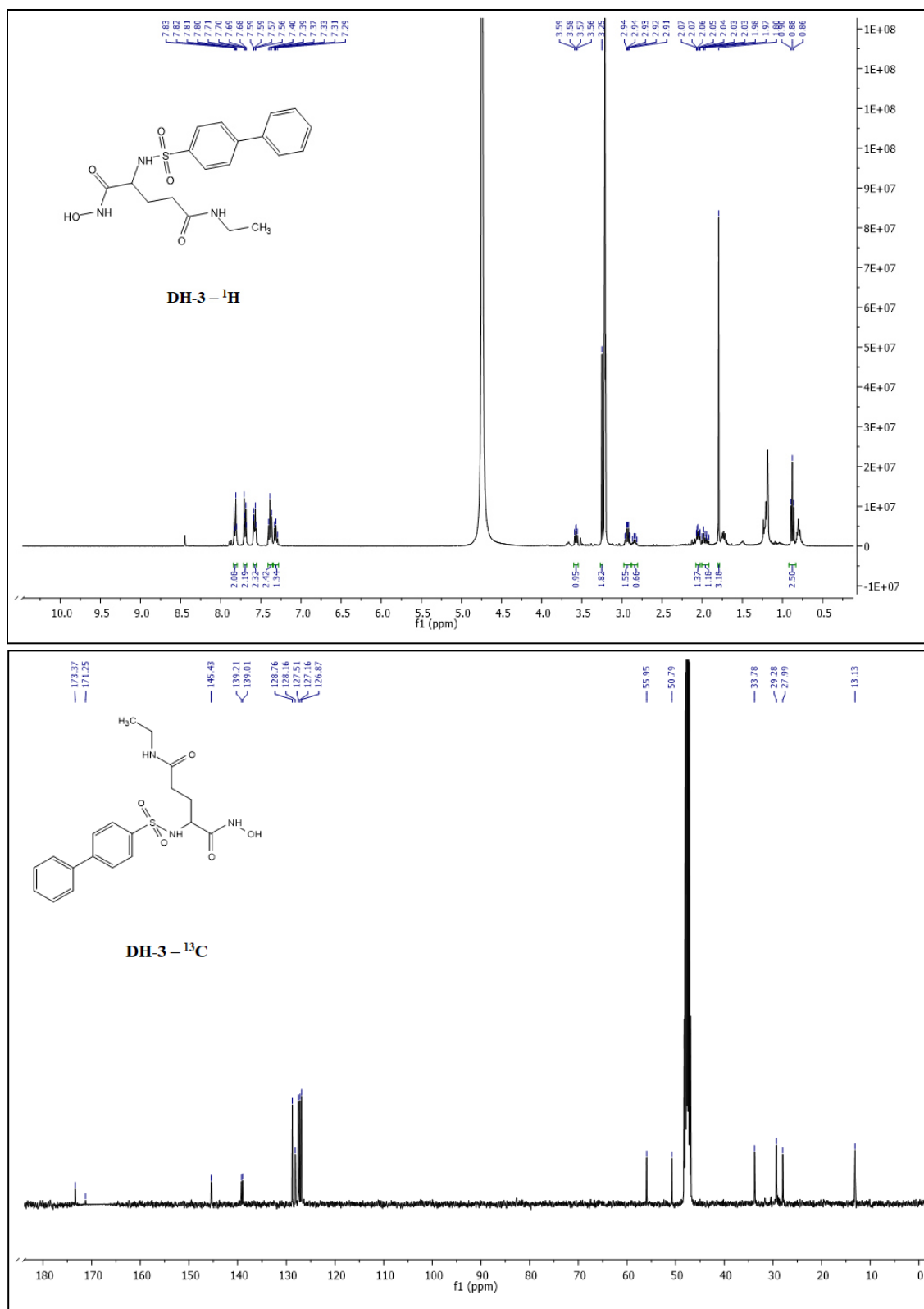


Figure A8. ^1H and ^{13}C NMR Spectra of Compound DH-3.

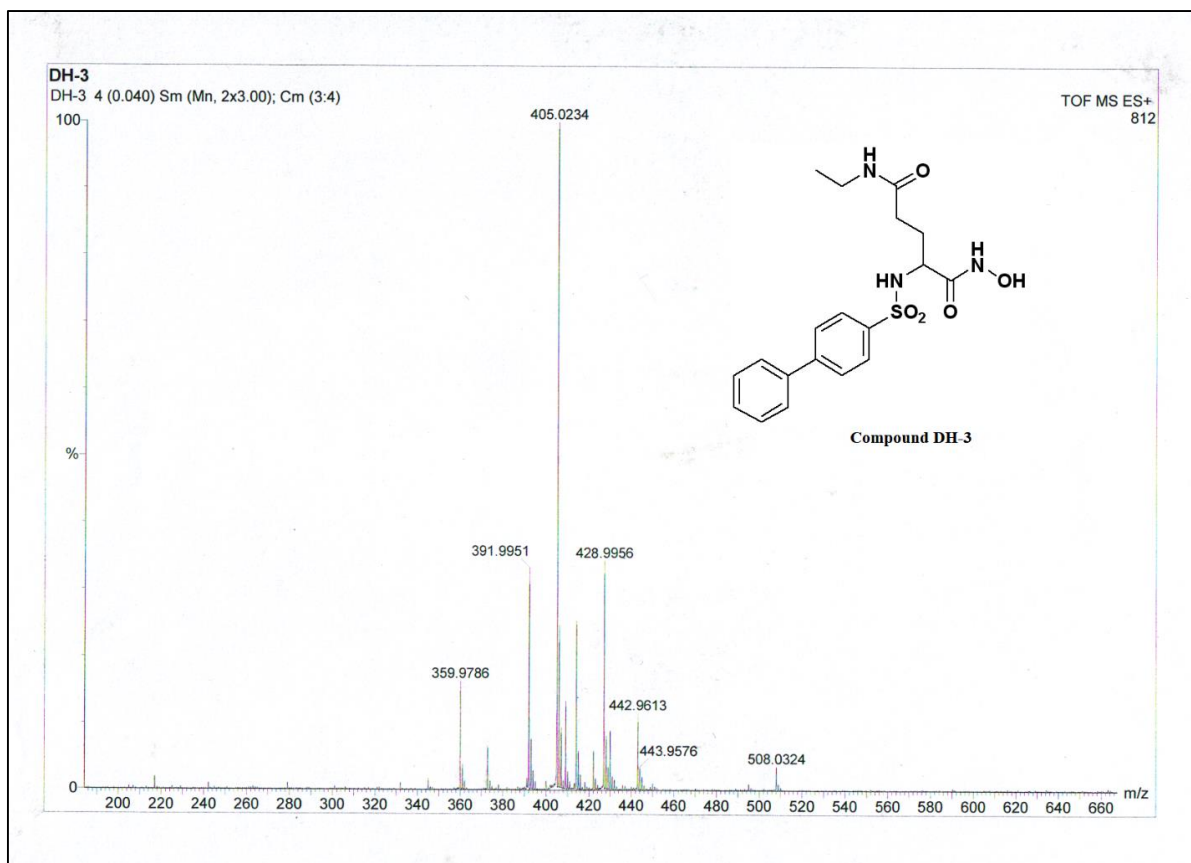


Figure A9. HRMS Spectra of Compound DH-3.

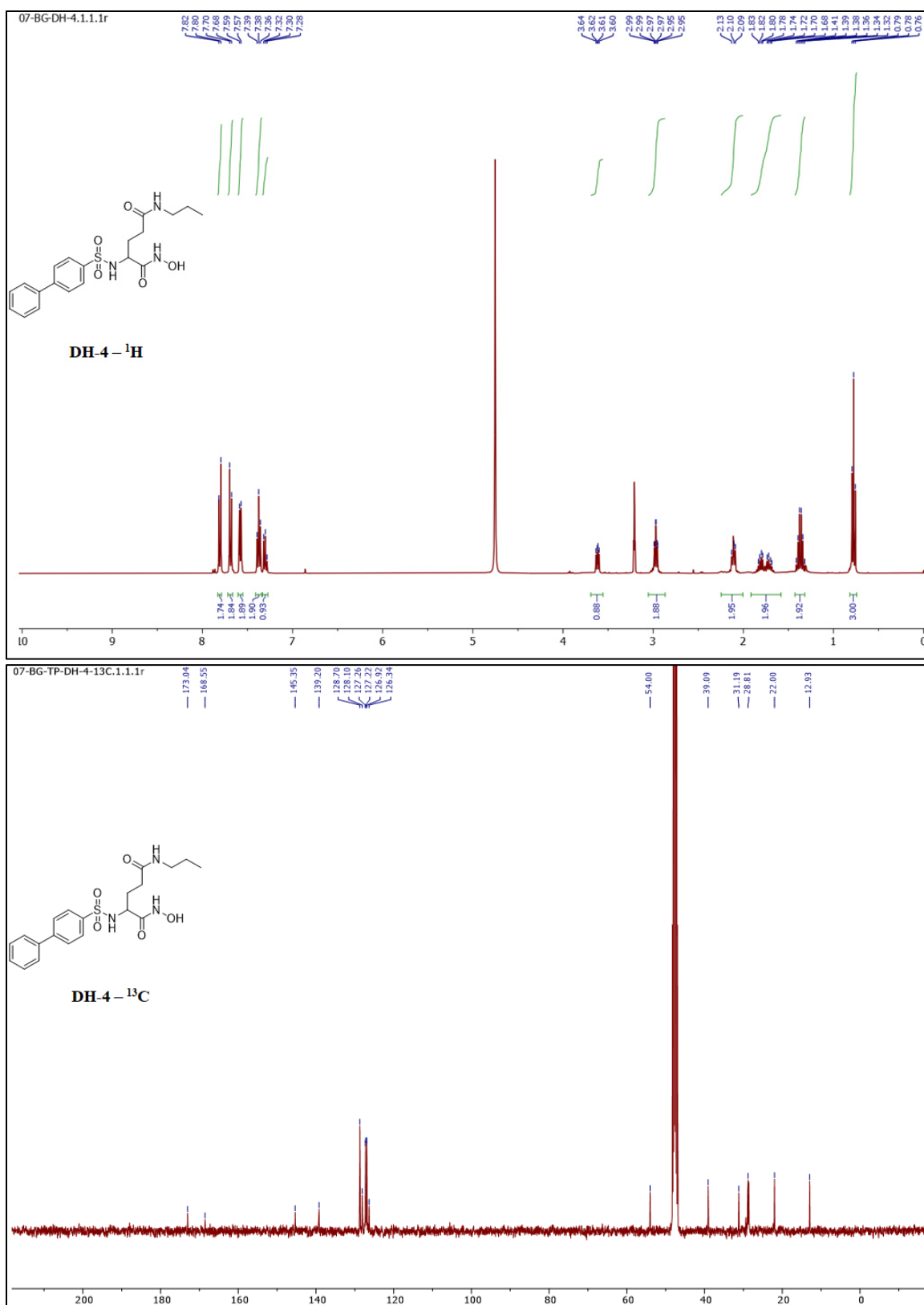


Figure A10. ^1H and ^{13}C NMR Spectra of Compound DH-4.

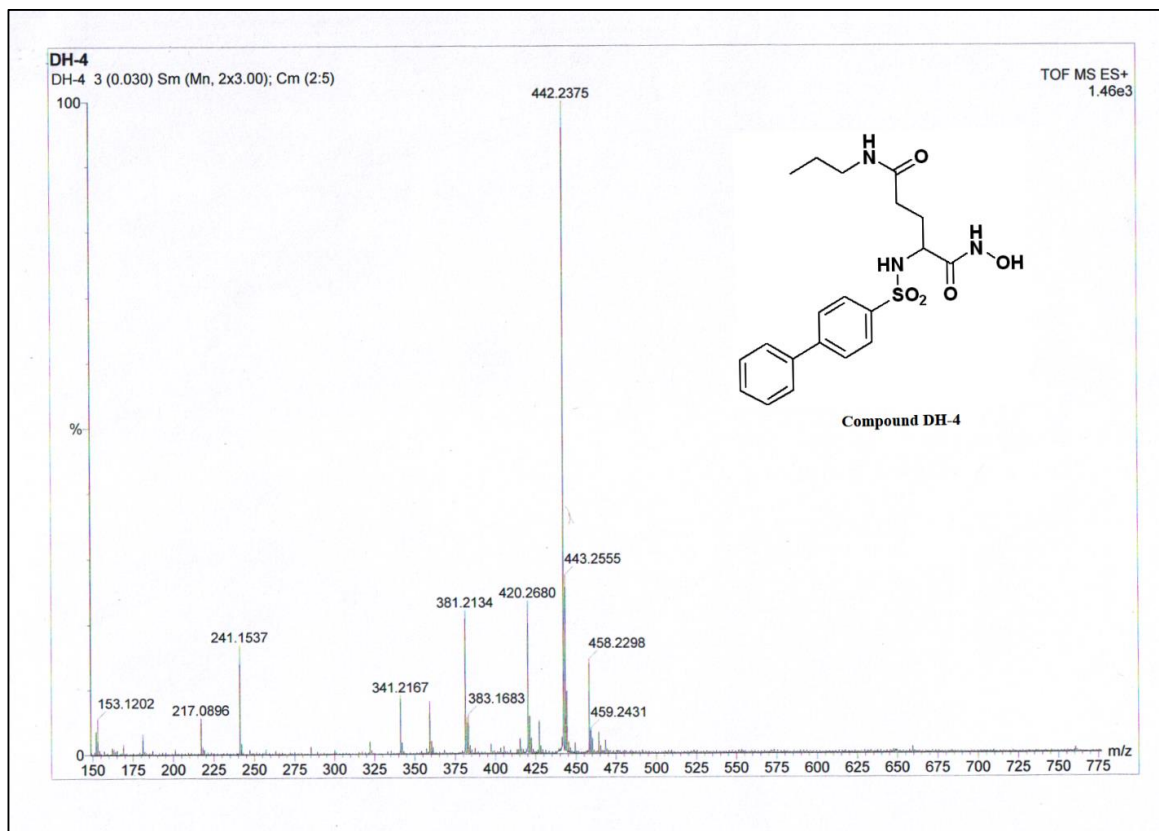
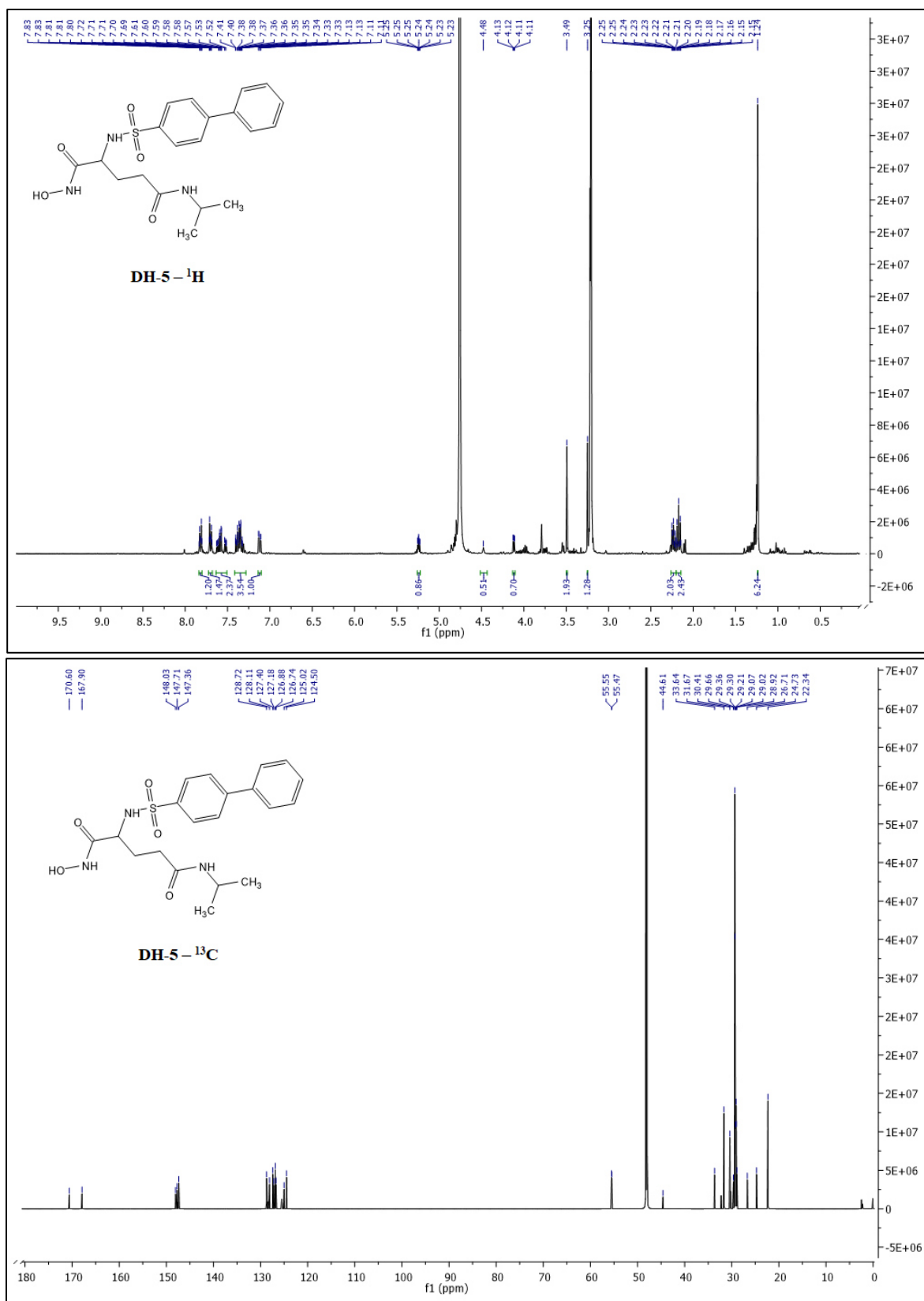


Figure A11. HRMS Spectra of Compound DH-4.



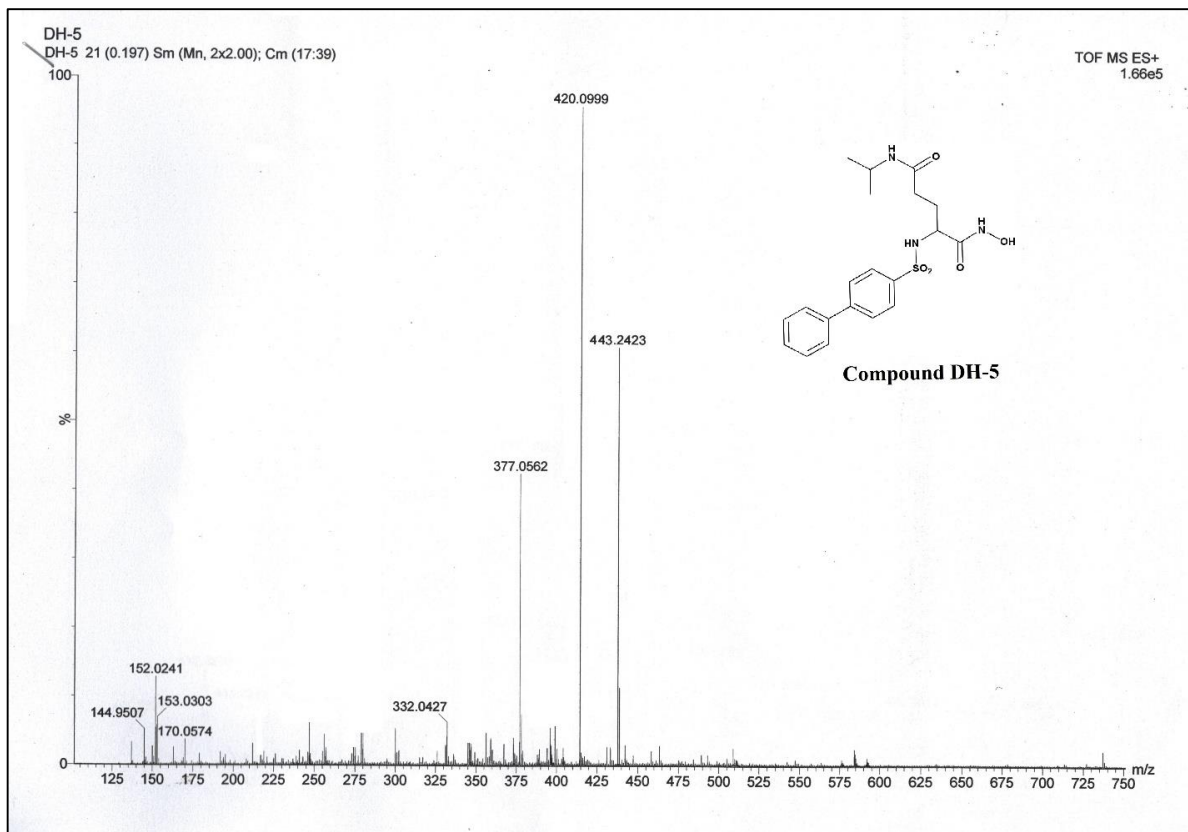
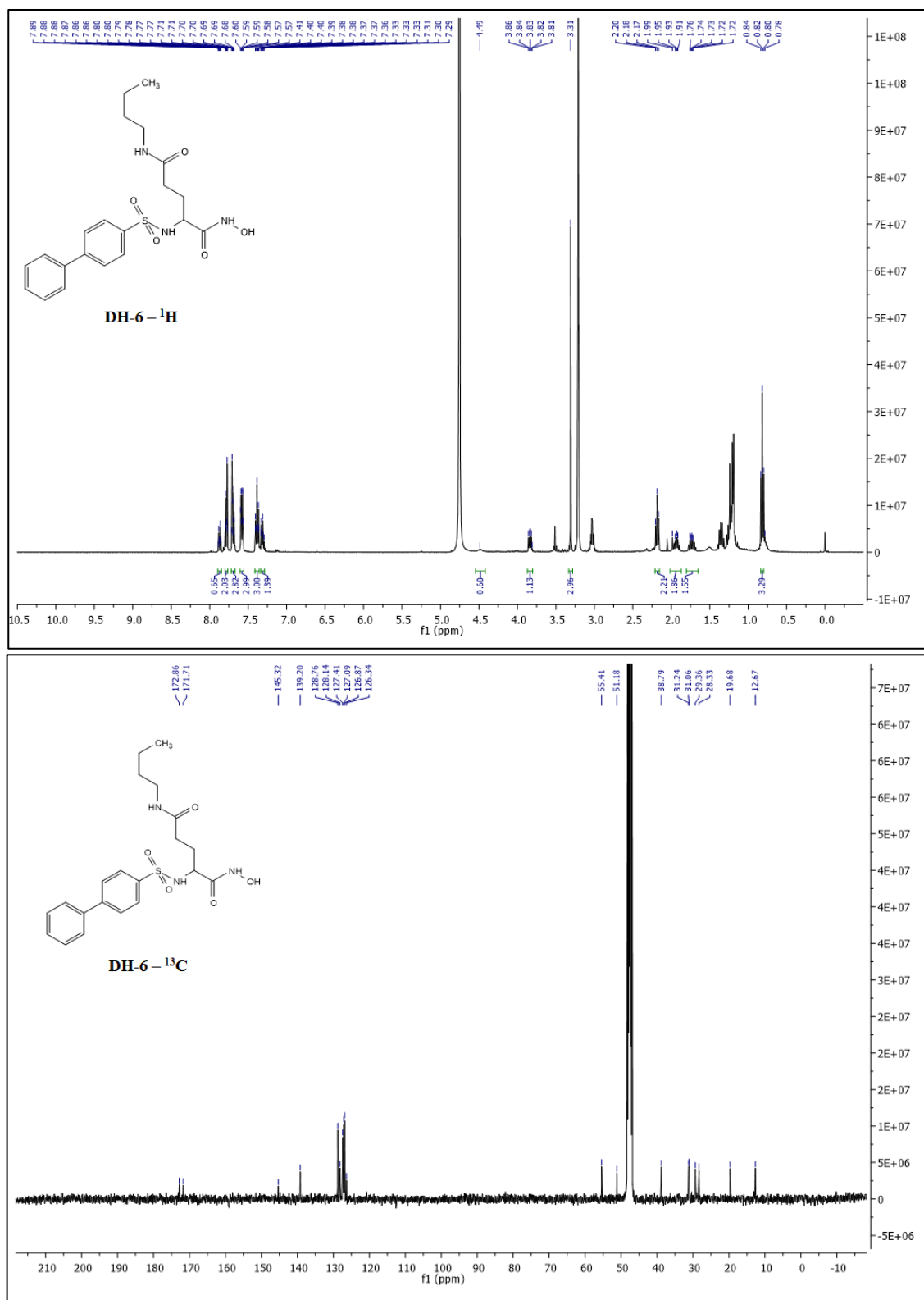


Figure A13. HRMS Spectra of Compound DH-5.



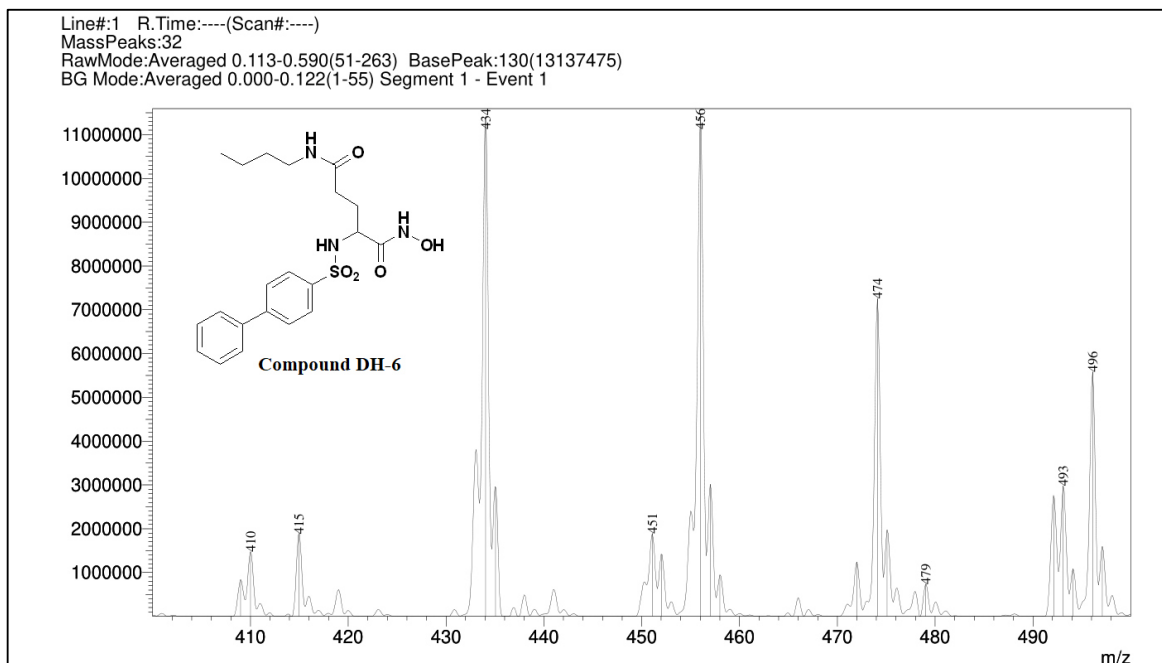


Figure A15. HRMS Spectra of Compound DH-6.

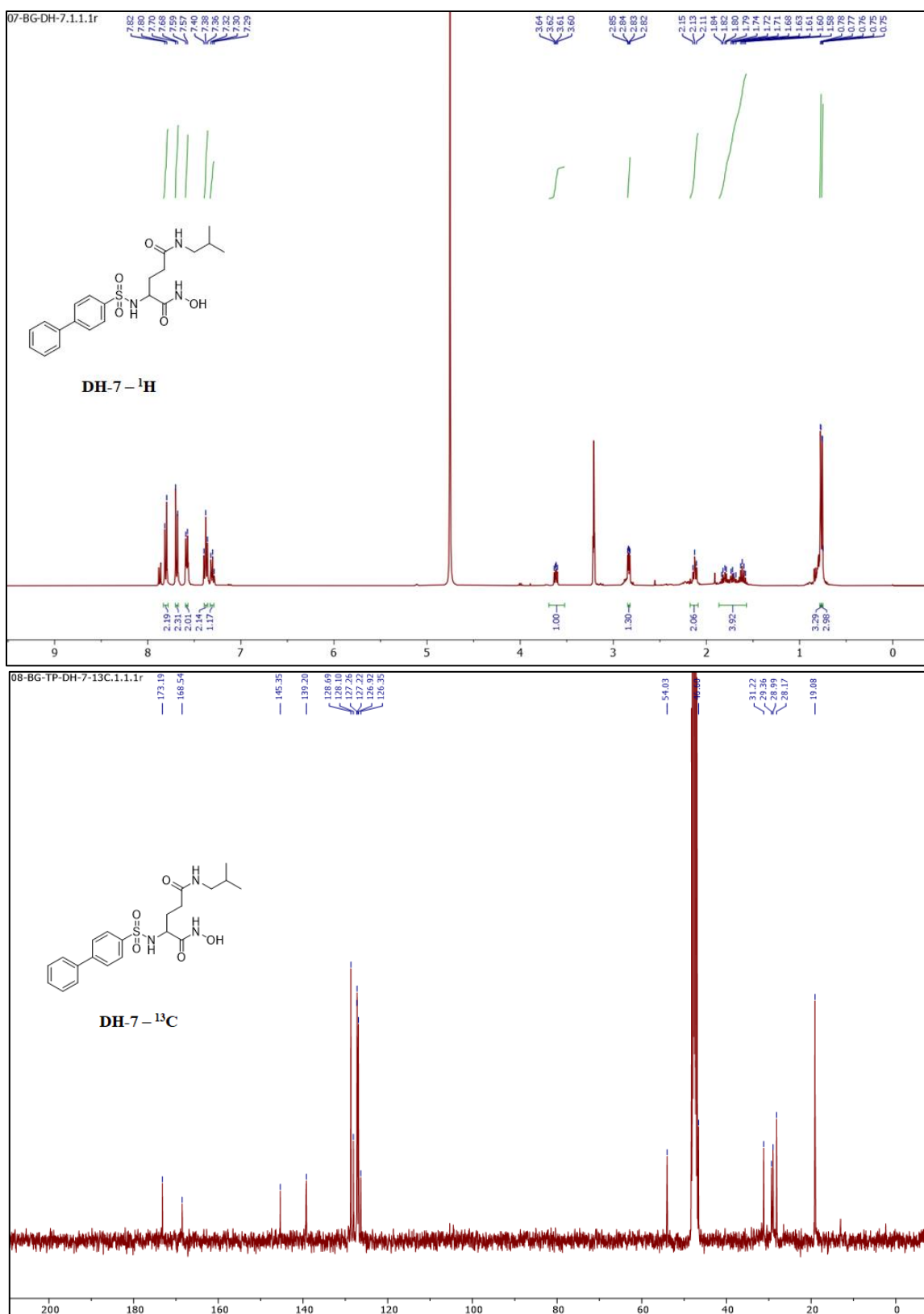


Figure A16. ^1H and ^{13}C NMR Spectra of Compound DH-7.

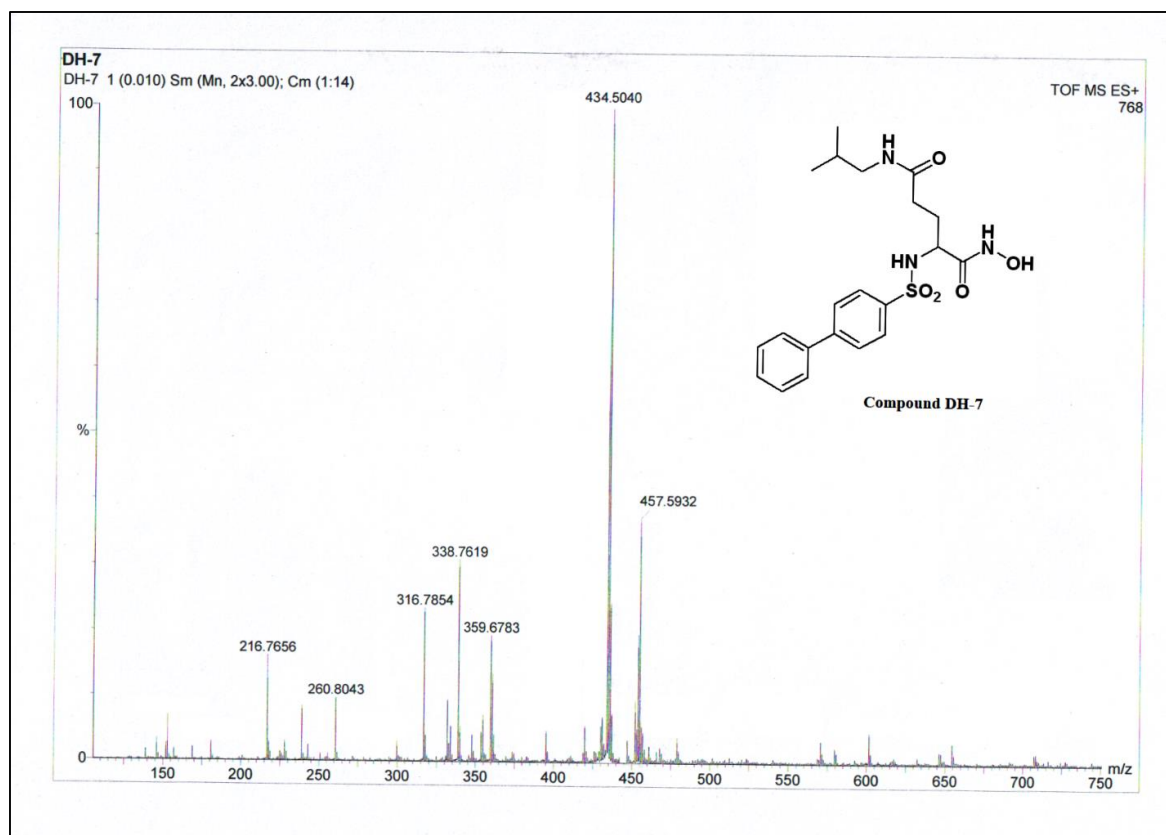


Figure A17. HRMS Spectra of Compound DH-7.

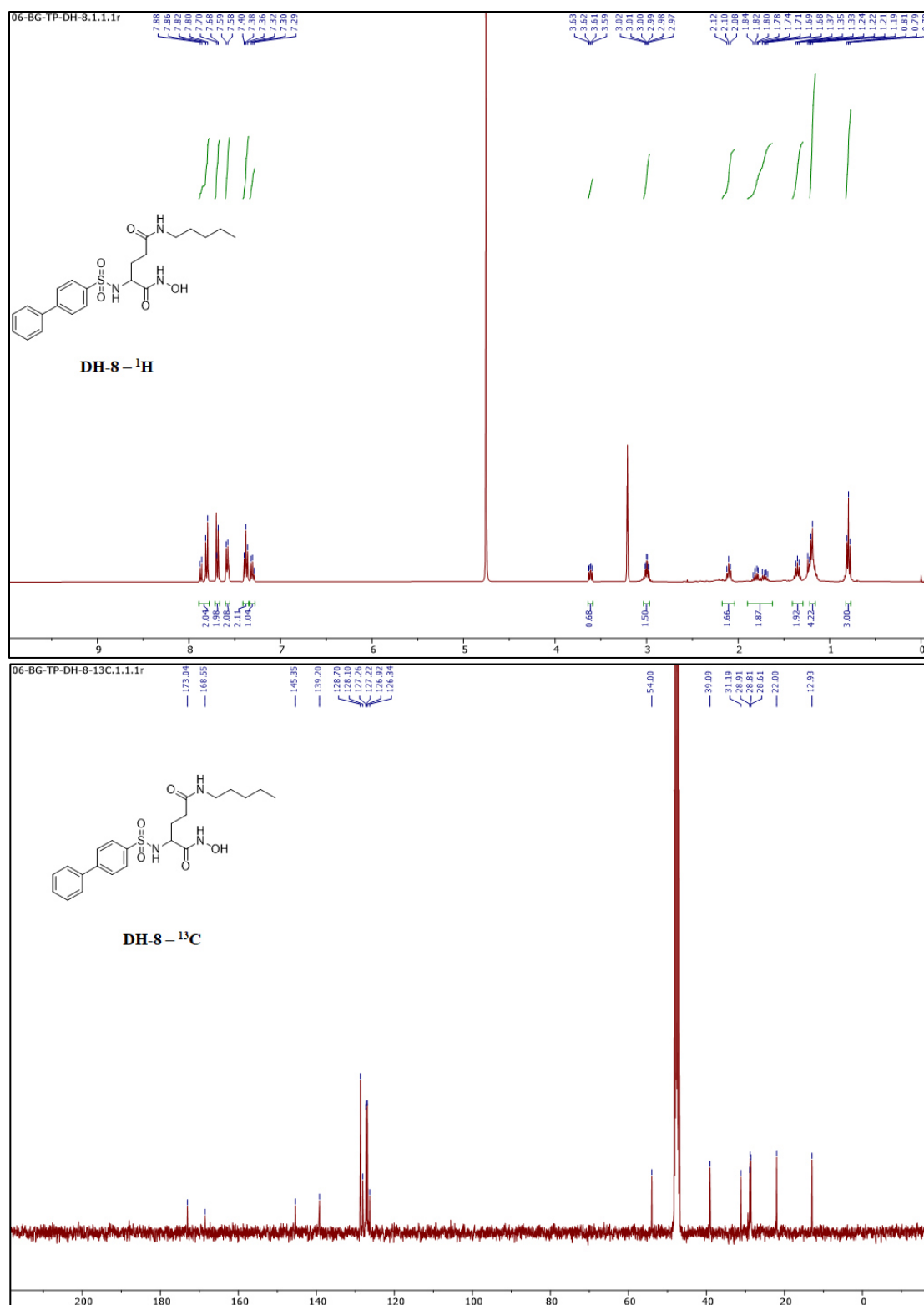


Figure A18. ^1H and ^{13}C NMR Spectra of Compound DH-8.

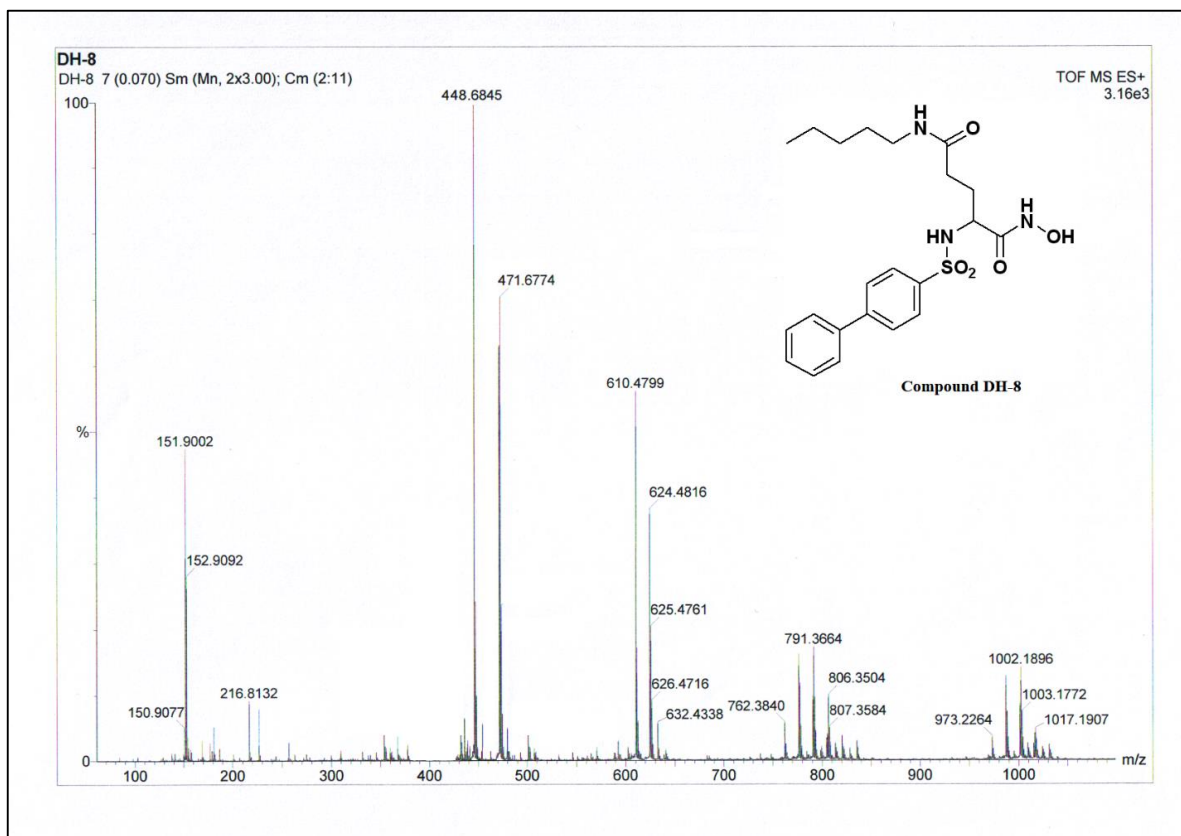


Figure A19. HRMS Spectra of Compound DH-8.

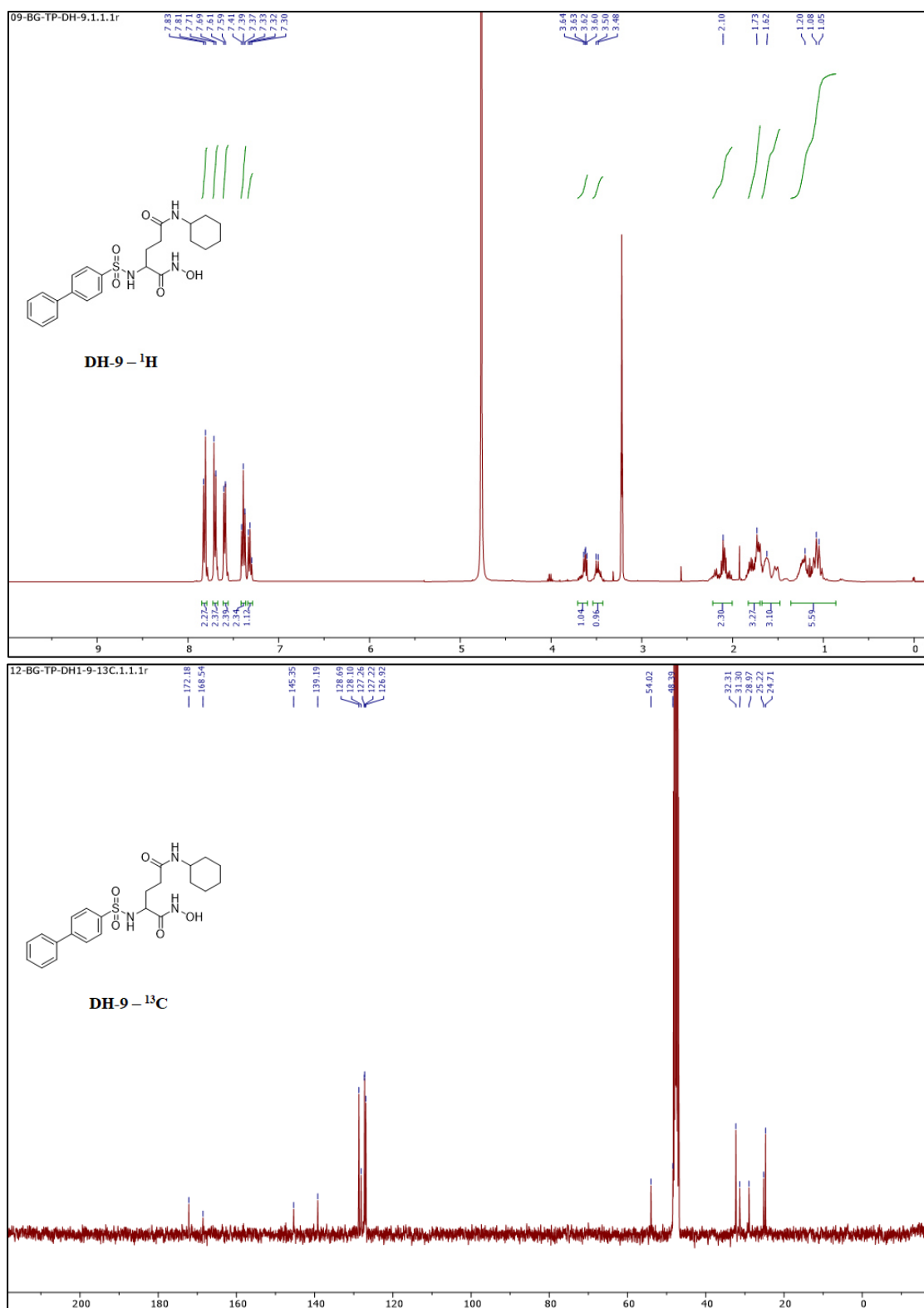


Figure A20. ^1H and ^{13}C NMR Spectra of Compound DH-9.

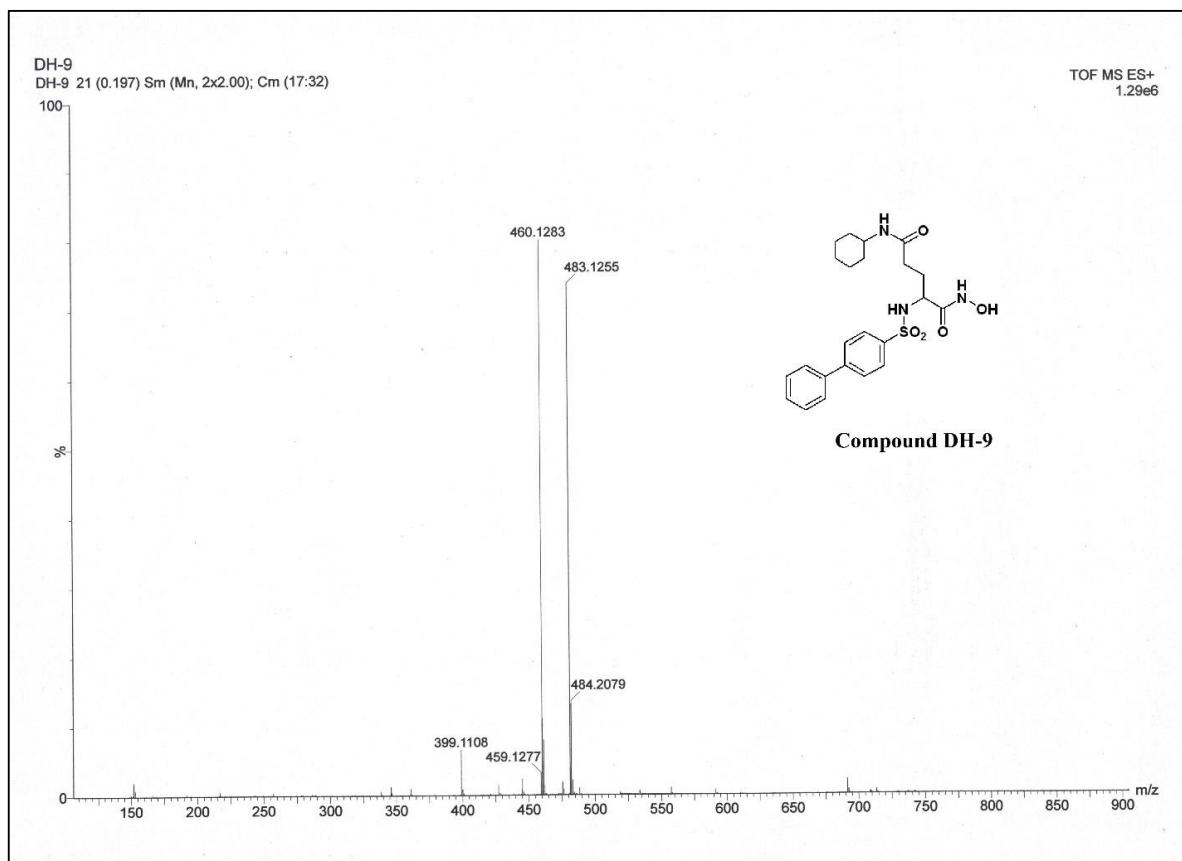


Figure A21. HRMS Spectra of Compound DH-9.

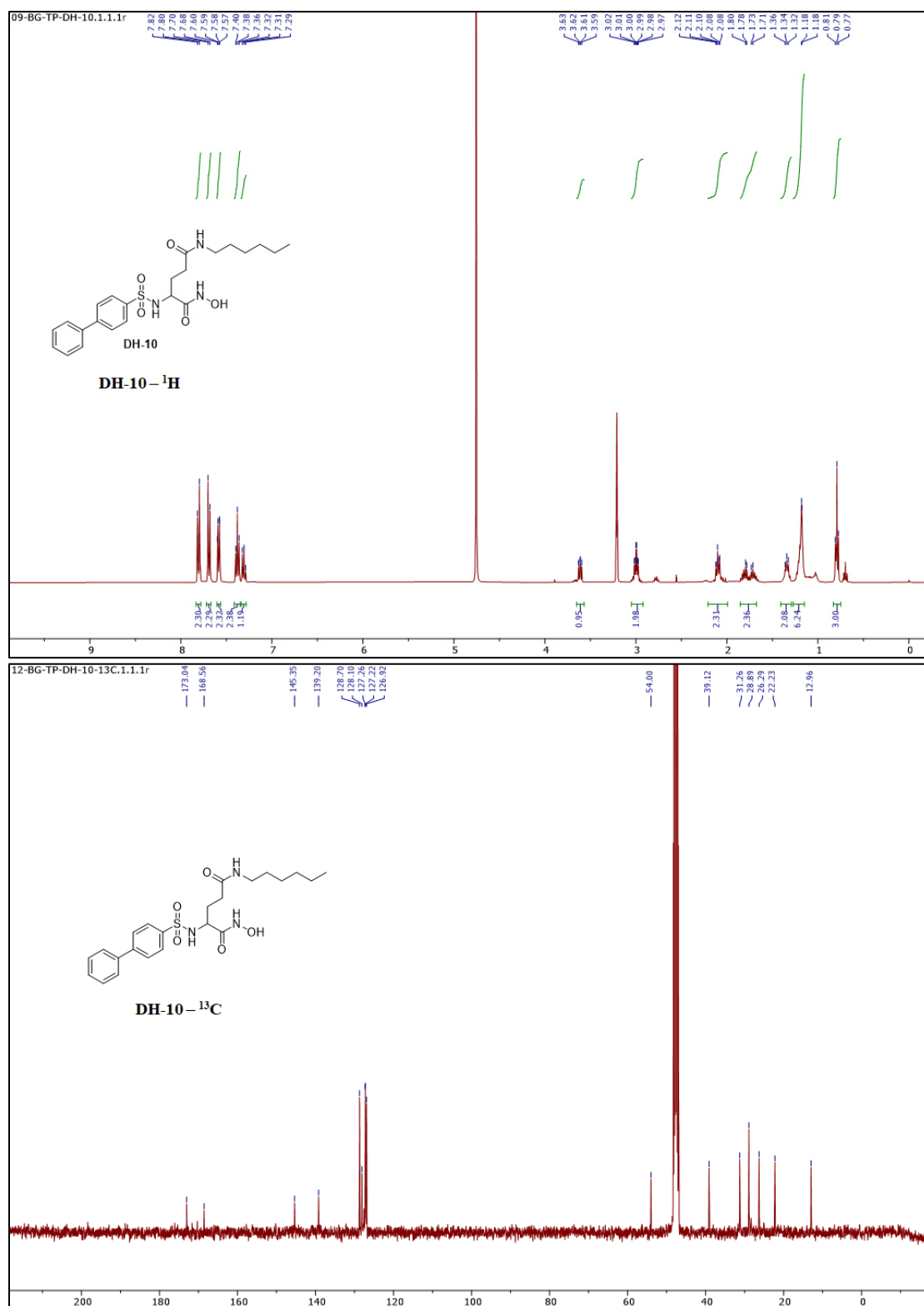


Figure A22. ^1H and ^{13}C NMR Spectra of Compound DH-10.

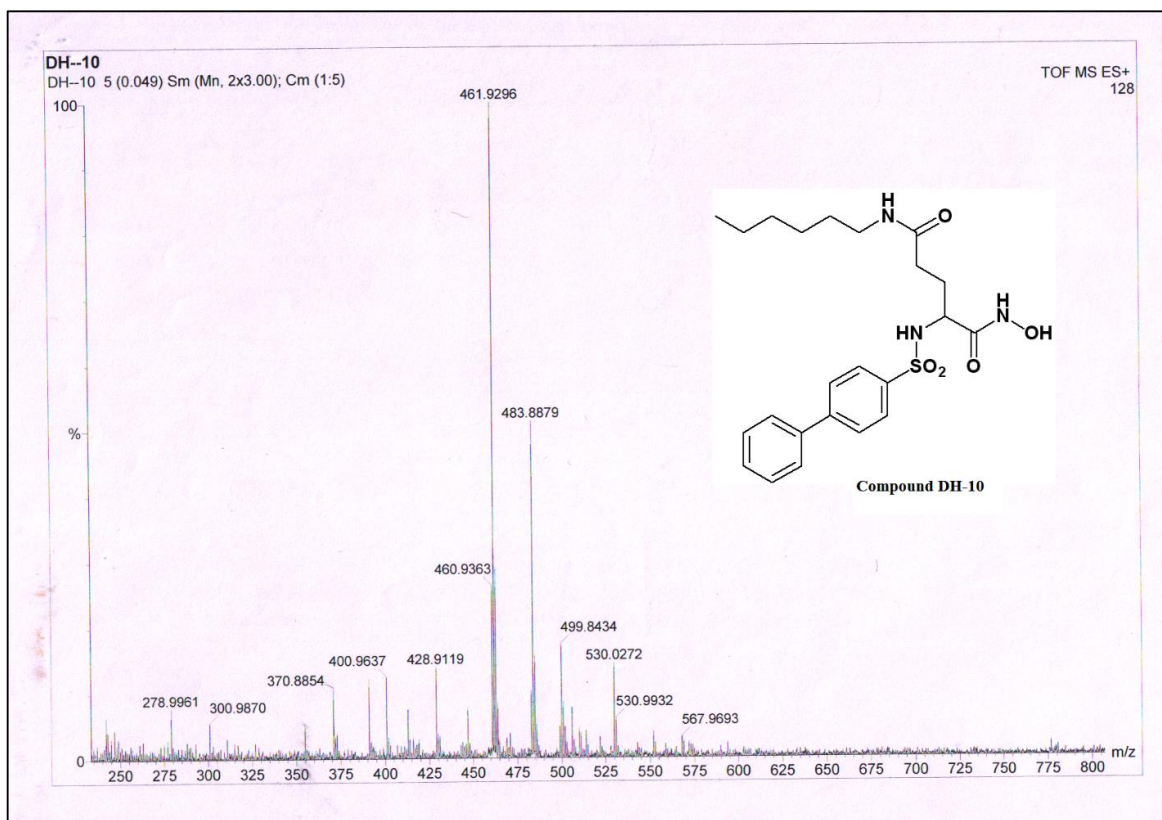


Figure A23. HRMS Spectra of Compound DH-10.

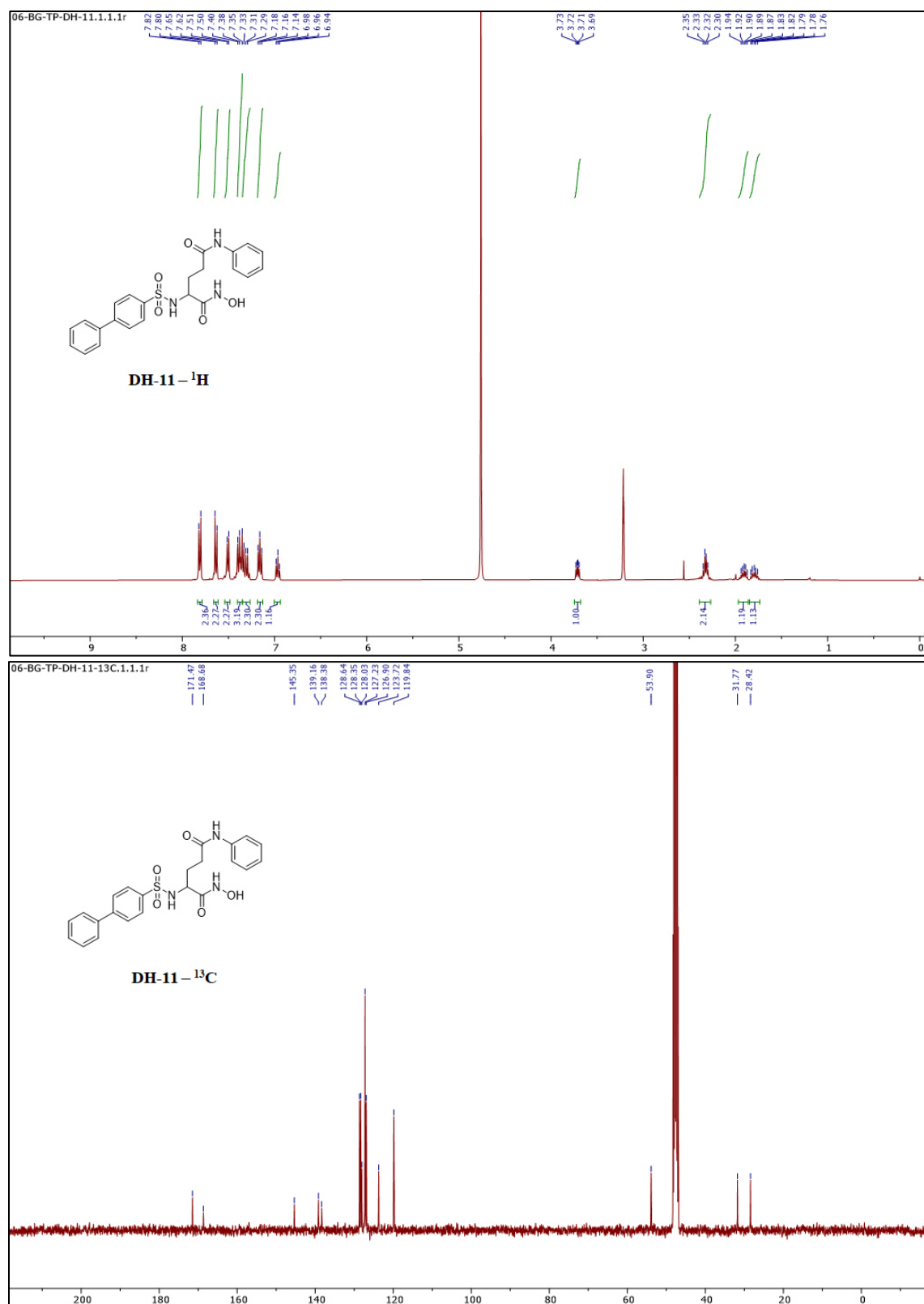


Figure A24. ^1H and ^{13}C NMR Spectra of Compound DH-11.

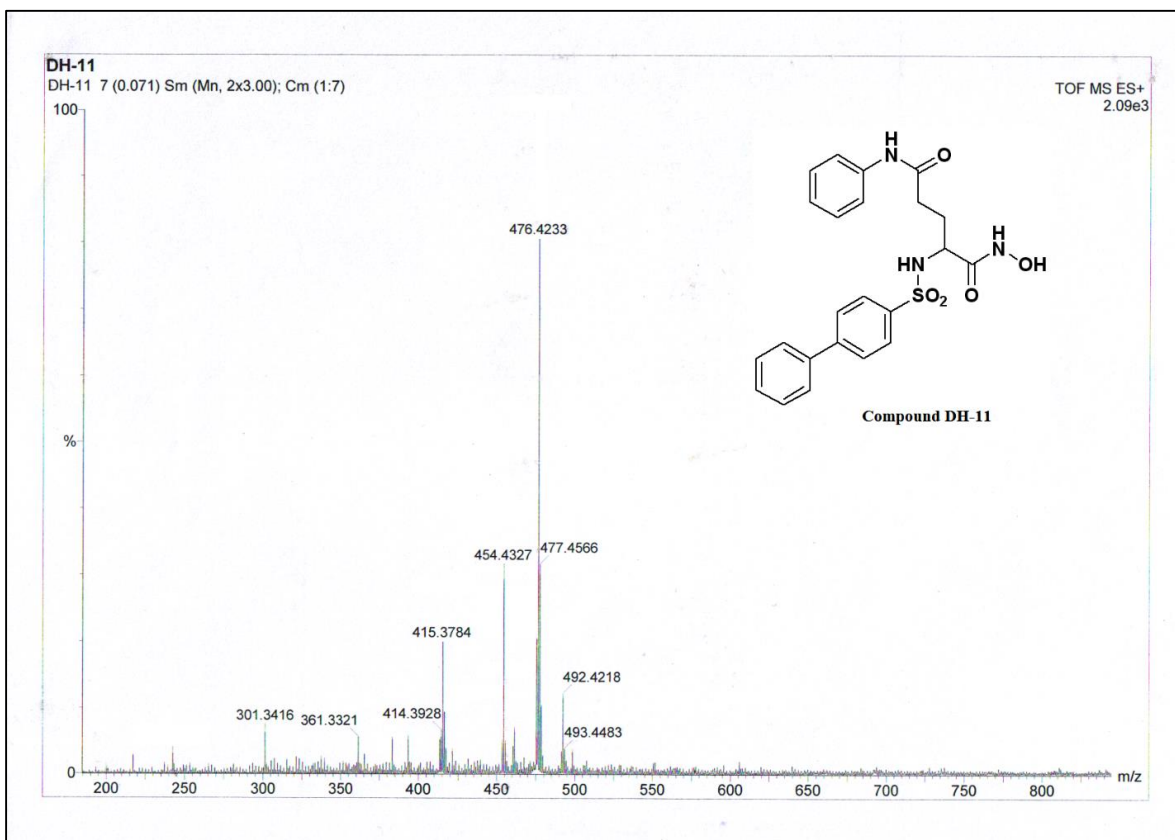


Figure A25. HRMS Spectra of Compound DH-11.

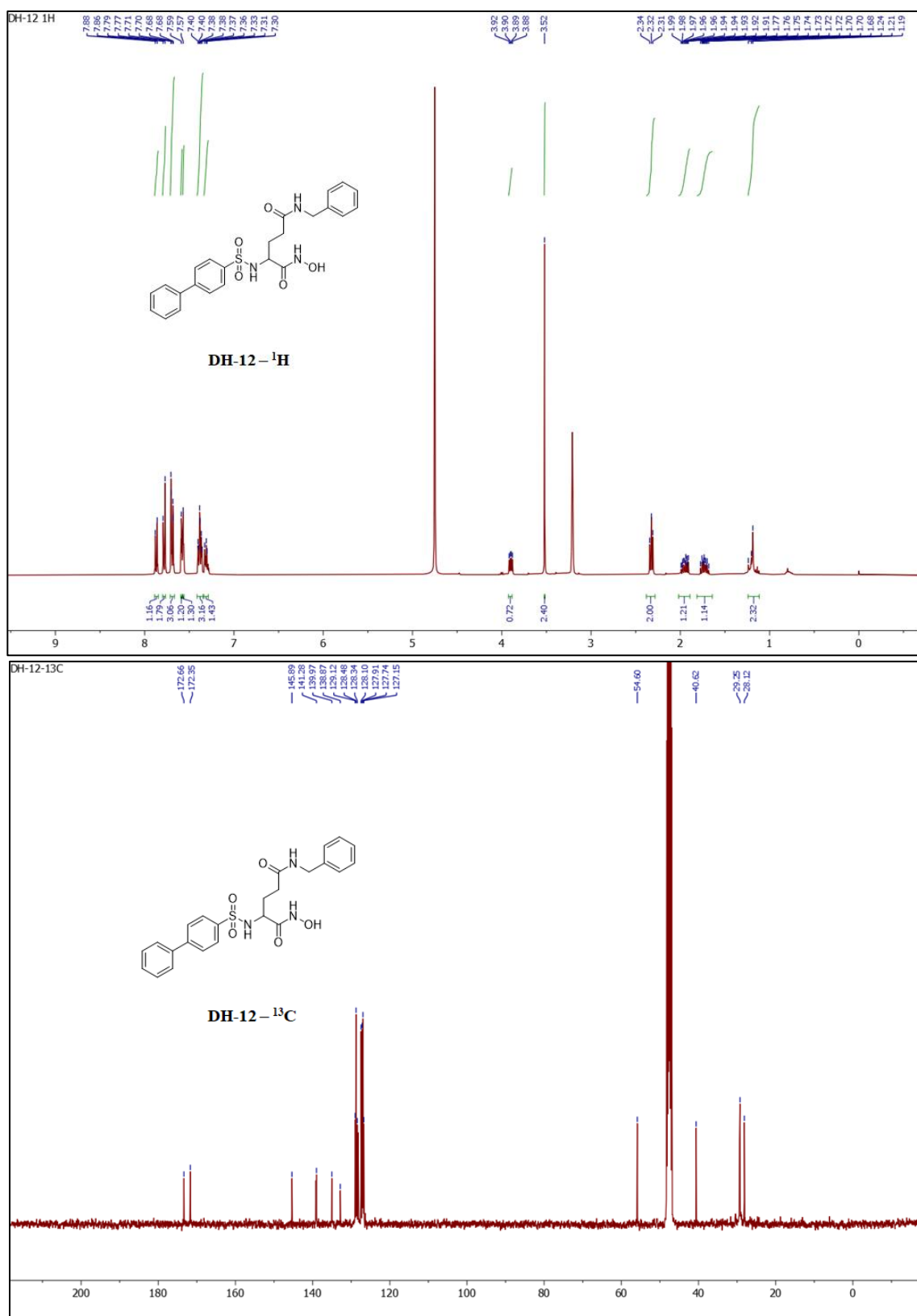


Figure A26. ¹H and ¹³C NMR Spectra of Compound DH-12.

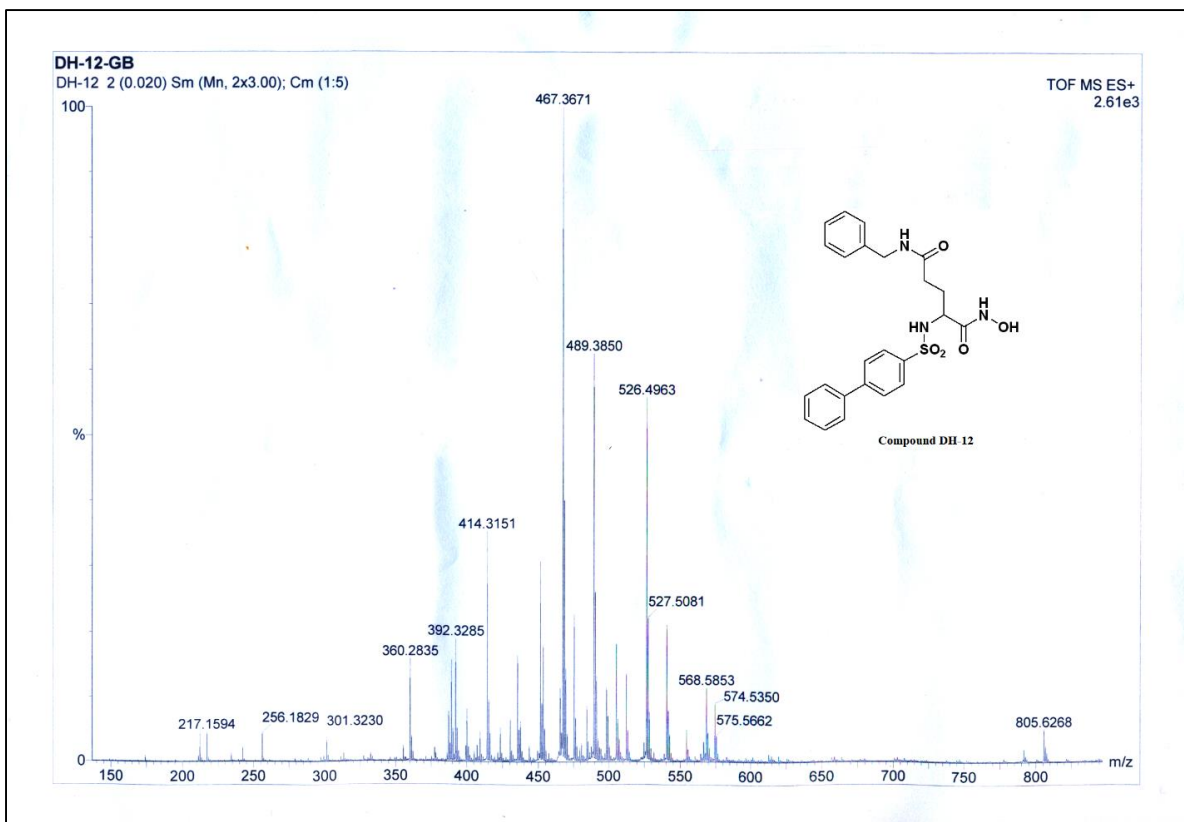


Figure A27. HRMS Spectra of Compound DH-12.

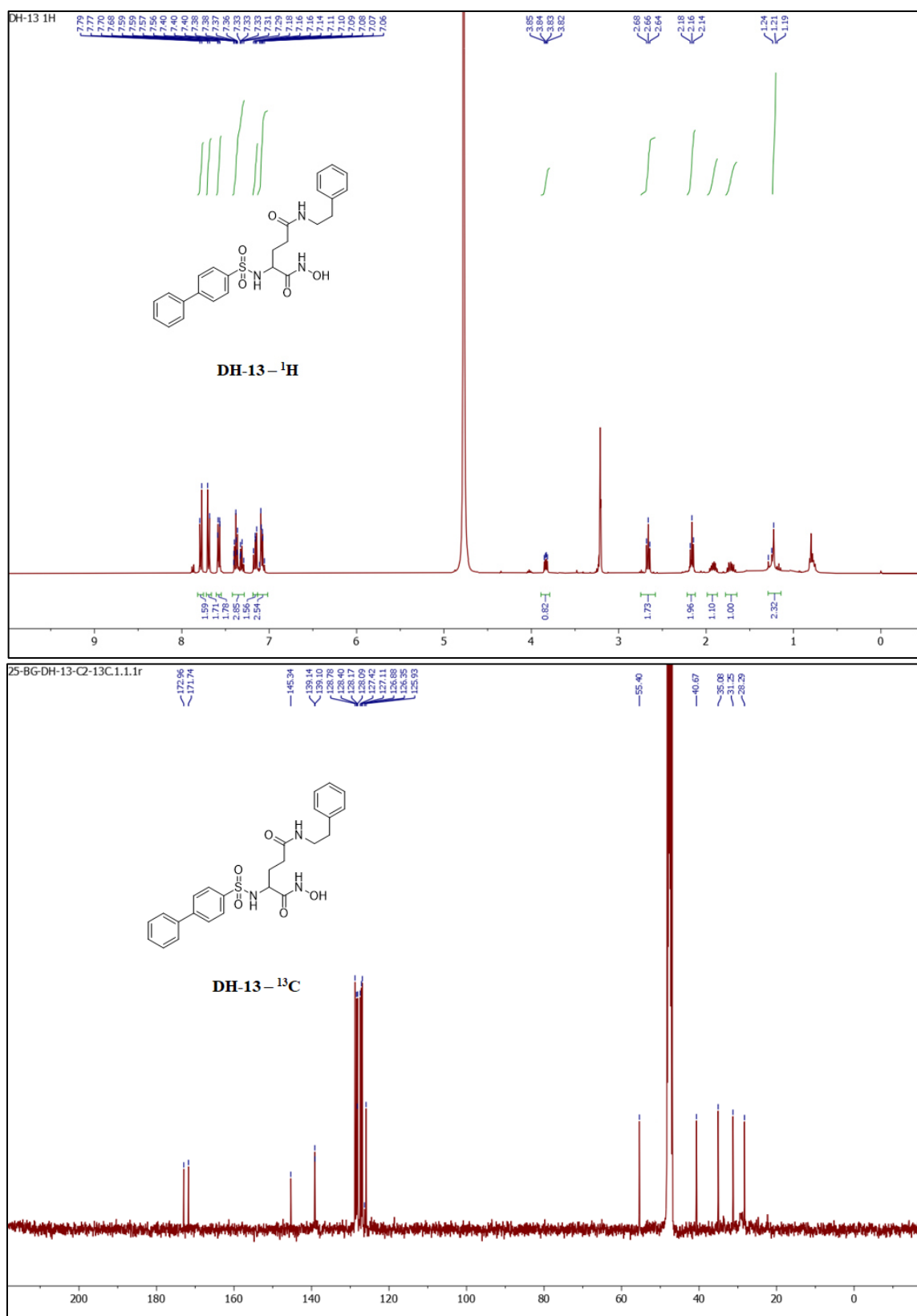


Figure A28. ¹H and ¹³C NMR Spectra of Compound DH-13.

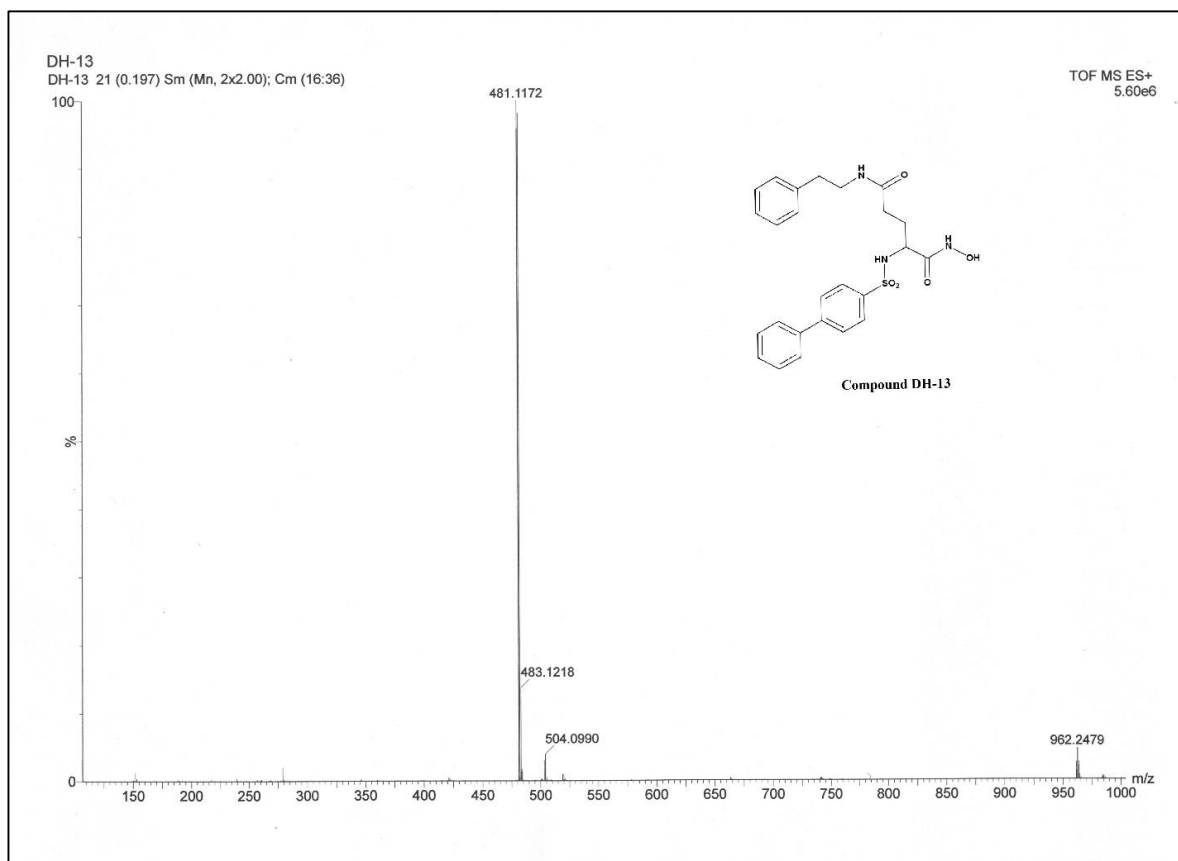


Figure A29. HRMS Spectra of Compound DH-13.

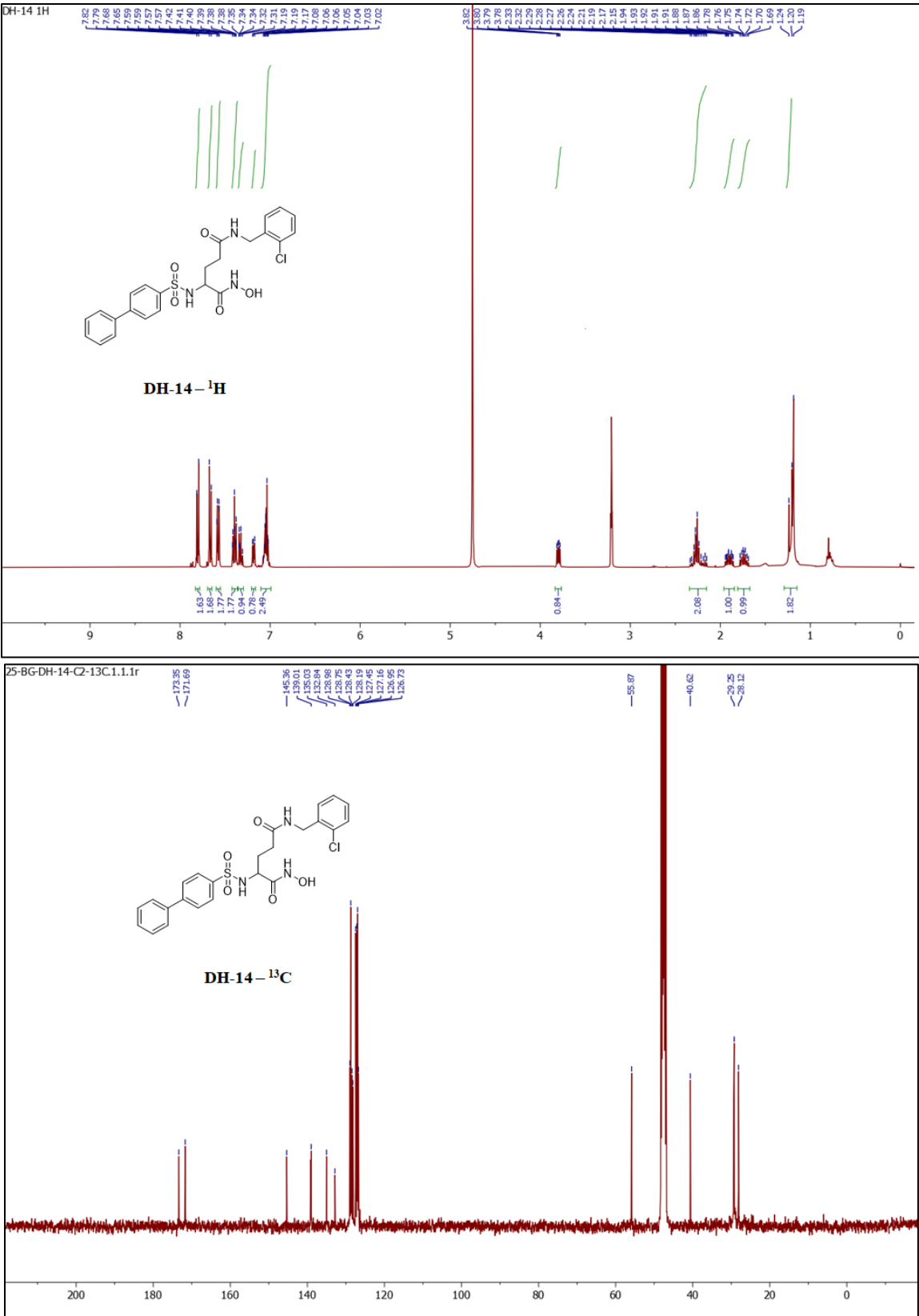


Figure A30. ^1H and ^{13}C NMR Spectra of Compound DH-14.

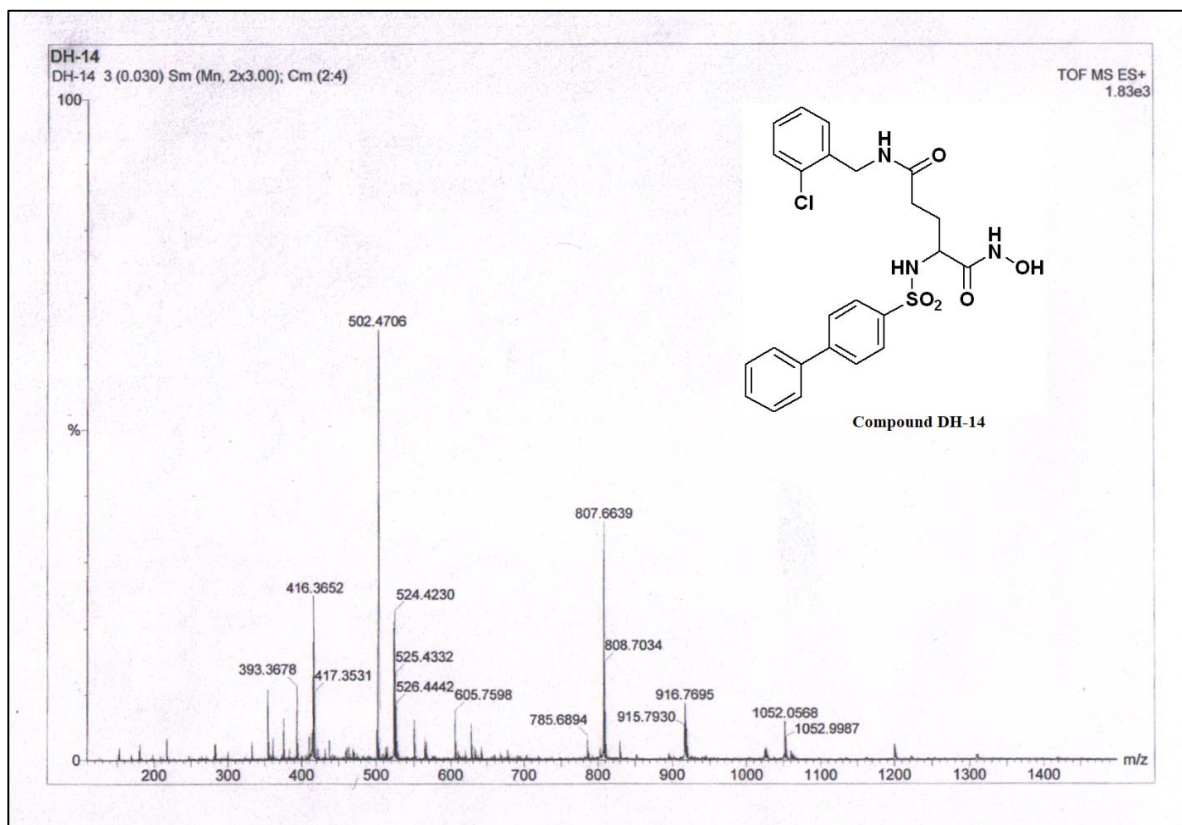


Figure A31. HRMS Spectra of Compound DH-14.

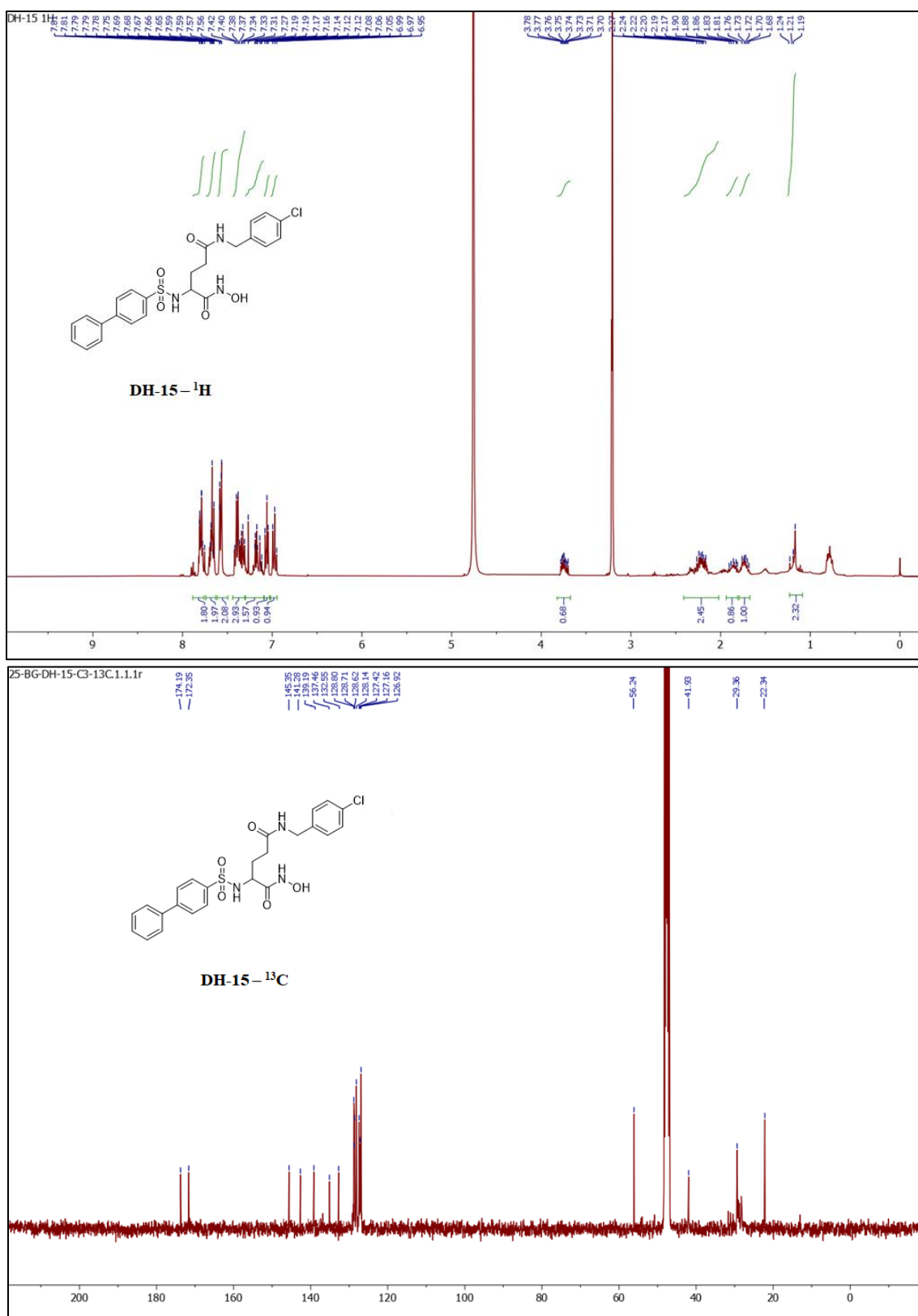


Figure A32. ¹H and ¹³C NMR Spectra of Compound DH-15.

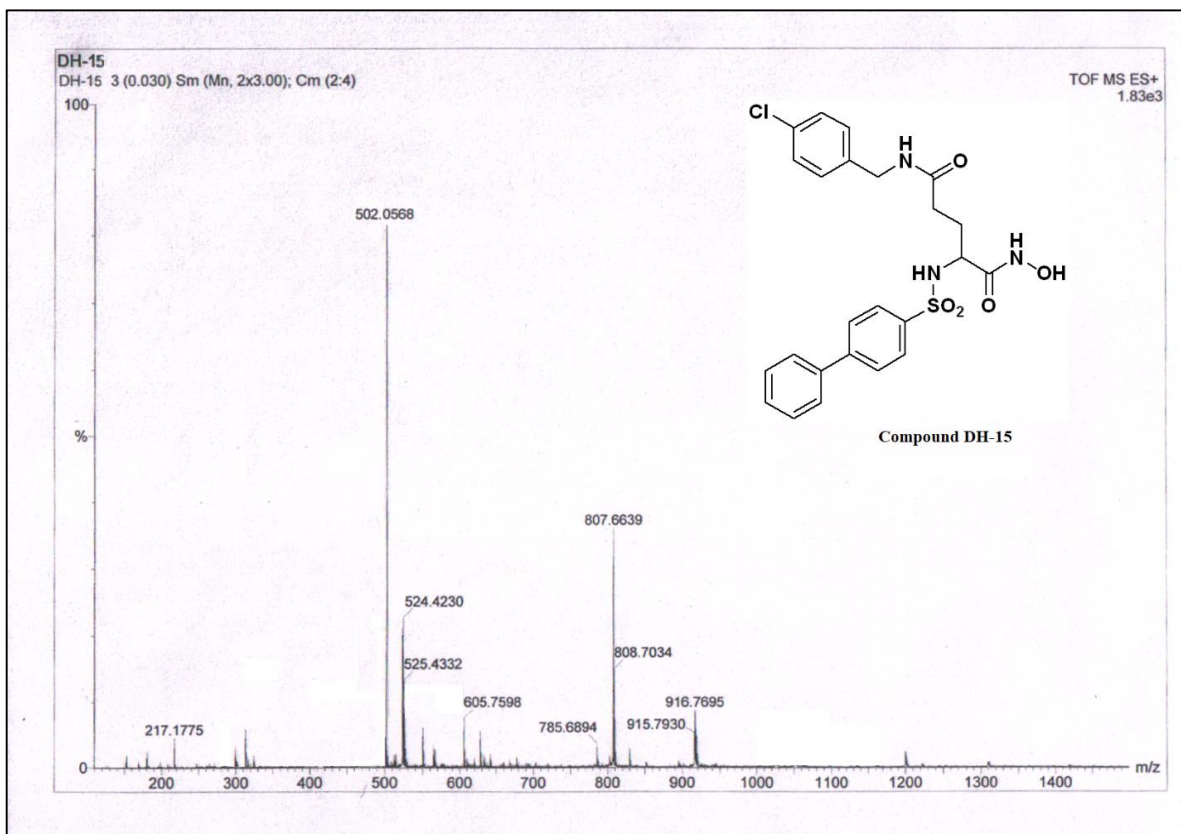


Figure A33. HRMS Spectra of Compound DH-15.

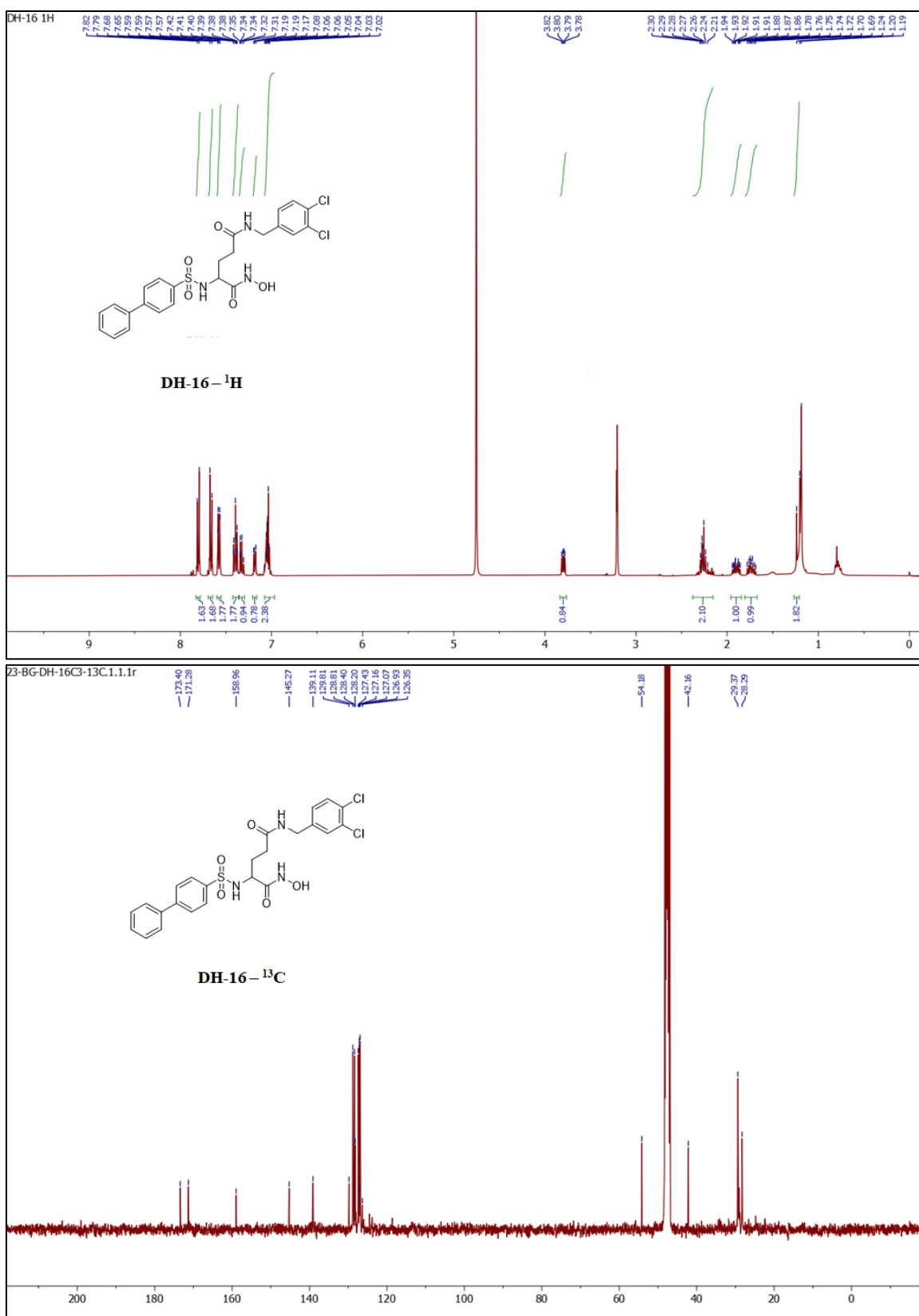


Figure A34. ¹H and ¹³C NMR Spectra of Compound DH-16.

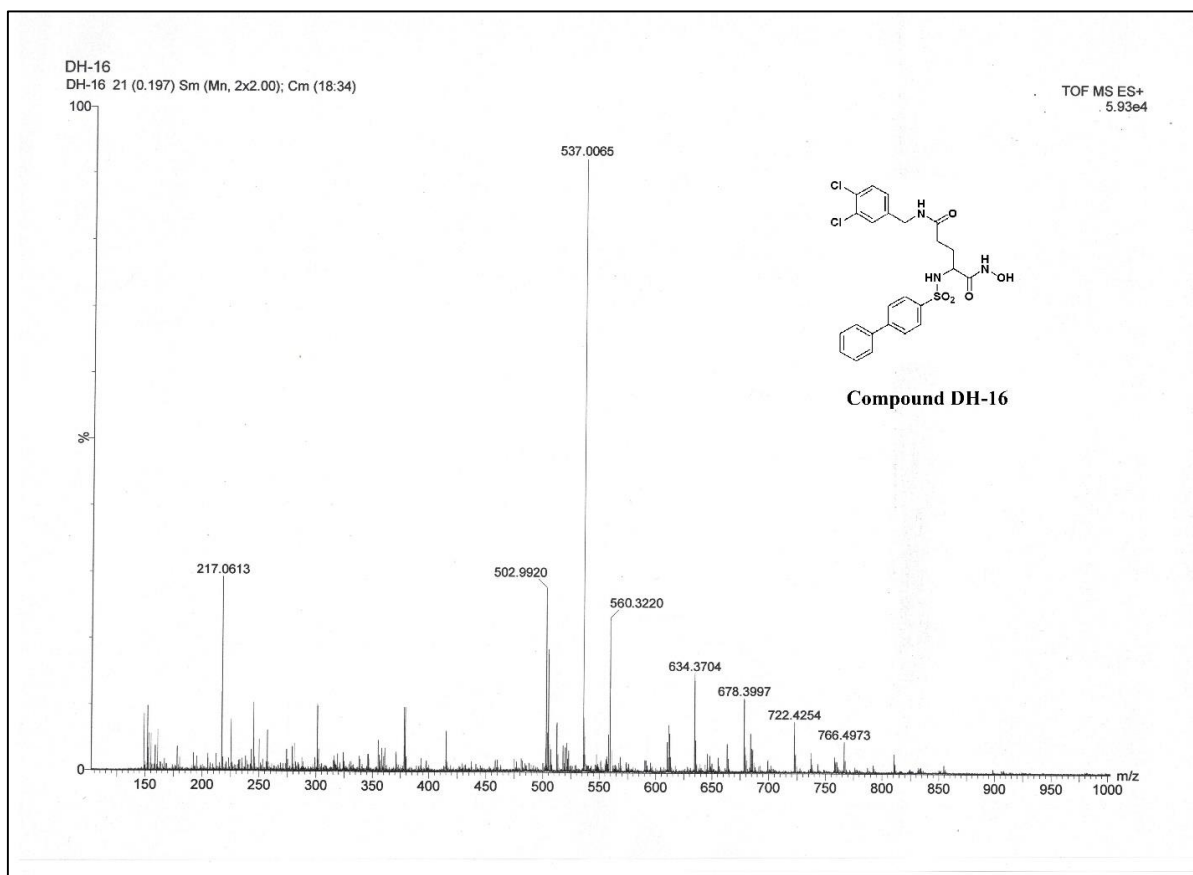


Figure A35. HRMS Spectra of Compound DH-16.

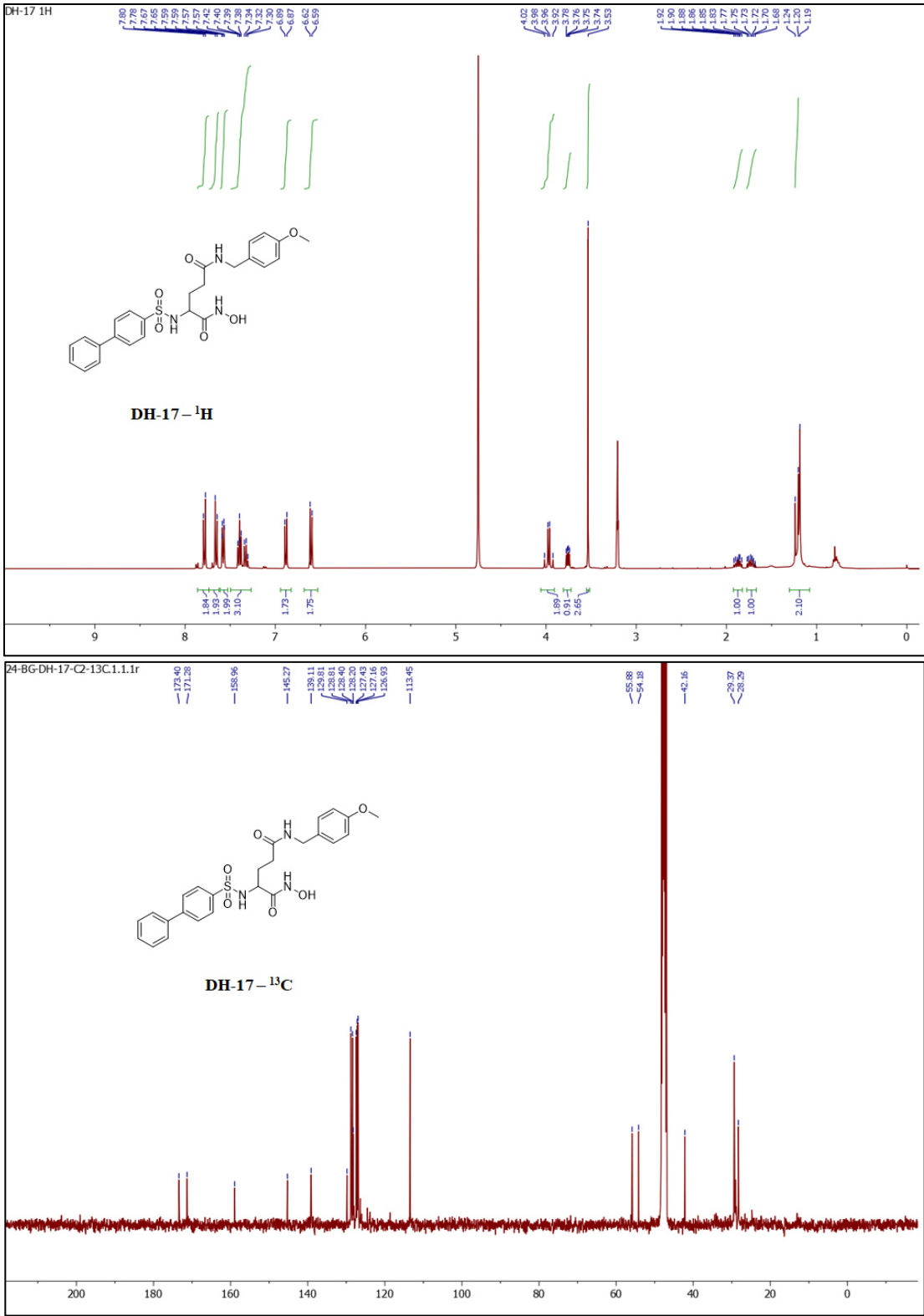


Figure A36. ^1H and ^{13}C NMR Spectra of Compound DH-17.

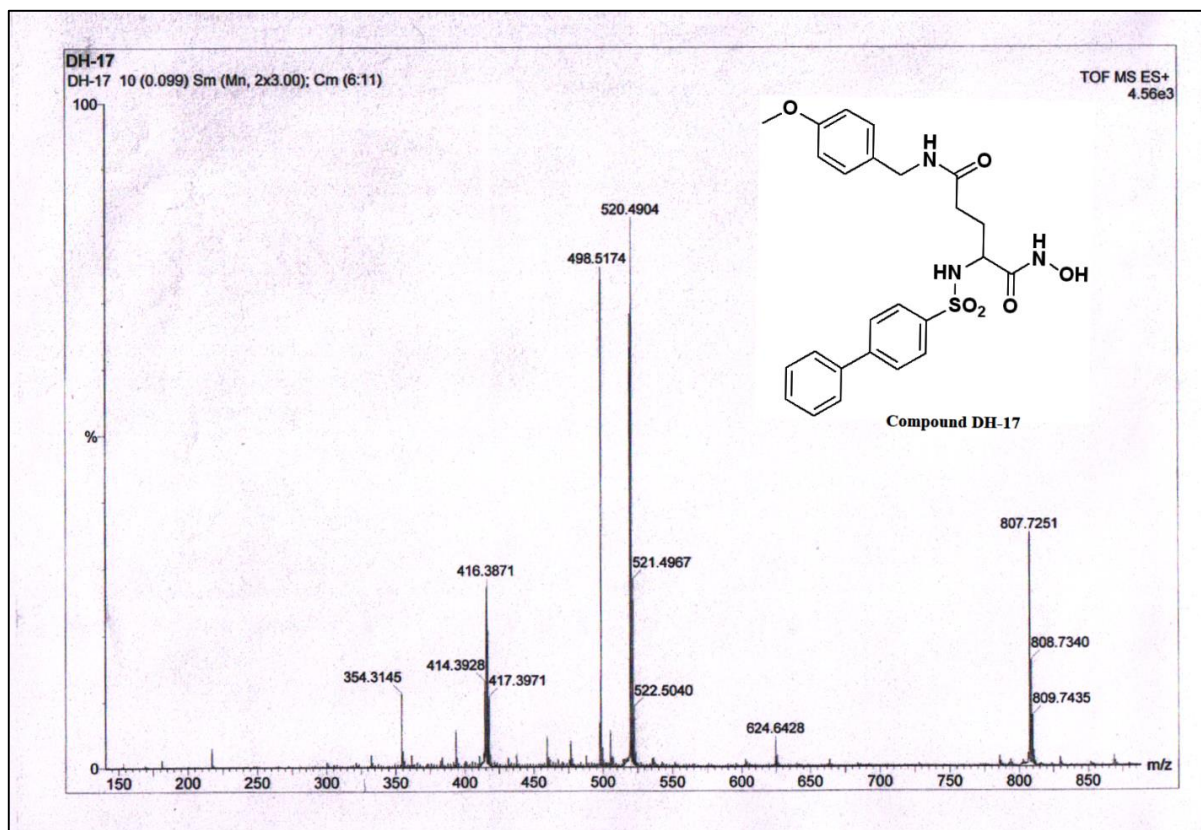


Figure A37. HRMS Spectra of Compound DH-17.

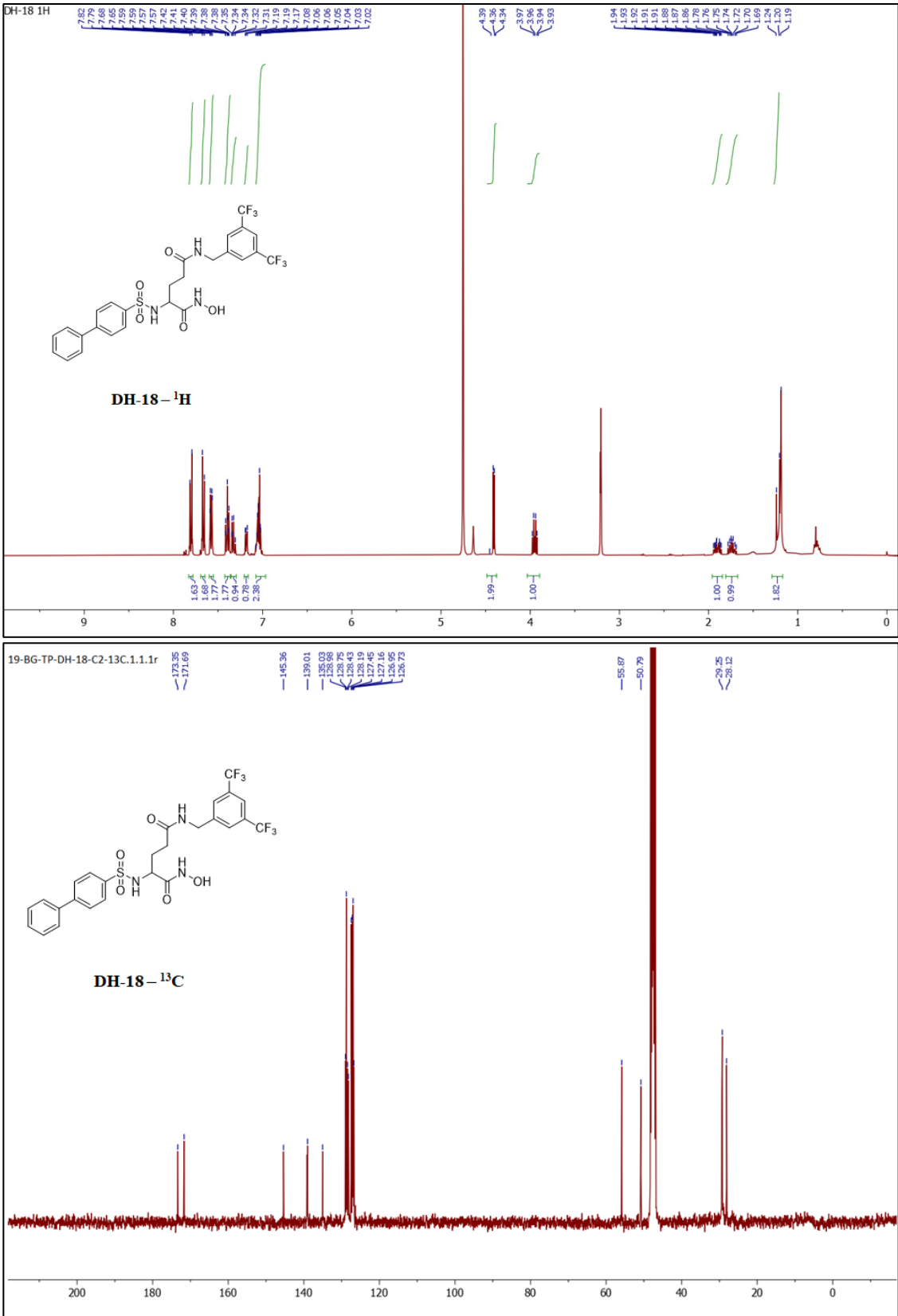


Figure A38. ^1H and ^{13}C NMR Spectra of Compound DH-18.

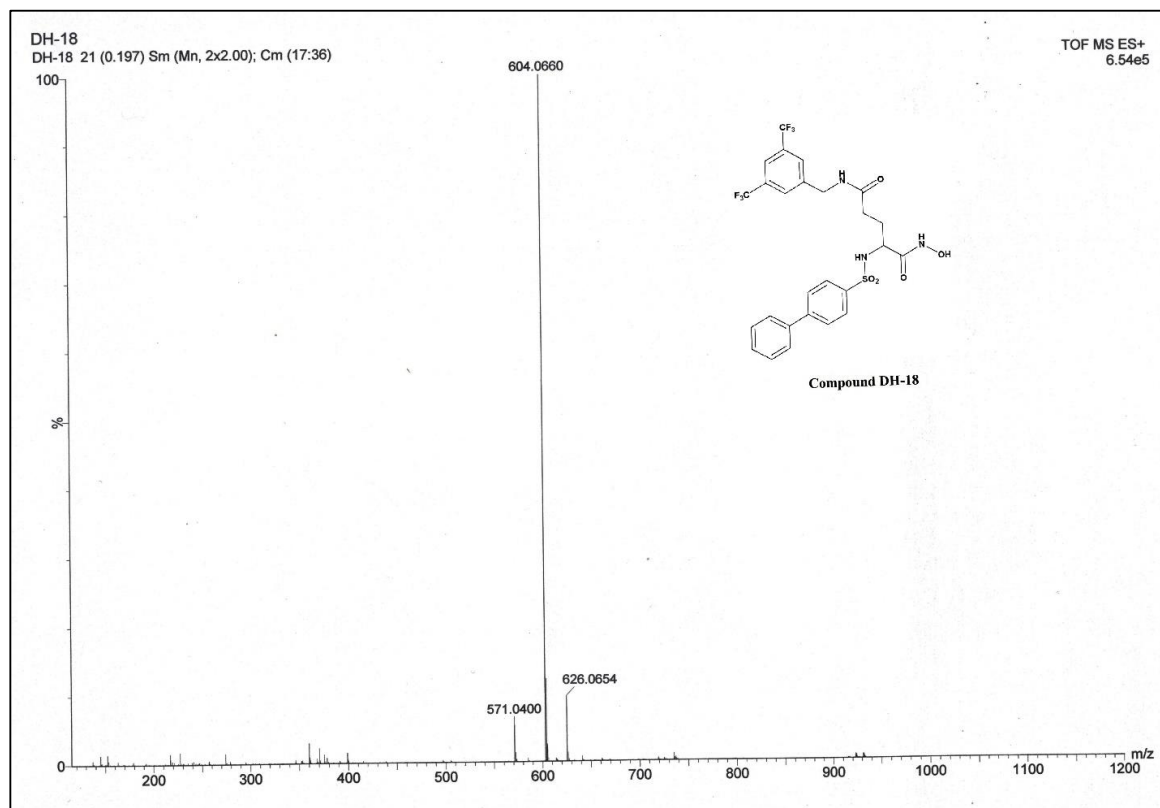
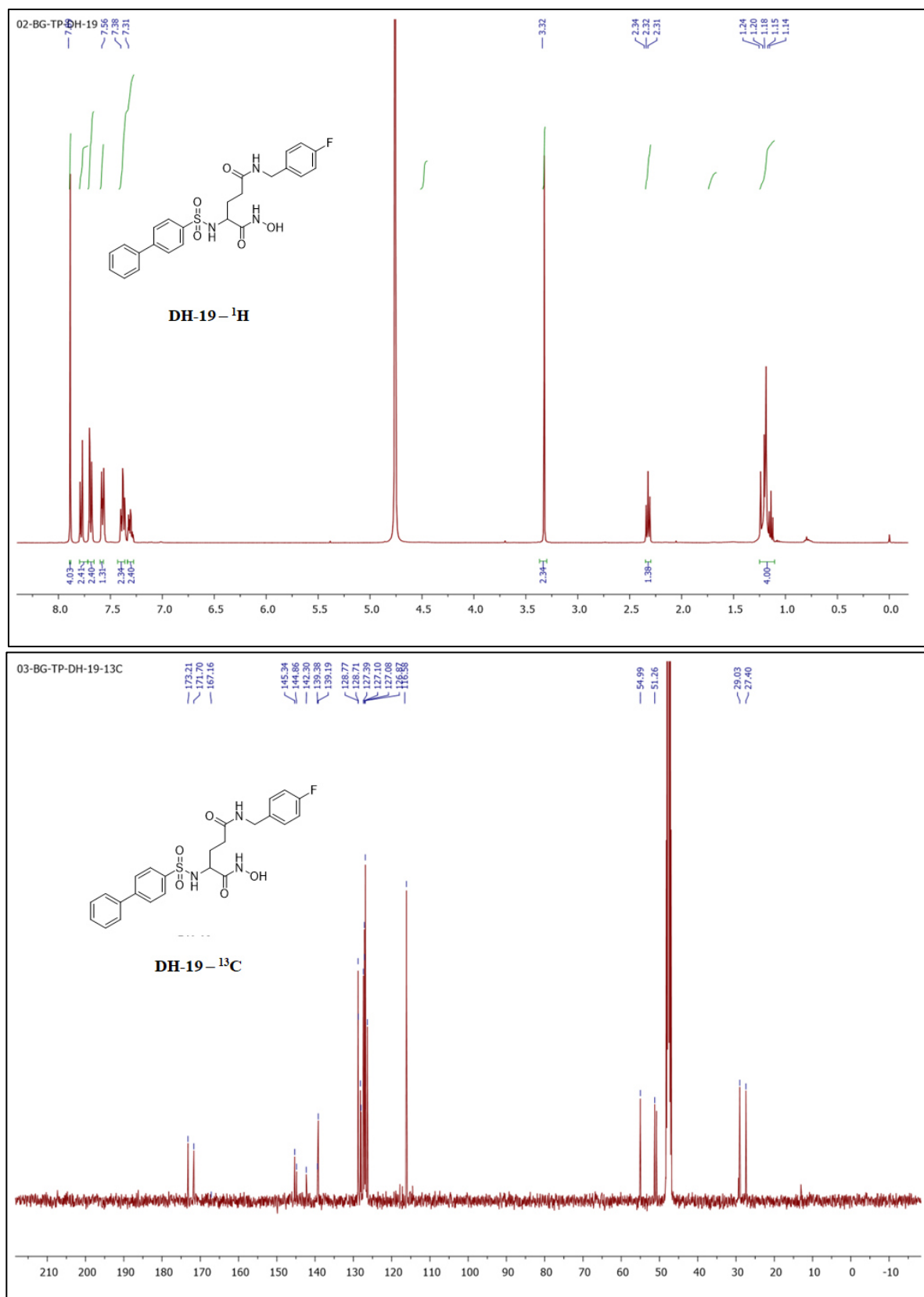


Figure A39. HRMS Spectra of Compound DH-18.

**Figure A40.** ^1H and ^{13}C NMR Spectra of Compound DH-19.

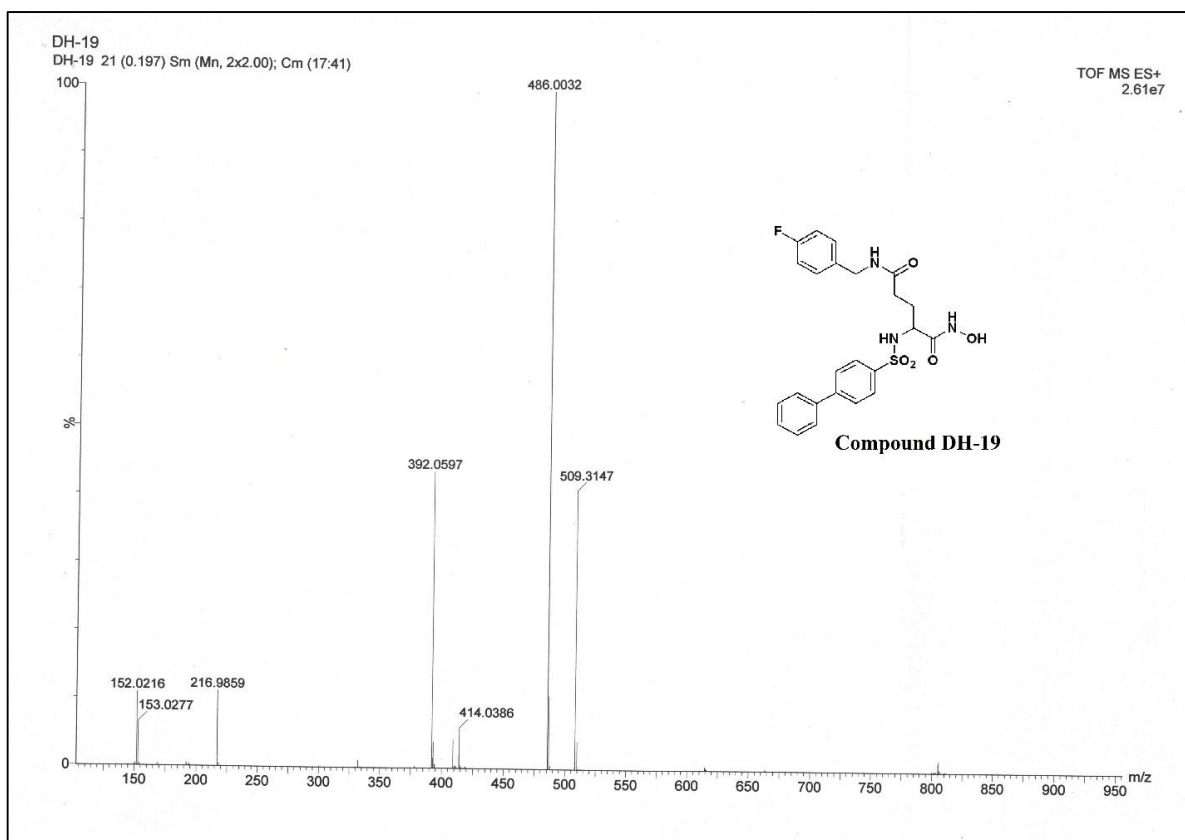


Figure A41. HRMS Spectra of Compound DH-19.

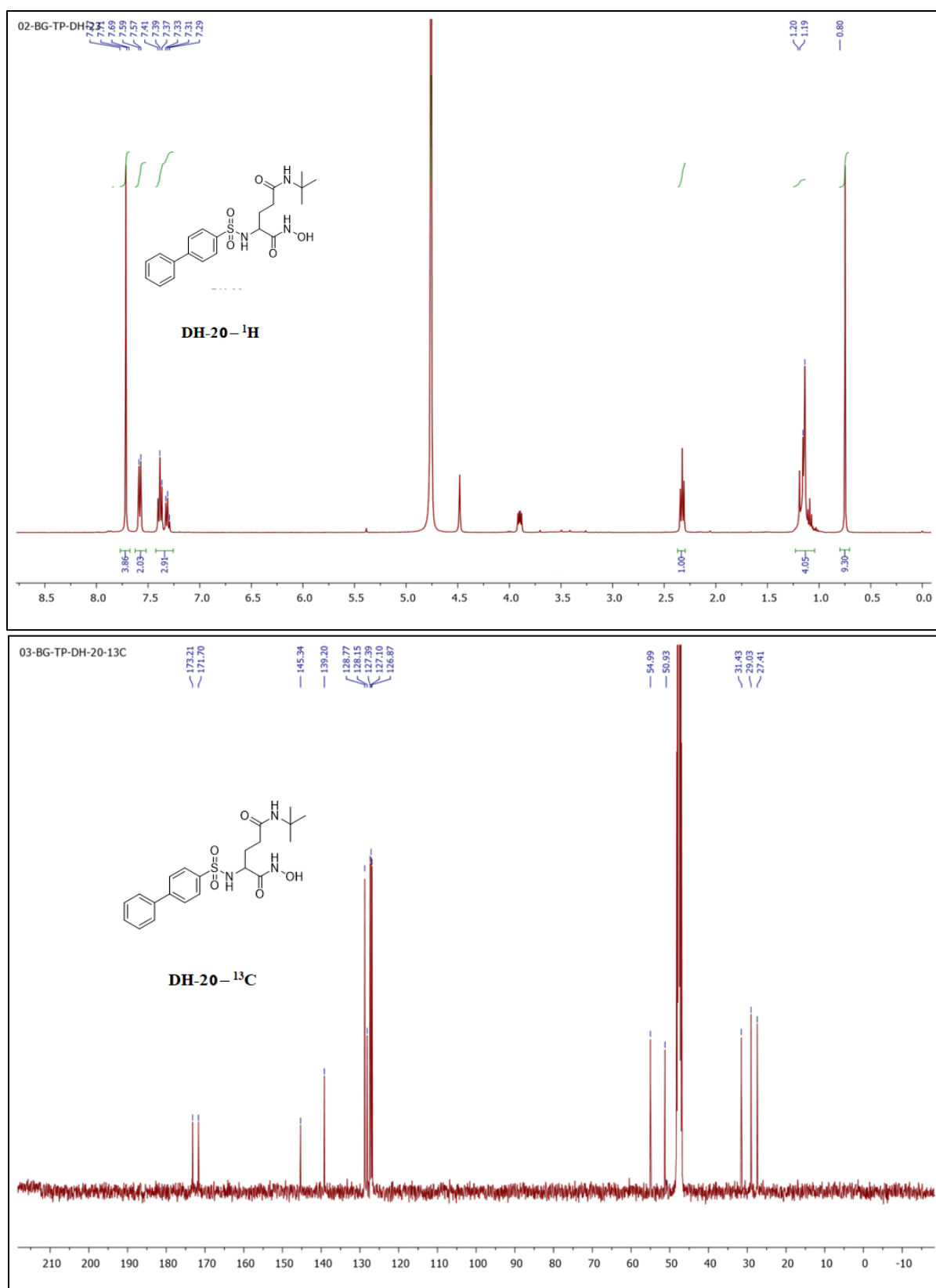


Figure A42. ¹H and ¹³C NMR Spectra of Compound DH-20.

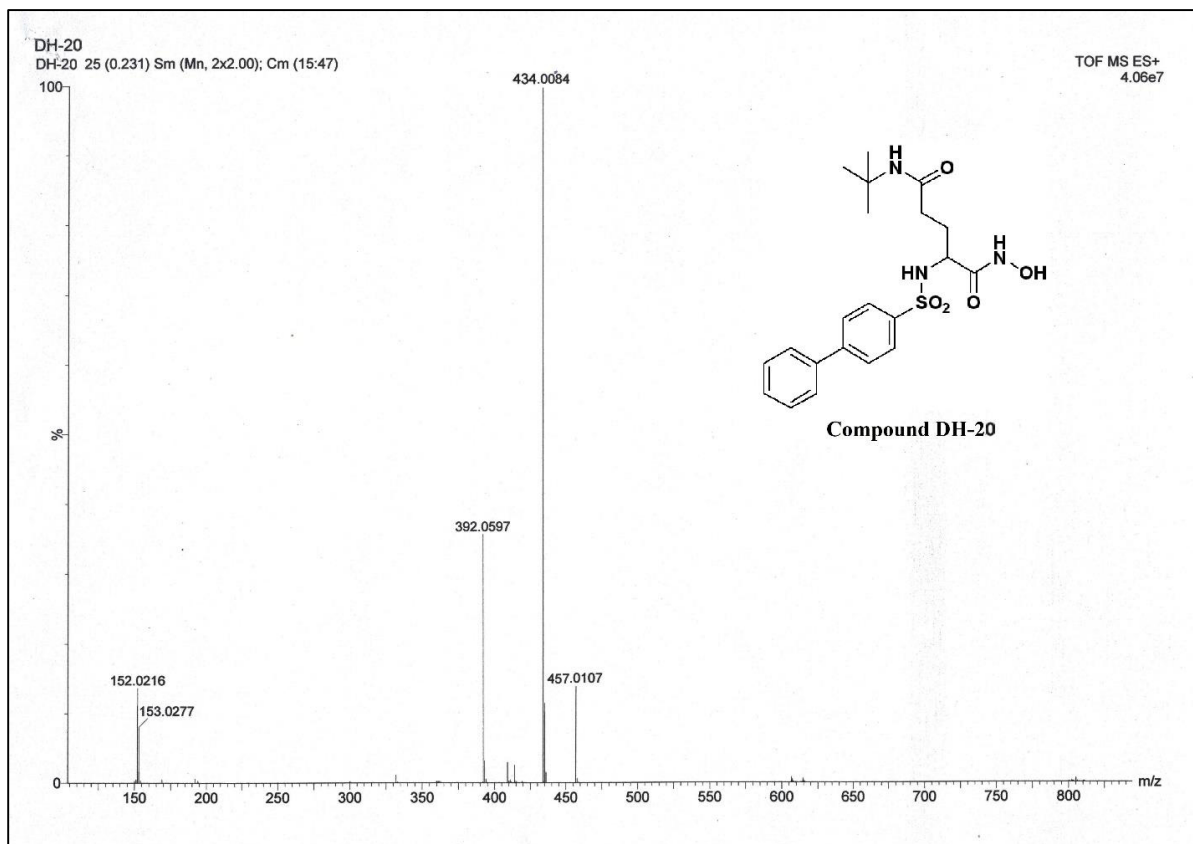


Figure A43. HRMS Spectra of Compound DH-20.

Table A1. Observed vs predicted MMP-2 inhibitory activity for all the first datasets molecules as per the MLR, HQSAR, and CoMSIA model.

<i>Compound</i>	<i>Observed (pIC₅₀)</i>	<i>MLR</i>	<i>HQSAR</i>	<i>CoMSIA Predicted</i>
1a	8.523	8.565	9.031	8.41
2a	8.222	8.565	8.474	8.635
3a	8.097	8.161	8.72	8.206
4a	8.097	8.565	8.432	8.629
5a	7.959	8.161	8.163	8.413
6a	7.921	8.161	8.121	8.413
7a	7	6.664	6.461	6.458
8a	7	6.664	6.819	6.61
9a	6.699	6.259	6.508	6.57
10a	6.699	6.664	6.262	6.466
11a	6.523	6.664	6.22	6.386
12a	6.398	5.933	6.461	5.895
13a	6.097	6.259	6.149	6.248
14a	5.959	6.259	5.951	6.294
15a	5.824	6.259	5.909	6.174
16a	5.699	5.528	6.149	5.766
17a	5.149	5.522	5.459	5.261
18a	5.022	4.791	5.459	4.998
19a	8.398	8.161	8.059	8.548
20a	8.155	7.806	7.939	7.457
21a	8	7.401	7.223	7.14
22a	7.699	7.424	7.352	7.518
23a	7.398	7.401	7.628	6.933
24a	7.398	7.52	7.065	7.06
25a	7.301	7.401	7.534	7.331
26a	7.046	7.116	6.753	6.6
27a	6.699	6.664	6.938	6.253
28a	6.699	6.664	6.349	6.791
29a	6.301	6.379	6.063	5.649
30a	6.155	6.259	6.532	6.132
31a	5.886	6.259	6.038	6.592
32a	5.82	4.939	5.461	5.722
33a	5.658	6.081	6.463	5.83
34a	5.569	5.676	6.151	6.199
35a	5.495	6.081	5.78	6.774
36a	5.456	5.676	5.468	6.571
37a	5.284	4.939	4.778	5.62
38a	5.051	5.522	5.348	5.587
39a	8.699	8.565	8.371	8.025
40a	6.569	5.933	5.95	5.798
41a	6.367	5.933	6.37	6.122

42a	6.337	5.933	5.994	5.994
43a	6.284	5.933	5.657	5.833
44a	6.143	5.933	6.077	6.272
45a	6.119	5.933	5.701	5.88
46a	6.06	5.933	5.865	5.956
47a	6.009	5.933	6.285	6.505
48a	5.987	5.933	5.909	5.918
49a	5.893	5.933	5.799	5.788
50a	5.818	5.528	5.554	5.69
51a	5.742	5.933	5.806	5.772
52a	5.712	5.933	5.506	4.922
53a	5.688	5.933	5.714	5.275
54a	5.684	5.528	5.973	5.416
55a	5.635	5.528	5.597	5.729
56a	5.567	5.933	5.513	5.864
57a	5.53	5.933	5.721	5.867
58a	5.474	5.933	5.897	5.502
59a	5.378	5.933	5.604	5.763
60a	5.361	5.933	5.812	5.578
61a	5.283	5.528	5.403	5.682
62a	5.24	5.528	5.41	6.824
63a	5.129	5.528	5.5	5.756
64a	6.991	6.503	7.073	7.115
65a	6.74	6.503	6.673	6.849

ANNEXURE

Biphenylsulfonamides as effective MMP-2 inhibitors with promising antileukemic efficacy: Synthesis, in vitro biological evaluation, molecular docking, and MD simulation analysis

Sandip K. Baidya^{1,2} | Tarun Patel³ | Ambati Himaja³ | Suvankar Banerjee¹ |
Sanjib Das^{1,2} | Balaram Ghosh³ | Tarun Jha¹  | Nilanjan Adhikari¹ 

¹Division of Medicinal and Pharmaceutical Chemistry, Department of Pharmaceutical Technology, Natural Science Laboratory, Jadavpur University, Kolkata, India

²School of Pharmacy, Sister Nivedita University, Kolkata, India

³Department of Pharmacy, Epigenetic Research Laboratory, Birla Institute of Technology and Science-Pilani, Hyderabad, India

Correspondence

Nilanjan Adhikari and Tarun Jha, Natural Science Laboratory, Division of Medicinal and Pharmaceutical Chemistry, Department of Pharmaceutical Technology, Jadavpur University, Kolkata, India.
Email: nilanjan_juphar@rediffmail.com and tjuphar@yahoo.com

Balaram Ghosh, Department of Pharmacy, Epigenetic Research Laboratory, Birla Institute of Technology and Science-Pilani, Hyderabad Campus, Shamirpet, Hyderabad 500078, India.
Email: balaram@hyderabad.bits-pilani.ac.in

Funding information

Department of Health Research, India; Indian Council of Medical Research

Abstract

Overexpression of matrix metalloproteinase-2 (MMP-2) possesses a correlation with leukemia especially chronic myeloid leukemia (CML). However, no such MMP-2 inhibitor has come out in the market to date for treating leukemia. In this study, synthesis, biological evaluation, and molecular modeling studies of a set of biphenylsulfonamide derivatives as promising MMP-2 inhibitors were performed, focusing on their potential applications as antileukemic therapeutics. Compounds DH-18 and DH-19 exerted the most effective MMP-2 inhibition (IC₅₀ of 139.45 nM and 115.16 nM, respectively) with potent antileukemic efficacy against the CML cell line K562 (IC₅₀ of 0.338 μM and 0.398 μM, respectively). The lead molecules DH-18 and DH-19 reduced the MMP-2 expression by 21.3% and 17.8%, respectively with effective apoptotic induction (45.4% and 39.8%, respectively) in the K562 cell line. Moreover, both these compounds significantly arrested different phases of the cell cycle. Again, both these molecules depicted promising antiangiogenic efficacy in the ACHN cell line. Nevertheless, the molecular docking and molecular dynamics (MD) simulation studies revealed that DH-18 formed strong bidentate chelation with the catalytic Zn²⁺ ion through the hydroxamate zinc binding group (ZBG). Apart from that, the MD simulation study also disclosed stable binding interactions of DH-18 and MMP-2 along with crucial interactions with active site amino acid residues namely His120, Glu121, His124, His130, Pro140, and Tyr142. In a nutshell, this study highlighted the importance of biphenylsulfonamide-based novel and promising MMP-2 inhibitors to open up a new avenue for potential therapy against CML.

KEYWORDS

angiogenesis, apoptosis, biphenylsulfonamides, CML, leukemia, MMP-2

1 | INTRODUCTION

Matrix metalloproteinases (MMPs), playing a major role in various disease conditions, are essential components of the extracellular matrix (ECM) (Page-McCaw et al., 2007). After a long journey to become recognized as the primary mediators of the ECM, MMPs

were initially discovered to play crucial roles in the metamorphosis of the anuran tadpole matrix (Gross & Lapiere, 1962; Gross & Nagai, 1965). In addition, MMPs are members of the metzincin family of metalloenzymes, which utilize the Zn²⁺ ion in their active site. The MMP family of zinc-dependent metalloenzymes consists of 26 members, and each has a variety of physiological and pathological



Pinpointing prime structural attributes of potential MMP-2 inhibitors comprising alkyl/arylsulfonyl pyrrolidine scaffold: a ligand-based molecular modelling approach validated by molecular dynamics simulation analysis

S.K. Baidya ^{a#}, S. Banerjee ^a, B. Ghosh ^b, T. Jha ^a and N. Adhikari ^a

^aNatural Science Laboratory, Division of Medicinal and Pharmaceutical Chemistry, Department of Pharmaceutical Technology, Jadavpur University, Kolkata, India; ^bEpigenetic Research Laboratory, Department of Pharmacy, Birla Institute of Technology and Science-Pilani, Hyderabad, India

ABSTRACT

MMP-2 overexpression is strongly related to several diseases including cancer. However, none of the MMP-2 inhibitors have been marketed as drug candidates due to various adverse effects. Here, a set of sulphonyl pyrrolidines was subjected to validation of molecular modelling followed by binding mode analysis to explore the crucial structural features required for the discovery of promising MMP-2 inhibitors. This study revealed the importance of hydroxamate as a potential zinc-binding group compared to the esters. Importantly, hydrophobic and sterical substituents were found favourable at the terminal aryl moiety attached to the sulphonyl group. The binding interaction study revealed that the S1' pocket of MMP-2 similar to '*a basketball passing through a hoop*' allows the aryl moiety for proper fitting and interaction at the active site to execute potential MMP-2 inhibition. Again, the sulphonyl pyrrolidine moiety can be a good fragment necessary for MMP-2 inhibition. Moreover, some novel MMP-2 inhibitors were also reported. They showed the significance of the 3rd position substitution of the pyrrolidine ring to produce interaction inside S2' pocket. The current study can assist in the design and development of potential MMP-2 inhibitors as effective drug candidates for the management of several diseases including cancers in the future.

ARTICLE HISTORY

Received 5 June 2024
Accepted 2 August 2024

KEYWORDS

MMP-2; HQSAR; Bayesian classification; CoMSIA; molecular docking; MD simulation

Introduction

Matrix metalloproteinases (MMPs) belong to the family of endopeptidases that are dependent on metal ions such as zinc and calcium and these MMPs are structurally and functionally related. MMPs are essential for the breakdown of the components of extracellular matrix (ECM), the remodelling of tissue, as well as the pathogenesis related to different diseases [1]. Furthermore, MMPs play a versatile role in a variety of physiological functions, like ovulation, development of embryos, angiogenesis, cellular diversity, as well

CONTACT N. Adhikari nilanjan_juphar@rediffmail.com

[#]Present Address: School of Pharmacy, Sister Nivedita University, DG Block (New Town), Action Area 1, 1/2, Newtown, Chakpachuria, Kolkata - 700156, India.

Supplemental data for this article can be accessed at: <https://doi.org/10.1080/1062936X.2024.2389822>

© 2024 Informa UK Limited, trading as Taylor & Francis Group



Research paper

Derivatives of *D*(–) glutamine-based MMP-2 inhibitors as an effective remedy for the management of chronic myeloid leukemia-Part-I: Synthesis, biological screening and *in silico* binding interaction analysis

Sanjib Das^{a,1}, Subha Mondal^a, Tarun Patel^b, Ambati Himaja^b, Nilanjan Adhikari^{a,**},
Suvankar Banerjee^a, Sandip Kumar Baidya^{a,1}, Asit Kumar De^c, Shovanlal Gayen^d,
Balaram Ghosh^{b,***}, Tarun Jha^{a,*}

^a Natural Science Laboratory, Division of Medicinal and Pharmaceutical Chemistry, Department of Pharmaceutical Technology, Jadavpur University, Kolkata, 700032, India

^b Epigenetic Research Laboratory, Department of Pharmacy, Birla Institute of Technology and Science-Pilani, Hyderabad, India

^c Department of Chemistry, Jadavpur University, Kolkata, India

^d Laboratory of Drug Design and Discovery, Department of Pharmaceutical Technology, Jadavpur University, Kolkata, 700032, India

ARTICLE INFO

Keywords:

D-glutamine derivatives
MMP-2
Chronic myeloid leukemia
Gelatinase
Apoptosis
Angiogenesis
Binding mode of interaction

ABSTRACT

Chronic myeloid leukemia (CML) is a global issue and the available drugs such as tyrosine kinase inhibitors (TKIs) comprise various toxic effects as well as resistance and cross-resistance. Therefore, novel molecules targeting specific enzymes may unravel a new direction in antileukemic drug discovery. In this context, targeting gelatinases (MMP-2 and MMP-9) can be an alternative option for the development of novel molecules effective against CML. In this article, some *D*(–)glutamine derivatives were synthesized and evaluated through cell-based antileukemic assays and tested against gelatinases. The lead compounds, i.e., benzyl analogs exerted the most promising antileukemic potential showing nontoxicity in normal cell line including efficacious gelatinase inhibition. Both these lead molecules yielded effective apoptosis and displayed marked reductions in MMP-2 expression in the K562 cell line. Not only that, but both of them also revealed effective antiangiogenic efficacy. Importantly, the most potent MMP-2 inhibitor, i.e., benzyl derivative of *p*-tosyl *D*(–)glutamine disclosed stable binding interaction at the MMP-2 active site correlating with the highly effective MMP-2 inhibitory activity. Therefore, such *D*(–)glutamine derivatives might be explored further as promising MMP-2 inhibitors with efficacious antileukemic profiles for the treatment of CML in the future.

1. Introduction

Chronic myelogenous leukemia (CML) is one of the most common forms of leukemia. The American Cancer Society reported a total of 1280 recorded fatalities and an anticipated 9280 new incidences of CML diagnosed in the United States in 2024 [1]. Notably, hematopoietic stem cells (HSCs) are affected by CML, like in other leukemias [2]. The translocation's breakpoints result in the fusion of two genes: breakpoint cluster region (BCR) on chromosome 22 and Abelson murine leukemia viral oncogene homolog 1 (ABL1) on chromosome 9. A key factor in the

pathophysiology of CML is the Philadelphia chromosome, which fundamentally stimulates tyrosine kinase (TK) via the BCR-ABL1 oncoprotein [2–4]. Tyrosine kinase inhibitors (TKIs) have changed the way CML is treated, and these are widely acknowledged [5]. Before TKIs were developed, CML was a disease with a high death rate for a longer period. Despite the adverse effects related to TKIs, these are still the first-line drugs for the treatment of CML, and the life expectancies of the patients are now similar to those of people without disease conditions [6–9]. However, the choice of physicians for TKI therapy is influenced by several criteria, including the patient's condition and several factors

* Corresponding author.

** Corresponding author.

*** Corresponding author.

E-mail addresses: nilanjan_juphar@rediffmail.com (N. Adhikari), balaram@hyderabad.bits-pilani.ac.in (B. Ghosh), tjupharm@yahoo.com (T. Jha).

¹ Present Address: School of Pharmacy, Sister Nivedita University, DG Block (New Town), Action Area 1, 1/2, Newtown, Chakpachuria, Kolkata - 700156, India.

REVIEW



An updated patent review of matrix metalloproteinase (MMP) inhibitors (2021-present)

Suvankar Banerjee , Sandip Kumar Baidya , Nilanjan Adhikari  and Tarun Jha 

Natural Science Laboratory, Division of Medicinal and Pharmaceutical Chemistry, Department of Pharmaceutical Technology, Jadavpur University, Kolkata, India

ABSTRACT

Introduction: Matrix metalloproteinases (MMPs) are strongly interlinked with the progression and mechanisms of several life-threatening diseases including cancer. Thus, novel MMP inhibitors (MMPIs) as promising drug candidates can be effective in combating these diseases. However, no MMPIs are marketed to date due to poor pharmacokinetics and lower selectivity. Therefore, this review was performed to study the newer MMPIs patented after the COVID-19 period for an updated perspective on MMPIs.

Areas covered: This review highlights patents related to MMPIs, and their therapeutic implications published between January 2021 and August 2023 available in the Google Patents, Patentscope, and Espacenet databases.

Expert opinion: Despite various MMP-related patents disclosed up to 2020, newer patent applications in the post-COVID-19 period decreased a lot. Besides major MMPs, other isoforms (i.e. MMP-3 and MMP-7) have gained attention recently for drug development. This may open up newer dimensions targeting these MMPs for therapeutic advancements. The isoform selectivity and bioavailability are major concerns for effective MMPI development. Thus, adopting theoretical approaches and experimental methodologies can unveil the development of novel MMPIs with improved pharmacokinetic profiles. Nevertheless, the involvement of MMPs in cancer, and the mechanisms of such MMPs in other diseases should be extensively studied for novel MMPI development.

ARTICLE HISTORY

Received 15 September 2023

Accepted 14 November 2023

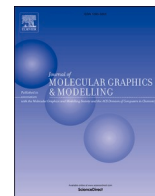
KEYWORDS

MMP; diseases; cancer; MMP inhibitor; clinical trials; binding interaction pattern

1. Introduction

Matrix metalloproteinases (MMPs), degrading various components of extracellular matrix (ECM), are found to be crucially interlinked with the modulation of normal physiological processes as well as versatile pathophysiological conditions and thus, have been established as promising biomolecular targets for the design and development of potential drug candidates to get rid of numerous life-threatening diseases [1]. In this context, the process of development of matrix metalloproteinase inhibitors (MMPIs) was initiated more than 30 years ago and continued to date [2–4]. However, such MMPIs failed to overcome the expectation to become drug candidates, though several extensive clinical studies were conducted [5]. Despite the setback of such MMPIs, research is still in progress as far as the patenting is concerned for the development of potential MMPIs suggesting their crucial implications to crusade against major classes of diverse disease conditions such as cancers, cardiovascular and neurological diseases, inflammatory conditions and immunological diseases [6–13]. Now, it has been already established that initial clinical studies were conducted in a premature fashion leading to erroneous conclusions as far as the wrong animal model studies were concerned [14]. Not only was that, but most clinical

studies were carried out considering those compounds exploring poor bioavailability, poor metabolic properties as well as broad-spectrum of MMP inhibition including inhibition of other classes of metalloenzymes [15]. The first-generation MMPIs are devoid of specificity toward specific MMPs and therefore, these MMPIs were found to exert numerous dose-mediated adverse effects such as arthralgia, musculoskeletal syndrome (MSS), myalgia, and gastrointestinal disorders [16]. Despite the crucial roles of each MMP in various disease states, structural similarity among them may be one of the prime reasons making the inhibitor designing approaches tremendously challenging that hinders overcoming such unintended adverse effects [17]. Mostly, the 1st generation MMPIs belong to the category of hydroxamate class. As the hydroxamate group has a poor selective feature as far as Zn²⁺ chelation is concerned, MMPIs comprising such zinc binding group (ZBG) are also often found to chelate strongly with the Zn²⁺ ion of other metalloenzymes namely A Disintegrin And Metalloprotease (ADAM) [18], carbonic anhydrases (CAs) [19], aggrecanases [20], meprins [21], etc. and subsequent inhibition. Nevertheless, the hydroxamate group may metabolically produce other lesser effective carboxylic acids or amides to induce the liberation of toxic hydroxylamine [9].



A fragment-based exploration of diverse MMP-9 inhibitors through classification-dependent structural assessment

Sandip Kumar Baidya^a, Suvankar Banerjee^a, Balaram Ghosh^b, Tarun Jha^{a, **},
Nilanjan Adhikari^{a, *}

^a Natural Science Laboratory, Division of Medicinal and Pharmaceutical Chemistry, Department of Pharmaceutical Technology, Jadavpur University, Kolkata, 700032, India

^b Epigenetic Research Laboratory, Department of Pharmacy, Birla Institute of Technology and Science-Pilani, Hyderabad Campus, Shamirpet, Hyderabad, 500078, India

ARTICLE INFO

Keywords:

MMP-9
Binding affinity
Bayesian classification
LDA
SARpy
Recursive partitioning

ABSTRACT

Matrix metalloproteinases (MMPs) are belonging to the Zn^{2+} -dependent metalloenzymes. These can degenerate the extracellular matrix (ECM) that is entailed with various biological processes. Among the MMP family members, MMP-9 is associated with several pathophysiological circumstances. Apart from wound healing, remodeling of bone, inflammatory mechanisms, and rheumatoid arthritis, MMP-9 has also significant roles in tumor invasion and metastasis. Therefore, MMP-9 has been in the spotlight of anticancer drug discovery programs for more than a decade. In this present study, classification-based QSAR techniques along with fragment-based data mining have been carried out on divergent MMP-9 inhibitors to point out the important structural attributes. This current study may be able to elucidate the importance of several pivotal molecular fragments such as sulfonamide, hydroxamate, *i*-butyl, and ethoxy functions for imparting potential MMP-9 inhibition. These observations are in correlation with the ligand-bound co-crystal structures of MMP-9. Therefore, these findings are beneficial for the design and discovery of effective MMP-9 inhibitors in the future.

1. Introduction

Zinc-dependent peptides are found to be encoded by 10 % of the genes in the human genome. Among all the metalloproteins, zinc-dependent proteins are the major part. The zinc ion of metalloenzymes plays a crucial role in the enzyme catalytic activity [1,2]. There are some significant zinc-dependent metalloenzymes like matrix metalloproteinases (MMPs), TNF- α converting enzyme (TACE), carbonic anhydrases (CAs), angiotensin-converting enzyme (ACE), carboxypeptidase A, thermolysin, etc. These metalloproteinases are responsible for executing various biological functions [3–7]. Therefore, these enzymes are an excellent target as they are engaged in a variety of human ailments namely cardiovascular and neurodegenerative disorders, rheumatoid arthritis, and cancer [2]. Regarding drug design and discovery, zinc-dependent metalloenzymes are the most desired and promising target [8]. Moreover, drug design may be beneficial for understanding the contribution of the zinc ion with the drug candidate physiochemically and quantitatively inside the zinc-containing proteins. Among

these metalloenzymes, MMPs, which are under the zinc-dependent endopeptidase classes, are found to be linked with the remodeling of extracellular matrix (ECM) and these are essential for many physiological processes like tissue repairing, morphogenesis, development, tissue homeostasis, etc [8,9]. Moreover, MMPs are associated with the availability of growth factors and take part extensively in cellular signaling to regulate crucial processes such as proliferation, migration, and apoptosis [10]. Generally, all MMPs are released as inactive forms. The ‘cysteine switch’ of MMPs is one of the prime reasons for the activation of MMP where the thiol function is unpaired, and the amino acid residue cysteine is restored with a water molecule [11]. Moreover, in this activation mechanism, the cysteine switch empowers the hydroxylation of the pro-peptide of the relatively activated MMPs. All MMPs are triggered in the cell except MT-MMPs, MMP-11, -23, and -28 [10]. There are 26 different types of MMPs. Their sequential homology as well as the biological consequences have already been reported [12]. MMPs are categorized into 5 distinct classes depending upon their specificity towards the particular substrate. These are (i) collagenase, (ii) gelatinase, (iii)

* Corresponding author.

** Corresponding author.

E-mail addresses: tjupharm@yahoo.com (T. Jha), nilanjan_juphar@rediffmail.com (N. Adhikari).

<https://doi.org/10.1016/j.jmgm.2023.108671>

Received 1 March 2023; Received in revised form 4 November 2023; Accepted 7 November 2023

Available online 11 November 2023

1093-3263/© 2023 Elsevier Inc. All rights reserved.



Assessing structural insights into in-house arylsulfonyl L-(+) glutamine MMP-2 inhibitors as promising anticancer agents through structure-based computational modelling approaches

S.K. Baidya ^a, S. Banerjee ^a, B. Ghosh ^b, T. Jha ^a and N. Adhikari ^a

^aNatural Science Laboratory, Division of Medicinal and Pharmaceutical Chemistry, Department of Pharmaceutical Technology, Jadavpur University, Kolkata, India; ^bEpigenetic Research Laboratory, Department of Pharmacy, Birla Institute of Technology and Science-Pilani, Hyderabad, India

ABSTRACT

MMP-2 is potentially contributing to several cancer progressions including leukaemias. Therefore, considering MMP-2 as a promising target, novel anticancer compounds may be designed. Here, 32 in-house arylsulfonyl L-(+) glutamines were subjected to various structure-based computational modelling approaches to recognize crucial structural attributes along with the spatial orientation for higher MMP-2 inhibition. Again, the docking-based 2D-QSAR study revealed that the Coulomb energy conferred by Tyr142 and total interaction energy conferred by Ala84 was crucial for MMP-2 inhibition. Importantly, the docking-dependent CoMFA and CoMSIA study revealed the importance of favourable steric, electrostatic, and hydrophobic substituents at the terminal phenyl ring. The MD simulation study revealed a lower fluctuation in the RMSD, RMSF, and Rg values indicating stable binding interactions of MMP-2 and these molecules. Moreover, the residual hydrogen bond and their interaction analysis disclosed crucial amino acid residues responsible for forming potential hydrogen bonding for higher MMP-2 inhibition. The results can effectively aid in the design and discovery of promising small-molecule drug-like MMP-2 inhibitors with greater anticancer potential in the future.

ARTICLE HISTORY

Received 3 July 2023



Accepted 17 September 2023


KEYWORDS

Arylsulfonamide; MMP-2; molecular docking-based QSAR; CoMFA; CoMSIA; molecular dynamics simulation

Introduction

Matrix metalloproteinases (MMPs) belong to zinc-dependent endopeptidases that are intimately associated with tissue remodelling, as well as degrading the extracellular matrix (ECM) [1]. Additionally, the activity of MMPs is enhanced in pathogenic circumstances, which causes tissue deterioration. MMPs are protease enzymes and are crucial biomarkers regarding cancer progression [2]. However, among all these MMPs, MMP-2, a key Zn^{2+} -dependent metalloenzyme, is one of the potential biomarkers of several diseases including various cancers, and thus, has already been established as a therapeutically valuable target due to its overexpression in numerous cancer conditions

CONTACT T. Jha  tjupharm@yahoo.com; N. Adhikari  nilanjan_juphar@rediffmail.com

 Supplemental data for this article can be accessed at: <https://doi.org/10.1080/1062936X.2023.2261842>.

© 2023 Informa UK Limited, trading as Taylor & Francis Group



Employing comparative QSAR techniques for the recognition of dibenzofuran and dibenzothiophene derivatives toward MMP-12 inhibition

Jigme Sangay Dorjay Tamang^a, Suvankar Banerjee^a , Sandip Kumar Baidya^a , Balaram Ghosh^b ,
Nilanjan Adhikari^a  and Tarun Jha^a 

^aNatural Science Laboratory, Division of Medicinal and Pharmaceutical Chemistry, Department of Pharmaceutical Technology, Jadavpur University, Kolkata, India; ^bEpigenetic Research Laboratory, Department of Pharmacy, Birla Institute of Technology and Science-Pilani, Hyderabad Campus, Shamirpet, Hyderabad, India

Communicated by Ramaswamy H. Sarma

ABSTRACT

Among various matrix metalloproteinases (MMPs), MMP-12 is one of the potential targets for cancer and other diseases. However, none of the MMP-12 inhibitors has passed the clinical trials to date. Therefore, designing potential MMP-12 inhibitors as new drug molecules can provide effective therapeutic strategies for several diseases. In this study, a series of dibenzofuran and dibenzothiophene derivatives were subjected to different 2D and 3D-QSAR techniques to point out the crucial structural contributions highly influential toward the MMP-12 inhibitory activity. These techniques identified some structural attributes of these compounds that are responsible for influencing their MMP-12 inhibition. The carboxylic group may enhance proper binding with catalytic Zn^{2+} ion at the MMP-12 active site. Again, the *i*-propyl sulfonamido carboxylic acid function contributed positively toward MMP-12 inhibition. Moreover, the dibenzofuran moiety conferred stable binding at the S1' pocket for higher MMP-12 inhibition. The steric and hydrophobic groups were found favourable near the furan ring substituted at the dibenzofuran moiety. Besides these ligand-based approaches, molecular docking and molecular dynamic (MD) simulation studies not only elucidated the importance of several aspects of these MMP-12 inhibitors while disclosing the significance of the finding of these QSAR studies and their influences toward MMP-12 inhibition. The MD simulation study also revealed stable and compact binding between such compounds at the MMP-12 active site. Therefore, the findings of these validated ligand-based and structure-based molecular modeling studies can aid the development of selective and potent lead molecules that can be used for the treatment of MMP-12-associated diseases.

ARTICLE HISTORY

Received 26 April 2023
Accepted 17 July 2023

KEYWORDS

MMP-12; dibenzofuran;
dibenzothiophene; QSAR;
topomer CoMFA; molecular
dynamic simulation

1. Introduction

The matrix metalloproteinases (MMPs) are known to consist of calcium and Zn^{2+} -dependent proteolytic enzymes that are engaged in the physiological and pathological processes in humans (Djuric & Zivkovic, 2017). Though the earlier studies speculated the limited activity of these MMPs against extracellular matrix (ECM), the involvement of these enzymes beyond ECM degradation was later discovered (Djuric & Zivkovic, 2017). Pro-peptide sequences, catalytic metalloproteinase domains with catalytic Zn^{2+} ions, hinge regions or linker peptides, and hemopexin domains are the typical structural components of MMPs (Cui et al., 2017). These MMPs are involved in a variety of pathophysiological conditions, that includes arthritis, cancer, neurodegenerative disorders, cardiovascular diseases, etc. There are 26 members in this protease family and depending on the structural and functional features they are grouped into six different subclasses such as gelatinases, collagenases, stromelysin, matrilysin, membrane-type, and other types of MMPs (Banerjee, Amin, et al., 2022).

Matrix metalloproteinase-12 (MMP-12) resides on chromosome 11q22 and is a member of the matrix metalloproteinase (MMP) family of peptidases called M10 (Guo & Jiang, 2022). MMP-12, which is also familiar as macrophage metalloelastase, was first discovered in 1975 as a form of metalloproteinase produced as a part of an inflammatory reaction (Li et al., 2021). The human MMP-12 that is in its inactive form consists of 54 kDa protein and then after processing it generates around 45 kDa form and then only 22 kDa is obtained as the active form due to loss from N- and C-terminal residues (He et al., 2018). Nonetheless, while MMPs are known to aid tumor formation, MMP-12 has a contentious role in cancer progression (Noel et al., 2021). Additionally, in tumor propagation in the lungs, it acts by cleaving with the elastin which is produced by the activated macrophages that are usually seen in lung diseases like chronic obstructive pulmonary disease (COPD) and emphysema (Ella et al., 2018). So far, very limited knowledge is obtained as to how the immune response can influence an individual with COPD and it may lead to lung cancer (Eide et al., 2016). MMP-12 is



Exploration of structural alerts and fingerprints for novel anticancer therapeutics: a robust classification-QSAR dependent structural analysis of drug-like MMP-9 inhibitors

S. Banerjee ^a, S.K. Baidya ^a, B. Ghosh ^b, T. Jha ^a and N. Adhikari ^a

^aNatural Science Laboratory, Division of Medicinal and Pharmaceutical Chemistry, Department of Pharmaceutical Technology, Jadavpur University, Kolkata, India; ^bEpigenetic Research Laboratory, Department of Pharmacy, Birla Institute of Technology and Science-Pilani, Hyderabad, India

ABSTRACT

Among various matrix metalloproteinases (MMPs), overexpression of MMP9 has been established as a key player in a variety of cancers. Therefore, MMP9 has emerged as a promising biomolecule that may be targeted to design potent inhibitors as novel anticancer therapeutics. In this study, a large database containing 1,123 drug-like MMP-9 inhibitors was considered for robust classification-dependent fragment-based QSAR study through SARpy, Bayesian classification, and recursive partitioning analyses and were validated by both internal and external validation techniques. In a nutshell, all these classification-dependent techniques revealed some common structural alerts and sub-structural fingerprints responsible for modulating MMP-9 inhibition. These observations are in agreement with the interactions obtained from the ligand-bound co-crystal structures of MMP-9 justifying the robustness of the current study. Finally, based on these crucial structural fragments, some new lead compounds were designed and further validated by the binding mode of interaction analysis. Therefore, these findings may be beneficial in designing novel and potential MMP-9 inhibitors in the future as a weapon to combat several cancers.

ARTICLE HISTORY




Received 22 February 2023
Accepted 27 April 2023

KEYWORDS

MMP-9; cancer; classification-based molecular modelling; SARpy; Bayesian classification; recursive partitioning

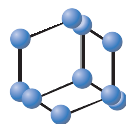
Introduction

Mortality by cancer is the main issue worldwide. Some studies revealed that enzymes like matrix metalloproteinases (MMPs) are the fundamental regulators of tumour microenvironment modification as identified during the cancer progression [1–3]. The MMP family contains 26 structurally related zinc-dependent MMPs [1]. MMPs are managing the disintegration of the extracellular matrix (ECM) and participate in playing key roles in several cellular mechanisms like angiogenesis, embryonic development, and normal tissue remodelling [3]. The enhancement turnover of ECM, metastasis, tumour growth, and angiogenesis are regulated by the signalling pathways related to MMPs due to their proteolytic activity [4]. MMPs are overexpressed in several types of human cancers [1]. Although,

CONTACT T. Jha  tjupharm@yahoo.com; N. Adhikari  nilanjan_juphar@rediffmail.com
 Supplemental data for this article can be accessed at: <https://doi.org/10.1080/1062936X.2023.2209737>

© 2023 Informa UK Limited, trading as Taylor & Francis Group

REVIEW ARTICLE

BENTHAM
SCIENCE

Hydrazides as Potential HDAC Inhibitors: Structure-activity Relationships and Biological Implications

Suvankar Banerjee¹, Sandip Kumar Baidya¹, Nilanjan Adhikari¹, Tarun Jha¹ and Balaram Ghosh^{2,*}

¹Natural Science Laboratory, Division of Medicinal and Pharmaceutical Chemistry, Department of Pharmaceutical Technology, P.O. Box 17020, Jadavpur University, Kolkata, 700032, West Bengal, India; ²Epigenetic Research Laboratory, Department of Pharmacy, Birla Institute of Technology and Science-Pilani, Hyderabad Campus, Shamirpet, Hyderabad, 500078, India

ARTICLE HISTORY

Received: December 13, 2022

Revised: February 03, 2023

Accepted: February 06, 2023

DOI:

10.2174/1568026623666230405124207



CrossMark

Abstract: Epigenetic modulations by HDACs are associated with multiple disease conditions. In this context, HDACs play vital roles in the progression of diseases including several cancers, neurodegenerative diseases, inflammatory diseases, and metabolic disorders. Though several HDAC inhibitors have been established as drug candidates, their usage has been restricted because of broad-spectrum inhibition, highly toxic character, and off-target adverse effects. Therefore, specific HDAC selectivity is essential to get rid of such adverse effects. Hydrazide-based compounds have already been proven to exert higher inhibitory efficacy and specific HDAC selectivity. In this article, the detailed structure-activity relationship (SAR) of the existing hydrazide-based HDAC inhibitors has been elucidated to gather crucial information that can be utilized further for the development of promising drug candidates for combating diverse diseases in the future.

Keywords: Epigenetics, HDAC, HDAC inhibitors, Hydrazide, Structure-activity relationship, Metabolic disorders.

1. INTRODUCTION

Epigenetic modifications are an essential cellular phenomenon regulating gene expression and genetic activity at transcriptional and post-transcriptional levels. Such epigenetic modifications, therefore, influence a wide variety of biological functions such as cellular morphogenesis, cell differentiation, variability as well as adaptability [1-3]. Nevertheless, the DNA methylation and modification of histone core proteins are also inevitable epigenetic modifications for the alteration of the chromatin structure and therefore regulating the genetic activity associated with cellular biology [1, 2]. The study of epigenetics has also disclosed the influences of these various epigenetic modulations related to different diseases and pathological conditions [2-4]. In this context, the acetylation and deacetylation of the histone proteins are crucial epigenetic mechanisms, governing the chromatin structure and gene expression. The two groups of enzymes namely the histone acetyltransferases (HATs) and the histone deacetylases (HDACs) are liable for the acetylation as well as the deacetylation of the N-terminal ϵ -Lysine residue, respectively [5-7]. The HATs due to their acetylating ability

are capable of introducing an acetate function at the N-terminal lysine residues that lead to a loose binding of DNA around the histone octamer, thus forming *open chromatin* conformation. Contradictorily, the deacetylation function of the HDAC enzymes allows them to eliminate the lysine acetate function for a tighter binding of the DNA around the histone octamer to form a *closed chromatin* conformation (Fig. 1).

Therefore, the activity conferred by HAT and HDAC on histone proteins is one of the crucial epigenetic functions regulating gene expression and epigenetic modifications [5, 7-9]. As far as the Zn^{2+} -dependant HDACs are concerned, these contribute to a wide variety of pathophysiological conditions [5, 6, 10] including neurological disorders [10-12], solid and hematological cancer conditions [5, 6, 13], several inflammatory diseases [12, 14-16], viral and parasitic infections [17-19], diabetes [20], and cardiovascular disorders [16]. Therefore, due to the major involvement of several HDAC isoforms in a variety of diseases and pathophysiological conditions, these HDACs have emerged as promising therapeutic targets for the development of potential drug candidates. Over time, the development of HDAC inhibitors has delivered some fruitful outcomes in disease management. However, only a few HDAC inhibitors namely vorinostat, belinostat, panobinostat, pracinostat, and romidepsin have been accepted by the United States Food and Drug Administration (US-FDA), whereas the benzamide-derived

*Address correspondence to this author at the Epigenetic Research Laboratory, Department of Pharmacy, Birla Institute of Technology and Science-Pilani, Hyderabad Campus, Shamirpet, Hyderabad, 500078, India; Tel: 91-4066303639; Mobile: 91-986-694-1923; E-mail: balaram@hyderabad.bits-pilani.ac.in



Cite this: *New J. Chem.*, 2023,
47, 7051

Quantitative structural assessments of potential meprin β inhibitors by non-linear QSAR approaches and validation by binding mode of interaction analysis†

Suvankar Banerjee,^a Sandip Kumar Baidya,^a Balaram Ghosh,^b
Suvendu Nandi,^c Mahitosh Mandal,^c Tarun Jha^{*a} and Nilanjan Adhikari^{*a}

The Zn^{2+} -dependent endopeptidase meprin β is an astacin family metalloenzyme that belongs to the metzincin superclass of metalloproteases. The presence of a wide variety of meprin β substrates has enabled this metalloenzyme to influence a range of biological pathways and processes that correspondingly correlate meprin β with several diseases and abnormal physiological conditions. The influences of the meprin β proteolytic activity have been observed in cancer, neurodegenerative disorders, hyperkeratosis, and inflammatory conditions, including fibrosis. Therefore, the development of effective inhibitors is an achievable method for therapeutic advancement against meprin β -related pathophysiological conditions. In this context, in this study, a combined quantitative structural assessment of a set of meprin β inhibitors is performed via fragment-based non-linear pattern recognition techniques and the binding mode of interaction analysis at the active site of the enzyme. This study has elucidated various structural attributes such as the presence of a chiral center, the orientation of halogenic groups, hydroxyl and carbonyl functions, and the effect of aryl sulfonamide moieties along with their effect on the binding of these compounds at the active site. Depending on the present outcomes, some new molecules were designed and these were highly effective meprin β inhibitors. The molecular dynamics (MD) simulation study also revealed the stability of both the best active and the designed compound at the meprin β active site. Therefore, the findings of this current study as well as the developed non-linear machine learning (ML) models of these meprin β inhibitors can be a valuable tool to identify and design potent and effective inhibitors for the treatment of meprin β -related pathophysiological conditions.

Received 26th September 2022,
Accepted 10th February 2023

DOI: 10.1039/d2nj04753e

rsc.li/njc

1. Introduction

The study of the metalloenzymes in normal and pathophysiological conditions has elucidated several crucial involvements of these enzymes in a wide range of disease states, including cancer, neurodegenerative disorders, inflammation, osteoarthritis, cardiovascular diseases, viral and parasitic infections, as well as in epigenetic abnormalities.^{1–7} Although several attempts were made to develop potential and selective inhibitors of such

metalloenzymes, a few novel molecules have been approved to date for targeting such metalloenzyme-related pathophysiology and associated disease conditions.⁸

Among these metalloenzymes, the Zn^{2+} -dependent metalloenzyme meprin β is one of the metzincin superfamily proteases that modulates several substrates such as procollagen I, collagen IV, triggered receptor expressed on myeloid cells 2 (TREM 2), interleukin (IL)-6R, cluster of differentiation (CD) 109, CD99, MUC-2, amyloid precursor protein (APP), E-cadherin, and IL-1 β .^{9,10} Meprin metalloenzyme was first discovered in mouse kidneys and human intestines in 1980.¹⁰ Both the meprin family members, i.e., meprin α and meprin β are the Zn^{2+} -dependent multi-domain proteases that belong to the astacin family of the metzincin endo-peptidase superfamily.^{9–12} The structure of meprin β consists of an N-terminal signal peptide followed by a pro-peptide domain, an astacin-like protease domain consisting of a Zn^{2+} -dependent catalytic active site, a meprin A5 protein tyrosine phosphatase μ (MAM) domain, a tumor necrosis factor receptor-associated factor (TRAF) domain, an epidermal growth

^a Natural Science Laboratory, Division of Medicinal and Pharmaceutical Chemistry, Department of Pharmaceutical Technology, Jadavpur University, Kolkata 700032, India. E-mail: tjupharm@yahoo.com, nilanjan_juphar@rediffmail.com

^b Epigenetic Research Laboratory, Department of Pharmacy, Birla Institute of Technology and Science-Pilani, Hyderabad Campus, Shamirpet, Hyderabad, 500078, India

^c Cancer Biology Laboratory, School of Medical Science & Technology, Indian Institute of Technology Kharagpur, Kharagpur, West Bengal 721302, India

† Electronic supplementary information (ESI) available. See DOI: <https://doi.org/10.1039/d2nj04753e>



A comparative quantitative structural assessment of benzothiazine-derived HDAC8 inhibitors by predictive ligand-based drug designing approaches

S. Banerjee , S.K. Baidya , N. Adhikari and T. Jha

Natural Science Laboratory, Division of Medicinal and Pharmaceutical Chemistry, Department of Pharmaceutical Technology, Jadavpur University, Kolkata, India

ABSTRACT

Histone deacetylase 8 (HDAC8) is a verified biomolecular target associated with diverse diseases including cancer. Though several HDAC inhibitors emerged effective against such diseases, no selective HDAC8 inhibitor is approved to date. Therefore, the development of potent HDAC8-selective inhibitors is inevitable to combat such diseases. Here, some benzothiazine-derived HDAC8 inhibitors were considered for a comparative QSAR analysis which may elucidate the prime structural components responsible for modulating their efficacy. Several outcomes from these diverse modelling techniques justified one another and thus validated each other. The ligand-based pharmacophore modelling study identified ring aromatic, positive ionizable, and hydrophobic features as essential structural attributes for HDAC8 inhibition. Besides, MLR, HQSAR and field-based 3D-QSAR studies signified the utility of the positive ionizable and hydrophobic features for potent HDAC8 inhibition. Again, the field-based 3D-QSAR study provided useful insight regarding the substitution in the fused phenyl ring. Moreover, the current observations also validated the previously reported molecular docking observations. Based on the outcomes, some new molecules were designed and predicted. Therefore, this comparative structural analysis of these HDAC8 inhibitors will surely assist in the development of potent HDAC8 inhibitors as promising anticancer therapeutics in the future.

ARTICLE HISTORY

Received 17 August 2022
Accepted 1 December 2022

KEYWORDS

Histone deacetylase 8;
benzothiazine derivatives;
pharmacophore mapping;
CoMFA; CoMSIA; binding
mode of analysis

Introduction

Histone deacetylases (HDACs) are known for discarding the acetyl groups from lysine residues of histone proteins to modulate diverse cellular functions through epigenetic modifications [1,2]. HDACs are involved in genetic transcription mechanisms and subsequently, modulate growth factors and tumour suppressors [3,4]. HDACs are correlated to different cellular signalling pathways and subsequently, abnormal expression of HDACs is associated with various diseases including cancer, neurodegenerative disorders, and immune diseases [2,5–7]. Therefore, HDACs can be targeted to achieve potential therapeutics against such diseases including cancer. HDAC inhibitors alone or in combination

CONTACT N. Adhikari nilanjan_juphar@rediffmail.com; T. Jha tjupharm@yahoo.com
 Supplemental data for this article can be accessed at: <https://doi.org/10.1080/1062936X.2022.2155241>

© 2022 Informa UK Limited, trading as Taylor & Francis Group



A quantitative structural analysis of AR-42 derivatives as HDAC1 inhibitors for the identification of promising structural contributors

R. Kundu, S. Banerjee , S.K. Baidya , N. Adhikari and T. Jha

Natural Science Laboratory, Division of Medicinal and Pharmaceutical Chemistry, Department of Pharmaceutical Technology, Jadavpur University, Kolkata, India

ABSTRACT

Alteration and abnormal epigenetic mechanisms can lead to the aberration of normal biological functions and the occurrence of several diseases. The histone deacetylase (HDAC) family of enzymes is one of the prime regulators of epigenetic functions modifying the histone proteins, and thus, regulating epigenetics directly. HDAC1 is one of those HDACs which have important contributions to cellular epigenetics. The abnormality of HDAC is correlated to the occurrence, progression, and poor prognosis in several disease conditions namely neurodegenerative disorders, cancer cell proliferation, metastasis, chemotherapy resistance, and survival in various cancers. Therefore, the progress of potent and effective HDAC1 inhibitors is one of the prime approaches to combat such diseases. In this study, both regression and classification-based molecular modelling studies were conducted on some AR-42 derivatives as HDAC1 inhibitors to elucidate the crucial structural aspects that are responsible for regulating their biological responses. This study revealed that the molecular polarizability, van der Waals volume, the presence of aromatic rings as well as the higher number of hydrogen bond acceptors might affect prominently their inhibitory activity and might be responsible for proper fitting and interactions at the HDAC1 active site to pertain effective inhibition.

ARTICLE HISTORY

Received 13 September 2022
Accepted 2 November 2022

KEYWORDS

HDAC1; AR-42; MLR; LDA;
Bayesian classification;
Molecular modelling study

Introduction

The term ‘cancer’ can be defined as the proliferation, uncontrolled growth, and differentiation of cells in the body. Nowadays, cancer is one of the prime health-related issues of our modern society that threatens the development as well as the well-being of the current worldwide population [1]. According to Globacan, a total number of 19,292,789 new cancer cases have been reported in the year 2020 along with 9,958,133 cancer-related deaths [2]. Among these newly diagnosed cases, a majority of cancer cases were observed for breast and lung cancers. Also, among the reported cancer-related deaths that occurred in the year 2020, most were due to lung cancer (18%), liver cancer (8.3%), and colorectal cancer (9.4%) [2].

CONTACT T. Jha tjupharm@yahoo.com; N. Adhikari nilanjan_juphar@rediffmail.com
 Supplemental data for this article can be accessed at: <https://doi.org/10.1080/1062936X.2022.2145353>

© 2022 Informa UK Limited, trading as Taylor & Francis Group

Selective Inhibitors of Medium-Size S1' Pocket Matrix Metalloproteinases: A Stepping Stone of Future Drug Discovery

Sandip Kumar Baidya, Suvankar Banerjee, Nilanjan Adhikari,* and Tarun Jha*

Cite This: *J. Med. Chem.* 2022, 65, 10709–10754

Read Online

ACCESS |



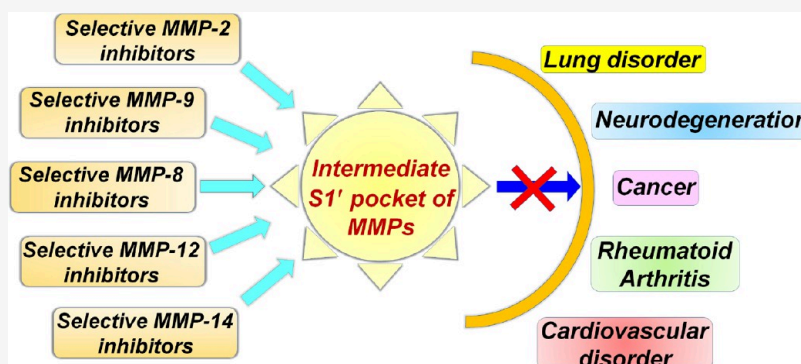
Metrics & More



Article Recommendations



Supporting Information



ABSTRACT: Among various matrix metalloproteinases (MMPs), MMPs having medium-size S1' pockets are established as promising biomolecular targets for executing crucial roles in cancer, cardiovascular diseases, and neurodegenerative diseases. However, no such MMP inhibitors (MMPIs) are available to date as drug candidates despite a lot of continuous research work for more than three decades. Due to a high degree of structural resemblance among these MMPs, designing selective MMPIs is quite challenging. However, the variability and uniqueness of the S1' pockets of these MMPs make them promising targets for designing selective MMPIs. In this perspective, the overall structural aspects of medium-size S1' pocket MMPs including the unique binding patterns of enzyme–inhibitor interactions have been discussed in detail to acquire knowledge regarding selective inhibitor designing. This overall knowledge will surely be a curtain raiser for the designing of selective MMPIs as drug candidates in the future.

■ INTRODUCTION

Matrix metalloproteinases (MMPs) are zinc-dependent endopeptidases. They are responsible for the degradation of the extracellular matrix (ECM). Several enzymes are involved in the remodeling of ECM, but these MMPs execute major roles.¹ Tissue remodeling is essential for the modulation of numerous physiological processes such as tissue repair, morphogenesis, growth, and development as well as tissue homeostasis. It could be a major reason for regulating several pathological conditions including cardiovascular diseases, neurodegenerative diseases, arthritis, and cancer. Therefore, matrix metalloproteinase inhibitors (MMPIs) have been evaluated as a potential pharmacological remedy for the management of osteoarthritis, cancer, and cardiovascular disorders. By regulating the ECM, MMPs are involved in growth factor availability and play crucial roles in the activity of cell surface signaling systems and, subsequently, influence cell proliferation, migration, and apoptosis.² In general, all these MMPs are secreted as inactive forms. The “cysteine switch” mechanism is one of the major MMP activation techniques where the thiol group is unpaired and the cysteine is replaced with a water molecule. At the time of this stepwise activation mechanism, it enables the hydroxylation of pro-peptides of

partially activated MMPs.³ Most of these MMPs are activated in the intercellular condition other than membrane-type MMPs (MT-MMPs), MMP-11, MMP-23, and MMP-28.² A total of 26 different types of MMPs have been identified, and their sequence homology along with biological effects has also been disclosed.⁴ These MMPs are grouped into six different classes based on their substrate specificity, i.e., (i) collagenases (MMP-1, MMP-8, MMP-13, MMP-18), (ii) gelatinases (MMP-2, MMP-9), (iii) matrilysins (MMP-7, MMP-26), (iv) stromelysins (MMP-3, MMP-10, MMP-11), (v) MT-MMPs (MMP-14, MMP-15, MMP-16, MMP-17, MMP-24, MMP-25), and (vi) miscellaneous MMPs (MMP-12, MMP-19, MMP-20, MMP-21, MMP-22, MMP-23, MMP-28, MMP-29). MMPs are found to execute significant roles in the

Received: October 28, 2021

Published: August 15, 2022





Cite this: DOI: 10.1039/d2nj01923j

The first report on predictive comparative ligand-based multi-QSAR modeling analysis of 4-pyrimidinone and 2-pyridinone based APJ inhibitors†

Suvankar Banerjee,^a Sandip Kumar Baidya,^a Balaram Ghosh,^b
Nilanjan Adhikari[✉] and Tarun Jha[✉]

The apelin–apelin receptor (APJ) system has been a promising biomolecular target participating crucially in several major disorders including cardiovascular diseases, neurodegenerative diseases, metabolic disorders, and lung, liver, and kidney-related diseases as well as in cancer. Though it is a promising therapeutic target for drug design for such diverse disease conditions, surprisingly no such molecular modeling study has been performed to date. This study reports the first predictive comparative multi-QSAR modeling analysis (like stepwise linear regression QSAR, MIA-QSAR, 3D-QSAR CoMFA, and CoMSIA) on a series of 4-pyrimidinone and 2-pyridinone-based APJ inhibitors to assimilate the knowledge regarding the crucial structural and physicochemical features responsible for the modulation of the APJ inhibitory effects. The statistically validated multi-QSAR modeling study unveils the importance of several crucial structural features responsible for modulating APJ inhibition. The presence of the 5-benzyl-1,3,4-oxadiazole ring, the higher number of hydrogen bond acceptor groups, and 4-chlorobenzyl, 4-bromobenzyl, and 2-methoxy groups may favor APJ inhibitory effects. However, bulky thiophenyl and *n*-butyl groups are detrimental to APJ inhibition. This current study may accelerate the process of the design and discovery of novel and highly potential APJ inhibitors for the effective treatment of multiple life-threatening disease conditions.

Received 19th April 2022,
Accepted 10th May 2022

DOI: 10.1039/d2nj01923j

rsc.li/njc

1. Introduction

The apelin receptor (APJ) is a rhodopsin-like class-A G-protein coupled receptor (GPCR) and was brought to light in the year 1993.^{1,2} However, this discovery is based on the sequence homology of the angiotensin II receptor and is further known as APJ.² The expression of APJ can be traced extensively in a broad spectrum of eukaryotes including human beings along with a higher expression in the CNS.³ Apelin is also secreted by the adipose tissue⁴ and the apelin receptor helps to inhibit glucose-simulated insulin secretion (GSIS).⁵ Interestingly, activation of APJ may lead to the reduction of insulin secretion which is responsible for the impairment of glucose elimination. Insulin binds to the APJ receptor on adipocytes along with the expression of apelin. Furthermore, these mechanisms provide negative

feedback on insulin production.⁵ The apelin-mediated activation of APJ is associated with several important physiological functions like fluid homeostasis, energy regulation, angiogenesis, vasodilation, and vasoconstriction along with the consolidation of heart muscle contractility.^{2,3,6} Similar to antidiuretic hormones such as vasopressin, apelin has potential regulatory roles in the fluid balance. However, several other studies have shown a clear diuretic effect for apelin with a decrease in the vasopressin expression.^{7,8} APJ was also found to be associated with the embryonic development of zebrafish when activated by Toddler/ELABELA, another indigenous peptide ligand.^{9,10} The combination of ELABELA and APJ is also associated with cardiovascular physiology and pathophysiology.¹¹ The primary pathophysiological conditions of APJ may be dependent on the context-related behavior of the GPCR.¹² From the aspects of the pathophysiology of APJ in terms of the drug development perspective, the APJ can be correlated with several physiological disorders such as cardiovascular diseases, neurological disorders, endothelial dysfunction-related diseases, respiratory diseases, inflammatory conditions, gastrointestinal diseases, hepatic disorders, kidney diseases, hypoxia-related diseases, metabolic disorders, and cancer progression.^{2,13–23}

Furthermore, the mechanism of action of apelin through the APJ is angiogenic, both in normal physiological conditions and

^a Natural Science Laboratory, Division of Medicinal and Pharmaceutical Chemistry, Department of Pharmaceutical Technology, Jadavpur University, Kolkata 700032, India. E-mail: nilanjan_juphar@rediffmail.com, tjupharm@yahoo.com

^b Epigenetic Research Laboratory, Department of Pharmacy, Birla Institute of Technology and Science–Pilani, Hyderabad Campus, Shamirpet, Hyderabad, 500078, India

† Electronic supplementary information (ESI) available. See DOI: <https://doi.org/10.1039/d2nj01923j>



Applying comparative molecular modelling techniques on diverse hydroxamate-based HDAC2 inhibitors: an attempt to identify promising structural features for potent HDAC2 inhibition

V. Yadav, S. Banerjee , S.K. Baidya , N. Adhikari and T. Jha

Natural Science Laboratory, Division of Medicinal and Pharmaceutical Chemistry, Department of Pharmaceutical Technology, Jadavpur University, Kolkata, India

ABSTRACT

Histone deacetylase 2 (HDAC2) has been implicated in a variety of cardiovascular and neurodegenerative disorders as well as in cancers. Thus, HDAC2 has become an exclusive target for anticancer drug development. Therefore, the development of newer HDAC2 inhibitors in disease conditions is a prime goal to restrain such a scenario. Although a handful of HDAC inhibitors was accepted for the treatment of HDAC-related disease conditions, the non-selective nature of these entities is one of the major setbacks in the treatment of specific HDAC isoform-related pathophysiology. In this framework, the analyses of pre-existing molecules are essential to identify the important structural features that can fulfil the requirements for the cap and linker moieties to obtain potent and effective HDAC2 inhibition. Thus, in this study, the implementation of a combined comparative 2D and 3D molecular modelling techniques was done on a group of 92 diverse hydroxamate derivatives having a wide range of HDAC2 inhibitory potency. Besides other crucial features, this study upheld the importance of groups like triazole and benzyl moieties along with the molecular fields that are crucial for regulating HDAC2 inhibition. The outcomes of this study may be employed for the designing of HDAC2 inhibitors in future.

ARTICLE HISTORY

Received 6 September 2021
Accepted 29 November 2021

KEYWORDS

HDAC2; MLR; LDA; recursive partitioning; CoMFA; CoMSIA

Introduction

The group of histone deacetylases (HDACs) are the Zn^{2+} /nicotinamide adenine dinucleotide (NAD^+)-dependent metalloenzymes having crucial contributions in transcriptional regulation. This is done by modulating the chromatin structure via erasing the acetate moiety from the acetylated N-terminal lysine ϵ -amino acid group of histone proteins. This process of acetate removal from the histone amino acids is known as deacetylation of histone [1,2].

CONTACT T. Jha tjupharm@yahoo.com

[#]Authors have equal contribution.

Supplemental data for this article can be accessed at: <https://doi.org/10.1080/1062936X.2021.2013317>

© 2022 Informa UK Limited, trading as Taylor & Francis Group



A robust classification-dependent multi-molecular modelling study on some biphenyl sulphonamide based MMP-8 inhibitors

S. Gutti, S.K. Baidya , S. Banerjee , N. Adhikari  and T. Jha 

Natural Science Laboratory, Division of Medicinal and Pharmaceutical Chemistry, Department of Pharmaceutical Technology, Jadavpur University, Kolkata, India

ABSTRACT

Matrix metalloproteinases (MMPs) are a group of zinc and calcium-dependent endopeptidases, which contribute to different physiological and biological activities via extracellular matrix (ECM) degradation. Matrix metalloproteinase-8 (MMP-8) belongs to type-II collagenases of the MMP family that has contribution in several physiological disorders such as cardiovascular diseases, joint, renal, digestive and respiratory disorders as well as in cancer. In clinical study, MMP-8 is found to be associated with periodontal disease condition. Therefore, MMP-8 specific inhibitors should be developed to target these disorders. The biphenyl sulphonamide (BPS) moiety is one of the crucial structural characteristics found in several MMP-8 inhibitors. Here, different classification-based molecular modelling methods were used to explore the structural features that lead to the activity variation of a series of MMP-8 inhibitors possessing a BPS moiety. Our current classification-based structural analysis of these BPS-derived MMP-8 inhibitors was able to identify the importance of several structural features such as the tetrahydroisoquinoline and N-Boc pyridyl groups, which have positive influences on MMP-8 inhibition. This study was also reflected the importance of the zinc-binding groups (ZBGs) like the hydroxamate and phosphonate for potent and sub-nanomolar range MMP-8 inhibition, which may benefit the development of highly potent MMP-8 inhibitors.

ARTICLE HISTORY

Received 10 August 2021
Accepted 1 September 2021


KEYWORDS

MMP-8 inhibitor;
classification-based QSAR;
LDA; Bayesian classification;
recursive partitioning; SARpy

Introduction

Matrix metalloproteinases (MMPs) are the zinc and calcium containing membrane-bound endopeptidases present intracellularly and classified under metzincin superfamily [1,2]. MMPs are multidomain proteins having common structural features like the amino terminal pre-domain, the conserved pro-domain, the catalytic domain and the hemopexin-like carboxy terminal domain [2]. Primarily, MMPs are biosynthesized as inactive form such as zymogen/pro-MMPs. However, MMPs are activated by the ‘cysteine-switch’ motif. The ‘cysteine switch’ model demonstrates that the interaction between cysteine in pro-peptide domain and the zinc ion in the catalytic domain [3]. MMPs are also

CONTACT T. Jha  tjupharm@yahoo.com

 Supplemental data for this article can be accessed at: <https://doi.org/10.1080/1062936X.2021.1976831>.

© 2021 Informa UK Limited, trading as Taylor & Francis Group



Review article

Outline of gelatinase inhibitors as anti-cancer agents: A patent mini-review for 2010-present



Sandip Kumar Baidya, Sk. Abdul Amin, Tarun Jha*

Natural Science Laboratory, Division of Medicinal and Pharmaceutical Chemistry, Department of Pharmaceutical Technology, P. O. Box 17020, Jadavpur University, Kolkata, 700032, West Bengal, India

ARTICLE INFO

Article history:

Received 13 August 2020

Received in revised form

15 October 2020

Accepted 18 November 2020

Available online 24 November 2020

Keywords:

Matrix metalloproteinase

Gelatinase inhibitor

Cancer

Medicinal chemistry

Hydroxamate

ABSTRACT

Matrix metalloproteinases (MMPs) are involved in several pathological and physiological functions. Gelatinases (MMP-2 and -9) have significant attention as therapeutic targets against cancer. Gelatinase inhibitors have demonstrated their effectiveness in several diseases including cancer. However, it is quite a challenging task to develop inhibitors as a therapeutic agent.

This review summarizes the patent dedicated to the medicinal chemistry of gelatinase inhibitor reported over last decades. We examine the patent being pursued for gelatinase inhibitor development to highlight the key issues. The main aim is to provide the scientific community with an overview of the patented gelatinase inhibitors to allow further development.

During early 2000s, some MMP inhibitors failed to pass the clinical trials. Hence, the lessons learned from early evidence and recent knowledge in that field will rejuvenate the development of selective inhibitors. Various studies and patents have continued in the recent years to expand knowledge. Continuously, our research team has been involved in the design of potent and selective gelatinase inhibitors for the past few years. This study is a part of our efforts. This study may be beneficial in the design and development of better gelatinase inhibitors in the future.

© 2020 Elsevier Masson SAS. All rights reserved.

Contents

1. Introduction	2
2. Pathophysiological role of gelatinase	2
3. Structure of gelatinase	2
4. Previous inhibitors in clinical trials	3
4.1. Collagen peptidomimetics	4
4.2. Non-peptidomimetics	4
4.3. Bisphosphonates & bisphosphonate esters	5
4.4. Tetracyclines	6
5. Outline of patent study of gelatinase inhibitors against cancer	6
5.1. Aryl-sulfonamide/aryl-sulfonide derivatives	6
5.2. Non-Arylsulfonamide derivatives	9
6. Expert opinion	10
Declaration of competing interest	10
Acknowledgement	10
References	11

* Corresponding author.

E-mail addresses: sandipbaidya@hotmail.com (S.K. Baidya), pharmacist.amin@gmail.com, skabdulamin.rs@jadavpuruniversity.in (Sk.A. Amin), tjupharm@yahoo.com (T. Jha).



Exploring the structural aspects of ureido-amino acid-based APN inhibitors: a validated comparative multi-QSAR modelling study

S. Banerjee, S.A. Amin , S.K. Baidya, N. Adhikari and T. Jha

Natural Science Laboratory, Division of Medicinal and Pharmaceutical Chemistry, Department of Pharmaceutical Technology, Jadavpur University, Kolkata, India

ABSTRACT

The zinc-dependent enzyme aminopeptidase N (APN) is a member of the M1 metalloenzyme family. The multi-functionality of APN as a peptidase, a receptor and a signalling molecule has provided it the access to influence a number of disease conditions namely viral diseases, angiogenesis, cellular metastasis and invasion including different cancer conditions. Hence, the development of potent APN inhibitors is a possible route for the treatment of diseases related to the activity of APN. In this study, different QSAR approaches have been adopted to identify the structural features of a group of hydroxamate-based ureido-amino acid derivative APN inhibitors. This study was able to identify different constitutional aspects of these APN inhibitors which are important for their inhibitory potency. Additionally, some of these observations were also aligned with the observations of previously performed QSAR studies conducted on different APN inhibitors. Therefore, the results of this study may help to design potent and effective APN inhibitors in the future.

ARTICLE HISTORY

Received 17 December 2019
Accepted 20 February 2020

KEYWORDS

Aminopeptidase-N; APN inhibitor; 2D-QSAR; LDA; Bayesian classification model

Introduction

Aminopeptidase N/CD13 is one of the members of the type-II Zn^{2+} dependent transmembrane exopeptidase enzymes belonging to the M1 family of the MA clan of metalloproteinases [1–5]. APN is frequently known as glunzicins and can be easily categorized due to the consensus HEXXH sequence present in it [2,5]. It is also popular as aminopeptidase N because of its ability to cleave the N-terminal amino acid residues from substrates [1,2,4]. Apart from this, the multifunctional ability of APN/CD13 allows it to act as a receptor for viral endocytosis and a signalling molecule for being a part of signal transduction. Therefore, it helps to influence a number of pathophysiological and disease conditions [1,2,4,5].

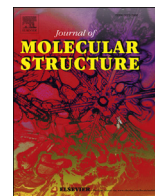
The APN mediated terminal degradation of peptides is associated with the deactivation of neuropeptide hormones such as enkephalins and endorphins [1]. Moreover, chemotactic peptides (MCP-1), angiotensin III (Ang-III) and kinins are associated with APN as substrates. APN has been found to be involved in the processing of cell surface

CONTACT T. Jha tjupharm@yahoo.com

This article was originally published with errors, which have now been corrected in the online version. Please see Correction (<http://dx.doi.org/10.1080/1062936X.2020.1744875>)

Supplementary data for this article can be accessed at: <https://doi.org/10.1080/1062936X.2020.1734080>.

© 2020 Informa UK Limited, trading as Taylor & Francis Group



Structural exploration of arylsulfonamide-based ADAM17 inhibitors through validated comparative multi-QSAR modelling studies

Sandip Kumar Baidya¹, Sk. Abdul Amin¹, Suvankar Banerjee, Nilanjan Adhikari², Tarun Jha^{*}

Natural Science Laboratory, Division of Medicinal and Pharmaceutical Chemistry, Department of Pharmaceutical Technology, Jadavpur University, P. O. Box 17020, Kolkata, 700032, West Bengal, India

ARTICLE INFO

Article history:

Received 11 December 2018

Received in revised form

19 February 2019

Accepted 21 February 2019

Available online 26 February 2019

Keywords:

ADAM17

2D-QSAR

HQSAR

Bayesian classification

Pharmacophore mapping

Molecular docking

ABSTRACT

Zinc-dependent ADAM17 takes part in a number of life-threatening conditions such as inflammatory diseases, cancer, Alzheimer's disease and rheumatoid arthritis. Therefore, ADAM17 may be a valuable target to design specific inhibitors for combating these diseases. In this scenario, it is a challenging task to design specific ADAM17 inhibitors as none of the earlier investigated compounds has come into the market as a potential drug candidate. Here, molecular modelling including 2D-QSAR, HQSAR, Bayesian classification, pharmacophore mapping and molecular docking studies of arylsulfonamides were performed to explore the structural and pharmacophoric requirements for exerting higher ADAM17 inhibitory activity. All these molecular modelling approaches were validated individually and these were statistically significant and reliable. The bulky steric and hydrophobic P1' substituents at the *para* position of the arylsulfonamido moiety favoured ADAM17 inhibition that supported and validated by molecular docking study. These crucial observations of arylsulfonamides may be considered for designing higher effective ADAM17 inhibitors in future.

© 2019 Elsevier B.V. All rights reserved.

1. Introduction

A disintegrin and metalloproteinase 17 (ADAM17), a zinc-dependant metalloenzyme, is a type I proteolytic enzyme adhered to the cell membrane. It belongs to the adamalysin family of protease enzymes under M12 subfamily of the subclan M under metalloproteinase clan MA [1–3]. ADAM17 is found to be involved in the shedding of several cytokines. The structural characterization of ADAM17, also known as Tumour necrosis factor- α converting enzyme (TACE), provides information about the large extracellular region comprising a number of domains. The cystine switch motif belongs to the prodomain regulates the activation and inactivation of the enzyme through coordination with the catalytic Zn^{2+} ion of the catalytic or metalloproteinase domain. The catalytic domain of the enzyme consists of the catalytic zinc ion which is responsible

for the proteolysis. The catalytic domain also provides the specific characteristics for the identification of the enzyme for being a member of the metalloproteinase family. The presence of the disintegrin domain next to the catalytic domain is known as the ectodomain having a C-shaped structure to increase the stiffness of the ectodomain. The membrane proximal domain (MPD) adjacent to the disintegrin domain supervises the enzymatic activity and substrate binding [4,5]. The Conserved Adam Seventeen Dynamic Interaction Sequence (CANDIS), a small amphiphilic helical region, is observed between the MPD and the transmembrane region. The CANDIS region assists the substrate recognition and substrate-enzyme interaction [6]. A transmembrane region helps the protein to remain attached to the cell surface where the cytosolic region is located inside the cell cytosol [4,5,7]. This structural feature of ADAM17 ectodomain resembles the structural characteristics of some other metalloenzymes such as snake venom metalloproteinases (SVMs), ADAM-thrombospondin motifs (ADAM-TS), membrane-type matrix metalloproteinases (MT-MMPs) and matrix metalloproteinases (MMPs) [5]. Structures of ADAM17 and ADAM10 ectodomains are almost identical to each other whereas the metalloproteinase domain of ADAM17 resembles with SVM, MT-MMP, MMPs and ADAM-TS that might explain the inhibition of

^{*} Corresponding author.

E-mail address: tjupharm@yahoo.com (T. Jha).

¹ Authors have equal contribution.

² Present Address: School of Pharmaceutical Technology, ADAMAS University, Barasat-Barrackpore Road, P. O. Jagannathpur, Kolkata – 700126, West Bengal, India.

Chapter 6

**DESIGN AND DEVELOPMENT OF MATRIX
METALLOPROTEINASE INHIBITORS CONTAINING
ZINC-BINDING GROUPS, WITHOUT ZINC-BINDING
GROUPS, AND MECHANISM-BASED**

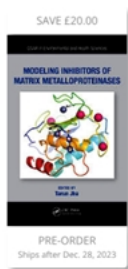
*Nilanjan Adhikari¹, Sandip Kumar Baidya¹,
Achintya Saha², Nahid Ali³ and Tarun Jha^{1,*}*

¹Natural Science Laboratory, Division of Medicinal and Pharmaceutical Chemistry,
Department of Pharmaceutical Technology,
Jadavpur University, Kolkata, India
²Department of Chemical Technology,
University of Calcutta, Kolkata, India
³Infectious Diseases and Immunology Division,
Council of Scientific and Industrial Research-Indian
Institute of Chemical Biology, Kolkata, West Bengal, India

ABSTRACT

Zinc metalloenzymes are ubiquitous in nature and are found in animals, plants and microbial organisms. Among different metalloenzymes, only the zinc-dependent matrix metalloproteinases (MMPs) have been widely studied and their potential inhibitors (MMPIs) have been mostly related to the chemicals that contain some zinc-binding group (ZBG). This chapter presents the design and discovery of important zinc-binding group containing MMPIs. Additionally, there also have been some MMPIs that do not contain any ZBG or those whose action is mechanism-based. This chapter presents an account of such inhibitors also along with their modes of action.

*Address for correspondence: Natural Science Laboratory, Division of Medicinal and Pharmaceutical Chemistry, Department of Pharmaceutical Technology, P.O. Box 17020, Jadavpur University, Kolkata 700032, India, E-mail: drtarunjha@yahoo.com.



1st Edition

Modeling Inhibitors of Matrix Metalloproteinases

Edited By Tarun Jha

Copyright 2024

Hardback

Available for pre-order. Item will ship after December 29, 2023

£99.99

GBP €79.99

1

PRE-ORDER

PURCHASE LOCALLY

ADD TO WISH LIST

ISBN 9781032289267

490 Pages 96 Color & 114 B/W Illustrations

December 29, 2023 by CRC Press

[Request Inspection Copy](#)Free Shipping (14-21 Business Days)
[shipping options](#)

Description

Matrix metalloproteinases (MMPs) have been established as promising biomolecular targets for novel drug design and discovery against numerous major disease conditions including various cancers, cardiovascular, neurodegenerative, inflammatory diseases, and more. This book covers various modern molecular modeling methodologies particularly related to MMP inhibitors. Included in the text are descriptions of ligand-based drug designing and structure-based drug designing modeling strategies for designing potential and target specific or selective MMPs. This book will benefit those who are looking for an in-depth text on the design and discovery processes of novel and selective MMPs.

Features

- Describes modeling strategies applied to MMPs
- Elaborates on the designing strategies of MMPs specifically
- Includes in-depth analyses of related case studies
- Acts as a guide for medicinal chemists, not only from pharmaceutical industries, but also from academia
- Covers various modern molecular modeling methodologies, particularly related to MMPs

Table of Contents

Part A: Fundamentals of molecular modeling

Chapter 1

2D-QSAR studies: Regression and classification-based QSAR studies

By Sanjib Das, Sk. Abdul Amin, Shovanai Gayen, and Tarun Jha

Chapter 2

3D-QSAR studies: CoMFA, CoMSIA and Topomer CoMFA methods

By Suvankar Banerjee, Sandip Kumar Baidya, Nilanjan Adhikari, and Tarun Jha

Chapter 3

Other modeling approaches: Pharmacophore mapping, molecular docking and molecular dynamic simulation studies

By Sk. Abdul Amin, Shovanai Gayen, Sanjib Das, and Tarun Jha

Part B: Matrix metalloproteinases and their inhibitors

Chapter 4

Collagenases and their inhibitors

By Sandip Kumar Baidya, Suvankar Banerjee, Nilanjan Adhikari, and Tarun Jha

Chapter 5

Gelatinases and their inhibitors

By Sk. Abdul Amin, Sanjib Das, Shovanai Gayen, and Tarun Jha

Chapter 6

Stromelysins and their inhibitors

By Sandip Kumar Baidya, Suvankar Banerjee, Nilanjan Adhikari, and Tarun Jha

Chapter 7

Matrilysins and their inhibitors

By Sandip Kumar Baidya, Suvankar Banerjee, Nilanjan Adhikari, and Tarun Jha

Chapter 8

Membrane-type MMPs and their inhibitors

By Suvankar Banerjee, Sandip Kumar Baidya, Nilanjan Adhikari, and Tarun Jha

Chapter 9

Other MMPs and their inhibitors

By Suvankar Banerjee, Sandip Kumar Baidya, Nilanjan Adhikari, and Tarun Jha

Part C: Modeling of MMP inhibitors

Chapter 10

Modeling inhibitors of Collagenases

By Sandip Kumar Baidya, Suvankar Banerjee, Nilanjan Adhikari, Balaram Ghosh, and Tarun Jha

Chapter 11

Modeling inhibitors of Gelatinases

By Samina Khatun, Sk. Abdul Amin, Suvankar Banerjee, Shovanai Gayen, and Tarun Jha

Chapter 12

Modeling inhibitors of Stromelysins

By Sandip Kumar Baidya, Suvankar Banerjee, Nilanjan Adhikari, and Tarun Jha

Chapter 13

Modeling inhibitors of Matrilysins

By Suvankar Banerjee, Sandip Kumar Baidya, Nilanjan Adhikari, and Tarun Jha

Chapter 14

Modeling inhibitors of membrane-type MMPs

By Suvankar Banerjee, Sandip Kumar Baidya, Nilanjan Adhikari, and Tarun Jha

Chapter 15

Modeling inhibitors of other MMPs

By Suvankar Banerjee, Sandip Kumar Baidya, Nilanjan Adhikari, and Tarun Jha

Part D: Conclusion and Future Perspective

Chapter 16

Conclusion and Future Perspectives

By Nilanjan Adhikari, Sandip Kumar Baidya, Suvankar Banerjee, and Tarun Jha

Sandeep Kumar Baidya
14/12/2023

Tarun Jha
14.12.23

TARUN JHA, Ph.D
Professor
Dept. of Pharm. Tech.
Jadavpur University
Kolkata-700 032

Nilanjan Adhikari
14/12/2023

DR. NILANJAN ADHIKARI
Assistant Professor
Dept. of Pharm. Tech.
Jadavpur University
Kolkata - 700 032